Studies of the role of nf-κb in controlling osteoclast differentiation and bone loss

Yao, Z.

STUDIES OF THE ROLE OF NF-κB IN CONTROLLING OSTEOCLAST DIFFERENTIATION AND BONE LOSS

ZHENQIANG YAO

A thesis submitted in fulfilment of the requirements of the University of Westminster for the degree of Doctor of Philosophy by publication

Collaborations

1. **Professor Brendan Boyce, Pathology and Laboratory Medicine, University of Rochester Medical Center, Rochester, NY, USA**
2. **Dr. Lianping Xing, Pathology and Laboratory Medicine, University of Rochester Medical Center, Rochester, NY, USA**
3. **Professor Brendan Lee, Baler College of Medicine, USA**

April 2016

CHAPTERS

Abstract

Increased osteoclast (OC) bone resorption and/or decreased osteoblast (OB) bone formation contribute to bone loss in osteoporosis and rheumatoid arthritis (RA). Findings of the basic and translational research presented in this thesis demonstrate a number of mechanisms by which cytokine-induced NF-κB activation controls bone resorption and formation: 1) Tumour necrosis factor-α (TNF) expands pool of OC precursors (OCPs) by promoting their proliferation through stimulation of the expression of macrophage colony stimulating factor (M-CSF) receptor, c-Fms, and switching M-CSF-induced resident (M2) to inflammatory (M1) macrophages with enhanced OC forming potential and increased production of inflammatory factors through induction of NF-κB RelB; 2) Similar to RANKL, TNF sequentially activates transcriptional factors NF-κB p50 and p52 followed by c-Fos and then NFATc1 to induce OC differentiation. However, TNF alone induces very limited OC differentiation. In contrast, it pre-activates OCPs to express cFos which cooperates with interleukin-1 (IL-1) produced by these OCPs in an autocrine mechanism by interacting with bone matrix to mediate the OC terminal differentiation and bone resorption from these pre-activated OCPs. 3) TNF-induced OC formation is independent of RANKL but it also induces NF-κB2 p100 to limit OC formation and bone resorption, and thus p100 deletion accelerates joint destruction and systemic bone loss in TNF-induced RA; 4) TNF receptor associated factor-3 (TRAF3) limits OC differentiation by negatively regulating non-canonical NF-κB activation and RANKL induces TRAF3 ubiquitination and lysosomal degradation to promote OC differentiation. Importantly, a lysosomal inhibitor that inhibits TRAF3 degradation prevents ovariectomy-induced bone loss; 5) RelB and Notch NICD bind RUNX2 to inhibit OB differentiation and RelB:p52 dimer association with NICD inhibit OB differentiation by enhancing the binding of RBPjκ to Hes1. These findings suggest that non-canonical NF-κB signaling could be targets to develop new therapies for RA or osteoporosis. For example 1) Agents that degrade TNF-induced RelB could block M1 macrophage differentiation to inhibit inflammation and joint destruction for the therapy of RA; 2) Agents that prevent p100 processing or TRAF3 degradation could inhibit bone resorption and also stimulate bone formation simultaneously for the therapy of osteoporosis.

List of abbreviations

ALP, alkaline phosphatase;

BM, bone marrow;

BSP, bone sialoprotein;

CFSE, Carboxyfluorescein Diacetate Succinimidyl Ester;

Chip, chromatin immunoprecipitation;

cKO, conditional knockout;

CQ, chloroquine;

μCT, micro–computed tomography;

dKO, double knockout;

DMARDs, disease modifying anti-rheumatic drugs;

DPP, dentin phosphoprotein;

DSP, dentin sialoprotein;

ELISA, enzyme-linked immunosorbent assay;

FACS, Fluorescence-activated cell sorting;

FBS, fetal bovine serum;

β-GP, β-glycerophosphate;

HRP, horseradish peroxidase;

IAP, inhibitor of apoptosis proteins;

IgG, immunoglobulin G;

IκB, inhibitory NF-κB protein;

IKK, IκB kinase;

IL-1, interleukin-1;

IL-1Ra, IL-1 receptor antagonist;

iNOS, inducible nitric oxide synthase;

KO, knockout;

M-CSF, macrophage colony stimulating factor;

MEM, modified essential medium;

MPC, mesenchymal progenitor cells;

NEMO, NF-κB essential modulator;

NFATc1, Nuclear factor of activated T-cells, cytoplasmic 1;

NF-κB, nuclear factor kappa-light-chain-enhancer of activated B cells;

NICD, Notch receptor intracellular domain;

NIK, NF-κB-inducing kinase;
OB, osteoblast;
OC, osteoclast;
OCIN, osteocalcin;
OCPs, osteoclast precursors;
OPG, osteoprotegerin;
OPN, osteopontin;
PBS, Phosphate-buffered saline;
PCR, polymerase chain reaction;
PPAR-γ, peroxisome proliferator-activated receptor gamma;
PTH, parathyroid hormone;
RA, rheumatoid arthritis;
RANKL, receptor activator of nuclear factor-kappa B ligand;
RBPjκ, recombination signal–binding protein jκ;
RUNX2, runt-related transcription factor 2;
SIBLING, small integrin-binding ligand, N-linked glycoprotein;
Smurf, Smad ubiquitin regulatory factor;
TGF-β1, transforming growth factor β1;
TNF, Tumour necrosis factor-α;
TNFR, TNF receptor;
TNF-Tg, transgenic mice with over-expression of human TNF-alpha;
TRAF, TNF receptor-associated factor;
TRAP, tartrate resistant acid phosphatase;

Chapter 1: Introduction

Bone is a dynamic structure that undergoes constant remodeling throughout life, in which mature bone tissue is removed from the skeleton by osteoclasts (OCs), a process called bone resorption, and new bone tissue is formed by osteoblasts (OBs), a process called bone formation. An OC, a multinucleated cell with 3 or more nuclei on the trabecular surface (Fig.1A), is originated from hematopoietic cell (Udagawa et al., 1990). The cytoplasm of an OC has a high concentration of vesicles and vacuoles including lysosomes filled with acid phosphatase, permitting the cell to be stained for high activity of tartrate resistant acid phosphatase (TRAP) (Fig.1 A-C) and Cathepin K. An activated OC is characterized by cytoskeletal reorganization, formation of sealing zones and specialized cell membrane called ruffled border that opposes the surface of the bone tissue, allowing it secretion of acids and lysosomal enzymes onto the resorbing surface (Boyce et al., 1992, Stenbeck, 2002). In contrast, an OB with single nuclei is specialized, terminally differentiated from a mesenchymal stem/progenitor cell (MSC/MPC) (Clarke, 2008) and it expresses activity of alkaline phosphatase (ALP) and thus is different from a MSC/MPC (Clarke, 2008). A number of connected OBs are organized as a group on the bone surface (Fig.1D), particularly OC resorbed lacunae, and this is essential for OBs to synthesize and secret bone matrix proteins called osteoid (Fig.1D lower panel), mainly composed of very dense, cross-linked collagen and several small amount of specialized proteins including osteocalcin and osteopontin (Clarke, 2008). The organized OBs then produce and deposit calcium-phosphate-hydroxide salt called hydroxyapatite on osteoid to finally form a very strong and dense mineralized bone tissue. Imbalance of bone remodeling, increased OC bone resorption and/or decreased

OB bone formation, results in bone loss contributing to common adult bone diseases including osteoporosis, rheumatoid arthritis (RA), bone metastatic cancer, aseptic loosening of arthroplasty and periodontitis (Boyle et al., 2003).

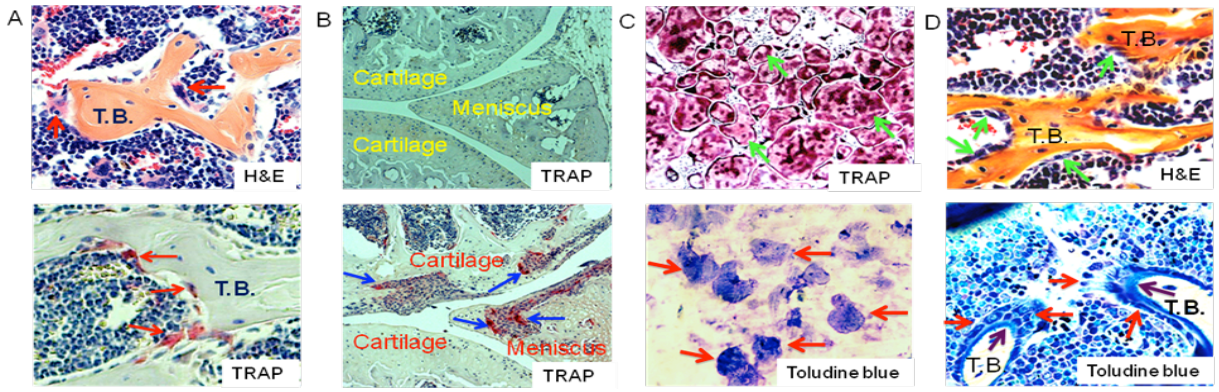

Fig.1. Features of OCs and OBs. (A) OCs locate on the surface of trabecular bone (T.B.) shown on H&E (upper panel)- and TARP (lower panel)-stained sections and are the TRAP+ (pink color) multinuclear cells (red arrow in the lower panel); (B) OCs do not exist in the joint surface normally (upper panel) while they are formed in the inflamed tissues adjacent to the articular surface to erode cartilage and bone (blue arrow) in a mouse RA model; (C) In vitro cultured OCs from mouse bone marrow cells by RANKL plus M-CSF stained with TRAP (pink color in the upper panel) and Toluidine blue to show resorption pits (red arrow, in the lower panel) on bone slices; (D) OBs are an organized groups of rectangle cells (green arrow) along with the trabecular surface (upper panel) and they produce osteoid (purple arrow in the lower panel, toluidine blue stained un-decalcified plastic section) between the organized OBs (red arrow) and T.B. along with the trabecular surfaces.

Osteoporosis is one of the leading diseases of aging, characterized by decreased bone mass and strength, resulting in increased fracture risk. It is estimated that 44 million people in the U.S. have low bone mineral density (BMD) and 10 million are

osteoporotic with low BMD. 1 in 2 Caucasian women and 25% of men over the age of 60 are likely to have osteoporotic fracture in their lifetime (Khosla, 2010, Keyak et al., 2011). Elderly patients with osteoporotic fractures develop complications, including pneumonia and deep vein thrombosis due to prolonged bed rest and up to 27% of them die within the first year after hip fracture (Panula et al., 2011). Currently, there are two classes of drugs for the treatment of osteoporosis: anti-resorptive and anabolic. The commonly used anti-resorptive drugs include a various bisphosphonates and the RANKL inhibitor Denosumab. Although anti-resorptive drugs effectively increase bone mass, they only reduce the rate of osteoporotic fracture by 50% (Wasnich and Miller, 2000). In addition, poor patient compliance and more recent fears about side-effects for anti-resorptive drugs such as bone necrosis have limited their use, and thus many patients go untreated (Rasmusson and Abtahi, 2014, Kennel and Drake, 2009). Teriparatide, a truncated form (amino acids 1-34) of PTH, is the first, and to date only, FDA approved agent for the treatment of osteoporosis by stimulating new bone formation however its use is limited to 2 years (Ponnapakkam et al., 2014) due to the potential to induce osteosarcoma (Cipriani et al., 2012). Developing new anti-resorptive and/or anabolic drugs is therefore an urgent need, particularly, there is no single drug with dual role that can simultaneously inhibit bone resorption and stimulate bone formation. Combined therapy with Teriparatide and a bisphosphonate does not appear to offer advantages over the use of the single agent alone (Black et al., 2003, Finkelstein et al., 2003) and therefore developing a drug with dual anti-resorptive and anabolic effect offers great promise for the prevention and treatment of osteoporosis.

RA is a chronic inflammatory disease characterized by synovial inflammation and joint destruction, leading to severe disability and premature mortality (Storheim and Zwart, 2014). About 1% of the world's population is afflicted by RA, women three times more often than men. Commonly there are three general classes of drugs used in the treatment of RA: non-steroidal anti-inflammatory agents (NSAIDs), corticosteroids, and disease modifying anti-rheumatic drugs (DMARDs). None of the treatments however can cure RA. Anti-TNF reagents such as Etanercept, Infliximab, Adalimumab, belong to the DMARDs and have significantly reduced the morbidity and joint destruction in RA, but they are expensive, and only ~50% of RA patients respond well to these agents (Hyrich et al., 2006, Symmons and Silman, 2006). In non-responding patients, TNF inhibitors are typically administered for several months before a decision is made to change to an alternative treatment, which is often another TNF inhibitor that may also be ineffective. Thus, there is an unmet need to develop new approaches to treat RA.

Generally, excessive differentiation and function of OCs, the unique cells that degrade bone, plays a central role in bone loss and destruction in RA and osteoporosis (Boyle et al., 2003) although the reduced bone formation is also considered to contribute these diseases. Normally, OCs don’t present in joint space, articular surface and the adjacent synovial tissue (Fig.1B upper panel). In RA, OCs are ectopically differentiated and activated on articular cartilage adjacent to the inflamed synovial tissue and thus erode the cartilage and subchondral bone (Fig.1B lower panel). In postmenopausal osteoporosis, both bone resorption and bone formation are increased (Garnero et al., 1994, Garnero et al., 1996, Eriksen et al., 1990) although some reported that bone formation was unchanged (Eriksen et al., 1990), resulting in the accelerated bone turnover and leading to bone loss finally. An unmet need therefore is

to perform extensive studies to shed light on the mechanism by which the differentiation and function of OCs may be controlled to suggest approaches to prevent/treat these diseases.

1.1 OC precursors and factors that control OC differentiation and activation

OCs are derived from the differentiation and fusion of myeloid lineage monocyte-macrophages (Udagawa et al., 1990) which are called OC precursors (OCPs). Macrophage colony stimulating factor (M-CSF) drives the myeloid progenitor cells to become monocyte OCPs and receptor activator of nuclear factor-kappa B (NF-κB) ligand (RANKL), a member of TNF superfamily of proteins, mediates the terminal differentiation and fusion of OCPs (Lacey et al., 1998, Dougall et al., 1999). Osteoprotegerin (OPG), a decoy receptor of RANKL, blocks RANKL-RANK interaction to inhibit OC formation and bone resorption (Boyce and Xing, 2007). However, OC lifespan and cell cycle of quiescent OCPs are less than a few weeks (Marks and Seifert, 1985, Mizoguchi et al., 2009), therefore patients with osteoporosis and RA must have an increased OCP pool to supplement the successive death of OCs. Indeed, it has been reported that the frequency of $CD14^{+}CD16^{+}$ blood monocytes in patients with active RA is increased (Kawanaka et al., 2002), and importantly that these macrophages present in RA joints actively produce inflammatory factors (Bingham, 2002).

Macrophages are classified as classically activated (inflammatory, M1) macrophages and alternatively activated (resident, M2) macrophages (Gordon, 2007, Gordon and Taylor, 2005, Wynn et al., 2013), which are linked to T helper 1 (TH1)- and TH2-type immune responses, respectively (Mosser and Edwards, 2008). M1 macrophages mediate inflammatory responses to a variety of bacterial, protozoal and

viral infections and produce many inflammatory cytokines, including TNF, IL-12, IL-18 and IL-23, which mediate immune reactions in several chronic inflammatory and autoimmune diseases, including RA, Crohn's disease, multiple sclerosis and autoimmune hepatitis (Murphy et al., 2003, Smith et al., 2009). M2 macrophages, in contrast, inhibit the production of a wide variety of pro-inflammatory mediators, through the production of cytokines such as IL-10, TGF-β and low levels of IL-12 and thus regulate wound healing (Murai et al., 2009). Thus, targeted depletion of M1 and boosting the activities of M2 macrophages are emerging as an attractive combined therapeutic strategy for autoimmune diseases (Leuschner et al., 2011, Li et al., 2012a, Li et al., 2012b). Better understanding of the mechanisms that regulate OCP pool expansion and M1/M2 differentiation is necessary to improve these therapeutic approaches and could lead to new strategies to reduce joint destruction in inflammatory arthritides.

Although RANKL generally activates OC formation to increase bone resorption in osteoporosis, published data also indicate that serum levels of RANKL are reduced (Kerschan-Schindl et al., 2008, Uemura et al., 2008) while OPG are increased with aging and in osteoporotic humans and other animals (Fichna et al., 2012, Abrahamsen et al., 2005). RANKL expression is also required for normal B cell development and lymph node formation (Franzoso et al., 1997), suggesting that it might have a role to promote joint inflammation in RA. However, transgenic mice that over-express human TNF-alpha, TNF-Tg mice, generated to have a deficiency of RANKL, still develop synovial inflammation although joint destruction is blocked due to OCs defect in these mice (Redlich et al., 2002a, Redlich et al., 2002b). In addition, preclinical and clinical

studies indicate that RANKL inhibitors do not significantly alter inflammatory processes and joint space narrowing in RA (Ferrari-Lacraz and Ferrari, 2011, Cohen et al., 2008). These findings suggest that factors other than RANKL/OPG may play a major role in inducing OC differentiation in osteoporosis and RA.

TNF can promote RANKL production and synergizes with it to induce OC formation (Lam et al., 2000, Zhang et al., 2001b). TNF also induce osteoclastogenesis in the presence of OPG from WT mouse OCPs (Kobayashi et al., 2000) and combined treatment of TNF and TGF-β1 also induce OC formation from *Rank*$^{-/-}$ OCPs *in vitro* (Kim et al., 2005). These suggest TNF induction of OC differentiation independent of RANKL so it was therefore puzzling that TNF did not induce OC formation when administered *in vivo* to *Rank*$^{-/-}$ mice (Li et al., 2000). Our findings indicated that TNF induced much smaller number of OCs than RANKL from WT mice OCPs (Yamashita et al., 2007), suggesting that TNF may mediate the inhibitory factors to limit OC differentiation. The precise conditions in which TNF limits or promotes OC formation and the factors that are critical for TNF induction or inhibition of OC formation therefore remain unclear.

Interleukin-1 (IL-1) has long been known to stimulate bone resorption (Boyce et al., 1989). It is produced by a variety of cell types at sites of inflammation in and around bones, including monocytes/macrophages, OCPs, and mature OC themselves (Xing et al., 2005, Teitelbaum, 2006). In general, IL-1 alone cannot directly mediate OC formation from OCPs *in vitro* (Kobayashi et al., 2000). Like TNF, it promotes RANKL expression by marrow osteoblastic stromal cells to induce osteoclastogenesis indirectly (Hofbauer et al., 1999) and also synergize with TNF to promote OC formation (Wei et al.,

2005), however the mechanism is unclear. Since only ~50% of RA patients respond well to anti-TNF treatment (Hyrich et al., 2006, Symmons and Silman, 2006), it is important to demonstrate if IL-1 synergizes with TNF to stimulate OC formation so as to design better approach to treat RA.

1.2 NF-κB signaling pathways in OC differentiation

Typically, for RANKL and other cytokines such as TNF and IL-1 signaling through their receptors is mediated by the recruitment of TNF receptor-associated factors (TRAFs) leading to activation of NF-κB, a family of transcription factors including RelA (also known as p65), p50, p52, RelB and c-Rel (Karin and Greten, 2005). P50 and p52 are formed from larger precursor proteins, p105, and p100, which are encoded by NF-κB1 and NF-κB2 gene, respectively (Karin and Greten, 2005). They were first identified binding to the κB site of the kappa light chain gene in B cells to regulate B lymphocyte differentiation (Karin and Greten, 2005, Courtois and Gilmore, 2006) but are actually involved in both innate and adaptive immune responses to pathogens and autoimmune stimuli and play critical roles in the initiation and maintenance of inflammatory responses. Each NF-κB subunit has a Rel homology domain in their N-terminus, allowing them to form homo- and heterodimers with one another and to bind to specific DNA sequences on gene promoters. Their binding to DNA requires a C-terminal transcription activation domain (TAD). RelA, RelB, and c-Rel possess TAD but p50 and p52 do not, and thus they rely on interactions with these three other family members to regulate gene transcription (Vallabhapurapu and Karin, 2009). RelA preferentially form heterodimers with p50 to activate cellular response, which is known as canonical NF-κB signaling (Fig.2). In many publications, NF-κB or NF-κB activity refers to RelA/p50-

mediated canonical NF-κB signaling. A non-canonical NF-κB pathway is activated several hours after canonical signaling has begun by translocation of RelB/52 heterodimers to the nucleus (Fig.2) and is sustained, lasting for many hours. This activation occurs efficiently in response to RANKL, but not to TNF (Novack et al., 2003).

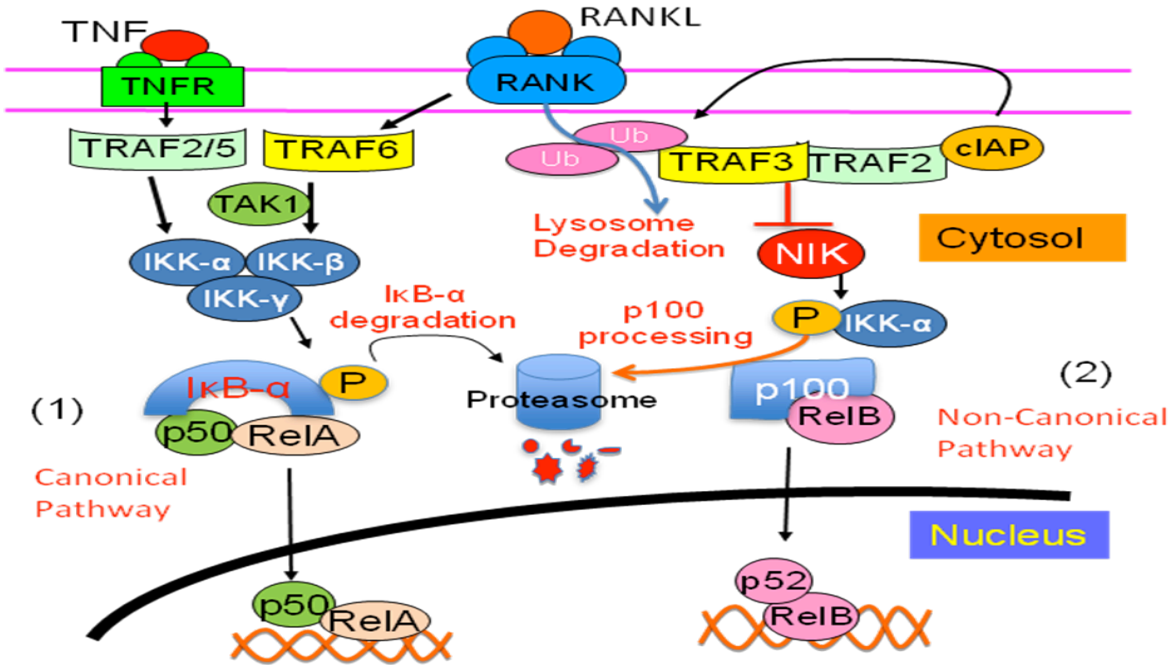

Fig.2. Canonical and Non-canonical NF-κB signaling. (1) Canonical NF-κB activation. Cytokines such as RANKL and TNF induce canonical signaling by recruiting TRAF6 and TRAF2/5, respectively, to their receptors to activate a complex consisting of IKK-α, IKK-β and IKK-γ (NEMO), which induces phosphorylation and degradation of IκB-α and the release of p65/p50 heterodimers, which translocate to the nucleus to activate the target gene expression. 2) Non-canonical NF-κB activation. In un-stimulated cells, TRAF3-TRA2 complex results in constitutive NIK degradation and thus p100 binds RelB to be remained trapped in cytoplasm. Cytokines such as CD40L and RANKL recruit cIAP to TRAF2-TRA3 complex, resulting in TRAF3 ubiquitin degradation and allowing newly synthesized NIK accumulation. NIK then phosphorylates IKK-α, which leads to proteasomal processing of p100 to p52, releasing RelB:p52 heterodimers for translocation to nucleus. TNF does not degrade TRAF3, and thus NIK is degraded, leading to the accumulation of p100 in the cytoplasm of osteoclast precursors to limit their differentiation. This figure was modified from Fig. 1 in our recent review (Boyce et al., 2015).

NF-κB activation comprises a number of steps that require ubiquitination and proteasomal degradation or processing of proteins that function as inhibitors that retain NF-κB dimers in the cytoplasm of un-stimulated cells. These inhibitory NF-κB proteins are known as IκB (Hayden and Ghosh, 2008). The IκB proteins have multiple ankyrin repeats that allow them to bind to NF-κB dimers to prevent their nuclear translocation. RelA/p50 heterodimers are held in an inactivate state in the cytoplasm mainly by their interaction with IκBα. The C-terminal portions of p105 and p100 also contain multiple ankyrin repeats, which endow them with IκB-like functions (Dobrzanski et al., 1995, Liou et al., 1992). The IκB portion of p105 binds to RelA and c-Rel retaining them in the cytoplasm, but it can also bind to p50 molecules in RelA/p50 heterodimers (Vallabhapurapu and Karin, 2009).

1.2.1 Canonical NF-κB signaling

Canonical NF-κB signaling is activated by a trimeric IκB kinase (IKK) complex, which is consists of two catalytic subunits (IKKα and IKKβ) and a regulatory subunit, IKKγ, also called NF-κB essential modulator (NEMO) (Vallabhapurapu and Karin, 2009, Shibata et al., 2007). This IKK complex phosphorylates IκBα, leading to its polyubiquitination and degradation by the 26S proteasome followed by the releasing of p50. As a result, RelA:p50 dimers are translocated to the nucleus to activate the target genes (Vallabhapurapu and Karin, 2009) (Fig.2).

1.2.2 Non-canonical NF-κB signaling

Non-canonical NF-κB signaling is activated by IKKα following its phosphorylation by NF-κB-inducing kinase (NIK). In un-stimulated cells, NIK undergoes constitutively ubiquitin degradation by TNF receptor-associated factor 3 (TRAF3)-TRAF2 complex.

Cytokine such as CD40L recruits the inhibitor of apoptosis proteins (IAP), cIAP1 and 2 through its receptor to TRAF3-TRAF2 complex, allowing TRAF3 ubiquitination and degradation to release NIK from this complex (Zarnegar et al., 2008). NIK then phosphorylates IKKα resulting in processing of p100 in the proteasome to p52, releasing RelB:p52 heterodimers (Bonizzi and Karin, 2004, Senftleben et al., 2001) Similarly, RANKL also induce TRAF3 ubiquitination followed by lysosomal degradation (Xiu et al., 2014, Yao et al., 2009), allowing newly synthesized NIK accumulation, and as a result, p100 is processed to p52 which forms heterodimers with RelB to translocate to nuclei (Fig.2). The IκB portion of p100 binds preferentially to RelB to retain it in the cytoplasm, but interestingly it also binds to and regulates RelA homodimers (Fusco et al., 2008).

A role for NF-κB in bone cells was first discovered unexpectedly 20 years ago by two groups generating NF-κB1/2 double knockout (dKO) mice to further investigate their role in immunity. In addition to the severe B cell and T cell defects, these dKO mice develop severe osteopetrosis due to an OC defect (Franzoso et al., 1997, Iotsova et al., 1997), all of which were reversed by transplantation of hematopoietic cells from WT mice, indicating that the defects were of hematopoietic cell origin (Franzoso et al., 1997). The similar defect of OC and immune cells occur in RANKL and RANK knockout mice generated by other groups later (Boyce and Xing, 2007). Cytokines, including TNF, IL-1, IL-6 and RANKL did not induce OC differentiation from hematopoietic progenitor cells of NF-κB p50/p52 dKO mice, indicating that NF-κB plays a central role in this cytokine-induced OC formation (Xing et al., 2003). However, murine single knockouts of either NF-κB1 p50 or NF-κB2 p52 have normal OC numbers and function *in vivo* (Xing et al.,

2003). This raises the question as to what is the role of NF-κB1 p50 or NF-κB2 p52 in OC differentiation in physiological and pathological conditions. RelA$^{-/-}$ mice die early during embryogenesis due to TNF-mediated massive hepatocyte apoptosis (Beg et al., 1995). A lack of RelA results in the apoptosis of the hematopoietic progenitor cells, resulting in reduced OC formation in response to RANKL (Vaira et al., 2008a), but was not involved in terminal OC formation (Vaira et al., 2008a). RelB$^{-/-}$ mice have normal OCs on their bone *in vivo*, but it is not fully understood why myeloid progenitor cells from RelB$^{-/-}$ mice have an impaired OC formation in response to RANKL *in vitro* (Vaira et al., 2008b). In summary, although it is known that NF-κB in general plays a critical role in OC differentiation, how each NF-κB member regulates OC differentiation in physiological and pathological conditions remain to be understood.

1.3 c-Fos and NFATc1 are master genes controlling OC differentiation

c-Fos is a member of Fos family of transcription factors including c-Fos, FosB, Fra-1 and Fra-2 as well as smaller FosB splice variants, FosB2 and ΔFosB (Milde-Langosch, 2005). c-Fos forms a heterodimer with c-jun, a member of Jun family of transcription factors, resulting in the formation of Activator Protein-1 (AP-1) complex which binds DNA at AP-1 specific sites at the promoter and enhancer regions of target genes and converts extracellular signals into changes of gene expression (Milde-Langosch, 2005). Mice lacking c-Fos develop osteopetrosis due to blockade of OC differentiation (Grigoriadis et al., 1994).

Nuclear factor of activated T-cells, cytoplasmic 1 (NFATc1), one of the five members of NFAT transcription factor family, was identified as a master gene controlling terminal OC differentiation since OCPs with over-expression of activated

form of NFATc1 automatically differentiate into mature OCs without addition of RANKL. Interestingly, over-expression of NFATc1 can rescue RANKL-induced OC defect from OCPs lacking c-Fos, suggesting that NFATc1 is a gene downstream from c-Fos (Matsuo et al., 2004). The relationship of NF-κB to c-Fos and NFATc1 for RANKL-induced osteoclastogenesis and how TNF mediate OC formation was however unknown.

1.4 TNF receptor-associated factors (TRAFs) in the control of OC differentiation.

RANKL and TNF signaling is mediated by recruitment of TRAFs (Darnay et al., 2007, Dempsey et al., 2003, Kim et al., 1999), leading to the activation of transcription factors including NF-κB, c-Fos, and NFATc1 (Takayanagi, 2007, Yamashita et al., 2007). The TRAF family of proteins includes 7 members, of which TRAF6 is thought to be essential for RANKL-induced OC differentiation *(Lomaga et al., 1999, Naito et al., 1999)*. However, the OC number on the bone surface of $TRAF6^{-/-}$ mice is normal (Lomaga et al., 1999) and combination of TNF with TGFβ1 can induce OC formation from $TRAF6^{-/-}$ OCPs (Kim et al., 2005). It was also reported that TRAF5 is involved in both RANKL- and TNF-induced OC formation (Kanazawa et al., 2003) and TRAF2 was required for TNF-induced OC formation (Kanazawa and Kudo, 2005). Others however have found that combined treatment of TNF and TGFβ1 also induced OC formation from OCPs lacking TRAF5 or TRAF2 (Kim et al., 2005). Thus much remain unknown concerning the mechanism by which TRAF transduce cytokine signaling to induce OC formation. TRAF3 has been identified as the key factor in the control of non-canonical NF-κB signaling (He et al., 2007, He et al., 2006). It forms a complex with TRAF2 to constitutively degrade NIK and thus prevents the processing of p100 into p52 while

cIAP1/2 induces TRAF3 ubiquitin degradation and thus activates NIK to process p100 to p52 (Gyrd-Hansen and Meier, 2010). Global deletion of TRAF3 resulted in death of mice within a week after birth due to aberrant p100 accumulation and interestingly, deletion of p100 partly rescued the phenotype of $TRAF3^{-/-}$ mice (He et al., 2006). It was not known if TRAF3 regulate OC formation and bone formation.

1.5 NF-κB in the control of bone formation

The role of NF-κB in OC formation and function has been studied in some depth (Franzoso et al., 1997, Iotsova et al., 1997, Yamashita et al., 2007, Yao et al., 2009, Vaira et al., 2008a, Vaira et al., 2008b). But the role of NF-κB signaling in bone formation is less well understood and published data are conflicting. Several groups have shown that activation of canonical NF-κB signaling inhibits bone formation based on an inhibitory effect of TNF induction of p65 on OB differentiation (Li et al., 2007, Gilbert et al., 2005, Gilbert et al., 2002, Yamazaki et al., 2009). Recently it was reported that inhibition of canonical NF-κB signaling specifically in mature OBs by genetic manipulation results in a transient increase in bone mass in young mice (Chang et al., 2009). Furthermore, the NF-κB inhibitor, S1627, promotes murine calvarial defect repair and increased bone mineral density in ovariectomized mice (Alles et al., 2010), providing additional evidences that canonical NF-κB signaling negatively regulates bone formation. Other groups however have reported that TNF-induced activation of canonical NF-κB signaling in mesenchymal progenitor cells (MPCs) promotes their differentiation into OBs (Cho et al., 2010, Hess et al., 2009, Lencel et al., 2011) through BMP-2-mediated up-regulation of runt-related transcription factor 2 (Runx2) and Osterix (Osx) expression (Hess et al., 2009). These findings indicate that there are complex

interactions involving cytokines and canonical NF-κB signaling that can have positive or negative regulatory effects on OBs to influence bone mass, depending upon the form of stimulation and the state of osteoblastic cell differentiation.

A role for non-canonical NF-κB signaling in bone formation has also been reported. For example, mice generated to have an accumulation of a non-processed form of NF-κB2 p100 have enhanced osteoblastic differentiation (Seo et al., 2012), and mice with deletion of p100, but retaining a functional p52, have osteopenia due to increased OC activity and impaired OB parameters (Soysa et al., 2010). Interestingly, deletion of both RelB and p100 in these latter mice prevented the osteopenia seen in the $p100^{-/-}$ mice and actually increased bone mass, accompanied by increased OB surfaces (Soysa et al., 2010), suggesting an important role of RelB to inhibit OB differentiation. These studies did not however include reports of the OB phenotype of single $RelB^{-/-}$ mice and did not examine the molecular mechanisms whereby RelB regulates OB differentiation or function. It was also unclear how NF-κB works with other signaling to control bone formation.

To address the above questions, the author and colleagues have performed extensive basic and translational studies and demonstrated a number of novel mechanisms by which cytokine-induced NF-κB activation controls osteoclastic bone resorption and osteoblastic bone formation in past ten years: 1) TNF expands OCP pool through promoting their proliferation (Yao et al., 2006) and switching M-CSF-induced resident to inflammatory macrophages via induction of NF-κB RelB (Zhao et al., 2015); 2) IL-1 produced in an autocrine mechanism by OCPs by interacting with bone matrix relays TNF that pre-activates NF-κB followed by c-Fos and NFATc1 to promote terminal

OC differentiation and bone resorption (Yamashita et al., 2007, Yao et al., 2008); 3) We provided first confirmed in vivo evidence that TNF induction of OC formation is independent of RANKL signaling but its capacity to make OCs is limited by its induction of NF-κB p100 (Yao et al., 2009); 4) We were the first to report that TRAF3 functions to inhibit OC differentiation by negatively regulating non-canonical NF-κB activation and RANKL induces TRAF3 ubiquitination and lysosomal degradation to promote OC differentiation (Yao et al., 2009). Importantly, a lysosomal inhibitor, chloroquine, that inhibits TRAF3 degradation prevents ovariectomy-induced bone loss (Xiu et al., 2014); 5) RelB and Notch NICD bind RUNX2 to inhibit OB differentiation and RelB:p52 dimer association with NICD inhibit OB differentiation by enhancing the binding of RBPjκ to Hes1 (Yao et al., 2014, Zhang et al., 2014).

Our findings also provide direction to develop new therapies for RA or osteoporosis. Currently, we are working with chemist to screen for agents that are able to degrade TNF-induced RelB and thus block M1 macrophage differentiation to inhibit inflammation and joint destruction for the therapy of RA. We are also working on small molecular chemicals to prevent p100 processing to inhibit bone resorption and also stimulate bone formation simultaneously for the therapy of osteoporosis.

Chapter 2 Method development

The research in the series of publications relating to this thesis was carried out both *in vitro* and *in vivo*. The methods used are briefly described below.

2.1 *Reagents*.

2.1.1 Table-1 Cytokines purchased from R&D systems, Minneapolis, MN, USA:

Cytokine	Cat #	Cytokine	Cat #	Cytokine	Cat #
TNF	410-MT;	M-CSF	416-ML;	RANKL,	462-Tec;
IL-1	401-ML;	TGF-β1	240-B;		

2.1.2 Cytokine inhibitors

a. TGFβ antibody, Cat# AB-100-NA, R&D systems, Minneapolis, MN, USA;

b. IL-1Ra, R&D Systems, Minneapolis, MN, USA;

c. TNF receptor fusion protein (ENBREL), gift from Amgen, Thousand Oaks, CA.

2.1.3 Antibodies (Abs) for Western blot and immunohistochemestry:

a. Table-2. Abs purchased from Santa Cruz Biotechnology, CA, USA:

Ab name	Clone	Cat. No.	Ab name	Clone	Cat. No.
P100/p52	C-5	sc-7386;	RelB	C19	sc-226;
P65	C20	sc-372;	P50	NLS	sc-114;
NFATc1	7A6	sc-7294;	c-Fos	4	sc-52;
NIK	H-248	sc-7211;	BECN1	H-300	sc-11427;
TRAF3	M20	sc-947;	TRAF2	H-249	sc-7187
TRAF5,	H-257	sc-7220;	TRAF6	D-10	sc-8409
HDAC2,	H-54	sc-7899	HES1	H-140	sc-25392
GAPDH	6C5	sc-32233	Runx2	M70	sc-10758
RBP-jk	D-20	sc-8213;	CyclinD1	H-295	sc-753;
Ubiquitin	P4D1	sc-8017;	VEGF-C	H-190	sc-9047;

b. Table-3 Antibodies purchased from Sigma-Aldrich:

Ab name	Clone	Cat. No.	Ab name	Clone	Cat. No.
HA,		H6908;	β-actin	AC-40,	A4700;
γ-tubulin	GTU-88	T6557;	FLAG	M2,	F3165.

c. Table-4 Antibodies purchased from Abcam, Cambridge, MA, USA

Ab name	Clone	Cat. No.	Ab name	Clone	Cat. No.
LAMP2	GL2A7	ab13524;	Cyclin E1,		ab-7959;
LYVE-1		ab10278.			

d. Table-5 Antibodies purchased from other sources:

Ab name	Cat. No.	Company	Address
Anti-rabbit IgG-HRP	1706515	Bio-Rad,	Hercules, CA, USA
Anti-mouse IgG-HRP	1721011	Bio-Rad,	Hercules, CA, USA
Anti-rabbit IgG/biotinylated	E0432	Dako,	Carpinteria, CA, USA
Anti-Runx2 ,	D130-3	MBL international,	Woburn, MA.
Anti-Smurf1,	AP2104B	Abgent, San Diego, CA	
CD3 (Mec13.3)		Biocare Medical,	Concord, CA, USA
Anti-hamster IgG/Fluor 488	A-21110,	ThermoFisher,	
Anti-rabbit IgG/Fluor 546 F	A-11018,	ThermoFisher.	
NOTCH2-NICD,	Developmental Studies Hybridoma Bank, University of Iowa		

2.1.4 Table-6 Reagents purchased from Sigma-Aldrich, Saint Louis, MS, USA:

Name	Cat. No.	Name	Cat. No.
Ascorbic acid,	A4544;	β-glycerophosphate,	9422;
MG132,	2211;	bafilomycin A1,	B1793;
3-Methyladenine,	M9281;	chloroquine (CQ),	C6628;
puromycin,	p9620;	ammonium chloride,	254134;
Calcein,	C0875.	CFSE	21888
Hoechst 33342,	B2261		

2.1.5 Table-7 siRNAs purchased from Santa Cruz Biotechnology, CA, USA:

Gene	Cat No.	Gene	Cat No.	Gene	Cat No.
TRAF3,	sc-36712;	RelA,	sc-29411;	RelB,	sc-36403;
ATG5,	sc-41445;	BECN1,	sc-29798;	ATG7,	sc-41447,
Non-specific, sc-37007.					

2.1.6 Reagents from other sources

Reagents purchased from Thermo Scientific, Rockford, IL, USA:

M-Per mammalian protein extraction reagent, cat# 78501;

The BCIP/NBT alkaline phosphatase substrate, cat# 34042.

Fugene 6 transfection reagent, cat# E2691, Promega, Madison, WI, USA.

Dual-Luciferase Reporter Assay system, cat# E1910, Promega, Madison, WI, USA.

FBS, Atlanta Biologicals, Lawrenceville, GA, USA.

NH_4Cl solution, Cat# 07850, Stem Cell Technologies, Vancouver, BC, Canada.

TRIzol reagent, Cat# 15596028, Life Technologies, Carlsbad, CA, USA.

iQ SYBR Green Supermix, Cat# 170-8882, Bio-Rad, Hercules, CA, USA.

iQ SYBR cDNA Synthesis Kit, Cat# 170-8891, Bio-Rad, Hercules, CA, USA.

hPTH(1–34 aa), cat# RP01001, GenScript, Piscataway, NJ, USA.

BrdU labeling reagent (Zymed),

Bone matrix proteins including OPN, DSP and BSP were gifts from Dr. Chunlin Qin, Department of Biomedical Science, Baylor College of Dentistry, Dallas, Texas.

2.1.7 ELISA kits

1. Mouse TNF-a ELISA Ready-Set-Go, Cat# 88-7324, eBioscience, San Diego, CA;
2. Human TNF-a ELISA Ready-Set-Go, Cat# 88-7346, eBioscience, San Diego, CA;
3. Mouse IL-1 β ELISA Ready-Set-Go, Cat# 88-7013, eBioscience, San Diego, CA;
4. Mouse TRaCP5b, Cat# SB-TR103, Immunodiagnostic Systems, NE35 PD, UK;
5. Mouse osteocalcin ELISA kit, Cat# MBS2020904, MyBioSource, San Diego, CA.

2.2 *Animals*.

Animals used in the publications documented here include: (1) C57Bl6 WT mice; (2) TNF-transgenic (TNF-Tg) mouse line 3647 (Keffer et al., 1991); (3) $RelB^{-/-}$ mice (Burkly et al., 1995, Elewaut et al., 2003); (4) *Nfkb2 (p52)*$^{-/-}$ mice C57BL/6 × 129 background (Franzoso et al., 1997); (5) $Nfkb1\ (p50)^{-/-}$ mice (Franzoso et al., 1997); (6) *Rankl*$^{-/-}$ (C57BL/6) mice (Kim et al., 2000) ; (7) *Rank*$^{-/-}$ mice C57BL/6 background (Li et al., 2000); (8) *Traf3*-floxed ($TRAF3^{f/f}$) mice (B6 background); (9) Lysozyme M $(LyM)^{Cre}$ mice (B6 background); (10) $CathepsinK^{Cre}$ mice (B6 background). TNF-Tg mice were crossed with $Nfkb2^{-/-}$ mice to generate TNF-Tg/$nfkb2^{-/-}$, single TNF-Tg (TNF-Tg/$nfkb2^{+/-}$) mice and their littermate mice. $TRAF3^{f/f}$ mice were crossed with LyM^{Cre} mice to generate TRAF3 conditional knockout mice in myeloid cells ($TRAF3^{f/f}LyM^{cre}$ mice) and their WT literate mice ($TRAF3^{f/f}$). University of Rochester Medical Center Institutional Animal Care and Use Committee approved all protocols for animal studies (see appendix 3).

2.3 *In vitro* studies:

2.3.1 Osteoclast related research methodology

2.3.1.1 Osteoclast culture and functional tests *in vitro* (Yao et al., 2006, Yao et al., 2009, Yao et al., 2008, Xiu et al., 2014, Yamashita et al., 2007):

Bone marrow (BM), spleen and peripheral blood cells were used to culture OCPs and OCs. BM was flushed from the long bones of mice using α-MEM containing 10% fetal bovine serum (FBS), passed through a 21-G and then through a 25-G needle to make single cell suspensions. The spleen was meshed on a cell strainer and, similarly, passed through a 21-G and then through a 25-G needle to make single cell suspensions. The cells were incubated in NH_4Cl solution for 10 min at room

temperature to lyse red blood cells. $5x10^4$ BM cells or $0.5\text{-}2x10^5$ spleen cells were seeded in a well of 96-well plates and cultured with 5 ng/ml M-CSF for 2 days, and then RANKL (10 ng/ml) or TNF (20 ng/ml) or both were added to the cultures for 48-56 hr at which time mature OCs could be observed using an inverted microscope. The cells were then fixed with 10% neutral formalin for 10 min and TRAP staining was performed. TRAP+ cells with three or more nuclei were considered as mature OCs. To test resorption function, the cells were seeded in wells containing a bovine cortical bone slice in each well followed by the regular culture procedure for 9 days (Yao et al., 2009, Yao et al., 2008). The bone slice was stained with TRAP to evaluate OC formation followed by toluidine blue staining to evaluate resorption pit formation.

2.3.1.2 OC differentiation in Trans-well assays (Yao et al., 2008):

GFP or c-Fos retrovirus-infected WT mouse OCPs were grown on bovine cortical bone slices in the presence of 5 ng/ml of M-CSF for 2 days. The bone slices were then transferred to the upper chamber of the Transwell culture plates and cross co-cultured with the GFP- or c-Fos-infected OCPs in the lower chamber of the Transwell for an additional 8 days in the presence of 5 ng/ml of M-CSF (Yao et al., 2008). When multinucleated cell formation was identified under an inverted microscope, the cells were fixed with 10% formalin and stained for TRAP activity to evaluate OC number.

2.3.1.3 TRAP staining (Yamashita et al., 2007, Yao et al., 2006, Yao et al., 2009, Yao et al., 2008):

Tartarate/Acetate Buffer (pH 5.0): dissolve 6.8 g of NaOAc $3H_2O$ (100mM) and 5.8 g of Na Tartrate $2H_2O$ (50mM) in 450 ml distilled water, add 1 ml of acetic acid, adjust pH to 5.0; add water to 500 ml.

TRAP solution 50 ml

1. Dissolve 5mg Naphthol AS-MX phosphate (Sigma N-4875) in 250 ul Ethylene Glycol Monoethyl Ether (Sigma E-2632)
2. Dissolve 30 mg Fast Red Violet LB salt (Sigma F-3381) in 50 ml Tartarate/Acetate Buffer;
3. Add 1 to 2 and mix well.

TRAP staining for cell culture

1. Fix the cells with 10% neutral Formalin;
2. Wash the cells three times with PBS;
3. TRAP staining solution 70 μl/well (96-well plate) 10 -30 min at room temp or 37°C.
4. After washing, counter stain with Mayer's Hematoxylin 30 sec followed by 0.5% Ammonia Water 30 sec.
5. Wash with H_2O and air dry.

Evaluation of OCs: TRAP+ cell is pink color. A TRAP+ cell with three or more nuclei is considered as a mature OC.

2.3.1.4 Resorption pit staining (Yao et al., 2009, Yamashita et al., 2007)**:**

Dipped a bone slice in the water and transferred it to the flat plate, brushed the bone slice each side for 10 times with a tooth-brush; Dipped the bone slice in 0.2% toluidine blue solution and wiped the remaining staining solution with a piece of soft paper. Observed the bone slice under a microscope and the pits were stained with light blue.

2.3.1.5 Retro-viral constructs and transfection (Yamashita et al., 2007, Yao et al., 2009, Yao et al., 2008)**:**

The coding regions of genes were amplified by PCR from cDNAs including murine origin of c-Fos, human origin of NFATc1, p52/p100, p50/p105, p65, RelB, and cloned into the pMX-puro retroviral vector (Matsuo et al., 2004, Kitamura et al., 1995). Each 5′ primer contains a Kozak sequence following the start codon. The retrovirus vectors were transiently transfected into the Plat-E retroviral packaging cell line (Morita et al., 2000), and viral supernatant was collected 48 h later. BM or spleen cells prepared as above were cultured with 5 ng/ml of M-CSF for 2 days to enrich for OCPs. The culture medium was then replaced with fresh medium containing M-CSF, 2 μg/ml polybrene and ¼ volume of retro-viral supernatant of target gene prepared from Plat-E packaging cells. After 24 hr of infection, RANKL or TNF was added to the cultures for an additional 48-56 hr to generate OCs.

2.3.2 Osteoblast studies

2.3.2.1 Generation of bone-derived MPCs (Yao et al., 2014, Zhang et al., 2014):

The mouse tibiae and femora were cut into small pieces after BM had been flushed out and the cavities had been washed extensively with PBS. The bone fragments were cultured for 4 days with α modified essential medium (α-MEM) containing 20% FBS at 37°C. Bone pieces were transferred into a new dish and cultured for an additional 4 to 5 days with α-MEM containing 10% FBS. The cells grown on the dish were passaged twice when they were 90% confluent, each time excluding cells tightly attached to the dishes. Third-passage cells contained over 99% MPCs, sufficient for our experiments. We named these cells “bone-derived MPCs” (bMPCs) (Yao et al., 2014) and they were frozen for use later in OB differentiation and mineralization experiments.

2.3.2.2 OB differentiation (Yao et al., 2014, Zhang et al., 2014):

BM was flushed from long bones of mice with α-MEM containing 20% FBS using a 25G needle. The cells were filtered with a 40-μm cell strainer, and 4×10^4 cells were cultured in 35-mm dishes at 37°C in 5% CO_2 for 4 days. Unattached cells were removed and replaced with 10% FBS in α-MEM containing 25 μg/mL L-ascorbic acid and 5 mM β-glycerophosphate (β-GP) to induce OB differentiation. After 5 to 7 days in inducing medium, the cells were stained for ALP activity using the ALP substrate, BCIP/NBT. Mineralization typically occurs after 10 to 14 days in culture, and the cells were stained with the von Kossa method for measurement of mineralized nodule formation. Calvariae from new born mice were cut into pieces and digested six times with a mixture of 0.5% collagenase I and 0.125% trypsin (both from Sigma) for 20 minutes at 37°C. Cells from the second to sixth digestions were collected for pre-OB cultures and OB differentiation experiments.

2.3.2.3 ALP staining (Yao et al., 2014, Zhang et al., 2014).

Cultured OBs or BM colonies induced for differentiation were fixed with 10% neutral Formalin for 10 min followed by washing three times with PBS; added BCIP/NBT alkaline phosphatase substrate to cover the dish and incubated the cells for 20-30 min at 37°C. Discarded the staining substrate, washed the dish with water followed by air dry. ALP+ cells will be stained with blue-black color. An alternative step is to count stain the cells with Eosin for 1 min and the cytoplasm of the cells are stained with red so that the percentage of ALP+ cells can be calculated.

2.3.2.4 Von Kossa staining (Yao et al., 2014, Zhang et al., 2014).

Cultured OBs or BM colonies induction for mineralization was fixed with 10% neutral formalin for 10 min followed by washing three times with PBS; added 1% silver nitrate to cover the dish and exposed the cells with bright light for 30 min. Washed the cells with water followed by air dry. Mineralized cells or colonies were stained with block.

2.4 *In vivo* studies:

2.4.1 TNF-induced osteoclastogenesis *in vivo* (Yao et al., 2009)**:**

TNF (0.5 µg) or PBS was injected over the calvariae of 3- to 4-week-old mice twice daily for 5 days. Mice were sacrificed on day 6, and calvariae and hind limbs were fixed in 10% formalin and decalcified with 10% EDTA. TRAP activity was assessed in paraffin-embedded sections, as described previously. OC numbers and surfaces as well as eroded surfaces were measured using an Osteometrics system (Yao et al., 2009).

2.4.2. Evaluation of arthritis and osteoporosis (Yao et al., 2009)**:**

Whilst the features of arthritis in the commonly used 197 line of TNF-Tg mice include paw swelling, deformation and reduced strength (Keffer et al., 1991), it was found that the only easily identifiable, reproducible parameter in 3647 line of TNF-Tg mice, was paw and finger deformation, including atrophy (Yao et al., 2009). We generated a deformation score (0, no deformation; 1, mild deformation; 2, moderate deformation; 3, severe deformation; 4, very severe deformation), which was blindly evaluated once each week to determine the clinical progress of arthritis. Each fore- and hind-paw was evaluated separately, and the deformation score was calculated as the sum of the 4 paws (Yao et al., 2009). Mice were euthanized to collect right tibiae for µCT scanning to evaluate cortical and trabecular bone volume, and left tibiae and forepaws were processed as paraffin slices for histologic evaluation of OCs and arthritis,

including inflammatory tissue area and carpal bone eroded cartilage surface (Yao et al., 2009).

2.4.3 Repairing of tibial bone defects (Yao et al., 2014, Zhang et al., 2014):

A 2-mm × 5-mm full-thickness cortical defect was made on the anterior surface of the left and right tibiae of SCID mice. Briefly, a hole was pierced through the cortex 1 mm below the growth plate using a 25G needle. Scissors were then inserted into the hole and a 2-mm × 5-mm defect was created by repeatedly cutting distally through the cortex (Yao et al., 2014). The defects were then almost completely filled with decalcified trabecular bone matrix, which had been extracted from bovine femoral necks using the following serial processing: 20% H_2O_2 for 2 days, 5 mmol Sodium Azide (NaN_3) overnight, 1 mol NaOH containing 1% Triton X-100 overnight, methanol/chloroform (1:1) for 24 hours, ether overnight, and 10% EDTA for 2 weeks (Yao et al., 2014). bMPCs (5×10^5) in 5 μL of Hank's solution were then injected into the bone matrix in the defects. The muscle fascia and skin overlying the defects were then sutured closed. Mice were euthanized 2, 4, and 8 weeks post-surgery, and the tibiae were fixed in 10% neutral buffered formalin for 2 days. The volume of new bone formed in the defects was measured using a VivaCT 40 μCT scanner. The bones were then processed through alcohols, decalcified, and embedded in paraffin. The volume of newly formed bone and fibrous tissue was quantified in H&E-stained sections using OsteoMeasure software.

2.5 Common methods used throughout this research

2.5.1 FACS analysis and cell sorting (Yao et al., 2006, Yao et al., 2014, Zhao et al., 2015)**:**

$2x10^6$ BM, spleen, peripheral blood mono-nuclear cells or cultured cells were stained with the fluorescent-conjugated antibodies listed in Table-8 for 30 min. Data were acquired using a FACScanto flow cytometer and analyzed using FlowJo software.

Table-8: Antibodies for FACS analysis

	Antibody name	Fluorescent label	Company
Monocye-Macrophages	CD11b	PE-cy7	eBioscience
	F4/80	PE-cy5	eBioscience
	Gr1 (Ly6G)	PE	eBioscience
	Ly6C	APC	eBioscience
	CD11c	FITC	eBioscience
	c-Fms	FITC	eBioscience
Lymphatic cells	CD8a	PE-cy7	eBioscience
	CD4	PE	eBioscience
	B220	PE-cy5	eBioscience
Mesenchymal Progenitor	CD105	PE	eBioscience
	CD45	APC	eBioscience
	Scal-1	FITC	eBioscience

Mesenchymal progenitors are CD45- cells.

2.5.2 Western blot analysis:

Cultured cells were lysed with M-Per mammalian protein extraction reagent (Thermo Scientific, Rockford, IL, USA) containing a protease inhibitor cocktail (Sigma, Saint Louis, MI, USA). Lysate proteins (10–20 µg) were loaded in 10% SDS-PAGE gels and transferred onto polyvinylidene difluoride membranes. Following blocking in 5% milk, membranes were incubated with a specific primary antibody or antibody to mouse β-actin (Table-3, 4 and 5) over-night at 4°C. After washing, the membranes were incubated with anti-rabbit (or mouse) IgG-HRP conjugate secondary antibody (Bio-Rad, Hercules, CA, USA) and exposed to ECL substrate. Signals were analyzed using a Bio-Rad (Hercules, CA, USA) imaging system.

2.5.3 Quantitative Real-Time PCR:

Total RNA was extracted from cultured cells using 1 ml TRIzol reagent, and 1 μg was used for synthesis of cDNA using a GeneAmp RNA PCR core kit. Quantitative PCR amplification was performed using an iCycler real-time PCR machine and iQ SYBR Green (Bio-Rad, Hercules, CA, USA). Relative mRNA expression levels of target genes were analyzed using the CT value of the gene, normalized to β-actin. The primer sequences used for real-time PCR are listed in Table-9.

Table-9: Primer sequence used for real-time PCR.

Gene	Forward primer	Reverse primer
c-Fms:	5′-GTCAGAGGCCCCGTTTGTT-3′;	5′-AGTAAATATAGAGGCTAGCACTGTG-
NFATc1:	5′-CACATTCTGGTCCATACGA-3′;	5′-CGTGTAGCTGCACAATGG-3′;
c-Fos:	5′-CTGTCAACACACAGGACTTTT-3′;	5′-AGGAGATAGCTGCTCTACTTTG-;
β-actin:	5′-ACCCAGATCATGTTTGAGAC-3′;	5′ GTCAGGATCTTCATGAGGTAGT-
TNFα:	5′-CACACTCAGATCATCTTCTCAA-3′;	5′-AGTAGACAAGGTACAACCCATC-3′
IL-1β:	5′-ATTAGACAGCTGCACTACAGG-3′;	5′-GGAGAATATCACTTGTTGGTTG-3′
Smurf1:	5′-AGTTCGTGGCCAAATAGTGG–3′,	5′-GTTCCTTCGTTCTCCAGCAG–3′
Smurf2:	5′-GTGAAGAGCTCGGTCCTTTG–3′;	5′-AGAGCCGGGGATCTGTAAAT–3′
ALP:	5′-CGGGACTGGTACTCGGATAA–3′;	5′-ATTCCACGTCGGTTCTGTTC–3′
OCIN:	5′-CTTGGTGCACACCTAGCAGA–3′;	5′-CTCCCTCATGTGTTGTCCCT–3′
VEGF-a:	5'-TTTACTGCTGTACCTCCACCA-3';	5'-ATCTCTCCTATGTGCTGGCTTT-3'
VEGF-b:	5'-CCTGGAAGAACACAGCCAAT-3';	5'-GGAGTGGGATGGATGATGTC-3'
VEGF-c:	5'-GGGAAGAAGTTCCACCATCA-3';	5'-ATGTGGCCTTTTCCAATACG-3'
VEGF-d:	5'-GCTGTCACTGTTGCCCACTA-3';	5'-CCCTTCCTTTCTGAGTGCTG-3'

2.5.4 Luciferase reporter assay:

The Luc reporter plasmids (NFATc1, Runx2, BECN1) were co-transfected with GFP or NF-κB subunit plasmid into plat-E cells or C2C12 cells using a FuGene6 reagent (Roche, Indianapolis, IN, USA). A 0.1μg aliquot of the SV40-Renilla Luc construct (Addgene, Cambridge, MA, USA) was also co-transfected with the above firefly

reporters to standardize results for transfection efficiency (Yao et al., 2014). Cell lysates were prepared using a reporter lysis buffer (Promega, Madison, WI, USA). Luciferase activity was measured using a Microplate Luminometer (PerkinElmer, Waltham, MA, USA) (Yao et al., 2014).

2.5.5 Chromatin immunoprecipitation (ChiP):

ChiP was performed using a MAGnify ChIP kit (Invitrogen, Carlsbad, CA, USA) following the instruction manual. Briefly, sheared chromatin from cultured cells that had been fixed with 1% formaldehyde was immunoprecipitated with 5 µg of antibody, negative control rabbit immunoglobulin G (IgG), or positive control H3 histone. Immunoprecipitated DNA was then used as a template for quantitative PCR using primers (Table-10) specific for the NF-κB binding sites of a gene promoter as well as a pair of unrelated primers designed in the region that was 3 kb apart from the specific binding sites (Yao et al., 2014).

Table-10: Primers specific for the NF-κB binding sites of a gene promoter.

Gene Promoter	Forward primer	Reverse primer
Runx2		
κB site- 1:	5′-TCAACTACACAGCCATGAT	5′-TAAGCTTGGGGATCTGTAAC
κB site- 2:	5′-CTTCTGAATGCCAGGAAGGC;	5′-TGGGACTGCCTACCACTGT
Unrelated site	5′-CACTGCTGACTGAAACAAGTC;	5′-AGTCTGAGTGAGCTTCCTGAT
BECN1 promoter:		
κB site:	5′-AAGAAGCCTAGAGTCCCTGG-3′;	5′-CCTGCGACAGCGGAGAAAAG-3′.
Unrelated site:	5′-GGGCAAGGCATCATAAAACAGG-3′;	5′-AGGAGATGAAGTTGACCTCC-3′.
Hes1 promoter		
RBPjκ site:	5′-CTCAGGCGCGCGCCATTGGCC-3′;	5′-GCTTACGTCCTTTTACTTGAC-3′;
Unrelated site:	5′-CCTAGGGAGAAGGAGCTGGCT-3′:	5′-TGGCCGTCAGGAGCCGGCACC-3′

2.5.6 Immunohistochemistry:

Bones were fixed in 10% phosphate-buffered formalin, decalcified in 10% EDTA, and embedded in paraffin wax. Deparaffinized sections were quenched with 3% hydrogen peroxide, treated for antigen retrieval for 30 min, and stained with a specific primary antibody and a biotinylated secondary antibody. The biotin was detected using standard avidin-biotin peroxidase technology and diaminobenzidine (Sigma, Saint Louis, MI, USA) as the chromogen.

2.5.7 Micro–computed tomography and bone histomorphometric analysis:

Mice were given injections of calcein (10 mg/kg) at 5 days and 1 day before euthanasia in a standard bone formation double-labeling protocol. Right tibiae were fixed in 10% neutral buffered formalin and subjected to micro–computed tomography (μCT) scanning using a VivaCT 40 mCT scanner for assessment of bone microstructure. Subsequently, un-decalcified plastic sections were processed to assess the dynamic and static parameters of bone formation using OsteoMeasure software. Left tibiae were fixed in 10% neutral buffered formalin for 2 days, decalcified and processed to paraffin sections to analyze bone volume, OB surface and OC surface on H&E and TRAP stained sections (Yao et al., 2014, Yao et al., 2009).

Chapter 3 Summary of research

The submitted publications forming the basis of this thesis cover five distinct, but related, areas of research:

1. TNF expands the pool of OCPs with enhanced OC forming potential (Yao et al., 2006, Zhao et al., 2015).
2. IL-1 produced in an autocrine mechanism by OCPs by interacting with bone matrix relays TNF that pre-activates NF-κB followed by c-Fos and NFATc1 to promote terminal OC differentiation (Yamashita et al., 2007, Yao et al., 2008).
3. NF-κB2 p100 limits OC formation and bone resorption (Yao et al., 2009).
4. TRAF3 negatively regulating OC differentiation (Yao et al., 2009, Xiu et al., 2014).
5. NF-κB inhibits bone formation by interacting with Notch signaling (Engin et al., 2008, Kaneki et al., 2006, Yao et al., 2014, Zhang et al., 2014).

The findings of each topic are briefly described respectively below.

3.1 TNF expansion of OCPs with enhanced OC forming potential by stimulating their proliferation and switching M-CSF-induced M2 to M1 macrophages via induction of NF-κB RelB.

These findings were reported in two publications.

a. **Yao Z**; Li P; Zhang Q; Schwarz EM; Keng P; Arbini A; Boyce BF; Xing L. "Tumor necrosis factor-alpha increases circulating osteoclast precursor numbers by promoting their proliferation and differentiation in the bone marrow through up-regulation of c-Fms expression." J. Biol. Chem. 2006; 281(17):11846-55.

b. Zhao Z, Hou X, Yin X, Li Y, Duan R, Boyce BF, **Yao Z**. TNF Induction of NF-κB RelB Enhances RANKL-Induced Osteoclastogenesis by Promoting Inflammatory

Macrophage Differentiation but also Limits It through Suppression of NFATc1 Expression. PLoS One. 2015;10(8):e0135728.

The main findings of these publications are outlined in Fig.3 and described below

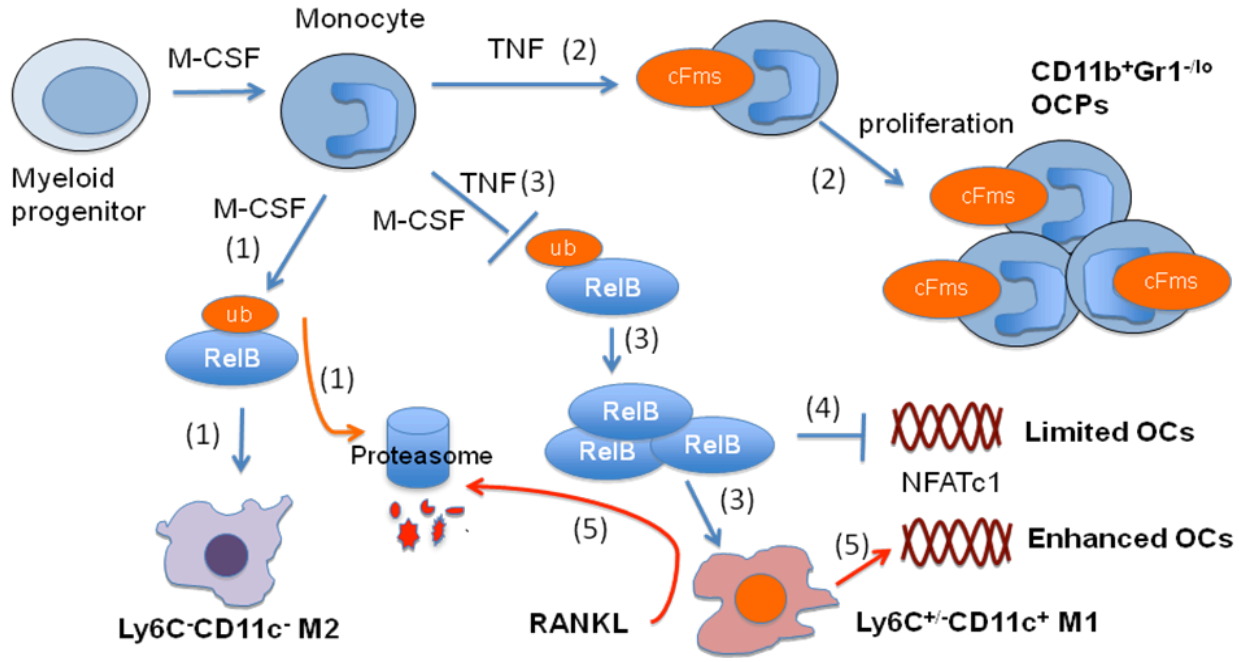

Fig.3. Mechanism by which TNF expand OCP pool to enhance OC formation (Yao et al., 2006, Zhao et al., 2015). (1) M-CSF drives myeloid progenitors differentiating into monocytes in which the newly synthesized RelB is constutitively degraded and these monocytes mainly differentiate into M2 macrophage with lesser OC formating potential (Zhao et al., 2015); (2) TNF stimulates the expression of c-Fms by the $CD11b^{+}Gr1^{-/lo}$ monocyte OCPs to promote their proliferation and thus expand OCP pool (Yao et al., 2006); (3) TNF inhibits the ubiquitin degradation of RelB and the accumulated RelB switches M-CSF-induced M2 to Ly6C+/-CD11c+ M1 macrophages with enhanced OC forming potenial (Zhao et al., 2015); (4) RelB itself inhibites NFATc1 expression and thus TNF alone has limited role to induce OC differentiation (Zhao et al., 2015); (5) RANKL induces RelB proteasomal degradation in M1 to release the inhibition of RelB and thus enhance OC differentiation (Zhao et al., 2015).

3.1.1 TNF increase myeloid OCP pool by stimulating their proliferation via up-regulation of the M-CSF receptor, cFms (Yao et al., 2006).

Previous findings indicated that peripheral blood $CD11b^+$ myeloid cell number was significantly increased in TNF-Tg mice (Li et al., 2004), but CD11b is also expressed on the granulocytes in addition to monocyte/ macrophages. To further identify the biological feature of OCPs, we stained mouse blood cells with fluorescent conjugated antibodies of CD11b and Gr-1 to sort different cell populations by flow cytometry for OC culture. We found that $CD11b^+/Gr\text{-}1^{-/lo}$ cells, but not $CD11b^+/Gr\text{-}1^{hi}$ and $CD11b^+/Gr\text{-}1^{-/-}$cells, gave rise to mature OCs in response to M-CSF and RANKL stimulation. Thus, $CD11b^+/Gr\text{-}1^{-/lo}$ cells are OCPs. Importantly, TNF promotes OCP proliferation by up-regulating the expression of M-CSF receptor, c-Fms. TNF-Tg mice had significantly increased $CD11b^+/Gr\text{-}1^{-/lo}$ cells in both blood and bone marrow, and administration of TNF to wild type mice also significantly increased the circulating and bone marrow $CD11b^+/Gr\text{-}1^{-/lo}$ cell population. Interestingly, dividing $CD11b^+/Gr\text{-}1^{-/lo}$ cells in the bone marrow from TNF-Tg mice and TNF treated mice were significantly increased when compared to their respective control mice, and *in vitro* culture indicated that TNF alone did not stimulate cell division but significantly enhanced M-CSF induced $CD11b^+/Gr\text{-}1^{-/lo}$ cell division. TNF stimulated conversion of $CD11b^+/Gr\text{-}1^{-/lo}/c\text{-}Fms^-$ to $CD11b^+/Gr\text{-}1^{-/lo}/c\text{-}Fms^+$ cells was not blocked by an M-CSF neutralizing antibody, suggesting that TNF directly stimulates the expression of the M-CSF receptor c-Fms to promote OCP proliferation.

3.1.2 $CD11b^+F4/80^+Gr1^-Ly6C^+$ macrophages are authentic OCPs (Zhao et al., 2015).

As described above, our early results show that $CD11b^+/Gr\text{-}1^{-/lo}$ cells are OCPs in TNF-Tg mouse studies (Yao et al., 2006). Recently, we cultured BM cells with M-CSF alone or in combination with TNF to enrich OCPs, which are called M-OCPs and T-

OCPs, respectively. Only $Gr1^-Ly6C^+$ cells but not $Gr1^-Ly6C^-$ cells of $CD11b^+F4/80^+$ M-OCPs form OCs in response to RANKL. Thus, $CD11b^+F4/80^+$ $Gr1^-Ly6C^+$ macrophages are authentic OCPs. However, both $Gr1^-Ly6C^+$ and $Gr1^-Ly6C^-$ cells from T-OCPs form OCs and their potential to form OCs are largely enhanced compared to that of M-OCPs. Interestingly, $Gr1^+Ly6C^+$ cells in $CD11b^+F4/80^+$ of T-OCPs also form OCPs and this population is corresponding to our early reported $CD11b^+/Gr1^{lo}$ OCPs.

3.1.3 TNF switches M-CSF-induced $Ly6C^-Gr1^-$ M2 to $Ly6C^+Gr1^-CD11c^+$ and $Ly6C^-Gr1^-CD11c^+$ inflammatory M1 macrophages with increased production of inflammatory factors and enhanced OC forming potential (Zhao et al., 2015).

CD11b and F4/80 are common macrophage surface markers; M1 cells are $CCR2^+Gr1^+CD62L^+CD11c^+$, while M2 cells are $CCR2^-Gr1^-CD62L^-CD11c^-$ in mice (Gordon, 2007, Gordon and Taylor, 2005). Ly6C is also widely used to differentiate M1 and M2 cells. $Ly6C^{+/hi}$ subsets are classified as M1 cells, while $Ly6C^{-/lo}$ subsets are classified as M2 cells (Yona and Jung, 2010, Mosser and Edwards, 2008). $Gr1^-Ly6C^+$ cells comprise 1/4 of $CD11b^+F4/80^+$ macrophages of M-OCPs while $Gr1^-Ly6C^-$ cells account for about 2/3 of $CD11b^+F4/80^+$ M-OCPs. In contrast, the frequency of $Gr1^-Ly6C^+$ and $Gr1^-Ly6C^-$ cells are respectively switched to 2/3 and 1/4 of $CD11b^+F4/80^+$ macrophages in T-OCPs. Interestingly, both $Gr1^-Ly6C^+$ and $Gr1^-Ly6C^-$ cells bear 2-fold more CD11c, a typical M1 surface marker (Gordon and Taylor, 2005). Importantly, $Gr1^-Ly6C^+$ cells from M-OCPs express higher M1 effector, iNOS, TNF, TGFβ1 and IL-1β, than that from $Ly6C^-Gr1^-$ cells, confirming that $Ly6C^+Gr1^-$ cells generally have a M1 profile. Consistently, $Ly6C^+Gr1^-$ cells from T-OCPs expressed higher iNOS, IL-1β and TGFβ1, but significantly lower M2 markers, IL-10 and PPAR-γ, than those from M-OCPs.

Of note, expression levels of iNOS and TGFβ1 were also increased, while IL-10 and PPAR-γ levels were decreased in $Ly6C^-Gr1^-$ cells from T-OCPs compared to M-OCPs cells, providing further support that $Ly6C^-Gr1^-$ cells from T-OCPs have a M1 phenotype.

We sorted each of these OCPs into four populations, $Ly6C^+Gr1^-$, $Ly6C^+Gr1^+$, $Ly6C^-Gr1^-$ and $Ly6C^-Gr1^+$ cells, to induce OC formation with RANKL or TNF in the presence of M-CSF. In M-OCPs, the OC forming potential of $Ly6C^+Gr1^-$ cells was much higher than $Ly6C^-Gr1^-$ cells: RANKL induced 125±16 OCs from $Ly6C^+Gr1^-$ cells, but only a few TRAP+ mononuclear cells were formed from $Ly6C^-Gr1^-$ cells. In contrast, both $Ly6C^+Gr1^-$ and $Ly6C^-Gr1^-$ cells from T- OCPs formed OCs in response to RANKL, the number being 398±26 and 413±17 respectively, and almost matching those from $Ly6C^-Gr1^-$ cells of R-OCPs (463±15).

3.1.4 RelB is required for TNF switching M-CSF-induced M2 to M1 macrophages (Zhao et al., 2015).

RelB is a member of the NF-κB family of transcription factors (Sun, 2011, Sun, 2012). RelB is required for dendritic cell development (Platzer et al., 2004) but the role of RelB in OC differentiation is not fully understood. OC numbers are normal in the bones of $RelB^{-/-}$ mice, but BM OCPs from $RelB^{-/-}$ mice form fewer OCs than WT OCPs *in vitro* in response to RANKL (Vaira et al., 2008b). We found that although both RANKL and TNF increased RelB mRNA level, TNF also significantly increased RelB protein level, whereas RANKL does not due to the fact that it also induces RelB proteasome degradation. It was also not known if RelB regulates M1 or M2 but we found that TNF induction of $Ly6C^+CD11c^+$ and $Ly6C^-CD11c^+$ M1 did not occur from $RelB^{-/-}$ BMCs, suggesting that RelB is required for TNF induction of M1.

3.1.5 TNF negatively regulates RANKL-induced OC formation via inhibition of NFATc1 but stimulates via an NFATc1 independent mechanism (Zhao et al., 2015).

TNF alone induces terminal differentiation of OCPs primed by M-CSF (Kobayashi et al., 2000, Yao et al., 2009), which is independent of RANKL. TNF also promotes RANKL expression by osteoblastic and other cells to enhance OC formation (Lam et al., 2000, Zhang et al., 2001b). However, TNF does not induce degradation of NIK and thus increases the level of the inhibitory NF-κB protein, p100, which reduces RANKL- and TNF-induced OCP differentiation (Yao et al., 2009). To further investigate the conditions in which TNF stimulates or inhibits RANKL-induced OC formation, M- and T-OCPs generated from WT mouse BM cells were then treated with TNF, RANKL or RANKL+TNF for an additional 48-60 hr to generate mature OCs. TNF alone induced relatively small numbers of OCs and significantly inhibited RANKL-induced OC formation from M-OCPs. Although the numbers of RANKL-induced OCs from T-OCPs were similar to those from M-OCPs, the total area of RANKL-induced OCs from T-OCPs was larger than that from M-OCPs ($p<0.05$), consistent with enhanced fusion, but we did not study the regulation of fusion. In addition, TNF did not inhibit RANKL-induced OC formation from T-OCPs, the number and area of RANKL+TNF-induced OCs being similar to those induced by RANKL alone. Similarly, the NFATc1 mRNA expression level matched the number of OCs. In OCs formed from M-OCPs, RANKL, but not TNF, increased NFATc1 mRNA expression, and TNF inhibited RANKL induction of NFATc1 expression within 24 hr of treatment, showing a 6-fold induction of NFATc1 mRNA for RANKL alone and a 2.1-fold induction for RANKL+TNF treated cells. In contrast, TNF did not inhibit RANKL-induced NFATc1 expression in T-OCPs. We next infected M-

OCPs with GFP or RelB retrovirus to over-express RelB followed by treatment of either TNF for 3 days or RANKL for 2 days to generate OCs. We found that over-expression of RelB significantly decreased RANKL-induced OC formation and NFATc1 mRNA expression. In contrast, over-expression of RelB increased TNF-induced OC formation but did not affect TNF-induced low level of NFATc1 mRNA. These findings suggest that TNF induction of RelB inhibits RANKL-induced osteoclastogenesis by directly inhibiting NFATc1 expression and in contrast, TNF alone induction of OC differentiation is through an NFATc1 independent mechanism.

3.2 IL-1 produced in an autocrine mechanism by OCPs by interacting with bone matrix relays TNF that pre-activates NF-κB followed by c-Fos and NFATc1 to promote terminal OC differentiation (Yamashita et al., 2007, Yao et al., 2008).

Two publications deal with the relationship of NF-κB to c-Fos and NFATc1 in cytokine-induced OC formation.

a. Yamashita T; **Yao Z** ***(co-first author)***; Li F; Zhang Q; Badell IR; Schwarz EM; Takeshita S; Wagner EF; Noda M; Matsuo K; Xing L; Boyce BF. "NF-kappaB p50 and p52 regulate receptor activator of NF-kappaB ligand (RANKL) and tumor necrosis factor-induced osteoclast precursor differentiation by activating c-Fos and NFATc1." J. Biol. Chem. 2007; 282(25):18245-53.

b. **Yao Z**; Xing L; Qin C; Schwarz EM; Boyce BF. "Osteoclast precursor interaction with bone matrix induces osteoclast formation directly by an interleukin-1-mediated autocrine mechanism." J. Biol. Chem. 2008; 283(15):9917-24.

The main findings of these publications are outlined in Fig.4 and described below.

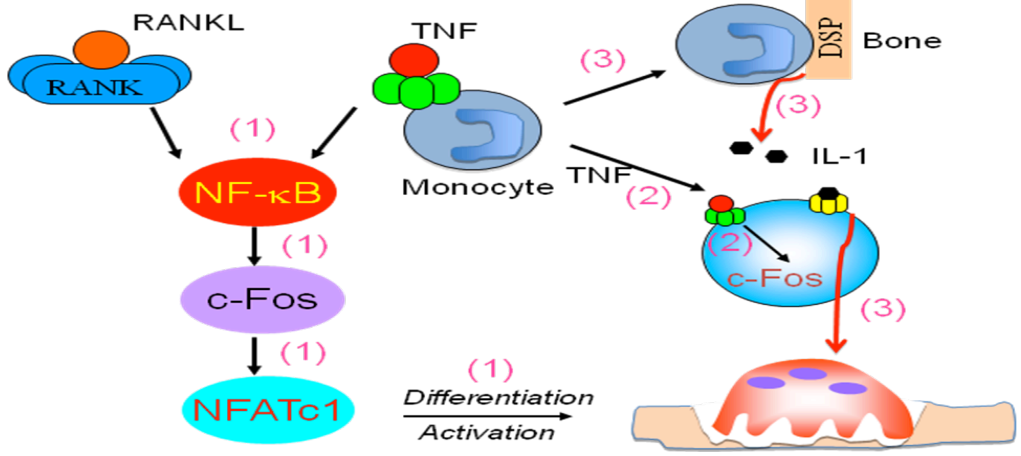

Fig.4. Cytokines sequentially activate NF-κB, c-Fos followed by NFATc1 to induce OC differentiation (Yamashita et al., 2007, Yao et al., 2008). (1) Similar to RANKL, TNF also sequentially activate NF-κB, c-Fos followed by NFATc1 to induce OC differentiation (Yamashita et al., 2007); (2) TNF induces monocyte OCPs to express c-Fos (Yamashita et al., 2007, Yao et al., 2008); (3) The pre-activated OCPs expressing c-Fos attach to bone and are stimulated by bone matrix proteins such as dentin sialoprotein **(**DSP) to produce IL-1 which mediates the terminal differentiation of OCPs into mature OCs to degrade bone (Yao et al., 2008).

3.2.1 c-Fos expression and activation to induce OC formation is NF-κB dependent (Yamashita et al., 2007).

RANKL does not induce OC formation from NF-κB p50/p52 dKO OCPs. RANKL- and TNF-induced c-Fos mRNA expression and activation were also impaired in the dKO OCPs. Importantly, c-Fos over-expression rescued RANKL- and TNF-induced OC formation from dKO OCPs, to a similar extent to p50+p52 over-expression, and these OCs functionally resorbed bone on bone slices *in vitro*. In addition, an NF-κB inhibitor prevented RANKL- or TNF-induced c-Fos expression and activation. Finally, NF-κB p50+p52 over-expression could not rescue OC defect from c-Fos-deficient cells. These findings indicate that RANKL- and TNF-induced c-Fos expression and activation is NF-

κB dependent and activated c-Fos by RANKL can efficiently substitute for the lack of p50 and p52 in dKO cells to induce OC formation and bone resorption.

3.2.2 c-Fos activates NFATc1 to induce OC formation in the absence of NF-κB p50 and p52 (Yamashita et al., 2007).

NFATc1 functions downstream of c-Fos during osteoclastogenesis in WT cells (Matsuo et al., 2004) but it is not known if this is the case in dKO cells. We found that RANKL increased NFATc1 mRNA and nuclear translocation in WT but not p50/ p52 dKO OCPs. However, c-Fos over-expression rescued RANKL- increased NFATc1 expression and activation in dKO cells. Interestingly, overexpression of a constitutively active form of NFATc1 in NF-κB dKO OCPs induced small number of OCs without addition of RANKL, and treatment of these NFATc1 over-expressing dKO cells with RANKL induced OC formation, the number being similar to that when NF-κB p50+p52 or c-Fos were overexpressed in dKO OCPs. Similarly, TNF also induced NFATc1 mRNA expression in dKO OCPs expressing c-Fos and induced OC formation from dKO OCPs with overexpression of NFATc1. Over-expression of c-Fos rescued RANKL- and TNF- induced NFATc1 expression and OC formation from NF-κB dKO OCPs, suggesting that c-Fos relays NF-κB signaling to mediate OC formation via NFATc1.

3.2.3 TNF induces the expression of c-Fos by OCPs with limited potential of mature OC formation (Yamashita et al., 2007).

TNF and RANKL induced a similar pattern of NF-κB, c-Fos and NFATc1 expression, increased c-Fos mRNA levels to similar extent as RANKL as early as 4 hr while increased NFATc1 expression much later, peaked at 48 hr for RANKL-treated cells and 1 day later for TNF-treated cells. Consistent with this, TNF induction of

osteoclastogenesis peaked one day later (3 days) than that of RANKL (2 days). Interestingly, OCs on the eroding inflamed joints of TNF-Tg mice had higher c-Fos expression compared with OCs at non-eroding site, suggesting that TNF may stimulate OCPs to express c-Fos to promote OC formation in the inflammatory joints. However, TNF alone-induced OC formation and bone resorption is very limited, suggesting that other factors may involve OC formation and bone resorption in TNF-Tg mice. Our later findings indicate that IL-1 produced in an autocrine mechanism from these OCPs and TNF induction of NF-κB2 p100 positively and negatively regulate TNF-induced OC differentiation, respectively, which will be discussed below.

3.2.4 *c*-Fos expressing OCPs automatically differentiate into mature OCs via IL-1 autocrine mechanism by interacting with bone matrix (Yao et al., 2008).

It has long been known that IL-1 is a potent stimulator of bone resorption in vitro and in vivo (Boyce et al., 1989). It enhances OCP fusion and OC survival in vitro (Lee et al., 2002, Jimi et al., 1999, Jimi et al., 1995) and promotes RANKL production by stromal cells (Hofbauer et al., 1999) and thus indirectly induces OC formation. It was however unknown if it has a direct action on OC formation. We found that c-Fos-expressing OCPs of WT mice formed mature OCs in response to IL-1 treatment directly, which is independent of NF-κB p50/p52 since the dKO OCPs expressing c-Fos also formed OCs in response to IL-1. Surprisingly, c-Fos-expressing OCPs from WT and dKO mice formed OCs spontaneously on bone slices without addition of cytokine. Interestingly, OCPs grown on bone slices produce IL-1β and OC formed from c-Fos expressing OCPs was blocked by inhibitor of IL-1β but not by inhibitor of TNF or TGFβ1.

Thus, TNF may pre-activate OCPs to express c-Fos and they will produce IL-1 by contacting bone matrix to further mediate their own differentiation and bone erosion.

3.2.5 The bone matrix proteins osteopontin (OPN) and dentin sialoprotein (DSP) stimulated OCP expression of IL-1 (Yao et al., 2008).

Bone matrix contains at least 20 non-collagenous proteins, including TGF-β1 and members of the SIBLING (small integrin-binding ligand, N-linked glycoprotein) family of proteins such as osteopontin (OPN), dentin sialoprotein (DSP), bone sialoprotein (BSP) and dentin phosphoprotein (DPP) (Qin et al., 2004, Fisher et al., 2001) which are released from the matrix during bone resorption. TGFβ1 has multiple effects on bone cells and has been proposed to be involved in coupling osteoblasts to sites of bone resorption (Chang et al., 2009). OPN appears to anchor OCs to bone matrix through interaction with the vitronectin receptor on the OC basolateral membrane (Reinholt et al., 1990) and is required for the activation of OC bone resorption in hindlimb unloading mouse model with disuse atrophy (Ishijima et al., 2001). Bone sialoprotein deficiency impairs osteoclastogenesis and mineral resorption in vitro (Boudiffa et al., 2010). Several of the bone matrix proteins have also been reported to stimulate macrophages to produce cytokines such as IL-1 (Silva et al., 2005). We found that DSP in particular, but also OPN, significantly increased IL-1 and to a lesser extent TNF mRNA expression in WT mouse OCPs, whereas DPP and TGF-β1 had no effect. Interestingly, none of these proteins induced OC formation from GFP retrovirus control-infected WT mouse OCPs. However, DSP or OPN induced OC formation from c-Fos retrovirus-infected WT mouse OCPs, which was partially blocked by IL-1Ra to the same extent as observed in cultures on bone slices (Yao et al., 2008). It could be concluded from these

observations that when TNF pre-activated OCPs expressing c-Fos adhere to bone matrix, interaction with bone matrix proteins including DSP and OPN leads to the production of IL-1 and as a result, the pre-activated OCPs expressing c-Fos further differentiate into mature OCs to degrade bone (Yao et al., 2008).

3.3 TNF induces OC differentiation independent of RANKL, but its induction of NF-κB2 p100 limits OC formation and bone resorption (Yao et al., 2009)

One publication in The Journal of Clinical Investigation reports the important progress in bone cell biology and rheumatology and provided the first confirmed *in vivo* evidence that TNF-induced OC formation is RANKL independent but its role is limited by NF-κB2 p100. Thus, increasing or stabilizing p100 could be a novel strategy to treat osteoporosis and RA. These findings made a breakthrough in bone cell biology as the JCI editor's comments (Tanaka and Nakano, 2009).

a. **Yao Z**; Xing L; Boyce BF. "NF-kappaB p100 limits TNF-induced bone resorption in mice by a TRAF3-dependent mechanism." J. Clin. Invest. 2009; 119(10):3024-34.

The major findings in this publication are outlined in Fig.5 and described below:

3.3.1 NF-κB2 p100 deficiency enhances TNF-induced OC formation (Yao et al., 2009).

TNF directly induces OC formation from WT mouse OCPs in the presence of OPG (Kobayashi et al., 2000) and combined treatment of TNF and TGF-β1 also induces OC differentiation from $Rank^{-/-}$ mice OCPs *in vitro* (Kim et al., 2005). However, TNF-induced OC number is much smaller than RANKL with less resorption function (Yamashita et al., 2007) and it was puzzling that TNF did not induce OC formation when it was administered in mice lacking RANK signaling (Li et al., 2000). In comparison with

RANKL that efficiently processes NF-κB2 p100 into p52, TNF does not activate the alternative NF-κB pathway and induces p100 accumulation (Novack et al., 2003). It was unknown if the limited OC formation induced by TNF was related to p100.

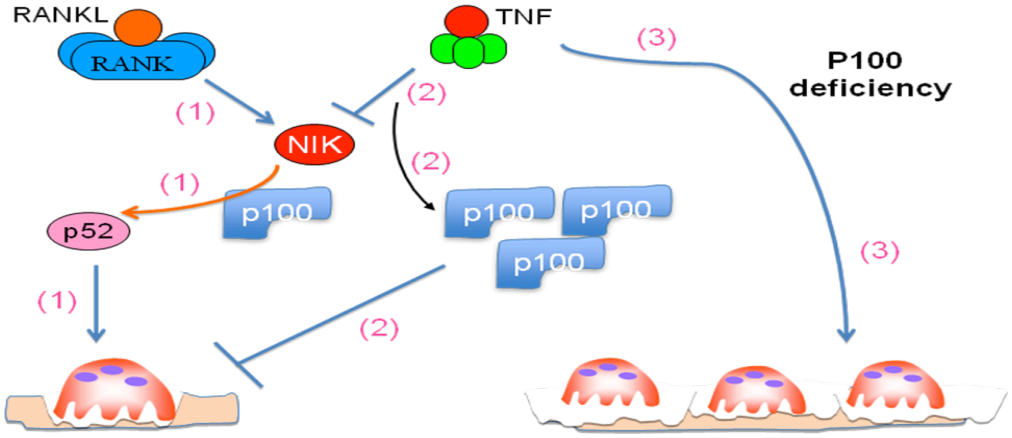

Fig.5. TNF-induced NF-kB2 p100 limits OC differentiation (Yao et al., 2009). (1) RANKL activates NIK to process p100 into p52, resulting in OC differentiation and activation from OCPs; (2) TNF does not activate NIK and thus newly synthesized p100 accumulates in the cells to limit OC formation; (3) P100 deficiency promotes TNF-induced OC formation and thus enhances joint erosion and systemic bone loss in RA.

We performed OC culture using *NFKB2* (p100/p52)$^{-/-}$ mice and found that TNF induced significantly more OCs from *NFKB2*$^{-/-}$ than from WT cells, the OC numbers and resorption pit being similar to those in RANKL-treated WT or *NFKB2*$^{-/-}$ cells. Consistent with this, TNF induced a greater c-Fos and NFATc1 expression in *NFKB2*$^{-/-}$ cells than WT cells, with their expression level in *NFKB2*$^{-/-}$ cells being similar to that induced by RANKL when mature OCs were forming. *NFKB2*$^{-/-}$ OCPs lack both p100 and p52 and our findings that over-expression of p100, but not p52, inhibited TNF- and RANKL-induced osteoclastogenesis significantly in both *NFKB2*$^{-/-}$ and WT OCPs, confirmed that p100 is responsible for TNF inhibition of OC differentiation. Next we injected TNF or PBS into the subcutaneous tissues of *NFKB2*$^{-/-}$ and *NFKB2*$^{+/-}$ control mice and found

that the parameters of bone resorption were significantly greater in *NFKB2*$^{-/-}$ mice than *NFKB2*$^{+/-}$ mice. Serum levels of TRAP5b, a specific marker of bone resorption released by OCs, were significantly higher in *NFKB2*$^{-/-}$ mice than in control mice treated with TNF, further confirming that *NFKB2* deficiency enhances TNF-induced bone resorption.

3.3.2 TNF induces robust OC formation *in vivo* in mice lacking RANKL or RANK when the mice also lack NF-κB2 p100 (Yao et al., 2009).

Similar to its effects in WT cells, TNF induced accumulation of p100 but not p52 protein in *RANK*$^{-/-}$ and *RANKL*$^{-/-}$ OCPs. We generated *RANK*$^{-/-}$/*NFKB2*$^{-/-}$ and *RANKL*$^{-/-}$/*NFKB2*$^{-/-}$ mice to culture OCs and found that spleen cells from *RANK*$^{-/-}$/*NFKB2*$^{-/-}$ and *RANKL*$^{-/-}$/*NFKB2*$^{-/-}$ mice treated with TNF formed significantly more OCs than did cells from *RANK*$^{-/-}$/*NFKB2*$^{+/-}$ and *RANKL*$^{-/-}$/*NFKB2*$^{+/-}$ mice. Next, we injected TNF to these mice to investigate if p100 also limits OC formation *in vivo* in the absence of RANK signaling. Although absence of *NFKB2* itself did not induce any OCs in *RANK*$^{-/-}$ or *RANKL*$^{-/-}$ mice (PBS injection), TNF induced many OCs and resorption lacunae in the calvarial bones of the *RANK*$^{-/-}$/*NFKB2*$^{-/-}$ and *RANKL*$^{-/-}$/*NFKB2*$^{-/-}$ mice following local injection, associated with increased OCs and eroded surfaces. Only occasional OCs were observed in the sections of TNF-injected *RANKL*$^{-/-}$ or *RANK*$^{-/-}$mice, as reported previously (Li et al., 2000). Of note, serum resorption marker, TRAP5b, was undetectable in *RANK*$^{-/-}$/*NFKB2*$^{+/-}$and *RANK*$^{-/-}$/*NFKB2*$^{-/-}$ mice and was slightly but significantly increased by TNF injection in *RANK*$^{-/-}$/*NFKB2*$^{+/-}$ mice. These values were increased further in *RANK*$^{-/-}$/*NFKB2*$^{-/-}$ mice after TNF injection, confirming that OCs induced by TNF in *RANK*$^{-/-}$ mice are functional and that NF-κB2 deficiency enhances

TNF-induced osteoclastogenesis and bone resorption in the mice lacking RANK signaling.

3.3.3 TNF attenuates RANKL-induced osteoclastogenesis *in vitro* through NF-κB2 p100 (Yao et al., 2009).

RANKL and TNF independently support the final stages of OCP differentiation to mature OCs and it is therefore important to study how TNF and RANKL work together to control osteoclastogenesis. A previous study reported that TNF synergized with RANKL to stimulate osteoclastogenesis *in vitro* (Lam et al., 2000). However, others reported that the synergistic effect occurred only in RANKL pretreated cells (Ochi et al., 2007). We found that TNF inhibited RANKL-induced osteoclastogenesis from M-CSF- enriched OCPs in a dose-dependent manner, and this inhibitory effect was abolished when *NFKB2 p100* was deleted, suggesting that TNF induction of p100 inhibits RANKL-induced OC formation. Thus, elevation of p100 or inhibition of p100 degradation could be a novel strategy to treat RA.

3.3.4 TNF-Tg mice lacking NF-κB2 p100 develop more severe systemic bone loss, joint erosion and inflammation than do TNF-Tg littermates (Yao et al., 2009).

To determine the possible pathological role of NF-κB2 absence in joint erosion in RA, we generated TNF-Tg/*NFKB2*$^{-/-}$ mice and found that they developed joint deformity earlier, with more severe joint inflammation and erosion than their TNF-Tg littermates. TNF-Tg/*NFKB2*$^{-/-}$ mice also had reduced trabecular bone volume and cortical thickness, associated with increased OC numbers and surfaces on the trabeculae compared with TNF-Tg/*NFKB2*$^{+/-}$ mice as evaluated by histomorphometry and 3-dimensional μCT imaging. However, serum TNF concentration in TNF-Tg/*NFKB2*$^{-/-}$ mice did not increase

compared with the TNF-Tg/*NFKB2*$^{+/-}$ littermate mice. Thus, the increased joint inflammation and bone erosion in TNF-Tg mice with *NFKB2* deficiency indicates an increased susceptibility to RA.

3.4 TRAF3 prevents bone loss by negatively regulating non-canonical NF-κB-mediated OC differentiation (Xiu et al., 2014, Yao et al., 2009).

These studies include two publications.

a. **Yao Z**; Xing L; Boyce BF. "NF-kappaB p100 limits TNF-induced bone resorption in mice by a TRAF3-dependent mechanism." J. Clin. Invest. 2009; 119(10):3024-34.

b. Xiu Y, Xu H, Zhao C, Li J, Morita Y, **Yao Z**, Xing L, Boyce BF. Chloroquine reduces osteoclastogenesis in murine osteoporosis by preventing TRAF3 degradation. J. Clin. Invest. 2014; 124(1):297–310.

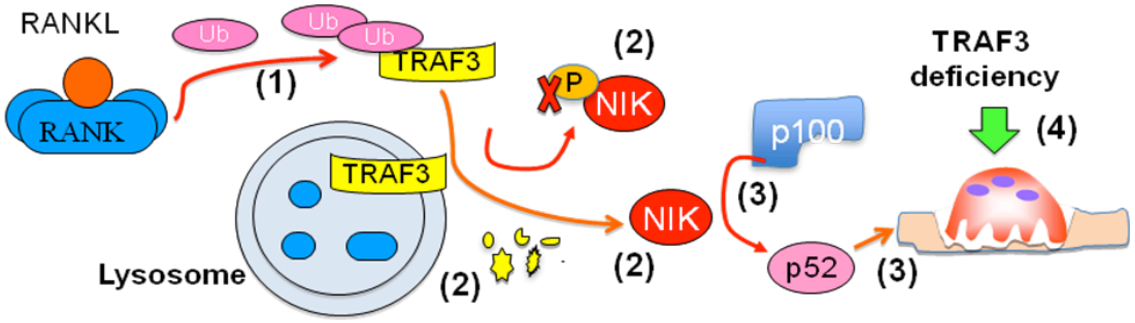

Fig.6. TRAF3 controls non-canonical NF-κB activation to limit OC formation (Xiu et al., 2014, Yao et al., 2009). (1) RANKL induces TRAF3 ubiquitination; (2) The ubiquitinated TRAF3 is moved to lysomome to be degraded, thus the newly synthesized NIK fails to be phosphorytion degraded, resulting in NIK accumulation in the cells; (3) The accumulated NIK process p100 into p52 and thus promote OC formation; (4) TRAF3 deficiency enhances RANKL-induced OC formation and bone resorption since NIK can continuely process p100.

The findings demonstrated a novel mechanism of TRAF3 controlled NF-κB activation during OC differentiation, in which RANKL induces TRAF3 autophagy/lysosome degradation to activate NF-κB and promote OC formation. These findings also indicate that pharmacological inhibition of TRAF3 degradation with compounds such as chloroquine may limit bone loss in common bone diseases. The main findings are outlined in Fig.6.

3.4.1 TRAF3 prevents OC differentiation by inhibiting p100 processing (Xiu et al., 2014, Yao et al., 2009).

The hallmark of non-canonical NF-κB activation is p100 processing into p52 by NIK and it has been reported that TRAF3 negatively regulates NIK to control non-canonical NF-κB signaling (He et al., 2007, He et al., 2006). We found that TRAF3 paralleled the change of p100 during RANKL- and TNF- induced OC formation, and importantly, treatment with TRAF3 siRNA prevented TNF-induced NF-κB2 p100 accumulation and inhibition of osteoclastogenesis. Importantly, over-expression of TRAF3 inhibited RANKL-induced OC formation directly. These findings confirmed that TRAF3 negatively regulates OC differentiation by preventing p100 processing. We then generated mice with conditional OC-specific deletion of *TRAF3* (cKO mice) and found that the cKO mice had mild osteoporosis associated with increased OC formation, further confirming that TRAF3 maintains bone homeostasis by inhibiting OC formation.

3.4.2 RANKL induces TRAF3 autophagy/lysosome degradation to mediate OC formation (Xiu et al., 2014).

CD40 or BAFF-R engagement in B cells induces rapid, proteasome-dependent TRAF3 degradation (Vallabhapurapu et al., 2008). Using a high-binding affinity ubiquitin

matrix to capture ubiquitinated proteins of OCPs followed by Western blotting analysis using an anti-TRAF3 Ab, we found that RANKL markedly increased TRAF3 ubiquitination allowing the ubiquitinated protein to be degraded in proteasomes or lysosomes (autophagosomes) (Clague and Urbe, 2010). In an earlier report, we found that RANKL-induced TRAF3 degradation was not blocked by proteasome inhibitor, MG132 (Yao et al., 2009), but was inhibited by the autophagy/lysosome inhibitor, chloroquine (CQ) (Xiu et al., 2014). Autophagy inhibitor Bafilomycin A1 (which blocks fusion of the autophagosome and the lysosome (Yamamoto et al., 1998)) increased TRAF3 accumulation, consistent with the finding that RANKL significantly increased co-localization of TRAF3 with LAMP2 (a lysosome marker), which was reduced by CQ. Importantly, CQ also inhibited RANKL induced OC formation from WT mouse OCPs but not from *TRAF3*$^{-/-}$ OCPs. These findings confirm that RANKL degrade TRAF3 through the lysosome to promote OC differentiation.

3.4.3 CQ inhibits pathological bone resorption *in vivo* via TRAF3 (Xiu et al., 2014).

Hyperparathyroidism is a disease with an excess of parathyroid hormone (PTH) due to overactivity of one or more of the body's four parathyroid glands, resulting in the increased serum calcium level, increased bone resorption and bone loss. High level of PTH can also induce bone marrow fibrosis, a hallmark of PTH-induced resorption. We found that CQ can prevent PTH-induced marrow fibrosis and OC activity in WT mice but not *TRAF3* conditional knockout mice in myeloid cells. In addition, CQ also prevented OVX-induced bone loss and increased OC numbers and surfaces in WT mice, but not in c-cKO mice. These suggest that PTH-induced marrow fibrosis and OVX-induced bone loss is through TRAF3.

3.4.4 RelB is required for RANKL-induced TRAF3 lysosomal degradation by regulating BECN1 expression (Xiu et al., 2014).

TRAF3 negatively regulates NIK to control non-canonical NF-κB signaling (Sun, 2011, Sun, 2012), a hallmark being the processing of p100 to p52. It is not known if NF-κB in turn regulates TRAF3. We found that basal TRAF3 protein levels in *RelB*$^{-/-}$ BM cells were 5-fold higher than in WT cells, and TRAF3 protein was also significantly accumulated in RANKL-treated *RelB*$^{-/-}$ OCPs in comparison with the time-dependent decreasing of TRAF3 in RANKL-treated WT OCPs. Consistent with these, RelB over-expression restored RANKL-induced TRAF3 degradation in RelB$^{-/-}$ OCPs. These findings suggest that RelB promotes RANKL-induced TRAF3 degradation.

As RANKL-induced TRAF3 degradation is lysosome/autophagosome-mediated, we examined the key molecules for autophagosome formation including ATG5, ATG7, ATG8 and beclin 1 (BECN1) in OCPs (Copetti et al., 2009). We found that RANKL upregulated BECN1 protein level approximately 3-fold while other autophagic proteins were not changed. Consistent with this, shRNA knockdown of BECN1 impaired RANKL-induced TRAF3 degradation and autolysosome formation. To determine if TRAF3 degradation and autolysosome formation induced by RANKL is through RelB-mediated BECN1, we investigated if RelB regulates the BECN1 promoter activity since the proximal 1.1 kb of the BECN1 promoter has 4 κB binding sites (Copetti et al., 2009). As expected, RelB significantly up-regulated BECN1 transcriptional activity in comparison with the minimal induction of its activity by RelA. ChIP assays confirmed that RelB directly binds to a conserved κB binding site of the BECN1 promoter. In summary, our

findings indicate that RANKL-induced TRAF3 lysosomal degradation is through RelB induction of BECN1-mediated lysosome/autophagosome formation.

3.5 TNF induction of non-canonical NF-κB inhibits bone formation by interacting with Notch signaling.

Bone remodeling is a coupled process, the old bone being removed by OCs followed by new bone formation to repair resorbed lacunae. OB cells produce RANKL to stimulate OC differentiation and OCs also produce factors to control bone formation (Boyce, 2013). This series of publications report the regulation of bone formation, in particular TNF induction of non-canonical NF-κB which inhibits bone formation by interacting with Notch signaling.

a. Kaneki H; Guo R; Chen D; **Yao Z**; Schwarz EM; Zhang YE; Boyce BF; Xing L. Tumor necrosis factor promotes Runx2 degradation through up-regulation of Smurf1 and Smurf2 in osteoblasts." J. Biol. Chem. 2006; 281(7):4326-33.
b. Engin F; **Yao Z**; Yang T; Zhou G; Bertin T; Jiang MM; Chen Y; Wang L; Zheng H; Sutton RE; Boyce BF; Lee B. "Dimorphic effects of Notch signaling in bone homeostasis." Nat. Med. 2008; 14(3):299-305.
c. **Yao Z**, Li Y, Yin X, Dong Y, Xing L, Boyce BF. NF-κB RelB negatively regulates osteoblast differentiation and bone formation. J Bone Miner Res. 2014; 29(4):866-77.
d. Zhang H, Hilton MJ, Anolik J, Welle S, Zhao C, **Yao Z**, Li X, Wang Z, Boyce B, Xing L. NOTCH inhibits osteoblast formation in inflammatory arthritis via noncanonical NF-κB. J. Clin. Invest. 2014 Jul 1;124(7):3200-14.

In addition to activating OC formation, TNF also inhibits OB differentiation (Li et al., 2007, Chang et al., 2009, Gilbert et al., 2002, Gilbert et al., 2005, Yamazaki et al., 2009). However, the mechanisms by which TNF inhibits OBs have not been fully determined. The findings that TNF induction of non-canonical NF-κB inhibits bone formation by interacting with Notch signaling are outlined in Fig.7 and discussed below.

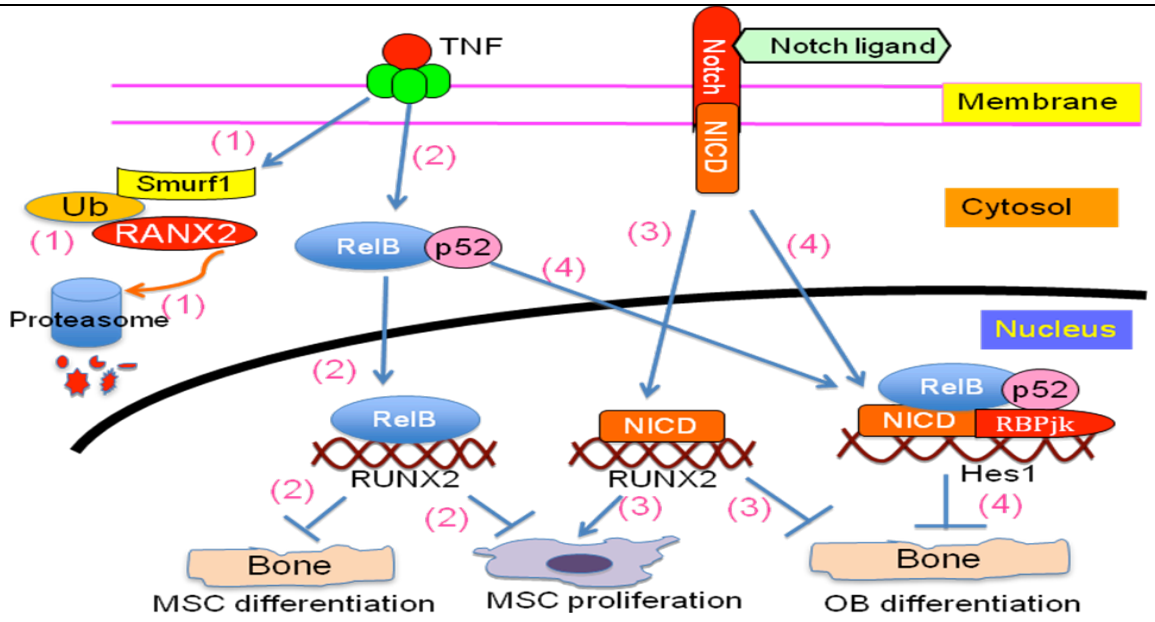

Fig.7. TNF-induced non-canonical NF-κB interacts with Notch to control bone fromation (Engin et al., 2008, Kaneki et al., 2006, Yao et al., 2014, Zhang et al., 2014). (1) TNF increases Smurf1 resulting in ubiquitination and degradation of Runx2 and thus inhibit OB differentiation; (2) TNF increase RelB which directly binds RUNX2 to inhibit MSC proliferation and OB differentiation (Yao et al., 2014); (3) Upon ligand binding, NICD is cleaved to translocate to the nucleus where it binds to RUNX2 promoter to promote MSC proliferation but inhibit OB differentiation (Engin et al., 2008); (4) RelB:p52 dimer association with NICD enhances RBPjκ binding to Hes1 to inhibit OB differentiation (Zhang et al., 2014).

3.5.1 TNF inhibits OB differentiation through Smurf-mediated RUNX2 Degradation

Runx2 is a critical transcription factor for OB differentiation and maturation. It is required for commitment of mesenchymal osteochondroprogenitors to the osteoblastic lineage and OB differentiation during both endochondral and intramembranous ossification (Komori, 2011). TNF inhibits osteoblast differentiation through TNFR1-mediated suppression of Runx2 gene transcription and destabilization of *Runx2* mRNA (Gilbert et al., 2002, Abbas et al., 2003, Gilbert et al., 2005). It was predicted that TNF also post-transcriptionally regulates *Runx2* since TNF reduction of nuclear *Runx2* protein (more than 90%) was greater than the reduction of total *Runx2* mRNA (50%) (Gilbert et al., 2002). Ubiquitin-mediated proteasomal degradation has been implicated in the regulation of BMP-2 and TGF-*β* signaling pathways in various cell types (Datto and Wang, 2005, Izzi and Attisano, 2004). The E3 ubiquitin ligase, Smad ubiquitin regulatory factor 1 (Smurf1), regulates OB differentiation by promoting proteasomal degradation of the BMP signaling proteins, Smad1, Smad5, and Runx2 (Zhu et al., 1999, Ying et al., 2003, Zhao et al., 2004). Smurf2, a closely related homolog of Smurf1, was shown to reduce the steady-state protein levels of Smad1 and 2, but not Smad3 and 4, in Smurf2-transfected cells (Lin et al., 2000, Zhang et al., 2001a).

Smurf1$^{-/-}$ mice exhibit an age-dependent increase in bone mass (Yamashita et al., 2005) and Col1a1-Smurf1 transgenic mice have decreased bone formation rates and decreased Runx2 protein expression in osteoblasts (Zhao et al., 2004), suggesting that Smurf1 negatively regulates OB differentiation and bone formation. We proposed a novel molecular mechanism of TNF inhibition of osteoblasts involving Smurf-mediated

ubiquitination and degradation of Runx2 through several lines of evidences (Kaneki et al., 2006): (i) TNF promoted ubiquitination and degradation of transfected and endogenous Runx2; (ii) TNF increased the expression of Smurf1 and Smurf2; (iii) TNF-induced ubiquitination and degradation of Runx2 were attenuated in cells overexpressing Smurf1 and Smurf2 siRNA; (iv) expression of Smurf1 and Smurf2 siRNA rescued the inhibitory effect of TNF on Runx2 reporter; (v) bones of mice that have elevated TNF levels have increased Smurf1 and decreased Runx2 protein expression.

3.5.2 Non-canonical NF-κB RelB negatively regulate OB differentiation

Several groups have shown that TNF induction of canonical NF-κB RelA inhibits OB differentiation (Gilbert et al., 2002, Gilbert et al., 2005, Li et al., 2007, Yamazaki et al., 2009, Chang et al., 2009), specifically in mature OBs (Chang et al., 2009). However, it was also reported that TNF-induced RelA in mesenchymal progenitor cells (MPCs) promotes their differentiation into OBs (Cho et al., 2010, Hess et al., 2009, Lencel et al., 2011). A role for non-canonical NF-κB signaling in bone formation has also been reported. Mice with accumulation of p100 have enhanced OB differentiation (Seo et al., 2012) and, consistently, mice with deletion of p100 but retention of a functional p52 have osteopenia due to increased OC activity and impaired OB parameters (Soysa et al., 2010). Interestingly, deletion of both RelB and p100 in these latter mice prevented the osteopenia in the $p100^{-/-}$ mice (Soysa et al., 2010), suggesting an important role of RelB to inhibit OB differentiation. The molecular mechanism whereby RelB regulates OB differentiation or function is however unclear. We found that RelB-/- mice had age-related increased bone mass due to increased OB precursor proliferation associated

with enhanced capacity of their MPCs to differentiate into OBs in vitro and to repair cortical bone defects in mice in vivo (Yao et al., 2014). Further analysis indicated that RelB directly targeted Runx2 promoter to inhibit its activation (Yao et al., 2014). But, it was still unclear how RelB determines the fate of MPCs.

3.5.3 TNF activates Notch signaling though the non-canonical NF-κB pathway

Notch is a family of evolutionarily conserved receptors that regulate cell fate. Upon ligand binding, the Notch receptor intracellular domain (NICD) is cleaved by γ-secretase and translocates to the nucleus, where it associates with the recombination signal–binding protein jκ (RBPjκ), leading to transcriptional activation of target genes such as *Hes1* and *Hey1* (Zanotti and Canalis, 2010). In collaboration with Dr. Lee's group (Baylor College of Medicine, Houston, USA), we found that OB-specific gain of Notch function increased proliferation of immature OBs by up-regulating the genes encoding cyclin D, cyclin E and osterix. NICD also regulated terminal OB differentiation by directly binding Runx2 and repressing its transactivation function (Engin et al., 2008).

We also investigated if NF-κB interacts with Notch signaling to regulate bone formation and MPC fate by performing RNA sequencing and pathway analyses in MPCs in a TNF- transgenic murine RA model, to identify pathways responsible for decreased OB differentiation. Among the 53 pathways dysregulated in MPCs, genes encoding Notch and non-canonical NF-κB pathway members were markedly elevated (Zhang et al., 2014). Interestingly, overexpression of p52 and RelB in murine MPCs increased NICD-dependent activation of RBPjκ reporter and level of Hes1. We also found that TNF promoted p52/RelB binding to NICD, which enhanced binding at the RBPjκ site within the Hes1 promoter (Zhang et al., 2014). These data suggest that TNF induction

of non-canonical NF-κB members activates Notch signaling to inhibit OB differentiation. Importantly, administration of Notch inhibitors to RA mice prevented bone loss by promoting OB differentiation, and CFU-fibroblasts treated with Notch inhibitors formed more new bone in recipient mice with tibial defects (Zhang et al., 2014). Together, these data indicate that persistent Notch activation in MPCs contributes to decreased OB differentiation associated with RA and suggest that Notch inhibitors could prevent inflammation-mediated bone loss.

Chapter 4 Discussion

RA and osteoporosis represent two common bone-related diseases that pose a major threat to public health. Although both conditions share some cellular and molecular mechanisms, for example, the excessive osteoclast differentiation and activation as well as the decreased bone formation during pathological process, their etiology, pathological features and treatment are very different. Thus, they will be discussed separately.

4.1 NF-κB control of joint destruction in RA

Macrophage/monocytes play central role in the pathological process of RA. They not only produce abundant inflammatory factors to mediate inflammation, but also differentiate into OCs involved in the destruction of cartilage and bone within the joint. A number of OC inhibitors such as bisphosphonates and Denosumab have been developed to treat osteoporosis. Bisphosphonates also have been used to treat bone loss in RA because of the high risk of osteoporosis in RA patients (Kim et al., 2010). RANKL inhibitors have also been tested in preclinical and clinical trials in RA but they did not alter the inflammatory processes (Ferrari-Lacraz and Ferrari, 2011), which is consistent with animal studies data showing that complete deletion of RANK signaling did not prevent synovial inflammation, despite blocking joint erosion due to an OC defect in TNF-induced RA (Redlich et al., 2002a, Redlich et al., 2002b). RANK deletion can result in increased number of macrophages since they do not further differentiate to form mature OCs (Dougall et al., 1999) but it is not known if failure of RANKL inhibitor for the treatment of joint inflammation in RA is related to the secondary increase in macrophages.

Macrophages are classified as inflammatory (M1) and anti-inflammatory (M2) (Mosser and Edwards, 2008). M1 macrophages produce many inflammatory cytokines, including TNF, IL-18, IL-12 and IL-23, to mediate inflammatory responses in a variety of autoimmune diseases (Murphy et al., 2003, Smith et al., 2009, Kaneki et al., 2006). M2 macrophages, in contrast, inhibit the production of a wide variety of pro-inflammatory factors, by inducing anti-inflammatory, pro-resolving mediators such as IL-10, and regulate wound healing (Murai et al., 2009). Thus, targeted depletion of M1 and boosting the activities of M2 macrophages is emerging as an attractive combined therapeutic strategy for autoimmune disease (Leuschner et al., 2011, Li et al., 2012a, Li et al., 2012b). Generally, M-CSF drives myeloid progenitor cell differentiation into monocyte-macrophages with M2-like phenotypes and an anti-inflammatory response (Sierra-Filardi et al., 2010). Indeed, we found that only small portion of M-CSF-induced OCPs have M1 phenotype which differentiate to OCs in response to RANKL but most of them have M2 phenotype which do not form OCs. Thus, targeting M-CSF or its receptor c-Fms to deplete macrophage populations would not be appropriate for the treatment of RA although TNF expands OCP pool via stimulating c-Fms expression (Yao et al., 2006). Our recent findings indicate that TNF switches M-CSF-induced M2 to M1 macrophages with enhanced OC forming potential in response to RANKL and increased production of inflammatory factors through induction of RelB (Zhao et al., 2015). TNF induction of RelB also however inhibits terminal OC differentiation by directly inhibiting NFATc1 expression and activation (Zhao et al., 2015). This could explain why TNF alone can significantly increase OCPs numbers through M2 to M1 switching, while having very limited ability to induce terminal OCP differentiation into OCs (Zhao et al.,

2015). In contrast, RANKL strikingly increases OC formation from TNF-primed OCPs compared to OCPs induced by M-CSF alone since it can efficiently degrade RelB protein, resulting in sustained activation of NFATc1 to promote OC formation (Zhao et al., 2015). Although over-expression of RelB can enhances TNF-induced OC formation, this effect is still lower than that of RANKL since it peaks one day later than that of RANKL (Zhao et al., 2015). Thus, TNF induction of RelB to induce terminal OC differentiation in physiological and pathologic conditions is limited, and the dominant role of TNF induction of RelB is to expand the pool of OCPs by switching the differentiation of M-CSF-induced M2 resident to M1 inflammatory macrophages. Thus, degrading TNF-induced RelB could be a novel strategy to specifically deplete TNF-induced M1 macrophages to decrease OC-induced joint destruction and inflammation in RA patients without affecting normal bone remodeling. Further study is needed to elucidate the detailed mechanism of TNF inhibition of RelB degradation in order to design a specific approach to degrade RelB as a therapeutic approach for RA.

TNF is one of the major pro-inflammatory cytokines that mediate pathological processes including joint inflammation and destruction (Boyce et al., 2005) and TNF-Tg mice develop arthritis that is very similar to human RA (Boyce et al., 2005, Keffer et al., 1991). Anti-TNF reagents have been developed to treat RA clinically, which have significantly improved RA treatment, but they are expensive and only ~50% RA patients respond well to these agents (Hyrich et al., 2006, Symmons and Silman, 2006). This suggests that other factors are involved in the TNF-induced pathological processes of RA, for example, IL-1 mediates TNF-induced osteoclastogenesis (Wei et al., 2005). We found that TNF shares the common critical transcriptional factors, NF-κB, c-Fos and

NFATc1 with RANKL to induce OC formation independent of RANKL signaling (Yamashita et al., 2007, Yao et al., 2009), but its potential to make OCs is limited (Yamashita et al., 2007, Yao et al., 2009). However, an auto-regulation of OC differentiation exists, in which OCPs interact with bone matrix to produce IL-1β which stimulates TNF pre-activated OCPs expressing c-Fos to further differentiate into mature OCs to erode bone (Yao et al., 2008). This may explain why a combined therapy of anti-TNF and anti-IL-1β seems to produce better results in RA patients (Williams et al., 2000).

The key step in non-canonical NF-κB activation is the processing of p100 to p52 (Bonizzi and Karin, 2004, Senftleben et al., 2001). RANKL efficiently processes p100 to p52 to induce full OC differentiation, but in contrast, TNF does not process p100 to p52 and thus induces a limited OC formation (Yao et al., 2009). Importantly, p100 deletion significantly enhances joint destruction and inflammation in the RA model of TNF-Tg mice but it does not however increase serum TNF concentrations in these mice (Yao et al., 2009). This suggests that p100 deficiency could increase the susceptibility to, or pathological progress of, rheumatoid arthritis. Mice with a mutation in *NFKB2* gene that prevents the processing of p100 into the active subunit, p52, express a complex phenotype with abnormalities in a variety of tissues including disorganized splenic architecture and disrupted B cell development due to activation of RelA (Tucker et al., 2007). It was recently reported that a common variable immunodeficiency (CVID) results from an 8bp deletion in the C-terminal part of *NFKB2* gene, resulting in a peptide that is 19 amino acids shorter due to a frameshift altering 17 C-terminal amino acids (Liu et al., 2014). It is currently unknown if an *NFKB2* genetic mutation results in p100

deficiency or enhanced processing to influence the susceptibility, disease severity and progress of human RA. Further study is also needed to determine if there are *NFKB2* genetic variations that limit the therapeutic response of RA patients to anti-TNF treatment. Similarly, since p100 deficiency also enhances RANKL-mediated bone destruction (Yao et al., 2009), further study is also needed to explore if agents that prevent p100 degradation, for example NIK inhibitors, can inhibit joint destruction to treat RA.

4.2 Targeting non-canonical NF-κB signaling to develop novel therapies for osteoporosis

A various bisphosphonates are the widely used anti-resorptive drugs for the treatment of osteoporosis and are prescribed at 73 percent of physician visits for osteoporosis (Stafford et al., 2004). About 4 percent of patients (Sedghizadeh et al., 2009) develop osteonecrosis of the jaw after taking oral bisphosphonates for 4.6 years (and a minimum of three years) (Zavras, 2011). The prevalence of bone necrosis is considerably higher in patients who are taking high-dose intravenous bisphosphonates (Ruggiero et al., 2004). Recently FDA approved anti-resorptive drug Denosumab can also results in bone necrosis (Aghaloo et al., 2010). PTH (teriparatide) is the only anabolic drug but its use is limited to 2 years (Ponnapakkam et al., 2014). PTH also has the risk to result in osteosarcoma (Cipriani et al., 2012) although this possibility is low in human. Thus, PTH is contraindicated in anyone: (1) with a history of osteosarcoma or any bone cancer (primary or metastatic); (2) at risk for osteosarcoma (Paget's disease of bone, previous radiation therapy to the skeleton or to other organs if skeletal tissue is exposed); or (3) children and young adults with open epiphyses (Cipriani et al., 2012).

Therefore, there is an unmet need to develop new anti-resorptive and/or anabolic drugs, particularly, the agents with dual anti-resorptive and anabolic effect simultaneously, for the treatment of osteoporosis since currently there is no single drug with dual role that can simultaneously inhibit bone resorption and stimulate bone formation, and combined therapy with teriparatide and a bisphosphonate does not appear to offer advantages over the use of the single agent alone (Black et al., 2003, Finkelstein et al., 2003). Our findings have demonstrated several new molecular targets for the development of new therapeutic approach of osteoporosis.

Numerous factors including hormones, cytokines and chemokines regulate multiple intracellular signaling pathways to act on bone formation and resorption, both positively and negatively, with aging (McLean, 2009, Ginaldi et al., 2005). It is unclear how these factors interact to result in osteoporotic bone loss through the stimulation of OC bone resorption and inhibition of OB bone formation. It is therefore crucial to identify the key molecules that control bone resorption and formation and to understand how other factors regulate them in order to develop agents with dual anti-resorptive and anabolic effects. Our findings and publications have indicated that non-canonical NF-κB activation plays a dual role in the stimulation of bone resorption and also inhibition of bone formation. Mice lacking functional NIK have impaired RANKL–stimulated osteoclastogenesis due to p100 accumulation (Aya et al., 2005). This is consistent with our findings that TNF induction of p100 accumulation inhibits TNF- and RANKL-induced OC formation, and that p100 deletion enhances TNF-induced systemic bone loss and joint destruction (Yao et al., 2009). More recently, it was reported that TNF also limits OC formation through RBP-jκ (Zhao et al., 2012) and IRF-8 (Zhao et al., 2009),

indicating that there are several potential mechanisms to restrict the destructive effects of TNF on bone. Interestingly, accumulation of p100 due to a loss-of-function of NIK also increased bone mass, associated with increased bone formation in mice (Soysa et al., 2010, Seo et al., 2012). Mice with a deletion of p100*,* but retaining a functional p52 protein however develop osteopenia with reduced osteoblast numbers (Soysa et al., 2010). These data suggest that increasing p100 protein levels not only inhibit bone resorption but also stimulate or maintain bone formation and thus, inhibiting non-canonical NF-κB activation could be a novel strategy to develop agents with both anti-resorptive and anabolic effect. Since the key step of non-canonical NF-κB activation is that NIK is activated to process p100 into p52, NIK could be an important target molecule to develop new therapeutic agents that inhibit non-canonical NF-κB activation. A number of NIK inhibitors have been reported (Mortier et al., 2010). No any reagent has reported to inhibit OC and/or stimulate OB differentiation but we are currently screening for if the reported NIK inhibitors can do so. The discovery of NIK crystal structure (Liu et al., 2012) enables us to design new class of NIK inhibitors for the purpose of development of dual anti-resorptive and anabolic agents for the treatment of osteoporosis.

TRAF3 is the key molecule that controls non-canonical NF-κB activation (He et al., 2007, He et al., 2006). It forms a complex with TRAF2 and cIAP1/2 to constitutively degrade NIK and thus prevent the processing of p100 into p52 (Gyrd-Hansen and Meier, 2010). We were the first to identify the role of TRAF3 in OC differentiation and function (Yao et al., 2009) and specific deletion of TRAF3 in myeloid cells results in the age-associated bone loss (Xiu et al., 2014). Interestingly, we recently found that a specific

deletion of TRAF3 in MPCs in mice also results in age-associated bone loss by decreasing OB differentiation and bone formation (un-published). These suggest that TRAF3 also play dual role to inhibit bone resorption and stimulate bone formation. Targeting TRAF3 could therefore be another strategy to develop new agents with dual anti-resorptive and anabolic effect. One of such approaches is to inhibit degradation of TRAF3. We also importantly showed that inhibition of TRAF3 degradation by lysosomal inhibitor chloroquine (CQ) that has long been used to treat malaria and RA prevents ovariectomy-induced osteoporosis and PTH-induced bone loss (Xiu et al., 2014). However, like many other anti-RA drugs, CQ also has severe side effects, for example, renal toxic and blindness in up to 0.5-1% of patients (Costedoat-Chalumeau et al., 2015, Taylor and White, 2004). An attractive strategy to minimize side effects of drugs used to treat bone diseases is to administer them in a form that specifically targets them to bone. This could allow drugs to be given to patients at doses with reduced risk of side effects, while also delivering effective concentrations specifically to bone. Based on the high bone affinity of bisphosphonates (BPs) that are currently used to osteoporosis, we have generated a Bone-Targeted CQ (BTCQ) analog using a BP that binds avidly to bone, but does not inhibit bone resorption. The preliminary results in vitro and in vivo are excited. Further in vivo testing for the treatment of osteoporosis is being undertaken. In addition, we will need to perform profound research to elucidate how TRAF3 ubiquitintion and degradation is controlled in order to design specific agents to prevent TRAF3 degradation for the therapy of osteoporosis.

4.3 Summary

Our studies have revealed a number of mechanisms by which cytokine-induced non-canonical NF-κB signaling controls both bone resorption and formation including:

1) TNF expands the pool of OCPs with enhanced OC forming potential (Yao et al., 2006, Zhao et al., 2015);

2) NF-κB p50 and p52 sequentially activate c-Fos and NFATc1 to induce OC differentiation (Yamashita et al., 2007, Yao et al., 2008);

3) NF-κB2 p100 limits OC formation and bone resorption (Yao et al., 2009);

4) TRAF3 negatively regulates OC differentiation (Xiu et al., 2014, Yao et al., 2009);

5) NF-κB inhibits bone formation by interacting with Notch signaling (Engin et al., 2008, Kaneki et al., 2006, Yao et al., 2014, Zhang et al., 2014).

Importantly, targeting non-canonical NF-κB signaling could be used to develop new agents for the therapy of RA or osteoporosis. For example, agents that degrade TNF-induced RelB could block M1 macrophage differentiation to inhibit inflammation and joint destruction for the therapy of RA. In addition, NIK inhibitors that prevent p100 processing or agents that prevent TRAF3 degradation could inhibit bone resorption and simultaneously stimulate bone formation for the therapy of osteoporosis. We are currently working with chemists to develop agents for the therapy of RA and/or osteoporosis based on the findings described in this thesis.

References

ABBAS, S., ZHANG, Y. H., CLOHISY, J. C. & ABU-AMER, Y. 2003. Tumor necrosis factor-alpha inhibits pre-osteoblast differentiation through its type-1 receptor. *Cytokine,* 22**,** 33-41.

ABRAHAMSEN, B., HJELMBORG, J. V., KOSTENUIK, P., STILGREN, L. S., KYVIK, K., ADAMU, S., BRIXEN, K. & LANGDAHL, B. L. 2005. Circulating amounts of osteoprotegerin and RANK ligand: genetic influence and relationship with BMD assessed in female twins. *Bone,* 36**,** 727-35.

AGHALOO, T. L., FELSENFELD, A. L. & TETRADIS, S. 2010. Osteonecrosis of the jaw in a patient on Denosumab. *J Oral Maxillofac Surg,* 68**,** 959-63.

ALLES, N., SOYSA, N. S., HAYASHI, J., KHAN, M., SHIMODA, A., SHIMOKAWA, H., RITZELER, O., AKIYOSHI, K., AOKI, K. & OHYA, K. 2010. Suppression of NF-kappaB increases bone formation and ameliorates osteopenia in ovariectomized mice. *Endocrinology,* 151**,** 4626-34.

AYA, K., ALHAWAGRI, M., HAGEN-STAPLETON, A., KITAURA, H., KANAGAWA, O. & NOVACK, D. V. 2005. NF-(kappa)B-inducing kinase controls lymphocyte and osteoclast activities in inflammatory arthritis. *J Clin Invest,* 115**,** 1848-54.

BEG, A. A., SHA, W. C., BRONSON, R. T., GHOSH, S. & BALTIMORE, D. 1995. Embryonic lethality and liver degeneration in mice lacking the RelA component of NF-kappa B. *Nature,* 376**,** 167-70.

BINGHAM, C. O., 3RD 2002. The pathogenesis of rheumatoid arthritis: pivotal cytokines involved in bone degradation and inflammation. *J Rheumatol Suppl,* 65**,** 3-9.

BLACK, D. M., GREENSPAN, S. L., ENSRUD, K. E., PALERMO, L., MCGOWAN, J. A., LANG, T. F., GARNERO, P., BOUXSEIN, M. L., BILEZIKIAN, J. P., ROSEN, C. J. & PA, T. H. S. I. 2003. The effects of parathyroid hormone and alendronate alone or in combination in postmenopausal osteoporosis. *N Engl J Med,* 349**,** 1207-15.

BONIZZI, G. & KARIN, M. 2004. The two NF-kappaB activation pathways and their role in innate and adaptive immunity. *Trends Immunol,* 25**,** 280-8.

BOUDIFFA, M., WADE-GUEYE, N. M., GUIGNANDON, A., VANDEN-BOSSCHE, A., SABIDO, O., AUBIN, J. E., JURDIC, P., VICO, L., LAFAGE-PROUST, M. H. & MALAVAL, L. 2010. Bone sialoprotein deficiency impairs osteoclastogenesis and mineral resorption in vitro. *J Bone Miner Res,* 25**,** 2669-79.

BOYCE, B. F. 2013. Advances in osteoclast biology reveal potential new drug targets and new roles for osteoclasts. *J Bone Miner Res,* 28**,** 711-22.

BOYCE, B. F., AUFDEMORTE, T. B., GARRETT, I. R., YATES, A. J. & MUNDY, G. R. 1989. Effects of interleukin-1 on bone turnover in normal mice. *Endocrinology,* 125**,** 1142-50.

BOYCE, B. F., LI, P., YAO, Z., ZHANG, Q., BADELL, I. R., SCHWARZ, E. M., O'KEEFE, R. J. & XING, L. 2005. TNF-alpha and pathologic bone resorption. *Keio J Med,* 54**,** 127-31.

BOYCE, B. F. & XING, L. 2007. Biology of RANK, RANKL, and osteoprotegerin. *Arthritis Res Ther,* 9 Suppl 1**,** S1.

BOYCE, B. F., XIU, Y., LI, J., XING, L. & YAO, Z. 2015. NF-kappaB-Mediated Regulation of Osteoclastogenesis. *Endocrinol Metab (Seoul),* 30**,** 35-44.

BOYCE, B. F., YONEDA, T., LOWE, C., SORIANO, P. & MUNDY, G. R. 1992. Requirement of pp60c-src expression for osteoclasts to form ruffled borders and resorb bone in mice. *J Clin Invest,* 90**,** 1622-7.

BOYLE, W. J., SIMONET, W. S. & LACEY, D. L. 2003. Osteoclast differentiation and activation. *Nature,* 423**,** 337-42.

BURKLY, L., HESSION, C., OGATA, L., REILLY, C., MARCONI, L. A., OLSON, D., TIZARD, R., CATE, R. & LO, D. 1995. Expression of relB is required for the development of thymic medulla and dendritic cells. *Nature,* 373**,** 531-6.

CHANG, J., WANG, Z., TANG, E., FAN, Z., MCCAULEY, L., FRANCESCHI, R., GUAN, K., KREBSBACH, P. H. & WANG, C. Y. 2009. Inhibition of osteoblastic bone formation by nuclear factor-kappaB. *Nat Med,* 15**,** 682-9.

CHO, H. H., SHIN, K. K., KIM, Y. J., SONG, J. S., KIM, J. M., BAE, Y. C., KIM, C. D. & JUNG, J. S. 2010. NF-kappaB activation stimulates osteogenic differentiation of mesenchymal stem cells derived from human adipose tissue by increasing TAZ expression. *J Cell Physiol,* 223**,** 168-77.

CIPRIANI, C., IRANI, D. & BILEZIKIAN, J. P. 2012. Safety of osteoanabolic therapy: a decade of experience. *J Bone Miner Res,* 27**,** 2419-28.

CLAGUE, M. J. & URBE, S. 2010. Ubiquitin: same molecule, different degradation pathways. *Cell,* 143**,** 682-5.

CLARKE, B. 2008. Normal bone anatomy and physiology. *Clin J Am Soc Nephrol,* 3 Suppl 3**,** S131-9.

COHEN, S. B., DORE, R. K., LANE, N. E., ORY, P. A., PETERFY, C. G., SHARP, J. T., VAN DER HEIJDE, D., ZHOU, L., TSUJI, W., NEWMARK, R. & DENOSUMAB RHEUMATOID ARTHRITIS STUDY, G. 2008. Denosumab treatment effects on structural damage, bone mineral density, and bone turnover in rheumatoid arthritis: a twelve-month, multicenter, randomized, double-blind, placebo-controlled, phase II clinical trial. *Arthritis Rheum,* 58**,** 1299-309.

COPETTI, T., BERTOLI, C., DALLA, E., DEMARCHI, F. & SCHNEIDER, C. 2009. p65/RelA modulates BECN1 transcription and autophagy. *Mol Cell Biol,* 29**,** 2594-608.

COSTEDOAT-CHALUMEAU, N., DUNOGUE, B., LEROUX, G., MOREL, N., JALLOULI, M., LE GUERN, V., PIETTE, J. C., BREZIN, A. P., MELLES, R. B. & MARMOR, M. F. 2015. A Critical Review of the Effects of Hydroxychloroquine and Chloroquine on the Eye. *Clin Rev Allergy Immunol,* 49**,** 317-26.

COURTOIS, G. & GILMORE, T. D. 2006. Mutations in the NF-kappaB signaling pathway: implications for human disease. *Oncogene,* 25**,** 6831-43.

DARNAY, B. G., BESSE, A., POBLENZ, A. T., LAMOTHE, B. & JACOBY, J. J. 2007. TRAFs in RANK signaling. *Adv Exp Med Biol,* 597**,** 152-9.

DATTO, M. & WANG, X. F. 2005. Ubiquitin-mediated degradation a mechanism for fine-tuning TGF-beta signaling. *Cell,* 121**,** 2-4.

DEMPSEY, P. W., DOYLE, S. E., HE, J. Q. & CHENG, G. 2003. The signaling adaptors and pathways activated by TNF superfamily. *Cytokine Growth Factor Rev,* 14**,** 193-209.

DOBRZANSKI, P., RYSECK, R. P. & BRAVO, R. 1995. Specific inhibition of RelB/p52 transcriptional activity by the C-terminal domain of p100. *Oncogene,* 10**,** 1003-7.

DOUGALL, W. C., GLACCUM, M., CHARRIER, K., ROHRBACH, K., BRASEL, K., DE SMEDT, T., DARO, E., SMITH, J., TOMETSKO, M. E., MALISZEWSKI, C. R., ARMSTRONG, A., SHEN, V., BAIN, S., COSMAN, D., ANDERSON, D., MORRISSEY, P. J., PESCHON, J. J. & SCHUH, J. 1999. RANK is essential for osteoclast and lymph node development. *Genes Dev,* 13**,** 2412-24.

ELEWAUT, D., SHAIKH, R. B., HAMMOND, K. J., DE WINTER, H., LEISHMAN, A. J., SIDOBRE, S., TUROVSKAYA, O., PRIGOZY, T. I., MA, L., BANKS, T. A., LO, D., WARE, C. F., CHEROUTRE, H. & KRONENBERG, M. 2003. NIK-dependent RelB activation defines a unique signaling pathway for the development of V alpha 14i NKT cells. *J Exp Med,* 197**,** 1623-33.

ENGIN, F., YAO, Z., YANG, T., ZHOU, G., BERTIN, T., JIANG, M. M., CHEN, Y., WANG, L., ZHENG, H., SUTTON, R. E., BOYCE, B. F. & LEE, B. 2008. Dimorphic effects of Notch signaling in bone homeostasis. *Nat Med,* 14**,** 299-305.

ERIKSEN, E. F., HODGSON, S. F., EASTELL, R., CEDEL, S. L., O'FALLON, W. M. & RIGGS, B. L. 1990. Cancellous bone remodeling in type I (postmenopausal) osteoporosis: quantitative assessment of rates of formation, resorption, and bone loss at tissue and cellular levels. *J Bone Miner Res,* 5**,** 311-9.

FERRARI-LACRAZ, S. & FERRARI, S. 2011. Do RANKL inhibitors (denosumab) affect inflammation and immunity? *Osteoporos Int,* 22**,** 435-46.

FICHNA, M., ZURAWEK, M., FICHNA, P., GRYCZYNSKA, M., NOWAK, J. & RUCHALA, M. 2012. Increased serum osteoprotegerin in patients with primary adrenal insufficiency receiving conventional hydrocortisone substitution. *J Physiol Pharmacol,* 63**,** 677-82.

FINKELSTEIN, J. S., HAYES, A., HUNZELMAN, J. L., WYLAND, J. J., LEE, H. & NEER, R. M. 2003. The effects of parathyroid hormone, alendronate, or both in men with osteoporosis. *N Engl J Med,* 349**,** 1216-26.

FISHER, L. W., TORCHIA, D. A., FOHR, B., YOUNG, M. F. & FEDARKO, N. S. 2001. Flexible structures of SIBLING proteins, bone sialoprotein, and osteopontin. *Biochem Biophys Res Commun,* 280**,** 460-5.

FRANZOSO, G., CARLSON, L., XING, L., POLJAK, L., SHORES, E. W., BROWN, K. D., LEONARDI, A., TRAN, T., BOYCE, B. F. & SIEBENLIST, U. 1997. Requirement for NF-kappaB in osteoclast and B-cell development. *Genes Dev,* 11**,** 3482-96.

FUSCO, A. J., SAVINOVA, O. V., TALWAR, R., KEARNS, J. D., HOFFMANN, A. & GHOSH, G. 2008. Stabilization of RelB requires multidomain interactions with p100/p52. *J Biol Chem,* 283**,** 12324-32.

GARNERO, P., SHIH, W. J., GINEYTS, E., KARPF, D. B. & DELMAS, P. D. 1994. Comparison of new biochemical markers of bone turnover in late postmenopausal osteoporotic women in response to alendronate treatment. *J Clin Endocrinol Metab,* 79**,** 1693-700.

GARNERO, P., SORNAY-RENDU, E., CHAPUY, M. C. & DELMAS, P. D. 1996. Increased bone turnover in late postmenopausal women is a major determinant of osteoporosis. *J Bone Miner Res,* 11**,** 337-49.

GILBERT, L., HE, X., FARMER, P., RUBIN, J., DRISSI, H., VAN WIJNEN, A. J., LIAN, J. B., STEIN, G. S. & NANES, M. S. 2002. Expression of the osteoblast

differentiation factor RUNX2 (Cbfa1/AML3/Pebp2alpha A) is inhibited by tumor necrosis factor-alpha. *J Biol Chem,* 277**,** 2695-701.
GILBERT, L. C., RUBIN, J. & NANES, M. S. 2005. The p55 TNF receptor mediates TNF inhibition of osteoblast differentiation independently of apoptosis. *Am J Physiol Endocrinol Metab,* 288**,** E1011-8.
GINALDI, L., DI BENEDETTO, M. C. & DE MARTINIS, M. 2005. Osteoporosis, inflammation and ageing. *Immun Ageing,* 2**,** 14.
GORDON, S. 2007. The macrophage: past, present and future. *Eur J Immunol,* 37 Suppl 1**,** S9-17.
GORDON, S. & TAYLOR, P. R. 2005. Monocyte and macrophage heterogeneity. *Nat Rev Immunol,* 5**,** 953-64.
GRIGORIADIS, A. E., WANG, Z. Q., CECCHINI, M. G., HOFSTETTER, W., FELIX, R., FLEISCH, H. A. & WAGNER, E. F. 1994. c-Fos: a key regulator of osteoclast-macrophage lineage determination and bone remodeling. *Science,* 266**,** 443-8.
GYRD-HANSEN, M. & MEIER, P. 2010. IAPs: from caspase inhibitors to modulators of NF-kappaB, inflammation and cancer. *Nat Rev Cancer,* 10**,** 561-74.
HAYDEN, M. S. & GHOSH, S. 2008. Shared principles in NF-kappaB signaling. *Cell,* 132**,** 344-62.
HE, J. Q., SAHA, S. K., KANG, J. R., ZARNEGAR, B. & CHENG, G. 2007. Specificity of TRAF3 in its negative regulation of the noncanonical NF-kappa B pathway. *J Biol Chem,* 282**,** 3688-94.
HE, J. Q., ZARNEGAR, B., OGANESYAN, G., SAHA, S. K., YAMAZAKI, S., DOYLE, S. E., DEMPSEY, P. W. & CHENG, G. 2006. Rescue of TRAF3-null mice by p100 NF-kappa B deficiency. *J Exp Med,* 203**,** 2413-8.
HESS, K., USHMOROV, A., FIEDLER, J., BRENNER, R. E. & WIRTH, T. 2009. TNFalpha promotes osteogenic differentiation of human mesenchymal stem cells by triggering the NF-kappaB signaling pathway. *Bone,* 45**,** 367-76.
HOFBAUER, L. C., LACEY, D. L., DUNSTAN, C. R., SPELSBERG, T. C., RIGGS, B. L. & KHOSLA, S. 1999. Interleukin-1beta and tumor necrosis factor-alpha, but not interleukin-6, stimulate osteoprotegerin ligand gene expression in human osteoblastic cells. *Bone,* 25**,** 255-9.
HYRICH, K. L., WATSON, K. D., SILMAN, A. J., SYMMONS, D. P. & BRITISH SOCIETY FOR RHEUMATOLOGY BIOLOGICS, R. 2006. Predictors of response to anti-TNF-alpha therapy among patients with rheumatoid arthritis: results from the British Society for Rheumatology Biologics Register. *Rheumatology (Oxford),* 45**,** 1558-65.
IOTSOVA, V., CAAMANO, J., LOY, J., YANG, Y., LEWIN, A. & BRAVO, R. 1997. Osteopetrosis in mice lacking NF-kappaB1 and NF-kappaB2. *Nat Med,* 3**,** 1285-9.
ISHIJIMA, M., RITTLING, S. R., YAMASHITA, T., TSUJI, K., KUROSAWA, H., NIFUJI, A., DENHARDT, D. T. & NODA, M. 2001. Enhancement of osteoclastic bone resorption and suppression of osteoblastic bone formation in response to reduced mechanical stress do not occur in the absence of osteopontin. *J Exp Med,* 193**,** 399-404.
IZZI, L. & ATTISANO, L. 2004. Regulation of the TGFbeta signalling pathway by ubiquitin-mediated degradation. *Oncogene,* 23**,** 2071-8.

JIMI, E., AKIYAMA, S., TSURUKAI, T., OKAHASHI, N., KOBAYASHI, K., UDAGAWA, N., NISHIHARA, T., TAKAHASHI, N. & SUDA, T. 1999. Osteoclast differentiation factor acts as a multifunctional regulator in murine osteoclast differentiation and function. *J Immunol,* 163**,** 434-42.

JIMI, E., SHUTO, T. & KOGA, T. 1995. Macrophage colony-stimulating factor and interleukin-1 alpha maintain the survival of osteoclast-like cells. *Endocrinology,* 136**,** 808-11.

KANAZAWA, K., AZUMA, Y., NAKANO, H. & KUDO, A. 2003. TRAF5 functions in both RANKL- and TNFalpha-induced osteoclastogenesis. *J Bone Miner Res,* 18**,** 443-50.

KANAZAWA, K. & KUDO, A. 2005. TRAF2 is essential for TNF-alpha-induced osteoclastogenesis. *J Bone Miner Res,* 20**,** 840-7.

KANEKI, H., GUO, R., CHEN, D., YAO, Z., SCHWARZ, E. M., ZHANG, Y. E., BOYCE, B. F. & XING, L. 2006. Tumor necrosis factor promotes Runx2 degradation through up-regulation of Smurf1 and Smurf2 in osteoblasts. *J Biol Chem,* 281**,** 4326-33.

KARIN, M. & GRETEN, F. R. 2005. NF-kappaB: linking inflammation and immunity to cancer development and progression. *Nat Rev Immunol,* 5**,** 749-59.

KAWANAKA, N., YAMAMURA, M., AITA, T., MORITA, Y., OKAMOTO, A., KAWASHIMA, M., IWAHASHI, M., UENO, A., OHMOTO, Y. & MAKINO, H. 2002. CD14+,CD16+ blood monocytes and joint inflammation in rheumatoid arthritis. *Arthritis Rheum,* 46**,** 2578-86.

KEFFER, J., PROBERT, L., CAZLARIS, H., GEORGOPOULOS, S., KASLARIS, E., KIOUSSIS, D. & KOLLIAS, G. 1991. Transgenic mice expressing human tumour necrosis factor: a predictive genetic model of arthritis. *EMBO J,* 10**,** 4025-31.

KENNEL, K. A. & DRAKE, M. T. 2009. Adverse effects of bisphosphonates: implications for osteoporosis management. *Mayo Clin Proc,* 84**,** 632-7; quiz 638.

KERSCHAN-SCHINDL, K., WENDLOVA, J., KUDLACEK, S., GLEISS, A., WOLOSZCZUK, W. & PIETSCHMANN, P. 2008. Serum levels of receptor activator of nuclear factor kappaB ligand (RANKL) in healthy women and men. *Exp Clin Endocrinol Diabetes,* 116**,** 491-5.

KEYAK, J. H., SIGURDSSON, S., KARLSDOTTIR, G., OSKARSDOTTIR, D., SIGMARSDOTTIR, A., ZHAO, S., KORNAK, J., HARRIS, T. B., SIGURDSSON, G., JONSSON, B. Y., SIGGEIRSDOTTIR, K., EIRIKSDOTTIR, G., GUDNASON, V. & LANG, T. F. 2011. Male-female differences in the association between incident hip fracture and proximal femoral strength: a finite element analysis study. *Bone,* 48**,** 1239-45.

KHOSLA, S. 2010. Update in male osteoporosis. *J Clin Endocrinol Metab,* 95**,** 3-10.

KIM, H. H., LEE, D. E., SHIN, J. N., LEE, Y. S., JEON, Y. M., CHUNG, C. H., NI, J., KWON, B. S. & LEE, Z. H. 1999. Receptor activator of NF-kappaB recruits multiple TRAF family adaptors and activates c-Jun N-terminal kinase. *FEBS Lett,* 443**,** 297-302.

KIM, N., KADONO, Y., TAKAMI, M., LEE, J., LEE, S. H., OKADA, F., KIM, J. H., KOBAYASHI, T., ODGREN, P. R., NAKANO, H., YEH, W. C., LEE, S. K., LORENZO, J. A. & CHOI, Y. 2005. Osteoclast differentiation independent of the TRANCE-RANK-TRAF6 axis. *J Exp Med,* 202**,** 589-95.

KIM, N., ODGREN, P. R., KIM, D. K., MARKS, S. C., JR. & CHOI, Y. 2000. Diverse roles of the tumor necrosis factor family member TRANCE in skeletal physiology revealed by TRANCE deficiency and partial rescue by a lymphocyte-expressed TRANCE transgene. *Proc Natl Acad Sci U S A,* 97**,** 10905-10.

KIM, S. Y., SCHNEEWEISS, S., LIU, J., DANIEL, G. W., CHANG, C. L., GARNEAU, K. & SOLOMON, D. H. 2010. Risk of osteoporotic fracture in a large population-based cohort of patients with rheumatoid arthritis. *Arthritis Res Ther,* 12**,** R154.

KITAMURA, T., ONISHI, M., KINOSHITA, S., SHIBUYA, A., MIYAJIMA, A. & NOLAN, G. P. 1995. Efficient screening of retroviral cDNA expression libraries. *Proc Natl Acad Sci U S A,* 92**,** 9146-50.

KOBAYASHI, K., TAKAHASHI, N., JIMI, E., UDAGAWA, N., TAKAMI, M., KOTAKE, S., NAKAGAWA, N., KINOSAKI, M., YAMAGUCHI, K., SHIMA, N., YASUDA, H., MORINAGA, T., HIGASHIO, K., MARTIN, T. J. & SUDA, T. 2000. Tumor necrosis factor alpha stimulates osteoclast differentiation by a mechanism independent of the ODF/RANKL-RANK interaction. *J Exp Med,* 191**,** 275-86.

KOMORI, T. 2011. Signaling networks in RUNX2-dependent bone development. *J Cell Biochem,* 112**,** 750-5.

LACEY, D. L., TIMMS, E., TAN, H. L., KELLEY, M. J., DUNSTAN, C. R., BURGESS, T., ELLIOTT, R., COLOMBERO, A., ELLIOTT, G., SCULLY, S., HSU, H., SULLIVAN, J., HAWKINS, N., DAVY, E., CAPPARELLI, C., ELI, A., QIAN, Y. X., KAUFMAN, S., SAROSI, I., SHALHOUB, V., SENALDI, G., GUO, J., DELANEY, J. & BOYLE, W. J. 1998. Osteoprotegerin ligand is a cytokine that regulates osteoclast differentiation and activation. *Cell,* 93**,** 165-76.

LAM, J., TAKESHITA, S., BARKER, J. E., KANAGAWA, O., ROSS, F. P. & TEITELBAUM, S. L. 2000. TNF-alpha induces osteoclastogenesis by direct stimulation of macrophages exposed to permissive levels of RANK ligand. *J Clin Invest,* 106**,** 1481-8.

LEE, Z. H., LEE, S. E., KIM, C. W., LEE, S. H., KIM, S. W., KWACK, K., WALSH, K. & KIM, H. H. 2002. IL-1alpha stimulation of osteoclast survival through the PI 3-kinase/Akt and ERK pathways. *J Biochem,* 131**,** 161-6.

LENCEL, P., DELPLACE, S., HARDOUIN, P. & MAGNE, D. 2011. TNF-alpha stimulates alkaline phosphatase and mineralization through PPARgamma inhibition in human osteoblasts. *Bone,* 48**,** 242-9.

LEUSCHNER, F., DUTTA, P., GORBATOV, R., NOVOBRANTSEVA, T. I., DONAHOE, J. S., COURTIES, G., LEE, K. M., KIM, J. I., MARKMANN, J. F., MARINELLI, B., PANIZZI, P., LEE, W. W., IWAMOTO, Y., MILSTEIN, S., EPSTEIN-BARASH, H., CANTLEY, W., WONG, J., CORTEZ-RETAMOZO, V., NEWTON, A., LOVE, K., LIBBY, P., PITTET, M. J., SWIRSKI, F. K., KOTELIANSKY, V., LANGER, R., WEISSLEDER, R., ANDERSON, D. G. & NAHRENDORF, M. 2011. Therapeutic siRNA silencing in inflammatory monocytes in mice. *Nat Biotechnol,* 29**,** 1005-10.

LI, J., HSU, H. C. & MOUNTZ, J. D. 2012a. Managing macrophages in rheumatoid arthritis by reform or removal. *Curr Rheumatol Rep,* 14**,** 445-54.

LI, J., HSU, H. C., YANG, P., WU, Q., LI, H., EDGINGTON, L. E., BOGYO, M., KIMBERLY, R. P. & MOUNTZ, J. D. 2012b. Treatment of arthritis by macrophage depletion and immunomodulation: testing an apoptosis-mediated therapy in a humanized death receptor mouse model. *Arthritis Rheum,* 64**,** 1098-109.

LI, J., SAROSI, I., YAN, X. Q., MORONY, S., CAPPARELLI, C., TAN, H. L., MCCABE, S., ELLIOTT, R., SCULLY, S., VAN, G., KAUFMAN, S., JUAN, S. C., SUN, Y., TARPLEY, J., MARTIN, L., CHRISTENSEN, K., MCCABE, J., KOSTENUIK, P., HSU, H., FLETCHER, F., DUNSTAN, C. R., LACEY, D. L. & BOYLE, W. J. 2000. RANK is the intrinsic hematopoietic cell surface receptor that controls osteoclastogenesis and regulation of bone mass and calcium metabolism. *Proc Natl Acad Sci U S A,* 97**,** 1566-71.

LI, P., SCHWARZ, E. M., O'KEEFE, R. J., MA, L., LOONEY, R. J., RITCHLIN, C. T., BOYCE, B. F. & XING, L. 2004. Systemic tumor necrosis factor alpha mediates an increase in peripheral CD11bhigh osteoclast precursors in tumor necrosis factor alpha-transgenic mice. *Arthritis Rheum,* 50**,** 265-76.

LI, Y., LI, A., STRAIT, K., ZHANG, H., NANES, M. S. & WEITZMANN, M. N. 2007. Endogenous TNFalpha lowers maximum peak bone mass and inhibits osteoblastic Smad activation through NF-kappaB. *J Bone Miner Res,* 22**,** 646-55.

LIN, X., LIANG, M. & FENG, X. H. 2000. Smurf2 is a ubiquitin E3 ligase mediating proteasome-dependent degradation of Smad2 in transforming growth factor-beta signaling. *J Biol Chem,* 275**,** 36818-22.

LIOU, H. C., NOLAN, G. P., GHOSH, S., FUJITA, T. & BALTIMORE, D. 1992. The NF-kappa B p50 precursor, p105, contains an internal I kappa B-like inhibitor that preferentially inhibits p50. *EMBO J,* 11**,** 3003-9.

LIU, J., SUDOM, A., MIN, X., CAO, Z., GAO, X., AYRES, M., LEE, F., CAO, P., JOHNSTONE, S., PLOTNIKOVA, O., WALKER, N., CHEN, G. & WANG, Z. 2012. Structure of the nuclear factor kappaB-inducing kinase (NIK) kinase domain reveals a constitutively active conformation. *J Biol Chem,* 287**,** 27326-34.

LIU, Y., HANSON, S., GURUGAMA, P., JONES, A., CLARK, B. & IBRAHIM, M. A. 2014. Novel NFKB2 mutation in early-onset CVID. *J Clin Immunol,* 34**,** 686-90.

LOMAGA, M. A., YEH, W. C., SAROSI, I., DUNCAN, G. S., FURLONGER, C., HO, A., MORONY, S., CAPPARELLI, C., VAN, G., KAUFMAN, S., VAN DER HEIDEN, A., ITIE, A., WAKEHAM, A., KHOO, W., SASAKI, T., CAO, Z., PENNINGER, J. M., PAIGE, C. J., LACEY, D. L., DUNSTAN, C. R., BOYLE, W. J., GOEDDEL, D. V. & MAK, T. W. 1999. TRAF6 deficiency results in osteopetrosis and defective interleukin-1, CD40, and LPS signaling. *Genes Dev,* 13**,** 1015-24.

MARKS, S. C., JR. & SEIFERT, M. F. 1985. The lifespan of osteoclasts: experimental studies using the giant granule cytoplasmic marker characteristic of beige mice. *Bone,* 6**,** 451-5.

MATSUO, K., GALSON, D. L., ZHAO, C., PENG, L., LAPLACE, C., WANG, K. Z., BACHLER, M. A., AMANO, H., ABURATANI, H., ISHIKAWA, H. & WAGNER, E. F. 2004. Nuclear factor of activated T-cells (NFAT) rescues osteoclastogenesis in precursors lacking c-Fos. *J Biol Chem,* 279**,** 26475-80.

MCLEAN, R. R. 2009. Proinflammatory cytokines and osteoporosis. *Curr Osteoporos Rep,* 7**,** 134-9.

MILDE-LANGOSCH, K. 2005. The Fos family of transcription factors and their role in tumourigenesis. *Eur J Cancer,* 41**,** 2449-61.

MIZOGUCHI, T., MUTO, A., UDAGAWA, N., ARAI, A., YAMASHITA, T., HOSOYA, A., NINOMIYA, T., NAKAMURA, H., YAMAMOTO, Y., KINUGAWA, S., NAKAMURA, M., NAKAMICHI, Y., KOBAYASHI, Y., NAGASAWA, S., ODA, K., TANAKA, H.,

TAGAYA, M., PENNINGER, J. M., ITO, M. & TAKAHASHI, N. 2009. Identification of cell cycle-arrested quiescent osteoclast precursors in vivo. *J Cell Biol,* 184**,** 541-54.

MORITA, S., KOJIMA, T. & KITAMURA, T. 2000. Plat-E: an efficient and stable system for transient packaging of retroviruses. *Gene Ther,* 7**,** 1063-6.

MORTIER, J., MASEREEL, B., REMOUCHAMPS, C., GANEFF, C., PIETTE, J. & FREDERICK, R. 2010. NF-kappaB inducing kinase (NIK) inhibitors: identification of new scaffolds using virtual screening. *Bioorg Med Chem Lett,* 20**,** 4515-20.

MOSSER, D. M. & EDWARDS, J. P. 2008. Exploring the full spectrum of macrophage activation. *Nat Rev Immunol,* 8**,** 958-69.

MURAI, M., TUROVSKAYA, O., KIM, G., MADAN, R., KARP, C. L., CHEROUTRE, H. & KRONENBERG, M. 2009. Interleukin 10 acts on regulatory T cells to maintain expression of the transcription factor Foxp3 and suppressive function in mice with colitis. *Nat Immunol,* 10**,** 1178-84.

MURPHY, C. A., LANGRISH, C. L., CHEN, Y., BLUMENSCHEIN, W., MCCLANAHAN, T., KASTELEIN, R. A., SEDGWICK, J. D. & CUA, D. J. 2003. Divergent pro- and antiinflammatory roles for IL-23 and IL-12 in joint autoimmune inflammation. *J Exp Med,* 198**,** 1951-7.

NAITO, A., AZUMA, S., TANAKA, S., MIYAZAKI, T., TAKAKI, S., TAKATSU, K., NAKAO, K., NAKAMURA, K., KATSUKI, M., YAMAMOTO, T. & INOUE, J. 1999. Severe osteopetrosis, defective interleukin-1 signalling and lymph node organogenesis in TRAF6-deficient mice. *Genes Cells,* 4**,** 353-62.

NOVACK, D. V., YIN, L., HAGEN-STAPLETON, A., SCHREIBER, R. D., GOEDDEL, D. V., ROSS, F. P. & TEITELBAUM, S. L. 2003. The IkappaB function of NF-kappaB2 p100 controls stimulated osteoclastogenesis. *J Exp Med,* 198**,** 771-81.

OCHI, S., SHINOHARA, M., SATO, K., GOBER, H. J., KOGA, T., KODAMA, T., TAKAI, T., MIYASAKA, N. & TAKAYANAGI, H. 2007. Pathological role of osteoclast costimulation in arthritis-induced bone loss. *Proc Natl Acad Sci U S A,* 104**,** 11394-9.

PANULA, J., PIHLAJAMAKI, H., MATTILA, V. M., JAATINEN, P., VAHLBERG, T., AARNIO, P. & KIVELA, S. L. 2011. Mortality and cause of death in hip fracture patients aged 65 or older: a population-based study. *BMC Musculoskelet Disord,* 12**,** 105.

PLATZER, B., JORGL, A., TASCHNER, S., HOCHER, B. & STROBL, H. 2004. RelB regulates human dendritic cell subset development by promoting monocyte intermediates. *Blood,* 104**,** 3655-63.

PONNAPAKKAM, T., KATIKANENI, R., SAKON, J., STRATFORD, R. & GENSURE, R. C. 2014. Treating osteoporosis by targeting parathyroid hormone to bone. *Drug Discov Today,* 19**,** 204-8.

QIN, C., BABA, O. & BUTLER, W. T. 2004. Post-translational modifications of sibling proteins and their roles in osteogenesis and dentinogenesis. *Crit Rev Oral Biol Med,* 15**,** 126-36.

RASMUSSON, L. & ABTAHI, J. 2014. Bisphosphonate associated osteonecrosis of the jaw: an update on pathophysiology, risk factors, and treatment. *Int J Dent,* 2014**,** 471035.

REDLICH, K., HAYER, S., MAIER, A., DUNSTAN, C. R., TOHIDAST-AKRAD, M., LANG, S., TURK, B., PIETSCHMANN, P., WOLOSZCZUK, W., HARALAMBOUS, S., KOLLIAS, G., STEINER, G., SMOLEN, J. S. & SCHETT, G. 2002a. Tumor necrosis factor alpha-mediated joint destruction is inhibited by targeting osteoclasts with osteoprotegerin. *Arthritis Rheum,* 46**,** 785-92.

REDLICH, K., HAYER, S., RICCI, R., DAVID, J. P., TOHIDAST-AKRAD, M., KOLLIAS, G., STEINER, G., SMOLEN, J. S., WAGNER, E. F. & SCHETT, G. 2002b. Osteoclasts are essential for TNF-alpha-mediated joint destruction. *J Clin Invest,* 110**,** 1419-27.

REINHOLT, F. P., HULTENBY, K., OLDBERG, A. & HEINEGARD, D. 1990. Osteopontin--a possible anchor of osteoclasts to bone. *Proc Natl Acad Sci U S A,* 87**,** 4473-5.

RUGGIERO, S. L., MEHROTRA, B., ROSENBERG, T. J. & ENGROFF, S. L. 2004. Osteonecrosis of the jaws associated with the use of bisphosphonates: a review of 63 cases. *J Oral Maxillofac Surg,* 62**,** 527-34.

SEDGHIZADEH, P. P., STANLEY, K., CALIGIURI, M., HOFKES, S., LOWRY, B. & SHULER, C. F. 2009. Oral bisphosphonate use and the prevalence of osteonecrosis of the jaw: an institutional inquiry. *J Am Dent Assoc,* 140**,** 61-6.

SENFTLEBEN, U., CAO, Y., XIAO, G., GRETEN, F. R., KRAHN, G., BONIZZI, G., CHEN, Y., HU, Y., FONG, A., SUN, S. C. & KARIN, M. 2001. Activation by IKKalpha of a second, evolutionary conserved, NF-kappa B signaling pathway. *Science,* 293**,** 1495-9.

SEO, Y., FUKUSHIMA, H., MARUYAMA, T., KUROISHI, K. N., OSAWA, K., NAGANO, K., AOKI, K., WEIH, F., DOI, T., ZHANG, M., OHYA, K., KATAGIRI, T., HOSOKAWA, R. & JIMI, E. 2012. Accumulation of p100, a precursor of NF-kappaB2, enhances osteoblastic differentiation in vitro and bone formation in vivo in aly/aly mice. *Mol Endocrinol,* 26**,** 414-22.

SHIBATA, W., MAEDA, S., HIKIBA, Y., YANAI, A., OHMAE, T., SAKAMOTO, K., NAKAGAWA, H., OGURA, K. & OMATA, M. 2007. Cutting edge: The IkappaB kinase (IKK) inhibitor, NEMO-binding domain peptide, blocks inflammatory injury in murine colitis. *J Immunol,* 179**,** 2681-5.

SIERRA-FILARDI, E., VEGA, M. A., SANCHEZ-MATEOS, P., CORBI, A. L. & PUIG-KROGER, A. 2010. Heme Oxygenase-1 expression in M-CSF-polarized M2 macrophages contributes to LPS-induced IL-10 release. *Immunobiology,* 215**,** 788-95.

SILVA, T. A., LARA, V. S., SILVA, J. S., OLIVEIRA, S. H., BUTLER, W. T. & CUNHA, F. Q. 2005. Macrophages and mast cells control the neutrophil migration induced by dentin proteins. *J Dent Res,* 84**,** 79-83.

SMITH, A. M., RAHMAN, F. Z., HAYEE, B., GRAHAM, S. J., MARKS, D. J., SEWELL, G. W., PALMER, C. D., WILDE, J., FOXWELL, B. M., GLOGER, I. S., SWEETING, T., MARSH, M., WALKER, A. P., BLOOM, S. L. & SEGAL, A. W. 2009. Disordered macrophage cytokine secretion underlies impaired acute inflammation and bacterial clearance in Crohn's disease. *J Exp Med,* 206**,** 1883-97.

SOYSA, N. S., ALLES, N., WEIH, D., LOVAS, A., MIAN, A. H., SHIMOKAWA, H., YASUDA, H., WEIH, F., JIMI, E., OHYA, K. & AOKI, K. 2010. The pivotal role of

the alternative NF-kappaB pathway in maintenance of basal bone homeostasis and osteoclastogenesis. *J Bone Miner Res,* 25**,** 809-18.
STAFFORD, R. S., DRIELING, R. L. & HERSH, A. L. 2004. National trends in osteoporosis visits and osteoporosis treatment, 1988-2003. *Arch Intern Med,* 164**,** 1525-30.
STENBECK, G. 2002. Formation and function of the ruffled border in osteoclasts. *Semin Cell Dev Biol,* 13**,** 285-92.
STORHEIM, K. & ZWART, J. A. 2014. Musculoskeletal disorders and the Global Burden of Disease study. *Ann Rheum Dis,* 73**,** 949-50.
SUN, S. C. 2011. Non-canonical NF-kappaB signaling pathway. *Cell Res,* 21**,** 71-85.
SUN, S. C. 2012. The noncanonical NF-kappaB pathway. *Immunol Rev,* 246**,** 125-40.
SYMMONS, D. P. & SILMAN, A. J. 2006. The world of biologics. *Lupus,* 15**,** 122-6.
TAKAYANAGI, H. 2007. Osteoimmunology: shared mechanisms and crosstalk between the immune and bone systems. *Nat Rev Immunol,* 7**,** 292-304.
TANAKA, S. & NAKANO, H. 2009. NF-kappaB2 (p100) limits TNF-alpha-induced osteoclastogenesis. *J Clin Invest,* 119**,** 2879-81.
TAYLOR, W. R. & WHITE, N. J. 2004. Antimalarial drug toxicity: a review. *Drug Saf,* 27**,** 25-61.
TEITELBAUM, S. L. 2006. Osteoclasts; culprits in inflammatory osteolysis. *Arthritis Res Ther,* 8**,** 201.
TUCKER, E., O'DONNELL, K., FUCHSBERGER, M., HILTON, A. A., METCALF, D., GREIG, K., SIMS, N. A., QUINN, J. M., ALEXANDER, W. S., HILTON, D. J., KILE, B. T., TARLINTON, D. M. & STARR, R. 2007. A novel mutation in the Nfkb2 gene generates an NF-kappa B2 "super repressor". *J Immunol,* 179**,** 7514-22.
UDAGAWA, N., TAKAHASHI, N., AKATSU, T., TANAKA, H., SASAKI, T., NISHIHARA, T., KOGA, T., MARTIN, T. J. & SUDA, T. 1990. Origin of osteoclasts: mature monocytes and macrophages are capable of differentiating into osteoclasts under a suitable microenvironment prepared by bone marrow-derived stromal cells. *Proc Natl Acad Sci U S A,* 87**,** 7260-4.
UEMURA, H., YASUI, T., MIYATANI, Y., YAMADA, M., HIYOSHI, M., ARISAWA, K. & IRAHARA, M. 2008. Circulating profiles of osteoprotegerin and soluble receptor activator of nuclear factor kappaB ligand in post-menopausal women. *J Endocrinol Invest,* 31**,** 163-8.
VAIRA, S., ALHAWAGRI, M., ANWISYE, I., KITAURA, H., FACCIO, R. & NOVACK, D. V. 2008a. RelA/p65 promotes osteoclast differentiation by blocking a RANKL-induced apoptotic JNK pathway in mice. *J Clin Invest,* 118**,** 2088-97.
VAIRA, S., JOHNSON, T., HIRBE, A. C., ALHAWAGRI, M., ANWISYE, I., SAMMUT, B., O'NEAL, J., ZOU, W., WEILBAECHER, K. N., FACCIO, R. & NOVACK, D. V. 2008b. RelB is the NF-kappaB subunit downstream of NIK responsible for osteoclast differentiation. *Proc Natl Acad Sci U S A,* 105**,** 3897-902.
VALLABHAPURAPU, S. & KARIN, M. 2009. Regulation and function of NF-kappaB transcription factors in the immune system. *Annu Rev Immunol,* 27**,** 693-733.
VALLABHAPURAPU, S., MATSUZAWA, A., ZHANG, W., TSENG, P. H., KEATS, J. J., WANG, H., VIGNALI, D. A., BERGSAGEL, P. L. & KARIN, M. 2008. Nonredundant and complementary functions of TRAF2 and TRAF3 in a

ubiquitination cascade that activates NIK-dependent alternative NF-kappaB signaling. *Nat Immunol,* 9**,** 1364-70.
WASNICH, R. D. & MILLER, P. D. 2000. Antifracture efficacy of antiresorptive agents are related to changes in bone density. *J Clin Endocrinol Metab,* 85**,** 231-6.
WEI, S., KITAURA, H., ZHOU, P., ROSS, F. P. & TEITELBAUM, S. L. 2005. IL-1 mediates TNF-induced osteoclastogenesis. *J Clin Invest,* 115**,** 282-90.
WILLIAMS, R. O., MARINOVA-MUTAFCHIEVA, L., FELDMANN, M. & MAINI, R. N. 2000. Evaluation of TNF-alpha and IL-1 blockade in collagen-induced arthritis and comparison with combined anti-TNF-alpha/anti-CD4 therapy. *J Immunol,* 165**,** 7240-5.
WYNN, T. A., CHAWLA, A. & POLLARD, J. W. 2013. Macrophage biology in development, homeostasis and disease. *Nature,* 496**,** 445-55.
XING, L., CARLSON, L., STORY, B., TAI, Z., KENG, P., SIEBENLIST, U. & BOYCE, B. F. 2003. Expression of either NF-kappaB p50 or p52 in osteoclast precursors is required for IL-1-induced bone resorption. *J Bone Miner Res,* 18**,** 260-9.
XING, L., SCHWARZ, E. M. & BOYCE, B. F. 2005. Osteoclast precursors, RANKL/RANK, and immunology. *Immunol Rev,* 208**,** 19-29.
XIU, Y., XU, H., ZHAO, C., LI, J., MORITA, Y., YAO, Z., XING, L. & BOYCE, B. F. 2014. Chloroquine reduces osteoclastogenesis in murine osteoporosis by preventing TRAF3 degradation. *J Clin Invest,* 124**,** 297-310.
YAMAMOTO, A., TAGAWA, Y., YOSHIMORI, T., MORIYAMA, Y., MASAKI, R. & TASHIRO, Y. 1998. Bafilomycin A1 prevents maturation of autophagic vacuoles by inhibiting fusion between autophagosomes and lysosomes in rat hepatoma cell line, H-4-II-E cells. *Cell Struct Funct,* 23**,** 33-42.
YAMASHITA, M., YING, S. X., ZHANG, G. M., LI, C., CHENG, S. Y., DENG, C. X. & ZHANG, Y. E. 2005. Ubiquitin ligase Smurf1 controls osteoblast activity and bone homeostasis by targeting MEKK2 for degradation. *Cell,* 121**,** 101-13.
YAMASHITA, T., YAO, Z., LI, F., ZHANG, Q., BADELL, I. R., SCHWARZ, E. M., TAKESHITA, S., WAGNER, E. F., NODA, M., MATSUO, K., XING, L. & BOYCE, B. F. 2007. NF-kappaB p50 and p52 regulate receptor activator of NF-kappaB ligand (RANKL) and tumor necrosis factor-induced osteoclast precursor differentiation by activating c-Fos and NFATc1. *J Biol Chem,* 282**,** 18245-53.
YAMAZAKI, M., FUKUSHIMA, H., SHIN, M., KATAGIRI, T., DOI, T., TAKAHASHI, T. & JIMI, E. 2009. Tumor necrosis factor alpha represses bone morphogenetic protein (BMP) signaling by interfering with the DNA binding of Smads through the activation of NF-kappaB. *J Biol Chem,* 284**,** 35987-95.
YAO, Z., LI, P., ZHANG, Q., SCHWARZ, E. M., KENG, P., ARBINI, A., BOYCE, B. F. & XING, L. 2006. Tumor necrosis factor-alpha increases circulating osteoclast precursor numbers by promoting their proliferation and differentiation in the bone marrow through up-regulation of c-Fms expression. *J Biol Chem,* 281**,** 11846-55.
YAO, Z., LI, Y., YIN, X., DONG, Y., XING, L. & BOYCE, B. F. 2014. NF-kappaB RelB negatively regulates osteoblast differentiation and bone formation. *J Bone Miner Res,* 29**,** 866-77.
YAO, Z., XING, L. & BOYCE, B. F. 2009. NF-kappaB p100 limits TNF-induced bone resorption in mice by a TRAF3-dependent mechanism. *J Clin Invest,* 119**,** 3024-34.

YAO, Z., XING, L., QIN, C., SCHWARZ, E. M. & BOYCE, B. F. 2008. Osteoclast precursor interaction with bone matrix induces osteoclast formation directly by an interleukin-1-mediated autocrine mechanism. *J Biol Chem,* 283**,** 9917-24.

YING, S. X., HUSSAIN, Z. J. & ZHANG, Y. E. 2003. Smurf1 facilitates myogenic differentiation and antagonizes the bone morphogenetic protein-2-induced osteoblast conversion by targeting Smad5 for degradation. *J Biol Chem,* 278**,** 39029-36.

YONA, S. & JUNG, S. 2010. Monocytes: subsets, origins, fates and functions. *Curr Opin Hematol,* 17**,** 53-9.

ZANOTTI, S. & CANALIS, E. 2010. Notch and the skeleton. *Mol Cell Biol,* 30**,** 886-96.

ZARNEGAR, B. J., WANG, Y., MAHONEY, D. J., DEMPSEY, P. W., CHEUNG, H. H., HE, J., SHIBA, T., YANG, X., YEH, W. C., MAK, T. W., KORNELUK, R. G. & CHENG, G. 2008. Noncanonical NF-kappaB activation requires coordinated assembly of a regulatory complex of the adaptors cIAP1, cIAP2, TRAF2 and TRAF3 and the kinase NIK. *Nat Immunol,* 9**,** 1371-8.

ZAVRAS, A. I. 2011. The impact of bisphosphonates on oral health: lessons from the past and opportunities for the future. *Ann N Y Acad Sci,* 1218**,** 55-61.

ZHANG, H., HILTON, M. J., ANOLIK, J. H., WELLE, S. L., ZHAO, C., YAO, Z., LI, X., WANG, Z., BOYCE, B. F. & XING, L. 2014. NOTCH inhibits osteoblast formation in inflammatory arthritis via noncanonical NF-kappaB. *J Clin Invest*.

ZHANG, Y., CHANG, C., GEHLING, D. J., HEMMATI-BRIVANLOU, A. & DERYNCK, R. 2001a. Regulation of Smad degradation and activity by Smurf2, an E3 ubiquitin ligase. *Proc Natl Acad Sci U S A,* 98**,** 974-9.

ZHANG, Y. H., HEULSMANN, A., TONDRAVI, M. M., MUKHERJEE, A. & ABU-AMER, Y. 2001b. Tumor necrosis factor-alpha (TNF) stimulates RANKL-induced osteoclastogenesis via coupling of TNF type 1 receptor and RANK signaling pathways. *J Biol Chem,* 276**,** 563-8.

ZHAO, B., GRIMES, S. N., LI, S., HU, X. & IVASHKIV, L. B. 2012. TNF-induced osteoclastogenesis and inflammatory bone resorption are inhibited by transcription factor RBP-J. *J Exp Med,* 209**,** 319-34.

ZHAO, B., TAKAMI, M., YAMADA, A., WANG, X., KOGA, T., HU, X., TAMURA, T., OZATO, K., CHOI, Y., IVASHKIV, L. B., TAKAYANAGI, H. & KAMIJO, R. 2009. Interferon regulatory factor-8 regulates bone metabolism by suppressing osteoclastogenesis. *Nat Med,* 15**,** 1066-71.

ZHAO, M., QIAO, M., HARRIS, S. E., OYAJOBI, B. O., MUNDY, G. R. & CHEN, D. 2004. Smurf1 inhibits osteoblast differentiation and bone formation in vitro and in vivo. *J Biol Chem,* 279**,** 12854-9.

ZHAO, Z., HOU, X., YIN, X., LI, Y., DUAN, R., BOYCE, B. F. & YAO, Z. 2015. TNF Induction of NF-kappaB RelB Enhances RANKL-Induced Osteoclastogenesis by Promoting Inflammatory Macrophage Differentiation but also Limits It through Suppression of NFATc1 Expression. *PLoS One,* 10**,** e0135728.

ZHU, H., KAVSAK, P., ABDOLLAH, S., WRANA, J. L. & THOMSEN, G. H. 1999. A SMAD ubiquitin ligase targets the BMP pathway and affects embryonic pattern formation. *Nature,* 400**,** 687-93.

***Appendix 1*: Publication lists for the application of a PhD by published work.**

Core publication lists:

1. **Yao Z**; Li P; Zhang Q; Schwarz EM; Keng P; Arbini A; Boyce BF; Xing L. "Tumor necrosis factor-alpha increases circulating osteoclast precursor numbers by promoting their proliferation and differentiation in the bone marrow through up-regulation of c-Fms expression." *The Journal of Biological Chemistry.* 2006; **281(17):**11846-55. http://www.jbc.org/content/281/17/11846.full.pdf+html
2. Zhao Z, Hou X, Yin X, Li Y, Duan R, Boyce BF, **Yao Z**. TNF Induction of NF-κB RelB Enhances RANKL-Induced Osteoclastogenesis by Promoting Inflammatory Macrophage Differentiation but also Limits It through Suppression of NFATc1 Expression. *PLoS One.* 2015;**10(8):**e0135728.. http://www.plosone.org/article/fetchObject.action?uri=info:doi/10.1371/journal.pone.0135728&representation=PDF
3. Yamashita T; **Yao Z *(co-first author)***; Li F; Zhang Q; Badell IR; Schwarz EM; Takeshita S; Wagner EF; Noda M; Matsuo K; Xing L; Boyce BF. "NF-kappaB p50 and p52 regulate receptor activator of NF-kappaB ligand (RANKL) and tumor necrosis factor-induced osteoclast precursor differentiation by activating c-Fos and NFATc1." *The Journal of Biological Chemistry.* 2007; **282(25):**18245-53. http://www.jbc.org/content/282/25/18245.long
4. **Yao Z**; Xing L; Qin C; Schwarz EM; Boyce BF. "Osteoclast precursor interaction with bone matrix induces osteoclast formation directly by an interleukin-1-mediated autocrine mechanism." *The Journal of Biological Chemistry.* 2008; **283(15):**9917-24. http://www.jbc.org/content/283/15/9917.full.pdf+html

5. **Yao Z**; Xing L; Boyce BF. "NF-kappaB p100 limits TNF-induced bone resorption in mice by a TRAF3-dependent mechanism." *The Journal of Clinical Investigation.* 2009; **119(10):**3024-34. http://www.ncbi.nlm.nih.gov/pmc/articles/PMC2752069/pdf/JCI38716.pdf

6. Xiu Y, Xu H, Zhao C, Li J, Morita Y, **Yao Z**, Xing L, Boyce BF. Chloroquine reduces osteoclastogenesis in murine osteoporosis by preventing TRAF3 degradation. *The Journal of Clinical Investigation.* 2014; **124(1):**297–310. http://www.ncbi.nlm.nih.gov/pmc/articles/PMC3871219/pdf/JCI66947.pdf

7. Kaneki H; Guo R; Chen D; **Yao Z**; Schwarz EM; Zhang YE; Boyce BF; Xing L. Tumor necrosis factor promotes Runx2 degradation through up-regulation of Smurf1 and Smurf2 in osteoblasts." *The Journal of Biological Chemistry.* 2006; **281(7):**4326-33. *http://www.jbc.org/content/281/7/4326.full.pdf+html*

8. Engin F; **Yao Z**; Yang T; Zhou G; Bertin T; Jiang MM; Chen Y; Wang L; Zheng H; Sutton RE; Boyce BF; Lee B. "Dimorphic effects of Notch signaling in bone homeostasis." *Nature Medicine.* 2008; **14(3):**299-305. *http://www.nature.com/nm/journal/v14/n3/pdf/nm1712.pdf*

9. **Yao Z**, Li Y, Yin X, Dong Y, Xing L, Boyce BF. NF-κB RelB negatively regulates osteoblast differentiation and bone formation. *Journal of Bone Mineral Research.* 2014; **29(4):**866-77. *http://onlinelibrary.wiley.com.ezpminer.urmc.rochester.edu/doi/10.1002/jbmr.2108/pdf*

10. Zhang H, Hilton MJ, Anolik J, Welle S, Zhao C, ***Yao Z***, Li X, Wang Z, Boyce B, Xing L. NOTCH inhibits osteoblast formation in inflammatory arthritis via non-canonical NF-κB. *The Journal of Clinical Investigation.* 2014 Jul 1;**124(7):**3200-14. http://www.jci.org/articles/view/68901/version/2/pdf/render

Supplemental list of publications:

11. Kiebala M, Polesskaya O, **Yao Z**, Perry SW, Maggirwar SB. Nuclear factor-kappa B family member RelB inhibits human immunodeficiency virus-1 Tat-induced tumor necrosis factor-alpha production. *PLoS One.* 2010; **5(7):**e11875. *http://www.plosone.org.ezpminer.urmc.rochester.edu/article/info%3Adoi%2F10.1371%2Fjournal.pone.0011875*

12. Zhang Q; Lu Y; Proulx ST; Guo R; **Yao Z**; Schwarz EM; Boyce BF; Xing L. "Increased lymphangiogenesis in joints of mice with inflammatory arthritis." *Arthritis Research & Therapy.* 2007; **9(6):**R118. *http://arthritis-research.com.ezpminer.urmc.rochester.edu/content/pdf/ar2326.pdf*

Appendix 2. Contribution statement to each publication in this thesis.

Publication	Contribution	Funding source
Article-1: JBC 2006	Conduct experiment of Fig.1, 2, 3 & 5.	NIH AR48697
	Writing paper	NIH AR43510
Article-2: PlosOne2015	Experimental Design	NSFC 81373191
	Conduct experiment of Fig.1, 2 &5	NIH AR43510
	Writing paper	
Article-3: JBC 2007	Conduct experiment of Fig.1,2,3,4,5&6	NIH AR43510
	Writing paper	
Article-4: JBC 2008	Experimental Design	NIH AR43510
	Conduct all the experiment	
	Writing paper	
Article-5: JCI 2009	Experimental Design	NIH AR43510
	Conduct all the experiment	
	Writing paper	
Article-6: JCI 2014	Experimental Design	NIH AR43510
	Supervise experiment	
Article-7: JBC 2006	Conduct experiment of Fig.1.	NIH AR48697
		NIH AR43510
Article-8: Nat Med 2008	Experimental Design	NIH ES11253
	Conduct experiment of Fig.1b, 3e & 4	NIH AR43510
Article-9: JBMR 2014	Experimental Design	NIH AR43510
	Conduct all the experiment	
	Writing paper	
Article-10: JCI 2014	Experimental Design.	NIH AR63650
	Develop model in Fig.4	NIH AR43510
Article-11: PlosOne2010	Conduct experiment of Fig. 2A, B&C	NIH NS054578
		NIH NS066801
Article-12: Arth Res Ther 2007	Conduct experiment of Fig. 1	NIH AR48697
		NIH AR43510

UNIVERSITY OF ROCHESTER MEDICAL CENTER

EASTMAN DENTAL CENTER
SCHOOL OF MEDICINE AND DENTISTRY
SCHOOL OF NURSING
STRONG MEMORIAL HOSPITAL
UNIVERSITY MEDICAL FACULTY GROUP

THE UNIVERSITY COMMITTEE ON ANIMAL RESOURCES

Verification of Protocol Review and Approval

University of Rochester
University Committee on Animal Resources

Title of Application:	**The Role of NF-kB RelB in Fracture Healing**
Principal Investigator:	**Zhenqiang Yao, Ph.D.**
Name of Institution:	**University of Rochester**
PHS Assurance:	**A-3292-01**
Application #:	**P30AR061307**
Species:	**Mouse**
Protocol Number:	**101373 / 2011-043**
Status:	**Approved**
Approval Date:	**December 13, 2011**

This letter certifies that the above protocol has been reviewed and approved by the University Committee on Animal Resources (UCAR). The protocol is effective for three (3) years from the date of approval. The approval date will be used as the anniversary date for Annual Protocol Reviews. The protocol may be subject to suspension if the conditions and requirements of the UCAR are not met.

Signed:

December 13, 2011

Suzanne Y. Stevens, Ph.D., UCAR Chair
or Christopher Stodgell, Ph.D., UCAR Vice-Chair
or Diane Moorman-White, D.V.M.
or Jeffrey D. Wyatt, D.V.M., M.P.H.

601 Elmwood Avenue, Box 674
Rochester, New York 14642
(Office) 585-275-1693 (Fax) 585-273-1337
E-mail: ucar@urmc.rochester.edu

UNIVERSITY OF ROCHESTER MEDICAL CENTER

EASTMAN DENTAL CENTER
SCHOOL OF MEDICINE AND DENTISTRY
SCHOOL OF NURSING
STRONG MEMORIAL HOSPITAL
UNIVERSITY MEDICAL FACULTY GROUP

THE UNIVERSITY COMMITTEE ON ANIMAL RESOURCES

Verification of Protocol Review and Approval

University of Rochester
University Committee on Animal Resources

Title of Application:	**Studies of the fate of the osteoclast**
Principal Investigator:	**Brendan Boyce, Ph.D.**
Name of Institution:	**University of Rochester**
PHS Assurance:	**A-3292-01**
Application #:	**RO1-AR43510**
Species:	**Mouse**
Protocol Number:	**101152 / 99-115**
Status:	**Approved**
Approval Date:	**March 31, 2011**

This letter certifies that the above protocol has been reviewed and approved by the University Committee on Animal Resources (UCAR). The protocol is effective for three (3) years from the date of approval. The approval date will be used as the anniversary date for Annual Protocol Reviews. The protocol may be subject to suspension if the conditions and requirements of the UCAR are not met.

Signed:

March 31, 2011

Suzanne Y. Stevens, Ph.D., UCAR Chair
or Christopher Stodgell, Ph.D., UCAR Vice-Chair
or Diane Moorman-White, D.V.M.
or Jeffrey D. Wyatt, D.V.M., M.P.H.

601 Elmwood Avenue, Box 674
Rochester, New York 14642
(Office) 585-275-1693 (Fax) 585-273-1337
E-mail: ucar@urmc.rochester.edu

UNIVERSITY OF ROCHESTER MEDICAL CENTER

EASTMAN DENTAL CENTER
SCHOOL OF MEDICINE AND DENTISTRY
SCHOOL OF NURSING
STRONG MEMORIAL HOSPITAL
UNIVERSITY MEDICAL FACULTY GROUP

THE UNIVERSITY COMMITTEE ON ANIMAL RESOURCES

Verification of Protocol Review and Approval

University of Rochester
University Committee on Animal Resources

Title of Application:	**Studies of the Fate of the Osteoclast**
Principal Investigator:	**Brendan Boyce, M.D.**
Name of Institution:	**University of Rochester**
PHS Assurance:	**A-3292-01**
Application:	**RO1-AR43510**
Species:	**Mouse**
Protocol Number:	**99-115 / 101152**
Status:	**Approved**
Approval Date:	**February 28, 2014**

This letter certifies that the above protocol has been reviewed and approved by the University Committee on Animal Resources (UCAR). The protocol is effective for three (3) years from the date of protocol approval. The approval date will be used as the anniversary date for Annual Protocol Reviews. The protocol may be subject to suspension if the conditions and requirements of the UCAR are not met.

Signed: February 28, 2014

Suzanne Y. Stevens, Ph.D., UCAR Chair
or Christopher Stodgell, Ph.D., UCAR Vice-Chair
or Diane Moorman-White, D.V.M.
or Jeffrey D. Wyatt, D.V.M., M.P.H.

601 Elmwood Avenue, Box 674
Rochester, New York 14642
(Office) 585-275-1693 (Fax) 585-273-1337
E-mail: ucar@urmc.rochester.edu

Mechanisms of Signal Transduction:

Tumor Necrosis Factor-α Increases Circulating Osteoclast Precursor Numbers by Promoting Their Proliferation and Differentiation in the Bone Marrow through Up-regulation of c-Fms Expression

Zhenqiang Yao, Ping Li, Qian Zhang, Edward M. Schwarz, Peter Keng, Arnaldo Arbini, Brendan F. Boyce and Lianping Xing

J. Biol. Chem. 2006, 281:11846-11855.
doi: 10.1074/jbc.M512624200 originally published online February 6, 2006

THE JOURNAL OF BIOLOGICAL CHEMISTRY VOL. 281, NO. 17, pp. 11846–11855, April 28, 2006

Tumor Necrosis Factor-α Increases Circulating Osteoclast Precursor Numbers by Promoting Their Proliferation and Differentiation in the Bone Marrow through Up-regulation of c-Fms Expression*

Received for publication, November 28, 2005 Published, JBC Papers in Press, February 6, 2006, DOI 10.1074/jbc.M512624200

Zhenqiang Yao[‡1], Ping Li[§1], Qian Zhang[‡], Edward M. Schwarz[§], Peter Keng[¶], Arnaldo Arbini[‡], Brendan F. Boyce[‡], and Lianping Xing[‡2]

From the [‡]Department of Pathology and the [§]Department of Orthopedics, [¶]Cancer Research Center, University of Rochester Medical Center, Rochester, New York 14642

Osteoclasts are essential cells for bone erosion in inflammatory arthritis and are derived from cells in the myeloid lineage. Recently, we reported that tumor necrosis factor-α (TNFα) increases the blood osteoclast precursor (OCP) numbers in arthritic patients and animals, which are reduced by anti-TNF therapy, implying that circulating OCPs may have an important role in the pathogenesis of erosive arthritis. The aim of this study is to investigate the mechanism by which TNFα induces this increase in OCP frequency. We found that TNFα stimulated cell division and conversion of $CD11b^+/Gr\text{-}1^{-/lo}$/c-$Fms^-$ to $CD11b^+/Gr\text{-}1^{-/lo}$/c-$Fms^+$ cells, which was not blocked by neutralizing macrophage colony-stimulating factor (M-CSF) antibody. *Ex vivo* analysis of monocytes demonstrated the following: (i) blood $CD11b^+/Gr\text{-}1^{-/lo}$ but not $CD11b^-/Gr\text{-}1^-$ cells give rise to osteoclasts when they were cultured with receptor activator NF-κB ligand and M-CSF; and (ii) TNF-transgenic mice have a significant increase in blood $CD11b^+/Gr\text{-}1^{-/lo}$ cells and bone marrow proliferating $CD11b^+/Gr\text{-}1^{-/lo}$ cells. Administration of TNFα to wild type mice induced bone marrow $CD11b^+/Gr\text{-}1^{-/lo}$ cell proliferation, which was associated with an increase in $CD11b^+/Gr\text{-}1^{-/lo}$ OCPs in the circulation. Thus, TNFα directly stimulates bone marrow OCP genesis by enhancing c-Fms expression. This results in progenitor cell proliferation and differentiation in response to M-CSF, leading to an enlargement of the marrow OCP pool. Increased marrow OCPs subsequently egress to the circulation, forming a basis for elevated OCP frequency. Therefore, the first step of TNF-induced osteoclastogenesis is at the level of OCP genesis in the bone marrow, which represents another layer of regulation to control erosive disease.

Mature osteoclasts are essential effector cells for normal bone remodeling and pathologic bone loss seen in many forms of erosive diseases, such as rheumatoid arthritis (RA).[3] The importance of osteoclastic resorption in this process has been proven in studies with various knock-out mice deficient in genes essential for osteoclastogenesis, which develop osteopetrosis because of the accumulation of un-resorbed bone matrix within the bone marrow cavity (1, 2). Similarly, these mice are completely resistant to bone destruction of affected joints when they are induced to develop erosive arthritis (3–5). Osteoclasts are derived from common osteoclast/monocyte precursors that are generated in bone marrow and travel to peripheral tissues through the bloodstream (6). In patients or animals with RA, these precursor cells constantly migrate to inflamed joints perhaps from the following two directions: "outside in," from blood to the pannus-bone interface, and "inside out," from epiphysial bone marrow to the subchondral bone. They then differentiate to mature osteoclasts in response to high levels of osteoclastogenic cytokines, including receptor activator NF-κB ligand (RANKL), macrophage-colony-stimulating factor (M-CSF), and tumor necrosis factor-α (TNFα), produced by inflammatory cells in the synovium (7, 8). Although the teams of mature osteoclasts mediate focal erosions via resorption of the periarticular and subchondral bone over long periods of time (months to years), the life span of individual osteoclasts is only a few weeks. Thus, mature osteoclasts must be constantly replaced by a perpetual supply of osteoclast precursors (OCPs). Currently, the molecular mechanism by which joint inflammation sustains the perpetual supply of OCPs is poorly understood.

OCPs are derived from c-Kit^+ multipotent hematopoietic stem cells in the bone marrow through a series of differentiation processes (9). The first step of OCP ontogeny is the commitment of hematopoietic stem cells to the myeloid lineage under the control of the Ets transcription factor PU.1 (10). Then the myeloid progenitors survive, proliferate, and differentiate into various "downstream" lineages, including OCPs. These events have been characterized by changes in the surface expression of distinct markers. For instance, early myeloid progenitors do not express detectable levels of c-Fms, the receptor for M-CSF, an essential survival factor for OCPs. As such, they exhibit lower proliferation and differentiation potency. However, under the influence of hematopoietic factors such as stem cell factor and perhaps M-CSF itself, c-Fms^- cells differentiate to c-Fms^+ cells (11). The conversion of c-Fms^- cells to c-Fms^+ cells is an important landmark for the progression of myelopoiesis because the M-CSF signal at this stage is critical for cell survival (anti-apoptosis), proliferation, and differentiation. However, the regulation of this conversion in chronic inflammatory bone diseases has not been well studied.

TNFα is one of the most potent pro-inflammatory cytokines, and its role in RA has been formally established by the development of anti-TNF therapy. Additional proof comes from studies of TNF transgenic (TNF-Tg)

* This work was supported by National Institutes of Health Grants AR48697 (to L. X.) and AR43510 (to B. F. B.). The costs of publication of this article were defrayed in part by the payment of page charges. This article must therefore be hereby marked "*advertisement*" in accordance with 18 U.S.C. Section 1734 solely to indicate this fact.

[1] Both authors contributed equally to this work.

[2] To whom correspondence should be addressed: Dept. of Pathology and Laboratory Medicine, 601 Elmwood Ave., Box 626, Rochester, NY 14642. Tel.: 585-273-4090; Fax: 585-756-4468; E-mail: Lianping_xing@urmc.rochester.edu.

[3] The abbreviations used are: RA, rheumatoid arthritis; RANK, receptor activator NF-κB; RANKL, receptor activator NF-κB ligand; TNFα, tumor necrosis factor-α; OCP, osteoclast precursor; WT, wild type; M-CSF, macrophage-colony-stimulating factor; FACS, fluorescence-activated cell sorting; PBMC, peripheral blood mononuclear cells; Tg, transgenic; RT, reverse transcription; PBS, phosphate-buffered saline; CFSE, carboxyfluorescein diacetate succinimidyl ester; TRAP, tartrate-resistant acid phosphatase; FITC, fluorescein isothiocyanate; PE, phycoerythrin.

mice that develop erosive arthritis featured with intense synovial inflammation and destruction of cartilage and bone (12). These mice have increased numbers of OCPs in spleen and blood and increased numbers of mature osteoclasts in the affected joints (13). The role of TNFα in osteoclastogenesis has been studied extensively in the last decade. Administration of TNFα into wild-type (WT) mice greatly increases the number of tartrate-resistant acid phosphatase (TRAP)-positive osteoclasts locally and systemically (13, 14). *In vitro*, TNFα directly stimulates mature osteoclast formation from OCPs in the absence of osteoblasts/stromal cells through activation of NF-κB and nuclear factor of activated T cells pathways (15). It also promotes the production of M-CSF by T lymphocytes and RANKL by osteoblasts, thereby indirectly stimulating osteoclast formation (16, 17). However, whether TNFα promotes OCP generation from early myeloid precursors and the mechanisms involved in this process have not been investigated.

In this study, we test the hypothesis that TNFα increases OCP numbers through regulation of c-Fms expression. We demonstrate that TNFα increases the proliferation of OCPs *in vivo* and *in vitro* and promotes the differentiation of c-Fms$^-$ cells to c-Fms$^+$ cells. TNFα-induced OCP genesis is directly related to increased blood OCP frequency. Thus, our results reveal a new mechanism for TNFα in the control of peripheral osteoclast numbers and provide an additional regulatory step to control osteoclast formation and bone resorption in inflammatory erosive diseases.

EXPERIMENTAL PROCEDURES

Reagents—Recombinant murine RANKL, TNFα, and human M-CSF were purchased from R & D Systems (Minneapolis, MN). Anti-murine CD11b (M1/70), c-Fms (AFS98), CD3 (145–2C11), B220 (RA3–6B2), and isotype controls were from eBioscience Inc. (San Diego, CA); anti-murine CD16/32 (FcγIII/II), c-Kit (2B8), Gr-1 (1A8), and isotype controls were from Pharmingen.

Animals—TNF-Tg mice in a CBA × C57Bl/6 background (3647 TNF-Tg line) were obtained from Dr. G. Kollias (12). Four-month-old TNF-Tg mice were used because this is the age when they typically develop severe joint disease with elevated serum human TNFα concentrations (13). Acute TNFα *in vivo* treatment was performed as we described previously (13). In brief, 2-month-old C57/B6 male mice were randomly divided into TNFα and PBS groups. Murine TNFα (0.5 μg in 25 μl of PBS) or the same volume of PBS was injected four times/day for 3 days into the subcutaneous layer overlying the calvariae of WT mice. Bone marrow and PBMCs were collected for cell cycle analysis, as described below. The Institutional Animal Care and Use Committee approved all animal studies.

Generation of Osteoclasts—Cells from several sources were used to generate osteoclasts: 1) freshly isolated bone marrow cells; 2) M-CSF or TNFα pretreated nonadherent bone marrow cells; and 3) flow-sorted bone marrow or blood cells. Cells were cultured in α-modified essential medium (Invitrogen) with 10% fetal calf serum (Hyclone Laboratories, Logan, UT), RANKL (5 ng/ml), and M-CSF (10 ng/ml) for 3–5 days when multinucleated cells typically were observed under an inverted microscope. Cells were then fixed and stained for TRAP activity, and TRAP$^+$ cells containing ≥3 nuclei were counted as mature osteoclasts as we described previously (13).

Fluorescence-activated Cell Sorting (FACS) Analysis and Cell Sorting—For FACS analysis, freshly isolated bone marrow, PBMCs or cultured OCPs were incubated with anti-murine CD16/32 to block Fc receptor-mediated antibody binding. Cells were then stained with various fluorescent-labeled antibodies. Data were acquired using a FACSCalibur flow cytometer (BD Biosciences) and analyzed using the Cellquest software (version 3.1), as described previously (13). For cell sorting, pooled bone marrow cells or peripheral blood cells from either TNF-Tg or WT mice were double-stained with FITC-anti-CD11b and PE-anti-Gr-1 antibodies, and then sorted by a FACSVantage SE Turbo sorter. CD11b$^+$/Gr-1$^{-/lo}$, CD11b$^-$/Gr-1$^-$, and CD11b$^+$/Gr-1^{hi} cells were collected separately, reanalyzed to ensure their purity (≥98%), and used for osteoclastogenesis assays, as described above.

Cell Cycle Analysis of Blood and Bone Marrow OCPs—PBMCs or bone marrow cells were stained with FITC anti-CD11b and PE anti-Gr-1 antibodies first, and the labeled cells were then incubated with Hoechst 33342 (5 μg/ml) for 45 min at 37 °C in a reaction buffer (19) prior to FACS analysis. Cell cycle distributions of CD11b$^+$ /Gr-1$^{-/lo}$, CD11b$^+$ /Gr-1^{hi}, and CD11b$^-$ /Gr-1$^-$ cells were analyzed using a FACSVantage flow cytometer (BD Biosciences) equipped with UV light and 488-nm laser excitations. The percentage of the cells in G_1, S, and G_2/M phases of the cell cycle was determined using the ModFit program (Verity Software, Topsham, ME).

In Vitro Carboxyfluorescein Diacetate Succinimidyl Ester (CFSE) Labeling—Fresh bone marrow cells were isolated from femur and tibia of WT mice. Red blood cells were removed using ACK lysis buffer (0.15 M NH_4Cl, 1.0 mM $KHCO_3$, 0.1 mM Na_2 EDTA). The cells were then resuspended in PBS at a density of 5×10^7/ml, and an equal volume of CFSE (10 μM) was added by drop while vortexing. The reaction was incubated at 37 °C for 10 min and mixed once during the incubation. The labeled cells were washed with α-minimum Eagle's medium plus 10% fetal bovine serum three times and seeded in a 6-well plate at a density of $4–5 \times 10^6$/well.

Quantitative Real Time RT-PCR—RNA from TNFα-treated and nontreated bone marrow cells or sorted CD11b$^+$/Gr-1$^{-/lo}$ cells was extracted using the RNeasy kit and the QiaShredder from Qiagen (Valencia, CA). cDNA was synthesized with the use of 20 μl of RT reaction solution containing 1 μg of total RNA, 10 mM Tris-HCl buffer (pH 8.3), 50 mM KCl, 5 mM $MgCl_2$, 1 mM deoxynucleoside triphosphates, 2.5 μM random hexamers, 20 units of RNase inhibitor, and 50 units of Moloney murine leukemia virus reverse transcriptase (all from Roche Applied Science). Quantitative PCR amplification was performed with gene-specific primers using a Rotor-Gene 2000 real time amplification operator (Corbett Research, Mortlake, Australia). The primer sequences included the following: 1) c-*Fms* primers, 5′-GTCAGAGGCCCCGTTTGTT-3′ and 5′-AGTAAATATAGAGGCTAGCACTGTGAGAAC-3′; and 2) actin primers, 5′-AGATGTGGATCAGCAAGCAG-3′ and 5′-GCGCAAGTTAGGTTTTGTCA-3′. The relative standard curve method was used to calculate the amplification difference for each primer set (20). The standard curve was made from four points corresponding to 10-fold cDNA dilution series for each gene. For each sample, the relative amount was calculated from their respective relative standard curves. The relative c-*Fms* expression value was then obtained by dividing each value by the actin value. Standards were run in triplicate, and samples were run three times in triplicate.

Statistics—All results are given as means ± S.E. Comparisons were made by analysis of variance and Student's *t* test for unpaired data. *p* values less than 0.05 were considered statistically significant.

RESULTS

CD11b and Gr-1 Are Cell Surface Markers for Blood and Bone Marrow OCPs—Previously, we have used CD11b as a single cell surface marker for OCPs in the spleen and demonstrated that TNF-Tg arthritic mice have increased CD11b$^+$ OCP frequency (13). However, CD11b protein is broadly expressed on the surface of various myeloid lineage cells, especially on granulocytes that consist of more than 70% of the

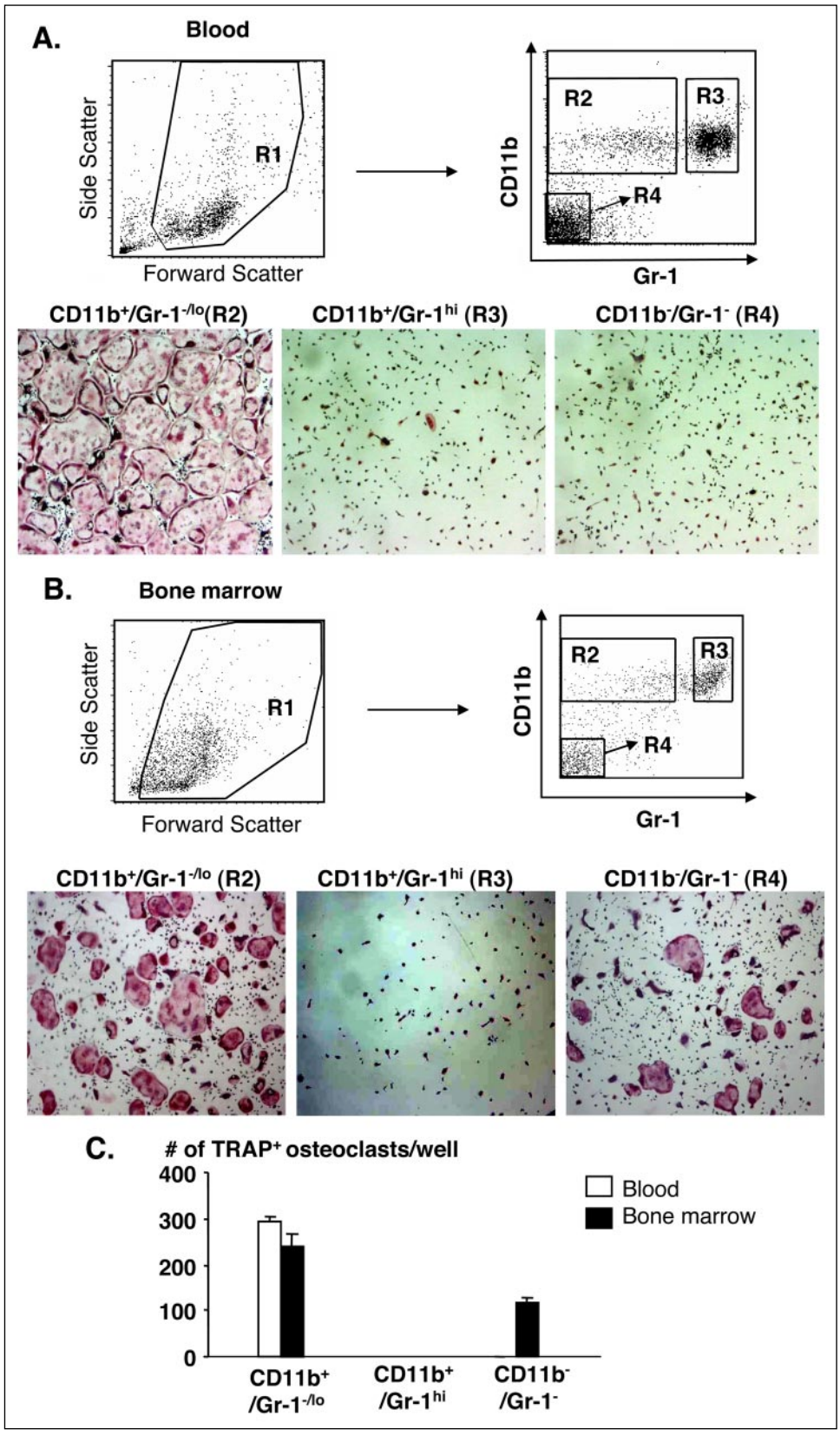

FIGURE 1. **Identification of cell populations with osteoclastogenic potential from peripheral blood and bone marrow cells.** *A,* PBMCs or bone marrow cells (*B*) from a pool of five WT mice were stained with FITC anti-CD11b and PE anti-Gr-1 antibodies and subjected to FACS analysis. The living cells were gated using forward and side scatter (*R1*). The $CD11b^{+}/Gr\text{-}1^{-/lo}$ (*R2*), $CD11b^{+}/Gr\text{-}1^{hi}$ (*R3*), and $CD11b^{-}/Gr\text{-}1^{-}$ (*R4*) populations were sorted and cultured with M-CSF and RANKL to generate osteoclasts. Photography (×4) of the $TRAP^{+}$ osteoclasts formed from purified PBMCs and from bone marrow are shown in the *upper* and *lower panels*, respectively. *C,* the number of $TRAP^{+}$ osteoclasts formed from above cultures was quantified and presented as means plus S.E. of three wells. Experiments were repeated once with similar results.

total blood (72.4 ± 3.4%) or bone marrow (77.4 ± 2%) $CD11b^{+}$ cells in adult C57/B6 mice. Because of this, OCP numbers may be overestimated if the frequency of $CD11b^{+}$ cells is used to assess the number of OCPs in these compartments. In this study, we first characterized the osteoclastogenic potential of blood and bone marrow cells using CD11b and Gr-1 to eliminate $CD11b^{+}/Gr\text{-}1^{hi}$ granulocytes (Fig. 1). Peripheral blood mononuclear cells (PBMC) and bone marrow cells from WT adult mice were stained with anti-CD11b and Gr-1 antibodies, and

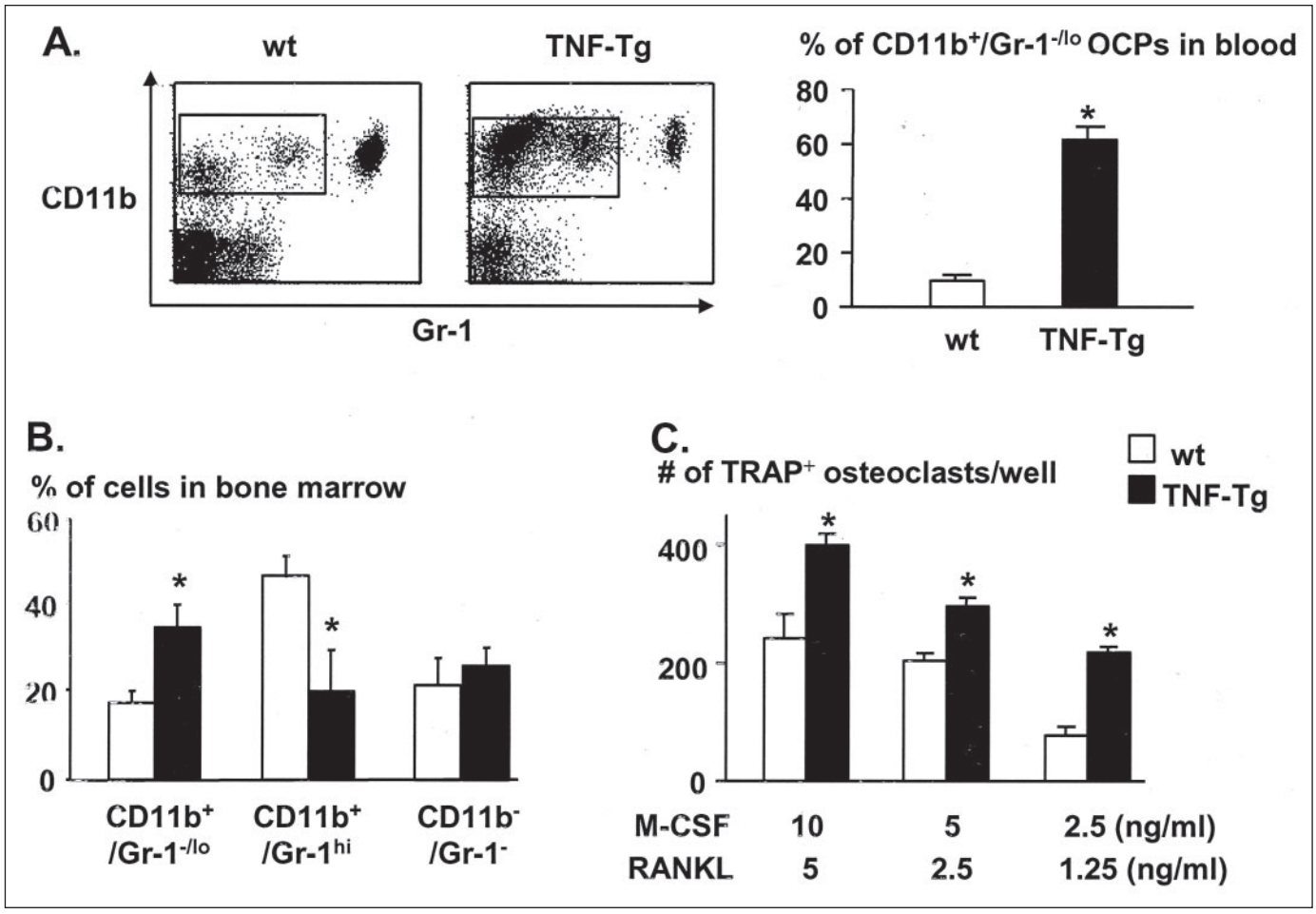

FIGURE 2. **Increased blood and bone marrow OCP frequency in TNF-Tg mice.** *A,* PBMCs from 4-month-old TNF-Tg mice and WT littermates were stained with anti-CD11b and anti-Gr-1 antibodies and subjected to FACS analysis. Representative histograms show the gated population of $CD11b^+/Gr\text{-}1^{-/lo}$ OCPs. The percentage of blood OCPs is shown as means plus S.E. from three pairs of TNF-Tg mice and WT littermates. *B,* bone marrow cells were stained with anti-CD11b and anti-Gr-1 antibodies and analyzed by FACS. The percentage of individual cell population is shown as means ± S.E. from three pairs of TNF-Tg mice and WT littermates. *C,* purified $CD11b^+/Gr\text{-}1^{-/lo}$ cells from bone marrow of TNF-Tg mice and WT littermates were cultured with M-CSF and RANKL to generate osteoclasts. The number of $TRAP^+$ osteoclasts was counted and shown as means ± S.E. of three wells. Similar results were obtained from two independent experiments. *, $p < 0.05$ *versus* WT mice.

three populations were fractionated by FACS on the basis of their surface expression: $CD11b^+/Gr\text{-}1^{-/lo}$ (R2), $CD11b^+/Gr\text{-}1^{hi}$ (R3), and $CD11b^-/Gr\text{-}1^-$ (R4). The sorted cells were cultured with M-CSF and RANKL to generate osteoclasts that were assessed by TRAP staining. In blood, only $CD11b^+/Gr\text{-}1^{-/lo}$ cells (R2) formed osteoclasts. Although both $CD11b^+/Gr\text{-}1^{-/lo}$ (R2) and $CD11b^-/Gr\text{-}1^-$ (R4) marrow cells gave rise to osteoclasts (Fig. 1), the number of $TRAP^+$ osteoclasts was much higher in the $CD11b^+/Gr\text{-}1^{-/lo}$ (R2) fraction than that in the $CD11b^-/Gr\text{-}1^-$ (R4) fraction (Fig. 1, *B* and *C*). The $CD11b^+/Gr\text{-}1^{hi}$ cells did not form $TRAP^+$ osteoclasts and died off under our culture conditions. Because it is likely that marrow $CD11b^-$ cells differentiate to $TRAP^+$ osteoclasts through the $CD11b^+$ stage and only blood $CD11b^+/Gr\text{-}1^{-/lo}$ cells give rise to osteoclasts, we reasoned that $CD11b^+/Gr\text{-}1^{-/lo}$ cells include the majority of OCPs and can be used as OCP surface markers.

TNF-Tg Mice Have Increased Blood and Bone Marrow OCPs—By using $CD11b^+/Gr\text{-}1^{-/lo}$ as OCP markers, we found that in TNF-Tg mice, the percentage of blood $CD11b^+/Gr\text{-}1^{-/lo}$ OCPs increased 5-fold (Fig. 2*A*), and their absolute number increased 14-fold, compared with WT littermates. TNF-Tg mice also had a 1-fold increase in bone marrow $CD11b^+/Gr\text{-}1^{-/lo}$ but not in $CD11b^-/Gr\text{-}1^-$ cells (Fig. 2*B*). Consistent with this change, the percentage of $CD11b^+/Gr\text{-}1^{hi}$ granulocyte numbers was reduced in these mice. However, the absolute number of granulocytes was unchanged both in blood (cell number (10^6/ml), 1.48 ± 0.21 in TNF-Tg mice *versus* 1.36 ± 0.16 in WT mice) and in bone marrow (cell number (10^6/femur), 3.53 ± 1.34 in TNF-Tg *versus* 3.32 ± 1.14 in WT mice, respectively). The osteoclast-forming potential of purified marrow $CD11b^+/Gr\text{-}1^{-/lo}$ cells from TNF-Tg mice and WT littermates was determined by cell culture in the presence of different amounts of M-CSF and RANKL. In all cases, TNF-Tg $CD11b^+/Gr\text{-}1^{-/lo}$ cells formed significantly more $TRAP^+$ osteoclasts (Fig. 2*C*), indicating that TNF-Tg mice have more OCPs within the $CD11b^+/Gr\text{-}1^{-/lo}$ population.

TNFα Promotes the Proliferation of Bone Marrow OCPs—To examine whether increased bone marrow $CD11b^+/Gr\text{-}1^{-/lo}$ OCPs in TNF-Tg mice results from an alteration in proliferation, cell cycle analysis was performed using a combination of anti-CD11b and Gr-1 antibodies and Hoechst 33342 DNA dye staining. This approach allows us to assess cell cycle status in different fractions of CD11b- and Gr-1-stained cells simultaneously and avoid cell sorting and *in vitro* labeling. Compared with $CD11b^-/Gr\text{-}1^-$ and $CD11b^+/Gr\text{-}1^{hi}$ cells, the $CD11b^+/Gr\text{-}1^{-/lo}$ population contained cells in the $S/G_2/M$ phase of the cell cycle in both TNF-Tg and WT mice (Fig. 3*A*). Furthermore, more TNF-Tg $CD11b^+/Gr\text{-}1^{-/lo}$ cells were in the $S/G_2/M$ phase than those of WT littermates, and there was no difference in the frequency of apoptosis (Fig. 3*B*, *upper panel*). In contrast to marrow cells, PBMCs were not in

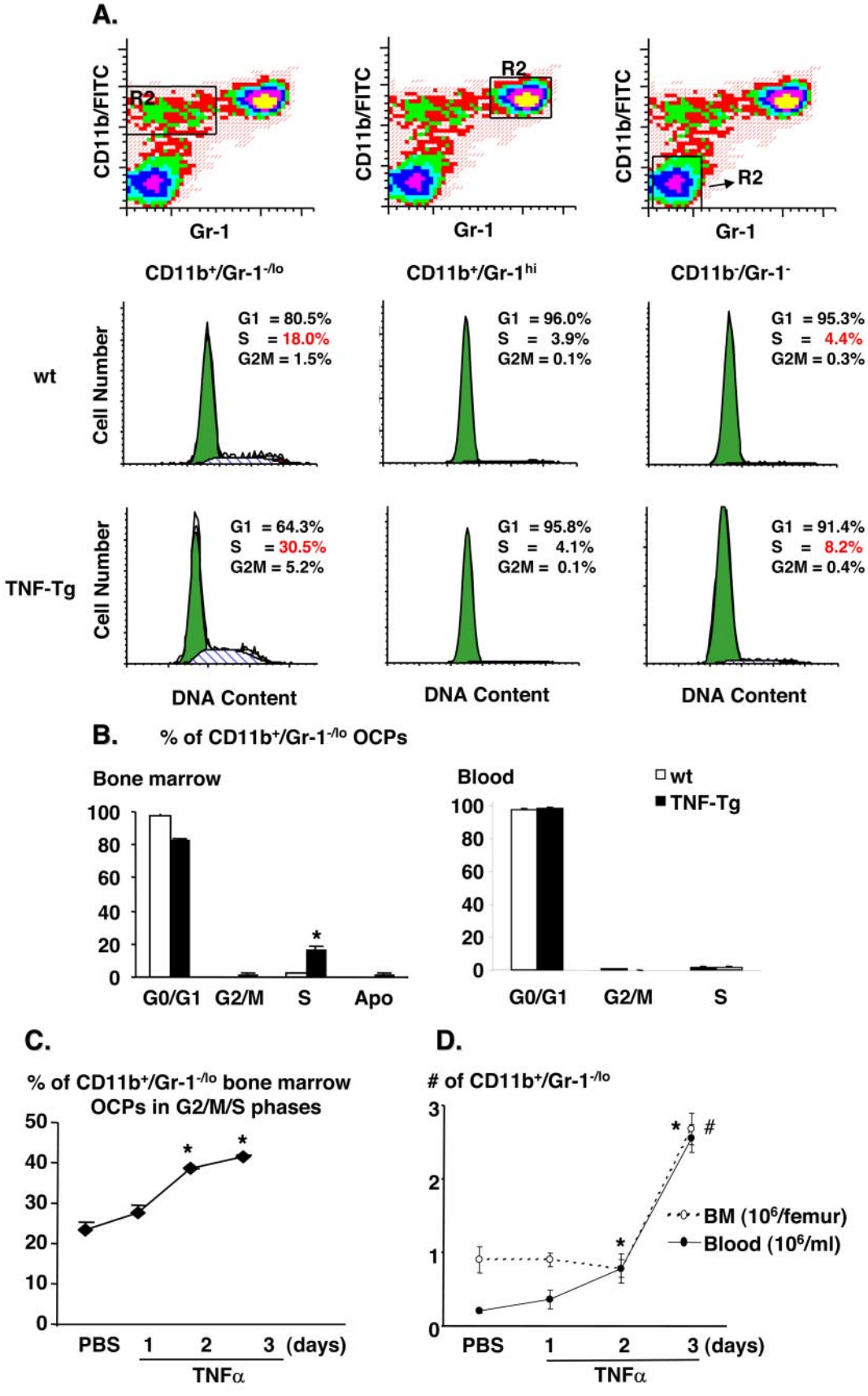

FIGURE 3. **Increased cycling OCPs in bone marrow, but not in blood, of TNF-Tg and TNFα-treated WT mice.** *A,* bone marrow cells from TNF-Tg mice and WT littermates were stained with anti-CD11b, anti-Gr-1 antibodies, and Hoechst 33342 DNA dye and subjected to FACS analysis. Representative histograms show cell cycle profiles of various gated cell populations. *B,* cell cycle analysis was performed for blood and bone marrow CD11b^{+}/Gr-1$^{-/lo}$ OCPs. The percentage of cells in various phases of cell cycles is shown as means ± S.E.

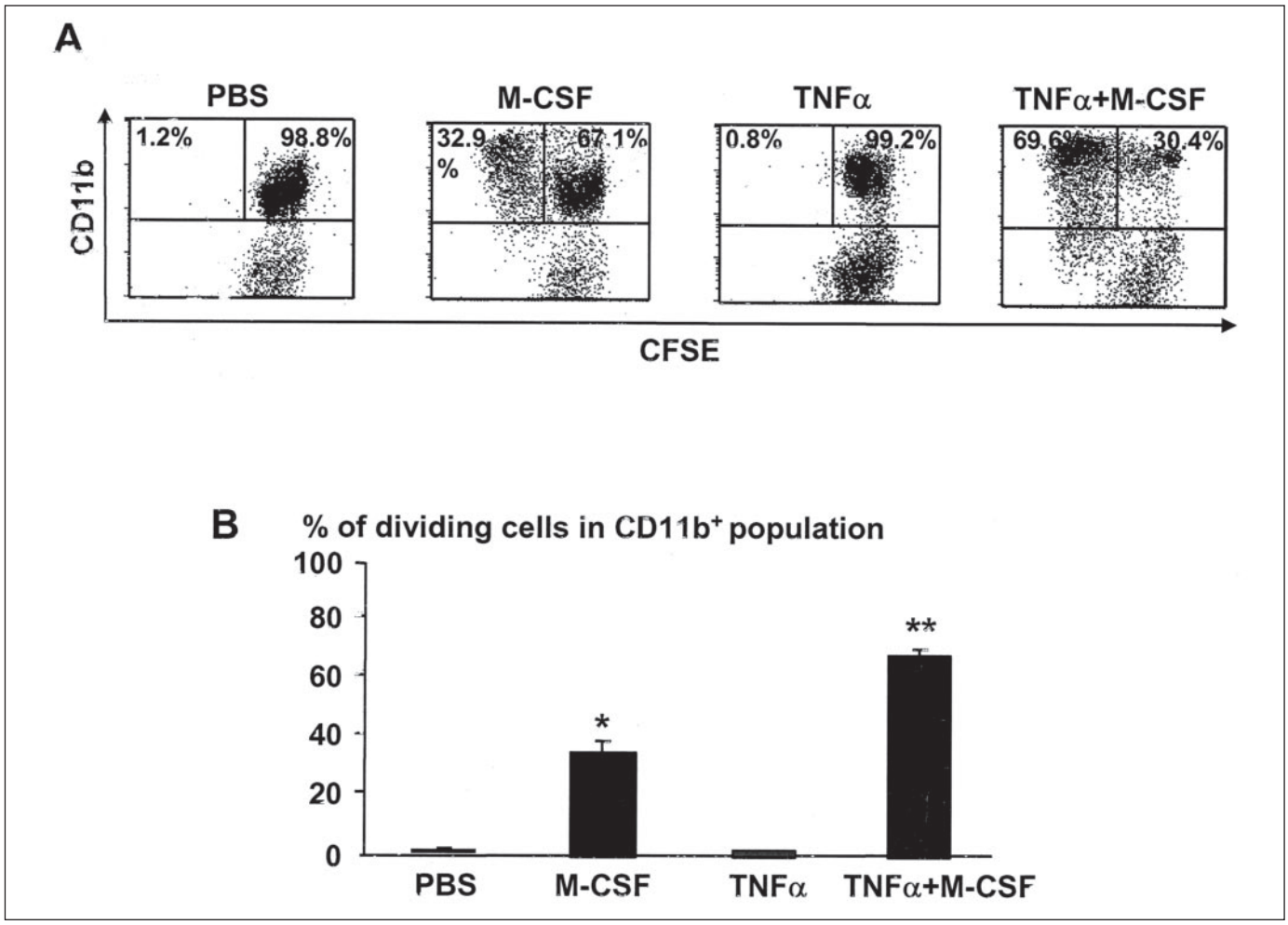

FIGURE 4. **TNFα enhances the proliferation of bone marrow OCPs that is dependent on M-CSF.** *A,* WT bone marrow cells were isolated, labeled with CFSE, and cultured *in vitro*. The cultures were treated with PBS, M-CSF (10 ng/ml), TNFα (10 ng/ml), and a combination of TNFα and M-CSF. Nonadherent cells were collected after 3 days and subjected to FACS analysis for CD11b and CFSE. The histograms are representative of three independent experiments. The percentage of fast-dividing cells (*upper left panels*) and non- or slow-dividing cells (*upper right panels*) in the $CD11b^+$ population is shown. *B,* the $CD11b^+$ cells were then gated, and the dividing cells with decrease CFSE labeling in this population were quantified. The results are presented as means ± S.E. of three independent experiments. *, $p < 0.05$ *versus* PBS-treated cultures; **, $p < 0.05$ *versus* M-CSF treated cultures.

the cell cycle, and the majority of them were at the G_0/G_1 phase (Fig. 3*B*, *lower panel*).

To investigate whether increased cycling of marrow OCPs leads to increased total numbers of OCPs in the bone marrow and subsequently in the peripheral blood, we injected TNFα (0.5 μg/injection, four times/day for 3 days) into WT mice and examined the cell cycle status of marrow OCPs, as well as the number of OCPs in blood and bone marrow by FACS analysis. A 3-day regimen was used because our preliminary experiments showed that it took 3 days for TNFα to increase blood OCPs (data not shown). TNFα significantly increased the percentage of cycling marrow OCPs, which started after the 2nd day and peaked after the 3rd day of injection. Correspondingly, total OCP numbers in bone marrow increased at 3 days. Blood OCPs were slightly elevated after 2 days and increased significantly after 3 days of TNFα treatment, in parallel with bone marrow cells (Fig. 3, *C* and *D*). Together, these findings suggest that TNFα may increase bone marrow OCP numbers by promoting their proliferation.

To determine the direct effects of TNF and M-CSF on OCP proliferation *in vitro*, we labeled WT bone marrow cells with 5-(and 6-)-carboxyfluorescein diacetate succinimidyl ester (CFSE) to monitor cell division. The labeled cells were then treated with PBS, M-CSF (10 ng/ml), TNFα (10 ng/ml), or M-CSF/TNFα for 24, 48, and 72 h, stained with anti-CD11b, and subjected to FACS analysis. The percentage of dividing cells in the $CD11b^+$ population was measured as an indicator of OCP division. Because our initial results demonstrated that 100% of $CD11b^+/Gr\text{-}1^{hi}$ cells die off, leaving only $CD11b^+$ $Gr\text{-}1^{-/lo}$ cells 24 h after culture (data not shown), Gr-1 staining was omitted in these experiments. TNFα alone had no effect on cell division at any time point, and M-CSF stimulated OCP division after treatment for 48 h (Fig. 4). In contrast, TNFα synergized with M-CSF to stimulate OCP division from 33% in M-CSF-treated cells alone up to 70% in TNFα plus M-CSF-treated cells (Fig. 4, *A* and *B*).

TNFα Induces c-Fms Expression of Bone Marrow OCPs—Increased M-CSF-dependent proliferation after TNFα treatment suggests that

from three pairs of TNF-Tg mice and WT littermates. *, $p < 0.05$ *versus* WT mice. *C,* TNFα was injected into WT mice (0.5 μg/mouse/injection, intraperitoneally, four times/day) for 1–3 days, or PBS was injected into WT mice for 3 days. The cell cycle analysis was performed for the $CD11b^+/Gr\text{-}1^{-/lo}$ OCP population. The percentage of cells in the $G_2/M/S$ phase of cell cycles is shown as means ± S.E. of three mice. *, $p < 0.05$ *versus* 3-day PBS-treated mice. *D,* the total number of $CD11b^+/Gr\text{-}1^{-/lo}$ OCPs in bone marrow and in blood was determined by FACS and cell counting. Values are the means ± S.E. from three pairs of mice. *, $p < 0.05$ *versus* blood cells; #, $p < 0.05$ *versus* bone marrow cells of PBS-treated mice, respectively.

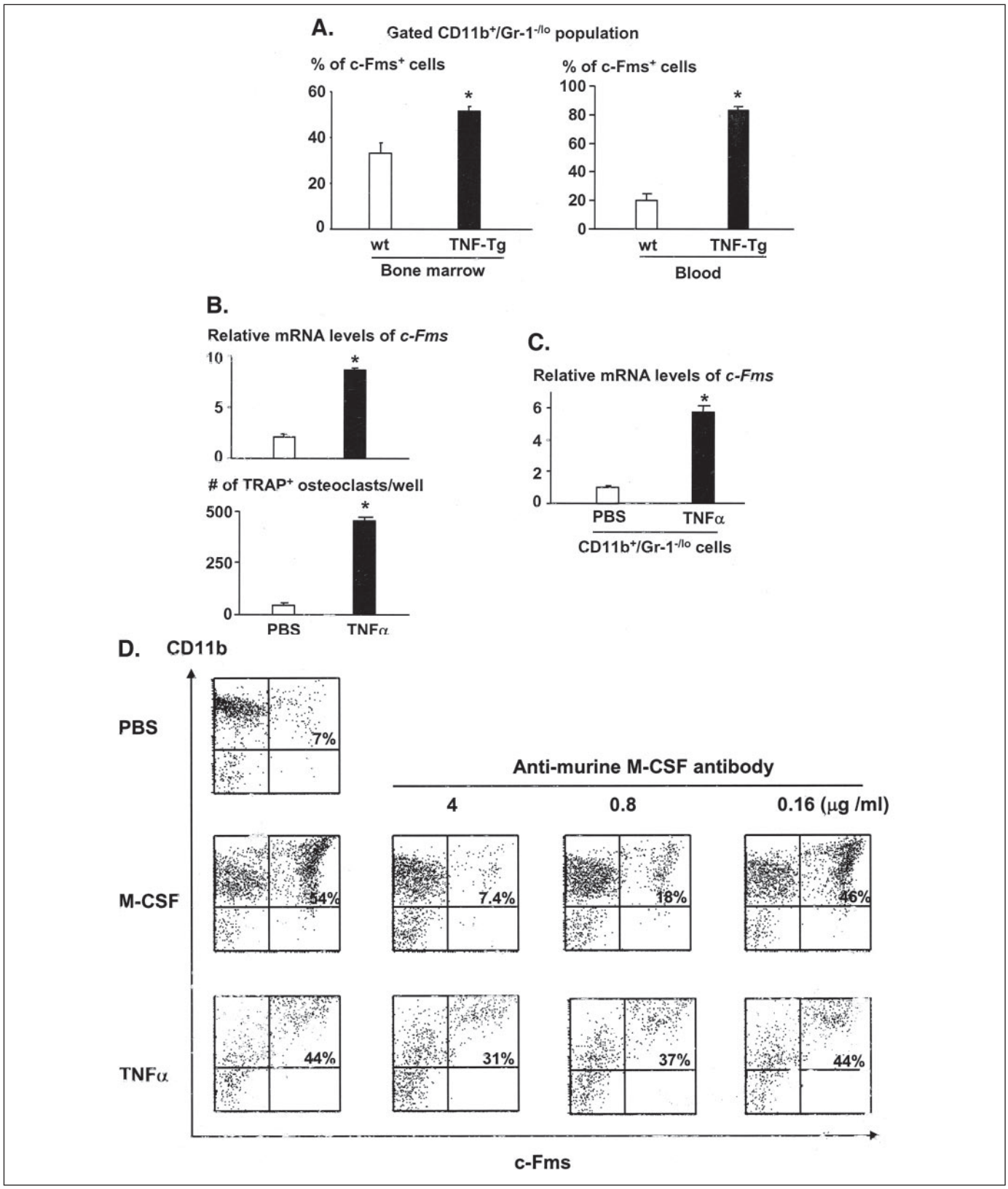

FIGURE 5. **TNFα increases c-Fms expression in OCPs.** *A,* bone marrow cells and PBMCs from TNF-Tg mice and WT littermates were stained with anti-CD11b, Gr-1, and c-Fms antibodies and subjected to FACS analysis. The percentage of c-Fms$^+$ cells within the CD11b$^+$ /Gr-1$^{-/lo}$ population was determined. Values are the means ± S.E. from four pairs of TNF-Tg mice and WT littermates. *B,* WT bone marrow cells were cultured with PBS or TNFα (10 ng/ml) for 3 days, and nonadherent cells were collected. The expression levels of *c-Fms* were determined by real time RT-PCR using *c-Fms*- and β-actin-specific primers and are shown as mean fold changes of TNF-treated cells over PBS-treated cells (*upper panels*). The osteoclast forming potential was examined by culturing cells with M-CSF and RANKL and is shown as means ± S.E. of number of TRAP$^+$ osteoclasts from three wells (*lower panel*). *C,* purified CD11b$^+$ /Gr-1$^{-/lo}$ cells from WT bone marrow were treated with TNFα (10 ng/ml) for 24 h, and *c-Fms* expression levels were determined by real time RT-PCR. *D,* WT bone marrow cells were incubated with PBS, M-CSF (10 ng/ml), or TNFα (10 ng/ml) in the presence of various doses of M-CSF neutralizing antibody for 3 days, and the percentage of CD11b$^+$ /c-Fms$^+$ cells was determined by FACS analysis. *, $p <$ 0.05 *versus* PBS-treated group. All experiments were repeated once with similar results.

TNFα may affect the factors essential for M-CSF signaling. Because the M-CSF receptor, c-Fms, is expressed on the surface of late stage of myeloid precursors, including OCPs (21), we hypothesized that TNF-Tg CD11b$^+$/Gr-1$^{-/lo}$ OCPs may contain more c-Fms$^+$ cells to account for the TNFα-induced M-CSF-dependent proliferation. To test this, we compared the percentage of c-Fms$^+$ cells in the gated CD11b$^+$/Gr-1$^{-/lo}$ population of TNF-Tg with that of WT mice, and we found that the TNF-Tg mice had significantly more c-Fms$^+$ cells in CD11b$^+$/Gr-1$^{-/lo}$ OCPs in both blood and bone marrow (Fig. 5*A*).

To determine whether TNFα promotes the differentiation of c-Fms$^-$ cells to c-Fms$^+$ cells, we examined the induction of CD11b$^+$/c-Fms$^+$ cells *in vitro* in response to TNFα. WT marrow cells were treated with PBS, M-CSF (10 ng/ml), TNFα (10 ng/ml), or M-CSF/TNFα, and the percentage of CD11b$^+$/c-Fms$^+$ cells was examined after 24, 48, and 72 h in nonadherent and adherent fractions (Fig. 5). TNFα increased the percentage of CD11b$^+$/c-Fms$^+$ cells at 24 h, and this peaked at 72 h. M-CSF decreased c-Fms expression over the first 12–24 h, which may reflect ligand-induced receptor internalization (22). However, after 48 h, M-CSF significantly stimulated c-Fms expression. TNFα alone increased the percentage of CD11b$^+$/c-Fms$^+$ cells in nonadherent cells by 9–10-fold and synergized with M-CSF to stimulate c-Fms expression in those cells (Fig. 5*B*). TNFα also stimulated the percentage of CD11b$^+$/c-Fms$^+$ cells in adherent cells, but to a lesser extent (by 3–4-fold, data not shown).

To confirm the functional consequence of increased c-Fms expression by TNFα in osteoclastogenesis, nonadherent TNFα- or PBS-treated cells were cultured to assess their osteoclast-forming potency. Cells primed by TNFα formed significantly more osteoclasts when they were subsequently cultured with M-CSF and RANKL (Fig. 5*B*). To examine if TNFα stimulates c-*Fms* gene transcription, mRNA expression levels of c-*Fms* were determined in TNFα-treated nonadherent cells or purified CD11b$^+$/Gr-1$^{-/lo}$ OCPs. TNFα significantly increased the c-*Fms* expression levels in both cell preparations (Fig. 5*C*). Finally, we treated cells with TNFα in the presence of M-CSF neutralizing antibody to determine whether TNF-induced c-Fms expression is mediated by M-CSF. This treatment completely prevented M-CSF-induced c-Fms expression in a dose-dependent manner but had little effect on TNFα-induced c-Fms up-regulation (Fig. 5*D*). These findings indicate that TNFα can directly stimulate c-Fms expression by OCPs.

DISCUSSION

TNFα is a pleiotropic cytokine that induces focal erosions in inflamed arthritic joints by several mechanisms. Recently, we have demonstrated that one of these mechanisms involves an increase in the frequency of peripheral blood CD11b$^+$ OCP in arthritic patients and in TNF-Tg arthritic mice. We also found that this increased OCP frequency is reduced by and associated with a successful outcome of anti-TNF therapy (4, 13), implying that circulating OCP numbers may have an important role in the pathogenesis of inflammatory erosive arthritis. However, the mechanism by which systemic TNFα induces this increase in OCP frequency remains unknown.

Although it has been well established that osteoclasts are derived from myeloid precursors (23, 24), the identity, function, and regulation of OCPs *in vivo* remain poorly understood, partly because of the absence of unique cell surface markers to identify them. We and other have previously used CD11b$^+$ as a single surface marker for spleen OCPs (13, 25). Recently, we established that many of these cells are blood granulocytes that express CD11b, and the number of OCP may be significantly overestimated by this method. Apart from CD11b, c-Fms and RANK expression also has been used to estimate OCPs, based on the essential role of M-CSF and RANKL for osteoclastogenesis (11). However, CD11b$^+$/c-Fms$^-$ and CD11b$^+$/c-Fms$^+$ cells as well as CD11b$^+$/RANK$^-$ and CD11b$^+$/RANK$^+$ cells all can give rise to osteoclasts. Thus, they also are suboptimal OCP markers (13, 26). To try to improve on this, here we assessed CD11b$^+$/Gr-1$^{-/lo}$ cells, excluding CD11b$^+$/Gr-1^{hi} granulocytes, which include both early (c-Fms$^-$ or/and RANK$^-$) and late OCPs (c-Fms$^+$ or/and RANK$^+$). We found that 60–70% of CD11b$^+$/Gr-1$^{-/lo}$ cells can differentiate to TRAP$^+$ mononuclear osteoclasts when cultured with M-CSF and RANKL, indicating that most of these cells have osteoclast-forming potential. However, it is important to realize that CD11b/Gr-1$^{-/lo}$ cells are not composed of only OCPs because they can differentiate into macrophages and dendritic cells under the appropriate conditions. At present, it is not known if there are committed mono-potential OCPs that can be separated from other precursor cells. Recently, Geissmann *et al.* (27) proposed that blood monocytes can be divided into two functional subsets according to expression patterns of an array of surface proteins: CD11b$^+$/Gr-1$^+$/CX3CR1^{lo}/CCR2$^+$/CD62L$^+$ cells are the cells that are actively recruited to inflamed tissues, and CD11b$^+$/Gr-1$^-$/CX3CR1$^+$/CCR2$^-$/CD62L$^-$ cells are resident monocytes that give rise to specialized cell types, including osteoclasts. According to this classification, our CD11b$^+$/Gr-1$^{-/lo}$ cells appear to belong to resident monocytes. Although the significance of this kind of classification *in vivo* is controversial (28), it may be possible to define further OCPs by using multiple surface markers.

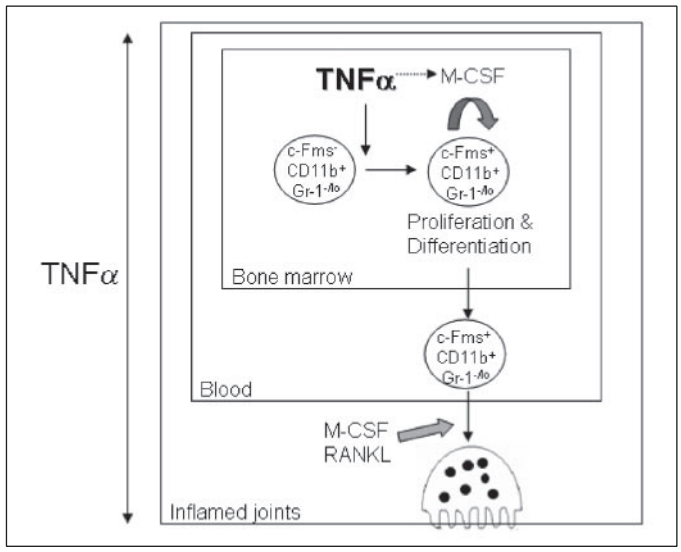

FIGURE 6. **TNFα-mediated osteoclast precursor genesis in chronic erosive arthritis.** During the early stages of osteoclastogenesis, TNFα increases the pool size of marrow osteoclast precursors by promoting their proliferation and differentiation in response to M-CSF and by stimulating c-Fms expression (TNFα in *boldface*) (this study). These osteoclast precursors then are released to the peripheral blood and differentiate to mature osteoclasts at the inflamed joints in the presence of M-CSF and RANKL, which are accelerated by TNFα.

Using CD11b$^+$/Gr-1$^{-/lo}$ as broad OCP markers, we demonstrated that TNFα promotes the differentiation of bone marrow CD11b$^+$/Gr-1$^{-/lo}$/c-Fms$^-$ cells to CD11b$^+$/Gr-1$^{-/lo}$/c-Fms$^+$ cells. Thus, the first step of TNFα-induced osteoclastogenesis is the conversion of c-Fms$^-$ OCPs to c-Fms$^+$ OCPs. This results in enhanced sensitization of precursor cells to M-CSF and provides more M-CSF-responding cells. TNFα-induced c-*Fms* mRNA expression has been reported in murine tissue macrophages (29). However, tissue macrophages are terminally differentiated cells that do not have osteoclast-forming potential (30), and the findings from macrophages may differ from those of osteoclasts or their precursors. Our findings provide the first experimental evidence of TNF increasing c-Fms expression by OCPs, and the functional consequence of this increased c-Fms expression on osteoclastogenesis (Fig. 5). In addi-

tion, the failure of neutralizing M-CSF antibodies to block TNFα-induced c-*Fms* expression indicates that this is a direct effect and is not secondary to M-CSF autoregulation (Fig. 5). Recently, Kitaura *et al.* (31) used chimerical WT and TNF receptor knock-out mice to dissect the contribution of cells in the osteoclast lineage from that of stromal cells in the response to TNFα-mediated osteoclastogenesis *in vivo*. From the findings of this elegant study, they conclude that in conditions where TNFα concentrations are high, TNFα can fully exert its bone erosive effects by directly promoting the differentiation of osteoclast precursors independent of cytokine-responsive stromal cells and T lymphocytes (31). Our results are consistent with their findings and further point out that one of the mechanisms by which TNF promotes OCP differentiation is though up-regulation of c-*Fms* expression.

We found that M-CSF alone increases c-Fms$^+$ cell numbers (Fig. 5), indicating that M-CSF can induce its own receptor expression and thereby forms an autocrine loop to amplify M-CSF-mediated signals. This is not a surprising because c-*Fms* expression is controlled by PU.1, one of the Ets transcription factors that is stimulated by M-CSF treatment (32). Because M-CSF is constitutively expressed in the bone microenvironment *in vivo*, and TNFα stimulates osteoblasts and T lymphocytes to up-regulate their expression of M-CSF (16, 17), TNFα-induced c-*Fms* expression must work through both M-CSF-dependent and -independent mechanisms. We have reported previously that TNFα promotes mature osteoclast survival (33). However, we did not observe clear changes in OCP apoptosis. Thus, TNFα likely has a different effect on OCPs *versus* mature osteoclasts; it stimulates proliferation and differentiation of the former to provide more OCPs and increases survival of the latter to prolong the duration of bone resorption (Fig. 6).

TNFα administration stimulates bone marrow OCP proliferation 1 day before the increase in total OCPs numbers are observed in both bone marrow and blood (Fig. 3). This finding, along with similar findings in TNF-Tg mice, suggests that TNFα-induced OCP proliferation and the subsequent increase in the bone marrow OCP pool may lead to the increased OCPs numbers in the peripheral blood. Based on these observations, we propose that in chronic inflammatory arthritis, where TNFα levels are elevated, TNFα increases marrow OCP numbers, which may directly result in a "push" of cells out of the bone marrow (marrow cell release) into the bloodstream because of the limited space available in the bone marrow cavity. Thus, chronic exposure to TNFα could increase the total turnover rate of OCPs. Unfortunately, we do not yet have experimental evidence to prove that the increase in blood OCP numbers in TNF-Tg mice is a direct consequence of an enlarged bone marrow pool. However, it is known that proliferation is not a pre-requisite for cell release from the bone marrow. In fact, the majority of common mobilizing factors stimulates marrow cell release without influencing their proliferation (18). Thus, TNFα-induced elevation in blood OCPs might result from different mechanisms than common mobilization and represent a unique response to chronic inflammation.

One important question regarding circulating OCPs is the role of these cells in normal bone remodeling, because this process occurs exclusively within the bone marrow cavity. Do OCPs need to travel in the blood to initiate physiological bone remodeling or do they simply receive signals from osteoblast/lining cells adjacent to them on or near bone surface identified for remodeling? We do not know the answers to these questions at this time. However, given that focal erosions develop from chronic inflammation over a number of years and the active osteoclasts that mediate these erosions have a half-life of only a few weeks, these cells must be replaced continuously. Because these osteoclasts are known to enter the joint through synovium as OCPs, our conclusion is that circulating OCPs serve as the pre-osteoclast reservoir. Identification of the mechanisms whereby OCP generation and trafficking are regulated should help answer these important questions.

In summary, our studies reveal a new mechanism by which TNFα stimulates osteoclast-mediated bone resorption in chronic inflammatory arthritis. We propose that the first influence of TNFα on osteoclastogenesis is to increase bone marrow OCP genesis through the following two mechanisms (Fig. 6): 1) TNFα directly stimulates the conversion of CD11b$^+$/Gr-1$^{-/lo}$/c-Fms$^-$ cells to c-Fms$^+$ cells; and 2) it stimulates osteoblasts/stromal cells to produce M-CSF, which subsequently increases c-Fms$^+$ cell proliferation. These CD11b$^+$/Gr-1$^{-/lo}$/c-Fms$^+$ cells are then released to the bloodstream, through a yet to be defined mechanism, and then home to inflamed joints where they differentiate in response to RANKL and other osteoclastogenic signals.

Acknowledgment—We thank Bianai Fan for technical assistance with the histological analysis.

REFERENCES

1. Teitelbaum, S. L., and Ross, F. P. (2003) *Nat. Rev. Genet.* **4,** 638–649
2. Boyle, W. J., Simonet, W. S., and Lacey, D. L. (2003) *Nature* **423,** 337–342
3. Kong, Y. Y., Feige, U., Sarosi, I., Bolon, B., Tafuri, A., Morony, S., Capparelli, C., Li, J., Elliott, R., McCabe, S., Wong, T., Campagnuolo, G., Moran, E., Bogoch, E. R., Van, G., Nguyen, L. T., Ohashi, P. S., Lacey, D. L., Fish, E., Boyle, W. J., and Penninger, J. M. (1999) *Nature* **402,** 304–309
4. Redlich, K., Hayer, S., Ricci, R., David, J. P., Tohidast-Akrad, M., Kollias, G., Steiner, G., Smolen, J. S., Wagner, E. F., and Schett, G. (2002) *J. Clin. Investig.* **110,** 1419–1427
5. Li, P., Schwarz, E. M., O'Keefe, R. J., Ma, L., Boyce, B. F., and Xing, L. (2004) *J. Bone Miner. Res.* **19,** 207–213
6. Xing, L., and Schwarz, E. M. (2005) *Curr. Rheu. Rev.* **1,** 21–28
7. Goldring, S. R. (2003) *Calcif. Tissue Int.* **73,** 97–100
8. Goldring, S. R. (2003) *Rheumatology* (*Oxf.*) **42,** Suppl. 2, ii, 11–16
9. Akashi, K., Traver, D., Miyamoto, T., and Weissman, I. L. (2000) *Nature* **404,** 193–197
10. Anderson, K. L., Smith, K. A., Conners, K., McKercher, S. R., Maki, R. A., and Torbett, B. E. (1998) *Blood* **91,** 3702–3710
11. Arai, F., Miyamoto, T., Ohneda, O., Inada, T., Sudo, T., Brasel, K., Miyata, T., Anderson, D. M., and Suda, T. (1999) *J. Exp. Med.* **190,** 1741–1754
12. Keffer, J., Probert, L., Cazlaris, H., Georgopoulos, S., Kaslaris, E., Kioussis, D., and Kollias, G. (1991) *EMBO J.* **10,** 4025–4031
13. Li, P., Schwarz, E. M., O'Keefe, R. J., Ma, L., Looney, R. J., Ritchlin, C. T., Boyce, B. F., and Xing, L. (2004) *Arthritis Rheum.* **50,** 265–276
14. Lam, J., Takeshita, S., Barker, J. E., Kanagawa, O., Ross, F. P., and Teitelbaum, S. L. (2000) *J. Clin. Investig.* **106,** 1481–1488
15. Kim, N., Kadono, Y., Takami, M., Lee, J., Lee, S. H., Okada, F., Kim, J. H., Kobayashi, T., Odgren, P. R., Nakano, H., Yeh, W. C., Lee, S. K., Lorenzo, J. A., and Choi, Y. (2005) *J. Exp. Med.* **202,** 589–595
16. Kaplan, D. L., Eielson, C. M., Horowitz, M. C., Insogna, K. L., and Weir, E. C. (1996) *J. Cell. Physiol.* **168,** 199–208
17. Cenci, S., Weitzmann, M. N., Roggia, C., Namba, N., Novack, D., Woodring, J., and Pacifici, R. (2000) *J. Clin. Investig.* **106,** 1229–1237
18. Cashman, J. D., Clark-Lewis, I., Eaves, A. C., and Eaves, C. J. (1999) *Blood* **94,** 3722–3729
19. Gothot, A., Pyatt, R., McMahel, J., Rice, S., and Srour, E. F. (1997) *Blood* **90,** 4384–4393
20. Johnson, M. R., Wang, K., Smith, J. B., Heslin, M. J., and Diasio, R. B. (2000) *Anal. Biochem.* **278,** 175–184
21. Dai, X. M., Ryan, G. R., Hapel, A. J., Dominguez, M. G., Russell, R. G., Kapp, S., Sylvestre, V., and Stanley, E. R. (2002) *Blood* **99,** 111–120
22. Fan, X., Biskobing, D. M., Fan, D., Hofstetter, W., and Rubin, J. (1997) *J. Bone Miner. Res.* **12,** 1387–1395
23. Roodman, G. D. (1999) *Exp. Hematol.* **27,** 1229–1241
24. Suda, T., Nakamura, I., Jimi, E., and Takahashi, N. (1997) *J. Bone Miner. Res.* **12,** 869–879
25. Lam, J., Abu-Amer, Y., Nelson, C. A., Fremont, D. H., Ross, F. P., and Teitelbaum, S. L.

(2002) *Ann. Rheum. Dis.* **61,** Suppl. 2, ii, 82–83
26. Xing, L., Bushnell, T. P., Carlson, L., Tai, Z., Tondravi, M., Siebenlist, U., Young, F., and Boyce, B. F. (2002) *J. Bone Miner. Res.* **17,** 1200–1210
27. Geissmann, F., Jung, S., and Littman, D. R. (2003) *Immunity* **19,** 71–82
28. Quinones, M. P., Ahuja, S. K., Jimenez, F., Schaefer, J., Garavito, E., Rao, A., Chenaux, G., Reddick, R. L., Kuziel, W. A., and Ahuja, S. S. (2004) *J. Clin. Investig.* **113,** 856–866
29. Alford, P. B., Xue, Y., and Shackelford, R. E. (1997) *Biochem. Biophys. Res. Commun.* **240,** 442–445
30. Huang, W., O'Keefe, R. J., and Schwarz, E. M. (2003) *Arthritis Res. Ther.* **5,** R49–R59
31. Kitaura, H., Sands, M. S., Aya, K., Zhou, P., Hirayama, T., Uthgenannt, B., Wei, S., Takeshita, S., Novack, D. V., Silva, M. J., Abu-Amer, Y., Ross, F. P., and Teitelbaum, S. L. (2004) *J. Immunol.* **173,** 4838–4846
32. Sevilla, L., Zaldumbide, A., Carlotti, F., Dayem, M. A., Pognonec, P., and Boulukos, K. E. (2001) *J. Biol. Chem.* **276,** 17800–17807
33. Zhang, Q., Badell, I. R., Schwarz, E. M., Boulukos, K. E., Yao, Z., Boyce, B. F., and Xing, L. (2005) *Arthritis Rheum.* **52,** 2708–2718

PLOS ONE

RESEARCH ARTICLE

TNF Induction of NF-κB RelB Enhances RANKL-Induced Osteoclastogenesis by Promoting Inflammatory Macrophage Differentiation but also Limits It through Suppression of NFATc1 Expression

Zhijun Zhao[1☯], Xiaodong Hou[1,2☯], Xiaoxiang Yin[1,2], Yanyun Li[2], Rong Duan[2], Brendan F. Boyce[2], Zhenqiang Yao[2]*

1 Department of Medical Imaging, Henan University First Affiliated Hospital, 357 Ximen Street, Kaifeng, Henan 475001, P.R. China, **2** University of Rochester Medical Center, Department of Pathology and Laboratory Medicine and Center for Musculoskeletal Research, Box 626, Room 1–2105, 601 Elmwood Ave, Rochester, NY 14642, United States of America

☯ These authors contributed equally to this work.
* zhenqiang_yao@urmc.rochester.edu

OPEN ACCESS

Citation: Zhao Z, Hou X, Yin X, Li Y, Duan R, Boyce BF, et al. (2015) TNF Induction of NF-κB RelB Enhances RANKL-Induced Osteoclastogenesis by Promoting Inflammatory Macrophage Differentiation but also Limits It through Suppression of NFATc1 Expression. PLoS ONE 10(8): e0135728. doi:10.1371/journal.pone.0135728

Editor: Juha Tuukkanen, University of Oulu, FINLAND

Received: December 29, 2014

Accepted: July 26, 2015

Published: August 19, 2015

Data Availability Statement: All relevant data are within the paper and its Supporting Information files.

Funding: This work was funded by National Natural Science Foundation of China 81373191 to ZY, National Institute for Arthritis, Musculoskeletal and Skin Diseases AR43510 to BFB, and P30AR061307 pilot grant (from Edward M. Schwarz) to ZY. The funders had no role in study design, data collection and analysis, decision to publish, or preparation of the manuscript.

Abstract

TNF induces bone loss in common bone diseases by promoting osteoclast formation directly and indirectly, but it also limits osteoclast formation by inducing expression of NF-κB p100. Osteoclast precursors (OCPs) are derived from M1 (inflammatory) and M2 (resident) macrophages. However, it is not known if TNF stimulates or limits osteoclast formation through regulation of M1 or M2 differentiation or if RelB, a partner of p100, is involved. To investigate these questions, we treated bone marrow cells (BMCs) with M-CSF alone or in combination with TNF to enrich for OCPs, which we called M-OCPs and T-OCPs, respectively. We found that TNF switched $CD11b^+F4/80^+$ M-OCPs from $Ly6C^-Gr1^-$ M2 to $Ly6C^+Gr1^-CD11c^+$ and $Ly6C^-Gr1^-CD11c^+$ M1 cells. RANKL induced osteoclast formation from both $Ly6C^+Gr1^-$ and $Ly6C^-Gr1^-$ T-OCPs, but only from $Ly6C^+Gr1^-$ M-OCPs, which formed significantly fewer osteoclasts than T-OCPs. Importantly, $Ly6C^+Gr1^-$ cells from both M- and T-OCPs have increased expression of the M1 marker genes, iNOS, TNF, IL-1β and TGFβ1, compared to $Ly6C^-Gr1^-$ cells, and $Ly6C^-Gr1^-$ cells from T-OCPs also have increased expression of iNOS and TGFβ1 compared to cells from M-OCPs. Both RANKL and TNF increased RelB mRNA expression. TNF significantly increased RelB protein levels, but RANKL did not because it also induced RelB proteasomal degradation. TNF inhibited RANKL-induced NFATc1 mRNA expression and osteoclast formation from M-OCPs, but not from T-OCPs, and it did not induce $Ly6C^+Gr1^-CD11c^+$ or $Ly6C^-Gr1^-CD11c^+$ M1 macrophages from RelB-/- BMCs. Furthermore, overexpression of RelB in M-OCPs reduced RANKL-induced osteoclast formation and NFATc1 mRNA expression, but it increased TNF-induced OC formation without affecting NFATc1 levels. Thus, TNF induction of RelB directly mediates terminal osteoclast differentiation independent of NFATc1 and limits RANKL-induced osteoclastogenesis by

Competing Interests: The authors have declared that no competing interests exist.

inhibiting NFATc1 activation. However, the dominant role of TNF is to expand the OCP pool by switching the differentiation of M-CSF-induced M2 to M1 macrophages with enhanced osteoclast forming potential. Strategies to degrade RelB could prevent TNF-induced M2/M1 switching and reduce osteoclast formation.

Introduction

TNF is the major cytokine driving inflammation in rheumatoid arthritis (RA), a chronic inflammatory disease affecting about 1% of the world's population and characterized by synovial inflammation and joint destruction, leading to severe morbidity and premature mortality [1]. Transgenic mice over-expressing TNF (TNF-Tg mice) develop a form of arthritis that is very similar to human RA [2]. Although anti-TNF therapies have significantly reduced the morbidity and joint destruction in RA, they are expensive, and only about 60% of patients have a good response to these agents [3, 4]. In non-responding patients, TNF inhibitors typically are administered for several months before a decision is made to switch to an alternative treatment, which is often another TNF inhibitor that also may be ineffective. Thus, there is a need to better understand how TNF induces joint inflammation and destruction.

Inflammatory cells, such as lymphocytes, macrophages and mast cells, drive chronic inflammatory processes, including synovial inflammation, by producing cytokines and autoantibodies at involved sites. Joint destruction in RA is mediated by ectopic differentiation of osteoclasts (OCs) from their monocyte-macrophage lineage precursors in affected joints. Receptor activator of nuclear factor-κB ligand (RANKL), a member of the TNF superfamily, mainly controls later phases of OC differentiation and activation [5], and its expression by synoviocytes and inflammatory cells in affected joints is promoted by TNF and other cytokines [6, 7]. RANKL expression is also required for normal B cell development and lymph node formation [8], suggesting that it might have a role to promote joint inflammation in RA. However, TNF-Tg mice generated to have deficiency of RANKL also develop synovial inflammation, but not joint destruction because OCs do not form in these mice [9, 10]. Preclinical and clinical studies indicate that RANKL inhibitors do not significantly alter inflammatory processes in RA [11]. These findings suggest that RANKL does not contribute significantly to TNF-induced inflammation in RA.

TNF can induce osteoclastogenesis directly from *Rank*$^{-/-}$OC precursors (OCPs) in vitro when the cells are co-cultured with [12] or without [13] TGF-β1, which is released from bone matrix during bone resorption and activated by the acidic microenvironment in resorption lacunae as a result of acid release from OCs [14, 15]. However, the numbers of OCs induced by TNF from WT OCPs are much lower than those induced by RANKL [16]. Despite these findings, it was puzzling that TNF did not induce OC formation when administered in vivo to *Rank*$^{-/-}$mice [17]. We have reported that TNF induces expression of NF-κB p100 and that p100 limits TNF- and RANKL-mediated OC formation [13]. Consistent with this inhibitory effect of p100, we also found that TNF efficiently induced OC formation in vivo when it was administered to RANKL$^{-/-}$ or RANK$^{-/-}$ mice also deficient in p100 [13]. TNF-Tg mice that we generated to be deficient in p100 have significantly accelerated development of arthritis and systemic bone loss, suggesting that p100 not only limits OC formation, but also joint inflammation induced by TNF [13]. More recently, it was reported that TNF also limits OC formation through RBP-j [18] and IRF-8 [19], indicating that there are several mechanisms to restrict the destructive effects of TNF on bone. In contrast, TNF can also synergize with RANKL to induce OC formation [20,

21]. However, the precise conditions in which TNF limits or promotes OC formation and the factors that are critical for TNF induction or inhibition of OC formation remain unclear.

OCPs comprise both classically activated (inflammatory, M1) macrophages and alternatively activated (resident, M2) macrophages [22–24]. LPS, which induces TNF production [25], promotes the differentiation of M1 macrophages [22, 24], and TNF increases the numbers of circulating OCPs by promoting their proliferation through up-regulation of expression of the receptor for M-CSF [26]. Expression of M-CSF, like RANKL, is essential for OC formation [27]. However, it is not known if TNF induction or inhibition of OC formation involves modulation of M1/M2 macrophage differentiation into OCs. We report here that TNF switches the differentiation of M-CSF-primed M2 into M1 macrophages to enhance osteoclastogenesis by inducing the expression of NF-κB RelB, the partner of p100/p52, and that RelB also directly targets NFATc1 to limit OC formation.

Materials and Methods

Reagents

Recombinant murine M-CSF, RANKL, TNF were purchased from R&D Systems (Minneapolis, MN). Antibodies of RelB for Western blot were purchased from Santa Cruz and anti-actin antibody was from Sigma. Goat anti-rabbit (or mouse) IgG-HRP conjugate secondary antibody was purchased from Bio-Rad. Fluorescent-labeled rat anti-mouse antibodies APC-Ly6C, PEcy7-CD11b, PE-Gr1 (also called Ly6G) and PECy5-F4/80 were purchased from eBioscience. Ammonium Chloride (NH_4Cl) solution was purchased from STEMCELL technologies.

Animals

Cells from 6–8 week-old C57Bl6 mice as well as RelB-/- and WT littermate mice on an inbred C57BL/6 background [28–30] were used for in vitro studies. This study was carried out in strict accordance with the administrative regulations of Laboratory Animals of the National Science and Technology Commission of People's Republic of China and the recommendations in the Guide for the Care and Use of Laboratory Animals of the National Institutes of Health. The protocols were approved by the Committee on the Ethics of Animal Experiments of Henan University and the University of Rochester Medical Center Institutional Animal Care and Use Committee. Mice were euthanized by CO_2 followed by neck dislocation according to AVMA guidelines.

Osteoclastogenesis

The culture procedure was modified from our previous reports [13, 16, 26, 31]. Briefly, bone marrow (BM) was flushed from the long bones of mice using α-MEM containing 10% FBS, passed through a 21-G and then through a 25-G needle to make single cell suspensions. The cells were incubated in NH_4Cl solution for 10 min at room temperature to lyse red blood cells. $6x10^4$ BM cells were seeded in 96-well plates and cultured with 5 ng/ml M-CSF for 2 days, and then RANKL (10 ng/ml) or TNF (20 ng/ml) or both were added to the cultures for 48–56 hr at which time mature OCs could be observed using an inverted microscope. The cells were then fixed with 10% neutral phosphate-buffered formalin for 10 min and TRAP staining was performed. TRAP+ cells with three or more nuclei were considered as mature OCs.

Over-expression of RelB

BM cells prepared as above were seeded in 96-well plates ($4x10^4$/well) for the evaluation of OC formation or in 60-mm dishes ($1.2x10^6$ cells per dish) for Western blot or FACS analysis

followed by culture with M-CSF for 2 days to enrich for OCPs. For over-expression of RelB, the culture medium was replaced with fresh medium containing M-CSF, 2 μg/ml polybrene and ¼ volume of retro-viral supernatant of pMX-GFP or pMX-GFP-RelB prepared from Plat-E packaging cells, as we described previously [13, 16, 31]. After 24 hr of infection, RANKL or TNF was added to the cultures for an additional 48–96 hr to generate OCs.

FACS analysis and cell sorting

2×10^6 BM or cultured cells were stained with APC-Ly6C, PEcy7-CD11b, PE-Gr1 and PECy5-F4/80 antibodies for 30 min. Data were acquired using a FACScanto flow cytometer and analyzed using FlowJo software, as described previously [26, 30]. For cell sorting, cultured OCPs from WT mice were stained with the above fluorescent-conjugated antibodies to confirm that each cell population was similar to those generated in our regular culture procedure, and the cells were then sorted by a Statler sorter to collect $Ly6C^+Gr1^-$, $Ly6C^+Gr1^+$, $Ly6C^-Gr1^-$ and $Ly6C^-Gr1^+$ cells separately. The sorted cells were reanalyzed to ensure their purity ($\geq$98%) and used for osteoclastogenesis assays, as we described previously [26].

Western blot analysis

Cultured cells were lysed with M-Per mammalian protein extraction reagent (Thermo Scientific) containing a protease inhibitor cocktail (Sigma). Lysate proteins (10–20 μg) were loaded in 10% SDS-PAGE gels and transferred onto polyvinylidene difluoride membranes. Following blocking in 5% milk, membranes were incubated with a specific primary antibody to RelB or mouse β-actin over-night at 4°C. After washing, the membranes were incubated with anti-rabbit (or mouse) IgG-HRP conjugate secondary antibody (Bio-Rad) and exposed to ECL substrate. Signals were analyzed using a Bio-Rad imaging system.

Quantitative Real-Time PCR

Total RNA was extracted from cultured cells using 1 ml TRIzol reagent, and 1 μg of RNA was used for synthesis of cDNA using a GeneAmp RNA PCR core kit. Quantitative PCR amplification was performed using an iCycler real-time PCR machine and iQ SYBR Green (Bio-Rad). Relative mRNA expression levels of target genes were analyzed using the CT value of the gene, normalized to β-actin.

Statistics

All results are given as the mean ± S.D. Comparisons between two groups were analyzed using Student's two-tailed unpaired t test. One-way analysis of variance and Dunnett's post hoc multiple comparisons were used for comparisons among three or more groups. p values <0.05 were considered statistically significant. Each experiment was repeated at least twice with similar results.

Results

TNF switches the differentiation of M-CSF-induced $Ly6C^-Gr1^-$ M2 to $Ly6C^+Gr1^-CD11c^+$ and $Ly6C^-Gr1^-CD11c^+$ inflammatory M1 macrophages

OCPs belong to the monocyte/macrophage lineage. Mouse $CD11b^+Gr1^{-/lo}$ cells are precursors that efficiently form OCs [26]. Since macrophages have been classified as M1 and M2 cells and TNF generally stimulates M1 differentiation [23], we investigated if TNF regulates M1/M2 cells and if this affects their OC formation potential. More than 30 cell surface markers are

used to classify M1 and M2 macrophages [22, 23]. CD11b and F4/80 are common macrophage surface markers; M1 cells are $CCR2^{+}Gr1^{+}CD62L^{+}CD11c^{+}$, while M2 cells are $CCR2^{-}Gr1^{-}CD62L^{-}CD11c^{-}$ in mice [22, 23]. Ly6C is also widely used to differentiate M1 and M2 cells. $Ly6C^{+/hi}$ subsets are classified as M1 cells, while $Ly6C^{-/lo}$ subsets are classified as M2 cells [32, 33].

To characterize TNF-induced OCPs, we examined expression of the cell surface markers: CD11b, F4/80, Ly6C, CD11c and Gr1. About 40% of primary BM cells were $CD11b^{+}F4/80^{+}$ cells and of these ~80% were $Ly6C^{+}Gr1^{hi+}$ granulocytes and ~15% were $Ly6C^{+}Gr1^{-/lo+}$ cells (Fig 1A), corresponding to our previously reported $CD11b^{+}Gr1^{-/lo+}$ OCPs [26]. We cultured BM cells with M-CSF alone or in combination with TNF or RANKL for 3 days to generate OCPs, which we called M-CSF-induced OCPs (M-OCPs), TNF-induced OCPs (T-OCPs) and RANKL-induced OCPs (R-OCPs), respectively. We found that the two common macrophage surface markers, $CD11b^{+}F4/80^{+}$, comprised ~75% and ~79% of T- and R-OCPs respectively, compared to ~87% of M-OCPs ($p<0.05$, Fig 1B upper panel and S1 Fig). We also found that in these $CD11b^{+}F4/80^{+}$ populations, $Ly6C^{+}Gr1^{-}$ cells comprised 23.9%, 50.8% and 15.9% of M-OCPs, T-OCPs and R-OCPs, respectively, while $Ly6C^{-}Gr1^{-}$ cells comprised 73%, 47% and 82.8% of these cells, respectively (Fig 1B middle panel), suggesting that TNF switched M-CSF-induced $Ly6C^{-}Gr1^{-}$ M2 to $Ly6C^{+}Gr1^{-}$ M1 macrophages, an effect similar to that induced by IFN-γ, which is a standard stimulator of M1 macrophage differentiation [22, 23]. In contrast, RANKL did not change the phenotype of M-CSF-induced macrophages. We also analyzed another M1 marker, CD11c, in $Ly6C^{+}Gr1^{-}$ and $Ly6C^{-}Gr1^{-}$ cells, and found that in the $Ly6C^{+-}Gr1^{-}$ cells from the $CD11b^{+}F4/80^{+}$ populations, the frequency of $CD11c^{+}$ cells in T-OCPs (5.96%) was double that in M-OCPs (3.18%), while it remained low in R-OCPs (1.83%, Fig 1B lowest panel). Similarly, in the $Ly6C^{-}Gr1^{-}$ cells from the $CD11b^{+}F4/80^{+}$ populations, $CD11c^{+}$ cells in T-OCPs (11.2%) were almost twice as frequent as those that in M-OCPs (6.67%) (Fig 1B lowest panel). We used IFN-γ as a positive control and found that it also increased $CD11c^{+}$ cells in both $Ly6C^{+}Gr1^{-}$ and $Ly6C^{-}Gr1^{-}$ cells from $CD11b^{+}F4/80^{+}$ populations, about four-fold more than those that in M-OCPs (Fig 1B lowest panel). These data suggest that $Ly6C^{-}Gr1^{-}$ cells from T-OCPs had also shifted to M1 macrophages.

TNF-induced $CD11b^{+}F4/80^{+}Ly6C^{+}Gr1^{-}$ and $CD11b^{+}F4/80^{+}Ly6C^{-}Gr1^{-}CD11c^{+}$ macrophages have higher OC forming potential than M-CSF-induced macrophages

M-, T-, and R-OCPs generated from WT mouse BM cells were stained with PEcy7-CD11b, PEcy5-F4/80, APC-Ly6C and PE-Gr1 antibodies to analyze their macrophage surface markers. We confirmed that the expression levels of cell surface markers in each OCP type (Fig 2A upper panel) were similar to those in OCPs in Fig 1B. We sorted each of these OCPs into four populations: $Ly6C^{+}Gr1^{-}$, $Ly6C^{+}Gr1^{+}$, $Ly6C^{-}Gr1^{-}$ and $Ly6C^{-}Gr1^{+}$ cells. $4x10^{4}$ of the sorted cells were seeded into 96-well plates and treated with RANKL or TNF in the presence of M-CSF to induce OC formation. In M-OCPs, the OC forming potential of $Ly6C^{+}Gr1^{-}$ cells was much higher than $Ly6C^{-}Gr1^{-}$ cells: RANKL induced 125±16 OCs from $Ly6C^{+}Gr1^{-}$ cells, but only a few TRAP+ mononuclear cells were formed from $Ly6C^{-}Gr1^{-}$ cells at this time point (Fig 2B). In contrast, both $Ly6C^{+}Gr1^{-}$ and $Ly6C^{-}Gr1^{-}$ cells from T- and R-OCPs formed many OCs, and both $Ly6C^{+}Gr1^{-}$ and $Ly6C^{-}Gr1^{-}$ cells from T-OCPs formed similar numbers of OCs, but $Ly6C^{-+}Gr1^{-}$ cells from R-OCPs formed more OCs than $Ly6C^{-}Gr1^{-}$ cells in response to RANKL ($p<0.01$). In addition, OC numbers from $Ly6C^{-}Gr1^{-}$ T-OCPs almost matched those from R-OCPs. TNF also induced large numbers of OCs from $Ly6C^{+}Gr1^{-}$ and $Ly6C^{-}Gr1^{-}$ cells from R-OCPs (Fig 2B) probably because R-OCPs had already undergone some further

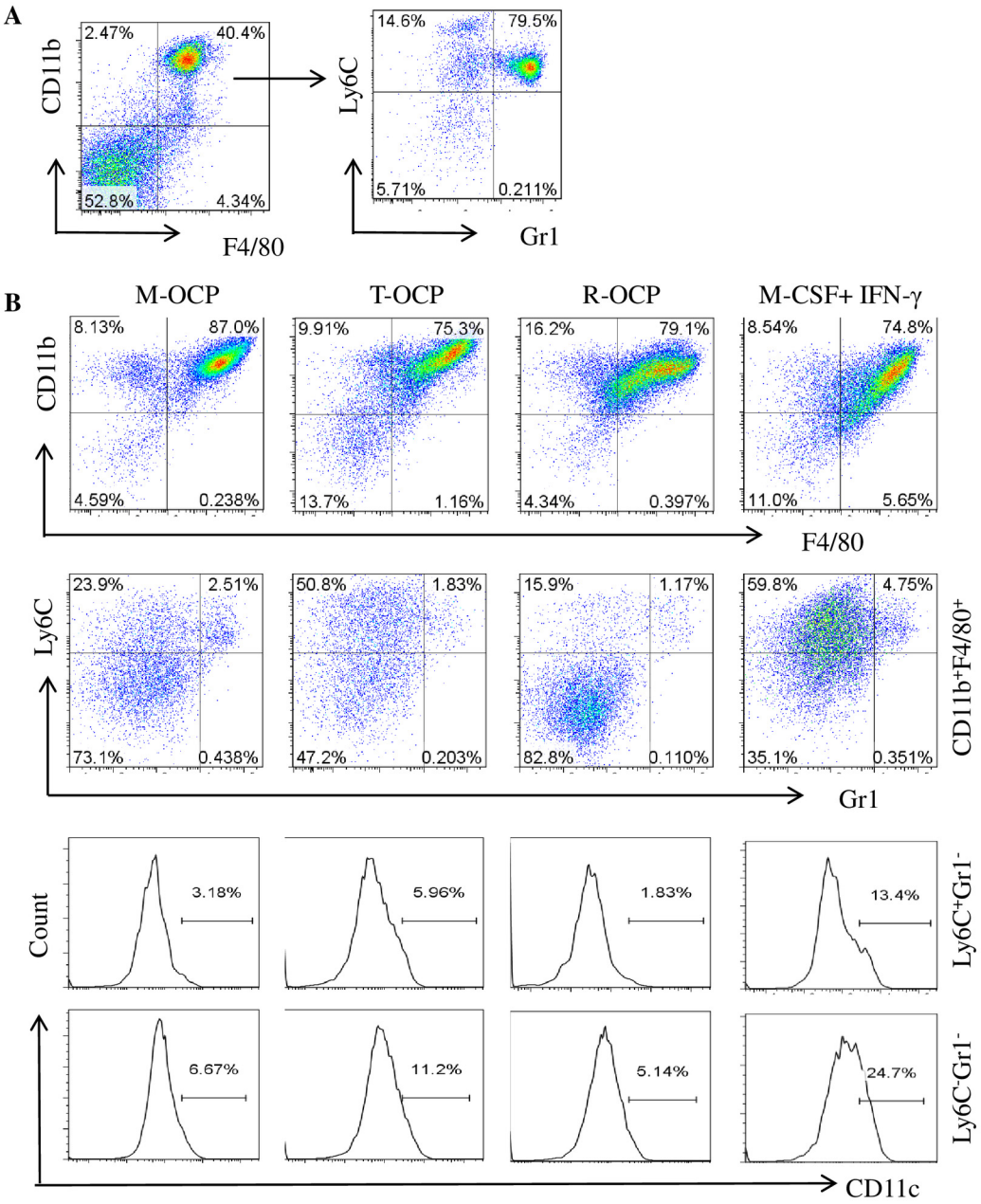

Fig 1. TNF promotes the differentiation of Ly6C$^+$Gr1$^-$CD11c$^+$ M1 macrophages. (A) Freshly isolated bone marrow cells (BMCs) from 3-month-old C57Bl6 mice were stained with anti-mouse APC-Ly6C, PEcy7-CD11b, PE-Gr1, FITC-CD11c and PEcy5-F4/80 antibodies and expression levels of these cell surface markers were analyzed by flow cytometry. (B) BMCs (2x10^6) from the mice in (A) were cultured with M-CSF, M-CSF+TNF (20ng/ml) or M-CSF +RANKL (10ng/ml) in 60 mm-dishes for 3 days to recruit OCPs, which we called M-CSF-induced OCPs (M-OCPs), TNF-induced OCPs (T-OCPs), and RANKL-induced OCPs (R-OCPs), respectively. IFN-γ (1ng/ml) was also added to M-CSF-treated cells as a positive control for M1 macrophage recruitment. Cells attached to the dishes were collected and stained with the above antibodies to analyze expression of cell surface markers by flow cytometry: CD11b$^+$F4/80$^+$ cells in the total cultured OCPs (upper panel), Ly6C$^+$Gr1$^-$ and Ly6C$^-$Gr1$^-$ cells in the CD11b$^+$F4/80$^+$ population (middle panel) and CD11c$^+$ cells in the Ly6C$^+$Gr1$^-$ and Ly6C$^-$Gr1$^-$ populations (lower panel). The experiment was repeated three times with similar results.

doi:10.1371/journal.pone.0135728.g001

differentiation. There were fewer Gr1$^+$ cells (Ly6C$^+$Gr1$^+$and Ly6C$^-$Gr1$^+$) in these cultured OCPs (Fig 2A) and the Gr1$^+$ cells from M-OCPs did not form OCs in response to TNF or RANKL (not shown). RANKL also induced OC formation from Ly6C$^+$Gr1$^+$ cells from T- and R-OCPs (not shown), but the total numbers of these cells were small.

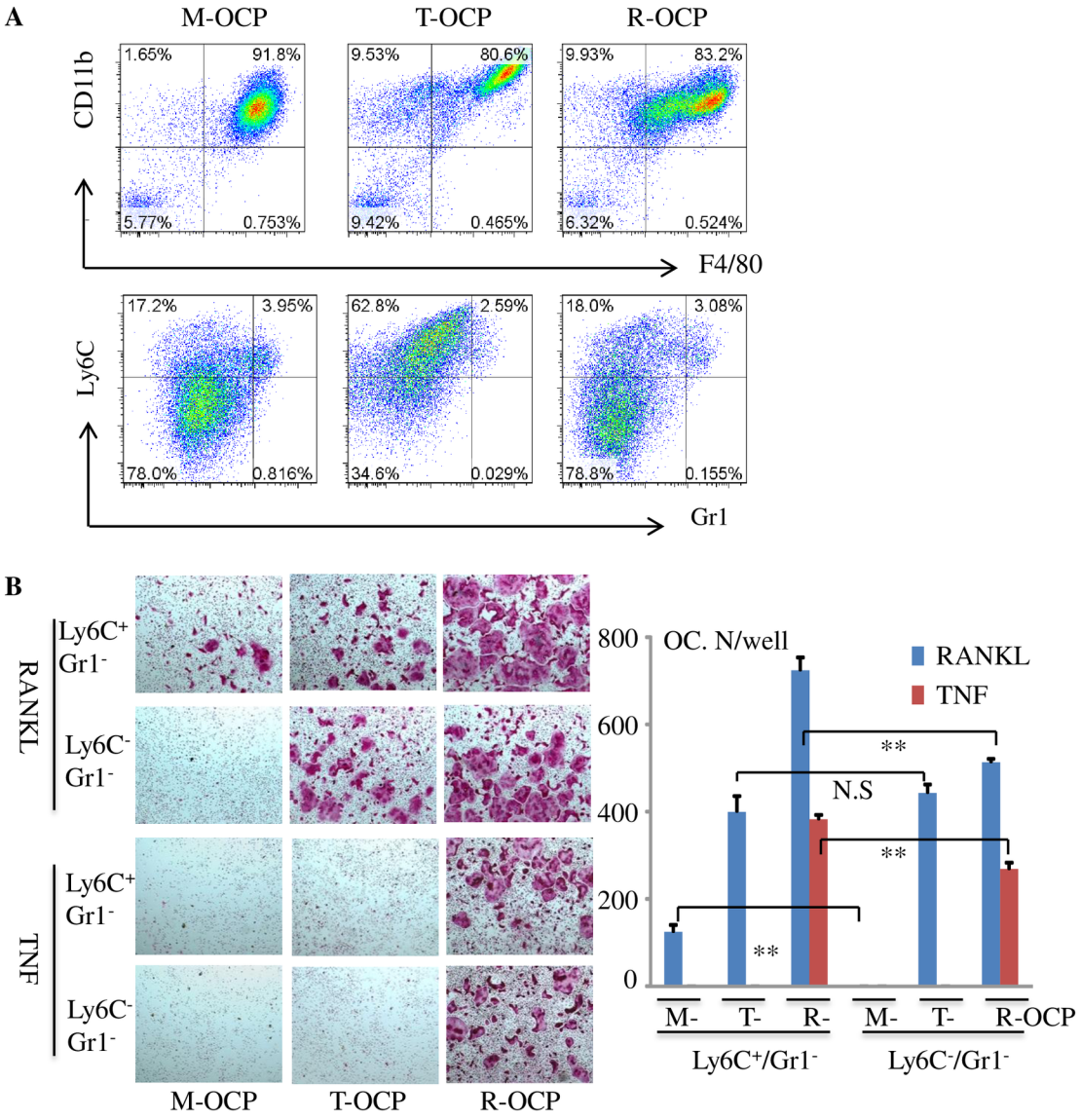

Fig 2. TNF-induced macrophages have higher OC forming potential than M-CSF-induced macrophages. (A) M-, T-, and R-OCPs cultured from BMCs from a 4-month-old C57Bl6 mouse were stained with the fluorescent-labeled antibodies as in Fig 1. $Ly6C^+Gr1^-$ and $Ly6C^-Gr1^-$ populations from $CD11b^+F4/80^+$ cells were sorted by flow cytometry. (B) The sorted cell populations were seeded in 96-well plates ($4x10^4$ cells/well) and treated with RANKL or TNF in the presence of M-CSF for 2 additional days to generate mature OCs, which were stained for TRAP activity. (C) Quantitation of numbers of OCs formed from each sorted population in (B), 4 wells per group, *p < 0.05, **p < 0.01. The experiment was repeated twice with similar results. M = M-CSF, P = PBS, R = RANKL, T = TNF, R+T = RANKL+TNF.

doi:10.1371/journal.pone.0135728.g002

$Ly6C^+Gr1^-$ cells express M1 macrophage markers and $Ly6C^-Gr1^-$ cells from T-OCPs are also polarized to M1 macrophages

We next sorted $Ly6C^+Gr1^-$ and $Ly6C^-Gr1^-$ cells from M-, T- and R-OCPs (Fig 3A) to extract total RNA. We used 1 μg RNA from each sample to reverse transcribe cDNA to test levels of the M1 marker genes, iNOS, TNF, TGFβ1 and IL-1β as well as the M2 markers, IL-10 and PPAR-γ, by real-time PCR. We found that the expression levels of iNOS, TNF, TGFβ1 and IL-1β were increased by 2.5, 1.95, 1.62 and 1.87 fold ($p<0.05$), respectively, in $Ly6C^+Gr1^-$ cells from M-OCPs compared to $Ly6C^-Gr1^-$ cells, while the levels of IL-10 and PPAR-γ were not

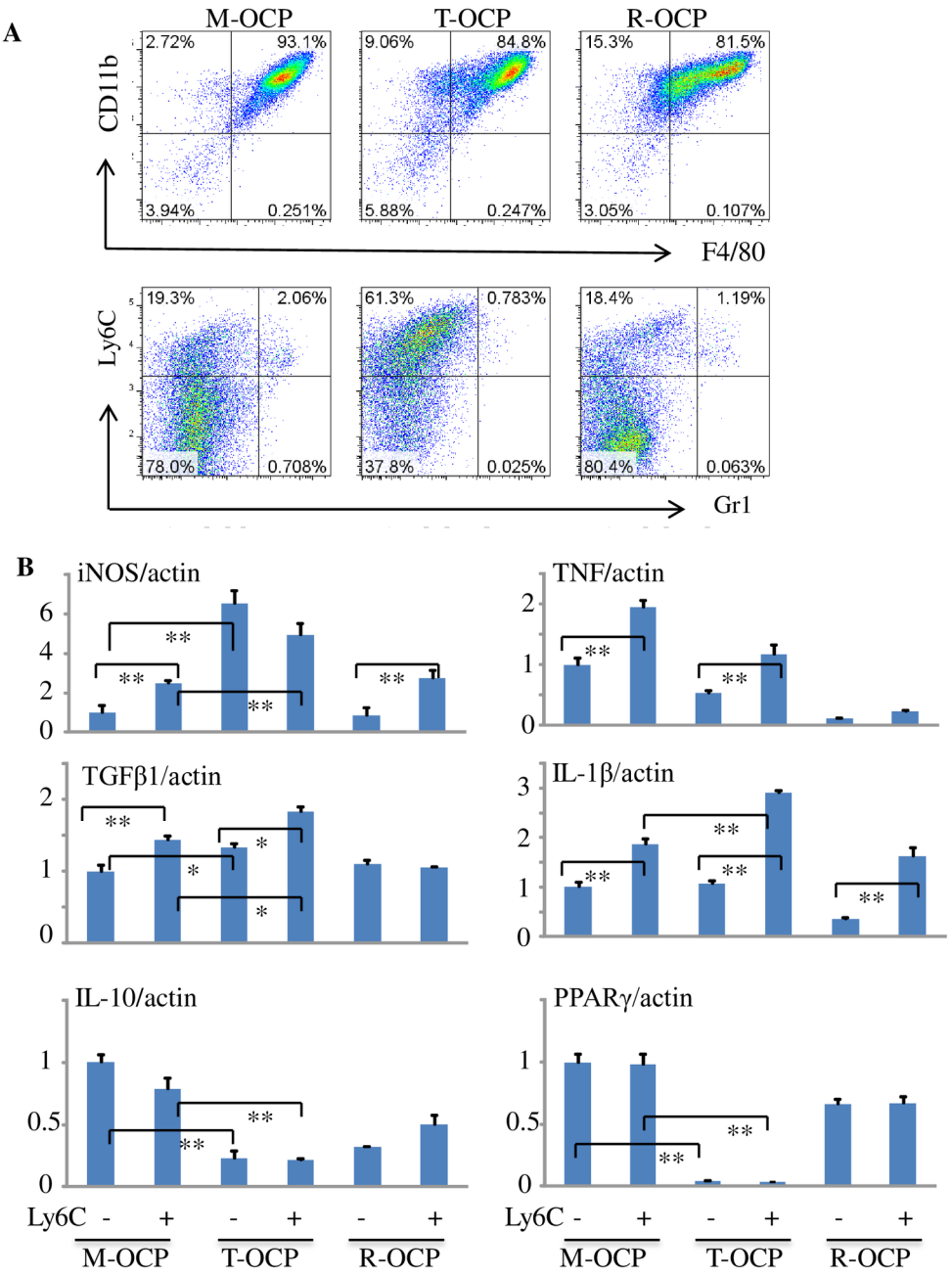

Fig 3. TNF-induced macrophages express M1 markers. Ly6C$^+$Gr1$^-$ and Ly6C$^-$Gr1$^-$ cells were sorted from cultured M-, T- and R-OCPs from 3-month-old C57Bl6 mice, as in Fig 2A (A). Total RNA was extracted from these sorted cells and mRNA expression levels of the M1 macrophage genes, TNF-α, iNOS, IL-1β and TGFβ1 as well as the M2 macrophage marker genes, PPAR-γ and IL-10, were tested by real-time PCR, normalized to β-actin (B). The data are representative of two independent experiments. *$p < 0.05$, **$p < 0.01$.

doi:10.1371/journal.pone.0135728.g003

significantly different (Fig 3B), confirming that Ly6C$^+$Gr1$^-$ cells generally have a M1 profile. Ly6C$^+$Gr1$^-$ cells from T-OCPs expressed higher iNOS, IL-1β and TGFβ1, but significantly lower IL-10 and PPAR-γ levels than those from M-OCPs ($p<0.05$). Of note, expression levels of iNOS and TGFβ1 were also increased, while IL-10 and PPAR-γ levels were decreased in Ly6C$^-$Gr1$^-$ cells from T-OCPs compared to M-OCPs cells (Fig 3B), providing further support

that Ly6C$^-$Gr1$^-$ cells from T-OCPs have a M1 phenotype. The expression level of iNOS in Ly6C$^+$Gr1$^-$ cells from T-OCPs was 2-fold higher than in Ly6C$^+$Gr1$^-$ cells from M-OCPs ($p<0.05$), but it was 6-fold higher in Ly6C$^-$Gr1$^-$ cells from T-OCPs than in Ly6C$^-$Gr1$^-$ cells from M-OCPs probably because the Ly6C$^-$Gr1$^-$ cells from T-OCPs had also switched to CD11c$^+$ M1 cells.

TNF induction of RelB promotes the differentiation of Ly6C$^+$Gr1$^-$ and Ly6C$^-$Gr1$^-$CD11c$^+$ macrophages

RelB is a member of the NF-κB family of transcription factors [34, 35]. OC numbers are normal in the bones of RelB-/- mice, but bone marrow OCPs from RelB-/- mice form fewer OCs than WT OCPs in vitro in response to RANKL [36]. To investigate the role of RelB in TNF-induced OC formation, we first tested RelB protein expression levels in M-, T- and R-OCPs from WT mouse BM cells, generated as in Fig 1B. We then used regular OC-inducing culture medium containing M-CSF and treated the cells with PBS, TNF, RANKL or a combination of TNF and RANKL for an additional 8 or 48 hr (mature OCs being formed at 48 hr). In M- and R-OCPs, RelB protein levels in RANKL-treated cells were similar to or lower than PBS-treated cells, while in contrast, TNF- and TNF+RANKL-treated cells had significantly higher RelB protein levels at both time-points (Fig 4A). After 8 hr treatment, the basal (PBS-treated cells) RelB protein level in T-OCPs was significantly higher than in M- and R-OCPs, while RANKL reduced and TNF increased it slightly (Fig 4A). At 48 hr, RelB protein levels remained low in PBS- and RANKL-treated M- and R-OCPs, while in T-OCPs they dropped to those of M- and R-OCPs and remained high in both TNF- and RANKL+TNF-treated OCPs (Fig 4A).

Increased protein levels can result from increased synthesis and/or decreased degradation. In general, both TNF and RANKL increased RelB mRNA expression (Fig 4B). Compared to PBS, RANKL and TNF increased RelB mRNA expression in M-OCPs by 4.5- and 7.5-fold, respectively, after 4 hr of treatment, and these remained high at 24 hr (Fig 4B). At 48 hr when mature OCs have begun to form, TNF or TNF+RANKL induced 3-fold higher RelB mRNA levels than PBS-treated M-OCPs, but RANKL did not change RelB levels at this time-point. Furthermore, in T- and R-OCPs treated with TNF or RANKL or both in combination RelB mRNA levels were still significantly increased when OCs had formed.

In contrast to the generally increased RelB mRNA, RelB protein levels in RANKL-treated OCPs or mature OCs was lower than or similar to PBS-treated cells (Fig 4A). In many cases, RelB protein levels in RANKL+TNF-treated M-OCPs were slightly lower than in cells treated with TNF alone, suggesting that RANKL may also induce RelB degradation. To test this hypothesis, M-OCPs generated from WT mouse BM cells were serum-starved for 2 hr followed by treatment of vehicle or the proteasome inhibitor, MG-132, for 3 hr. We found that RelB protein levels increased by 7.5- and 9-fold in PBS- and RANKL-treated cells, respectively, in the presence of MG-132, but by only 2-fold in TNF-treated cells (Fig 4C), suggesting that RelB undergoes strong constitutive degradation and that the additional RelB induced by RANKL is also efficiently degraded.

To determine if TNF induction of Ly6C$^+$Gr1$^-$ and Ly6C$^-$Gr1$^-$CD11c$^+$ macrophages requires RelB expression, we used RelB-/- mouse BM cells to examine expression of macrophage markers in cytokine-induced OCPs. RelB-/- mice develop multiorgan inflammation [28], and consistent with this, the % CD11b$^+$ myeloid cells in freshly isolated RelB-/- BM was higher than in WT cells. For example, CD11b$^+$F4/80$^+$ cells comprised ~76% of RelB-/- BM cells compared to 45% in WT mice (not shown), and Ly6C$^+$ cells were also increased in the CD11b$^+$F4/80$^+$ population from the RelB-/- mice (not shown). After 3 days of culture, the total percentage of CD11b$^+$F4/80$^+$ cells from RelB-/- mice was ~93–94% in M-, T- and R-OCPs (Fig 5A).

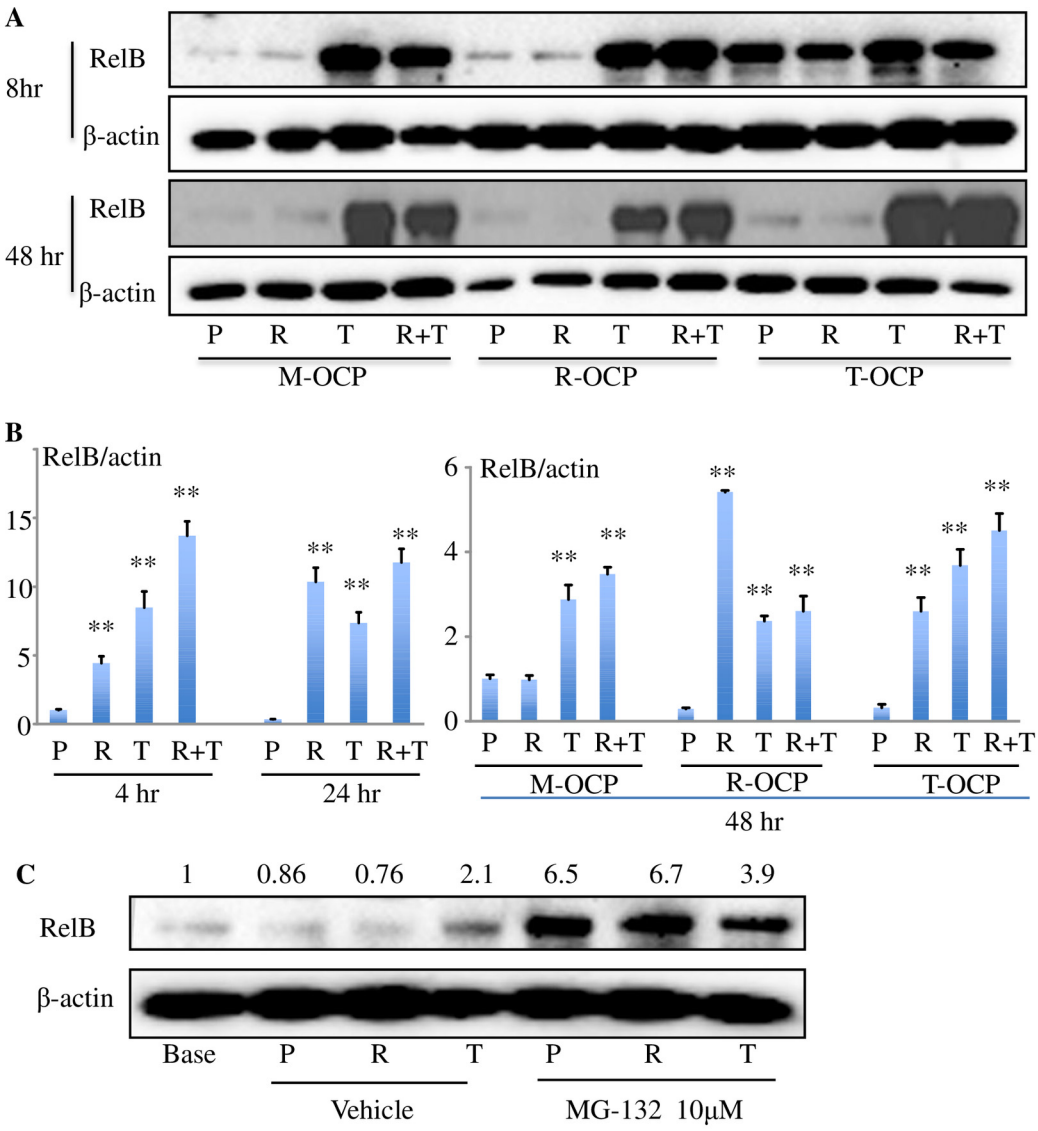

Fig 4. TNF increases expression of RelB mRNA and prevents RelB protein degradation. (A) M-, R-, and T- OCPs generated as in Fig 1B were treated with PBS (P), R, T or R+T for 8 hr or for 48 hr by which time mature OCs had formed. Cell lysates were subjected to Western blot analysis of RelB and β-actin. (B) M-OCPs were treated with P, R, T or R+T for 4 and 24 hr (left panel), or M-, R- and T-OCPs were treated with P, R, T or R+T for 48 hr by which time mature OCs had formed (right panel). Total RNA was extracted to test mRNA expression of NFATc1 normalized to β-actin. **p < 0.01 vs. the respective PBS-treated cells. (C) M-OCPs were serum-starved for 2 hr followed by treatment of P, R or T in the presence of 10 μM MG-132 for 3 hr. Protein levels of RelB and β-actin were tested by Western blot. The data are the band levels measured densitometrically, normalized to β-actin.

doi:10.1371/journal.pone.0135728.g004

However, TNF did not induce $Ly6C^+Gr1^-$ cells from the RelB-/- $CD11b^+F4/80^+$ population (Fig 5B). Similarly, although the percentage of $CD11c^+$ cells in the $Ly6C^+Gr1^-$ and $Ly6C^-Gr1^-$ population of M-OCPs was higher (18% and 8.84%) in RelB-/- cells than in WT cells (2.98% and 4.55%) (Fig 5C), the frequency of $CD11c^+$ cells did not change (~12%) in $Ly6C^+Gr1^-$, but was reduced to 7.84% in $Ly6C^-Gr1^-$ cells from RelB-/- T-OCPs compared to their respective WT T-OCPs (12.4% and 20.6%). These data suggest that RelB is required for TNF induction of $Ly6C^+Gr1^-$ and $Ly6C^-Gr1^-CD11c^+$ cells and that the increase in $CD11c^+$ cells seen in RelB-/- mice in vivo is independent of TNF.

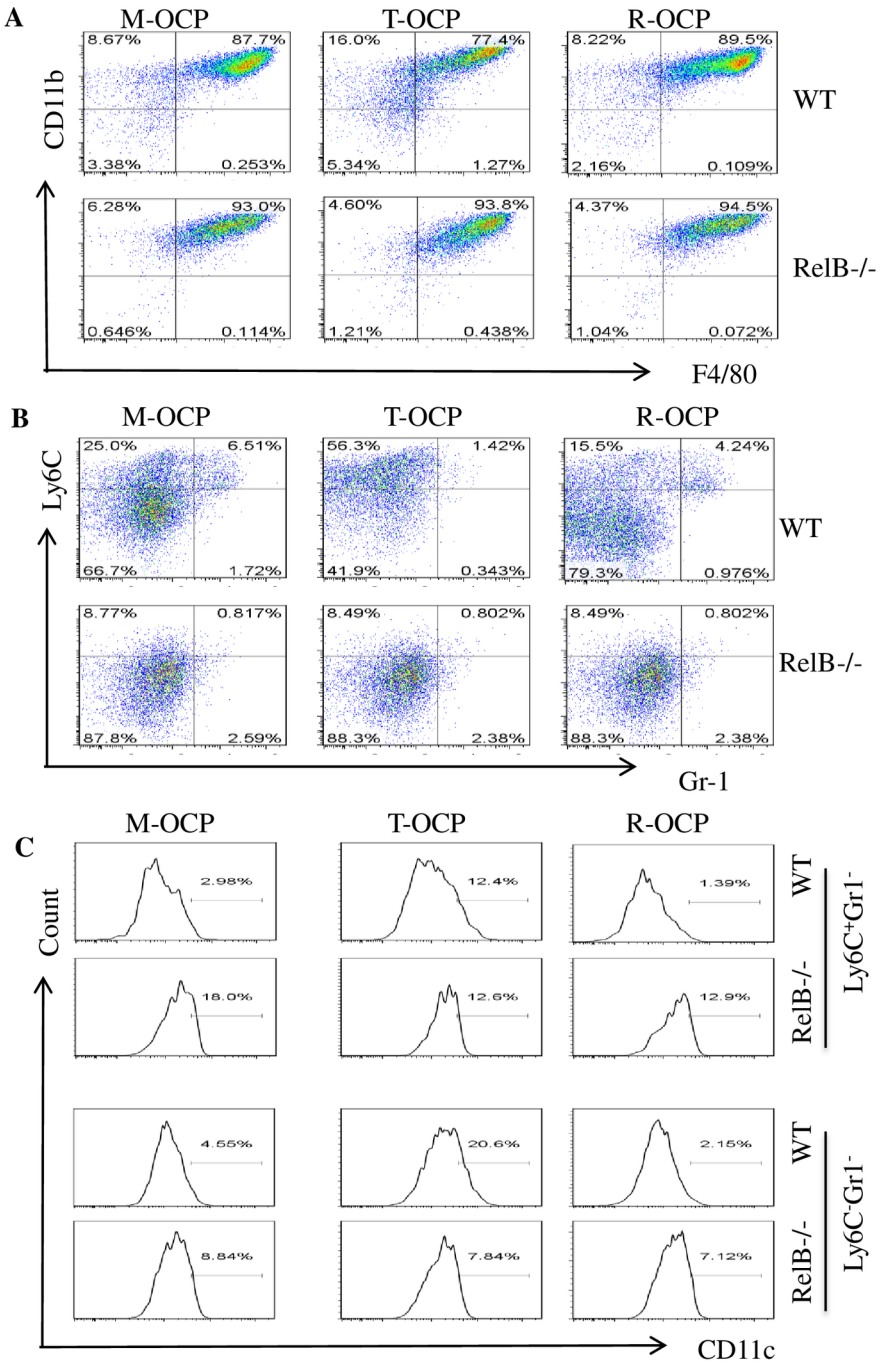

Fig 5. RelB deficiency prevents TNF-induced M1 macrophage differentiation. BMCs from 4-month-old RelB-/- and WT littermate mice were cultured to produce M-, R- and T-OCPs, as in Fig 1B. Cells were subjected to flow cytometry to analyze expression of CD11b and F4/80 (A), Ly6C and Gr1 cells in the $CD11b^{+}F4/80^{+}$ population (B), and $CD11c^{+}$ cells in the $Ly6C^{+}Gr1^{-}$ and $Ly6C^{-}Gr1^{-}$ populations (C), as in Fig 1B. The experiment was repeated twice with similar results.

doi:10.1371/journal.pone.0135728.g005

TNF inhibits RANKL-induced osteoclastogenesis from OCPs primed by M-CSF alone, but not by RANKL and TNF

TNF or RANKL alone induces terminal differentiation of OCPs primed by M-CSF [13, 37]. However, TNF induces significantly fewer osteoclasts than RANKL [16]. TNF increases levels of TNF receptor-associated factor 3 (TRAF3) in OCPs and this induces degradation of NF-κB-inducing kinase (NIK) leading to increased cytoplasmic levels of the inhibitory NF-κB protein, p100, and reduced RANKL- and TNF-induced OCP differentiation [13]. However, TNF also promotes RANKL expression by osteoblastic and other cells to enhance OC formation [20, 21]. To further investigate the conditions in which TNF stimulates or inhibits RANKL-induced OC formation, we cultured BM cells with M-CSF alone or in combination with RANKL or TNF for 2 days to generate M-, R- and T-OCPs, as in Fig 1B. The culture medium was replaced with freshly made medium containing M-CSF and the cells were then treated with TNF, RANKL or RANKL+TNF for an additional 48–60 hr to generate mature OCs. We found that TNF alone induced relatively small numbers of OCs and significantly inhibited RANKL-induced OC formation from M-OCPs (Fig 6A). TNF induced fewer OCs here than in our earlier reports [13, 16] because we stopped these experiments one day earlier to examine early events in OC formation (Fig 6B). In contrast, the numbers and area of OCs induced by TNF from R-OCPs almost matched those induced by RANKL (Fig 6B). The area of OCs induced by TNF+RANKL from R-OCPs was larger than that induced by RANKL alone ($p< 0.01$, but there was no difference in OC numbers (Fig 6B). Furthermore, RANKL induced more OCs (number and area) from R-OCPs than from M-OCPs (Fig 6B). Although the numbers of RANKL-induced OCs from T-OCPs were similar to those from M-OCPs, the total area of RANKL-induced OCs from T-OCPs was larger than that from M-OCPs ($p<0.01$), consistent with enhanced fusion. In addition, TNF did not inhibit RANKL-induced OC formation from T-OCPs, the number and area of RANKL+TNF-induced OCs being similar to those induced by RANKL alone (Fig 6B).

To further investigate the conditions in which TNF stimulates or inhibits RANKL-induced OC formation, we next tested mRNA expression levels of NFATc1, the master gene controlling terminal OC differentiation and maturation [38, 39], by real-time PCR. In general, the NFATc1 mRNA expression level matched the number of OCs (Fig 6C). After 4 hr of treatment, neither RANKL nor TNF changed NFATc1 mRNA expression levels (S2 Fig) in M-OCPs, but after 24 hr, RANKL increased NFATc1 mRNA expression by 13-fold. In contrast TNF increased NFATc1 expression by only 2-fold and significantly inhibited RANKL induction of its expression (S2 Fig). After 48 hr, the expression patterns of NFATc1 in mature OCs from M-OCPs in response to RANKL, TNF or RANKL+TNF (Fig 6C) were very similar to those at 24hr (S2 Fig). In contrast, TNF and RANKL+TNF induced similar levels of NFATc1 mRNA expression as RANKL alone in mature OCs from R-OCPs after 48 hr (Fig 6C). In addition, RANKL increased NFATc1 mRNA levels in OCs from T-OCPs significantly more than TNF (Fig 6C). However, the expression level of NFATc1 in OCs induced by RANKL from T-OCPs was only about half of that from M- or R-OCPs (Fig 6C). This may be due to the low basal expression level of NFATc1 in T-OCPs (PBS-treated cells). Of note, TNF did not inhibit RANKL-induced NFATc1 expression in T-OCPs (Fig 6C).

Biphasic effect of RelB on OC formation

The precise role of RelB in OC differentiation remains incompletely understood. For example, RANKL-induced OC formation from RelB-/- precursors is impaired in vitro, but the basal OC numbers in RelB-/- mice in vivo are normal [36]. To further investigate the role of RelB in OCP differentiation and OC formation, we over-expressed RelB in WT BM cells using a RelB retrovirus. GFP protein expression in pMX-GFP- and pMX-GFP-RelB retrovirus-infected cells

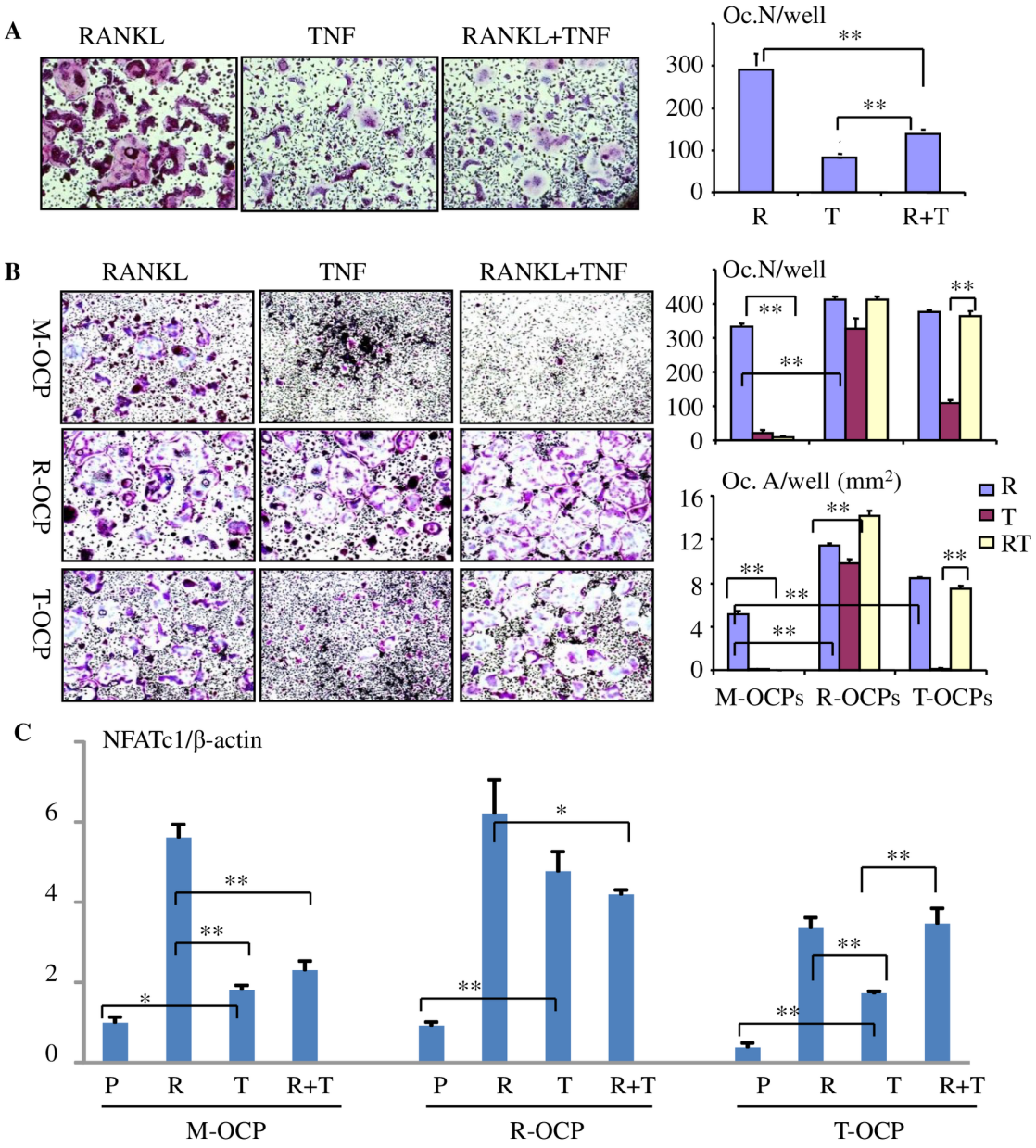

Fig 6. TNF inhibits RANKL-induced osteoclastogenesis from M-OCPs, but not from T-OCPs. (A) BMCs ($1x10^5$ per well) from 2-month-old C57Bl6 mice were cultured for M-OCPs in 96-well plates for 2 days, as in Fig 1B. R, T or both were added to the cultures for an additional 2.5 days to generate mature OCs. TRAP staining was performed to evaluate OC numbers, 4 wells per group (*p<0.05, **p<0.01). (B)&(C) BMCs ($1x10^5$ per well) from 3-month-old C57Bl6 mice were cultured for M-, R- and T-OCPs in 96-well plates for 2 days. RANKL, TNF or both were added for an additional 2 days in the presence of M-CSF to generate mature OCs. (B) The cells were fixed with 10% neutral buffered formalin for 10 min and TRAP staining was performed to evaluate OC numbers (N) and area (A), 4 wells per group (*p<0.05, **p<0.01). (C) Total RNA was extracted from mature OCs generated from M-, R- and T-OCPs treated with the above cytokines for 48 hr. NFATc1 mRNA expression was tested by real-time PCR normalized to β-actin, **p<0.01. The experiment was repeated twice with similar results.

doi:10.1371/journal.pone.0135728.g006

analyzed by flow cytometry and Western blot confirmed RelB over-expression (Fig 7A). We treated the infected cells with RANKL or TNF for 3 or 4 days and found that over-expression of RelB significantly decreased RANKL- but increased TNF-induced OC formation (number and area) after 3 days (Fig 7B). In contrast, after 4 days, the number and area of RANKL-

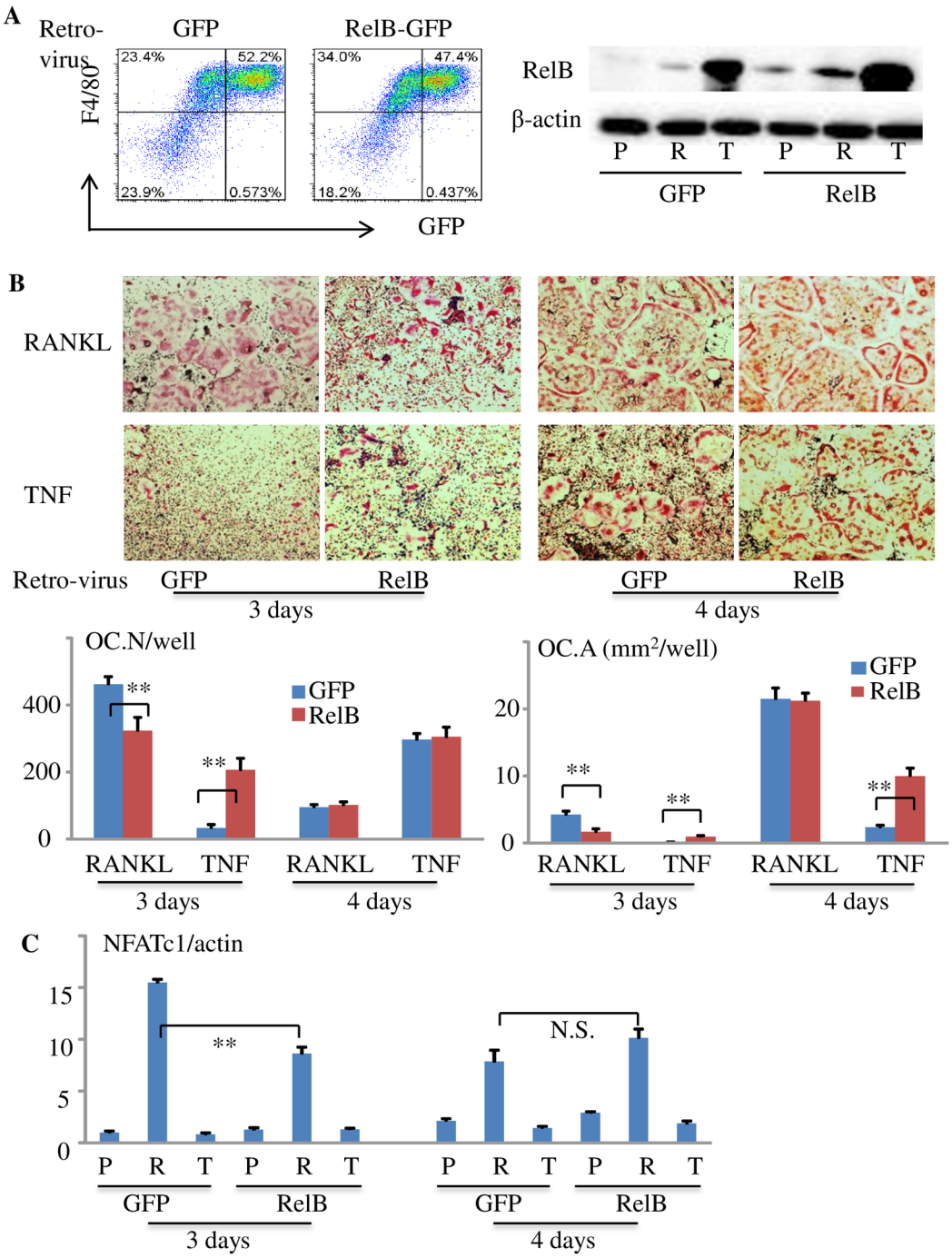

Fig 7. Over-expression of RelB inhibits RANKL-, but enhances TNF-induced OC differentiation. (A) BMCs from 3-month-old C57Bl6 mice were cultured with M-CSF for 2 days followed by treatment of ¼ volume of pMX-GFP or pMX-GFP-RelB retroviral supernatant in the presence of 2 ng/ml of polybrene for 3 days. $GFP^{+}F4/80^{+}$ cells were analyzed by flow cytometry (left panel) and RelB protein levels in GFP or RelB expressing cells that had been treated with P, R or T for 8 hr were tested by Western blot (right panel). (B) M-OCPs were infected with pMX-GFP or pMX-GFP-RelB retrovirus as above. After 24 hr of infection, the cells were treated with RANKL or TNF for 3 days or 4 days in the presence of M-CSF when mature OCs were observed under inverted microscopy. TRAP staining was performed to evaluate OC numbers and area, 4 wells per group, *p< 0.05, **p< 0.01. (C) M-OCPs were infected with GFP or GFP-RelB retrovirus and cultured with P, R or T for 3 or 4 days as above (B). Total RNA was extracted from these cells using Trizol reagent, and mRNA expression of NFATc1 normalized to β-actin was tested by real-time PCR. *p< 0.05, **p< 0.01 vs. GFP. The in vitro experiment was repeated twice with similar results.

doi:10.1371/journal.pone.0135728.g007

induced OCs were similar in GFP- and RelB-overexpressing cells, reflecting a plateau in OC formation, while OC area induced by TNF from RelB-overexpressing cells was still significantly larger than that from GFP-overexpressing cells, although OC numbers were similar (Fig 7B). We also tested NFATc1 mRNA expression in control and RelB retrovirus-infected M-OCPs treated with TNF or RANKL for 3 or 4 days. We found that TNF did not affect NFATc1 mRNA expression levels in either GFP- or RelB-infected cells. However, RANKL-induced NFATc1 mRNA levels in RelB overexpressing cells were significantly reduced compared to GFP-infected cells after 3 days, but not after 4 days, probably because mature OCs begin to die after 3–4 days (Fig 7C).

Discussion

M1 and M2 macrophages are linked to T helper 1 (TH1)- and TH2-type immune responses, respectively [33]. M1 macrophages mediate inflammatory responses to a variety of bacterial, protozoal and viral infections and produce many inflammatory cytokines, including TNF, IL-18, IL-12 and IL-23, which mediate immune reactions in several chronic inflammatory and autoimmune diseases, including rheumatoid arthritis, Crohn's disease, multiple sclerosis and autoimmune hepatitis [40–42]. M2 macrophages, in contrast, inhibit the production of a wide variety of pro-inflammatory mediators, such as IL-10, and regulate wound healing [43]. Thus, targeted depletion of M1 and boosting the activities of M2 macrophages are emerging as an attractive combined therapeutic strategy for autoimmune diseases [44–46]. Better understanding of the mechanisms that regulate M1/M2 differentiation should improve these therapeutic approaches and could lead to reduced joint destruction in inflammatory arthritides.

Granulocyte macrophage-colony stimulating factor (GM-CSF) drives myeloid progenitor differentiation into granulocytes and M1 monocyte/macrophages with a pro-inflammatory cytokine profile (e.g. TNF and IL-23 expression) and also into cells with dendritic cell (DC) properties, and thus it is often employed in studies of DC development and function [47, 48]. However, GM-CSF is not critical for macrophage development since mice lacking GM-CSF do not have notable defects in tissue macrophages [49]. In contrast, targeted ablation of M-CSF or its receptor causes severe depletion of macrophages in many tissues associated with failure of osteoclast formation and osteopetrosis, indicating that M-CSF plays a major role in the generation of macrophages [24].

Macrophages induced in response to M-CSF alone have an anti-inflammatory cytokine profile (e.g. IL-10 expression) and are similar to M2 macrophages [50]. In general, M2 macrophages switch to a M1 phenotype in response to IFN-γ and LPS and secrete large amounts of cytokines involved in autoimmune responses [22, 24, 33, 51]. We previously reported that TNF increases $CD11b^+Gr\text{-}1^{-/lo}$ OCP numbers by stimulating expression of the M-CSF receptor, c-fms [26], which has important roles in OCP proliferation [52], OC formation and survival [53]. However, it was not known if these are M1 or M2 macrophages or if the positive or negative regulatory effects of TNF on OC formation involve modulation of M1/M2 differentiation. Here, we have shown that TNF promotes a switch of M-CSF-induced $F4/80^+CD11b^{+-}$ $Ly6C^-Gr1^-$ M2 to $F4/80^+CD11b^+Ly6C^+Gr1^-$ and $F4/80^+CD11b^+Ly6C^-Gr1^-CD11c^+$ M1 macrophages based on our findings that: 1) the $Ly6C^+$ $Gr1^-$ cells comprise 50–63% of $CD11b^+F4/80^+$ from T-OCPs and only 17–25% from M-OCPs; and in contrast, $Ly6C^-Gr1^-$ cells comprise 34–47% of the $CD11b^+F4/80^+$ T-OCPs compared to 67–78% of these cells from M-OCPs (Figs 1B, 2A, 3A and 5B); 2) $CD11c^+$ cells in both $Ly6C^+Gr1^-$ and $Ly6C^-Gr1^-$ populations from T-OCPs are also increased compared to the respective populations from M-OCPs (Figs 1B and 5B); and 3) importantly, $Ly6C^+Gr1^-$ cells from both M- and T-OCPs have increased expression of the M1 marker genes, iNOS, TNF, IL-1β and TGFβ1, compared to $Ly6C^-$ $Gr1^-$ cells. $Ly6C^-Gr1^-$

cells from T-OCPs also have increased expression of iNOS and TGFβ1 compared to those from M-OCPs, and both $Ly6C^+Gr1^-$ and $Ly6C^-Gr1^-$ cells from T-OCPs have decreased expression of the M2 genes, IL-10 and PPAR-γ (Fig 3B).

A switch from a M2 to a M1 phenotype can also change the OC forming potential of these cells. For example, Raw264.7 cells, a murine macrophage cell line that can differentiate into OCs in response to RANKL without the need to add M-CSF, have enhanced OC forming potential when they are induced to a M1 phenotype by IFN-γ and LPS [54]. We found that only $Ly6C^+Gr1^-$ M1 cells, but not $Ly6C^-Gr1^-$ M2 cells in the $CD11b^+F4/80^+$ population from M-OCPs formed OCs in response to RANKL. Thus, $CD11b^+F4/80^+Ly6C^+Gr1^-$ M1 macrophages are authentic OCPs. However, both $Ly6C^+Gr1^-$ and $Ly6C^-Gr1^-$ cells primed by TNF have significantly enhanced OC forming potential, and both cell populations have increased expression of the M1 surface marker, CD11c, and express the M1 effector molecules, iNOS, TGFβ1 and IL-1β, suggesting that these cells have been switched to a M1 phenotype. In addition, TNF-primed $Ly6C^{+/-}Gr1^+CD11b^+F4/80^+$ cells form OCs in response to RANKL, although the numbers are small. This population could be similar to our previously identified $CD11b^+Gr1^{+/-}$ OCPs in TNF-Tg mice [26]. With all of these features, it is not surprising that TNF did not inhibit RANKL-induced OC formation from TNF-primed OCPs. Robust induction of OC formation by TNF from RANKL-primed OCPs probably reflects the fact that these cells are already well along the OC differentiation process since NFATc1 expression was significantly increased within 24 hours of RANKL treatment [16].

In general, the transcription factor, PU.1, controls the global macrophage-specific enhancer repertoire, irrespective of polarization [55]. In response to M1-inducing stimuli, transcription factors, signal transducer and activator of transcription 1 (STAT1) and interferon-regulatory factor 5 (IRF5) are activated to polarize M1 macrophages [55], while factors that activate STAT6, IRF4 and peroxisome proliferator activated receptor-γ (PPAR-γ) control the polarization of M2 macrophages [55]. NF-κB p50 and p65 have been identified as regulators of macrophage polarization and cytokine production [56, 57]. p50 is considered as a key component in the orchestration of M2-driven inflammatory reactions. It inhibits M1-polarization and IFN-β production, and p50-deficient mice show exacerbated M1-driven inflammation and defective capacity to mount allergy-driven M2-polarized inflammatory reactions [57]. Similarly, transfection of p50 siRNA into M2-like macrophages resulted in a significant decrease in expression of the M2 marker, IL-10, and increased production of the M1 markers, IL-12, TNF-α and IL-6 [58]. Hyperacetylated p65 and increased NF-κB binding activity in bone marrow cells with targeted deletion of mammalian sirtuin member 1 (SIRT1) in myeloid cells resulted in increased M1 polarization, migration, and pro-inflammatory cytokine production, suggesting that p65 also plays an important role in M1 activation [56]. Here, we report a novel mechanism by which TNF induction of M1 macrophages is through NF-κB RelB, based on our findings that TNF significantly increased RelB protein levels associated with switching of M-CSF-induced $Ly6C^-Gr1^-CD11c^-$ M2 to $Ly6C^+Gr1^-$ and $Ly6C^-Gr1^-CD11c^+$ M1 $F4/80^+CD11b^+$ macrophages, while TNF induction of $Ly6C^+Gr1^-$ and $Ly6C^-Gr1^-CD11c^+$ M1 macrophages does not occur in RelB-/- bone marrow cells (Fig 5).

The role of RelB in OC differentiation is also poorly understood. OC numbers in the bones of RelB-/- mice are normal in vivo, while RANKL-induced OC formation from RelB-/- myeloid progenitors is impaired in vitro, and cancer-induced osteolysis is reduced in RelB-/- mice in vivo [26]. These findings suggest that RelB is not required for basal OC formation, but appears to play a positive role in the enhanced osteoclastogenesis in pathologic conditions. Contrary to the reported positive role for RelB in OC differentiation [26], we found that RelB itself functions as a transcriptional repressor of NFATc1 to inhibit terminal OC differentiation based on our findings that: 1) TNF inhibits RANKL-induced OC formation and NFATc1 mRNA

expression in M-CSF-primed OCPs; and 2) over-expression of RelB significantly inhibits RANKL-induced OC formation and NFATc1 mRNA expression. These are consistent with the reports that RelB acts as a transcriptional repressor of inflammatory mediators by forming an inactive complex with RelA [59–62]. TNF induction of RelB to inhibit NFATc1 activation could explain why TNF alone can significantly increase OCPs numbers through M2 to M1 switching, while having very limited ability to induce terminal OCP differentiation into OCs. In contrast, RANKL strikingly increases OC formation from TNF-primed OCPs compared to OCPs induced by M-CSF alone since it can efficiently degrade RelB protein, resulting in sustained activation of NFATc1 to promote OC formation. Although over-expression of RelB can significantly enhance TNF-induced OC formation, this effect is still lower than that of RANKL since it peaks one day later than that of RANKL. Thus, the ability of TNF alone to induce terminal OC differentiation in physiological and pathologic conditions is limited.

In summary, our findings provide further evidence of positive and negative effects of TNF on OC formation through its induction of RelB. TNF induction of RelB in OCPs limits OC differentiation in the absence of other stimulators and it also directly limits RANKL-induced OC formation by inhibiting NFATc1 activation. However, TNF-induced RelB also directly mediates terminal OC differentiation independently of NFATc1. Our findings show that the dominant role of TNF is to expand the pool of OCPs with enhanced OC forming potential by switching the differentiation of M-CSF-induced M2 resident to M1 inflammatory macrophages. Thus, strategies to degrade RelB could reverse the differentiation of TNF-induced M1 to M2 macrophages and would represent a novel therapeutic approach for inflammatory arthritides.

Supporting Information

S1 Fig. TNF-induced OCPs have reduced frequency of $CD11b^{+}F4/80^{+}$ macrophages.
(TIFF)

S2 Fig. TNF inhibits RANKL-induced NFATc1 mRNA expression.
(TIFF)

Author Contributions

Conceived and designed the experiments: ZY. Performed the experiments: ZZ XY XH YL RD ZY. Analyzed the data: ZZ XH ZY. Contributed reagents/materials/analysis tools: BFB ZY. Wrote the paper: ZY BFB.

References

1. Storheim K, Zwart JA. Musculoskeletal disorders and the Global Burden of Disease study. Annals of the rheumatic diseases. 2014; 73(6):949–50. doi: 10.1136/annrheumdis-2014-205327 PMID: 24790065.
2. Keffer J, Probert L, Cazlaris H, Georgopoulos S, Kaslaris E, Kioussis D, et al. Transgenic mice expressing human tumour necrosis factor: a predictive genetic model of arthritis. The EMBO journal. 1991; 10 (13):4025–31. PMID: 1721867; PubMed Central PMCID: PMC453150.
3. Hyrich KL, Watson KD, Silman AJ, Symmons DP, British Society for Rheumatology Biologics R. Predictors of response to anti-TNF-alpha therapy among patients with rheumatoid arthritis: results from the British Society for Rheumatology Biologics Register. Rheumatology. 2006; 45(12):1558–65. doi: 10.1093/rheumatology/kel149 PMID: 16705046.
4. Symmons DP, Silman AJ. The world of biologics. Lupus. 2006; 15(3):122–6. PMID: 16634363.
5. Hodge JM, Kirkland MA, Nicholson GC. Multiple roles of M-CSF in human osteoclastogenesis. Journal of cellular biochemistry. 2007; 102(3):759–68. PMID: 17516513.
6. Abu-Amer Y, Abbas S, Hirayama T. TNF receptor type 1 regulates RANK ligand expression by stromal cells and modulates osteoclastogenesis. Journal of cellular biochemistry. 2004; 93(5):980–9. PMID: 15389885.

7. Wei S, Kitaura H, Zhou P, Ross FP, Teitelbaum SL. IL-1 mediates TNF-induced osteoclastogenesis. The Journal of clinical investigation. 2005; 115(2):282–90. doi: 10.1172/JCI23394 PMID: 15668736; PubMed Central PMCID: PMC544608.
8. Franzoso G, Carlson L, Xing L, Poljak L, Shores EW, Brown KD, et al. Requirement for NF-kappaB in osteoclast and B-cell development. Genes & development. 1997; 11(24):3482–96. PMID: 9407039; PubMed Central PMCID: PMC316809.
9. Redlich K, Hayer S, Maier A, Dunstan CR, Tohidast-Akrad M, Lang S, et al. Tumor necrosis factor alpha-mediated joint destruction is inhibited by targeting osteoclasts with osteoprotegerin. Arthritis and rheumatism. 2002; 46(3):785–92. PMID: 11920416.
10. Redlich K, Hayer S, Ricci R, David JP, Tohidast-Akrad M, Kollias G, et al. Osteoclasts are essential for TNF-alpha-mediated joint destruction. The Journal of clinical investigation. 2002; 110(10):1419–27. doi: 10.1172/JCI15582 PMID: 12438440; PubMed Central PMCID: PMC151809.
11. Ferrari-Lacraz S, Ferrari S. Do RANKL inhibitors (denosumab) affect inflammation and immunity? Osteoporos Int. 2011; 22(2):435–46. doi: 10.1007/s00198-010-1326-y PMID: 20571772.
12. Kim N, Kadono Y, Takami M, Lee J, Lee SH, Okada F, et al. Osteoclast differentiation independent of the TRANCE-RANK-TRAF6 axis. The Journal of experimental medicine. 2005; 202(5):589–95. doi: 10.1084/jem.20050978 PMID: 16147974; PubMed Central PMCID: PMC2212875.
13. Yao Z, Xing L, Boyce BF. NF-kappaB p100 limits TNF-induced bone resorption in mice by a TRAF3-dependent mechanism. The Journal of clinical investigation. 2009; 119(10):3024–34. doi: 10.1172/JCI38716 PMID: 19770515; PubMed Central PMCID: PMC2752069.
14. Takai H, Kanematsu M, Yano K, Tsuda E, Higashio K, Ikeda K, et al. Transforming growth factor-beta stimulates the production of osteoprotegerin/osteoclastogenesis inhibitory factor by bone marrow stromal cells. The Journal of biological chemistry. 1998; 273(42):27091–6. PMID: 9765225.
15. Tang SY, Alliston T. Regulation of postnatal bone homeostasis by TGFbeta. BoneKEy reports. 2013; 2:255. doi: 10.1038/bonekey.2012.255 PMID: 24404376; PubMed Central PMCID: PMC3722719.
16. Yamashita T, Yao Z, Li F, Zhang Q, Badell IR, Schwarz EM, et al. NF-kappaB p50 and p52 regulate receptor activator of NF-kappaB ligand (RANKL) and tumor necrosis factor-induced osteoclast precursor differentiation by activating c-Fos and NFATc1. The Journal of biological chemistry. 2007; 282(25):18245–53. doi: 10.1074/jbc.M610701200 PMID: 17485464.
17. Li J, Sarosi I, Yan XQ, Morony S, Capparelli C, Tan HL, et al. RANK is the intrinsic hematopoietic cell surface receptor that controls osteoclastogenesis and regulation of bone mass and calcium metabolism. Proceedings of the National Academy of Sciences of the United States of America. 2000; 97(4):1566–71. PMID: 10677500; PubMed Central PMCID: PMC26475.
18. Zhao B, Grimes SN, Li S, Hu X, Ivashkiv LB. TNF-induced osteoclastogenesis and inflammatory bone resorption are inhibited by transcription factor RBP-J. The Journal of experimental medicine. 2012; 209(2):319–34. doi: 10.1084/jem.20111566 PMID: 22249448; PubMed Central PMCID: PMC3280875.
19. Zhao B, Takami M, Yamada A, Wang X, Koga T, Hu X, et al. Interferon regulatory factor-8 regulates bone metabolism by suppressing osteoclastogenesis. Nature medicine. 2009; 15(9):1066–71. doi: 10.1038/nm.2007 PMID: 19718038; PubMed Central PMCID: PMC2755267.
20. Lam J, Takeshita S, Barker JE, Kanagawa O, Ross FP, Teitelbaum SL. TNF-alpha induces osteoclastogenesis by direct stimulation of macrophages exposed to permissive levels of RANK ligand. The Journal of clinical investigation. 2000; 106(12):1481–8. doi: 10.1172/JCI11176 PMID: 11120755; PubMed Central PMCID: PMC387259.
21. Zhang YH, Heulsmann A, Tondravi MM, Mukherjee A, Abu-Amer Y. Tumor necrosis factor-alpha (TNF) stimulates RANKL-induced osteoclastogenesis via coupling of TNF type 1 receptor and RANK signaling pathways. The Journal of biological chemistry. 2001; 276(1):563–8. doi: 10.1074/jbc.M008198200 PMID: 11032840.
22. Gordon S. The macrophage: past, present and future. European journal of immunology. 2007; 37 Suppl 1:S9–17. PMID: 17972350.
23. Gordon S, Taylor PR. Monocyte and macrophage heterogeneity. Nature reviews Immunology. 2005; 5(12):953–64. doi: 10.1038/nri1733 PMID: 16322748.
24. Wynn TA, Chawla A, Pollard JW. Macrophage biology in development, homeostasis and disease. Nature. 2013; 496(7446):445–55. doi: 10.1038/nature12034 PMID: 23619691; PubMed Central PMCID: PMC3725458.
25. Comstock KL, Krown KA, Page MT, Martin D, Ho P, Pedraza M, et al. LPS-induced TNF-alpha release from and apoptosis in rat cardiomyocytes: obligatory role for CD14 in mediating the LPS response. Journal of molecular and cellular cardiology. 1998; 30(12):2761–75. PMID: 9990546.
26. Yao Z, Li P, Zhang Q, Schwarz EM, Keng P, Arbini A, et al. Tumor necrosis factor-alpha increases circulating osteoclast precursor numbers by promoting their proliferation and differentiation in the bone

marrow through up-regulation of c-Fms expression. The Journal of biological chemistry. 2006; 281 (17):11846–55. doi: 10.1074/jbc.M512624200 PMID: 16461346.

27. Yoshida H, Hayashi S, Kunisada T, Ogawa M, Nishikawa S, Okamura H, et al. The murine mutation osteopetrosis is in the coding region of the macrophage colony stimulating factor gene. Nature. 1990; 345(6274):442–4. doi: 10.1038/345442a0 PMID: 2188141.

28. Burkly L, Hession C, Ogata L, Reilly C, Marconi LA, Olson D, et al. Expression of relB is required for the development of thymic medulla and dendritic cells. Nature. 1995; 373(6514):531–6. doi: 10.1038/373531a0 PMID: 7845467.

29. Elewaut D, Shaikh RB, Hammond KJ, De Winter H, Leishman AJ, Sidobre S, et al. NIK-dependent RelB activation defines a unique signaling pathway for the development of V alpha 14i NKT cells. The Journal of experimental medicine. 2003; 197(12):1623–33. doi: 10.1084/jem.20030141 PMID: 12810685; PubMed Central PMCID: PMC2193960.

30. Yao Z, Li Y, Yin X, Dong Y, Xing L, Boyce BF. NF-kappaB RelB negatively regulates osteoblast differentiation and bone formation. Journal of bone and mineral research: the official journal of the American Society for Bone and Mineral Research. 2014; 29(4):866–77. PMID: 24115294; PubMed Central PMCID: PMC3961566.

31. Yao Z, Xing L, Qin C, Schwarz EM, Boyce BF. Osteoclast precursor interaction with bone matrix induces osteoclast formation directly by an interleukin-1-mediated autocrine mechanism. The Journal of biological chemistry. 2008; 283(15):9917–24. doi: 10.1074/jbc.M706415200 PMID: 18250170; PubMed Central PMCID: PMC2442286.

32. Yona S, Jung S. Monocytes: subsets, origins, fates and functions. Current opinion in hematology. 2010; 17(1):53–9. PMID: 19770654.

33. Mosser DM, Edwards JP. Exploring the full spectrum of macrophage activation. Nature reviews Immunology. 2008; 8(12):958–69. doi: 10.1038/nri2448 PMID: 19029990; PubMed Central PMCID: PMC2724991.

34. Sun SC. The noncanonical NF-kappaB pathway. Immunological reviews. 2012; 246(1):125–40. PMID: 22435551; PubMed Central PMCID: PMC3313452.

35. Vallabhapurapu S, Matsuzawa A, Zhang W, Tseng PH, Keats JJ, Wang H, et al. Nonredundant and complementary functions of TRAF2 and TRAF3 in a ubiquitination cascade that activates NIK-dependent alternative NF-kappaB signaling. Nature immunology. 2008; 9(12):1364–70. doi: 10.1038/ni.1678 PMID: 18997792; PubMed Central PMCID: PMC2671996.

36. Vaira S, Johnson T, Hirbe AC, Alhawagri M, Anwisye I, Sammut B, et al. RelB is the NF-kappaB subunit downstream of NIK responsible for osteoclast differentiation. Proceedings of the National Academy of Sciences of the United States of America. 2008; 105(10):3897–902. doi: 10.1073/pnas.0708576105 PMID: 18322009; PubMed Central PMCID: PMC2268780.

37. Kobayashi K, Takahashi N, Jimi E, Udagawa N, Takami M, Kotake S, et al. Tumor necrosis factor alpha stimulates osteoclast differentiation by a mechanism independent of the ODF/RANKL-RANK interaction. The Journal of experimental medicine. 2000; 191(2):275–86. PMID: 10637272; PubMed Central PMCID: PMC2195746.

38. Takayanagi H. The role of NFAT in osteoclast formation. Annals of the New York Academy of Sciences. 2007; 1116:227–37. PMID: 18083930.

39. Takayanagi H, Kim S, Koga T, Nishina H, Isshiki M, Yoshida H, et al. Induction and activation of the transcription factor NFATc1 (NFAT2) integrate RANKL signaling in terminal differentiation of osteoclasts. Developmental cell. 2002; 3(6):889–901. PMID: 12479813.

40. Murphy CA, Langrish CL, Chen Y, Blumenschein W, McClanahan T, Kastelein RA, et al. Divergent pro- and antiinflammatory roles for IL-23 and IL-12 in joint autoimmune inflammation. The Journal of experimental medicine. 2003; 198(12):1951–7. doi: 10.1084/jem.20030896 PMID: 14662908; PubMed Central PMCID: PMC2194162.

41. Smith AM, Rahman FZ, Hayee B, Graham SJ, Marks DJ, Sewell GW, et al. Disordered macrophage cytokine secretion underlies impaired acute inflammation and bacterial clearance in Crohn's disease. The Journal of experimental medicine. 2009; 206(9):1883–97. doi: 10.1084/jem.20091233 PMID: 19652016; PubMed Central PMCID: PMC2737162.

42. Kaneki H, Guo R, Chen D, Yao Z, Schwarz EM, Zhang YE, et al. Tumor necrosis factor promotes Runx2 degradation through up-regulation of Smurf1 and Smurf2 in osteoblasts. The Journal of biological chemistry. 2006; 281(7):4326–33. doi: 10.1074/jbc.M509430200 PMID: 16373342; PubMed Central PMCID: PMC2647592.

43. Murai M, Turovskaya O, Kim G, Madan R, Karp CL, Cheroutre H, et al. Interleukin 10 acts on regulatory T cells to maintain expression of the transcription factor Foxp3 and suppressive function in mice with colitis. Nature immunology. 2009; 10(11):1178–84. doi: 10.1038/ni.1791 PMID: 19783988; PubMed Central PMCID: PMC2898179.

44. Leuschner F, Dutta P, Gorbatov R, Novobrantseva TI, Donahoe JS, Courties G, et al. Therapeutic siRNA silencing in inflammatory monocytes in mice. Nature biotechnology. 2011; 29(11):1005–10. doi: 10.1038/nbt.1989 PMID: 21983520; PubMed Central PMCID: PMC3212614.

45. Li J, Hsu HC, Mountz JD. Managing macrophages in rheumatoid arthritis by reform or removal. Current rheumatology reports. 2012; 14(5):445–54. doi: 10.1007/s11926-012-0272-4 PMID: 22855296; PubMed Central PMCID: PMC3638732.

46. Li J, Hsu HC, Yang P, Wu Q, Li H, Edgington LE, et al. Treatment of arthritis by macrophage depletion and immunomodulation: testing an apoptosis-mediated therapy in a humanized death receptor mouse model. Arthritis and rheumatism. 2012; 64(4):1098–109. PMID: 22006294; PubMed Central PMCID: PMC3596268.

47. Jackson SH, Alicea C, Owens JW, Eigsti CL, Malech HL. Characterization of an early dendritic cell precursor derived from murine lineage-negative hematopoietic progenitor cells. Experimental hematology. 2002; 30(5):430–9. PMID: 12031649.

48. Schmid MA, Kingston D, Boddupalli S, Manz MG. Instructive cytokine signals in dendritic cell lineage commitment. Immunological reviews. 2010; 234(1):32–44. PMID: 20193010.

49. Pollard JW. Trophic macrophages in development and disease. Nature reviews Immunology. 2009; 9 (4):259–70. doi: 10.1038/nri2528 PMID: 19282852; PubMed Central PMCID: PMC3648866.

50. Sierra-Filardi E, Vega MA, Sanchez-Mateos P, Corbi AL, Puig-Kroger A. Heme Oxygenase-1 expression in M-CSF-polarized M2 macrophages contributes to LPS-induced IL-10 release. Immunobiology. 2010; 215(9–10):788–95. doi: 10.1016/j.imbio.2010.05.020 PMID: 20580464.

51. Ginhoux F, Jung S. Monocytes and macrophages: developmental pathways and tissue homeostasis. Nature reviews Immunology. 2014; 14(6):392–404. doi: 10.1038/nri3671 PMID: 24854589.

52. Mizoguchi T, Muto A, Udagawa N, Arai A, Yamashita T, Hosoya A, et al. Identification of cell cycle-arrested quiescent osteoclast precursors in vivo. The Journal of cell biology. 2009; 184(4):541–54. doi: 10.1083/jcb.200806139 PMID: 19237598; PubMed Central PMCID: PMC2654120.

53. Marks SC Jr., Seifert MF. The lifespan of osteoclasts: experimental studies using the giant granule cytoplasmic marker characteristic of beige mice. Bone. 1985; 6(6):451–5. PMID: 3006733

54. Jeganathan S, Fiorino C, Naik U, Sun HS, Harrison RE. Modulation of osteoclastogenesis with macrophage M1- and M2-inducing stimuli. PloS one. 2014; 9(8):e104498. doi: 10.1371/journal.pone.0104498 PMID: 25101660; PubMed Central PMCID: PMC4125219.

55. Lawrence T, Natoli G. Transcriptional regulation of macrophage polarization: enabling diversity with identity. Nature reviews Immunology. 2011; 11(11):750–61. doi: 10.1038/nri3088 PMID: 22025054.

56. Hah YS, Cheon YH, Lim HS, Cho HY, Park BH, Ka SO, et al. Myeloid deletion of SIRT1 aggravates serum transfer arthritis in mice via nuclear factor-kappaB activation. PloS one. 2014; 9(2):e87733. doi: 10.1371/journal.pone.0087733 PMID: 24498364; PubMed Central PMCID: PMC3912001.

57. Porta C, Rimoldi M, Raes G, Brys L, Ghezzi P, Di Liberto D, et al. Tolerance and M2 (alternative) macrophage polarization are related processes orchestrated by p50 nuclear factor kappaB. Proceedings of the National Academy of Sciences of the United States of America. 2009; 106(35):14978–83. doi: 10.1073/pnas.0809784106 PMID: 19706447; PubMed Central PMCID: PMC2736429.

58. Kono Y, Kawakami S, Higuchi Y, Yamashita F, Hashida M. In vitro evaluation of inhibitory effect of nuclear factor-kappaB activity by small interfering RNA on pro-tumor characteristics of M2-like macrophages. Biological & pharmaceutical bulletin. 2014; 37(1):137–44. PMID: 24141263.

59. Marienfeld R, May MJ, Berberich I, Serfling E, Ghosh S, Neumann M. RelB forms transcriptionally inactive complexes with RelA/p65. The Journal of biological chemistry. 2003; 278(22):19852–60. doi: 10.1074/jbc.M301945200 PMID: 12657634.

60. Kiebala M, Polesskaya O, Yao Z, Perry SW, Maggirwar SB. Nuclear factor-kappa B family member RelB inhibits human immunodeficiency virus-1 Tat-induced tumor necrosis factor-alpha production. PloS one. 2010; 5(7):e11875. doi: 10.1371/journal.pone.0011875 PMID: 20686703; PubMed Central PMCID: PMC2912378.

61. Madge LA, May MJ. The NFkappaB paradox: RelB induces and inhibits gene expression. Cell cycle. 2011; 10(1):6–7. PMID: 21191180.

62. Overgaard M, Borch J, Gerdes K. RelB and RelE of Escherichia coli form a tight complex that represses transcription via the ribbon-helix-helix motif in RelB. Journal of molecular biology. 2009; 394(2):183–96. doi: 10.1016/j.jmb.2009.09.006 PMID: 19747491; PubMed Central PMCID: PMC2812701.

Mechanisms of Signal Transduction:

NF-κB p50 and p52 Regulate Receptor Activator of NF- κB Ligand (RANKL) and Tumor Necrosis Factor-induced Osteoclast Precursor Differentiation by Activating c-Fos and NFATc1

Teruhito Yamashita, Zhenqiang Yao, Fang Li, Qian Zhang, I. Raul Badell, Edward M. Schwarz, Sunao Takeshita, Erwin F. Wagner, Masaki Noda, Koichi Matsuo, Lianping Xing and Brendan F. Boyce

J. Biol. Chem. 2007, 282:18245-18253.
doi: 10.1074/jbc.M610701200 originally published online May 7, 2007

THE JOURNAL OF BIOLOGICAL CHEMISTRY VOL. 282, NO. 25, pp. 18245–18253, June 22, 2007

NF-κB p50 and p52 Regulate Receptor Activator of NF-κB Ligand (RANKL) and Tumor Necrosis Factor-induced Osteoclast Precursor Differentiation by Activating c-Fos and NFATc1*

Received for publication, November 17, 2006, and in revised form, May 2, 2007 Published, JBC Papers in Press, May 7, 2007, DOI 10.1074/jbc.M610701200

Teruhito Yamashita[‡1], Zhenqiang Yao[‡1], Fang Li[‡], Qian Zhang[‡], I. Raul Badell[‡], Edward M. Schwarz[§], Sunao Takeshita[¶], Erwin F. Wagner[‖], Masaki Noda[**], Koichi Matsuo[‡‡], Lianping Xing[‡§], and Brendan F. Boyce[‡§2]

From the [‡]Department of Pathology and Laboratory Medicine and [§]Center for Musculoskeletal Research, University of Rochester Medical Center, Rochester, New York 14642, the [¶]Department of Bone and Joint Disease, Research Institute, National Center for Geriatrics and Gerontology, Obu 474-8522, Japan, the [‖]Research Institute of Molecular Pathology, A-1030 Vienna, Austria, the [**]Tokyo Medical and Dental University, Tokyo 101-0062, Japan, and the [‡‡]Department of Microbiology and Immunology, School of Medicine, Keio University, Tokyo 160-8582, Japan

Postmenopausal osteoporosis and rheumatoid joint destruction result from increased osteoclast formation and bone resorption induced by receptor activator of NF-κB ligand (RANKL) and tumor necrosis factor (TNF). Osteoclast formation induced by these cytokines requires NF-κB p50 and p52, c-Fos, and NFATc1 expression in osteoclast precursors. c-Fos induces NFATc1, but the relationship between NF-κB and these other transcription factors in osteoclastogenesis remains poorly understood. We report that RANKL and TNF can induce osteoclast formation directly from NF-κB p50/p52 double knockout (dKO) osteoclast precursors when either c-Fos or NFATc1 is expressed. RANKL- or TNF-induced c-Fos up-regulation and activation are abolished in dKO cells and in wild-type cells treated with an NF-κB inhibitor. c-Fos expression requires concomitant RANKL or TNF treatment to induce NFATc1 activation in the dKO cells. Furthermore, c-Fos expression increases the number and resorptive capacity of wild-type osteoclasts induced by TNF *in vitro*. We conclude that NF-κB controls early osteoclast differentiation from precursors induced directly by RANKL and TNF, leading to activation of c-Fos followed by NFATc1. Inhibition of NF-κB should prevent RANKL- and TNF-induced bone resorption.

Osteoclasts are specialized bone-resorbing cells derived from multipotent myeloid progenitor cells. They play a crucial homeostatic role in skeletal modeling and remodeling and destroy bone in many pathologic conditions (1, 2). Understanding of the regulation of osteoclast formation, activation, and survival has increased dramatically in recent years following the identification of osteoprotegerin and of receptor activator of NF-κB (RANK)[3] and its ligand, RANKL (3–5). RANKL is a member of the TNF superfamily (6, 7). It is expressed by a variety of cell types, particularly osteoblast/stromal cells, and its expression by these cells increases in response to a variety of factors, including cytokines, growth factors, and hormones, to induce osteoclast formation, activation, and survival in normal and disease states (2, 8, 9). Osteoprotegerin is a decoy receptor for RANKL that negatively regulates bone resorption by binding to RANKL, and thus, preventing it binding to RANK on osteoclasts or their precursors. Thus, in many circumstances, osteoclast formation is regulated indirectly by accessory cells.

In addition to passively responding to RANKL, osteoclasts also actively regulate their own formation, activation, and survival, both positively and negatively. For example, they produce both ligands (10, 11) and receptors (12–14) for positive regulatory cytokines, such as TNF and interleukin-1, as well as for interferon-β, which negatively regulates their formation (15, 16). TNF has been implicated in postmenopausal and inflammation-associated bone loss mainly by inducing expression of RANKL (8, 17) and macrophage colony-stimulating factor (M-CSF) (18, 19) by accessory cells. By this mechanism, these cytokines indirectly increase osteoclastogenesis. In addition, TNF increases expression of RANK and c-Fms on the surface of osteoclast precursors to amplify RANKL and M-CSF signaling (20, 21). TNF also induces activation of the transcription factors NF-κB, AP-1, and nuclear factor of activated T cells c1 (NFATc1, also known as NFAT2) in osteoclast precursors (reviewed in Refs. 1 and 22, 23), thereby directly controlling the differentiation of these precursors to osteoclasts (24–27).

NF-κB, AP-1 and NFATc1 are essential for RANKL-induced osteoclastogenesis (28–31) and are activated downstream in the RANKL/RANK signaling pathway to induce a variety of responses in osteoclast precursors (29, 32). c-Fos, a component of the dimeric transcription factor, AP-1 (reviewed by Karsenty

* This work is supported by National Institutes of Health Grants AR43510 (to B. F. B.) and AR48697 (to L. X.). The costs of publication of this article were defrayed in part by the payment of page charges. This article must therefore be hereby marked "*advertisement*" in accordance with 18 U.S.C. Section 1734 solely to indicate this fact.

[1] These authors contributed equally to the work.

[2] To whom correspondence should be addressed: Dept. of Pathology and Laboratory Medicine, 601 Elmwood Ave., Box 626, Rochester, NY 14642. Tel.: 585-275-5837; Fax: 585-273-3637; E-mail: Brendan_Boyce@urmc.rochester.edu.

[3] The abbreviations used are: RANK, receptor activator of NF-κB; RANKL, RANK ligand; TNF, tumor necrosis factor; dKO, double knock-out; WT, wild type; M-CSF, macrophage colony-stimulating factor; MDS, M-CSF-dependent splenocytes; GFP, green fluorescent protein; RT, reverse transcription; NFAT, nuclear factor of activated T cells; PBS, phosphate-buffered saline; EMSA, electrophoretic mobility shift assay.

and Wagner (23)), mediates RANKL stimulation of osteoclast formation by transcriptionally inducing NFATc1 (29, 33). NFATc1 is a member of the NFAT transcription factor family of five proteins that regulate the expression of cytokines and immunoregulatory genes in several cell types (34–36). NFATc1 rescues osteoclastogenesis in cells lacking c-Fos (29, 33, 37–39), indicating that c-Fos is upstream of NFATc1.

NF-κB comprises a family of five transcription factors, and expression of both p50 and p52 is required for osteoclast formation (30, 31). NF-κB p50/p52 double knock-out (dKO) mice do not form osteoclasts, whereas osteoclast formation in p50 or p52 single knock-out mice is normal. The dKO mice have increased numbers of $CD11b^+/RANK^+$ osteoclast precursors in their spleens (40), indicating that p50/p52 expression is required for progression of these cells along the osteoclast differentiation pathway. The defect cannot be rescued by treatment of dKO splenocytes with RANKL or TNF (40), each of which activates NF-κB in wild-type (WT) osteoclasts (25, 26). This is important because TNF can induce osteoclast formation *in vitro* from WT, $RANKL^{-/-}$, or $RANK^{-/-}$ osteoclast precursors (41–43), indicating that p50 and p52 expression is required for this *in vitro* effect of TNF. Despite these observations, the mechanism whereby TNF induces osteoclast formation *in vitro* in the absence of RANKL/RANK signaling remains unknown.

Although it is established that RANKL activates c-Fos and NFATc1 in osteoclasts or their precursors (29, 33), there are conflicting data on its effects on NF-κB activation (44). Recent studies have indicated that NF-κB p65 and to a lesser extent p50 proteins are recruited along with NFATc2 to the NFATc1 promoter within 1 h of treatment of osteoclast precursors with RANKL (45). c-Fos is not recruited to the NFATc1 promoter until much later (at 24 h), by which time NFATc2 and NF-κB p65 and p50 are no longer detectable. Interestingly, by this time, NFATc1 has been recruited to its own promoter. These investigators suggested that RANKL induces cooperation of NFATc2 pre-existing in precursors with other transcription factors, such as NF-κB to activate initial induction of NFATc1, followed by a later auto-amplification phase of NFATc1 to induce osteoclast formation. Despite these demonstrations of transient NF-κB p65 and p50 association with NFATc2, but not NFATc1, on the NFATc1 promoter, it is still not clear what the relationship is among NF-κB, c-Fos, and NFATc1 during the early events that mediate RANKL or TNF-induced osteoclast formation. This is exemplified by the pathways illustrated in recent review papers of signaling downstream from RANK (46, 47). Thus, it is still not clear whether the essential role of NF-κB p50 and p52 in osteoclast formation is up- or downstream of c-Fos given that expression of both is required for osteoclastogenesis *in vitro* and *in vivo*, nor is it clear whether it is necessary for NF-κB p50 and p52 to interact with NFATc1 in osteoclast precursors for their differentiation into osteoclasts.

Here, we report that RANKL or TNF can induce osteoclast formation from NF-κB dKO osteoclast precursors when c-Fos is expressed, indicating that NF-κB is upstream of c-Fos. RANKL or TNF treatment and c-Fos expression in dKO cells also induces NFATc1 expression, and retroviral expression of NFATc1 plus treatment with these cytokines rescue the defect in osteoclast formation. These findings indicate that interaction between NFATc1 and NF-κB p50 or p52 is not required for NFATc1 to execute its osteoclastogenic effect.

MATERIALS AND METHODS

Animals—Generation of NF-κB p50/p52 dKO mice (C57Bl/6 × 129) was described previously (30), and mice were used when they were 3–6 weeks old. Littermates of dKO mice that have normal teeth eruption and skeletal development were used as WT controls. The Institutional Animal Care and Use Committee approved all animal studies.

Reagents—Recombinant human M-CSF, murine RANKL, interleukin-1β, and TNFα were purchased from R&D Systems, Inc. (Minneapolis, MN). Polybrene and puromycin were obtained from Sigma. NF-κB activation inhibitor was purchased from Calbiochem.

Constructs and Transfection—The coding regions of genes were amplified by PCR from cDNAs and cloned into the pMX-puro retroviral vector (33, 48). Each 5′ primer contains a Kozak sequence following the start codon. c-Fos was murine, and NF-κB p50 and p52 were of human origin. The pMSCV-caNFATc1 construct was a gift from Dr. N. Clipstone (Northwestern University, Chicago, IL) (49). The pMX-GFP-puro vector was used as a control for infection efficiency. These retrovirus vectors were transiently transfected into the Plat-E retroviral packaging cell line (50), and viral supernatant was collected 48 h later.

Osteoclastogenesis and Viral Infection—Splenocytes were extracted from spleens through a fine wire mesh and cultured with conditioned medium from a M-CSF-producing cell line (51) (1:20 dilution) for 3 days in α-modified essential medium with 10% fetal calf serum (Hyclone Laboratories, Logan, UT) to enrich for osteoclast precursors, which we named M-CSF-dependent splenocytes (MDS). Then the cells were infected with the retroviral supernatants in the presence of M-CSF (10 ng/ml) and Polybrene (8 μg/ml). On day 2 after infection, puromycin (2 μg/ml) was added to the cultures to select for gene-integrated cells. ~50–80% of MDS were GFP-positive under fluorescence microscopy 2 days after infection, and this increased to >90% following puromycin treatment. The cells were cultured with M-CSF (10 ng/ml) for 3–7 days. RANKL (10 ng/ml) and TNF (20 ng/ml) (these doses for RANKL and TNF effectively induce osteoclast formation from WT spleen cells) were added every other day. The experiments were stopped during this time based on a visual assessment of multinucleated cell formation using an inverted microscope. Optimal osteoclast formation occurs in WT cell preparations 1–2 days after those from the dKO mice. The cells were fixed, stained for tartrate-resistant acid phosphatase (TRAP) activity to identify osteoclasts as $TRAP^+$ cells containing ≥3 nuclei, and counted, as described previously (52). For functional studies, infected cells were cultured on bone slices for 10 days under the same conditions as described above. Osteoclasts were then removed, resorption pits were visualized after 0.1% toluidine blue staining, and the mean pit area was measured, as described previously (53).

Quantitative Real-time RT-PCR—RNA from MDS or infected cells was extracted using the RNeasy kit and the

QiaShredder from Qiagen (Valencia, CA). cDNA synthesis was performed as described previously (40). Quantitative PCR amplification was performed with gene-specific primers using an iCycler real-time PCR machine using iQ SYBR Green supermix (both from Bio-Rad Laboratories) according to the manufacturer's instructions. The primer sequences are as follows: *NFATc1*, forward, 5′-CACATTCTGGTCCATACGA-3′, and reverse, 5′-CGTGTAGCTGCACAATGG-3′; c-*fos*, forward, 5′-CTGTCAACACACAGGACTTTT-3′, and reverse, 5′-AGGAGATAGCTGCTCTACTTTG-3′; β-actin, forward, 5′-ACCCAGATCATGTTTGAGAC-3′, and reverse, 5′-GTCAGGATCTTCATGAGGTAGT-3′. The relative standard curve method was used to calculate the amplification difference for each primer set (54). The standard curve was made from four points corresponding to 10-fold cDNA serial dilution for each gene. For each sample, the relative amount was calculated from its respective standard curve. The quantity of c-*fos* or *NFATc1* mRNA was then obtained by division of each value by the *actin* value. Standards and samples were run in triplicate.

Western Blot Analysis—Infected cells were lysed with radioimmunoprecipitation buffer (50 mM HEPES at pH 7, 1% Triton X-100, 1 mM EDTA, 0.1% sodium dodecyl sulfate, 1% sodium deoxycholate, 150 mM NaCl with protease inhibitors, and sodium orthovanadate). The lysates (20 μg of protein) were resolved by 10% SDS-PAGE and immunoblotted with a rabbit anti-c-Fos, mouse anti-NFATc1 (both from Santa Cruz Biotechnology, Santa Cruz, CA), or a mouse anti-actin (Sigma) antibody.

NFATc1 Nuclear Translocation—c-Fos or GFP virus-infected MDS were cultured with M-CSF and RANKL in 96-well culture plates to generate osteoclasts. After mature osteoclasts were observed, cells were fixed with 10% neutral buffered formalin and permeabilized using 0.1% Triton X-100. Immunofluorescent staining was performed using mouse anti-NFATc1 antibody followed by Cy3-conjugated anti-murine immunoglobulin (Jackson ImmunoResearch, West Grove, PA). Subcellular localization of Cy3-labeled NFATc1 was observed using fluorescence microscopy.

Electrophoretic Mobility Shift Assay (EMSA)—To assess c-Fos activation, EMSA was performed as described previously (55). Briefly, 5 μg of nuclear extracts prepared from untreated MDS or RANKL- or TNF-treated MDS were incubated with ^{32}P-end-labeled 21-mer double-stranded oligonucleotide containing the consensus AP-1 site (5′-CGCTTGATGACTCAGCCGGAA-3′) (Santa Cruz Biotechnology) for 30 min at room temperature. The DNA-protein complex formed was then separated from free oligonucleotide on 5% native polyacrylamide gels. Binding specificity was examined by competition with 30-fold excess unlabeled AP-1 oligonucleotide. SP-1 binding sequence 5′-CGAGCCGGCCCCGCCCATC-3′ (Invitrogen) was used as a loading control.

Statistics—All experiments were performed more than once with similar results. Results are given as mean ± S.E. Comparisons were made by analysis of variance and Mann-Whitney's *U* test for unpaired data. p values <0.05 were considered statistically significant.

RESULTS

NF-κB Is Upstream from c-Fos in RANKL and TNF-induced Osteoclast Formation—c-Fos, like NF-κB, is activated by RANKL and TNF to induce osteoclast formation (15), but it is not known whether c-Fos can substitute for NF-κB expression in osteoclast precursors. To examine this question, we overexpressed c-Fos in NF-κB p50/p52 dKO MDS. MDS were used as osteoclast precursors in our study because NF-κB dKO mice have severe osteopetrosis, which prevents harvesting of bone marrow cells. We first examined whether NF-κB p50, p52, and p50+p52 retroviral expression would rescue the defect in osteoclast formation in dKO MDS when the cells were treated with RANKL. Overexpression of p50+p52 in dKO cells rescued osteoclast formation, inducing ~150 osteoclasts/96 wells (Fig. 1*A*). In comparison, RANKL-treated GFP-infected WT cells typically formed ~300 TRAP$^+$ osteoclasts (data not shown), indicating that the maximal rescue efficiency of our system is ~50% of that of WT cells. c-Fos expression alone, like p50, p52, or p50+p52, did not induce osteoclasts in the absence of RANKL (Fig. 1, *A* and *B*). However, when RANKL was added to c-Fos-expressing dKO cells, the combination rescued the osteoclast formation defect, inducing ~150 osteoclasts (Fig. 1, *B* and *C*). The TRAP$^+$ cells that formed on plastic dishes and bone slices from dKO cells overexpressing c-Fos appeared similar to those of WT MDS treated with M-CSF and RANKL, and they formed numerous resorption pits on bone slices, typical of mature WT osteoclasts (Fig. 1*D*). These data indicate that c-Fos activated by RANKL can efficiently substitute for the lack of p50 and p52 in dKO cells in these culture conditions and that the resulting c-Fos-overexpressing osteoclasts have a bone resorptive capacity similar to that of WT cells.

TNF plays important roles in osteoclast formation, activation, and survival in a number of pathologic conditions (9, 56) by stimulating RANKL expression in stromal and other cell types. To determine whether TNF, like RANKL, could induce osteoclast formation directly when c-Fos was overexpressed in dKO MDS, we treated c-Fos-expressing dKO MDS with TNF. We observed numerous TRAP$^+$ osteoclasts. However, the number of osteoclasts formed (~80/well) was less than in the c-Fos/RANKL-treated cultures (~150/well; Fig. 1*B*).

To determine whether there is impaired RANKL or TNF-induced c-Fos up-regulation and AP-1 binding activity in the absence of NF-κB p50 and p52, we compared c-Fos mRNA expression and activation in dKO and WT MDS. RANKL or TNF stimulated c-Fos mRNA expression in WT cells but not in dKO cells (Fig. 2*A*). Accordingly, RANKL or TNF induced binding of c-Fos protein to an AP-1 oligonucleotide probe in an EMSA using nuclear extracts from WT MDS but not using dKO cells. In contrast, binding to the SP-1 control probe was similar between dKO and WT nuclear extracts, indicating equal loading in the EMSA (Fig. 2*B*). To further determine whether NF-κB is upstream from c-Fos induced by RANKL or TNF, we treated WT cells with a newly developed NF-κB inhibitor (57) and demonstrated that NF-κB inhibitor treatment prevented RANKL or TNF-induced c-Fos expression (Fig. 2*C*) and activation (data not shown). Finally, we infected c-Fos-deficient cells with NF-κB p50+p52 retroviral constructs and treated

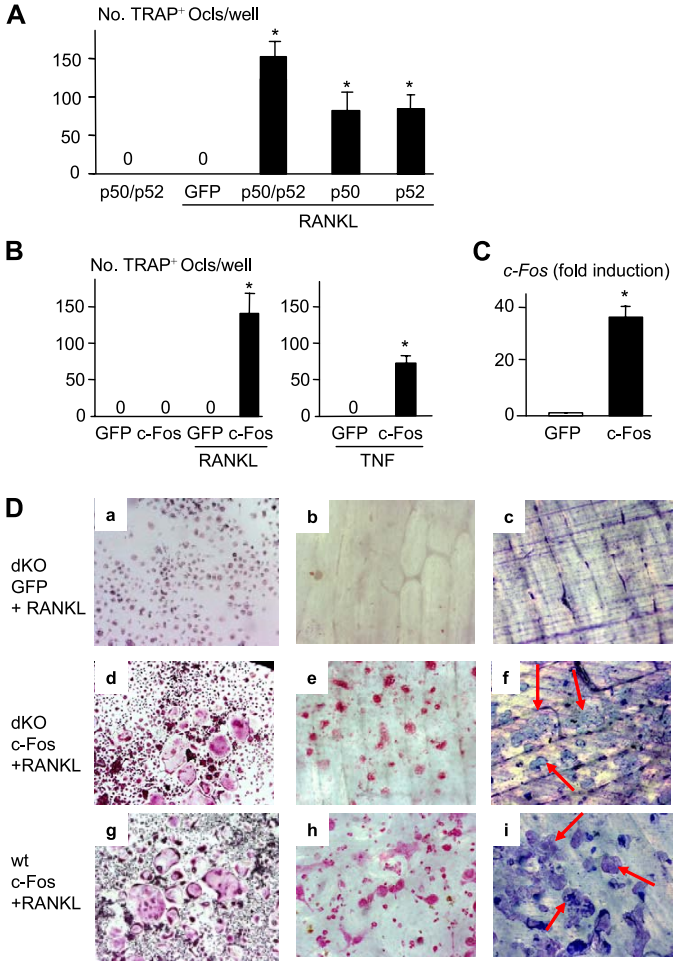

FIGURE 1. **c-Fos is downstream of NF-κB in RANKL-induced osteoclastogenesis.** *A* and *B*, NF-κB dKO splenocytes were cultured with M-CSF for 3 days to generate osteoclast precursors, called MDS (as described above). MDS were infected with retroviral supernatant containing NF-κB p50+p52, p50, or p52 (*A*) or c-Fos (*B*) with M-CSF for 2 days, selected in medium containing puromycin (2 μg/ml) plus M-CSF (10 ng/ml) for 2 days, and cultured with M-CSF and RANKL (10 ng/ml) or TNF (20 ng/ml) for 5 days ($n = 4$ wells/group), and $TRAP^+$ osteoclasts were counted. *C*, *c-fos* mRNA was assessed by real-time RT PCR using total RNA from c-Fos- or GFP-infected MDS after culture for 4 days. Values (means of triplicate loadings plus S.E.) are the -fold changes of *c-fos*/actin in c-Fos- over GFP-infected samples. *D*, TRAP-stained c-Fos- or GFP-infected dKO cells cultured with RANKL on plastic dishes (*panels a* and *d*) or bone slices (*panels b* and *e*). Resorption pits (*panel f*, *arrows*) produced by these cells (*panels c* and *f*) stained with toluidine blue; osteoclasts and resorption pits from WT cells were induced by c-Fos/RANKL (*panels g–i*). *, $p < 0.05$ *versus* GFP-treated groups.

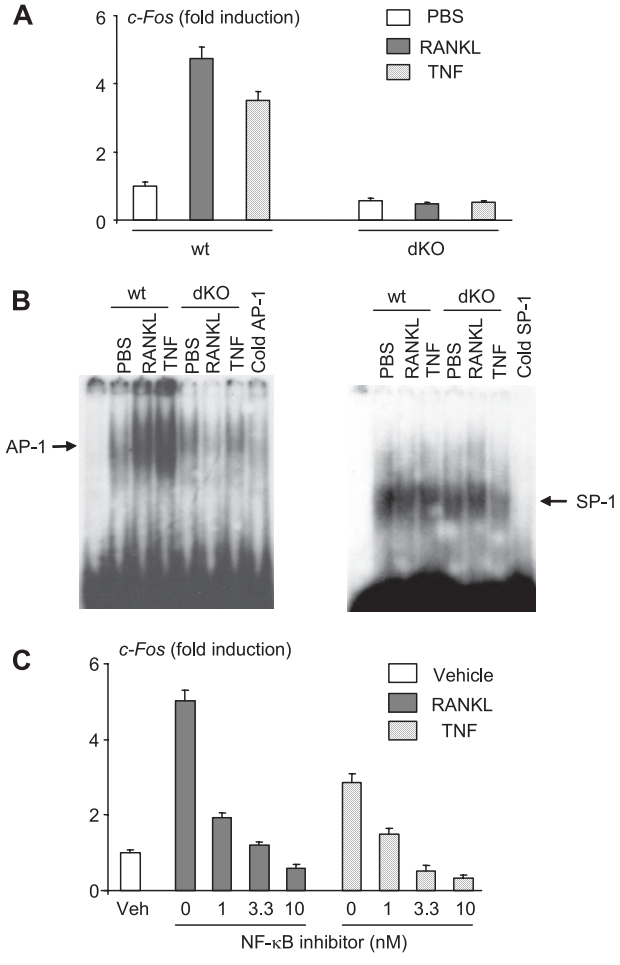

FIGURE 2. **Impaired RANKL or TNF-induced c-Fos activation in NF-κB dKO osteoclast precursors.** *A*, NF-κB dKO or WT MDS were treated with RANKL, TNF, or PBS. Total RNA was extracted, and expression of *c-fos* mRNA was measured by real-time RT-PCR at 4 h as in Fig. 1. Values are the -fold changes of *c-fos*/actin in cytokine-treated over PBS-treated samples and are the means of triplicate loading plus S.E. *B*, WT and NF-κB dKO MDS were treated with RANKL, TNF, or PBS control for 8 h. Nuclear protein (5 μg) was subjected to EMSA for AP-1 binding activity. AP-1 bands are indicated by the *arrowhead*, and SP-1 probe was used as a loading control. *C*, WT MDS were treated with various doses of NF-κB inhibitor in the presence of RANKL or TNF for 4 h. The expression of *c-fos* mRNA was determined by real-time RT-PCR. Values are the -fold changes of *c-fos*/actin in cytokine-treated over vehicle (*Veh*) (Me_2SO)-treated samples.

them with RANKL. As expected, overexpression of NF-κB in these cells did not rescue their defect in osteoclast formation (data not shown). These findings indicate that c-Fos is downstream of NF-κB in RANKL and TNF-induced osteoclast formation.

c-Fos Up-regulates NFATc1 Expression in NF-κB dKO Osteoclast Precursors, and NFATc1 Overexpression Rescues the Defect in Osteoclast Formation in NF-κB dKO Cells—NFATc1 functions downstream of c-Fos during osteoclastogenesis in WT cells (29). If this is also the case in dKO cells, we should not observe increased NFATc1 expression in RANKL-treated dKO cells, and NFATc1 expression should be rescued by c-Fos overexpression. We found that RANKL treatment of WT, but not dKO MDS, increased NFATc1 mRNA 5-fold. In contrast, c-Fos overexpression plus RANKL induced NFATc1 mRNA in both WT and dKO cells, as assessed by real-time RT-PCR (Fig. 3*A*). Consistent with this, c-Fos/RANKL-induced dKO osteoclasts had increased NFATc1 protein expression (Fig. 3*B*), but RANKL alone did not induce endogenous c-Fos or NFATc1 expression in dKO MDS in the absence of c-Fos retroviral infection (Fig. 3*B*). NFATc1 activation by RANKL in both WT and dKO osteoclasts was examined by immunofluorescence staining using an anti-NFATc1 antibody. In WT or dKO osteoclast precursors cultured in the absence of RANKL, NFATc1 is detectable only in the cytoplasm regardless of c-Fos overexpression (Fig. 3*C*, *panels a–d*). In mature WT osteoclasts, NFATc1 translocated to nuclei in response to RANKL plus either GFP or c-Fos infection (Fig. 3*C*, *panels e* and *f*). By contrast, in dKO MDS only infected with c-Fos, no mature osteoclasts formed, and therefore, no NFATc1 translocation was observed (Fig. 3*C*, *panel g*). However, NFATc1 was observed in

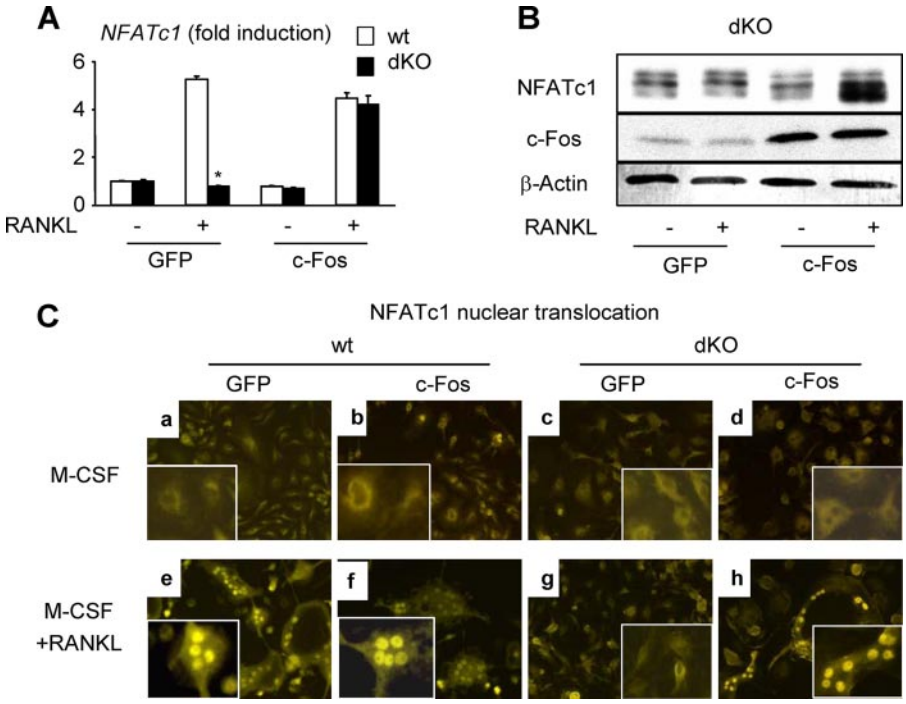

FIGURE 3. **c-Fos expression and RANKL induce NFATc1 expression and activation in NF-κB dKO osteoclast precursors during osteoclast differentiation.** *A*, WT or NF-κB dKO MDS were generated, infected with c-Fos or GFP, and treated with M-CSF ± RANKL, and *NFATc1* expression was assessed as described in the legend for Fig. 1. *, $p < 0.05$ *versus* WT cells. *B*, c-Fos and NFATc1 protein expression levels in c-Fos and GFP-infected dKO cultures treated with and without RANKL for 5 days were assessed by Western blot analysis. *C*, mature osteoclasts were generated from WT or NF-κB dKO MDS that were infected with c-Fos or GFP retroviral supernatants in the presence of M-CSF ± RANKL or PBS. When multinucleated cells with the morphologic features of osteoclasts were observed under an inverted microscope, the cells were stained with anti-NFATc1 antibody to identify nuclear translocation (×10; *insets* are ×40).

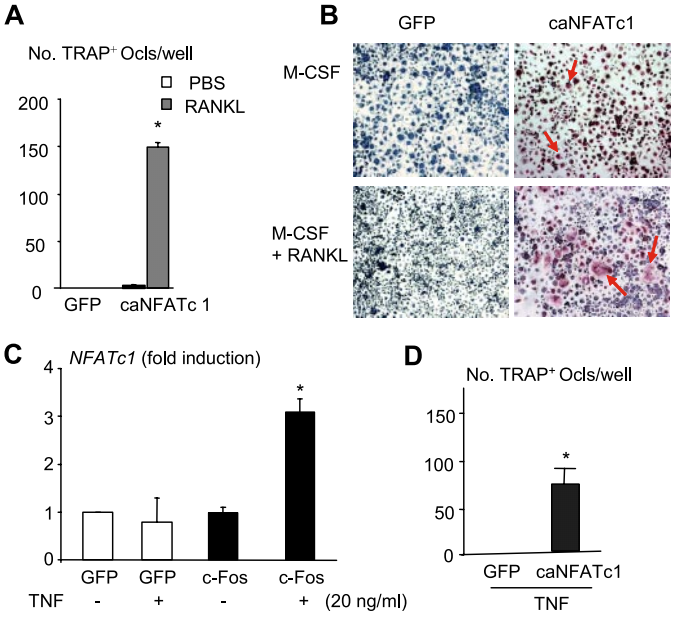

FIGURE 4. **NFATc1 expression and RANKL or TNF treatment induce osteoclast formation from NF-κB dKO osteoclast precursors.** *A*, NF-κB dKO MDS were generated, infected with NFATc1, c-Fos or GFP, and treated with M-CSF ± RANKL or PBS, and TRAP+ osteoclast formation was assessed as described in the legend for Fig. 1. *B*, TRAP+ osteoclasts (*Ocls*, *arrows*) formed in the NFATc1-infected cultures treated with PBS, but their numbers were much smaller than in the cultures treated with RANKL. *C*, NF-κB dKO MDS were generated, infected with NFATc1 or GFP, and treated with M-CSF ± TNF or PBS, and TRAP+ osteoclast formation was assessed, as described in the legend for Fig. 1. *D*, *NFATc1* mRNA was assessed by real-time RT PCR using total RNA from c-Fos- or GFP-infected MDS. *, $p < 0.05$ *versus* GFP-infected group.

nuclei of c-Fos/RANKL-induced mature osteoclasts from NF-κB dKO MDS (Fig. 3*C*, *panel h*). These data indicate that NFATc1 nuclear translocation is associated with multinucleated mature osteoclast formation downstream from NF-κB in RANKL-stimulated cells.

We next overexpressed a constitutively active form of NFATc1 in NF-κB dKO MDS to determine whether it could rescue their defect in osteoclast formation. Treatment of these NFATc1-expressing dKO cells with RANKL induced osteoclast formation (Fig. 4, *A* and *B*). Maximal osteoclast numbers appeared 1 day earlier than with c-Fos overexpression in the same experiment (data not shown). The number of osteoclasts formed when NFATc1 was overexpressed in the dKO cultures (Fig. 4*A*) was similar to that when NF-κB p50+p52 or c-Fos were overexpressed in dKO MDS, consistent with sequential activation of NF-κB, c-Fos, and then NFATc1 in RANKL-induced osteoclastogenesis. Notably, small numbers of osteoclasts formed in the dKO cultures expressing NFATc1 alone (Fig. 4*B*), presumably because unlike the c-Fos or NF-κB constructs, this NFAT construct is constitutively active because it is not phosphorylated.

We next determined whether TNF-induced dKO osteoclast formation, like RANKL, is mediated through NFATc1. We observed induction of NFATc1 expression in c-Fos-expressing dKO MDS treated with TNF (Fig. 4*C*). TNF also induced osteoclast formation from NF-κB dKO cells when NFATc1 was overexpressed in these cells (Fig. 4*D*).

RANKL and TNF Induce a Similar Pattern of c-Fos or NFATc1 Expression during Osteoclastogenesis from WT Splenocytes—Both RANKL and TNF plus c-Fos overexpression rescued the defect in osteoclastogenesis and increased NFATc1 expression in osteoclasts formed from NF-κB dKO MDS, suggesting that TNF may trigger osteoclastogenesis by up-regulating c-Fos and NFATc1 sequentially, like RANKL, as described previously in WT cells (15). Wild-type MDS were treated with RANKL or TNF for various times, and expression levels of c-Fos and NFATc1 and osteoclast formation were examined. TNF increased c-*fos* mRNA levels to the same extent as RANKL as early as 4 h, although c-*fos* levels were significantly higher in the RANKL-treated than in the TNF-treated cultures thereafter (Fig. 5*A*). NFATc1 expression increased much later than c-Fos (Fig. 5, *A* and *B*). Notably, RANKL-induced NFATc1 expression peaked at 48 h when mature osteoclasts formed (Fig. 5*C*). In contrast, TNF-induced NFATc1 expression and osteoclast formation

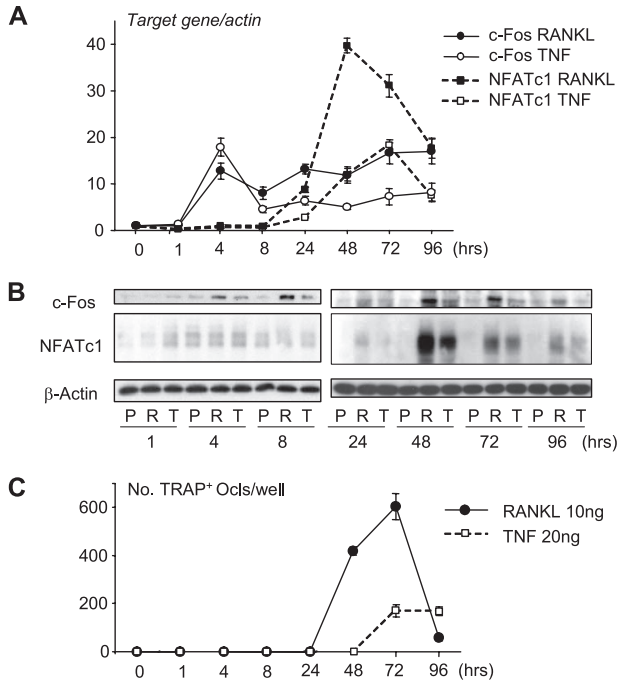

FIGURE 5. **RANKL and TNF induce c-Fos followed by NFATc1 expression in WT osteoclast precursors.** *A* and *B*, WT MDS were generated and treated with M-CSF ± RANKL (10 ng/ml) or TNF (20 ng/ml), and c-Fos and NFATc1 mRNA (*A*) and protein (*B*) expression was assessed by real-time RT-PCR and Western blot analysis, respectively, at the times indicated. *C*, TRAP$^+$ osteoclast formation was assessed, as described in the legend for Fig. 1 in parallel experiments. *P*, PBS; *R*, RANKL; *T*, TNF.

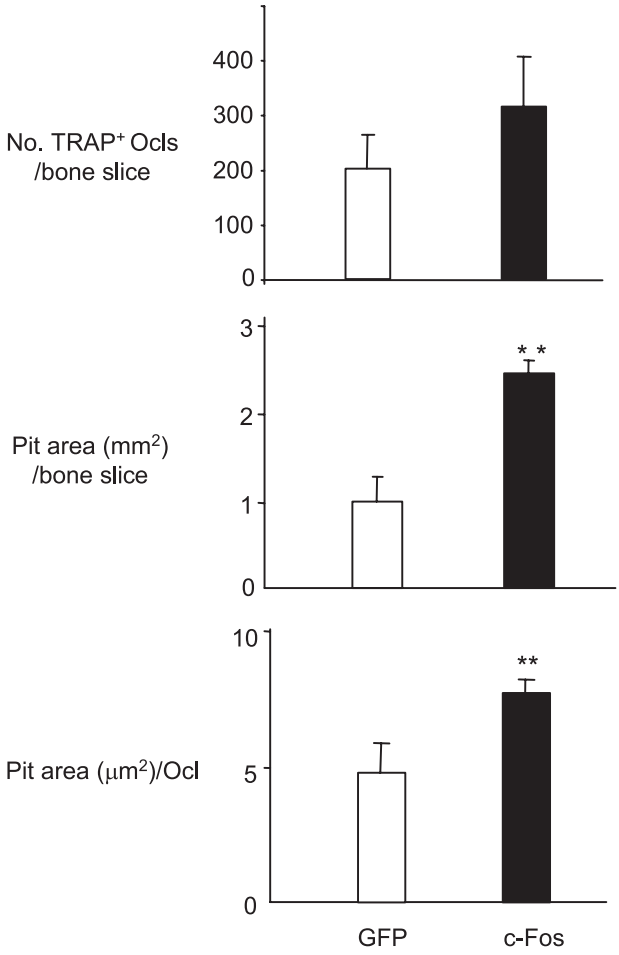

FIGURE 6. **c-Fos expression increases the resorptive activity of WT osteoclasts (*Ocls*) treated with TNF.** WT MDS were generated, infected with c-Fos or GFP, and treated with TNF (20 ng/ml) for 8 days. Osteoclast formation and resorption pit area were assessed. *, $p < 0.05$ *versus* TNF-treated GFP-infected group.

peaked 1 day later (Fig. 5, *A*–*C*), associated with lower levels of NFATc1 expression and fewer osteoclasts. This suggests that the weaker osteoclastogenic effect of TNF in comparison with RANKL in these cultures may be due to lower induced NFATc1 expression.

c-Fos Expression Increases the Resorptive Activity of Osteoclasts Induced from WT MDS by TNF—Having demonstrated that c-Fos can substitute for NF-κB in osteoclast formation, we next examined whether c-Fos could increase the bone-resorbing capacity of mature osteoclasts induced by TNF. The ability of TNF to induce osteoclast formation and bone resorption *in vitro* has been controversial (13). However, we found that TNF-induced osteoclasts do resorb bone (Fig. 6), although the pits were smaller and shallower than those formed in response to RANKL (data not shown). c-Fos also significantly increased the TNF-induced pit area (Fig. 6).

DISCUSSION

Expression of NF-κB, c-Fos, and NFATc1 is required for osteoclast precursors to differentiate into osteoclasts in response to RANKL. Here, we show that c-Fos and NFATc1 induction is downstream of NF-κB p50 and p52 activation in RANKL-mediated signaling in osteoclast precursor differentiation because either c-Fos or NFATc1 can efficiently substitute for NF-κB p50 and p52 in RANKL-treated NF-κB p50/p52 dKO cells to induce osteoclast formation and bone resorption. Furthermore unexpectedly, c-Fos or NFATc1 can substitute for NF-κB in TNF-stimulated osteoclast formation from NF-κB dKO cells *in vitro*. NFATc1 has been described as the master switch for regulating terminal differentiation of osteoclasts downstream from RANKL, and its expression is regulated by c-Fos (29, 33). Our findings indicate that NF-κB p50 and p52 play an essential role regulating the early differentiation of osteoclast precursors upstream from c-Fos and NFATc1 in response to RANKL and TNF, both of which can induce osteoclast formation directly from osteoclast precursors *in vitro*.

The importance of these findings is that expression of RANKL and TNF is increased in a variety of common bone diseases associated with increased bone resorption, including postmenopausal osteoporosis, rheumatoid arthritis, and periodontal disease (2, 58, 59). These two cytokines can increase the expression of each other by accessory cells and of TNF by osteoclasts and their precursors (60, 61). By this latter mechanism, TNF could amplify its osteoclastogenic effects in an autocrine auto-amplifying manner, setting up what we propose is an auto-amplifying cycle of increasing osteoclastogenesis whereby TNF induces more osteoclasts and their precursors, which produce more TNF to induce formation of more osteoclasts, and so on. Excessive production of TNF in joints of patients with rheumatoid arthritis could account in large part for the aggressive bone resorption seen in affected joints of these patients. The

efficacy of anti-TNF therapy in many rheumatic patients supports this assertion (62).

Overexpression of NF-κB p50 and p52 or c-Fos alone in dKO MDS did not induce osteoclast formation in our cultures. Although NFATc1 overexpression alone did induce small numbers of osteoclasts, as with NF-κB p50 and p52 or c-Fos, concomitant treatment with cytokines was required to rescue the osteoclast formation defect efficiently. Currently, we do not know why cytokines are required for this efficient rescue of the osteoclast formation defect. When c-Fos or NFATc1 was overexpressed alone in c-*fos*$^{-/-}$ cells, this, too, did not rescue the osteoclastogenesis defect and needed the addition of RANKL for efficient rescue (33). We therefore speculate that this retroviral rescue system has an intrinsic deficiency that prevents full recovery of osteoclastogenesis or that to initiate the osteoclast formation program, these virus-encoded transcription factors need to be activated through RANKL signaling and interact with a yet to be identified RANKL-induced molecule. However, it is also possible that other mechanisms are involved in RANKL-induced osteoclast formation. Further studies will be required to address this particular issue.

To date, there is no evidence that NF-κB activates c-Fos directly, and there are no consensus NF-κB binding sites on the c-Fos promoter. Indirect activation of c-Fos by NF-κB through serum-response factors has been described in embryonic fibroblasts (63). Recently, we have found that NF-κB binding activity was significantly higher in c-*fos*$^{-/-}$ MDS when compared with WT cells, supporting the argument that NF-κB is upstream rather than downstream of c-Fos (64). The report that NF-κB p65 and p50 transiently interact with NFATc2, but not with NFATc1, on the NFAT2c1 promoter is intriguing and warrants further study to determine exactly what the role of NF-κB p50 and p52 and NFAT2 proteins is in the early stages of osteoclastogenesis.

TNF, like RANKL, can activate a variety of signaling pathways in osteoclasts and their precursors (reviewed in Refs. 8, 58, and 65) that induce osteoclast formation and activation. Our observation of a sequence of induction by RANKL and TNF beginning with NF-κB followed by c-Fos and NFATc1 suggests that these cytokines may share a common pathway to induce osteoclast precursor differentiation in addition to activating c-Fos. However, RANKL and TNF recruit different adapter proteins, TNF receptor-associated factor (TRAF) 6 (66) and TRAF2 (67), respectively, to their receptors to mediate downstream signaling, suggesting that they should activate different pathways. RANKL has been reported to regulate stimulated, but not basal, osteoclast formation by a pathway involving NF-κB-inducing kinase and NF-κB p100 processing to p52 in the NF-κB alternative pathway (68). However, these authors did not observe this effect with short term TNF treatment, again suggesting that RANKL and TNF may use different pathways. Further studies will be required to determine what these are.

In the later stages of our cultures after 24–48 h when osteoclasts begin to form, RANKL and TNF induced expression of NFATc1 in c-Fos-infected dKO MDS. That NFATc1 is essential for osteoclastogenesis and works downstream of c-Fos has been established by genetic studies (29, 33). For example, overexpression of NFATc1 retrovirus plus RANKL treatment rescued the osteoclastogenesis defect in *Fos*$^{-/-}$ osteoclast precursors (33). The recent studies by Asagiri *et al.* (45) reporting that NF-κB p65 and p50 bind transiently to the promoter region of NFATc1 along with NFATc2 within 1 h of treatment with RANKL highlight the complexity of the signaling downstream from RANKL/RANK interaction and our limited understanding of how RANKL mediates osteoclast formation.

The current paradigm on osteoclastogenesis posits that most cytokines, hormones, and growth factors induce osteoclast formation and bone resorption predominantly by an indirect mechanism whereby they promote RANKL and M-CSF expression in osteoblast/stromal cells, rather than by directly acting on osteoclast precursors to mediate the differentiation of RANK-expressing precursors into mature osteoclasts. Indeed, it has been proposed recently that stromal cells expressing M-CSF make a greater contribution to TNF-mediated osteoclast formation than osteoclast precursors (18) and that osteoclast formation *in vitro* requires prior priming of these precursors by RANKL (69). However, the claim in this latter study has now been disproved (42, 43). Thus, it is now clear that TNF can induce osteoclast formation both directly and indirectly at least *in vitro*, although the relative contributions of these two mechanisms *in vivo* remain uncertain.

Our findings suggest that osteoclastogenesis is controlled by a hierarchical transcriptional program in which NF-κB activation appears to be the first event and is followed by c-Fos and NFATc1 activation. NF-κB is not essential for the commitment of hematopoietic stem cells to the osteoclast progenitor cells because these cells can give rise to functional osteoclasts if the downstream transcription factors, c-Fos or NFATc1, are overexpressed in these cells. Thus, inhibitors of NF-κB should prevent osteoclast formation induced directly or indirectly by RANKL or TNF in the early stages of osteoclast precursor differentiation, rather than during the later stages where an NFATc1 inhibitor would be predicted to work, based on published data (70, 71) and on our data. Blockade of NF-κB signaling using such an approach may be an effective therapeutic strategy to prevent bone loss in a variety of common bone diseases. This overall beneficial effect of NF-κB inhibition in preclinical studies contrasts with the disappointing results with the calcineurin inhibitor, cyclosporin A, which induces osteoporosis in humans (72), presumably because it inhibits not only NFATc1 activation in osteoclasts but also in osteoblasts by down-regulating expression of the NFATc1 target gene, osterix, in osteoblasts, and thus, reducing bone formation directly (73).

Acknowledgments—We thank Neil A. Clipstone for providing the constitutively active form of the NFATc1 construct, Ulrich Siebenlist for providing the human NF-κB p52 cDNA, and Toshio Kitamura for the Plat-E cell line.

REFERENCES

1. Boyle, W. J., Simonet, W. S., and Lacey, D. L. (2003) *Nature* **423,** 337–342
2. Teitelbaum, S. L. (2000) *J. Bone Miner. Metab.* **18,** 344–349
3. Lacey, D. L., Timms, E., Tan, H. L., Kelley, M. J., Dunstan, C. R., Burgess, T., Elliott, R., Colombero, A., Elliott, G., Scully, S., Hsu, H., Sullivan, J.,

Hawkins, N., Davy, E., Capparelli, C., Eli, A., Qian, Y. X., Kaufman, S., Sarosi, I., Shalhoub, V., Senaldi, G., Guo, J., Delaney, J., and Boyle, W. J. (1998) *Cell* **93,** 165–176
4. Dougall, W. C., Glaccum, M., Charrier, K., K., R., Brasel, K., Smedt, T., Daro, E., Smith, J., Tometsko, M. E., Maliszewski, C. R., Armstrong, A., Shen, V., Bain, S., Cosman, D., Anderson, D., Morrissey, P. J., J. J., P., and Schuh, J. (1999) *Genes Dev.* **13,** 2412–2424
5. Simonet, W. S., Lacey, D. L., Dunstan, C. R., Kelley, M., Chang, M. S., Luthy, R., Nguyen, H. Q., Wooden, S., Bennett, L., Boone, T., Shimamoto, G., DeRose, M., Elliott, R., Colombero, A., Tan, H. L., Trail, G., Sullivan, J., Davy, E., Bucay, N., Renshaw-Gegg, L., Hughes, T. M., Hill, D., Pattison, W., Campbell, P., and Boyle, W. J. (1997) *Cell* **89,** 309–319
6. Wong, B. R., Rho, J., Arron, J., Robinson, E., Orlinick, J., Chao, M., Kalachikov, S., Cayani, E., Bartlett, F. S., III, Frankel, W. N., Lee, S. Y., and Choi, Y. (1997) *J. Biol. Chem.* **272,** 25190–25194
7. Kong, Y. Y., Boyle, W. J., and Penninger, J. M. (1999) *Immunol. Cell Biol.* **77,** 188–193
8. Goldring, S. R. (2003) *Calcif. Tissue Int.* **73,** 97–100
9. Udagawa, N., Kotake, S., Kamatani, N., Takahashi, N., and Suda, T. (2002) *Arthritis Res.* **4,** 281–289
10. O'Keefe, R. J., Teot, L. A., Singh, D., Puzas, J. E., Rosier, R. N., and Hicks, D. G. (1997) *Lab. Investig.* **76,** 457–465
11. Cappellen, D., Luong-Nguyen, N. H., Bongiovanni, S., Grenet, O., Wanke, C., and Susa, M. (2002) *J. Biol. Chem.* **277,** 21971–21982
12. Jimi, E., Nakamura, I., Duong, L. T., Ikebe, T., Takahashi, N., Rodan, G. A., and Suda, T. (1999) *Exp. Cell Res.* **247,** 84–93
13. Kobayashi, K., Takahashi, N., Jimi, E., Udagawa, N., Takami, M., Kotake, S., Nakagawa, N., Kinosaki, M., Yamaguchi, K., Shima, N., Yasuda, H., Morinaga, T., Higashio, K., Martin, T. J., and Suda, T. (2000) *J. Exp. Med.* **191,** 275–286
14. Dougall, W. C., Glaccum, M., Charrier, K., Rohrbach, K., Brasel, K., De Smedt, T., Daro, E., Smith, J., Tometsko, M. E., Maliszewski, C. R., Armstrong, A., Shen, V., Bain, S., Cosman, D., Anderson, D., Morrissey, P. J., Peschon, J. J., and Schuh, J. (1999) *Genes Dev.* **13,** 2412–2424
15. Takayanagi, H., Kim, S., Matsuo, K., Suzuki, H., Suzuki, T., Sato, K., Yokochi, T., Oda, H., Nakamura, K., Ida, N., Wagner, E. F., and Taniguchi, T. (2002) *Nature* **416,** 744–749
16. Takayanagi, H., Ogasawara, K., Hida, S., Chiba, T., Murata, S., Sato, K., Takaoka, A., Yokochi, T., Oda, H., Tanaka, K., Nakamura, K., and Taniguchi, T. (2000) *Nature* **408,** 600–605
17. Suda, T., Kobayashi, K., Jimi, E., Udagawa, N., and Takahashi, N. (2001) *Novartis Found. Symp.* **232,** 235–250
18. Kitaura, H., Zhou, P., Kim, H. J., Novack, D. V., Ross, F. P., and Teitelbaum, S. L. (2005) *J. Clin. Investig.* **115,** 3418–3427
19. Tanabe, N., Maeno, M., Suzuki, N., Fujisaki, K., Tanaka, H., Ogiso, B., and Ito, K. (2005) *Life Sci.* **77,** 615–626
20. Yao, Z., Li, P., Zhang, Q., Schwarz, E. M., Keng, P., Arbini, A., Boyce, B. F., and Xing, L. (2006) *J. Biol. Chem.* **281,** 11846–11855
21. Zhang, Y. H., Heulsmann, A., Tondravi, M. M., Mukherjee, A., and Abu-Amer, Y. (2001) *J. Biol. Chem.* **276,** 563–568
22. Boyce, B. F., Yamashita, T., Yao, Z., Zhang, Q., Li, F., and Xing, L. (2005) *J. Bone Miner. Metab.* **23,** (suppl.) 11–15
23. Karsenty, G., and Wagner, E. F. (2002) *Dev. Cell* **2,** 389–406
24. Takayanagi, H. (2005) *J. Mol. Med.* **83,** 170–179
25. Kong, Y. Y., Yoshida, H., Sarosi, I., Tan, H. L., Timms, E., Capparelli, C., Morony, S., Oliveira-dos-Santos, A. J., Van, G., Itie, A., Khoo, W., Wakeham, A., Dunstan, C. R., Lacey, D. L., Mak, T. W., Boyle, W. J., and Penninger, J. M. (1999) *Nature* **397,** 315–323
26. Abu-Amer, Y., Ross, F. P., McHugh, K. P., Livolsi, A., Peyron, J. F., and Teitelbaum, S. L. (1998) *J. Biol. Chem.* **273,** 29417–29423
27. Jimi, E., Ikebe, T., Takahashi, N., Hirata, M., Suda, T., and Koga, T. (1996) *J. Biol. Chem.* **271,** 4605–4608
28. Grigoriadis, A. E., Wang, Z.-Q., Cecchini, M. G., Hofstetter, W., Felix, R., Fleisch, H. A., and Wagner, E. F. (1994) *Science* **266,** 443–448
29. Takayanagi, H., Kim, S., Koga, T., Nishina, H., Isshiki, M., Yoshida, H., Saiura, A., Isobe, M., Yokochi, T., Inoue, J., Wagner, E. F., Mak, T. W., Kodama, T., and Taniguchi, T. (2002) *Dev. Cell* **3,** 889–901
30. Franzoso, G., Carlson, L., Xing, L., Poljak, L., Shores, E. W., Brown, K. D., Leonardi, A., Tran, T., Boyce, B. F., and Siebenlist, U. (1997) *Genes Dev.* **11,** 3482–3496
31. Iotsova, V., Caamano, J., Loy, J., Lewin, A., and Bravo, R. (1997) *Nat. Med.* **3,** 1285–1289
32. Miyazaki, T., Katagiri, H., Kanegae, Y., Takayanagi, H., Sawada, Y., Yamamoto, A., Pando, M., Asano, T., Verma, I., Oda, H., Nakamura, K., and Tanaka, S. (2000) *J. Cell Biol.* **148,** 333–342
33. Matsuo, K., Galson, D. L., Zhao, C., Peng, L., Laplace, C., Wang, K. Z., Bachler, M. A., Amano, H., Aburatani, H., Ishikawa, H., and Wagner, E. F. (2004) *J. Biol. Chem.* **279,** 26475–26480
34. Crabtree, G. R., and Olson, E. N. (2002) *Cell* **109,** (suppl.) S67–S79
35. Rao, A., Luo, C., and Hogan, P. G. (1997) *Annu. Rev. Immunol.* **15,** 707–747
36. Macian, F. (2005) *Nat. Rev. Immunol.* **5,** 472–484
37. Koga, T., Inui, M., Inoue, K., Kim, S., Suematsu, A., Kobayashi, E., Iwata, T., Ohnishi, H., Matozaki, T., Kodama, T., Taniguchi, T., Takayanagi, H., and Takai, T. (2004) *Nature* **428,** 758–763
38. Ishida, N., Hayashi, K., Hoshijima, M., Ogawa, T., Koga, S., Miyatake, Y., Kumegawa, M., Kimura, T., and Takeya, T. (2002) *J. Biol. Chem.* **277,** 41147–41156
39. Hirotani, H., Tuohy, N. A., Woo, J. T., Stern, P. H., and Clipstone, N. A. (2004) *J. Biol. Chem.* **279,** 13984–13992
40. Xing, L., Bushnell, T. P., Carlson, L., Tai, Z., Tondravi, M., Siebenlist, U., Young, F., and Boyce, B. F. (2002) *J. Bone Miner. Res.* **17,** 1200–1210
41. Yamashita, T., Xing, L., Li, P., Schwarz, E. M., Dougall, W. C., and Boyce, B. F. (2002) *J. Bone Miner. Res.* **17,** Suppl. 1, S131
42. Armstrong, A. P., Tometsko, M. E., Glaccum, M., Sutherland, C. L., Cosman, D., and Dougall, W. C. (2002) *J. Biol. Chem.* **277,** 44347–44356
43. Kim, N., Kadono, Y., Takami, M., Lee, J., Lee, S. H., Okada, F., Kim, J. H., Kobayashi, T., Odgren, P. R., Nakano, H., Yeh, W. C., Lee, S. K., Lorenzo, J. A., and Choi, Y. (2005) *J. Exp. Med.* **202,** 589–595
44. Zhu, L. L., Zaidi, S., Moonga, B. S., Troen, B. R., and Sun, L. (2005) *Biochem. Biophys. Res. Commun.* **326,** 131–135
45. Asagiri, M., Sato, K., Usami, T., Ochi, S., Nishina, H., Yoshida, H., Morita, I., Wagner, E. F., Mak, T. W., Serfling, E., and Takayanagi, H. (2005) *J. Exp. Med.* **202,** 1261–1269
46. Takayanagi, H. (2007) *Nat. Rev. Immunol.* **7,** 292–304
47. Asagiri, M., and Takayanagi, H. (2007) *Bone* **40,** 251–264
48. Kitamura, T., Onishi, M., Kinoshita, S., Shibuya, A., Miyajima, A., and Nolan, G. P. (1995) *Proc. Natl. Acad. Sci. U. S. A.* **92,** 9146–9150
49. Neal, J. W., and Clipstone, N. A. (2001) *J. Biol. Chem.* **276,** 3666–3673
50. Morita, S., Kojima, T., and Kitamura, T. (2000) *Gene Ther.* **7,** 1063–1066
51. Takeshita, S., Kaji, K., and Kudo, A. (2000) *J. Bone Miner. Res.* **15,** 1477–1488
52. Hughes, D. E., Dai, A., Tiffee, J. C., Li, H. H., Mundy, G. R., and Boyce, B. F. (1996) *Nat. Med.* **2,** 1132–1136
53. Li, P., Schwarz, E. M., O'Keefe, R. J., Ma, L., Looney, R. J., Ritchlin, C. T., Boyce, B. F., and Xing, L. (2004) *Arthritis Rheum.* **50,** 265–276
54. Johnson, M. R., Wang, K., Smith, J. B., Heslin, M. J., and Diasio, R. B. (2000) *Anal. Biochem.* **278,** 175–184
55. Feng, J. Q., Xing, L., Zhang, J. H., Zhao, M., Horn, D., Chan, J., Boyce, B. F., Harris, S. E., Mundy, G. R., and Chen, D. (2003) *J. Biol. Chem.* **278,** 29130–29135
56. Goldring, S. R. (2003) *Rheumatology* (*Oxf.*) **42,** Suppl. 2, ii11–ii16
57. Tobe, M., Isobe, Y., Tomizawa, H., Nagasaki, T., Takahashi, H., and Hayashi, H. (2003) *Bioorg. Med. Chem.* **11,** 3869–3878
58. Kaplan, C., and Finnegan, A. (2003) *Front Biosci.* **8,** d1018–1029
59. Sato, K., and Takayanagi, H. (2006) *Curr. Opin. Rheumatol.* **18,** 419–426
60. Xing, L., and Schwarz, E. (2005) *Curr. Rheumatol. Rev.* **1,** 21–28
61. Teitelbaum, S. L. (2006) *Arthritis Res. Ther.* **8,** 201
62. Feldmann, M., and Maini, R. N. (2003) *Nat. Med.* **9,** 1245–1250
63. Fujioka, S., Niu, J., Schmidt, C., Sclabas, G. M., Peng, B., Uwagawa, T., Li, Z., Evans, D. B., Abbruzzese, J. L., and Chiao, P. J. (2004) *Mol. Cell. Biol.* **24,** 7806–7819
64. Ray, N., Kuwahara, M., Takada, Y., Maruyama, K., Kawaguchi, T., Tsubone, H., Ishikawa, H., and Matsuo, K. (2006) *Int. Immunol.* **18,** 671–677
65. Xing, L., and Schwarz, E. (2005) *Curr. Rheumatol. Res.* **1,** 21–28
66. Mizukami, J., Takaesu, G., Akatsuka, H., Sakurai, H., Ninomiya-Tsuji, J.,

Matsumoto, K., and Sakurai, N. (2002) *Mol. Cell. Biol.* **22,** 992–1000
67. Kanazawa, K., and Kudo, A. (2005) *J. Bone Miner. Res.* **20,** 840–847
68. Novack, D. V., Yin, L., Hagen-Stapleton, A., Schreiber, R. D., Goeddel, D. V., Ross, F. P., and Teitelbaum, S. L. (2003) *J. Exp. Med.* **198,** 771–781
69. Lam, J., Takeshita, S., Barker, J. E., Kanagawa, O., Ross, F. P., and Teitelbaum, S. L. (2000) *J. Clin. Investig.* **106,** 1481–1488
70. Urushibara, M., Takayanagi, H., Koga, T., Kim, S., Isobe, M., Morishita, Y., Nakagawa, T., Loeffler, M., Kodama, T., Kurosawa, H., and Taniguchi, T. (2004) *Arthritis Rheum.* **50,** 794–804
71. Jimi, E., Aoki, K., Saito, H., D'Acquisto, F., May, M. J., Nakamura, I., Sudo, T., Kojima, T., Okamoto, F., Fukushima, H., Okabe, K., Ohya, K., and Ghosh, S. (2004) *Nat. Med.* **10,** 617–624
72. Rich, G. M., Mudge, G. H., Laffel, G. L., and LeBoff, M. S. (1992) *J. Heart Lung Transplant.* **11,** 950–958
73. Koga, T., Matsui, Y., Asagiri, M., Kodama, T., de Crombrugghe, B., Nakashima, K., and Takayanagi, H. (2005) *Nat. Med.* **11,** 880–885

Molecular Basis of Cell and Developmental Biology:

Osteoclast Precursor Interaction with Bone Matrix Induces Osteoclast Formation Directly by an Interleukin-1-mediated Autocrine Mechanism

Zhenqiang Yao, Lianping Xing, Chunlin Qin, Edward M. Schwarz and Brendan F. Boyce

J. Biol. Chem. 2008, 283:9917-9924.
doi: 10.1074/jbc.M706415200 originally published online February 4, 2008

THE JOURNAL OF BIOLOGICAL CHEMISTRY VOL. 283, NO. 15, pp. 9917–9924, April 11, 2008

Osteoclast Precursor Interaction with Bone Matrix Induces Osteoclast Formation Directly by an Interleukin-1-mediated Autocrine Mechanism*

Received for publication, August 3, 2007, and in revised form, February 1, 2008 Published, JBC Papers in Press, February 4, 2008, DOI 10.1074/jbc.M706415200

Zhenqiang Yao[‡], Lianping Xing[‡§], Chunlin Qin[¶], Edward M. Schwarz[§], and Brendan F. Boyce[‡§1]

From the [‡]Department of Pathology and Laboratory Medicine and the [§]Center for Musculoskeletal Research, University of Rochester Medical Center, Rochester, New York 14642 and the [¶]Department of Biomedical Sciences, Baylor College of Dentistry, Texas A&M University System Health Science Center, Dallas, Texas 75246

Interleukin-1 (IL-1) and tumor necrosis factor (TNF) mediate bone resorption in a variety of diseases affecting bone. Like TNF, IL-1 is secreted by osteoclast precursors (OCPs), but unlike TNF, it does not induce osteoclast formation directly from OCPs *in vitro*. TNF induces IL-1 expression and activates c-Fos, a transcription factor required in OCPs for osteoclast formation. Here, we examined whether IL-1 can induce osteoclast formation directly from OCPs overexpressing c-Fos and whether interaction with bone matrix affects OCP cytokine expression. We infected OCPs with c-Fos or green fluorescent protein retrovirus, cultured them with macrophage colony-stimulating factor and IL-1 on bone slices or plastic dishes, and assessed osteoclast and resorption pit formation and expression of IL-1 by OCPs. We used a Transwell assay to determine whether OCPs secrete IL-1 when they interact with bone matrix. IL-1 induced osteoclast formation directly from c-Fos-expressing OCPs on plastic. c-Fos-expressing OCPs formed osteoclasts spontaneously on bone slices without addition of cytokines. OCPs on bone secreted IL-1, which induced osteoclast formation from c-Fos-expressing OCPs in the lower Transwell dishes. The bone matrix proteins dentin sialoprotein and osteopontin, but not transforming growth factor-β, stimulated OCP expression of IL-1 and induced c-Fos-expressing OCP differentiation into osteoclasts. Osteoclasts eroding inflamed joints have higher c-Fos expression compared with osteoclasts inside bone. We conclude that OCPs expressing c-Fos may induce their differentiation directly into osteoclasts by an autocrine mechanism in which they produce IL-1 through interaction with bone matrix. TNF could induce c-Fos expression in OCPs at sites of inflammation in bone to promote this autocrine mechanism and thus amplify bone loss.

Increased osteoclast formation and activity are responsible for bone loss in common bone diseases such as postmenopausal osteoporosis, rheumatoid arthritis, periodontal disease, and orthopedic implant loosening (1). Osteoclast differentiation and function are controlled primarily by macrophage colony-stimulating factor (M-CSF)[2] and RANKL (receptor activator of NF-κB ligand) expressed by osteoblast/stromal cells and by signaling downstream from their receptors in osteoclast precursors (OCPs) (2–5). M-CSF induces expression of RANK, the receptor for RANKL, in OCPs (6). Binding of RANKL to RANK completes the differentiation of OCPs into mature osteoclasts through sequential activation of the transcription factors NF-κB, c-Fos, and NFATc1 (nuclear factor of activated T cells c1) (7). Expression of each of these transcription factors is required in OCPs for osteoclastogenesis (1, 8, 9). c-Fos is a component of the dimeric transcription factor AP-1 (10, 11), which mediates RANKL-stimulated osteoclast formation by transcriptionally activating NFATc1 (12–14). Overexpression of c-Fos in *fos*$^{-/-}$ OCPs rescues the defect in RANKL-mediated osteoclast formation from these cells (12), although overexpression of c-Fos is not sufficient by itself for induction of OCP differentiation into osteoclasts on plastic culture plates (12–14). We have reported recently that c-Fos can substitute for NF-κB p50 and p52 in OCPs from mice lacking NF-κB p50 and p52 and that, under these circumstances, RANKL or tumor necrosis factor (TNF) can induce osteoclast formation from these cells, but not when the cells express green fluorescent protein (GFP) (7).

Interleukin-1 (IL-1) and TNF are pro-inflammatory cytokines that stimulate bone resorption and are expressed in abundance at sites of inflammation in and around bones (15–17). They are produced by a variety of cell types, including monocytes/macrophages, OCPs, and mature osteoclasts themselves (18, 19). Like TNF, IL-1 promotes RANKL expression by marrow osteoblastic stromal cells (20) and by this mechanism induces osteoclastogenesis indirectly. However, unlike TNF, IL-1 alone cannot directly mediate osteoclast formation from OCPs *in vitro* (21). OCPs and osteoclasts express IL-1 receptors, and IL-1 appears to enhance osteoclast differentiation by promoting fusion of OCPs (22) and supporting the survival of mature osteoclasts (23–25).

* This work was supported by National Institutes of Health Grants AR43510 (to B. F. B.) and AR48697 (to L. X.). The costs of publication of this article were defrayed in part by the payment of page charges. This article must therefore be hereby marked "*advertisement*" in accordance with 18 U.S.C. Section 1734 solely to indicate this fact.

[1] To whom correspondence should be addressed: Dept. of Pathology and Laboratory Medicine, University of Rochester Medical Center, 601 Elmwood Ave, P. O. Box 626, Rochester, NY 14642. Tel.: 585-275-5837; Fax: 585-273-3637; E-mail: Brendan_Boyce@urmc.rochester.edu.

[2] The abbreviations used are: M-CSF, macrophage colony-stimulating factor; OCPs, osteoclast precursors; TNF, tumor necrosis factor; GFP, green fluorescent protein; IL-1, interleukin-1; TGFβ, transforming growth factor-β; OPN, osteopontin; DSP, dentin sialoprotein; IL-1Ra, IL-1 receptor antagonist; DPP, dentin phosphoprotein; WT, wild-type; dKO, double knock-out; TNF-Tg, TNF transgenic; MDS, M-CSF-dependent splenocytes; TRAP, tartrate-resistant acid phosphatase; RT, reverse transcription.

OCPs are attracted to bone surfaces by signaling, which appears to involve bone-lining cells (26) and osteocytes (27). Once they are attached to bone matrix, osteoclasts and OCPs receive survival-enhancing signals through integrin-mediated signaling (28), and they secrete cytokines such as IL-1 and TNF (29) as well as factors that can affect the differentiation of osteoblast precursors (30). Bone matrix contains several non-collagenous proteins, including transforming growth factor-β (TGFβ) (31, 32) and members of the SIBLING (small integrin-binding ligand, *N*-linked glycoprotein) family of proteins such as osteopontin (OPN), dentin sialoprotein (DSP), and bone sialoprotein (33, 34). These proteins are released from the matrix during bone resorption. TGFβ has multiple effects on bone cells and has been proposed to be involved in coupling osteoblasts to sites of bone resorption (31, 32). OPN appears to anchor osteoclasts to bone matrix through interaction with the vitronectin receptor on the osteoclast basolateral membrane (35) and is required for the activation of osteoclastic bone resorption in unloaded mice (36). Overexpression of bone sialoprotein in osteoblasts leads to bone loss indirectly in mice by enhancing RANKL expression by osteoblastic cells and thus inducing osteoclast differentiation (37). However, it is not known if any of the bone matrix proteins play a more direct role in osteoclast formation.

Here, we report that when OCPs interact with bone matrix or are treated with DSP or OPN, they increase their expression of IL-1. This induces differentiation of c-Fos-expressing OCPs directly into osteoclasts in the absence of RANKL by an autocrine/paracrine mechanism.

MATERIALS AND METHODS

Reagents and Animals—Recombinant human M-CSF, murine RANKL, IL-1, TNF, IL-1 receptor antagonist (IL-1Ra), TGFβ1, and a pan-specific TGFβ antibody were purchased from R&D Systems, Inc. (Minneapolis, MN). TNF receptor fusion protein (ENBREL) was from Amgen (Thousand Oaks, CA). DSP and dentin phosphoprotein (DPP) were extracted from rat dentin, and OPN was extracted from rat long bone cortex as we reported previously (38). Wild-type (WT) mice (C57Bl/6), NF-κB p50/p52 double knock-out (dKO) mice (C57Bl/6×129), and human TNF transgenic (TNF-Tg) mice (line 3647, CBA×C57Bl/6) were used as we described previously (7, 39). The Institutional Animal Care and Use Committee approved all animal studies.

Osteoclastogenesis and Viral Infection—Splenocytes were extracted from spleens through a fine wire mesh and cultured with conditioned medium from a M-CSF-producing cell line (1:20 dilution) (40) for 3 days in α-modified essential medium with 10% fetal calf serum (HyClone Laboratories, Logan, UT) to enrich for osteoclast precursors, which we named M-CSF-dependent splenocytes (MDS). The cells were then infected with retroviral supernatants of c-Fos-, NFATc1-, or GFP control-infected Plat-E packaging cells in the presence of M-CSF (10 ng/ml) and Polybrene (8 μg/ml) as we described previously (7).

For Transwell assays, GFP or c-Fos retrovirus-infected WT MDS were seeded directly on bovine cortical bone slices (4 × 4 × 0.2 mm) in 96-well plates or on plastic in the wells of the lower chamber of a 24-well Transwell dish and cultured in the presence of M-CSF for 2 days. The bone slices were then transferred to the upper chamber of the Transwell culture plates and co-cultured with the GFP- or c-Fos-infected MDS in the lower chamber for an additional 8 days in the presence of M-CSF. When multinucleated cell formation was identified under an inverted microscope, the cells were fixed with 10% formalin and stained for tartrate-resistant acid phosphatase (TRAP) activity to identify osteoclasts as $TRAP^+$ cells containing three or more nuclei, and these cells were counted as described previously (7).

For cytokine blockade experiments using different inhibitors, GFP- or c-Fos-infected MDS were cultured directly on plastic plates or bone slices for 2 days in the presence of M-CSF and then treated with cytokines ± inhibitors. When primary spleen cells were used, they were cultured with M-CSF for 3 days prior to inhibitor treatment.

For functional assays, infected cells were cultured on bone slices for 10 days under the same conditions as described above. Osteoclasts were then removed; resorption pits were visualized after 0.1% toluidine blue staining; and the mean pit area (mm^2/slice) was measured as described previously (7).

Quantitative Real-time Reverse Transcription (RT)-PCR—RNA from MDS or retrovirus-infected cells cultured on either plastic dishes or bone slices was extracted using TRIzol reagent (Invitrogen), and cDNA synthesis was performed using the GeneAmp RNA PCR core kit (Applied Biosystems, Foster City, CA). Quantitative PCR amplification was performed with gene-specific primers using an iCycler real-time PCR machine and iQ SYBR Green Supermix (both from Bio-Rad) according to the manufacturer's instruction. The murine primer sequences used were as follows: TNFα, 5′-CACACTCAGATCATCTTCTCAA-3′ (forward) and 5′-AGTAGACAAGGTACAACCCATC-3′ (reverse); IL-1β, 5′-ATTAGACAGCTGCACTACAGG-3′ (forward) and 5′-GGAGAATATCACTTGTTGGTTG-3′ (reverse); c-*fos*, 5′-CTGTCAACACACAGGACTTTT-3′ (forward) and reverse 5′-AGGAGATAGCTGCTCTACTTTG-3′ (reverse); and β-actin, 5′-ACCCAGATCATGTTTGAGAC-3′ (forward) and 5′-GTCAGGATCTTCATGAGGTAGT-3′ (reverse). The relative standard curve method was used to calculate the amplification difference for each primer set (41). A standard curve was made from four points corresponding to 5-fold cDNA serial dilutions for each gene. For each sample, the relative amount was calculated from its respective standard curve. The quantity of the target gene mRNA was then obtained by division of each value by the actin value. Standards and samples were run in triplicate.

Immunohistochemistry—Long bones from 4-month-old TNF-Tg mice and WT littermates (three/group) were fixed in 10% phosphate-buffered formalin, decalcified in 10% EDTA, and embedded in paraffin wax. Deparaffinized sections were quenched with 3% hydrogen peroxide, treated for antigen retrieval for 30 min, and stained with a rabbit anti-c-Fos antibody (Santa Cruz Biotechnology, Inc., Santa Cruz, CA) and a biotinylated goat anti-rabbit secondary antibody (Dako, Carpinteria, CA). The biotin was detected using standard avidin-biotin peroxidase technology (Dako) and diaminobenzidine (Sigma) as the chromogen. An adjacent section was used for TRAP staining to identify mature osteoclasts as described previously (42). c-Fos-positive and -negative osteoclasts on the

joint surfaces and in the primary spongiosa of the metaphyses were counted, and the number of c-Fos-positive osteoclasts was expressed as a percentage of the total number of osteoclasts at each site.

IL-1 Protein Measurement—Culture medium from GFP- or c-Fos-infected cells grown on plastic or bone slices in 96-well plates or in the Transwell assay system was collected at the time when osteoclasts could be seen on the plastic of the culture wells or around bone slices using an inverted microscope (generally after 7–9 days). A mouse IL-1β enzyme-linked immunosorbent assay kit (eBioscience, San Diego, CA) was used to measure IL-1 concentration according to the manufacturer's instructions.

Statistics—All results are given as the mean ± S.D. Comparisons between two groups were analyzed using Student's two-tailed unpaired *t* test. One-way analysis of variance and Dunnett's post hoc multiple comparisons were used for comparisons among three or more groups. p values <0.05 were considered statistically significant. Each experiment was repeated at least twice with similar results.

RESULTS

IL-1 Induces Osteoclast Formation Directly from Osteoclast Precursors Overexpressing c-Fos or NFATc1 and Synergizes with RANKL—To determine whether IL-1 can induce osteoclast formation from WT OCPs overexpressing c-Fos, we infected WT MDS with c-Fos retrovirus and cultured them on plastic culture plates in the presence of M-CSF. c-Fos-expressing MDS alone did not give rise to osteoclasts on plastic plates, but they formed numerous TRAP$^+$ osteoclasts when they were treated with IL-1 (Fig. 1*A*). These cells also formed resorption pits when they were cultured on bone slices with IL-1 (data not shown). Furthermore, like TNF and RANKL (7), IL-1 induced osteoclast formation directly from NF-κB dKO OCPs overexpressing c-Fos (Fig. 1*A*). In addition, suboptimal doses of IL-1 and RANKL induced osteoclast formation synergistically (Fig. 1*E*).

c-Fos induces expression of NFATc1, which is critical for osteoclastogenesis (12). We found that expression of NFATc1 was up-regulated in cells overexpressing c-Fos when they were treated with IL-1 for 72–96 h, the time when osteoclasts were forming in these cultures (data not shown). IL-1 induced osteoclast formation from both WT and NF-κB dKO MDS expressing NFATc1 (Fig. 1*B*), and notably, NFATc1 induced osteoclast formation 1 day earlier than c-Fos, although both ultimately induced similar numbers of osteoclasts (data not shown).

Overexpression of c-Fos in Osteoclast Precursors on Bone Slices Promotes Osteoclast Differentiation through Production of Soluble Factors—When we cultured c-Fos-expressing WT or NF-κB dKO MDS on bone slices without IL-1, we found unexpectedly that they gave rise to osteoclasts, and these cells also formed resorption pits (Fig. 1*C*, *panels a–d*, and *D*). Interestingly, osteoclasts also formed from c-Fos-expressing OCPs on the plastic around the bone slices (Fig. 1*C*, *panels e* and *f*). Because there was no other cytokine added to these bone slice cultures except M-CSF and because c-Fos-overexpressing OCPs cultured on plastic did not form osteoclasts in the absence of IL-1, we hypothesized that c-Fos-expressing OCPs

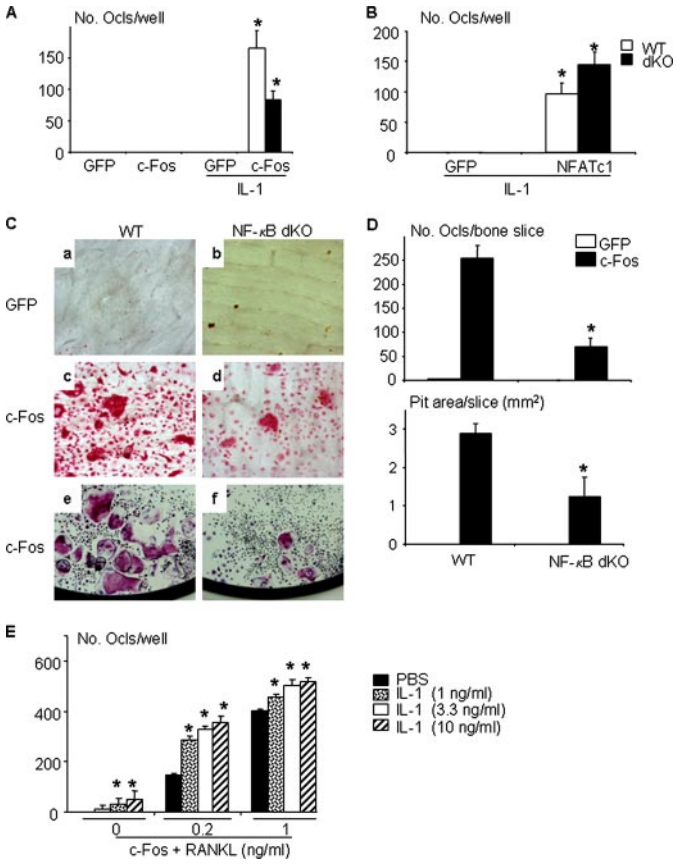

FIGURE 1. **c-Fos overexpression in osteoclast precursors directly induces their differentiation into osteoclasts on bone slices.** GFP, c-Fos, or NFATc1 retrovirus-infected WT and NF-κB p50/p52 dKO MDS were cultured on plastic culture plates ± IL-1 or on bone slices + M-CSF to form osteoclasts. Osteoclasts were identified by TRAP staining, and resorption pits were visualized by toluidine blue staining. The number of osteoclasts (*Ocls*) that formed on plastic dishes from GFP- or c-Fos-infected (*A*) or NFATc1-infected (*B*) cells was assessed. TRAP$^+$ osteoclasts in c-Fos-overexpressing cells on bone slices (*C*, *panels a–d*) and TRAP$^+$ cells that formed on the plastic dish around bone slices (*panels e* and *f*) and the number of osteoclasts on bone slices and pit area (*D*) were assessed. c-Fos retrovirus-infected WT MDS were cultured with various doses of IL-1 and RANKL on plastic plates to form osteoclasts. The numbers of osteoclasts were assessed (*E*). Values are the mean ± S.D. of four plastic culture wells or bone slices. *, $p < 0.05$ *versus* the respective value for GFP-infected cells or phosphate-buffered saline (*PBS*)-treated cells.

grown on bone produce and release a soluble factor(s) to drive differentiation of the precursors on the adjacent plastic into mature osteoclasts or that osteoclasts or OCPs migrate from the bone onto the plastic.

To examine whether c-Fos-expressing OCPs grown on bone secrete a soluble factor(s), we used a Transwell assay system. GFP- or c-Fos-expressing OCPs were cultured on bone slices in the upper chamber, and either GFP- or c-Fos-infected cells were cultured on plastic in the lower chamber of the Transwell culture system (Fig. 2*A*). These cultures also contained M-CSF. We found that c-Fos-expressing cells grown on the bone slices in the upper chamber induced mature osteoclasts from c-Fos- but not GFP-infected cells in the lower chamber (Fig. 2*B*). Furthermore, GFP-expressing OCPs cultured on bone slices in the upper chamber induced more osteoclasts in the lower chambers compared with c-Fos-expressing OCPs (Fig. 2*B*). Bone slices placed alone in the upper chamber without cells did not induce osteoclast formation from c-Fos-expressing OCPs.

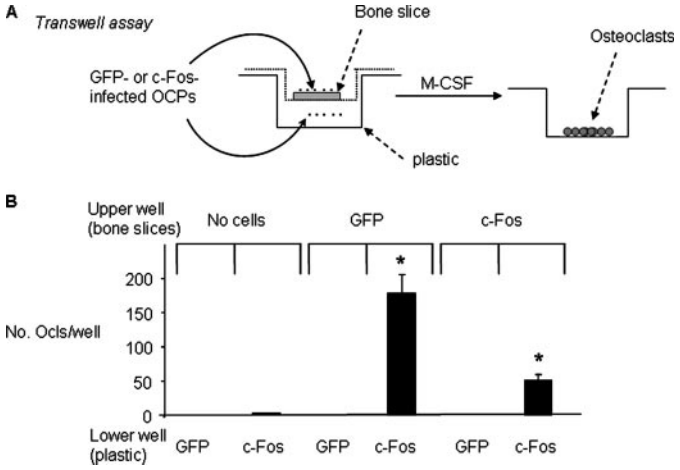

FIGURE 2. **Osteoclast precursors grown on bone slices induce osteoclast formation from c-Fos-overexpressing precursors on plastic below them.** *A*, GFP or c-Fos retrovirus-infected WT MDS were cultured on bone slices or plastic in 24-well plates for 2 days in the presence of added M-CSF. Bone slices with either GFP- or c-Fos-infected cells or control slices with no cells were moved into the upper chambers of the Transwells and co-cultured with cells on plastic in the lower chambers as indicated in the presence of added M-CSF. *B*, the cells in the lower chambers were stained for TRAP activity, and the number of osteoclasts (*Ocls*) was counted. Values are the mean ± S.D. of three wells. *, $p < 0.05$ *versus* the co-culture of c-Fos-infected cells in the lower chamber with blank bone.

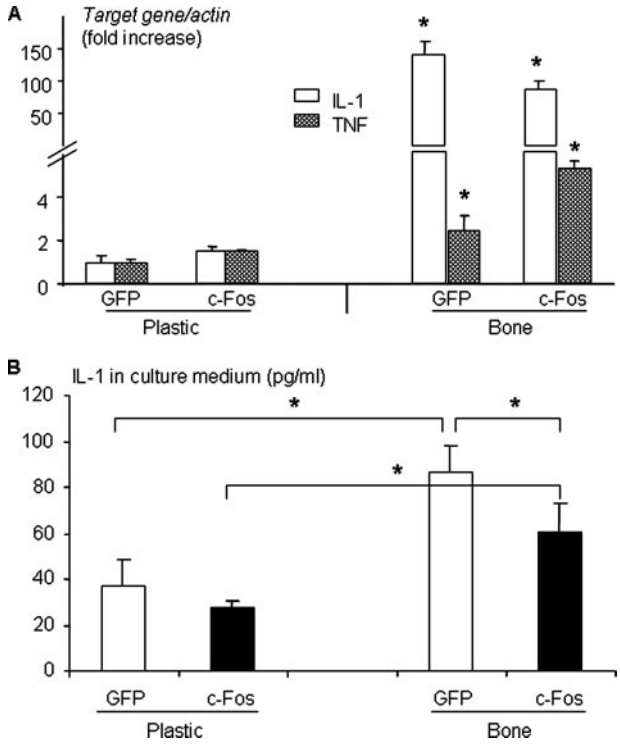

FIGURE 3. **Osteoclast precursors grown on bone slices express markedly more IL-1 than those cultured on plastic plates.** GFP or c-Fos retrovirus-infected WT MDS were cultured on plastic or bone slices in the presence of M-CSF for 9 days. *A*, total RNA was extracted and subjected to real-time RT-PCR to determine the expression levels of IL-1 and TNF. The -fold changes were calculated by dividing the value of the target gene by that of the GFP-infected samples on plastic. Values are the mean ± S.D. of triplicate loadings. *, $p < 0.05$ *versus* cells grown on plastic. *B*, IL-1β protein concentrations were measured by enzyme-linked immunosorbent assay in the culture medium collected from the cultures described in *A* at the end of the culture. Data are the mean ± S.D. of five wells from one independent experiment representative of three. *, $p < 0.05$ between the two groups indicated.

IL-1 Is Produced by Osteoclast Precursors Interacting with Bone and Promotes Osteoclastogenesis from c-Fos-expressing Precursors—TNF and IL-1 are pro-inflammatory cytokines known to be secreted by osteoclasts and OCPs (29). Thus, we considered both as candidate factors that could be produced by OCPs on bone slices to induce osteoclast formation. Both GFP- and c-Fos-expressing OCPs grown on bone slices expressed markedly more IL-1 mRNA (100–150-fold higher) compared with similar OCPs cultured on plastic dishes after 9 days of culture (Fig. 3*A*), the time when osteoclast formation begins. In contrast, the expression of TNF mRNA by the OCPs was increased by only 3–5-fold on bone slices. Furthermore, GFP-expressing OCPs expressed significantly higher levels of IL-1 mRNA on bone slices (Fig. 3*A*) and secreted more IL-1 protein into the culture medium compared with c-Fos-expressing OCPs (Fig. 3*B*).

To determine whether IL-1 or TNF is responsible for the differentiation of c-Fos-expressing OCPs on bone slices and functions as a soluble factor, OCPs were infected with c-Fos retrovirus and cultured on bone slices in the presence of IL-1Ra or the TNF inhibitor ENBREL. IL-1Ra reduced c-Fos-induced osteoclast formation by ~50% (Fig. 4*A*), an effect similar to that reported as the maximal effect of this protein to inhibit IL-1-induced osteoclast activity (29). In contrast, ENBREL at doses that completely blocked TNF-induced osteoclast formation on plastic had no inhibitory effect on c-Fos-induced osteoclast formation on bone slices (Fig. 4*B*). Furthermore, IL-1Ra reduced osteoclast formation (Fig. 4*C*) induced by IL-1 in c-Fos-expressing OCPs cultured on plastic to a similar extent as in c-Fos-expressing OCPs without IL-1 on bone slices (Fig. 4*A*).

Bone Matrix Proteins Stimulate Osteoclast Precursors to Produce IL-1 and Induce Their Differentiation into Osteoclasts When c-Fos Is Overexpressed—Bone matrix contains at least 20 non-collagenous proteins, several of which have been reported to stimulate macrophages to produce cytokines such as IL-1 (43). To examine whether this is also the case for OCPs, we cultured OCPs on plastic, treated them with the bone matrix proteins (DSP, DPP, OPN, or TGFβ), and determined their effects on the levels of IL-1 and TNF mRNA expression by real-time RT-PCR. DSP in particular and also OPN significantly increased IL-1 and to a lesser extent TNF mRNA expression, whereas DPP and TGFβ had no effect (Fig. 5*A*).

To determine whether IL-1 induced by DSP or OPN can substitute for exogenous IL-1 and stimulate c-Fos-expressing OCPs to differentiate into osteoclasts, we treated GFP- or c-Fos-infected cells with DSP or OPN on plastic. As expected, these proteins did not induce osteoclast formation from GFP-infected cells. However, they induced osteoclast formation from c-Fos-expressing precursors, which was partially blocked by IL-1Ra (Fig. 5*B*) to the same extent as observed in cultures on bone slices (Fig. 4*A*) or in IL-1-induced osteoclast formation (Fig. 4*C*).

TNF, but Not IL-1, Increases c-Fos Expression in Osteoclast Precursors—Our experiments demonstrated that IL-1-induced osteoclast formation requires forced c-Fos expression in OCPs. We reasoned that IL-1 would not have this effect by itself, otherwise IL-1 alone should be able to induce osteoclast formation. TNF has been reported to induce osteoclast differentiation

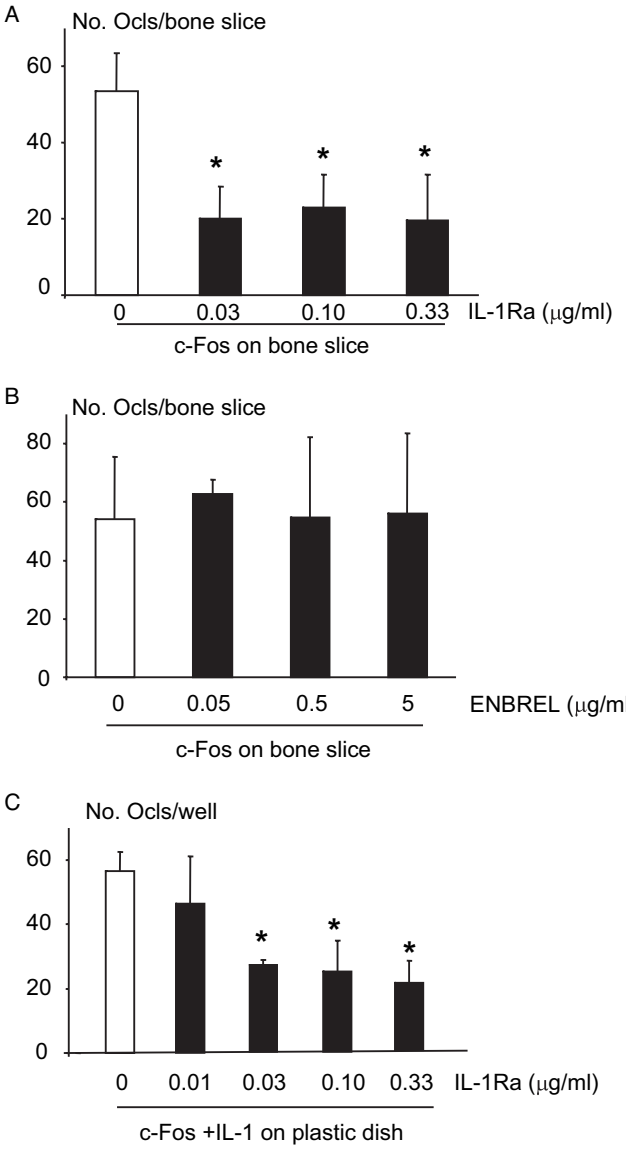

FIGURE 4. **IL-1Ra decreases c-Fos expression-induced osteoclast formation on bone slices.** c-Fos retrovirus-infected WT MDS were cultured on bone slices and treated with the indicated doses of IL-1Ra (*A*) or ENBREL (*B*) or cultured on plastic plates and treated with IL-1 (10 ng/ml) plus the indicated doses of IL-1Ra (*C*) in the presence of M-CSF. The number of $TRAP^+$ osteoclasts (*Ocls*) was counted. Values are the mean ± S.D. of four bone slices or wells. *, $p < 0.05$ *versus* the non-blocker control.

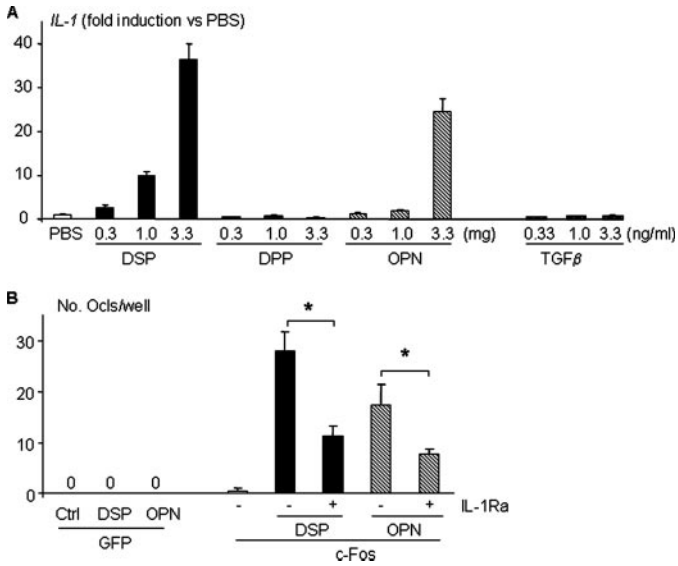

FIGURE 5. **Bone matrix proteins stimulate osteoclast precursors to express IL-1, which induces c-Fos-expressing precursors to form osteoclasts.** *A*, WT MDS were treated with DSP, DPP, OPN, or TGFβ for 4 h at the indicated doses. The expression levels of IL-1 mRNA were evaluated by real-time RT-PCR. The -fold changes were calculated by dividing the value of the treated cells by that of the phosphate-buffered saline (*PBS*)-treated samples. Values are the mean ± S.D. of triplicate loadings. *B*, GFP or c-Fos retrovirus-infected WT MDS were treated with DSP (3 μg/ml) or OPN (3 μg/ml) in the absence or presence of IL-1Ra (0.1 μg/ml) for 6 days. The number of $TRAP^+$ osteoclasts (*Ocls*) was counted. Values are the mean ± S.D. of four wells. *, $p < 0.05$ *versus* the non-blocker control (*Ctrl*).

directly from OCPs in the absence of RANKL (7, 44). To examine whether TNF induces high c-Fos expression in OCPs *in vitro*, we first treated OCPs with TNF and compared its effects on the expression of c-Fos by OCPs with that of IL-1 and RANKL, which was included here as a positive control. TNF induced sustained c-Fos expression from 8 to 96 h and induced osteoclast formation. RANKL had a similar but less pronounced effect. In contrast, IL-1 did not have any stimulatory effect on c-Fos expression or induce osteoclast differentiation (Fig. 6*A*).

We then examined the effect of TNF on c-Fos expression by osteoclasts *in vivo* using TNF-Tg mice, which develop an inflammatory erosive arthritis similar to rheumatoid arthritis (45). In bone sections from TNF-Tg mice with erosive arthritis, we found a strong signal for c-Fos in the cytoplasm and nuclei of many osteoclasts (43 ± 10%) eroding the bone on the outer surfaces of inflamed joints (Fig. 6*B*), where local concentrations of IL-1 and TNF are increased (46, 47). In contrast, fewer osteoclasts (21 ± 1%) in the subjacent primary spongiosa away from the inflammation expressed c-Fos, and the intensity of the staining in the same sections was much weaker (Fig. 6*B*). In the primary spongiosa, c-Fos was expressed strongly in osteoblasts, cells known to up-regulate their expression of c-Fos in response to factors such as parathyroid hormone (48, 49), indicating that the lower intensity of the signal for c-Fos in osteoclasts inside the bones was not due to suboptimal specimen fixation or processing.

DISCUSSION

IL-1 is a potent stimulator of bone resorption *in vitro* and *in vivo* (50). It enhances osteoclast precursor fusion and osteoclast survival *in vitro* (23–25). However, unlike TNF and RANKL, IL-1 cannot induce osteoclast formation directly from OCPs *in vitro*. In this study, we have demonstrated that IL-1 can induce osteoclast formation directly from OCPs when they are overexpressing c-Fos and that these cells can resorb bone *in vitro*. Thus, under conditions in which c-Fos expression is increased in OCPs, IL-1 could potentially induce osteoclast formation directly to mediate bone loss in addition to its known effect to induce osteoclast formation indirectly through up-regulation of RANKL expression by accessory cells such as osteoblast/stromal cells or synoviocytes.

c-Fos plays an essential role in osteoclast formation. Its expression is required in OCPs for RANKL- and TNF-induced osteoclast formation (7, 12). c-Fos acts downstream from NF-κB in RANKL- and TNF-induced OCP differentiation into

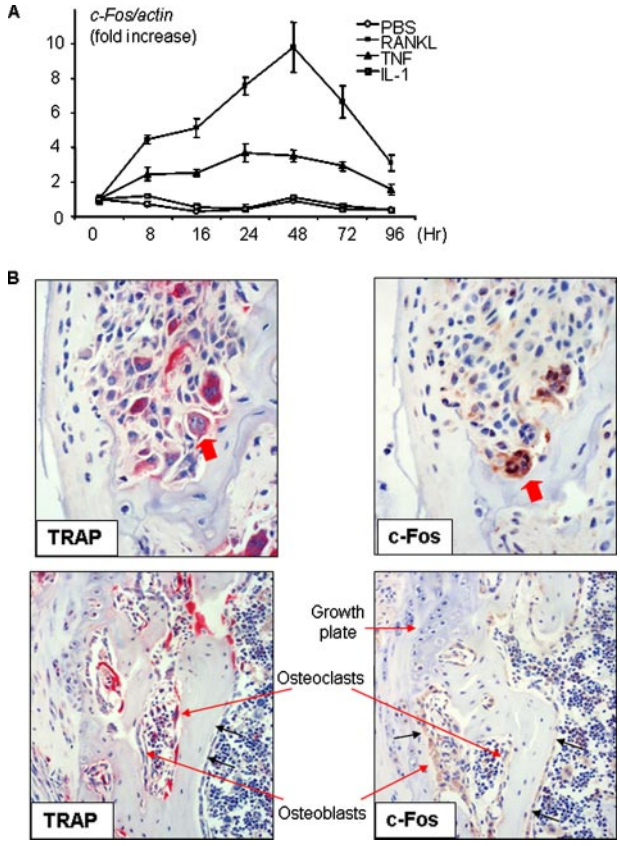

FIGURE 6. **TNF increases c-Fos expression in osteoclasts and precursors.** *A*, WT MDS were treated with IL-1 (10 ng/ml), TNF (20 ng/ml), RANKL (10 ng/ml), or phosphate-buffered saline (*PBS*) for the indicated time points. Expression of c-Fos mRNA was measured by real-time RT-PCR. The -fold changes were calculated by dividing the value of the treated cells by that of the untreated base-line samples. Values are the mean ± S.D. of triplicate loadings. *B*, long bone sections from a knee joint of a 4-month-old TNF-Tg mouse showing severe synovial inflammation and adjacent bone and cartilage erosion were stained for TRAP activity. Adjacent sections were stained with anti-c-Fos antibody. The *upper panels* show $TRAP^+$ osteoclasts actively resorbing subchondral bone and also strongly expressing c-Fos (*arrows*). The *lower panels* show the primary spongiosa of the same animal below the growth plate, where osteoclasts were actively resorbing bone as part of normal endochondral ossification, with these $TRAP^+$ osteoclasts having low or no c-Fos protein expression. Data are representative of three TNF-Tg mice.

osteoclasts and can substitute for NF-κB p50 and p52 in this process (7). We found that TNF and RANKL, but not IL-1, increase c-Fos expression by OCPs *in vitro*. This failure of IL-1 to induce c-Fos expression in OCPs could explain its inability to induce osteoclast formation directly from these cells. We found that c-Fos expression is increased in osteoclasts on the eroded surfaces of joints and to a lesser extent in the metaphyseal bones of TNF-Tg mice. TNF and RANKL expression is increased in the joints of these mice and of patients with rheumatoid arthritis, where IL-1 expression is also increased (46). Thus, TNF and RANKL could increase the expression of c-Fos in OCPs in rheumatoid arthritis and other inflammatory bone diseases, and IL-1 could directly induce differentiation of these OCPs into osteoclasts. Our finding that IL-1 acts synergistically with RANKL at very low doses to induce osteoclast formation directly from c-Fos-expressing WT OCPs suggests that this osteoclast-inducing effect of IL-1 could be further enhanced by RANKL. This would represent a new role for IL-1 to increase osteoclast formation by a direct autocrine mechanism that would amplify the bone-resorbing effects of TNF and RANKL and contribute to the vicious cycle we have proposed for cytokine-induced bone loss (7). This effect would be similar to that reported previously for bone sialoprotein, which contributes to RANKL-mediated bone resorption by inducing osteoclastogenesis and osteoclast survival and decreasing osteoclast apoptosis (51).

NFATc1, the master transcription factor regulating late-stage osteoclast differentiation, is activated downstream from c-Fos (7, 12). In NF-κB p50/p52 dKO OCPs treated with RANKL or TNF, NFATc1 rescues the defect in osteoclast formation as effectively as c-Fos (7). We found that NFATc1 also rescues this defect in dKO OCPs treated with IL-1 and that it mediates osteoclast formation from WT OCPs treated with IL-1. These findings indicate that although IL-1 is unable to induce osteoclast formation on its own, its downstream signaling can lead to osteoclast formation in a pathway that requires c-Fos and NFATc1.

Surprisingly, we also found that when OCPs overexpressing c-Fos were cultured on bone slices along with M-CSF, they released sufficient amounts of IL-1 to promote their differentiation into mature bone-resorbing osteoclasts in the absence of other cytokines. This induction of osteoclast formation was inhibited significantly by IL-1Ra, but not by the TNF inhibitor ENBREL, indicating that IL-1 largely mediated the effect. The failure of the IL-1Ra to completely prevent osteoclast formation in any of our assays, including IL-1-treated c-Fos-expressing OCPs, suggests that osteoclast interaction with bone matrix may induce the expression by OCPs of another factor(s). However, a previous study using this reagent (29) and our experience with it indicate that these reagents do not completely prevent IL-1-induced effects on osteoclasts or OCPs. Thus, further studies will be required to resolve this issue.

Our Transwell culture assays showed that GFP-expressing OCPs express more IL-1 and thus support more osteoclast formation from precursors in the lower chamber compared with c-Fos-expressing OCPs. RANKL induces c-Fos expression in OCPs, but it also induces expression of interferon-β, which limits osteoclast formation by down-regulating c-Fos expression (52). However, we found that c-Fos- and GFP-expressing OCPs express similar levels of interferon-β (data not shown). At this time, we do not have a definitive explanation for this difference between these culture conditions. It may represent another autoregulatory mechanism within OCPs to limit excess osteoclast differentiation.

Interaction of osteoclasts with bone matrix is known to increase osteoclast survival (53) through integrin-mediated signaling (28). Our findings indicate a previously unknown effect of interaction of osteoclastic cells with bone matrix, *viz.* release of IL-1 and differentiation of c-Fos-expressing precursors into mature bone-resorbing osteoclasts. We found that the bone matrix proteins DSP and OPN stimulate expression of IL-1 by OCPs. A previous study has shown that dental matrix proteins stimulate macrophages to release cytokines, including IL-1, TNF, and MCP-1 (monocyte chemoattractant protein-1) (43). Furthermore, we found that DSP and OPN stimulate differentiation of c-Fos-expressing OCPs into osteoclasts and that

IL-1Ra significantly inhibits this effect. It could be concluded from these observations that when OCPs adhere to bone matrix, they begin to resorb it and so cause release of these proteins, which in turn could stimulate the OCPs to produce IL-1. However, GFP-expressing OCPs also express increased amounts of IL-1, and they do not form resorption pits even after they have been on the matrix for >10 days. Thus, resorption does not seem to be required for OCPs to increase their expression of IL-1. Furthermore, neither NF-κB p50 nor NF-κB p52 expression appears to be required for OCPs to produce IL-1 because c-Fos-overexpressing NF-κB dKO OCPs also form osteoclasts on bone slices (Fig. 1*C*). Nevertheless, release of DSP and OPN from bone matrix by osteoclasts during resorption could augment the effect of this interaction.

It is becoming increasingly clear that osteoclasts are involved in more complex processes than simply resorption of bone. Their precursors are formed in the marrow cavity, where they increase their proliferation and expression of c-Fms, the receptor for M-CSF, in response to cytokines such as TNF (54). OCPs circulate in the blood and are attracted to sites of inflammation, where pro-inflammatory cytokine concentrations are high (18), and to sites destined for resorption. OCPs enter resorption lacunae through blood vessels, where they appear to be separated from the adjacent marrow cells by a membrane inside which osteoclasts, osteoblasts, and other cells interact (55). OCPs and osteoclasts secrete cytokines to modulate the activities of cells around them and, in that respect at least, can be considered to be immune cells at sites of inflammation in bone (8, 18, 56). Recent studies indicate that OCPs not only respond to osteoblasts to have their formation regulated either positively or negatively (1) but also regulate osteoblast formation both positively and negatively (30, 57). Our studies indicate that OCPs also react to signals coming from bone matrix by secreting IL-1. It is likely that this interaction between OCPs and osteoblastic cells is more complicated than these recent studies suggest and that other proteins released from the matrix will affect the function of osteoclasts and other cells in the resorption lacunae. IL-1 has multiple ways of promoting bone resorption, including mediating the pro-osteoclastogenic effects of TNF through osteoblast/stromal cells (29). IL-1 is generally a more powerful stimulator of bone resorption than TNF, and this direct action mediated through interaction with bone matrix may be one of the mechanisms that accounts for these differences.

In conclusion, our findings have defined novel interactions among OCPs, bone matrix, and cytokines at sites of bone resorption. These involve an autocrine role for IL-1 to induce osteoclast formation from OCPs in which c-Fos expression has been up-regulated by cytokines such as TNF and RANKL to amplify their effects at sites in bone where their concentrations are increased. They also support involvement of a paracrine loop in which matrix proteins such as DSP and OPN could induce increased secretion of IL-1 by OCPs to induce the differentiation of c-Fos-expressing OCPs into bone-resorbing osteoclasts. Collectively, these processes could account for the aggressive resorption observed in common inflammatory bone diseases.

Acknowledgments—We thank Dr. Toshio Kitamura for the Plat-E cell line and Bianai Fan for technical assistance with histology.

REFERENCES

1. Boyle, W. J., Simonet, W. S., and Lacey, D. L. (2003) *Nature* **423,** 337–342
2. Lacey, D. L., Timms, E., Tan, H. L., Kelley, M. J., Dunstan, C. R., Burgess, T., Elliott, R., Colombero, A., Elliott, G., Scully, S., Hsu, H., Sullivan, J., Hawkins, N., Davy, E., Capparelli, C., Eli, A., Qian, Y. X., Kaufman, S., Sarosi, I., Shalhoub, V., Senaldi, G., Guo, J., Delaney, J., and Boyle, W. J. (1998) *Cell* **93,** 165–176
3. Kong, Y. Y., Yoshida, H., Sarosi, I., Tan, H. L., Timms, E., Capparelli, C., Morony, S., Oliveira-dos-Santos, A. J., Van, G., Itie, A., Khoo, W., Wakeham, A., Dunstan, C. R., Lacey, D. L., Mak, T. W., Boyle, W. J., and Penninger, J. M. (1999) *Nature* **397,** 315–323
4. Li, J., Sarosi, I., Yan, X. Q., Morony, S., Capparelli, C., Tan, H. L., McCabe, S., Elliott, R., Scully, S., Van, G., Kaufman, S., Juan, S. C., Sun, Y., Tarpley, J., Martin, L., Christensen, K., McCabe, J., Kostenuik, P., Hsu, H., Fletcher, F., Dunstan, C. R., Lacey, D. L., and Boyle, W. J. (2000) *Proc. Natl. Acad. Sci. U. S. A.* **97,** 1566–1571
5. Kapur, R. P., Yao, Z., Iida, M. H., Clarke, C. M., Doggett, B., Xing, L., and Boyce, B. F. (2004) *J. Bone Miner. Res.* **19,** 1689–1697
6. Arai, F., Miyamoto, T., Ohneda, O., Inada, T., Sudo, T., Brasel, K., Miyata, T., Anderson, D. M., and Suda, T. (1999) *J. Exp. Med.* **190,** 1741–1754
7. Yamashita, T., Yao, Z., Li, F., Zhang, Q., Badell, I. R., Schwarz, E. M., Takeshita, S., Wagner, E. F., Noda, M., Matsuo, K., Xing, L., and Boyce, B. F. (2007) *J. Biol. Chem.* **282,** 18245–18253
8. Takayanagi, H. (2007) *Nat. Rev. Immunol.* **7,** 292–304
9. Boyce, B. F., Yamashita, T., Yao, Z., Zhang, Q., Li, F., and Xing, L. (2005) *J. Bone Miner. Metab.* **23,** (suppl.) 11–15
10. Karsenty, G., and Wagner, E. F. (2002) *Dev. Cell* **2,** 389–406
11. Matsuo, K., Owens, J. M., Tonko, M., Elliott, C., Chambers, T. J., and Wagner, E. F. (2000) *Nat. Genet.* **24,** 184–187
12. Matsuo, K., Galson, D. L., Zhao, C., Peng, L., Laplace, C., Wang, K. Z., Bachler, M. A., Amano, H., Aburatani, H., Ishikawa, H., and Wagner, E. F. (2004) *J. Biol. Chem.* **279,** 26475–26480
13. Takayanagi, H., Kim, S., Koga, T., Nishina, H., Isshiki, M., Yoshida, H., Saiura, A., Isobe, M., Yokochi, T., Inoue, J., Wagner, E. F., Mak, T. W., Kodama, T., and Taniguchi, T. (2002) *Dev. Cell* **3,** 889–901
14. Asagiri, M., Sato, K., Usami, T., Ochi, S., Nishina, H., Yoshida, H., Morita, I., Wagner, E. F., Mak, T. W., Serfling, E., and Takayanagi, H. (2005) *J. Exp. Med.* **202,** 1261–1269
15. Kaplan, C., and Finnegan, A. (2003) *Front. Biosci.* **8,** d1018–d1029
16. Sato, K., and Takayanagi, H. (2006) *Curr. Opin. Rheumatol.* **18,** 419–426
17. Teitelbaum, S. L. (2000) *J. Bone Miner. Metab.* **18,** 344–349
18. Xing, L., Schwarz, E. M., and Boyce, B. F. (2005) *Immunol. Rev.* **208,** 19–29
19. Teitelbaum, S. L. (2006) *Arthritis Res. Ther.* **8,** 201–209
20. Hofbauer, L. C., Lacey, D. L., Dunstan, C. R., Spelsberg, T. C., BRiggs, B. L., and Khosla, S. (1999) *Bone* **25,** 255–259
21. Kobayashi, K., Takahashi, N., Jimi, E., Udagawa, N., Takami, M., Kotake, S., Nakagawa, N., Kinosaki, M., Yamaguchi, K., Shima, N., Yasuda, H., Morinaga, T., Higashio, K., Martin, T. J., and Suda, T. (2000) *J. Exp. Med.* **191,** 275–286
22. Jimi, E., Nakamura, I., Duong, L. T., Ikebe, T., Takahashi, N., Rodan, G. A., and Suda, T. (1999) *Exp. Cell Res.* **247,** 84–93
23. Lee, Z. H., Lee, S. E., Kim, C. W., Lee, S. H., Kim, S. W., Kwack, K., Walsh, K., and Kim, H. H. (2002) *J. Biochem.* (*Tokyo*) **131,** 161–166
24. Jimi, E., Akiyama, S., Tsurukai, T., Okahashi, N., Kobayashi, K., Udagawa, N., Nishihara, T., Takahashi, N., and Suda, T. (1999) *J. Immunol.* **163,** 434–442
25. Jimi, E., Shuto, T., and Koga, T. (1995) *Endocrinology* **136,** 808–811
26. Chambers, T. J. (1981) *J. Pathol.* **135,** 1–7
27. Tatsumi, S., Ishii, K., Amizuka, N., Li, M., Kobayashi, T., Kohno, K., Ito, M., Takeshita, S., and Ikeda, K. (2007) *Cell Metab.* **5,** 464–475
28. Teitelbaum, S. L. (2006) *Ann. N. Y. Acad. Sci.* **1068,** 95–99
29. Wei, S., Kitaura, H., Zhou, P., Ross, F. P., and Teitelbaum, S. L. (2005) *J. Clin. Investig.* **115,** 282–290

30. Lee, S. H., Rho, J., Jeong, D., Sul, J. Y., Kim, T., Kim, N., Kang, J. S., Miyamoto, T., Suda, T., Lee, S. K., Pignolo, R. J., Koczon-Jaremko, B., Lorenzo, J., and Choi, Y. (2006) *Nat. Med.* **12,** 1403–1409
31. Mundy, G. R., and Bonewald, L. F. (1990) *Ann. N. Y. Acad. Sci.* **593,** 91–97
32. Zwerina, J., Hayer, S., Tohidast-Akrad, M., Bergmeister, H., Redlich, K., Feige, U., Dunstan, C., Kollias, G., Steiner, G., Smolen, J., and Schett, G. (2004) *Arthritis Rheum.* **50,** 277–290
33. Qin, C., Baba, O., and Butler, W. T. (2004) *Crit. Rev. Oral Biol. Med.* **15,** 126–136
34. Fisher, L. W., Torchia, D. A., Fohr, B., Young, M. F., and Fedarko, N. S. (2001) *Biochem. Biophys. Res. Commun.* **280,** 460–465
35. Reinholt, F. P., Hultenby, K., Oldberg, A., and Heinegard, D. (1990) *Proc. Natl. Acad. Sci. U. S. A.* **87,** 4473–4475
36. Ishijima, M., Rittling, S. R., Yamashita, T., Tsuji, K., Kurosawa, H., Nifuji, A., Denhardt, D. T., and Noda, M. (2001) *J. Exp. Med.* **193,** 399–404
37. Valverde, P., and Chen, J. (2006) *J. Bone Miner. Res.* **21,** Suppl. 1, S167 (abstr.)
38. Qin, C., Brunn, J. C., Cadena, E., Ridall, A., Tsujigiwa, H., Nagatsuka, H., Nagai, N., and Butler, W. T. (2002) *J. Dent. Res.* **81,** 392–394
39. Li, P., Schwarz, E. M., O'Keefe, R. J., Ma, L., Looney, R. J., Ritchlin, C. T., Boyce, B. F., and Xing, L. (2004) *Arthritis Rheum.* **50,** 265–276
40. Takeshita, S., Kaji, K., and Kudo, A. (2000) *J. Bone Miner. Res.* **15,** 1477–1488
41. Johnson, M. R., Wang, K., Smith, J. B., Heslin, M. J., and Diasio, R. B. (2000) *Anal. Biochem.* **278,** 175–184
42. Xing, L., Bushnell, T. P., Carlson, L., Tai, Z., Tondravi, M., Siebenlist, U., Young, F., and Boyce, B. F. (2002) *J. Bone Miner. Res.* **17,** 1200–1210
43. Silva, T. A., Lara, V. S., Silva, J. S., Oliveira, S. H., Butler, W. T., and Cunha, F. Q. (2005) *J. Dent. Res.* **84,** 79–83
44. Kim, N., Kadono, Y., Takami, M., Lee, J., Lee, S. H., Okada, F., Kim, J. H., Kobayashi, T., Odgren, P. R., Nakano, H., Yeh, W. C., Lee, S. K., Lorenzo, J. A., and Choi, Y. (2005) *J. Exp. Med.* **202,** 589–595
45. Keffer, J., Probert, L., Cazlaris, H., Georgopoulos, S., Kaslaris, E., Kioussis, D., and Kollias, G. (1991) *EMBO J.* **10,** 4025–4031
46. Goldring, S. R. (2003) *Calcif. Tissue Int.* **73,** 97–100
47. Sfikakis, P. P., and Kollias, G. (2003) *Curr. Opin. Rheumatol.* **15,** 380–386
48. Lee, E., Miura, M., Yoshinari, M., Iwai, H., and Kariya, K. (1994) *Biochem. Biophys. Res. Commun.* **202,** 128–134
49. Clohisy, J. C., Scott, D. K., Brakenhoff, K. D., Quinn, C. O., and Partridge, N. C. (1992) *Mol. Endocrinol.* **6,** 1834–1842
50. Boyce, B. F., Aufdemorte, T. B., Garrett, I. R., Yates, A. J., and Mundy, G. R. (1989) *Endocrinology* **125,** 1142–1150
51. Valverde, P., Tu, Q., and Chen, J. (2005) *J. Bone Miner. Res.* **20,** 1669–1679
52. Takayanagi, H., Kim, S., Matsuo, K., Suzuki, H., Suzuki, T., Sato, K., Yokochi, T., Oda, H., Nakamura, K., Ida, N., Wagner, E. F., and Taniguchi, T. (2002) *Nature* **416,** 744–749
53. Hughes, D. E., Wright, K. R., Uy, H. L., Sasaki, A., Yoneda, T., Roodman, G. D., Mundy, G. R., and Boyce, B. F. (1995) *J. Bone Miner. Res.* **10,** 1478–1487
54. Yao, Z., Li, P., Zhang, Q., Schwarz, E. M., Keng, P., Arbini, A., Boyce, B. F., and Xing, L. (2006) *J. Biol. Chem.* **281,** 11846–11855
55. Hauge, E. M., Qvesel, D., Eriksen, E. F., Mosekilde, L., and Melsen, F. (2001) *J. Bone Miner. Res.* **16,** 1575–1582
56. Baron, R. (2004) *Nat. Med.* **10,** 458–460
57. Zhao, C., Irie, N., Takada, Y., Shimoda, K., Miyamoto, T., Nishiwaki, T., Suda, T., and Matsuo, K. (2006) *Cell Metab.* **4,** 111–121

 Related Commentary, page 2879

NF-κB p100 limits TNF-induced bone resorption in mice by a TRAF3-dependent mechanism

Zhenqiang Yao, Lianping Xing, and Brendan F. Boyce

Department of Pathology and Laboratory Medicine, University of Rochester Medical Center, Rochester, New York, USA.

TNF and RANKL mediate bone destruction in common bone diseases, including osteoarthritis and RA. They activate NF-κB canonical signaling directly in osteoclast precursors (OCPs) to induce osteoclast formation in vitro. However, unlike RANKL, TNF does not activate the alternative NF-κB pathway efficiently to process the IκB protein NF-κB p100 to NF-κB p52, nor does it appear to induce osteoclast formation in vivo in the absence of RANKL. Here, we show that TNF limits RANKL- and TNF-induced osteoclast formation in vitro and in vivo by increasing NF-κB p100 protein accumulation in OCPs. In contrast, TNF induced robust osteoclast formation in vivo in mice lacking RANKL or RANK when the mice also lacked NF-κB p100, and TNF-Tg mice lacking NF-κB p100 had more severe joint erosion and inflammation than did TNF-Tg littermates. TNF, but not RANKL, increased OCP expression of TNF receptor–associated factor 3 (TRAF3), an adapter protein that regulates NF-κB p100 levels in B cells. TRAF3 siRNA prevented TNF-induced NF-κB p100 accumulation and inhibition of osteoclastogenesis. These findings suggest that upregulation of TRAF3 or NF-κB p100 expression or inhibition of NF-κB p100 degradation in OCPs could limit bone destruction and inflammation-induced bone loss in common bone diseases.

Introduction

Osteoclasts, the cells that degrade bone, play a central role in bone destruction in common erosive bone diseases, including postmenopausal osteoporosis, RA, and periodontitis (1). In these conditions there is increased production of the proinflammatory cytokines TNF (2) and RANKL (3), members of the TNF superfamily (4) that stimulate bone resorption by osteoclasts (5, 6). Signaling through their receptors is mediated by recruitment of TNF receptor–associated factors (TRAFs) (7–9) and leads to activation of transcription factors including NF-κB, c-Fos, and NFATc1 (10, 11). Among the TRAF family of proteins, TRAF6 is essential for RANKL-induced osteoclast differentiation in vitro but not in vivo (12, 13), while TRAF2 may be required for TNF-induced osteoclast formation (14). TRAF5 is involved in both RANKL- and TNF-induced osteoclast formation (15). Similar to RANKL, but not many other osteoclast-stimulating factors, TNF can induce osteoclast formation directly from osteoclast precursors (OCPs) in vitro in the presence of M-CSF independent of RANKL/RANK signaling (16–18), by activation of NF-κB (10, 11). TNF induces fewer osteoclasts from WT OCPs and less bone resorption in vitro than RANKL (11, 17), but the molecular basis for this difference is unknown.

The NF-κB family of proteins includes NF-κB p105 (also known as NF-κB1), NF-κB p100 (also known as NF-κB2) (precursor proteins, which can act as inhibitory κB proteins by binding to other NF-κB proteins), RelA (p65), RelB, and c-Rel (19, 20). In response to RANKL and TNF, p105 is processed constitutively to p50 (19–21), which forms dimers, typically with RelA (19, 20). RANKL and TNF activate these p50/RelA dimers in the canonical NF-κB pathway to promote OCP differentiation, but they also induce expression of p100 in these cells (22). p100 undergoes efficient proteasomal processing to p52 in response to RANKL through activation of NF-κB–inducing kinase (NIK) and IKKα in the alternative pathway (23), thus releasing p52/RelB complexes to translocate to nuclei. In mice lacking NIK, unprocessed p100 can accumulate in OCPs and limit pathologic, but not basal, osteoclastogenesis induced by RANKL (23). TNF increases p100 protein levels slightly in OCPs (24), but it is not known whether TNF limits osteoclastogenesis through this mechanism. NIK is also involved in canonical NF-κB signaling (25). Its activity is regulated negatively by constitutive proteasomal degradation as a result of its association with TRAF3 (26–28), which limits p100 processing and inhibits noncanonical NF-κB signaling. Thus, ablation of TRAF3 protein in B cells in which CD40 or BAFF-R activation induces TRAF3 degradation and prevents NIK degradation, resulting in progressive accumulation of NIK and activation of the noncanonical NF-κB pathway through processing of p100 (26–28). Further, early postnatal lethality occurs in *TRAF3*$^{-/-}$ mice because of uncontrolled NIK activity; this is rescued by crossing the mice with *Nfkb2*$^{-/-}$ mice (28). However, it is not known whether TNF affects TRAF3 or NIK levels in OCPs as a mechanism to control osteoclast numbers or activity.

Basal osteoclast formation requires expression of RANKL (29), RANK (30), and NF-κB p105 and p100 (31, 32), but not of TNF, TNF receptors (p55 and p75) (33), or TRAF2, -5, or -6 (12, 14, 15, 18), although the precise roles of TRAF2, -5, and -6 in osteoclasts are controversial (12, 14, 15, 18). Despite compelling evidence for a strong proresorptive function of TNF, which induces osteoclast formation from *Rankl*$^{-/-}$ and *Rank*$^{-/-}$ OCPs in vitro when costimulated with TGF-β (17, 18), TNF does not induce osteoclast formation in vivo when administered to *Rank*$^{-/-}$ mice (34). These findings have led to the conclusion that RANKL/RANK signaling is a prerequisite for osteoclast differentiation in vivo (35). Here we report an unexpected role for TNF to limit TNF- and RANKL-induced osteoclastogenesis by inducing expression of NF-κB p100 and TRAF3 in OCPs. TNF also induces robust osteoclast formation in vivo in *Rankl*$^{-/-}$ and *Rank*$^{-/-}$ mice when they also lack NF-κB

Conflict of interest: The authors have declared that no conflict of interest exists.

Citation for this article: *J. Clin. Invest.* **119**:3024–3034 (2009). doi:10.1172/JCI38716.

p100. Importantly, deficiency of NF-κB2 accelerates TNF-induced bone loss and joint inflammation in a model of RA, pointing to a role for NF-κB p100 to limit bone resorption and inflammation in diseases in which TNF expression is increased.

Results

TNF induces expression of noncanonical NF-κB proteins differently from RANKL in OCPs. To investigate the possibility that TNF induces fewer osteoclasts from OCPs than RANKL by promoting accumulation of the inhibitory NF-κB p100 protein, we examined the expression pattern of p100 in WT OCPs. Both RANKL and TNF increased *p100/p52* mRNA levels within 4 hours of treatment by 11- and 7-fold, respectively, and these remained elevated by 7- and 5-fold, respectively, at 8 hours (data not shown). We examined p100 and p52 protein expression levels during our typical culture period (1–96 hours). TNF induced sustained accumulation of p100 between 4 and 72 hours (Figure 1A). In contrast, RANKL more efficiently processed p100 to p52 during this period (Figure 1A), and this was associated with the formation of larger numbers of osteoclasts (Figure 1B). p100 levels in TNF-treated cells were not different from those of PBS-treated controls at 96 hours, by which time osteoclast formation has peaked in these cultures (11). TNF also induced increased p52 levels, but to a lesser extent than RANKL between 8 and 48 hours, confirming that p100 is processed in response to TNF (24), especially at 72 and 96 hours, when TNF induces peak osteoclast formation (11). Both TNF and RANKL markedly increased RelB levels, but the effect of TNF was greater than that of RANKL from 48 to 96 hours (Figure 1A). Deficiency of p100 did not affect either TNF- or RANKL-mediated nuclear translocation of RelB (Supplemental Figure 1A; supplemental material available online with this article; doi:10.1172/JCI38716DS1), presumably because RelB also can associate with p50 and translocate into nuclei (36). In contrast, TNF and RANKL overall had similar stimulatory effects on the expression levels of the canonical NF-κB p50 and p65 proteins during osteoclastogenesis (24–96 hours), with some variation at each time point (Figure 1A). Of note, although both TNF and RANKL mediated rapid NF-κB p65 nuclear translocation, the effect of TNF was more sustained than that of RANKL (Supplemental Figure 1, B and C). We had observed this previously in OCPs from NF-κB1/2 double-knockout mice that do not form osteoclasts (11).

TNF-induced NF-κB p100 limits osteoclastogenesis. To determine whether TNF-induced NF-κB p100 limits the number of osteoclasts formed in response to TNF, we treated *Nfkb2*$^{-/-}$ and WT OCPs with TNF and found significantly more osteoclasts from *Nfkb2*$^{-/-}$ than from WT cells, the numbers being similar to those in RANKL-treated WT or *Nfkb2*$^{-/-}$ cells (Figure 1B). This effect was not associated with induction in vitro or in vivo in OCPs of IFN-β (data not shown), which limits RANKL-induced osteoclastogenesis by downregulating c-Fos expression in OCPs (37). Importantly, osteoclasts induced by TNF from *Nfkb2*$^{-/-}$ OCPs formed resorption pits as effectively as those induced by RANKL (Figure 1B). TNF activates c-Fos and NFATc1, the same critical transcriptional factors activated by RANKL to induce osteoclast differentiation, but TNF induces these to a lesser extent than RANKL when mature osteoclasts are formed (11). However, we found that TNF induced a fold induction of c-Fos and NFATc1 similar to that of RANKL when osteoclasts were forming in *Nfkb2*$^{-/-}$ cells (data not shown). Erk and p38 signaling are also involved in osteoclast differentiation and are activated in response to RANKL and TNF (38). We found that TNF induced stronger activation of both Erk and p38 than RANKL, and this was observed in both WT and *Nfkb2*$^{-/-}$ cells (data not shown).

Nfkb2$^{-/-}$ *OCPs lack both p100 and p52.* To determine whether p100 or p52 is responsible for the inhibitory effect of TNF, we infected *Nfkb2*$^{-/-}$ and WT OCPs with *p100, p52*, or *GFP* control retrovirus and treated them with TNF. p100 inhibited TNF- and RANKL-induced osteoclastogenesis significantly in both *Nfkb2*$^{-/-}$ and WT OCPs (Figure 1C). p52 also caused a small but significant reduction in osteoclast numbers (Figure 1C), which may be due to a minor inhibitory effect of p52 homodimers, but this effect was much less than that of p100. High expression of these retrovirally induced proteins was confirmed in infected WT OCPs (Figure 1C).

To determine whether p100 limits TNF-induced osteoclastogenesis in vivo, we injected TNF or PBS vehicle into the supra-calvarial subcutaneous tissues of *Nfkb2*$^{-/-}$ and *Nfkb2*$^{+/-}$ control mice twice daily for 5 days and examined its effects on osteoclastogenesis and resorption. Basal osteoclast numbers as well as osteoclast surface and eroded surface were similar in *Nfkb2*$^{-/-}$ and *Nfkb2*$^{+/-}$ mice (Figure 1D). Mean values for these parameters of bone resorption increased significantly in the *Nfkb2*$^{+/-}$ and *Nfkb2*$^{-/-}$ mice in response to TNF, but the increase was significantly greater in the *Nfkb2*$^{-/-}$ mice (Figure 1D). Serum levels of tartrate-resistant acid phosphatase 5b (TRAP5b), a specific marker of bone resorption released by osteoclasts, were significantly higher in *Nfkb2*$^{-/-}$ mice than in control mice treated with TNF (7.3 ± 0.5 vs. 5.4 ± 0.8 U/l; $P < 0.01$), confirming that *Nfkb2* deficiency enhances TNF-induced bone resorption. We also found that basal TRAP5b levels were higher in *Nfkb2*$^{-/-}$ mice than in their littermate controls (6.2 ± 0.1 vs 3.6 ± 0.4 U/l; $P < 0.01$), which suggests that osteoclasts in *Nfkb2*$^{-/-}$ mice are more active than WT osteoclasts, as we did not observe any difference in the number of osteoclasts at this time point. This effect differs from those we reported previously with IL-1, which induced similarly increased numbers of osteoclasts in *Nfkb2*$^{+/-}$ and *Nfkb2*$^{-/-}$ mice (39). IL-1 does not induce osteoclast formation from WT OCPs in the absence of RANKL but can do so when the cells overexpress c-Fos, which is activated by, and downstream of, NF-κB (40).

TNF induces osteoclastogenesis in Rank$^{-/-}$ *or Rankl*$^{-/-}$ *mice in the absence of NF-κB2.* TNF induces p100 expression through canonical NF-κB signaling (41). To test the hypothesis that p100 induced by TNF prevents osteoclast formation in vivo in *Rank*$^{-/-}$ mice, we first examined whether TNF increases the expression of NF-κB p100 protein in *Rank*$^{-/-}$ or *Rankl*$^{-/-}$ OCPs. Similar to its effects in WT cells, TNF induced p100 accumulation but not p52 protein in *Rank*$^{-/-}$ and *Rankl*$^{-/-}$ cells (Figure 2A), indicating that TNF-induced p100 protein expression is independent of RANK signaling. There was some variability in basal levels of p100 expression from one experiment to another, which is a recognized feature of currently available antibodies to this protein, but basal levels of expression overall did not vary significantly among WT, *Rank*$^{-/-}$, and *Rankl*$^{-/-}$ OCPs. As expected, RANKL did not have any effect on p100/p52 protein in *Rank*$^{-/-}$ cells, while it clearly increased p52 in *Rankl*$^{-/-}$ cells (Figure 2A). Of note, different from WT cells, RANKL did not increase p100 levels in *Rankl*$^{-/-}$ OCPs, possibly because they had not encountered RANKL previously and therefore might be more sensitive to RANKL and completely process p100 to p52.

We next generated *Rank*$^{-/-}$*/Nfkb2*$^{-/-}$ and *Rankl*$^{-/-}$*/Nfkb2*$^{-/-}$ mice to determine whether TNF could induce osteoclastogenesis in the absence of NF-κB2 and either RANK or RANKL. First, we treated OCPs from *Rank*$^{-/-}$*/Nfkb2*$^{+/-}$ and *Rankl*$^{-/-}$*/Nfkb2*$^{+/-}$ mice with TNF

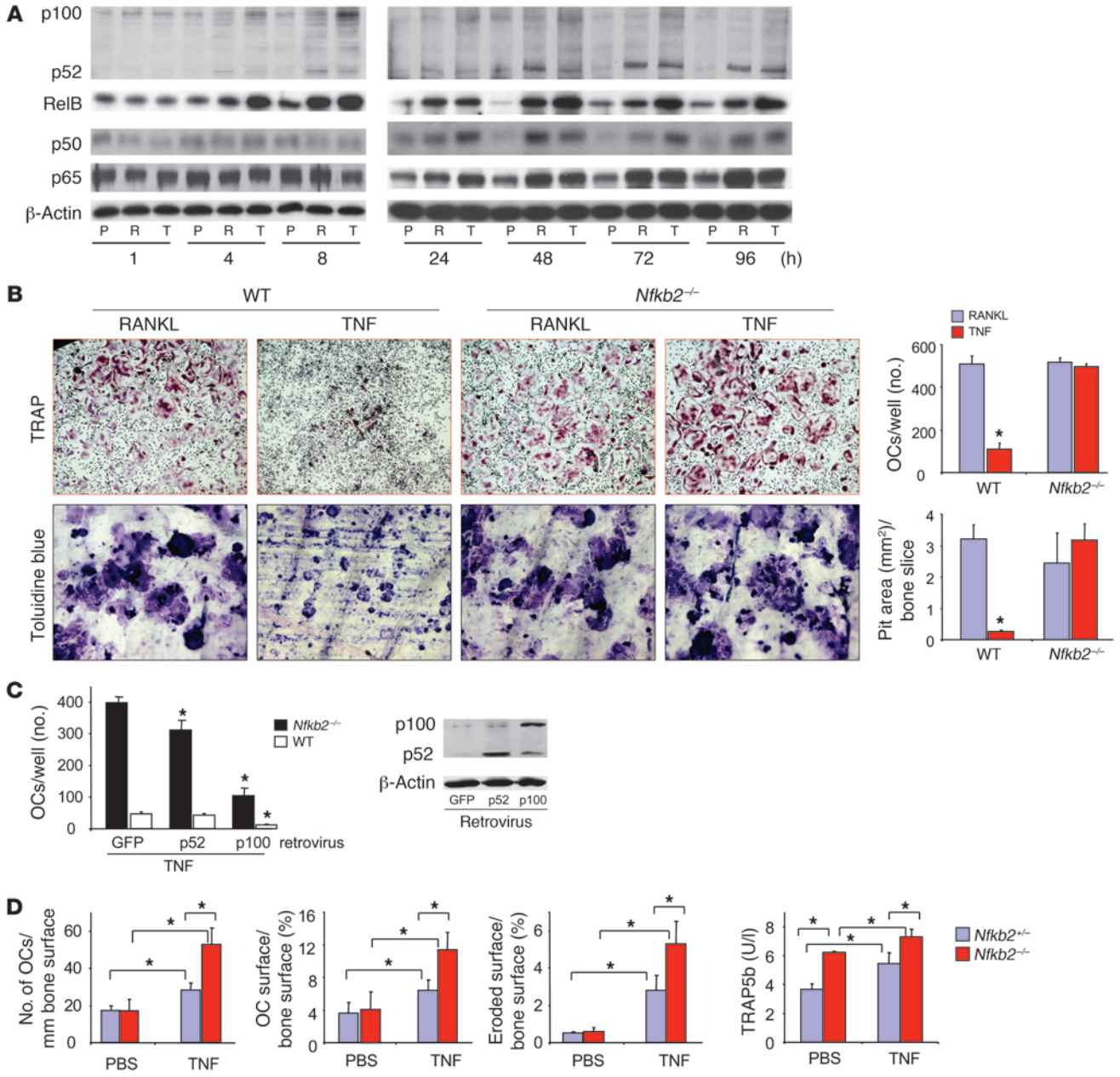

Figure 1

TNF-induced expression of NF-κB p100 inhibits osteoclastogenesis. (**A**) WT mouse OCPs, cultured from splenocytes with M-CSF for 3 days, were treated with RANKL or TNF for the indicated times. NF-κB proteins in whole-cell lysates were determined by Western blot. Experiments were repeated at least twice with similar results. P, PBS; R, RANKL 10 ng/ml; T, TNF 20 ng/ml. (**B**) WT or *Nfkb2*$^{-/-}$ OCPs were treated with RANKL or TNF directly on plastic or bone slices in 96-well plates in the presence of M-CSF for 2 and 5 days, respectively, to induce osteoclasts (OCs) and resorption pits. Top: Representative TRAP-stained osteoclasts (original magnification, ×4) and toluidine blue–stained pits (original magnification, ×20). Bottom: Osteoclast number and resorption pit area (n = 4/group; *P < 0.05 vs RANKL). (**C**) *Nfkb2*$^{-/-}$ or WT OCPs were infected with GFP, p100, or p52 retroviruses for 2 days and treated with TNF for 2 more days. Osteoclast numbers were counted (left panel; *P < 0.05 versus GFP), and the infection efficiency was confirmed by Western blot from the infected WT OCPs (right panels). (**D**) Murine TNF (0.5 μg in 10 μl PBS) or 10 μl PBS were injected twice daily over the calvariae of 4-week-old *Nfkb2*$^{-/-}$ or *Nfkb2*$^{+/-}$ control mice for 5 days (n = 4/group). The number of osteoclasts/mm bone surface, percentage of osteoclast surface/bone surface, and percentage of eroded surface/bone surface were measured in TRAP-stained calvarial bone sections, and serum TRAP5b was tested with ELISA.

and found that they formed slightly but significantly more osteoclasts than did OCPs from *Nfkb2*$^{+/-}$ littermates (Figure 2B). This likely reflects the fact that *Rank*$^{-/-}$ (42) and *Rankl*$^{-/-}$ (data not shown) mouse spleens contain more OCPs than do spleens of WT mice because of extramedullary hematopoiesis that results from their lack of an adequate marrow cavity. OCPs from *Rank*$^{-/-}$/*Nfkb2*$^{-/-}$ and *Rankl*$^{-/-}$/*Nfkb2*$^{-/-}$ mice treated with TNF formed significantly more osteoclasts than did OCPs from *Rank*$^{-/-}$/*Nfkb2*$^{+/-}$ and *Rankl*$^{-/-}$/

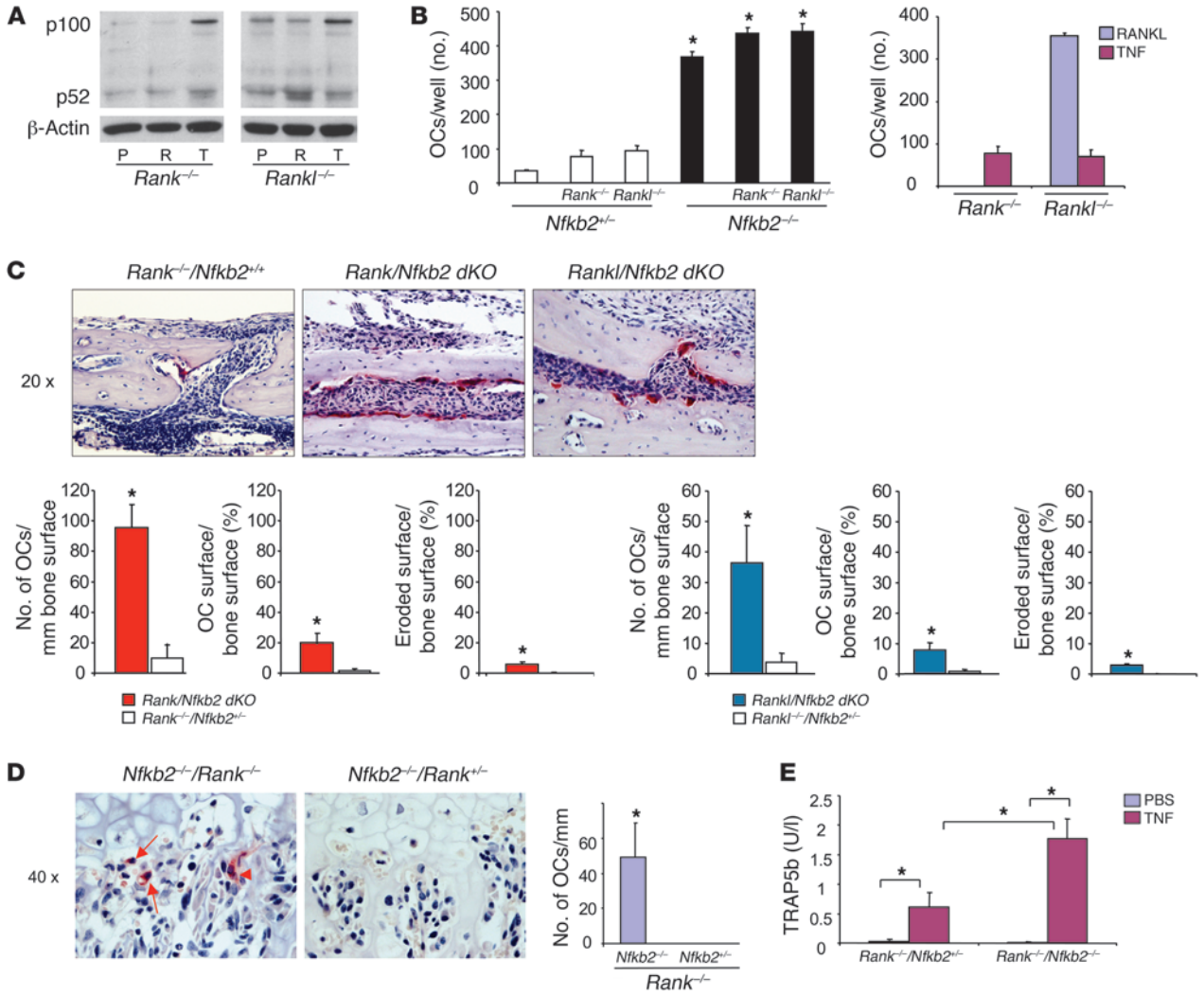

Figure 2

NF-κB2 deficiency enhances TNF-induced osteoclastogenesis in *Rank*$^{-/-}$ or *Rankl*$^{-/-}$ mice in vitro and in vivo. (**A**) NF-κB p100 and p52 were analyzed by Western blot in whole-cell lysates of PBS-, RANKL-, or TNF-treated (8 hours) OCPs from *Rank*$^{-/-}$ or *Rankl*$^{-/-}$ mice. (**B**) Left: OCPs from *Rank*$^{-/-}$/*Nfkb2*$^{-/-}$ or *Rankl*$^{-/-}$/*Nfkb2*$^{-/-}$ mice and their *Nfkb2*$^{+/-}$ littermates were treated with TNF for 2 days to evaluate osteoclast formation using TRAP staining (*$P < 0.05$ vs. *Nfkb2*$^{+/-}$). Right: OCPs from *Rank*$^{-/-}$/*Nfkb2*$^{+/+}$ and *Rankl*$^{-/-}$/*Nfkb2*$^{+/+}$ mice were treated with RANKL or TNF for comparison with *Rank*$^{-/-}$/*Nfkb2*$^{+/-}$ and *Rankl*$^{-/-}$/*Nfkb2*$^{+/-}$ mice to determine the effects of haploinsufficiency of *Nfkb2*. (**C**) Murine TNF (0.5 μg in 10 μl PBS) or 10 μl PBS was injected twice daily over the calvariae of *Rank*$^{-/-}$/*Nfkb2*$^{-/-}$ or *Rankl*$^{-/-}$/*Nfkb2*$^{-/-}$ mice and *Rank*$^{-/-}$ or *Rankl*$^{-/-}$ littermates. Top: TRAP-stained sections show numerous actively resorbing TRAP^{+} osteoclasts locally in calvarial sections (original magnification, ×20) from TNF-injected *Rank*$^{-/-}$/*Nfkb2*$^{-/-}$ or *Rankl*$^{-/-}$/*Nfkb2*$^{-/-}$ mice. Bottom: Numbers and surface extent of osteoclasts (n = 3/genotype). Occasional osteoclasts induced by TNF from a *Rank*$^{-/-}$/*Nfkb2*$^{+/+}$ mouse are illustrated in the left panels. *$P < 0.05$ vs. single KO mice. (**D**) Left: Occasional binucleate (arrowhead), but mainly mononuclear (arrows), TRAP^{+} cells (left panel) formed beneath hypertrophic chondrocytes in the growth plate of the tibia of a *Rank*$^{-/-}$/*Nfkb2*$^{-/-}$ mouse (original magnification, ×40), but not of *Rank*$^{-/-}$/*Nfkb2*$^{+/-}$ littermates injected with TNF as described in **C**. Right: Osteoclast numbers (expressed per mm of length of growth plate) counted in representative sections. (**E**) Serum TRAP5b levels were tested with ELISA from TNF- or PBS-injected *Rank*$^{-/-}$/*Nfkb2*$^{-/-}$ and *Rank*$^{-/-}$/*Nfkb2*$^{+/-}$ mice (n = 3/group; *$P < 0.05$).

Nfkb2$^{+/-}$ mice, the numbers being slightly higher than those from *Nfkb2*$^{-/-}$ OCPs (Figure 2B). We also found that TNF induced the formation of bone-resorbing osteoclasts from *Rank*$^{-/-}$/*Nfkb2*$^{+/-}$ and *Rankl*$^{-/-}$/*Nfkb2*$^{+/-}$ OCPs without the addition of TGF-β, which was suggested to be necessary as a pretreatment (18). A neutralizing TGF-β antibody did not prevent these effects, nor did the addition of TGF-β increase TNF-induced osteoclast numbers (data not shown). To exclude the possibility that haploinsufficiency of *Nfkb2* affects the status of *Rank*$^{-/-}$ and *Rankl*$^{-/-}$ osteoclast differentiation, we treated spleen cells from *Rank*$^{-/-}$ and *Rankl*$^{-/-}$ mice with TNF in the presence of M-CSF and found that similar osteoclast numbers were formed as with OCPs from *Rank*$^{-/-}$ and *Rankl*$^{-/-}$ mice with *Nfkb2* haploinsufficiency (Figure 2B, right panel). We believe that we were able to induce osteoclastogenesis in our cultures because we used lower numbers of M-CSF–dependent OCPs from these KO mice than we used from WT controls. The KO mice had higher numbers of OCPs in their spleens, as described above, and when we used similar numbers of OCPs from *Rankl*$^{-/-}$ or *Rank*$^{-/-}$ mice as from WT mice,

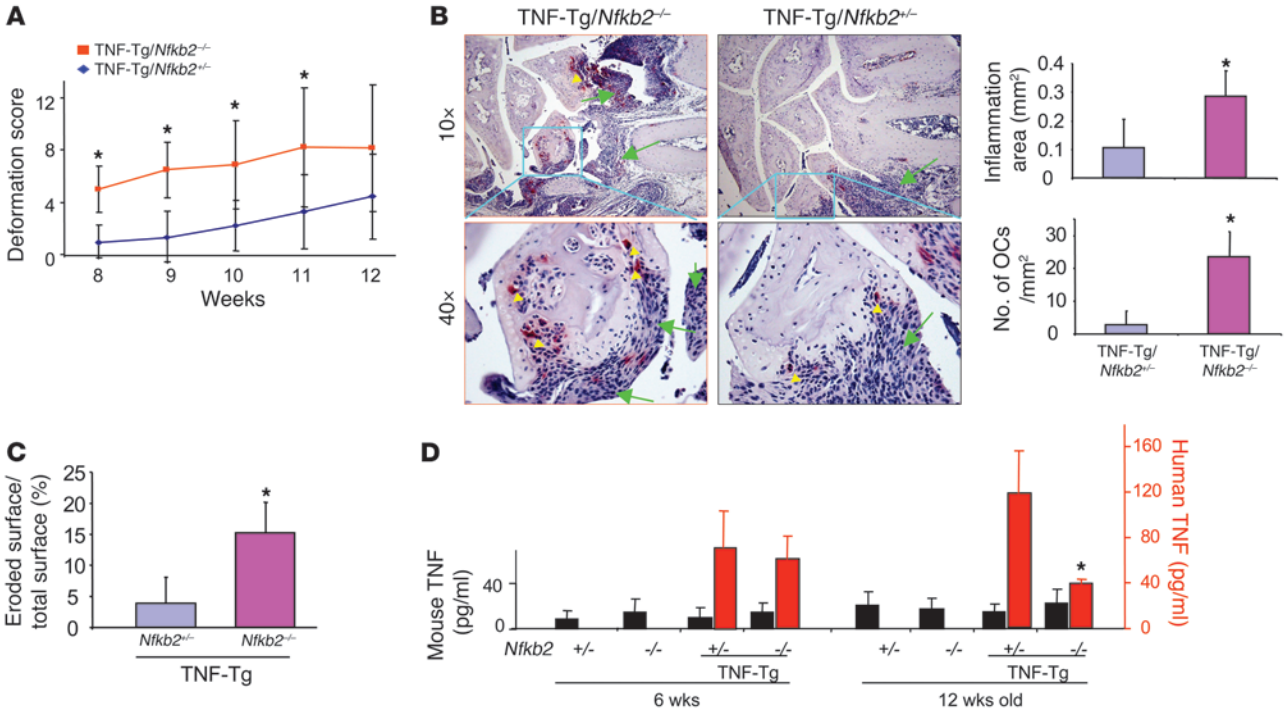

Figure 3
Increased joint inflammation and osteoclastogenesis in TNF-Tg/*Nfkb2*$^{-/-}$ mice. (**A**) Age-related changes in clinically assessed joint deformation scores showed that joint deformation occurred earlier in the TNF-Tg/*Nfkb2*$^{-/-}$ mice (n = 7) than in their TNF-Tg/*Nfkb2*$^{+/-}$ littermates (n = 8). (**B**) Representative TRAP-stained sections (original magnification, ×20) from 12-week-old animals showed more severe wrist joint inflammation (green arrows) and more osteoclasts (yellow arrowheads) in a TNF-Tg/*Nfkb2*$^{-/-}$ mouse than in a TNF-Tg/*Nfkb2*$^{+/-}$ mouse. Histomorphometric analysis showed that the area of inflammatory tissue (upper panel) and osteoclast numbers (lower panel) were increased in the wrists of TNF-Tg/*Nfkb2*$^{-/-}$ mice. *P < 0.05. (**C**) The percentage of cartilage eroded surface/total joint surface was measured in carpal bones of 6-week-old mice (n = 5/group). (**D**) Serum levels of murine TNF (black bars) and human TNF (red bars) were tested with ELISA at 6 and 12 weeks of age (*P < 0.05 vs. TNF-Tg/*Nfkb*$^{+/-}$ littermates).

TNF did not induce osteoclastogenesis (data not shown), presumably because their increased density inhibits differentiation.

Although absence of *Nfkb2* itself did not induce any osteoclasts in *Rank*$^{-/-}$ or *Rankl*$^{-/-}$ mice (PBS injection; data not shown), TNF induced many osteoclasts and resorption lacunae in the calvarial bones of the *Rank*$^{-/-}$/*Nfkb2*$^{-/-}$ and *Rankl*$^{-/-}$/*Nfkb2*$^{-/-}$ mice following local injection, associated with increased osteoclast and eroded surfaces (Figure 2, C and D). Only occasional osteoclasts were observed in the sections of TNF-injected *Rankl*$^{-/-}$ or *Rank*$^{-/-}$ mice, as reported previously (34). We also observed small numbers of TRAP^{+} osteoclasts in the long bones of the TNF-injected *Rank*$^{-/-}$/*Nfkb2*$^{-/-}$ and *Rankl*$^{-/-}$/*Nfkb2*$^{-/-}$ mice, although in contrast to those formed in the calvariae, these were mainly mononuclear cells located predominantly along the edge of the growth plates (Figure 2D) or in the centers of the physes. These cells had no effect on the increased bone volume in these osteopetrotic mice, presumably reflecting the short period of 5-day administration and their small size. To assess the possible function of these cells further, we measured serum TRAP5b levels. TRAP5b was undetectable in *Rank*$^{-/-}$/*Nfkb2*$^{+/-}$and *Rank*$^{-/-}$/*Nfkb2*$^{-/-}$ mice and was slightly but significantly increased by TNF injection in *Rank*$^{-/-}$/*Nfkb2*$^{+/-}$mice (0.61 ± 0.25 U/l). These values were increased further in *Rank*$^{-/-}$/*Nfkb2*$^{-/-}$ mice after TNF injection (1.77 ± 0.34 U/l; Figure 2E), confirming that osteoclasts induced by TNF in *Rank*$^{-/-}$ mice are functional and that NF-κB2 deficiency enhances TNF-induced osteoclastogenesis and bone resorption in the mice lacking RANK signaling. TRAP5b was not observed in serum or osteoclasts in bone sections from vehicle-treated *Rank*$^{-/-}$/*Nfkb2*$^{-/-}$ or *Rankl*$^{-/-}$/*Nfkb2*$^{-/-}$ mice, presumably because the concentration of endogenous TNF in the marrow cavities of these mice is low and not sufficiently high to induce OCP differentiation even in the absence of p100.

TNF-Tg mice lacking NF-κB p100 have more severe joint erosion and inflammation and systemic bone loss than TNF-Tg mice. To determine whether the absence of NF-κB2 would enhance joint erosion in TNF-Tg mice, we generated TNF-Tg/*Nfkb2*$^{-/-}$ mice and found that they developed joint deformity earlier than their TNF-Tg littermates, that is, at 8 weeks versus 12 weeks of age (Figure 3A). At 12 weeks of age, TNF-Tg/*Nfkb2*$^{-/-}$ mice had significantly increased areas of inflammation and osteoclast numbers in their forepaw joints assessed histomorphometrically (Figure 3B). However, we observed no significant difference in the types of inflammatory cells or in the appearance of the hyperplastic synoviocytes in the TNF-Tg/*Nfkb2*$^{-/-}$ mice compared with control mice upon histologic analysis. FACS analysis showed that *Nfkb2*$^{-/-}$ mice had significantly reduced numbers of B220^{+} B cells in their spleens and peripheral blood compared with *Nfkb2*$^{+/-}$ control mice. This feature was also present in TNF-Tg/*Nfkb2*$^{-/-}$ mice. In contrast, there was no difference in numbers of CD3^{+}, CD4^{+}, or CD8^{+} cells among the *Nfkb2*$^{+/-}$, *Nfkb2*$^{-/-}$, TNF-Tg/*Nfkb2*$^{+/-}$, and TNF-Tg/*Nfkb2*$^{-/-}$ mice (data not shown).

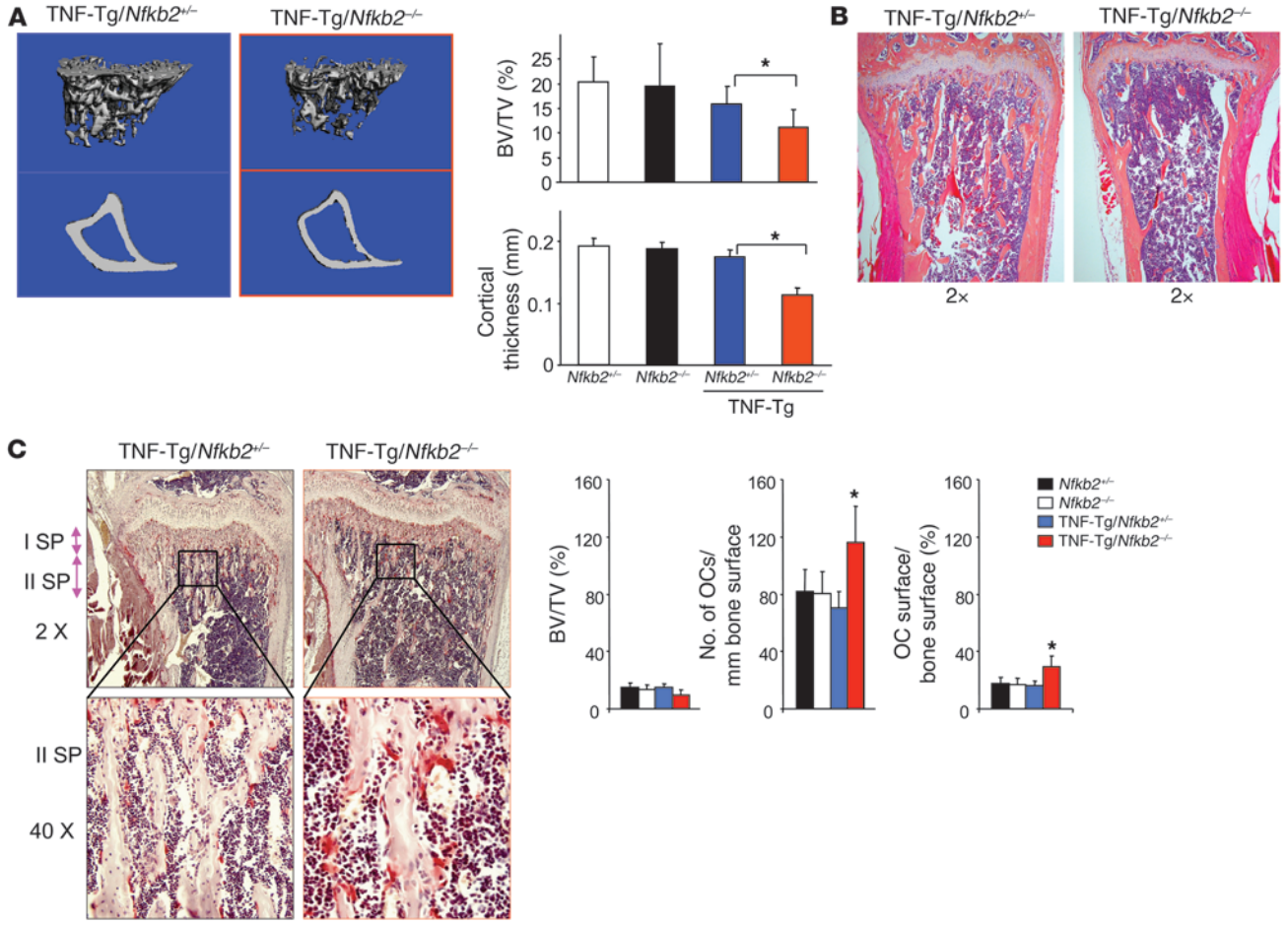

Figure 4

More severe systemic bone loss in TNF-Tg/*Nfkb2*$^{-/-}$ mice. (**A**) Tibiae from 12-week-old *Nfkb*$^{+/-}$ (n = 4), *Nfkb2*$^{-/-}$ (n = 4), TNF-Tg/*Nfkb2*$^{+/-}$ (n = 7), and TNF-Tg/*Nfkb2*$^{-/-}$ mice (n = 8) were subjected to μCT scanning. Representative images (left) and data analysis (right) showed reduced trabecular bone volume and cortical bone thickness in TNF-Tg/*Nfkb2*$^{-/-}$ mice. (**B**) H&E-stained sections of tibiae (original magnification, ×2) showed decreased trabecular bone in the metaphyseal regions and thinner cortices (green arrow) in TNF-Tg/*Nfkb2*$^{-/-}$ mice. (**C**) TRAP-stained sections of 6-week-old mice showed increased numbers of osteoclasts in the secondary spongiosa of the proximal tibia of a TNF-Tg/*Nfkb2*$^{-/-}$ mouse (left panels), which was confirmed by histomorphometric analysis (right panels). BV/TV, bone volume/tissue volume. *P < 0.05 vs. TNF-Tg/*Nfkb2*$^{+/-}$ mice. Original magnification, ×2 (top), ×40 (bottom).

TNF-Tg/*Nfkb2*$^{-/-}$ mice also had reduced long bone trabecular bone volume and cortical thickness compared with TNF-Tg/*Nfkb2*$^{+/-}$ mice (Figure 4A), which we confirmed morphometrically by 3-dimensional μCT imaging (Figure 4B). These TNF-Tg/*Nfkb2*$^{-/-}$ mice had lost almost all of their metaphyseal trabecular bone (Figure 4A), making it difficult to quantify and normalize osteoclast parameters histomorphometrically. However, in 6-week-old TNF-Tg/*Nfkb2*$^{-/-}$ mice, which had slightly but not significantly lower trabecular bone volume/tissue volume ratios than TNF-Tg mice, metaphyseal osteoclast numbers and surfaces were increased significantly (Figure 4C). These mice also had enhanced erosion of cartilage on their carpal bone joint surfaces compared with TNF-Tg/*Nfkb2*$^{+/-}$ littermates (Figure 3C). Bone formation rates assessed in undecalcified bone sections following double calcein labeling were similar in the TNF-Tg/*Nfkb2*$^{-/-}$ and control mice (data not shown).

We next determined whether NF-κB2 deficiency influences human (Tg) or mouse serum TNF concentrations in these mice. Murine TNF values were similar among the groups in both 6- and 12-week-old mice. NF-κB2 deficienc0y did not affect human TNF concentrations in 6-week-old TNF-Tg mice, but mean values were significantly lower in TNF-Tg/*Nfkb2*$^{-/-}$ mice than in TNF-Tg/*Nfkb2*$^{+/-}$ littermates aged 12 weeks. We do not have an explanation for the reduction of TNF in these mice, but by this age TNF-Tg/*Nfkb2*$^{-/-}$mice were much smaller than control mice, and some had already died. The cause of this early mortality requires further study.

TNF attenuates RANKL-induced osteoclastogenesis in vitro through NF-κB p100. Many cytokines, including RANKL, TNF, IL-1, and M-CSF, are involved in bone destruction in pathological conditions. Of these, RANKL and TNF can support the final stages of OCP differentiation to osteoclasts. Therefore, it is important to study how TNF and RANKL work together to control osteoclastogenesis. A previous study reported that TNF synergizes with RANKL to stimulate osteoclastogenesis in vitro (35) when both cytokines are added at the beginning of the culture period. However, the synergistic effect occurs only in RANKL pretreated cells (43), which we confirmed (data not shown). We then used a dif-

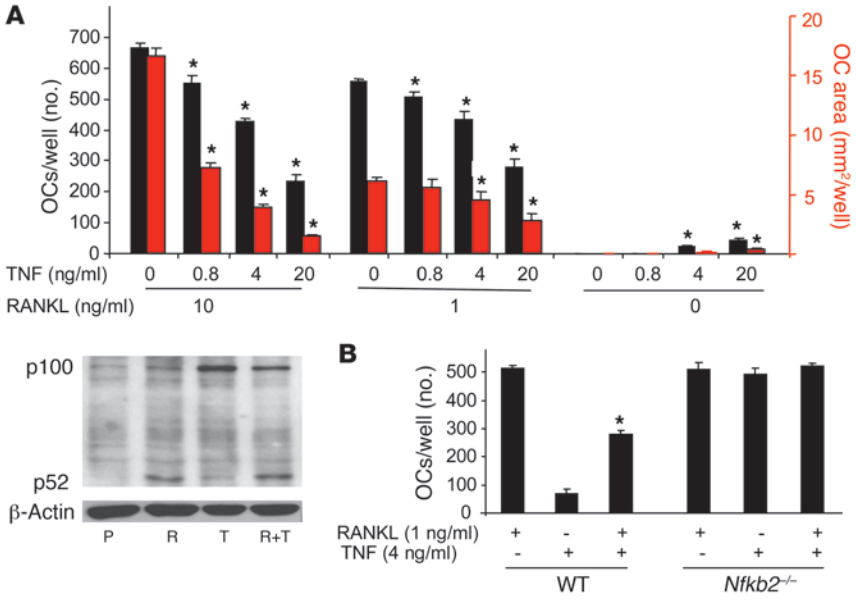

Figure 5
TNF-induced NF-κB p100 inhibits RANKL-induced osteoclastogenesis. (**A**) WT mouse spleen cells were cultured with M-CSF for 3 days, and RANKL and/or TNF were added at the indicated doses for 2 more days to generate osteoclasts. Top: TNF dose-dependently inhibited RANKL-induced osteoclastogenesis, assessed by osteoclast number (black bars) and area (red bars) per well. Bottom: The protein levels of NF-κB p100 and p52 were analyzed with Western blot and assessed in whole-cell lysates extracted from RANKL-treated (10 ng/ml) and/or TNF-treated (20 ng/ml) WT mouse OCPs at 8 hours. (**B**) The inhibitory effect of TNF on RANKL-induced osteoclastogenesis was abolished in *Nfkb2*$^{-/-}$ OCPs (*$P < 0.05$ vs. RANKL treatment alone; 4 wells/group). The same experiments were repeated at least twice with similar results.

ferent osteoclastogenesis protocol in which spleen cells are first cultured with M-CSF for 3 days, to enrich for OCPs, and then TNF with or without RANKL was added to these cells for a further 2–3 days. TNF inhibited RANKL-induced osteoclastogenesis in a dose-dependent (0.8–20 ng/ml) manner (Figure 5A) at both optimal (10 ng/ml) and low (1 ng/ml) RANKL concentrations. Of note, although the number of osteoclasts induced by 1 ng/ml RANKL was just slightly less than the optimal dose, osteoclasts formed later and were smaller in these cultures, and this was evident as a reduced osteoclast area (Figure 5A). TNF alone (4 and 20 ng/ml) induced small numbers of osteoclasts in the absence of RANKL, as expected. In these experiments, NF-κB p100 levels in WT OCPs treated with TNF (20 ng/ml) plus RANKL (10 ng/ml) were significantly higher than in cells treated with RANKL alone, but the levels were less than those in cells treated with TNF alone, presumably because RANKL induced some proteasomal degradation of p100 through NIK, despite the inhibitory effect of TNF (Figure 5A). Accordingly, p52 expression was higher in the cultures of RANKL plus TNF than in those treated with TNF alone.

We next treated WT and *Nfkb2*$^{-/-}$ OCPs with low but effective doses of TNF with or without RANKL and found that TNF (4 ng/ml) significantly reduced osteoclastogenesis induced by RANKL (1 ng/ml) in WT cultures but had no inhibitory effect in *Nfkb2*$^{-/-}$ cultures in which both cytokines had nearly maximal osteoclastogenic effects either alone or in combination (Figure 5B), confirming that NF-κB p100 mediates this TNF-induced inhibition of osteoclastogenesis.

TNF induction of NF-κB p100 and inhibition of osteoclastogenesis is mediated by TRAF3. To determine the mechanism whereby TNF-induced NF-κB p100 accumulation limits osteoclastogenesis, we examined the effects of TNF and RANKL on the expression of TRAFs in OCPs. TRAFs directly interact with TNF superfamily receptors and trigger intracellular signaling events, including NIK-mediated processing of p100 to p52 (7). In addition, TRAF2 and -3 can also mediate proteasomal degradation of signaling molecules (26, 27). We found that neither RANKL nor TNF affected the mRNA expression levels of TRAF3 or -6 (data not shown). However, both RANKL and TNF increased the protein levels of TRAF6, which activates NIK, and this is consistent with our observation that both cytokines slightly elevated NIK protein levels (Figure 6A). Importantly, TNF induced significantly higher levels of TRAF3, paralleling the elevated NF-κB p100 levels (Figure 6A). RANKL alone slightly reduced TRAF3, but it significantly decreased TNF-induced TRAF3 protein levels, which was matched by relatively lower levels of p100 (Figure 6A). Neither TNF nor RANKL affected protein levels of TRAF2 or -5 significantly in these cultures (data not shown).

To determine how TRAF3 is regulated by TNF, we added cycloheximide to the cultures of WT OCPs treated with PBS, RANKL, or TNF to prevent the synthesis of new protein and thus observe degradation of TRAF3 by Western blot. RANKL accelerated the degradation of TRAF3, starting at 1 hour and continuing through 4 hours (Figure 6B). In contrast, TNF prevented TRAF3 degradation, suggesting that TNF induction of TRAF3 results in the accumulation of NF-κB p100 and inhibition of osteoclastogenesis. To test this possibility, WT OCPs were transfected with TRAF3 siRNA to examine its effects on expression of NIK and p100 and on osteoclastogenesis. Transfection of TRAF3 siRNA reduced TRAF3 protein levels, and this was associated with higher levels of NIK and lower p100 levels in the TNF-treated cells compared with control siRNA-treated cells (Figure 6C). Surprisingly, we did not detect a significant change in p52 levels in either cytoplasmic or nuclear extracts using TRAF3 siRNA. This was a consistent finding that will require further study to determine whether TRAF3 also regulates p52 expression. TRAF3 siRNA significantly increased TNF-induced nuclear and cytoplasmic RelB, the typical partner of p52, which was reported recently to be involved in RANKL-induced osteoclastogenesis in vitro (44). Consistent with these results, TRAF3 siRNA significantly increased TNF-induced osteoclastogenesis (Figure 6D), although it had no effect on osteoclast numbers in RANKL-treated cultures, presumably because RANKL can degrade TRAF3 and TRAF3 siRNA likely would not have an additional effect on TRAF3 degradation. Of note, inhibition of TRAF3 attenuated the TNF-induced reduction of RANKL-mediated osteoclastogenesis.

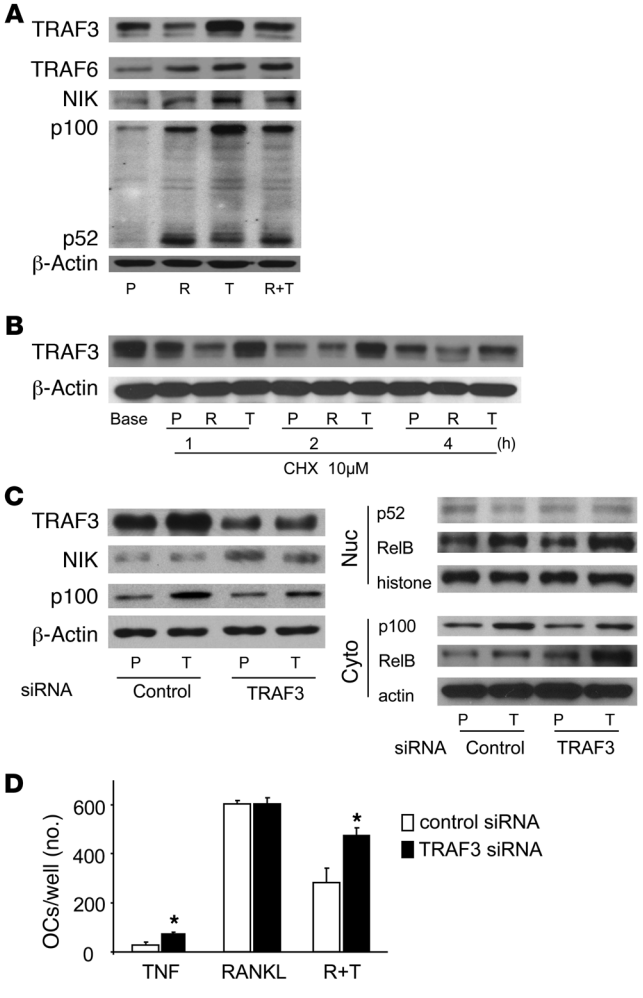

Figure 6
TNF-induced TRAF3 negatively regulates osteoclastogenesis through NIK. (**A**) WT mouse OCPs were treated with RANKL and/or TNF for 8 hours, and whole-cell lysate protein was extracted and subjected to Western blotting for TRAF3, TRAF6, NIK, and NF-κB p100 and p52. (**B**) Cycloheximide (10 μM) was added to WT mouse OCPs treated with RANKL (10 ng/ml), TNF (20 ng/ml), or PBS control for the indicated times. Whole-cell lysates were subjected to Western blotting for TRAF3. (**C**) WT mouse OCPs were transfected with TRAF3 siRNA or a nonspecific control siRNA for 8 hours. The cells were treated with TNF (20 ng/ml) or PBS for an additional 8 hours. Whole-cell lysates were subjected to Western blotting to determine the levels of cytoplasmic TRAF3, NIK, and NF-κB p100 (left panel) and either nuclear p52 or cytoplasmic p100 and RelB (right panels). (**D**) TRAF3 siRNA–transfected cells were treated with TNF and/or RANKL (10 ng/ml) for 3 days in the presence of M-CSF to generate osteoclasts. *$P < 0.05$ vs. control).

Discussion

There is compelling evidence for a strong proresorptive function of TNF, which has long been implicated in the pathogenesis of bone loss and inflammation in a variety of common bone diseases (1, 4, 10, 45) and, more recently, cherubism (46). TNF induces bone loss by indirect and direct mechanisms, including promotion of RANKL expression by accessory cells (4, 6) and induction of OCP proliferation and differentiation (47). These cells can then secrete proinflammatory osteoclastogenic cytokines and thus lead to the initiation of autocrine and paracrine self-amplifying cycles that increase bone loss (48). A pivotal role of TNF in pathologic bone loss is evidenced by the efficacy of anti-TNF therapy to limit disease progression in approximately 70% of patients with RA (49) and to reduce bone erosion soon after menopause (2).

Despite this evidence, TNF does not induce osteoclast formation when administered in vivo to *Rankl*$^{-/-}$ or *Rank*$^{-/-}$ mice (34), although it can induce osteoclastogenesis directly from *Rank*$^{-/-}$ OCPs in vitro when costimulated with TGF-β (18), leading some to suggest that prior priming of OCPs by RANKL (35) or IL-1 expression by stromal cells (50) is necessary for TNF-induced bone resorption. Here we explain these discrepant findings by showing that locally injected TNF fails to induce osteoclastogenesis in *Rankl*$^{-/-}$ and *Rank*$^{-/-}$ mice because of the inhibitory effects NF-κB p100 and provide conclusive evidence that TNF can induce osteoclastogenesis in these mice when they are deficient also in NF-κB p100.

The osteoclastogenesis induced locally by TNF in calvariae of *Rank*$^{-/-}$/*Nfkb2*$^{-/-}$ or *Rankl*$^{-/-}$/*Nfkb2*$^{-/-}$ mice was associated with systemic induction of small numbers of mainly mononuclear TRAP^{+} cells along epiphyseal growth plates. We have reported that RANKL induced by BMP2 in hypertrophic chondrocytes at the growth plate attracts OCPs to this site to remove bone (51), which is formed rapidly and must be removed to prevent development of osteopetrosis during development. Our findings suggest that the administered TNF directed OCPs to this site independently of RANKL. However, further studies are required to determine whether this was by a direct or indirect mechanism and whether TNF induces expression of chemokines here as it also does to attract circulating OCPs to inflamed joints (52).

Our observation that TRAP^{+} cells do not form in untreated *Rank*$^{-/-}$/*Nfkb2*$^{-/-}$ or *Rankl*$^{-/-}$/*Nfkb2*$^{-/-}$ mice is important because it suggests that TNF levels at the growth plate during endochondral ossification are too low to induce OCP differentiation to osteoclasts and that TNF does not have an important positive or negative regulatory role in this physiologic process. However, TRAP5b released from osteoclasts induced by locally injected TNF resulted in slightly increased serum TRAP5b levels in *Rank*$^{-/-}$/*Nfkb2*$^{+/-}$ mice and significantly increased levels in *Rank*$^{-/-}$/*Nfkb2*$^{-/-}$ mice, supporting our conclusion that TNF-induced resorption in pathologic bone remodeling is attenuated by NF-κB2. The inhibitory role for NF-κB p100 in osteoclastogenesis is further supported by the development of erosive arthritis and systemic bone loss in TNF-Tg/*Nfkb2*$^{-/-}$ mice much earlier than TNF-Tg/*Nfkb2*$^{+/-}$ littermates.

The reports that TNF induces RANKL expression in the joints of TNF-Tg mice (53, 54) led us to consider whether NF-κB p100 also limits RANKL-induced resorption in TNF-Tg mice. Indeed, we found that TNF limits RANKL-induced differentiation of WT OCPs in vitro through induced NF-κB p100 and that retroviral expression of NF-κB2 in OCPs reduced RANKL-induced osteoclastogenesis. Interestingly, inhibition of osteoclastogenesis alone does not prevent TNF-induced synovial inflammation, since TNF-Tg/*c-Fos*$^{-/-}$ hybrid mice lack osteoclasts and joint destruction but still have synovial inflammation (55). Therefore, inhibition of osteoclasts alone is likely to have a limited role in the treatment of RA. Unexpectedly and importantly, we found that the TNF-Tg/*Nfkb2*$^{-/-}$ mice also had significantly increased inflammation in their joints, indicating that NF-κB p100 limits not only OCP differentiation

but also the number of inflammatory cells attracted to the joints of the mice in response to TNF.

Deficiency of Nfkb2 dramatically accelerated TNF-Tg–induced arthritic bone erosion and inflammation, but this was not associated with an increase in their serum concentrations of either human or murine TNF, suggesting that deficiency of NF-κB p100 could be associated with more severe joint inflammation in RA patients. This might be of great importance in the clinical setting of arthritis, but it will require further study to determine whether there are variations in the transcription, function, or degradation of p100 that could increase the susceptibility of RA patients to TNF. Similarly, further study is also required to determine the precise mechanism whereby p100 limits the inflammatory infiltration, and specifically whether NF-κB p100 can be further increased locally, for example by using local adenoviral gene delivery, to inhibit inflammation and bone resorption in these mice.

TNF stimulates *Nfkb2* mRNA expression through the canonical NF-κB p65/p50 pathway to increase the total amount of NF-κB p100 transcripts and protein (24). At the same time, TNF activates the noncanonical pathway leading to some processing of NF-κB p100 to NF-κB p52 (24), but the molecular mechanisms have not been identified. We found that TNF stabilized TRAF3, resulting in its accumulation in OCPs in parallel with p100 levels, a finding that, to our knowledge, has not been reported previously in any cell type. This could account for limited NF-κB p100 degradation by NIK because TRAF3 induces degradation of NIK in B cells (26, 27). These effects of TNF differ from those of RANKL, which does not increase TRAF3 protein levels and activates NIK to induce efficient processing of p100 to p52 (23). TRAF3 negatively regulates p100 processing to p52 by promoting proteasomal degradation of NIK through its physical association with the TRAF3 binding motif in NIK (25, 26). Loss of TRAF3 results in accumulation of NIK and constitutive p100 processing in $TRAF3^{-/-}$ B cells (25, 28). TRAF6, which mediates RANKL/RANK-activated canonical NF-κB signaling, cannot associate with NIK directly and therefore does not inhibit it (56).

TRAF3 siRNA reduced TRAF3 protein levels in WT OCPs associated with increased NIK levels and p100 processing, which released more RelB to go to nuclei in the cells and increased osteoclastogenesis. TNF induced only a slight increase NIK levels in the OCPs, but this in part may reflect the difficulty in detecting low levels of NIK in cells with currently available reagents (57) and the fact that most published studies were able to detect changes in NIK levels only when NIK was overexpressed (26, 57). Although some investigators have suggested that TRAF2 is required for TNF-induced osteoclastogenesis (14) and TRAF5 is involved in both RANKL- and TNF-induced osteoclastogenesis (15), others have found that TRAF2- or TRAF5-deficient OCPs can differentiate into mature osteoclasts in response to TNF (18). TRAF2 functions along with TRAF3 in B cells to degrade NIK (26). However, TRAF2, -5, and -6 do not appear to play a major role in p100 processing in OCPs, based on our observation that their protein levels are similar in TNF- and RANKL-treated cells. Currently, we do not know the precise molecular mechanism by which TNF increases TRAF3 protein levels in OCPs. TNF does not affect TRAF3 mRNA, but it clearly prevents its degradation. It will be important to work this out in further studies, since stabilization of TRAF3 could potentially be one mechanism to limit bone resorption and possibly inflammation in inflammatory arthritis.

Our findings, coupled with the fact that TNF, RANKL, and IL-1 can all induce TNF expression by OCPs (40), support an important direct role for TNF in osteoclastogenesis in conditions such as RA and postmenopausal osteoporosis, in which production of these cytokines is increased beyond physiologic levels (58), while physiologic levels of the cytokines are unable to induce osteoclastogenesis in $Rankl^{-/-}$ and $Rank^{-/-}$ mice. However, they also identify an important negative regulatory role for TNF to limit its effects and those of RANKL. Given the important role that TNF has in inducing inflammation and bone destruction in many common bone diseases, we propose that this negative regulatory role for TNF in limiting bone resorption and inflammation might be harnessed to help reduce the high morbidity associated with many common diseases in which its expression is increased. These might include increasing the stability or expression of p100 or TRAF3 and inhibiting NIK in OCPs.

Methods

Reagents and animals. Recombinant M-CSF, RANKL, and TNF for cell cultures were from R&D Systems. TNF for in vivo experiments was a gift from Amgen. Cycloheximide was from Calbiochem. The sources of $Nfkb2^{-/-}$ (C57BL/6 × 129) (11, 31), human TNF-Tg (CBA × C57BL/6, TNF-Tg line 3647) (40), $Rankl^{-/-}$ (C57BL/6) (59), and $Rank^{-/-}$ (C57BL/6) mice (30) were described previously. $Nfkb2^{-/-}$ mice were crossed with $Rank^{+/-}$ or $Rankl^{+/-}$ mice to generate $Nfkb2^{+/-}/Rankl^{-/-}$ or $Nfkb^{+/-}/Rankl^{-/-}$ and $Nfkb2^{-/-}/Rank^{-/-}$ or $Nfkb2^{-/-}/Rank^{-/-}$ mice. $Nfkb2^{-/-}$ mice were crossed with TNF-Tg mice to generate TNF-Tg/$Nfkb2^{+/-}$ and TNF-Tg/$Nfkb2^{-/-}$ mice. The University of Rochester Medical Center Institutional Animal Care and Use Committee approved all animal studies.

Osteoclast formation and functional assays. Spleen cells (1.75×10^5/well in 96-well plates) from WT mice were cultured with M-CSF (10 ng/ml) for 2–3 days in α-MEM with 10% FBS to enrich for OCPs. To generate osteoclasts from $Rankl^{-/-}$ and $Rank^{-/-}$ mice in response to TNF, we seeded about 1/5th the number of splenocytes we used from WT cells. This allowed us to obtain comparable numbers of OCPs after 3-day treatment with M-CSF and to induce osteoclastogenesis from these splenocytes. OCPs were treated with RANKL (10 ng/ml) and/or TNF (20 ng/ml) for 2–3 days to generate mature osteoclasts. To test the role of NF-κB p100 on OCP differentiation, $Nfkb2^{-/-}$ and WT littermate OCPs were infected with retroviral supernatants of p100, p52, or GFP controls for 2 days and then treated with TNF or RANKL for 2–4 days, as described previously (11, 40). To test the role of TRAF3 in TNF-induced osteoclastogenesis, WT OCPs were transfected with a pool of 3 TRAF3-specific siRNAs (Santa Cruz Biotechnology Inc.) or nonspecific control siRNA for 8 hours, and then treated with TNF and/or RANKL for 3–4 days. For functional assays of osteoclasts, spleen cells were seeded in 96-well plates containing bovine cortical bone slices and cultured with TNF or RANKL, and resorption pit formation was assessed, as reported previously (11, 40). Cells were costimulated with M-CSF in all experiments.

Western blot analysis. Whole-cell lysate protein from OCPs or mature osteoclasts and nuclear protein from TRAF3 siRNA–transfected OCPs cultured in 60- or 100-mm dishes were prepared as described previously (11). Lysates (10 μg) were loaded in 10% SDS-PAGE gels and immunoblotted with antibodies to NF-κB1, NF-κB2, p65, RelB, TRAF2, TRAF3, TRAF5, TRAF6, and NIK (Santa Cruz Biotechnology Inc.) or mouse actin (Sigma-Aldrich). To test for degradation of the TRAF3 protein, 10 μM CHX was added to WT OCPs treated with RANKL (10 ng/ml), TNF (20 ng/ml), or PBS control to inhibit new protein synthesis, and whole-cell lysates were subjected to Western blot for TRAF3.

TNF-induced osteoclastogenesis in vivo. TNF (0.5 μg) or PBS was injected over the calvariae of 3- to 4-week-old mice twice daily for 5 days. Mice were sacrificed on day 6, and calvariae and hind limbs were fixed in 10% formalin

and decalcified with 10% EDTA. TRAP activity was assessed in paraffin-embedded sections, as described previously (11, 40). Osteoclast numbers and surfaces and eroded surfaces were measured using an Osteometrics system, as described previously (11, 40).

Evaluation of arthritis and osteoporosis. Although the features of arthritis in the commonly used 197 line of TNF-Tg mice include paw swelling, reduced strength, and deformation (60), we found that the only easily identifiable, reproducible parameter in our 3647 line of TNF-Tg mice, which carry only 1 copy of the TNF transgene (40), is paw and finger deformation, including atrophy. We generated a deformation score (0, no deformation; 1, mild deformation; 2, moderate deformation; 3, severe deformation; 4, very severe deformation), which was evaluated once each week to determine the clinical progress of arthritis. Each forepaw and hindpaw was evaluated separately, and the deformation score was calculated as the sum of the 4 paws. Mice were sacrificed in a CO_2 container. Right tibiae were collected for μCT scanning to evaluate cortical and trabecular bone volume. Left tibiae and forepaws were fixed, decalcified, and processed through paraffin for histologic evaluation of osteoclasts and arthritis, including inflammatory tissue area and carpal bone eroded cartilage surface.

ELISA. Mouse TRAP5b (Immunodiagnostic Systems) were assessed in serum collected from TNF- or PBS-injected *Nfkb2*$^{-/-}$ and *Rank*$^{-/-}$/*Nfkb2*$^{-/-}$ mice and their littermate controls, and human and mouse TNF (eBioscience) were determined in serum of TNF-Tg/*Nfkb2*$^{-/-}$ mice and their littermate controls according to the manufacturer's instructions

Statistics. All results are given as mean ± SD. Comparisons between 2 groups were analyzed using the 2-tailed unpaired Student's *t* test. One-way ANOVA and Dunnett's post-hoc multiple comparisons were used for comparisons among 3 or more groups. *P* values less than 0.05 were considered statistically significant.

Acknowledgments

We thank Hani A. Awad for help with μCT analysis and Xiaoyun Zhang and Yanyun Li for histology. This work was supported by NIH grants AR43510 to B.F. Boyce and AR48697 to L. Xing.

Received for publication January 26, 2009, and accepted in revised form August 19, 2009.

Address correspondence to: Brendan F. Boyce, Department of Pathology and Laboratory Medicine, 601 Elmwood Ave., Box 626, Rochester, New York 14642, USA. Phone: (585) 275-5837; Fax: (585) 273-3637; E-mail: Brendan_Boyce@urmc.rochester.edu.

1. Novack, D.V., and Teitelbaum, S.L. 2008. The osteoclast: friend or foe? *Annu. Rev. Pathol.* **3**:457–484.
2. Charatcharoenwitthaya, N., Khosla, S., Atkinson, E.J., McCready, L.K., and Riggs, B.L. 2007. Effect of blockade of TNF-alpha and interleukin-1 action on bone resorption in early postmenopausal women. *J. Bone Miner. Res.* **22**:724–729.
3. Eghbali-Fatourechi, G., et al. 2003. Role of RANK ligand in mediating increased bone resorption in early postmenopausal women. *J. Clin. Invest.* **111**:1221–1230.
4. Feng, X. 2005. Regulatory roles and molecular signaling of TNF family members in osteoclasts. *Gene.* **350**:1–13.
5. Teitelbaum, S.L. 2000. Bone resorption by osteoclasts. *Science.* **289**:1504–1508.
6. Boyce, B.F., and Xing, L. 2008. Functions of RANKL/RANK/OPG in bone modeling and remodeling. *Arch. Biochem. Biophys.* **473**:139–146.
7. Dempsey, P.W., Doyle, S.E., He, J.Q., and Cheng, G. 2003. The signaling adaptors and pathways activated by TNF superfamily. *Cytokine Growth Factor Rev.* **14**:193–209.
8. Darnay, B.G., Besse, A., Poblenz, A.T., Lamothe, B., and Jacoby, J.J. 2007. TRAFs in RANK signaling. *Adv. Exp. Med. Biol.* **597**:152–159.
9. Kim, H.H., et al. 1999. Receptor activator of NF-kappaB recruits multiple TRAF family adaptors and activates c-Jun N-terminal kinase. *FEBS Lett.* **443**:297–302.
10. Takayanagi, H. 2007. Osteoimmunology: shared mechanisms and crosstalk between the immune and bone systems. *Nat. Rev. Immunol.* **7**:292–304.
11. Yamashita, T., et al. 2007. NF-kappaB p50 and p52 regulate receptor activator of NF-kappaB ligand (RANKL) and tumor necrosis factor-induced osteoclast precursor differentiation by activating c-Fos and NFATc1. *J. Biol. Chem.* **282**:18245–18253.
12. Lomaga, M.A., et al. 1999. TRAF6 deficiency results in osteopetrosis and defective interleukin-1, CD40, and LPS signaling. *Genes Dev.* **13**:1015–1024.
13. Naito, A., et al. 1999. Severe osteopetrosis, defective interleukin-1 signalling and lymph node organogenesis in TRAF6-deficient mice. *Genes Cells.* **4**:353–362.
14. Kanazawa, K., and Kudo, A. 2005. TRAF2 is essential for TNF-alpha-induced osteoclastogenesis. *J. Bone Miner. Res.* **20**:840–847.
15. Kanazawa, K., Azuma, Y., Nakano, H., and Kudo, A. 2003. TRAF5 functions in both RANKL- and TNFalpha-induced osteoclastogenesis. *J. Bone Miner. Res.* **18**:443–450.
16. Ross, F.P. 2006. M-CSF, c-Fms, and signaling in osteoclasts and their precursors. *Ann. N. Y. Acad. Sci.* **1068**:110–116.
17. Kobayashi, K., et al. 2000. Tumor necrosis factor alpha stimulates osteoclast differentiation by a mechanism independent of the ODF/RANKL-RANK interaction. *J. Exp. Med.* **191**:275–286.
18. Kim, N., et al. 2005. Osteoclast differentiation independent of the TRANCE-RANK-TRAF6 axis. *J. Exp. Med.* **202**:589–595.
19. Hayden, M.S., and Ghosh, S. 2004. Signaling to NF-kappaB. *Genes Dev.* **18**:2195–2224.
20. Beinke, S., and Ley, S.C. 2004. Functions of NF-kappaB1 and NF-kappaB2 in immune cell biology. *Biochem. J.* **382**:393–409.
21. Coux, O., and Goldberg, A.L. 1998. Enzymes catalyzing ubiquitination and proteolytic processing of the p105 precursor of nuclear factor kappaB1. *J. Biol. Chem.* **273**:8820–8828.
22. Yilmaz, Z.B., Weih, D.S., Sivakumar, V., and Weih, F. 2003. RelB is required for Peyer's patch development: differential regulation of p52-RelB by lymphotoxin and TNF. *EMBO J.* **22**:121–130.
23. Novack, D.V., et al. 2003. The IkappaB function of NF-kappaB2 p100 controls stimulated osteoclastogenesis. *J. Exp. Med.* **198**:771–781.
24. Chaisson, M.L., et al. 2004. Osteoclast differentiation is impaired in the absence of inhibitor of kappa B kinase alpha. *J. Biol. Chem.* **279**:54841–54848.
25. Zarnegar, B., Yamazaki, S., He, J.Q., and Cheng, G. 2008. Control of canonical NF-kappaB activation through the NIK-IKK complex pathway. *Proc. Natl. Acad. Sci. U. S. A.* **105**:3503–3508.
26. Vallabhapurapu, S., et al. 2008. Nonredundant and complementary functions of TRAF2 and TRAF3 in a ubiquitination cascade that activates NIK-dependent alternative NF-kappaB signaling. *Nat. Immunol.* **9**:1364–1370.
27. Hauer, J., et al. 2005. TNF receptor (TNFR)-associated factor (TRAF) 3 serves as an inhibitor of TRAF2/5-mediated activation of the noncanonical NF-kappaB pathway by TRAF-binding TNFRs. *Proc. Natl. Acad. Sci. U. S. A.* **102**:2874–2879.
28. He, J.Q., et al. 2006. Rescue of TRAF3-null mice by p100 NF-kappa B deficiency. *J. Exp. Med.* **203**:2413–2418.
29. Lacey, D.L., et al. 1998. Osteoprotegerin ligand is a cytokine that regulates osteoclast differentiation and activation. *Cell.* **93**:165–176.
30. Dougall, W.C., et al. 1999. RANK is essential for osteoclast and lymph node development. *Genes Dev.* **13**:2412–2424.
31. Franzoso, G., et al. 1997. Requirement for NF-kappaB in osteoclast and B-cell development. *Genes Dev.* **11**:3482–3496.
32. Iotsova, V., Caamano, J., Loy, J., Lewin, A., and Bravo, R. 1997. Osteopetrosis in mice lacking NF-κB1 and NF-κB2. *Nat. Med.* **3**:1285–1289.
33. Abu-Amer, Y., et al. 2000. Tumor necrosis factor receptors types 1 and 2 differentially regulate osteoclastogenesis. *J. Biol. Chem.* **275**:27307–27310.
34. Li, J., et al. 2000. RANK is the intrinsic hematopoietic cell surface receptor that controls osteoclastogenesis and regulation of bone mass and calcium metabolism. *Proc. Natl. Acad. Sci. U. S. A.* **97**:1566–1571.
35. Lam, J., et al. 2000. TNF-alpha induces osteoclastogenesis by direct stimulation of macrophages exposed to permissive levels of RANK ligand. *J. Clin. Invest.* **106**:1481–1488.
36. Derudder, E., et al. 2003. RelB/p50 dimers are differentially regulated by tumor necrosis factor-alpha and lymphotoxin-beta receptor activation: critical roles for p100. *J. Biol. Chem.* **278**:23278–23284.
37. Takayanagi, H., et al. 2002. RANKL maintains bone homeostasis through c-Fos-dependent induction of interferon-beta.[see comment]. *Nature.* **416**:744–749.
38. Boyle, W.J., Simonet, W.S., and Lacey, D.L. 2003. Osteoclast differentiation and activation. *Nature.* **423**:337–342.
39. Xing, L., et al. 2003. Expression of either NF-kappaB p50 or p52 in osteoclast precursors is required for IL-1-induced bone resorption. *J. Bone Miner. Res.* **18**:260–269.
40. Yao, Z., Xing, L., Qin, C., Schwarz, E.M., and Boyce, B.F. 2008. Osteoclast precursor interaction with bone matrix induces osteoclast formation directly by an interleukin-1-mediated autocrine mechanism. *J. Biol. Chem.* **283**:9917–9924.
41. Basak, S., et al. 2007. A fourth IkappaB protein within the NF-kappaB signaling module. *Cell.* **128**:369–381.
42. Li, P., et al. 2004. RANK signaling is not required for TNFalpha-mediated increase in CD11(hi) osteoclast precursors but is essential for mature osteoclast formation in TNFalpha-mediated inflammatory arthritis. *J. Bone Miner. Res.* **19**:207–213.
43. Ochi, S., et al. 2007. Pathological role of osteoclast costimulation in arthritis-induced bone loss. *Proc.*

Natl. Acad. Sci. U. S. A. **104**:11394–11399.
44. Vaira, S., et al. 2008. RelB is the NF-kappaB subunit downstream of NIK responsible for osteoclast differentiation. *Proc. Natl. Acad. Sci. U. S. A.* **105**:3897–3902.
45. Boyce, B.F., et al. 2005. TNF-alpha and pathologic bone resorption. *Keio J. Med.* **54**:127–131.
46. Aliprantis, A.O., et al. 2008. NFATc1 in mice represses osteoprotegerin during osteoclastogenesis and dissociates systemic osteopenia from inflammation in cherubism. *J. Clin. Invest.* **118**:3775–3789.
47. Yao, Z., et al. 2006. Tumor necrosis factor-{alpha} increases circulating osteoclast precursor numbers by promoting their proliferation and differentiation in the bone marrow through up-regulation of c-Fms expression. *J. Biol. Chem.* **281**:11846–11855.
48. Boyce, B.F., Schwarz, E.M., and Xing, L. 2006. Osteoclast precursors: cytokine-stimulated immunomodulators of inflammatory bone disease. *Curr. Opin. Rheumatol.* **18**:427–432.
49. Shealy, D.J., and Visvanathan, S. 2008. Anti-TNF antibodies: lessons from the past, roadmap for the future. *Handb. Exp. Pharmacol.* **181**:101–129.
50. Wei, S., Kitaura, H., Zhou, P., Ross, F.P., and Teitelbaum, S.L. 2005. IL-1 mediates TNF-induced osteoclastogenesis. *J. Clin. Invest.* **115**:282–290.
51. Usui, M., et al. 2008. Murine and chicken chondrocytes regulate osteoclastogenesis by producing RANKL in response to BMP2. *J. Bone Miner. Res.* **23**:314–325.
52. Xing, L., Schwarz, E.M., and Boyce, B.F. 2005. Osteoclast precursors, RANKL/RANK, and immunology. *Immunol. Rev.* **208**:19–29.
53. Zhang, Q., et al. 2008. VEGF-C, a lymphatic growth factor, is a RANKL target gene in osteoclasts that enhances osteoclastic bone resorption through an autocrine mechanism. *J. Biol. Chem.* **283**:13491–13499.
54. Schwarz, E.M., et al. 2006. Autoimmunity and bone. *Ann. N. Y. Acad. Sci.* **1068**:275–283.
55. Redlich, K., et al. 2002. Osteoclasts are essential for TNF-alpha-mediated joint destruction. *J. Clin. Invest.* **110**:1419–1427.
56. He, J.Q., Saha, S.K., Kang, J.R., Zarnegar, B., and Cheng, G. 2007. Specificity of TRAF3 in its negative regulation of the noncanonical NF-kappa B pathway. *J. Biol. Chem.* **282**:3688–3694.
57. Sasaki, Y., et al. 2008. NIK overexpression amplifies, whereas ablation of its TRAF3-binding domain replaces BAFF:BAFF-R-mediated survival signals in B cells. *Proc. Natl. Acad. Sci. U. S. A.* **105**:10883–10888.
58. O'Gradaigh, D., Ireland, D., Bord, S., and Compston, J.E. 2004. Joint erosion in rheumatoid arthritis: interactions between tumour necrosis factor alpha, interleukin 1, and receptor activator of nuclear factor kappaB ligand (RANKL) regulate osteoclasts. *Ann. Rheum. Dis.* **63**:354–359.
59. Kim, N., Odgren, P.R., Kim, D.K., Marks, S.C., Jr., and Choi, Y. 2000. Diverse roles of the tumor necrosis factor family member TRANCE in skeletal physiology revealed by TRANCE deficiency and partial rescue by a lymphocyte-expressed TRANCE transgene. *Proc. Natl. Acad. Sci. U. S. A.* **97**:10905–10910.
60. Keffer, J., et al. 1991. Transgenic mice expressing human tumour necrosis factor: a predictive genetic model of arthritis. *EMBO J.* **10**:4025–4031.

Chloroquine reduces osteoclastogenesis in murine osteoporosis by preventing TRAF3 degradation

Yan Xiu,[1] Hao Xu,[1] Chen Zhao,[1] Jinbo Li,[1] Yoshikazu Morita,[1] Zhenqiang Yao,[1,2] Lianping Xing,[1,2] and Brendan F. Boyce[1,2]

[1]Department of Pathology and Laboratory Medicine, and [2]Center for Musculoskeletal Research, University of Rochester Medical Center, Rochester, New York, USA.

The cytokines RANKL and TNF activate NF-κB signaling in osteoclast precursors (OCPs) to induce osteoclast (OC) formation. Conversely, TNF can limit OC formation through NF-κB p100, which acts as an inhibitor, and TNF receptor–associated receptor 3 (TRAF3); however, a role for TRAF3 in RANKL-mediated OC formation is unknown. We found that TRAF3 limits RANKL-induced osteoclastogenesis by suppressing canonical and noncanonical NF-κB signaling. Conditional OC-specific *Traf3*-KO (cKO) mice had mild osteoporosis and increased OC formation. RANKL induced TRAF3 degradation via the lysosome/autophagy system. The autophagy/lysosome inhibitor chloroquine reduced RANKL-induced OC formation and function by increasing TRAF3 expression in OCPs in vitro and in vivo. Although chloroquine had no effect on basal bone resorption, it inhibited parathyroid hormone– and ovariectomy-induced OC activation in WT, but not cKO, mice. Deletion of the transcription factor gene *Relb* resulted in increased TRAF3 expression in OCPs, which was associated with decreased RANKL-induced TRAF3 degradation. RelB directly increased expression of BECN1, a key autophagy regulator, by binding to its promoter. These data indicate that autophagic/lysosomal degradation of TRAF3 is an important step in RANKL-induced NF-κB activation in OCPs. Furthermore, treatments that increase TRAF3 levels in OCPs, including pharmacological inhibition of its degradation with compounds such as chloroquine, may limit bone destruction in common bone diseases.

Introduction

Bone homeostasis is maintained by a delicate balance between osteoclastic bone resorption and osteoblastic bone formation. Disruption of this balance with a higher rate of bone resorption occurs in metabolic and inflammatory bone disorders, such as postmenopausal osteoporosis and RA, resulting in increased risk of fracture and joint destruction, respectively (1). Osteoclasts (OCs) resorb bone in physiologic and pathologic conditions (2), and their formation and activity are increased in osteoporosis and RA as a result of increased production of proinflammatory cytokines, such as TNF and RANKL, which activate NF-κB (3).

NF-κB transcriptional factors regulate immune and numerous other cellular responses and play critical roles in skeletal development, endochondral ossification, OC and osteoblast functions, and common bone diseases (4). In mammals, there are 5 NF-κB family members: RelA (p65), RelB, and c-Rel, and the precursor proteins NF-κB1 (p105) and NF-κB2 (p100), which are processed into p50 and p52, respectively (5). Canonical NF-κB signals through IKKβ and NF-κB essential modulator (NEMO), leading to phosphorylation of IκBα and translocation of p65/p50 heterodimers into nuclei in response to cytokines; noncanonical NF-κB stimulates IKKα-mediated phosphorylation of p100 through activation of NF-κB–inducing kinase (NIK) and leads to processing of p100 to p52 and release of RelB/p52 complexes. Noncanonical signaling is induced by TNF family members, including RANKL, CD40 ligand, BAFF, and lymphotoxin-β (5).

A role for NF-κB signaling in bone was first identified in reports of defective cytokine-induced osteoclastogenesis in NF-κB1/2 double-KO mice (6, 7), but NF-κB–induced osteoclastogenesis by cytokines remains incompletely understood. NF-κB is a pivotal regulator of RANKL- and TNF-induced osteoclast precursor (OCP) differentiation and is activated via TNF receptor–associated factors (TRAFs), which share a common C-terminal structural TRAF domain that mediates oligomerization and receptor binding. RANKL activates both canonical and noncanonical NF-κB signaling in OCPs through TRAF6 and NIK, leading to activation of IKKβ and IKKα, respectively (4, 8), and to stimulatory and inhibitory signaling in the cells (5). Similarly, TNF stimulates OC formation directly, but it also limits RANKL-and TNF-mediated OC formation by increasing cellular levels of NF-κB p100 (9) and other inhibitory proteins (4, 10). TNF typically induces fewer OCs than RANKL in vitro when WT OCPs are used, but it induces similar numbers of OCs from *Nfkb2*$^{-/-}$ OCPs as RANKL and also robust OC formation in *Rankl*$^{-/-}$ and *Rank*$^{-/-}$ mice deficient in p100. These findings indicate that p100 inhibits TNF-induced osteoclastogenesis by a TNF receptor–associated receptor 3–dependent (TRAF3-dependent) mechanism (9), but the mechanism whereby TRAF3 inhibits osteoclastogenesis has been unclear, although it does involve NIK degradation (11).

Apart from their role as adaptor proteins, TRAFs also act as E3 ubiquitin ligases, a function crucial for the activation of NF-κB signaling (12). Overexpression and genetic studies identified positive activation roles for TRAF2, -5, and -6 in canonical NF-κB signaling (13–15). However, study of the role of TRAF3 in NF-κB signaling has been difficult because most *Traf3*-KO mice die within the first week after birth (16). A report that TRAF3 is constitutively bound to NIK and mediates NIK ubiquitination and degradation in B cells identified a critical negative regulatory role of TRAF3

Conflict of interest: The authors have declared that no conflict of interest exists.
Citation for this article: *J Clin Invest.* 2014;124(1):297–310. doi:10.1172/JCI66947.

in noncanonical signaling (17). Furthermore, *Traf3*$^{-/-}$ mice have marked B cell accumulation of NIK, and compound deficiency of NF-κB p100 rescued their early postnatal lethality (18). Although deficiency of NIK or its downstream signaling molecule, RelB, appears to have little effect on basal bone homeostasis, *Nik*$^{-/-}$ and *RelB*$^{-/-}$ mice have defective osteoclastogenesis in response to pathologic osteolysis in vivo (8, 19). Additionally, transgenic mice with OC-targeted overexpression of a mutant NIK lacking the TRAF3-binding domain have decreased bone mass and increased bone erosion in a serum-transfer model of RA (11). Collectively, these data indicate that NIK and TRAF3 play important negative regulatory roles in noncanonical NF-κB signaling.

Results

Mice with OC-specific deletion of TRAF3 have increased osteoclastogenesis and osteoporosis, mediated by increased canonical and noncanonical NF-κB signaling. Culture of WT BM cells with M-CSF for 2 days followed by RANKL typically results in microscopically recognizable OCs 4 days later (data not shown). Expression of NFATc1, the master regulator of osteoclastogenesis (4), increased significantly 4 days after RANKL treatment, while TRAF3 protein levels decreased progressively (Figure 1A) and *TRAF3* mRNA levels remained unchanged (Supplemental Figure 1A; supplemental material available online with this article; doi:10.1172/JCI66947DS1). We generated a TRAF3 retroviral expression vector by inserting a human TRAF3 cDNA fragment into a pMX-IRES-GFP retroviral expression vector. After transfecting pMX-IRES-GFP or pMX-TRAF3-IRES-GFP vectors into PlatE packaging cells using Fugene 6, virus supernatants were collected and added to WT OCPs generated by culturing BM cells with M-CSF for 3 days (20). Approximately 60%–70% infection efficiency was confirmed in all samples by flow cytometry (data not shown). GFP$^+$ cells were sorted and cultured with M-CSF plus RANKL. Numerous tartrate-resistant acid phosphatase–positive (TRAP$^+$) OCs were observed in pMX-GFP–infected cells, but OC formation was decreased approximately 3-fold in pMX-TRAF3-IRES-GFP–infected cells (Figure 1B).

We next generated 2 new lines of mice with TRAF3 expression targeted to OC lineage cells: *Traf3*$^{f/f}$*;cathepsin K*^{cre} (which we call C-cKO) and *Traf3*$^{f/f}$*;lysozyme M*^{cre} (L-cKO) mice, and found that C-cKO BM cells cultured with M-CSF plus RANKL for 3 days formed TRAP$^+$ multinucleated OCs, but WT cultures did not (Supplemental Figure 1B). Although C-cKO and WT cells had formed similar numbers of OCs 2 days later, C-cKO OCs were larger, resulting in significantly increased OC area (Supplemental Figure 1B) and suggesting that TRAF3 negatively regulates osteoclastogenesis and perhaps fusion. We observed similar findings in cells from L-cKO mice (data not shown). L-cKO and C-cKO mice have normal bone phenotypes, similar to WT mice (Supplemental Figure 1C). Thus, we used Cre littermates as WT controls for future experiments. When we used RANKL at low concentrations (≤5 μg/ml), WT OCs generally formed later and were smaller (data not shown), but C-cKO cells in these conditions had greater OC-forming ability than WT cells (Figure 1C) and increased resorption pit areas when cultured on bone slices with M-CSF plus RANKL for 9 days, although OC numbers were similar by this time (Supplemental Figure 2). We also cultured these cells on 6-well plates for 6 days, resuspended the cells with 0.25% trypsin/EDTA, and replated equal numbers of OCs on bone slices in 96-well plates for an additional 4 days. Resorption pit area and numbers were similar between C-cKO and WT OCs (data not shown), consistent with TRAF3 having its major role in RANKL-induced OC formation rather than function.

Importantly, we found that 2-month-old C-cKO mice have mild osteoporosis, as indicated by significantly reduced tibial trabecular bone volume (BV) (Figure 1D), trabecular number, and thickness, with mean values for trabecular connectivity and separation being numerically lower and higher, respectively, but these did not reach statistical significance (Supplemental Figure 1D). These were associated with increased OC numbers and surfaces (Figure 1E), compared with control mice.

Previous TRAF3 overexpression studies in B cells suggested that TRAF3 suppresses canonical NF-κB activation (21). To test the mechanism by which TRAF3 inhibits osteoclastogenesis, we examined canonical and noncanonical protein levels in OCPs overexpressing TRAF3 in response to RANKL and observed markedly increased expression of NFATc1, NIK, p52, RelB, and RelA in pMX-GFP–infected OCPs (Figure 1F). In RANKL-treated pMX-TRAF3-IRES-GFP–infected OCPs, induction of NFATc1, NIK, RelA, and RelB was reduced compared with GFP-infected controls, accompanied by decreased p100 to p52 processing (Figure 1F). Consistent with these findings, we observed increased RelA, RelB, and NIK levels and increased p100 to p52 processing in L-cKO OCPs, even without RANKL stimulation (Figure 1G). Further addition of RANKL did not affect expression levels of these molecules, presumably reflecting prior exposure of primary cells to RANKL in vivo or the effects of constitutively active NIK. Furthermore, RelA nuclear translocation is increased in L-cKO OCPs under basal and RANKL-induced conditions (Figure 1H), indicating enhanced NF-κB signaling. We observed similar findings in C-cKO cells (data not shown).

TRAF3 ring finger domain is required for RANKL-induced TRAF3 degradation through a lysosome/autophagosome-dependent mechanism. TRAF3 contains 3 major domains: a ring finger (RF), required for suppression of NIK (22); a zinc finger (ZF), required for NF-κB activation (23); and a TRAF domain, which binds degradation-targeted proteins, such as NIK (22). We overexpressed RANK and TRAF3 in 293T cells to examine which TRAF3 domain or domains are required for its degradation. TRAF3 protein levels decreased significantly in these cells with serum starvation, which can induce autophagy in many cell types (24), and with RANKL treatment (Figure 2A). In contrast, TRAF3 accumulated with serum starvation or RANKL in cells expressing TRAF3 deletion mutants lacking either the RF or the RF and ZF domains. In contrast, with serum-starvation or RANKL treatment, TRAF3 levels decreased slightly in cells with the TRAF domain deleted. We observed similar findings in L-cKO OCPs infected with WT and mutant TRAF3 retroviruses. These findings contrast with a report that a NIK mutant lacking the TRAF3-binding domain is constitutively active (11). They suggest that the TRAF3-binding domain of NIK is necessary for NIK proteasomal degradation, while the TRAF domain of TRAF3 is not essential for TRAF3 degradation.

CD40 or BAFF-R engagement in B cells induces rapid, proteasome-dependent TRAF3 degradation (25). To determine whether RANKL induces TRAF3 ubiquitination and degradation in OCPs, we incubated endogenous TRAF3 proteins with a high-binding affinity ubiquitin matrix and captured ubiquitinated proteins using an anti-TRAF3 Ab. RANKL markedly increased TRAF3 ubiquitination (Figure 2B), which can occur in proteasomes, lysosomes, and autophagosomes in mammalian cells (26). To examine the mechanism involved, we pretreated WT OCPs with the lyso-

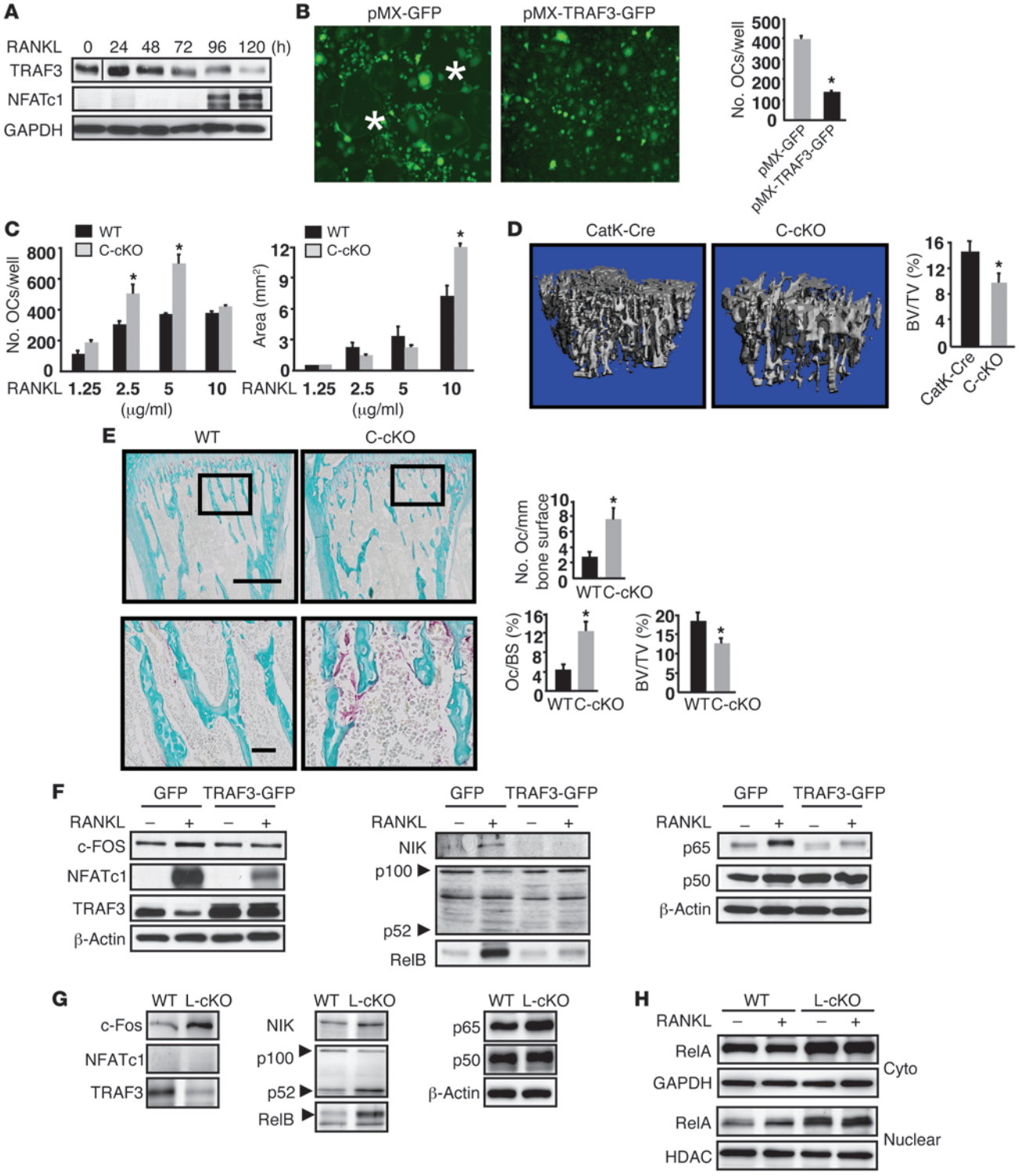

Figure 1

Mice with OC-specific deletion of TRAF3 have increased osteoclastogenesis and mild osteoporosis mediated by increased canonical and noncanonical NF-κB signaling. (**A**) WBs of TRAF3 and NFATc1 expression in WT BM cells treated with M-CSF plus RANKL. Lanes were run on the same gel, but were noncontiguous. (**B**) OCs formed from FACSAria-sorted WT OCPs infected with GFP or TRAF3-IRES-GFP (TRAF3-GFP) retroviruses treated with RANKL. Original magnification, ×10. *OC centers. TRAP+ OCs were counted. (**C**) BM-derived C-cKO or WT cells cultured with RANKL. *$P < 0.05$. (**D**) Representative tibial μCT scans from 2-month-old CatK-Cre or C-cKO mice. *$P < 0.05$. (**E**) Representative TRAP-stained tibial sections and bone histomorphometry from 2-month-old WT or C-cKO mice; boxed areas in lower images. Scale bars: 500 μm (upper panels); 50 μm (lower panels). OcS/BS, OC surface/bone surface (%). *$P < 0.05$. (**F**) WBs of whole cell lysates of WT OCPs infected with GFP or TRAF3-IRES-GFP retroviruses and cultured with RANKL for 5 days. (**G** and **H**) WBs of WT and L-cKO OCPs treated with RANKL for 48 hours. Cyto, cytoplasmic.

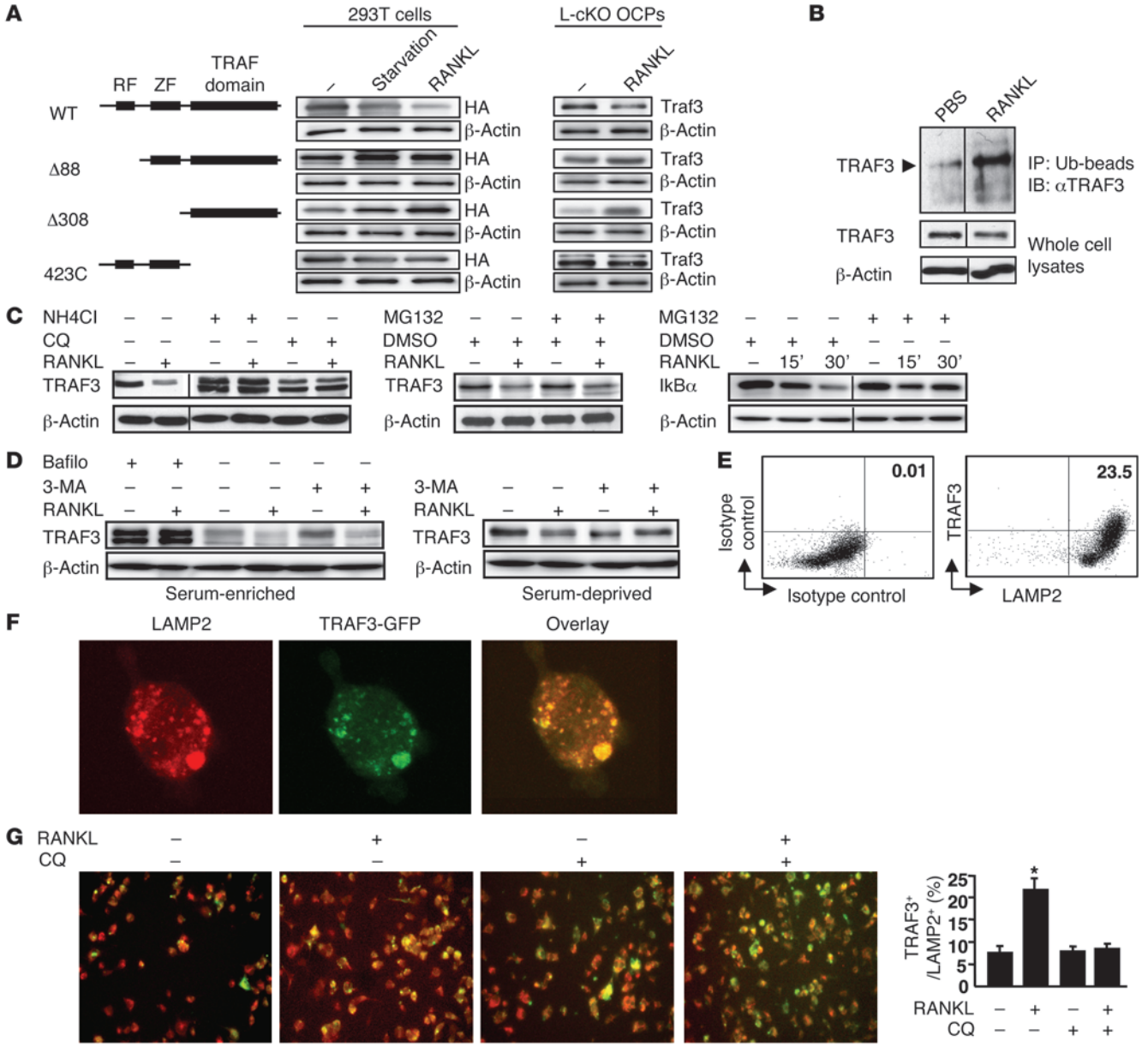

Figure 2

RANKL-induced TRAF3 degradation is lysosome mediated. (**A**) 293T cells transfected with HA-tagged WT or mutant TRAF3 constructs. L-cKO BM-derived OCPs infected with WT or mutant pMX-TRAF3 viruses were serum deprived or treated with RANKL for 8 hours. (**B**) Ubiquitinated (Ub) proteins from whole cell lysates of RANKL-treated (2 hours) WT OCPs using UbiQapture-Q Matrix blotted with anti-TRAF3 Ab. (**C**) WT OCPs pretreated with NH_4Cl (50 mM) for 1 hour, CQ (50 mM) for 6 hours, or MG132 (20 mM) for 4 hours were treated with RANKL for 8 hours. For IκBα, WT OCPs were treated with DMSO or MG132 with or without RANKL for indicated times. Lanes were run on the same gel, but were noncontiguous in **B** and **C**. (**D**) WT OCPs pretreated with bafilomycin (Bafilo; 50 ng/ml) for 16 hours or 3-MA (3-MA (5 mM) for 2 hours were treated with or without RANKL for 8 hours in serum-enriched or -deprived conditions. (**E**) TRAF3-GFP retrovirus–infected WT OCPs treated with RANKL for 8 hours were fixed and double-stained with TRAF3 and LAMP2 Abs. Left plot shows background staining with isotype control Abs. (**F**) TRAF3-GFP retrovirus–infected WT OCPs stained with anti-LAMP2 Ab. Colocalization assessed using confocal microscopy. Original magnification, ×60. (**G**) TRAF3-GFP retrovirus–infected WT OCPs treated with or without RANKL or CQ (2 mM) were stained with anti-LAMP2 Ab. TRAF3/LAMP2 double-positive cells were counted. Original magnification, ×20. *$P < 0.05$.

some inhibitors chloroquine (CQ) for 6 hours or NH_4Cl for 1 hour or with the proteasome inhibitor MG132 for 4 hours, followed by RANKL, and evaluated the extent of TRAF3 degradation by Western blot (WB). Pretreatment with either CQ or NH_4Cl, but not MG132, markedly increased TRAF3 levels in response to RANKL (Figure 2C). To confirm that MG132 functioned effectively as a proteasome inhibitor (27), we treated WT OCPs with RANKL plus MG132 for 15 and 30 minutes and found that compared with DMSO control, MG132 blocked RANKL-induced IκBα degradation (Figure 2C).

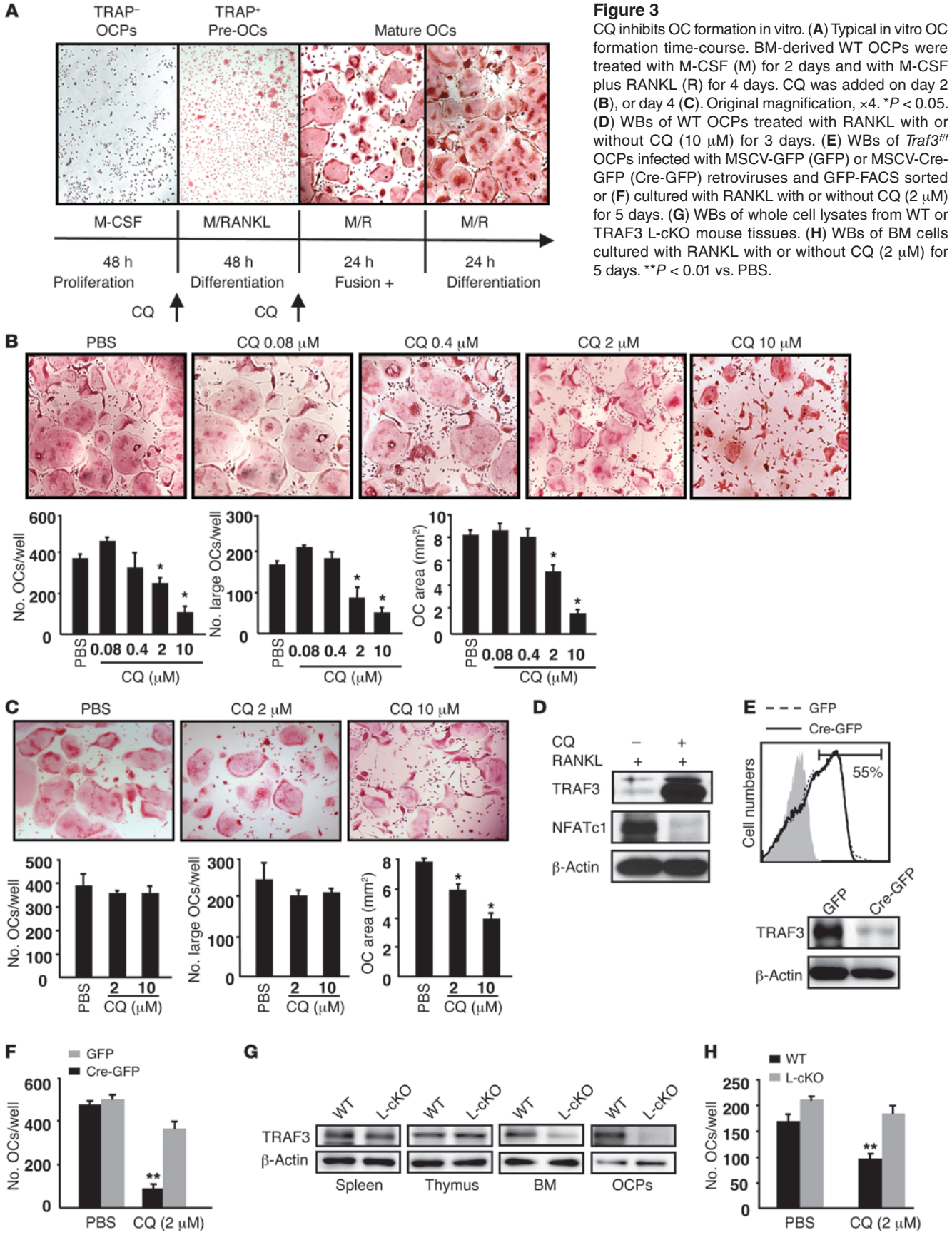

Figure 3

CQ inhibits OC formation in vitro. (**A**) Typical in vitro OC formation time-course. BM-derived WT OCPs were treated with M-CSF (M) for 2 days and with M-CSF plus RANKL (R) for 4 days. CQ was added on day 2 (**B**), or day 4 (**C**). Original magnification, ×4. $^{*}P < 0.05$. (**D**) WBs of WT OCPs treated with RANKL with or without CQ (10 μM) for 3 days. (**E**) WBs of *Traf3*$^{f/f}$ OCPs infected with MSCV-GFP (GFP) or MSCV-Cre-GFP (Cre-GFP) retroviruses and GFP-FACS sorted or (**F**) cultured with RANKL with or without CQ (2 μM) for 5 days. (**G**) WBs of whole cell lysates from WT or TRAF3 L-cKO mouse tissues. (**H**) WBs of BM cells cultured with RANKL with or without CQ (2 μM) for 5 days. $^{**}P < 0.01$ vs. PBS.

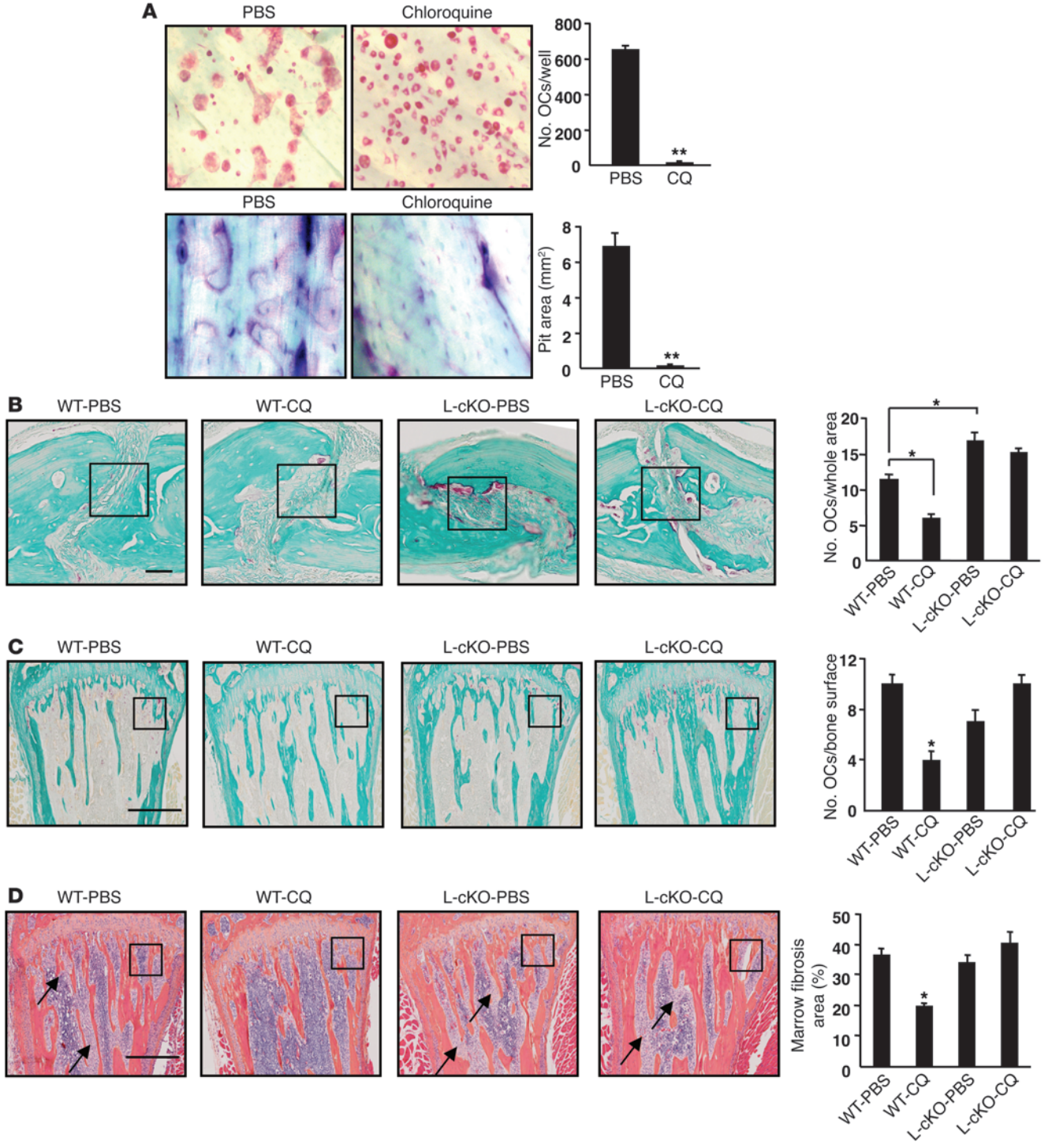

Figure 4

CQ affects OC function in vitro and in vivo. (**A**) WT OCPs cultured with RANKL with or without CQ (5 μM) for 9 days. TRAP staining (left panels) and toluidine blue (right panels, to highlight resorption pits). Values are means + SEM of 4 wells. $^{**}P < 0.01$ vs PBS. Original magnification, ×20. (**B**–**D**) Representative TRAP-stained sections and OC numbers in calvarial (**B**) and tibial (**C**) sections from 10- to 12-week-old male WT or L-cKO mice treated with CQ (50 mg/kg/d i.p. for 10 days) and given supracalvarial injections of hPTH(1-34 aa) (10 μg/mouse) 4×/d for 3 days beginning on day 7. (**D**) Representative H&E-stained tibial sections from the mice in **C** illustrating marrow fibrosis (arrows) and values for percentage of marrow space occupied by marrow fibrosis. Values are means + SEM of 4 mice/group. $^{*}P < 0.05$. Boxed areas in **B**–**D** are illustrated at higher magnification in Supplemental Figure 5. Scale bars: 50 μm (**B**); 500 μm (**C** and **D**).

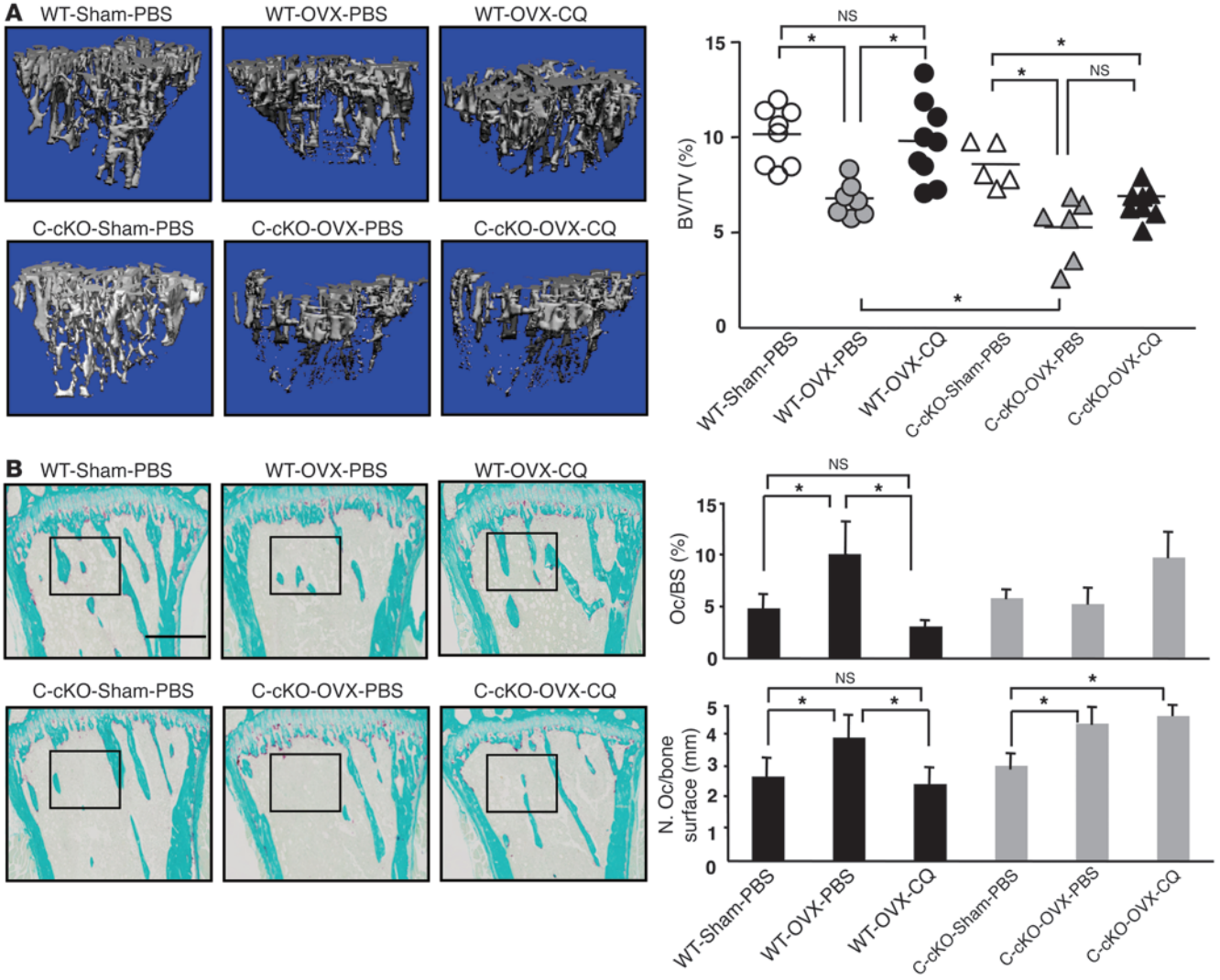

Figure 5

CQ prevents OVX-induced bone loss in WT, but not in C-cKO mice. OVX or sham-operated 8- to 9-week-old WT and C-cKO mice treated with PBS or CQ (50 mg/kg/d i.p. for 28 days). (**A**) Representative μCT images of tibiae and trabecular BVs. (**B**) Representative TRAP-stained tibial sections and histomorphometric data for OC surface and numbers. Values are the mean + SEM of 5–9 mice/group. *$P < 0.05$. Boxed areas are shown at higher magnification in Supplemental Figure 6B. Scale bar: 500 μm.

We next tested autophagy inhibitors on RANKL-induced TRAF3 degradation. Bafilomycin A1 blocks fusion of the autophagosome and the lysosome (28); it increased accumulation of TRAF3 (Figure 2D). 3-Methyladenine (3-MA), which blocks PI3K, had no effect on TRAF3 degradation in serum-enriched conditions. However, TRAF3 accumulated in serum-deprived OCPs treated with 3-MA (Figure 2D), consistent with 3-MA–inhibiting autophagy only in serum-deprived cells (29). We next infected WT OCPs with a pMX-TRAF3-GFP retrovirus and found that TRAF3 and LAMP2 (a lysosome marker) were coexpressed in approximately 23% of RANKL-treated cells (Figure 2E). Confocal microscopy showed that the TRAF3-GFP fusion protein was localized mostly in the cytosol in OCPs (Figure 2F). RANKL significantly increased colocalization of TRAF3 and LAMP2, which was reduced by CQ (Figure 2G).

CQ inhibits RANKL-induced OC formation by preventing lysosomal degradation of TRAF3. To determine whether CQ affects OC formation, we cultured WT BM cells with M-CSF for 2 days, added RANKL, and stained them for TRAP activity on days 2, 4, 5, and 6. Two days after RANKL addition, OCPs differentiated into TRAP$^+$ mononuclear cells, which we called pre-OCs, that ultimately fused to form OCs over the following 2 days (Figure 3A). When we added CQ during the initial stages of OC formation, the total number of OCs and large OCs and OC area were significantly reduced dose dependently, with the highest dose (10 μM) inducing a 3-fold reduction in OC numbers (Figure 3B). Addition of CQ during the later stages of OC formation reduced OC area, with no effect on total and large OC numbers (Figure 3C). Furthermore, when these OCPs were treated with RANKL plus CQ for 3 days, the percentage of apoptotic and dead cells was similar to that in controls (6.1 vs. 5.3%, data not shown). Thus, CQ inhibits OCP differentiation, but not OCP fusion or OC survival.

CQ is an anti-malarial agent, and like its derivative, hydroxychloroquine, has been used early in the treatment of systemic lupus

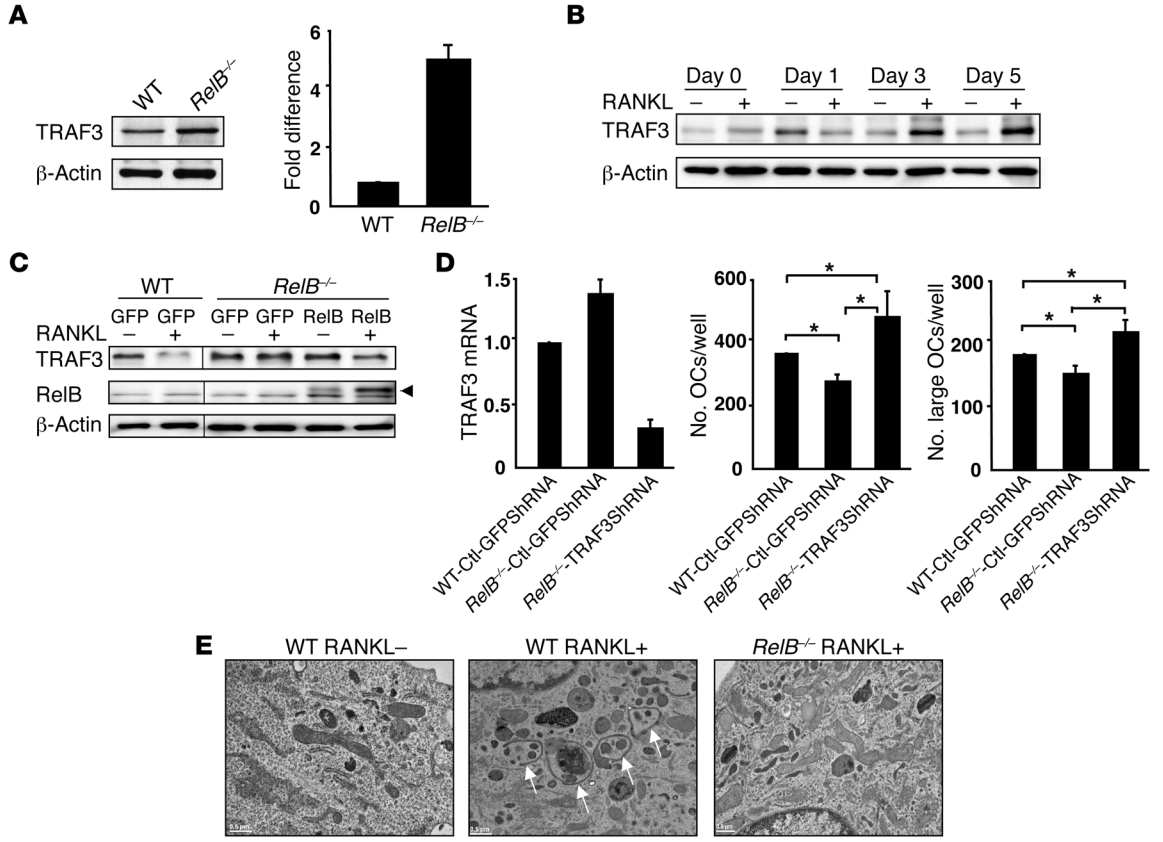

Figure 6

RelB positively regulates RANKL-induced TRAF3 degradation. (**A**) WBs of WT and *RelB*$^{-/-}$ BM whole cell lysates and TRAF3 levels quantified densitometrically (mean + SEM of 3 blots). (**B**) WBs of RANKL-treated *RelB*$^{-/-}$ OCPs. (**C**) WBs of WT or *RelB*$^{-/-}$ OCPs infected with pMY-GFP or pMY-RelB-GFP retrovirus for 2 days and treated with RANKL for 8 hours. Arrowhead, specific RelB band. Lanes were run on the same gel, but were noncontiguous. (**D**) WT or *RelB*$^{-/-}$ OCPs infected with control GFP shRNA (Ctl-shRNA) or TRAF3 shRNA lentiviruses for 2 days were cultured with MCSF plus RANKL for 4 days. TRAF3 knockdown was confirmed by RT-PCR. Total numbers of OCs and large OCs were counted. (**E**) EM images of WT or *RelB*$^{-/-}$ OCPs treated with RANKL for 4 days in 2-well culture chambers showing autophagosomes (arrows).

erythematosus and RA, but the precise mechanism of action in autoimmune diseases is not clear (30). We found that TRAF3 levels increased markedly in OCPs after CQ treatment (10 μM for 3 days); this was accompanied by decreased NFATc1 expression (Figure 3D). We infected OCPs from *Traf3*$^{f/f}$ mice with MSCV-Cre-GFP (where MSCV indicates murine stem cell virus) or MSCV-GFP retrovirus and sorted GFP$^+$ cells to verify deletion of TRAF3 (Figure 3E). Sorted GFP$^+$ cells then were cultured with or without CQ in OC formation assays. TRAF3-deficient and WT OCPs formed similar numbers of OCs, and CQ reduced OC numbers from WT cells (~80%), but had no effect on TRAF3-deficient cells (Figure 3F). We next confirmed specific deletion of TRAF3 protein in BM cells and OCPs from L-cKO mice (Figure 3G) and found that CQ did not inhibit RANKL-induced OC formation in TRAF3-deficient cells (Figure 3H).

CQ inhibits OC formation in vitro and PTH- and ovariectomy-induced bone resorption in vivo via TRAF3. We next cultured WT OCPs on bone slices with RANKL for 9 days and found that CQ-treated cells formed few TRAP$^+$ OCs (12 ± 3 vs. 656 ± 17 in controls) and few resorption pits, which covered very little of the bone slices (0.04 ± 0.01 mm^2) compared with controls where pits occupied most of the surface (6.9 ± 0.7 mm^2) (Figure 4A). We then treated 3-week- or 3-month-old WT and C-cKO mice with CQ (25 mg/kg i.p, once daily) for 28 days and found no significant difference in BV or other structural parameter values assessed by μCT in tibiae compared with those of vehicle-treated mice (Supplemental Figure 3, A and B), suggesting that this regimen of CQ has no effect on basal bone resorption or bone mass. Further time-course and dose-response studies will be required to determine whether CQ can inhibit basal bone resorption.

To determine whether CQ affects osteoblast formation or function, we performed CFU-F, CFU–alkaline phosphatase (CFU-ALP), and bone nodule formation assays using 2 μM CQ, which inhibits OC formation. We found that CQ had no effects on any of these indices of osteoblast function in WT BM stromal cells (Supplemental Figure 4A), suggesting that the predominant effect of CQ is on OCs. Parathyroid hormone (PTH) is a primary regulator of calcium homeostasis and has both anabolic and catabolic effects, associated with intermittent or continuous administration, respectively (31, 32). To test whether CQ affects PTH-induced bone formation, we administered PTH (2 μg/kg, 3×/d) intermittently to WT mice for 14 days along with CQ (50 mg/kg, 1×/d). PTH treatment significantly increased trabecular BV, trabecular thickness, and mineral apposition (MAR) and bone formation rates (BFR), but CQ had no effect (Supplemental Figure 4, B–D).

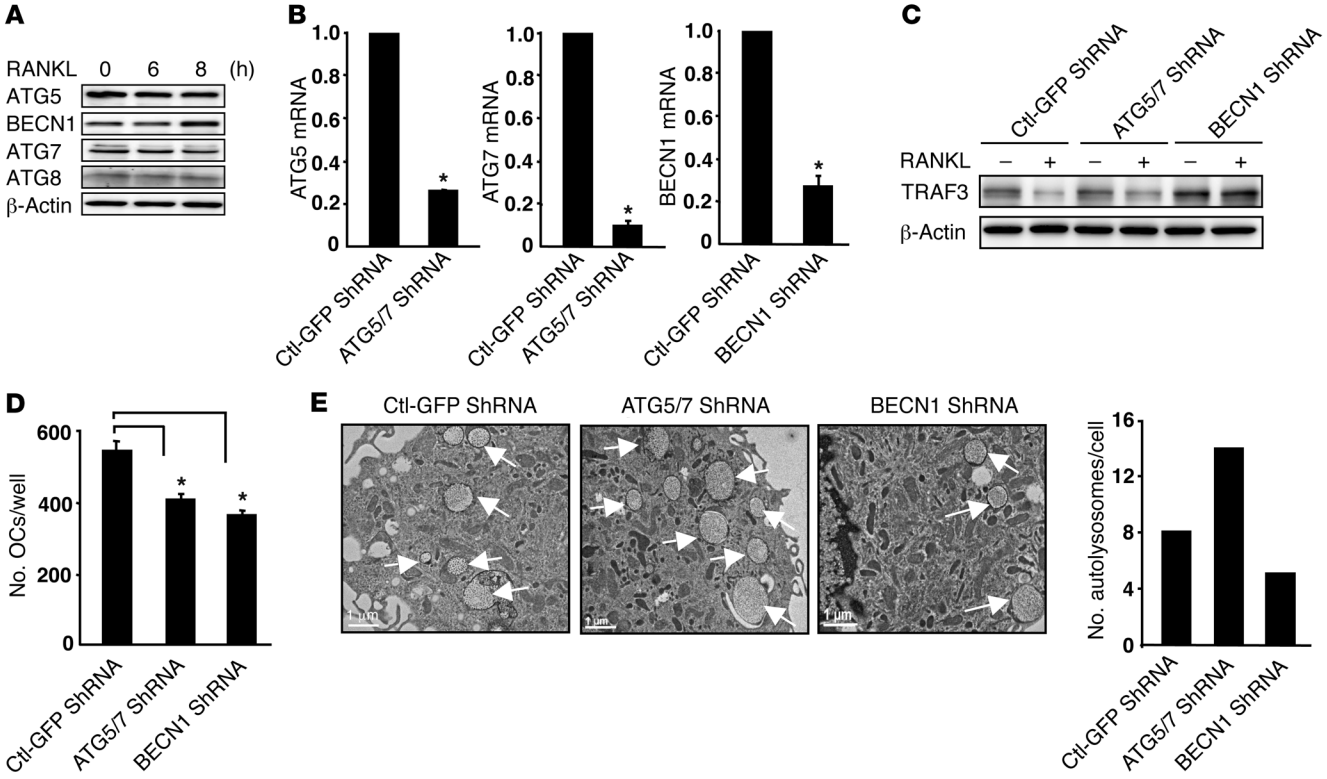

Figure 7

RANKL-induced TRAF3 degradation is absent in BECN1, but not in ATG5/7 knockdown OCPs. (**A**) WBs of WT OCPs treated with RANKL. (**B**–**E**) WT OCPs infected with Ctl-GFP, BECN1, or ATG5 and ATG7 shRNA lentiviruses for 2 days. (**B**) mRNA levels of BECN1, ATG5, and ATG7. (**C**) WB of infected cells treated with RANKL for 8 hours. (**D**) OCs formed from infected cells cultured with RANKL for 5 days. **P* < 0.05 vs. Ctl-GFP shRNA. (**E**) EM images and numbers of autophagosomes (arrows, expressed/cell in at least 50 cells/preparation from 2 independent experiments) in infected cells.

We next examined the effects of CQ in an in vivo model of pathologic bone resorption in which PTH stimulates OC formation by inducing RANKL expression (33). We treated L-cKO or Cre-negative control mice with CQ (50 mg/kg, 1×/d) for 7 days followed by CQ plus PTH (10 μg/mouse, 4×/d, s.c. over calvariae) for another 3 days (34). CQ markedly reduced PTH-induced OC formation in calvariae and tibiae in WT mice compared with PBS treatment, but not in L-cKO mice (Figure 4, B and C, and Supplemental Figure 5, A and B). A similar pattern of change was observed in serum TRAP5b levels (Supplemental Figure 5D). Furthermore, marrow fibrosis (a hallmark of PTH-induced resorption) was observed in all groups except the WT mice treated with CQ and PTH (Figure 4D and Supplemental Figure 5C). Similar results were obtained in a separate experiment using C-cKO mice (data not shown).

To further evaluate the effects of CQ on bone resorption in vivo, we used 8- to 9-week-old female C-cKO or Cre-negative control mice in an ovariectomy (OVX) model. Two days after surgery, mice were treated with PBS or CQ (50 mg/kg, i.p. 1×/d) for 28 days, and tibiae were analyzed using μCT and histology. Four weeks after surgery, uterine weights and tibial BVs in OVX mice were markedly reduced compared with those of sham-operated WT and C-cKO mice, consistent with OVX, and BVs were significantly lower in C-cKO than in WT mice (Figure 5A and Supplemental Figure 6A). In addition, CQ prevented OVX-induced bone loss and increased OC numbers and surfaces in WT mice, but not in C-cKO mice (Figure 5, A and B, and Supplemental Figure 6, B and C).

RelB is required for RANKL-induced TRAF3 lysosomal degradation by regulating BECN1 expression. We next investigated basal and inducible TRAF3 levels in *RelB*$^{-/-}$ OCPs, in part because RANKL/NIK/p100 signaling activates RelB (5) and also to determine whether RelB regulates TRAF3 degradation. Basal TRAF3 protein levels were 5-fold higher in *RelB*$^{-/-}$ BM cells than in WT cells (Figure 6A). In addition, in contrast to the time-dependent decrease in TRAF3 levels induced by RANKL in WT OCPs (Figure 1A), significant accumulation of TRAF3 protein was observed in RANKL-treated *RelB*$^{-/-}$ OCPs (Figure 6B), suggesting that RelB promotes RANKL-induced TRAF3 degradation. To test this, we infected *RelB*$^{-/-}$ OCPs with pMY-RelB to determine whether adding back RelB could restore RANKL-induced TRAF3 degradation. TRAF3 levels decreased significantly in GFP control virus–infected OCPs 8 hours after RANKL stimulation (similar to Figure 2C). This decrease did not occur in GFP control virus–infected *RelB*$^{-/-}$ OCPs, but was seen in *RelB*$^{-/-}$ OCPs overexpressing pMY-RelB (Figure 6C).

M-CSF plus RANKL–treated *RelB*$^{-/-}$ BM cells generated significantly fewer mature OCs than WT cells (8). To further investigate the role of TRAF3 in these conditions, we infected WT and *RelB*$^{-/-}$ OCPs with control GFP (Ctl-GFP) or TRAF3 shRNA lentivirus and confirmed TRAF3 knockdown by RT-PCR. *TRAF3* mRNA levels were 35% higher in *RelB*$^{-/-}$ than in control OCPs (Figure 6D), and *RelB*$^{-/-}$ cells formed fewer OCs than WT cells. TRAF3 knockdown induced significantly more OCs from *RelB*$^{-/-}$ cells (267 ± 18 to 490 ± 54) and to a greater extent than WT virus-infected cells (367 ± 6; Figure 6D).

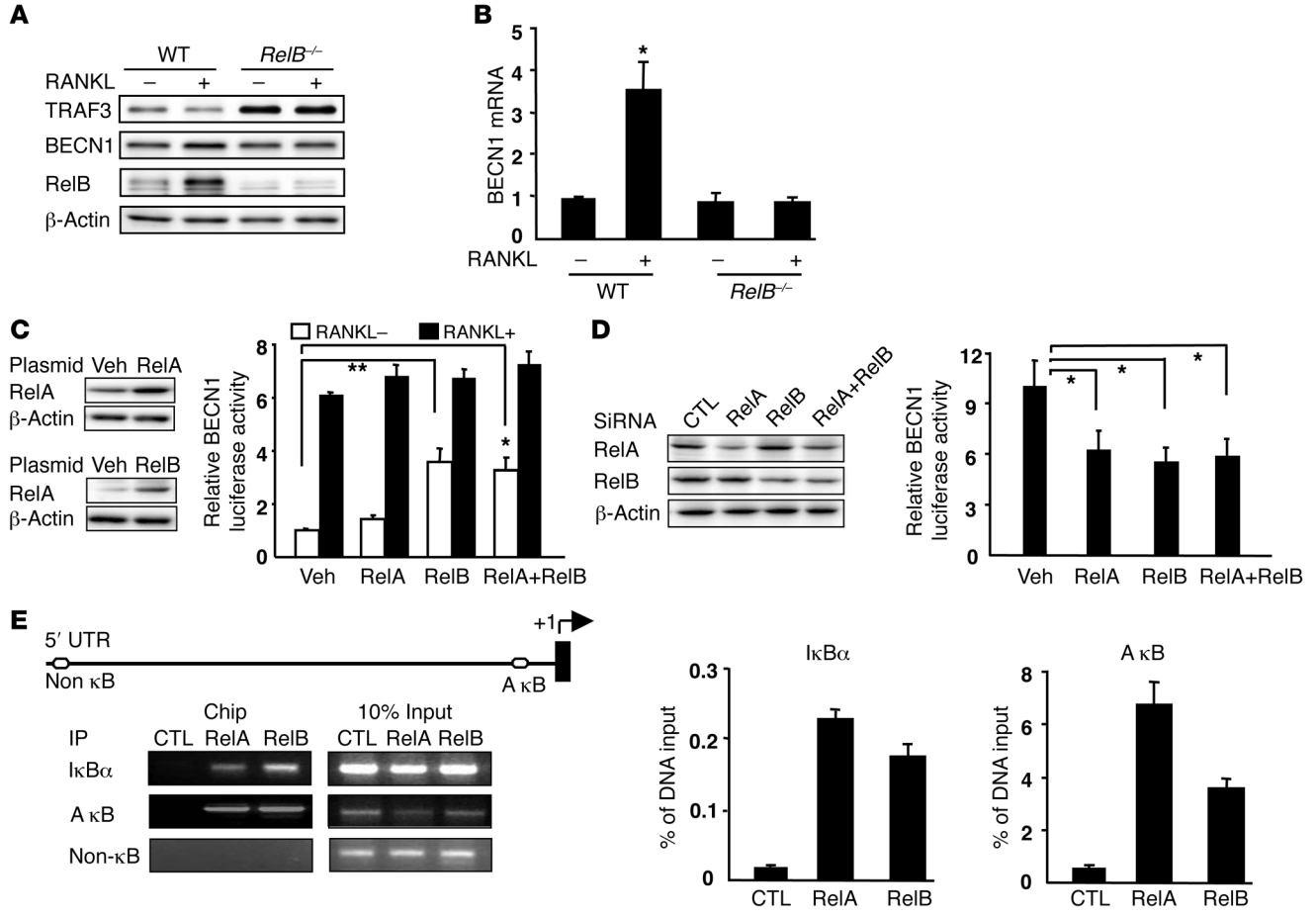

Figure 8

RelB binds to the BECN1 promoter and regulates its expression. Whole cell lysate WBs (**A**) and RT-PCR–detected *BECN1* mRNA levels (**B**) in WT or *RelB*$^{-/-}$ OCPs treated with RANKL or vehicle for 8 hours. (**C**) 293T cells transfected with RelA- or RelB-expressing plasmids or cotransfected with a human BECN1 promoter pGL3-Luc reporter and a Renilla luciferase plasmid and RelA- and/or RelB-expressing plasmids. RANKL-treated samples were cotransfected with a hRANK plasmid. (**D**) RelA- or RelB siRNAs were transfected into 293T cells 48 hours before cotransfection with pGL3-Luc and Renilla plasmids. Protein levels were assessed by WB. Dual-luciferase assays were performed 24 hours after transfection. Values in **C** and **D** are means + SEM from 3 independent experiments. **P* < 0.05; ***P* < 0.01. (**E**) WT OCPs treated with RANKL for 8 hours and sheared chromatin precipitated with RelA- or RelB-specific Abs, or IgG (negative control [CTL]). Recovered DNA was used as a template for PCR. Primers for the A κB site inside the IκBα promoter and a non-κB site in the proximal BECN1 promoter region were positive and negative controls, respectively. RelA or RelB binding to the indicated promoters was quantified by real-time PCR. Data are representative of 2 independent experiments.

To further explore the role of RelB in RANKL-induced TRAF3 lysosomal degradation, we used transmission EM (widely used to monitor autophagy) (35) to evaluate the ability of WT and *RelB*$^{-/-}$ cells to form autophagosomes. Initial steps in autophagy include formation and expansion of an isolation membrane, also called a phagophore, the edges of which fuse to form an autophagosome, a double-membraned vesicle that sequesters cytoplasmic material. Autophagosomes then fuse with lysosomes to form autolysosomes where the captured material, together with the inner membrane is degraded (36). Autophagic vacuoles with their characteristic double membranes formed in WT, but not in *RelB*$^{-/-}$, cells in response to RANKL (Figure 6E).

Having demonstrated that RANKL-induced TRAF3 degradation is lysosome/autophagy-mediated, we next examined protein levels in OCPs of ATG5, ATG7, ATG8, and beclin 1 (BECN1), key molecules in autophagosome formation (37). RANKL upregulated expression of BECN1 (~3-fold), but not of the other autophagic proteins (Figure 7A). Moreover, RANKL-induced TRAF3 degradation and autolysosome formation were impaired in cells with shRNA knockdown of BECN1, but not of ATG5/7 (Figure 7, B, C, and E), associated with a significant reduction in OC numbers (Figure 7D). TRAF3 levels in OCPs treated with ATG5/7 shRNA fell in response to RANKL, similar to control shRNA, but this was associated with reduced osteoclastogenesis and increased autolysosome numbers, suggesting that ATG5/7 may regulate the degradation of other modulators that contribute to RANKL-induced OC formation.

BECN1 associates with PI3KIII/Vps34 as a platform that modulates autophagosome formation during early steps of autophagy (37). The reduction in TRAF3 induced by RANKL was accompanied by increased RelB and BECN1 protein and mRNA levels in WT OCPS, but not in *RelB*$^{-/-}$ OCPs (Figure 8, A and B), suggesting an association between RelB and BECN1. There are 4 κB binding sites in the BECN1 promoter and in its first intron region, and RelA upregulates BECN1 transcriptional activity (37). We there-

fore cotransfected a pGL3-BECN1 reporter vector, including 1.1 kbp upstream of the human BECN1 promoter (37), together with RelA or RelB expression vectors into 293T cells and performed dual luciferase assays. We confirmed RelA and RelB overexpression in 293T cells by WB (Figure 8C). BECN1 transcriptional activity was upregulated significantly by RelB, but only minimally by RelA, overexpression (Figure 8C), which may reflect RelA protein levels being relatively low in our assays compared with published levels (37). RANKL markedly increased BECN1 transcriptional activity, consistent with the increased BECN1 protein level induced by RANKL (Figure 8C). However, RANKL did not increase BECN1 activity further when RelA or RelB was overexpressed. Furthermore, siRNA knockdown of RelA or RelB in 293T cells resulted in reduced protein levels and an approximately 50% reduction in BECN1 promoter activity (Figure 8D). To further assess interaction of RelB with the BECN1 promoter, we performed ChIP assays. An A κB site is conserved in humans and mice (37), and real-time PCR and standard PCR analyses of ChIP DNA revealed that RelB binds to this A κB site with a lower binding ability than RelA. Neither nonspecific IgG nor primers covering the proximal BECN1 promoter region displayed detectable binding (Figure 8E).

Discussion

TRAF3, a relatively understudied TRAF family member, has been shown recently to act as an important multifunctional regulator of type I IFN and balanced cytokine production by serving as an adaptor molecule that facilitates assembly of a NIK/TRAF2/activated/cellular inhibitor of apoptosis (cIAP) complex (38). NIK plays a key role in noncanonical NF-κB signaling, and its stability is regulated by TRAF3 in B cells (17) and in OCPs (11). Here, we have shown using gain- and loss-of-function approaches that TRAF3 suppresses RANKL-induced OC formation, consistent with TRAF3 being a negative regulator of noncanonical signaling (11). Mice that we generated with conditional KO of TRAF3 in OCPs were osteoporotic with increased OC numbers (Figure 1, D and E), indicating that TRAF3 plays an important protective role in physiological bone remodeling.

Our finding that TRAF3 also inhibits expression of p65 is consistent with the increased p65-binding activity in *Traf3*$^{-/-}$ cells (39) and increased phospho-p65 level in TRAF3 knockdown cells in response to TNF or LTβR (40), but the mechanism whereby TRAF3 inhibits NF-κB signaling is unclear. TRAF3 deficiency did not alter protein levels of RANK or DC-STAMP (Supplemental Figure 7, A and B), key regulators of RANKL-induced OCP differentiation and fusion (41, 42). TRAF3 could inhibit both NF-κB pathways by affecting NIK-IKKα signaling because IKKα is required for formation of IKKα/IKKβ/IKKγ and IKKα/IKKα complexes in the canonical and noncanonical pathways, respectively (43, 44). In addition, TRAF3 overexpression upregulated expression of type I IFN (Supplemental Figure 7C), which can act as a negative regulator of osteoclastogenesis (45). Thus, TRAF3 might also suppress OC formation through RANKL/IFN-α signaling crosstalk. The primary role of canonical signaling appears to be to mediate OCP survival (46). However, when we inhibited RANKL-induced OC formation with CQ to prevent TRAF3 lysosomal degradation, we found no change in OCP proliferation or apoptosis rates (Figure 3, C and D), despite seeing a CQ-induced reduction in levels of the p65 target gene *NFATc1* (Figure 4A) and a reduction in p65 levels in OCPs when TRAF3 was overexpressed (Figure 1F). Further studies will be required to determine exactly how TRAF3 functions in these NF-κB pathways and also whether it might have positive regulatory roles, as reported in other cell types (12).

In normal eukaryotic cells, autophagosomes digest damaged organelles and misfolded and long-lived proteins (47) and ultimately fuse with lysosomes, leading to degradation of their contents. Human genome-wide association data suggest a link between autophagy genes and osteoporosis (48), and the OC ruffled border membrane has been described as an autophagosome that fuses with lysosomes to facilitate secretion of matrix-degrading enzymes, especially cathepsin K. Furthermore, autophagy proteins, including Atg5, Atg7, Atg4B, and LC3, are important for generating the ruffled border (49). However, a potential role for autophagy in OC formation has not been reported. Here, we demonstrate for what we believe is the first time that autophagy also plays a role in osteoclastogenesis by regulating degradation of TRAF3, which we show undergoes ubiquitination and sequential autophagic-lysosomal degradation in response to RANKL. Our data are supported by a report that proteasome inhibition only marginally reduced TRAF3 degradation upon LTβR stimulation in 293T cells (50). However, TRAF3 can undergo K48-linked polyubiquitination by Triad3A and subsequent proteasomal degradation following virus infection in A549 human epithelial cells (51). Thus, the fate of TRAF3 may vary in response to different stimuli and be cell context dependent. In B cells, CD40 or BAFF receptor activation reduced TRAF3 degradation in a TRAF2/cIAP1/2-dependent manner, and CD40-induced TRAF3 degradation was inhibited by a small-molecule mimetic, which inhibits cIAPs (52). We found that knockdown of cIAP1/2 reduced RANKL-induced TRAF3 degradation and decreased OC formation (Supplemental Figure 8), but the precise function of cIAPs in RANKL-induced TRAF3 lysosomal degradation will require further study.

Our finding that RelB is required for RANKL-induced TRAF3 lysosomal degradation is important because it points to a negative feedback loop between NF-κB signaling and TRAF3. Many factors known to induce autophagy, including TNF (53), also act as NF-κB activators. Depletion of essential autophagy modulators, including Atg5, Atg7, BECN1, and Vsp34 by RNAi inhibited TNF-driven NF-κB activation in human cancer cell lines (54). Similarly, KO of the genes encoding IKKα, IKKβ, IKKγ, or their upstream activator, TAK1, reduced autophagy induced by nutrient depletion or by treatment with rapamycin or other autophagy stimulators (55). However, the detailed molecular mechanisms are still unclear. We found that RANKL-induced TRAF3 degradation is absent in *RelB*$^{-/-}$ OCPs (Figure 8A). Our data suggest that RelB induction of TRAF3 lysosomal degradation is through transcriptional modulation of the early autophagic protein BECN1 (Figure 8E), with degradation of TRAF3 leading to activation of NF-κB signaling. Although the mechanism by which BECN1 might target TRAF3 for transfer to the lysosome is unclear, our findings have identified a RelB-regulated autophagy pathway involving NF-κB activation.

Given the essential functions of NF-κB in inflammation, autoimmune disease, and oncogenesis, large numbers of natural or synthetic NF-κB inhibitors have been produced (56). Although many of these inhibitors suppress osteoclastogenesis and bone resorption, none of them has progressed to clinical trials for the treatment of common bone diseases, such as postmenopausal osteoporosis or RA (4). Biologic inhibitors directed at pathogenetic cytokines, such as TNF, IL-1, and IL-6, have been approved for the treatment of inflammatory arthritis (57, 58). However, these treatments fail to achieve remission in up to 40% of patients (57). Thus, additional insights

into the pathogenesis of joint destruction in this common disease and new drugs are needed. Our identification of TRAF3 as an inhibitor of osteoclastogenesis suggests a new target for treatment of RA.

CQ was used for many years to reduce inflammation in RA until it was replaced by hydroxychloroquine because the latter has fewer ophthalmic side effects. However, clinical studies indicate that, when given alone or in combination with methotrexate, hydroxychloroquine does not prevent joint destruction in 60%–70% of affected patients (58), suggesting that it may have limited use as an antiresorptive in most RA patients. CQ and hydroxychloroquine prevent acidification of the lysosomal compartment, but their mechanism of action is unclear, and reports of the effects of these drugs on OCs in vitro have been contradictory. For example, hydroxychloroquine had no inhibitory effect on human OCP differentiation (59), while CQ inhibited the formation of large OCs in the later phases of osteoclastogenesis (60). This latter finding differs from our in vitro observations and may reflect differences in culture conditions, but it does support a role for this class of compounds as inhibitors of bone resorption. Our finding that CQ inhibits OC formation in vitro and in vivo by preventing TRAF3 lysosomal degradation suggests that CQ could inhibit bone resorption in humans by this mechanism. The dose of CQ that we used in our in vivo studies (50 mg/kg) is higher than the dose of hydroxychloroquine given to patients (~5 mg/kg), and this could account for the efficacy we observed in our mouse studies coupled with the fact that PTH- and OVX-induced resorption is less complex than the severe inflammatory milieu in RA. Recent studies indicate that CQ can have therapeutic efficacy in a number of other diseases, including cancer and pulmonary hypertension, and there are more than 30 clinical trials underway examining combinations of hydroxychloroquine with anticancer agents (61, 62). Other CQ derivatives could possibly have better anti-OC efficacy and fewer side effects, but further studies will be required to examine this.

In addition to this newly identified function of TRAF3 in bone homeostasis, TRAF3 has been implicated in the pathogenesis of a number of diseases, including multiple myeloma (63) and experimental autoimmune encephalomyelitis/multiple sclerosis (64). TRAF3 mutations in humans with multiple myeloma result in the accumulation of NIK and constitutive activation of NF-κB, thereby promoting myeloma cell survival. Strategies to increase TRAF3 levels in OCPs by CQ or CQ derivatives should inhibit bone resorption in conditions in which RANKL is increased. Manipulating TRAF3 expression levels in other cell types, such as B cells, could also have beneficial therapeutic effects in patients with RA.

Methods

Mice. All animals were 6 to 12 weeks old. WT C57BL/6 (B6) mice were from the National Cancer Institute (Frederick, Maryland, USA). *RelB*$^{-/-}$ mice have been described previously (65). *Traf3*-floxed mice (B6 background) were from L. Rui (University of Michigan, Ann Arbor, Michigan, USA) (66). Lysozyme M-Cre (*Lyz2tm1(cre)Ifo*/J; B6 background) mice were purchased from the Jackson Laboratories. Cathepsin K-Cre mice (B6 background) were provided by Y.-P. Li (University of Alabama at Birmingham, Birmingham, Alabama, USA). To generate cKO mice, *Traf3*-floxed mice were bred with cathepsin K-Cre or lysozyme M-Cre transgenic mice. Cathepsin K-Cre, lysozyme M-Cre, and *Traf3*-floxed mice all have normal bone phenotypes (BV/tissue volume [TV], Tb. N, Tb.Th, and Tb. Sp values; data not shown). Cre-negative littermates were used as WT controls in all in vivo experiments.

Abs and reagents. The following Abs were from Santa Cruz Biotechnology Inc.: TRAF3 (clone M20), NFATc1 (clone 7A6), c-Fos (clone 4), NIK (clone H-248), RelB (clone C19), p65 (clone C20), p50 (clone NLS), and BECN1 (clone H-300). p100/p52 Ab was from Millipore. HA (clone H6908) and β-actin (clone AC-40) Abs were from Sigma-Aldrich. Recombinant M-CSF and RANKL were from R&D Systems. MG132, bafilomycin A1, 3-MA, NH_4Cl, and CQ were from Sigma-Aldrich. LAMP2 Ab, clone GL2A7, was from Abcam.

Plasmid construction and retroviral transfer Abs and reagents. The retroviral vector pMX-TRAF3-IRES-GFP WT and mutants were generated by inserting a cDNA fragment encoding TRAF3 WT and mutants into a pMX-IRES-GFP retroviral expression vector from K. Matsuo (Keio University, Minato, Tokyo, Japan). A pMX-TRAF3-GFP fusion protein vector was generated by inserting a TRAF3 PCR fragment into BamHI-NcoI sites of pMX-TRAF3-IRES-GFP. pMY-GFP vector, was from A. Hirao (Keio University). We generated pMY-RelB-GFP by inserting a RelB cDNA fragment into the pMY-GFP vector. MSCV-Cre and MSCV-Cre-GFP were from T. Reya (UCSD, La Jolla, California, USA). Retrovirus packaging was performed by transfecting plasmids into Plat-E cells (pMY virus) or 293T cells (MSCV virus) using Fugene 6 (Roche) following the manufacturer's protocol. WT and mutant TRAF3 constructs were from S.C. Sun (17) (University of Texas, MD Anderson Cancer Center, Houston, Texas, USA). These plasmids were transfected into 293T cells using Fugene 6.

In vitro OC formation and functional assays. BM cells (4×10^4) were cultured in 96-well plates in α-MEM with 10% FBS and recombinant M-CSF (10 ng/ml
in all experiments) for 2 days to enrich for OCPs. OCPs were infected with retrovirus for 2 days followed by RANKL (10 ng/ml in all experiments, unless otherwise stated; R&D Systems) for 5 to 7 days. OC formation was assessed by counting TRAP$^+$ multinucleated cells with 3 or more nuclei. OC area was assessed using standard stereologic methods, an ocular eyepiece grid, an Olympus TH4-100 microscope, and a ×4 objective lens. WT BM cells were cultured with M-CSF for 2 days on bone slices to generate OCPs and then CQ (5 μM) and RANKL were added. Cells were fixed and stained for TRAP activity to allow counting of OCs, which were then removed; bone slices were stained with 0.5% toluidine blue to visualize resorption pits, as described (67).

In vitro CFU-F, CFU-ALP, and bone nodule formation assays. For CFU-F and CFU-ALP colony formation assays, BM cells from long bones were cultured in 10-cm dishes with 10^6 cells/dish in 10 ml α-MEM plus 10% FCS with or without 50 μg/ml ascorbic acid and 10 mM β-glycerophosphate. Media were changed every 3 to 4 days, and cultures were maintained for 24 days when cells were stained with H&E or for ALP activity. For bone nodule formation, BM cells were cultured in α-MEM plus 10% FCS for 7 to 10 days and cultured in osteoblast-inducing medium containing 50 μg/ml ascorbic acid and 10 mM β-glycerophosphate for 21 to 28 days; mineralized bone nodules were examined after Von Kossa staining.

WB analysis. Whole-cell lysate protein from retrovirus-infected OCPs, TRAF3 plasmid-transfected 293T cells, WT, or cKO OCPs were cultured in 60-mm dishes and lysed with RIPA Lysis Buffer (Millipore) containing a protease inhibitor cocktail (Roche). Lysates (10–40 μg) were loaded in 10% SDS-PAGE gels and immunoblotted with Abs to TRAF3, NFATc1, c-Fos, p65, RelB, p50, GAPDH, NIK, p100, HA, HDAC, BECN1, RANK, DC-STAMP, or mouse actin.

In vitro ubiquitination assays. WT BM cells were treated with M-CSF for 2 days and RANKL was added for 2 hours. Whole cell lysates were prepared using lysis buffer containing 20 mM HEPES, 250 mM NaCl, 20 mM Tris-HCl, 0.5% NP-40, 2 mM EDTA, 2 μg/ml leupeptin, 2 μg/ml aprotinin, 1 mM DTT, 1 mM PMSF, and 1 mM N-ethylmaleimide (Sigma-Aldrich) to limit deubiquitination and incubated with UbiQapture-Q matrix (Enzo Life Sciences) to pull down all ubiquitinated proteins, following the manufacturer's protocol. Precipitates were subjected to WB using anti-TRAF3 Abs.

Flow cytometry and cell sorting. WT OCPs were infected with pMX-TRAF3-GFP retrovirus for 3 days, and the cells were stained using an intracellular

staining kit (BD Bioscience). In brief, the cells were fixed and permeabilized by Cytofix/Cytoperm buffer, then stained with PE-*Traf3* Ab and Rat anti-mouse LAMP2 Ab (Santa Cruz Biotechnology Inc.). The secondary Ab (biotinylated anti-rat IgG; Vector Laboratories) was visualized by APC-streptavidin (BD Biosciences). WT OCPs were treated with RANKL and 10 μM CQ for 3 days and stained with FITC–annexin V and propidium iodide (BD Biosciences) for 15 minutes. Cytometric analyses were performed using a flow cytometer (FACS LSR II; BD Biosciences) and FlowJo software. GFP-positive retrovirus-infected OCPs were sorted using FACSAria (BD Biosciences).

Immunocytochemistry and confocal microscopy. pMX-TRAF3-GFP–infected OCPs were seeded into 8-well chamber slides (Lab-Tek, NUNC), fixed with 4% paraformaldehyde, and permeabilized with 0.1% Triton X-100. After blocking with 5% goat serum in PBS for 4 hours, cells were incubated with anti-LAMP2 Ab (Abcam) in a humidity chamber at 4°C overnight. The next day, cells were washed and incubated with secondary Alexa Fluor 350–labeled anti-rat Ab. Colocalization of TRAF3 and LAMP2 in single cells was assessed using a FV1000 Olympus Laser Scanning Confocal Microscope.

In vivo PTH and CQ treatment and histological analysis. CQ (50 mg/kg/d) was administered i.p. for 10 days to female WT or L-cKO mice (10 to 12 weeks old; 4/group), as described (68). On day 7, mice were given supracalvarial injections of vehicle or hPTH(1–34 aa) (EMD Biosciences; 10 μg/injection) 4×/d for 3 days, (using a protocol that induces hypercalcemia and bone resorption; ref. 34), and killed 16 hours after the last injection. Calvarial and tibial sections were prepared as described (9). OC numbers and marrow fibrosis were measured in TRAP- and H&E-stained sections using an eyepiece grid and an Olympus TH4-100 microscope.

Six-week-old female WT mice (7–8/group) were injected i.p. daily with 50 mg/kg CQ and with hPTH (2 μg/mouse s.c.) 3×/d for 14 days to induce bone formation, as described (69). Tibiae were used for μCT scanning. Calcein labeling was described previously (70). MAR and BFR in endocortical and trabecular bone were measured using standard procedures and Visiopharm Integrator System image analysis software.

OVX-induced bone loss. OVX or sham surgeries were performed in WT or C-cKO mice (8 to 9 weeks old; 5–9/group). CQ treatment (50 mg/kg i.p. daily injection for 28 days) was started 2 days after surgery. Controls received PBS. Calcein labeling was performed as described above. OVX was confirmed by uterine weight and histology. Tibiae were assessed by micro-CT and histomorphometry.

Electron microscopy. WT or *RelB*$^{-/-}$ OCPs were infected with Ctl-GFP, ATG5 shRNA, BECN1 shRNA, or ATG7 shRNA (Santa Cruz Biotechnology Inc.) for 2 days, cultured on glass chamber slides for 4 days with RANKL, fixed in 0.1 M sodium cacodylate–buffered 2.5% glutaraldehyde for 24 hours, and post-fixed in 1% buffered osmium tetroxide for 30 minutes. Slides were transitioned through graded ethanols to 100% and infiltrated with Spurr's epoxy resin overnight. The slides were dipped into liquid nitrogen, and the entrapped cells were popped off and thin sectioned, then placed onto nickel grids, stained with aqueous uranyl acetate and lead citrate and examined using a Hitachi 7650 Transmission EM.

Reporter assay. A pGL3 luciferase reporter containing 1.1 kbp of the human BECN1 promoter (CHET4) was from C. Schneider (Università degli Studi di Udine, Udine, Italy) (37). CHET4 and pcDNA3-RelA-cFlag (Addgene) or pcDNA3-RelB-cFlag plasmids (Addgene) was cotransfected into 293T cells together with a Renilla luciferase plasmid with or without an hRANK construct. Cells were treated with RANKL or PBS, and dual-luciferase assays were performed 24 hours after transfection. siRNA targeting RelA or RelB (Santa Cruz Biotechnology Inc.) was transfected into 293T cells following the manufacturer's instructions. CHET4 and a Renilla luciferase plasmid were cotransfected by Fugene 6 48 hours later.

ChIP assay. ChIP was performed as described (37). In brief, BM-derived OCPs were treated with RANKL for 8 hours and fixed in 1% formaldehyde. Chromatin was sheared by sonication (16 rounds of 20 pulses with 2 minutes between rounds (Qsonica 125 sonicator). Then samples were incubated overnight at 4°C with Abs to p65, RelB, and IgG (negative control). Precipitated DNAs were analyzed by real-time PCR. Primers for the mIkBa promoter (–316 to –15) were a positive control: 5′-GGACCCCAAACCAAAATCG-3′ and 5′-TCAGGCGCGGGGAA-TTTCC-3′ as described (71). A primer set that covers the BECN1 proximal promoter region (–1897 to approximately –1513) was used as a negative control: 5′-GGGCAAGGCATCATAAAACAGG-3′ and 5′-AGGAGATGAAGTTGACCTCC-3′. Specific primers for the A κB site in the BECN1 promoter region (–241 to approximately –1) are: 5′-AAGAAGCCTAGAGTCCCTGG-3′ and 5′-CCTGCGACAGCGGAGAAAAG-3′.

Statistics. Values are shown as means + SEM of 4 samples unless otherwise stated. One-way ANOVA and nonparametric comparison (Bonferroni's multiple comparison test) were used with Prism software version 4.0b for experiments with more than 2 groups. Two-tailed Student's *t* test was used for other statistical analyses, and significance was set at $P < 0.05$.

Study approval. All animal experiments were performed using University of Rochester Medical Center ACUAC–approved protocols and conformed to the *Guide for the Care and Use of Laboratory Animals* (NIH. Revised 2011).

Acknowledgments

We thank Yanyun Li, Michael Thullen, and Karen Bentley for technical support. This work was supported by the following grants from the National Institute for Arthritis, Musculoskeletal and Skin Diseases: AR43510 and 1S10RR027340 (to B.F. Boyce); AR48697 (to L. Xing); P30AR061307, and T32AR053459.

Received for publication August 19, 2013, and accepted in revised form October 3, 2013.

Address correspondence to: Brendan F. Boyce, Department of Pathology and Laboratory Medicine, University of Rochester Medical Center, 601 Elmwood Avenue, Box 626, Rochester, New York 14642, USA. Phone: 585.275.5837; Fax: 585.273.3637; E-mail: Brendan_Boyce@URMC.Rochester.edu.

Yan Xiu's present address is: Department of Physical Medicine and Rehabilitation, Perelman School of Medicine, University of Pennsylvania, Philadelphia, Pennsylvania, USA.

Chen Zhao's present address is: Department of Pathology and Laboratory Medicine, University of Pennsylvania Medical Center, Philadelphia, Pennsylvania, USA

Yoshikazu Morita's present address is: Milk Science Research Institute, Megmilk Snow Brand Co., Saitama, Japan.

1. Sitara D, Aliprantis AO. Transcriptional regulation of bone and joint remodeling by NFAT. *Immunol Rev*. 2010;233(1):286–300.
2. Teitelbaum SL. Osteoclasts. What do they do and how do they do it? *Am J Pathol*. 2007;170(2):427–435.
3. Braun T, Zwerina J. Positive regulators of osteoclastogenesis and bone resorption in rheumatoid arthritis. *Arthritis Res Ther*. 2011;13(4):235.
4. Boyce BF. Advances in osteoclast biology reveal potential new drug targets and new roles for osteoclasts. *J Bone Miner Res*. 2013;28(4):711–722.
5. Oeckinghaus A, Hayden MS, Ghosh S. Crosstalk in NF-κB signaling pathways. *Nat Immunol*. 2011;12(8):695–708.
6. Franzoso G, et al. Requirement for NF-κB in osteoclast and B-cell development. *Genes Dev*. 1997; 11(24):3482–3496.
7. Iotsova V, et al. Osteopetrosis in mice lacking NF-κB1

and NF-κB2. *Nat Med*. 1997;3(11):1285–1289.
8. Vaira S, et al. RelB is the NF-κB subunit downstream of NIK responsible for osteoclast differentiation. *Proc Natl Acad Sci U S A*. 2008;105(10):3897–3902.
9. Yao Z, Xing L, Boyce BF. NF-κB p100 limits TNF-induced bone resorption in mice by a TRAF3-dependent mechanism. *J Clin Invest*. 2009; 119(10):3024–3034.
10. Zhao B, Grimes SN, Li S, Hu X, Ivashkiv LB. TNF-induced osteoclastogenesis and inflammatory bone resorption are inhibited by transcription factor RBP-J. *J Exp Med*. 2012;209(2):319–334.
11. Yang C, et al. NIK stabilization in osteoclasts results in osteoporosis and enhanced inflammatory osteolysis. *PLoS One*. 2010;5(11):e15383.
12. Hacker H, Tseng PH, Karin M. Expanding TRAF function. TRAF3 as a tri-faced immune regulator. *Nat Rev Immunol*. 2011;11(7):457–468.
13. Bishop GA. The multifaceted roles of TRAFs in the regulation of B-cell function. *Nat Rev Immunol*. 2004; 4(10):775–786.
14. Rothe M, Sarma V, Dixit VM, Goeddel DV. TRAF2-mediated activation of NF-κB by TNF receptor 2 and CD40. *Science*. 1995;269(5229):1424–1427.
15. Cao Z, Xiong J, Takeuchi M, Kurama T, Goeddel DV. TRAF6 is a signal transducer for interleukin-1. *Nature*. 1996;383(6599):443–446.
16. Xu Y, Cheng G, Baltimore D. Targeted disruption of TRAF3 leads to postnatal lethality and defective T-dependent immune responses. *Immunity*. 1996; 5(5):407–415.
17. Liao G, Zhang M, Harhaj EW, Sun SC. Regulation of the NF-κB-inducing kinase by tumor necrosis factor receptor-associated factor 3-induced degradation. *J Biol Chem*. 2004;279(25):26243–26250.
18. He JQ, et al. Rescue of TRAF3-null mice by p100 NF-κB deficiency. *J Exp Med*. 2006;203(11):2413–2418.
19. Novack DV, et al. The IκB function of NF-κB2 p100 controls stimulated osteoclastogenesis. *J Exp Med*. 2003;198(5):771–781.
20. Li P, et al. Systemic tumor necrosis factor alpha mediates an increase in peripheral CD11bhigh osteoclast precursors in tumor necrosis factor α-transgenic mice. *Arthritis Rheum*. 2004;50(1):265–276.
21. Cheng G, et al. Involvement of CRAF1, a relative of TRAF, in CD40 signaling. *Science*. 1995; 267(5203):1494–1498.
22. He JQ, Saha SK, Kang JR, Zarnegar B, Cheng G. Specificity of TRAF3 in its negative regulation of the noncanonical NF-κB pathway. *J Biol Chem*. 2007; 282(6):3688–3694.
23. Dadgostar H, Cheng G. An intact zinc ring finger is required for tumor necrosis factor receptor-associated factor-mediated nuclear factor-κB activation but is dispensable for c-Jun N-terminal kinase signaling. *J Biol Chem*. 1998;273(38):24775–24780.
24. Mizushima N. Autophagy: process and function. *Genes Dev*. 2007;21(22):2861–2873.
25. Vallabhapurapu S, et al. Nonredundant and complementary functions of TRAF2 and TRAF3 in a ubiquitination cascade that activates NIK-dependent alternative NF-κB signaling. *Nat Immunol*. 2008;9(12):1364–1370.
26. Clague MJ, Urbe S. Ubiquitin. same molecule, different degradation pathways. *Cell*. 2010; 143(5):682–685.
27. Ang E, et al. Proteasome inhibitors impair RANKL-induced NF-kappaB activity in osteoclast-like cells via disruption of p62, TRAF6, CYLD, and IκBα signaling cascades. *J Cell Physiol*. 2009;220(2):450–459.
28. Yamamoto A, et al. Bafilomycin A1 prevents maturation of autophagic vacuoles by inhibiting fusion between autophagosomes and lysosomes in rat hepatoma cell line, H-4-II-E cells. *Cell Struct Funct*. 1998;23(1):33–42.
29. Wu YT, et al. Dual role of 3-methyladenine in modulation of autophagy via different temporal patterns of inhibition on class I and III phosphoinositide 3-kinase. *J Biol Chem*. 2010; 285(14):10850–10861.
30. Ben-Zvi I, Kivity S, Langevitz P, Shoenfeld Y. Hydroxychloroquine. From malaria to autoimmunity. *Clin Rev Allergy Immunol*. 2012;42(2):145–153.
31. Tam CS, Heersche JN, Murray TM, Parsons JA. Parathyroid hormone stimulates the bone apposition rate independently of its resorptive action. differential effects of intermittent and continuous administration. *Endocrinology*. 1982;110(2):506–512.
32. Hock JM, Gera I. Effects of continuous and intermittent administration and inhibition of resorption on the anabolic response of bone to parathyroid hormone. *J Bone Miner Res*. 1992;7(1):65–72.
33. Ma YL, et al. Catabolic effects of continuous human PTH (1–38) in vivo is associated with sustained stimulation of RANKL and inhibition of osteoprotegerin and gene-associated bone formation. *Endocrinology*. 2001;142(9):4047–4054.
34. Yates AJ, et al. Effects of a synthetic peptide of a parathyroid hormone-related protein on calcium homeostasis, renal tubular calcium reabsorption, and bone metabolism in vivo and in vitro in rodents. *J Clin Invest*. 1988;81(3):932–938.
35. Klionsky DJ, et al. Guidelines for the use and interpretation of assays for monitoring autophagy in higher eukaryotes. *Autophagy*. 2008;4(2):151–175.
36. Levine B, Kroemer G. Autophagy in the pathogenesis of disease. *Cell*. 2008;132(1):27–42.
37. Copetti T, Bertoli C, Dalla E, Demarchi F, Schneider C. p65/RelA modulates BECN1 transcription and autophagy. *Mol Cell Biol*. 2009;29(10):2594–2608.
38. Tseng PH, et al. Different modes of ubiquitination of the adaptor TRAF3 selectively activate the expression of type I interferons and proinflammatory cytokines. *Nat Immunol*. 2010;11(1):70–75.
39. Zarnegar B, Yamazaki S, He JQ, Cheng G. Control of canonical NF-κB activation through the NIK-IKK complex pathway. *Proc Natl Acad Sci U S A*. 2008; 105(9):3503–3508.
40. Bista P, et al. TRAF3 controls activation of the canonical and alternative NFκB by the lymphotoxin beta receptor. *J Biol Chem*. 2010;285(17):12971–12978.
41. Simonet WS, et al. Osteoprotegerin. a novel secreted protein involved in the regulation of bone density. *Cell*. 1997;89(2):309–319.
42. Kukita T, et al. RANKL-induced DC-STAMP is essential for osteoclastogenesis. *J Exp Med*. 2004; 200(7):941–946.
43. Senftleben U, et al. Activation by IKKα of a second, evolutionary conserved, NF-κB signaling pathway. *Science*. 2001;293(5534):1495–1499.
44. Zandi E, Rothwarf DM, Delhase M, Hayakawa M, Karin M. The IκB kinase complex (IKK) contains two kinase subunits, IKKα and IKKβ, necessary for IκB phosphorylation and NF-κB activation. *Cell*. 1997;91(2):243–252.
45. Takayanagi H, et al. RANKL maintains bone homeostasis through c-Fos-dependent induction of interferon-β. *Nature*. 2002;416(6882):744–749.
46. Vaira S, et al. RelA/p65 promotes osteoclast differentiation by blocking a RANKL-induced apoptotic JNK pathway in mice. *J Clin Invest*. 2008; 118(6):2088–2097.
47. Deretic V, Jiang S, Dupont N. Autophagy intersections with conventional and unconventional secretion in tissue development, remodeling and inflammation. *Trends Cell Biol*. 2012;22(8):397–406.
48. Zhang L, et al. Pathway-based genome-wide association analysis identified the importance of regulation-of-autophagy pathway for ultradistal radius BMD. *J Bone Miner Res*. 2010;25(7):1572–1580.
49. DeSelm CJ, et al. Autophagy proteins regulate the secretory component of osteoclastic bone resorption. *Dev Cell*. 2011;21(5):966–974.
50. Ganeff C, et al. Induction of the alternative NF-κB pathway by lymphotoxin αβ (LTαβ) relies on internalization of LTβ receptor. *Mol Cell Biol*. 2011; 31(21):4319–4334.
51. Nakhaei P, et al. The E3 ubiquitin ligase Triad3A negatively regulates the RIG-I/MAVS signaling pathway by targeting TRAF3 for degradation. *PLoS Pathog*. 2009;5(11):e1000650.
52. Zarnegar BJ, et al. Noncanonical NF-κB activation requires coordinated assembly of a regulatory complex of the adaptors cIAP1, cIAP2, TRAF2 and TRAF3 and the kinase NIK. *Nat Immunol*. 2008; 9(12):1371–1378.
53. Djavaheri-Mergny M, et al. NF-κB activation represses tumor necrosis factor-α-induced autophagy. *J Biol Chem*. 2006;281(41):30373–30382.
54. Criollo A, et al. Autophagy is required for the activation of NFκB. *Cell Cycle*. 2012;11(1):194–199.
55. Criollo A, et al. The IKK complex contributes to the induction of autophagy. *EMBO J*. 2010; 29(3):619–631.
56. Ben-Neriah Y, Karin M. Inflammation meets cancer, with NF-κB as the matchmaker. *Nat Immunol*. 2011; 12(8):715–723.
57. Smolen JS, Aletaha D, Koeller M, Weisman MH, Emery P. New therapies for treatment of rheumatoid arthritis. *Lancet*. 2007;370(9602):1861–1874.
58. Davila L, Ranganathan P. Pharmacogenetics. implications for therapy in rheumatic diseases. *Nat Rev Rheumatol*. 2011;7(9):537–550.
59. Lee CK, et al. Effects of disease-modifying antirheumatic drugs and antiinflammatory cytokines on human osteoclastogenesis through interaction with receptor activator of nuclear factor κB, osteoprotegerin, and receptor activator of nuclear factor κB ligand. *Arthritis Rheum*. 2004;50(12):3831–3843.
60. Voronov I, et al. The R740S mutation in the V-ATPase a3 subunit increases lysosomal pH, impairs NFATc1 translocation and decreases in vitro osteoclastogenesis. *J Bone Miner Res*. 2013; 28(1):108–118.
61. Kimura T, Takabatake Y, Takahashi A, Isaka Y. Chloroquine in cancer therapy. a double-edged sword of autophagy. *Cancer Res*. 2013;73(1):3–7.
62. Lotze MT, Maranchie J, Appleman L. Inhibiting autophagy. a novel approach for the treatment of renal cell carcinoma. *Cancer J*. 2013;19(4):341–347.
63. Keats JJ, et al. Promiscuous mutations activate the noncanonical NF-κB pathway in multiple myeloma. *Cancer Cell*. 2007;12(2):131–144.
64. Xiao Y, et al. Peli1 promotes microglia-mediated CNS inflammation by regulating Traf3 degradation. *Nat Med*. 2013;19(5):595–602.
65. Burkly L, et al. Expression of relB is required for the development of thymic medulla and dendritic cells. *Nature*. 1995;373(6514):531–536.
66. Gardam S, Sierro F, Basten A, Mackay F, Brink R. TRAF2 and TRAF3 signal adapters act cooperatively to control the maturation and survival signals delivered to B cells by the BAFF receptor. *Immunity*. 2008;28(3):391–401.
67. Zhang Q, et al. VEGF-C, a lymphatic growth factor, is a RANKL target gene in osteoclasts that enhances osteoclastic bone resorption through an autocrine mechanism. *J Biol Chem*. 2008; 283(19):13491–13499.
68. Parkhitko A, et al. Tumorigenesis in tuberous sclerosis complex is autophagy and p62/sequestosome 1 (SQSTM1)-dependent. *Proc Natl Acad Sci U S A*. 2011;108(30):12455–12460.
69. Calvi LM, et al. Osteoblastic expansion induced by parathyroid hormone receptor signaling in murine osteocytes is not sufficient to increase hematopoietic stem cells. *Blood*. 2012;119(11):2489–2499.
70. Schwarz EM, et al. Tumor necrosis factor-α/nuclear transcription factor-κB signaling in periprosthetic osteolysis. *J Orthop Res*. 2000;18(3):472–480.
71. Yamamoto Y, Verma UN, Prajapati S, Kwak YT, Gaynor RB. Histone H3 phosphorylation by IKK-α is critical for cytokine-induced gene expression. *Nature*. 2003;423(6940):655–659.

Mechanisms of Signal Transduction:

Tumor Necrosis Factor Promotes Runx2 Degradation through Up-regulation of Smurf1 and Smurf2 in Osteoblasts

Hiroyuki Kaneki, Ruolin Guo, Di Chen, Zhenqiang Yao, Edward M. Schwarz, Ying E. Zhang, Brendan F. Boyce and Lianping Xing

J. Biol. Chem. 2006, 281:4326-4333.
doi: 10.1074/jbc.M509430200 originally published online December 22, 2005

THE JOURNAL OF BIOLOGICAL CHEMISTRY VOL. 281, NO. 7, pp. 4326–4333, February 17, 2006
Printed in the U.S.A.

Tumor Necrosis Factor Promotes Runx2 Degradation through Up-regulation of Smurf1 and Smurf2 in Osteoblasts*

Received for publication, August 25, 2005, and in revised form, November 10, 2005 Published, JBC Papers in Press, December 22, 2005, DOI 10.1074/jbc.M509430200

Hiroyuki Kaneki[‡], Ruolin Guo[‡], Di Chen[§], Zhenqiang Yao[‡], Edward M. Schwarz[§], Ying E. Zhang[¶], Brendan F. Boyce[‡], and Lianping Xing[‡1]

From the [‡]Department of Pathology and Laboratory Medicine and [§]Department of Orthopaedics, Center for Musculoskeletal Research, University of Rochester, School of Medicine and Dentistry, Rochester, New York 14642, and the [¶]Laboratory of Cellular and Molecular Biology, Center for Cancer Research, NCI, National Institutes of Health, Bethesda, Maryland 20892

Tumor necrosis factor (TNF) plays an important role in the pathogenesis of inflammatory bone loss through stimulation of osteoclastic bone resorption and inhibition of osteoblastic bone formation. Compared with the well established role of TNF in osteoclastogenesis, mechanisms by which TNF inhibits osteoblast function have not been fully determined. Runx2 is an osteoblast-specific transcription factor whose steady-state protein levels are regulated by proteasomal degradation, mediated by the E3 ubiquitin ligases, Smurf1 and Smurf2. We hypothesized that TNF inhibits osteoblast function through Smurf-mediated Runx2 degradation. We treated C2C12 and 2T3 osteoblast precursor cell lines and primary osteoblasts with TNF and found that TNF, but not interleukin-1, significantly increased Smurf1 and Smurf2 expression. TNF increased the degradation of endogenous or transfected Runx2 protein, which was blocked by treating cells with a proteasomal inhibitor or by infecting cells with small interfering (si)RNA against Smurf1 or Smurf2. TNF inhibited the expression of bone morphogenetic protein and transforming growth factor-β signaling reporter constructs, and the inhibition of each was blocked by Smurf1 siRNA and Smurf2 siRNA, respectively. Overexpression of Smurf1 and/or Smurf2 siRNAs prevented the inhibitory effect of TNF on Runx2 reporter. Consistent with these *in vitro* findings, bones from TNF transgenic mice or TNF-injected wild type mice had increased Smurf1 and decreased Runx2 protein levels. We propose that one of the mechanisms by which TNF inhibits bone formation in inflammatory bone disorders is by promoting Runx2 proteasomal degradation through up-regulation of Smurf1 and Smurf2 expression.

Tumor necrosis factor (TNF)[2] is a major contributor to pathologic bone loss through stimulation of osteoclastic bone resorption and inhibition of osteoblastic bone formation. In patients with rheumatoid arthritis, TNF and other cytokines are overproduced in inflamed joints by various cells infiltrating the synovial membrane. This leads to severe local erosion of cartilage and bone, periarticular osteopenia, as well as systemic osteoporosis (1, 2). Under these conditions, osteoblasts do not catch up with the accelerated bone resorption, indicating impaired osteoblast function (3). The inhibitory effects of TNF on bone formation *in vitro* were first described in 1987 in neonatal rat calvarial organ cultures (4). Subsequent studies demonstrated that TNF inhibits recruitment of osteoblast progenitors, reduces expression of genes produced by mature osteoblasts, and promotes osteoblast apoptosis through nuclear factor-κB signaling pathway (5–9). However, compared with our understanding of the role of TNF in osteoclast biology, little is known of the molecular mechanisms that mediate the effect of TNF on osteoblast inhibition.

To date, the most important mechanistic finding of TNF-mediated osteoblast inhibition was the demonstration that TNF decreases Runt-related gene 2 (Runx2) expression and its DNA binding activity in osteoblasts (10). This is partially through suppression of Runx2 gene transcription and destabilization of *Runx2* mRNA through the TNF receptor 1 signaling pathway (10–12). However, because TNF-induced reduction in nuclear Runx2 protein (more than 90%) was greater than expected, compared with the decrease in total *Runx2* mRNA (50%), it has been predicted that TNF may also have post-transcriptional effects. Furthermore, pharmacological inhibitors of the cell survival-promoting kinases, Akt, phosphatidylinositol 3-kinase, and extracellular signal-regulated kinases, fail to reverse the inhibitory effects of TNF on osteoblast differentiation *in vitro* (11), suggesting that other signal pathways may be involved.

In the past several years, ubiquitin-mediated proteasomal degradation has been implicated in the regulation of bone morphogenetic protein (BMP)-2 and transforming growth factor-β (TGF-β) signaling pathways in various cell types (13, 14). We and others have demonstrated that the E3 ubiquitin ligase, Smad ubiquitin regulatory factor (Smurf)1, regulates osteoblast differentiation by promoting proteasomal degradation of the BMP signaling protein, Smad1 and Smad5, and of the osteoblast transcription factor, Runx2 (15–18). Smurf2, a closely related homolog of Smurf1, was shown to reduce the steady-state protein levels of Smad1 and 2, but not Smad3 and 4, in Smurf2-transfected cells (19, 20). Ectopic expression of Smurf1 in 2T3 osteoblast precursors and C2C12 myoblast/osteoblast precursors induces the proteasomal degradation of Smad1 and Runx2 proteins, leading to inhibition of osteoblast differentiation (17). Smurf1 blocks BMP-induced osteogenic conversion of C2C12 cells and facilitates their myogenic differentiation by inducing degradation of Smad5 (16). *In vitro*, Smurf1 also targets a member of the Rho family of small GTPases, RhoA, for ubiquitination and degradation (21, 22). *In vivo*, overexpression of Smurf1 in osteoblasts by the osteoblast-specific type I collagen (Col1a1) promoter leads to reduction in osteoblast proliferation and activity. Col1a1-Smurf1 transgenic mice have decreased bone formation rates and decreased Runx2 protein expression in osteoblasts (18). Smurf1 knock-out

* This work was supported by National Institutes of Health Grants AR48697 (to L. X.), AR43510 (to B. F. B), and AR051189 (to D. C.). The costs of publication of this article were defrayed in part by the payment of page charges. This article must therefore be hereby marked "*advertisement*" in accordance with 18 U.S.C. Section 1734 solely to indicate this fact.

[1] To whom correspondence should be addressed: Dept. of Pathology and Laboratory Medicine, University of Rochester, 601 Elmwood Ave., Box 626, Rochester, NY 14642. Tel.: 585-273-4090; Fax: 585-756-4468; E-mail: Lianping_xing@urmc.rochester.edu.

[2] The abbreviations used are: TNF, tumor necrosis factor; ALP, alkaline phosphatase; BMP, bone morphogenetic protein; CMV, cytomegalovirus; E3, ubiquitin-protein isopeptide ligase; IL-1, interleukin-1; Luc, luciferase; MTT, 3-(4,5-dimethylthiazol-2-yl)-2,5-diphenyltetrazolium bromide; OC, osteocalcin; PBS, phosphate-buffered saline; RANKL, receptor activator NF-κB ligand; RT, reverse transcription; siRNA, small interfering RNA; Smurf, Smad ubiquitin regulatory factor; Tg, transgenic; TGF-β, transforming growth factor-β; TRAF, TNF receptor-associated factor; wt, wild type.

TABLE 1
Sequences of primers used in the real time PCR

Genes	GenBank™ accession number	Sequences of primers[a]	Target sites on genes	Product sizes
				bp
Smurf1	NM029438	F: 5′-AGTTCGTGGCCAAATAGTGG-3′ R: 5′-GTTCCTTCGTTCTCCAGCAG-3′	687–785	99
Smurf2	NM 025481	F: 5′-GTGAAGAGCTCGGTCCTTTG-3′ R: 5′-AGAGCCGGGGATCTGTAAAT-3′	1041–1154	114
ALP	AF285233	F: 5′-CGGGACTGGTACTCGGATAA-3′ R: 5′-ATTCCACGTCGGTTCTGTTC-3′	550–706	157
OC	AH004426	F: 5′-CTTGGTGCACACCTAGCAGA-3′ R: 5′-CTCCCTCATGTGTTGTCCCT-3′	638–824	186
β-actin	NM 001101	F: 5′-AGATGTGGATCAGCAAGCAG-3′ R: 5′-GCGCAAGTTAGGTTTTGTCA-3′	1134–1251	118

[a] F, forward primer; R, reverse primer.

(Smurf1−/−) mice were generated recently. Although they survive to adulthood, they exhibit an age-dependent increase in bone mass (23). Interestingly, osteoblasts from Smurf1−/− mice have normal levels of the BMP receptors, Smad1, 2, 3, and 5, and Runx2, all of which have been defined previously as targets of Smurf1. Because Smurf1 and Smurf2 possess overlapping functions, it is possible that Smurf2 compensates for the loss of Smurf1 in these knock-out animals (19, 20, 24). Currently, the role of Smurf2 in osteoblast function *in vivo* and the role of Smurf E3 ligases in the pathogenesis of bone diseases remain poorly understood. Additionally, there is little information on the regulation of Smurfs expression under physiological and pathological conditions.

To explore the molecular mechanisms of TNF-mediated osteoblast inhibition, we tested the hypothesis that TNF inhibits osteoblastic bone formation by up-regulating Smurf E3 ligases that degrade Runx2 protein. We found that TNF increased Smurf1 and Smurf2 expression in osteoblasts, leading to enhanced ubiquitination and degradation of Runx2 protein. This TNF-induced Runx2 degradation was reversed by proteasome inhibitors and by knocking down endogenous Smurf1 or Smurf2 using small interfering RNA (siRNA) against Smurf1 or Smurf2. Bones from TNF-overexpressing mice exhibited increased Smurf1 and decreased Runx2 protein levels. Taken together, our findings point to a novel molecular mechanism of TNF inhibition of osteoblasts, which involves post-transcriptional regulation of protein function through Smurf E3 ligase-mediated proteasomal degradation.

MATERIALS AND METHODS

Animals—TNF transgenic (Tg) mice in a CBA × C57BL/6 background (3647 TNF-Tg line) were obtained from Dr. G. Kollias. C57BL/6 mice were purchased from Jackson Laboratories (Bar Harbor, ME). The Institutional Animal Care and Use Committee approved all animal studies.

Antibodies—Monoclonal antibodies specific for FLAG and β-actin were purchased from Sigma. Anti-Runx2 monoclonal antibody was from MBL (Woburn, MA). Anti-ubiquitin monoclonal antibody was from Santa Cruz (Santa Cruz, CA). Anti-Smurf1 polyclonal antibody was from Abgent (San Diego, CA).

Cell Culture and Transfection Conditions—C2C12 myoblast/osteoblast precursors were cultured in Dulbecco's modified Eagle's medium, and 2T3 osteoblast precursors were cultured in α-minimal essential medium supplemented with 1% penicillin-streptomycin (all from Invitrogen) and 10% fetal calf serum (JRH Biosciences, Lenexa, KS). When cells were grown to 90% confluence, the cDNA expression plasmid, pCMV-FLAG-tagged Runx2 (F-Runx2) and/or a pCMV-Myc-tagged Smurf1 (M-Smurf1) were transiently transfected into the cells using Lipofectamine 2000 transfection reagent (Invitrogen) according to the manufacturer's instructions. Total amounts of transfected plasmids in each group were equalized by the addition of empty vector. After transfection (24 h), the cells were cultured further in the presence and absence of murine TNF (R&D Systems) and subjected to reverse transcription (RT)-PCR or Western blot analysis.

Bone Nodule Formation—Bone marrow cells were flushed from the tibiae and femur of wild type (wt) and TNF-Tg mice, and the cells were seeded at a density of 2×10^6/ml. The cells were cultured in 37 °C with a humidified 5% CO_2 atmosphere. When the cells reached confluence (day 0), the medium was changed to an osteoblast-inducing medium (α-minimal essential medium-supplemented 10% fetal calf serum with 100 μg/ml L-ascorbic acid and 5 mM β-glycerophosphate) with or without 40 ng/ml BMP-2, and the medium was changed twice a week. After an 18-day incubation, the cells were fixed with 10% formalin and stained by the von-Kossa method. The area of mineralized bone nodules was determined under light microscopy by point counting, as described previously (25).

Quantitative Real Time RT-PCR—Cells were homogenized using 1 ml of TRIzol reagent (Invitrogen), and total RNA was extracted according to the manufacturer's protocol. cDNA was synthesized using 20 μl of reverse transcription reaction solution containing 1 μg of total RNA, 10 mM Tris-HCl buffer (pH 8.3), 50 mM KCl, 5 mM $MgCl_2$, 1 mM deoxynucleoside triphosphates, 2.5 μM random hexamers, 20 units RNase inhibitor, and 50 units of Moloney murine leukemia virus reverse transcriptase (all from Roche Applied Science). Quantitative real time PCR amplifications were performed in an iCycler real time PCR machine using iQ SYBR Green supermix (both from Bio-Rad Laboratories) according to the manufacturer's instruction. The sequences of primer sets for *Smurf1*, *Smurf2*, alkaline phosphatase (*ALP*), osteocalcin (*OC*), and *β-actin* mRNAs, target sites on mRNAs and product sizes by PCR are shown in Table 1. To minimize the background of products amplified from genomic DNAs, these primers were designed to exist on two different exons. The quantity of *Smurf1*, *Smurf2*, *ALP*, and *OC* mRNA in each sample was normalized using the C_T (threshold cycle) value obtained for the *β-actin* mRNA amplifications.

Western Blot Analysis—Cells were washed with cold phosphate-buffered saline (PBS), and whole cell lysates were prepared by the addition of M-PER mammalian protein extraction reagent (Pierce) containing a protease inhibitor mixture (Roche Applied Science). Twenty μg of protein was loaded per lane and separated on a 10% polyacrylamide gel, followed by transfer to a nitrocellulose membrane (Bio-Rad) by electroblotting. Membrane was blocked for nonspecific binding in 3% nonfat dry milk and followed by incubation with an antibody at 4 °C. After membrane was washed, the blots were probed with a horseradish peroxidase-conjugated secondary antibody (Bio-Rad) and visualized by an enhanced chemiluminescence system (Amersham Biosciences) according to the manufacturer's instructions.

TABLE 2
Sequences of siRNA used in the infection

Target genes[a]	Sequences of siRNA[b]	Target sites on mRNA
Smurf1 (NM 029438)	5′-GATTCGAACCTTGCAAAGAAAGAC ttcaagagaGTCTTTCTTTGCAAGGTTCTTTTTTC-3′	372–390
Smurf2 (NM 025481)	5′-GATTCGACCAACAGCAACAGCAAG ttcaagagaCTTGCTGTTGCTGTTGGTCTTTTTTC-3′	1199–1217

[a] Parentheses indicate GenBank™ accession numbers.
[b] siRNAs are designated to encode two complementary sequences of 19 nucleotides homologous to a segment of Smurf1 or Smurf2 mRNA (underlined) separated by a nine-nucleotide space (small characters), and have a terminator signal (TTTTTTC) at a 3′ terminus.

Ubiquitination of Runx2—2T3 cells were incubated in medium containing 7.5 ng/ml TNF for 72 h in the presence of PBS or 0.1 mM MG132 (Calbiochem) for the last 12 h of TNF treatment. For the immunoprecipitation, cell lysate was incubated with anti-Runx2 antibody overnight at 4 °C followed by the addition of protein G-agarose (Roche Applied Science) overnight at 4 °C. The immunoprecipitates were washed with 50 mM Tris-HCl buffer (pH 8.0), containing 150 mM NaCl, 1% Nonidet P-40, 0.05% deoxycholate, and 0.1% SDS, resuspended in 1 × reducing sample buffer, and subjected to Western blot analysis with an anti-ubiquitin antibody. The same membrane was stripped and reprobed for Runx2.

siRNA and Virus Infection—Platinum-E cells were transfected with a retrovirus vector (pRetro-H1G) that encodes Smurf1 or Smurf2 siRNA, or an empty vector using FuGENE 6 reagent (Roche Applied Science). The sequences of Smurf1 and Smurf2 siRNAs are shown in Table 2. After 2 days, viral supernatants were harvested and filtered using a 0.45-μm membrane filter. 2T3 cells were infected with virus supernatant in the presence of Polybrene. After 4 h, 2 ml of α-minimal essential medium was added to the cells to dilute Polybrene. The cells were cultured for an additional 48 h in α-minimal essential medium containing 10% fetal bovine serum. The cells were then used for RNA extraction or Western blot analysis.

Luciferase Assay—2T3 cells were transfected with the BMP, 12×SBE-OC-Luc (17) or the TGF-β, p3TP-Lux (18), signaling reporter construct using Lipofectamine 2000 transfection reagent. After 6 h, cells were treated with 10 ng/ml TNF for 48 h, followed by a 24-h incubation in the presence or absence of 50 ng/ml BMP-2 or 2 ng/ml TGF-β (both from R&D Systems). For determination of the effect of TNF on Runx2 expression, 2T3 cells were cotransfected with a Runx2 expression vector, F-Runx2, and the Runx2 reporter construct, 6×OSE2-OC-pGL3 (17) followed by a 48-h TNF treatment. Cell lysates were extracted, and luciferase activity was measured using a Dual Luciferase Reporter Assay System (Promega) and normalized by *Renilla* luciferase activity.

Caspase-3 Assay—2T3 cells were treated with TNF (2.5, 5, and 7.5 ng/ml) for 24, 48, and 72 h and then lysed in a buffer containing 1% Nonidet P-40, 200 mM NaCl, 20 mM Tris-HCl (pH 7.4), 10 μg/ml leupeptin, and aprotinin (0.27 mM trypsin inhibitor/ml). Caspase-3 activity was determined by incubation of cell lysate (containing 25 μg of total protein) with 50 μM fluorogenic substrate, *N*-acetyl-Asp-Glu-Val-Asp-7-amino-4-methylcoumarin (Calbiochem) in 200 μl of 10 mM HEPES (pH 7.4), containing 220 mM mannitol, 68 mM sucrose, 2 mM NaCl, 2.5 mM KH_2PO_4, 0.5 mM EGTA, 2 mM $MgCl_2$, 5 mM pyruvate, 0.1 mM phenylmethylsulfonyl fluoride, and 1 mM dithiothreitol. The release of fluorescent 7-amino-4-methylcoumarin was measured by spectrofluorometry (excitation/emission, 499/521 nm).

MTT Cell Viability Assay—Cell viability was determined by the 3-(4,5-dimethylthiazol-2-yl)-2,5-diphenyltetrazolium bromide (MTT, Sigma) dye reduction assay according to the method of Green *et al.* (26). Briefly, after cells in 96-well plates were treated with various concentrations of TNF for 24, 48, or 96 h, 10 μl of MTT was added for 3 h, and the absorbance was read at 540 nm. Cell viability was calculated as the ratio of optical densities in wells with and without TNF.

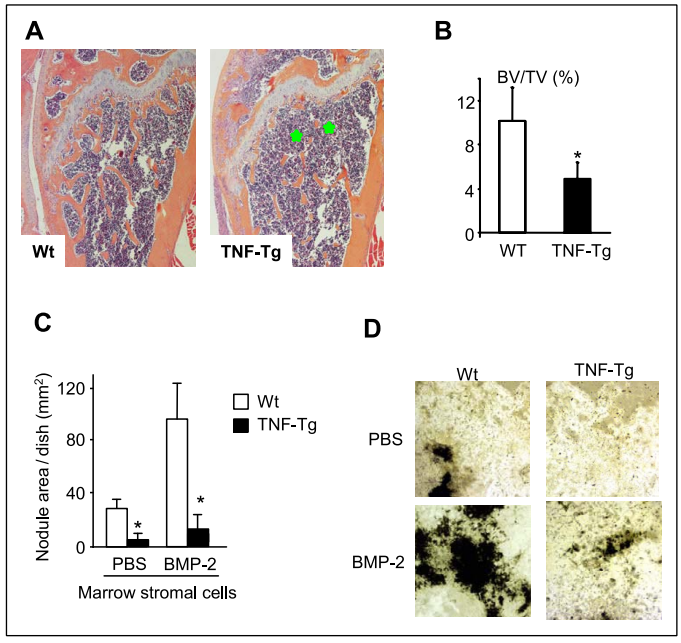

FIGURE 1. **Decreased bone volume and osteoblast functions in TNF-Tg mice.** *A*, femur from a 4-month-old TNF-Tg mouse and a wt littermate were fixed and processed. Paraffin-embedded sections were stained with hematoxylin and eosin. Lower bone volume in the metaphysis of the femur (*green stars*) is present in the TNF-Tg mouse (magnification, ×4). *B*, the distal femoral trabecular bone volume was measured as described previously (38). The values are the mean ± S.E. of eight or nine mice. *, $p < 0.05$ *versus* wt mice. *C*, bone marrow stromal cells were isolated from 4-month-old TNF-Tg mice and wt littermates and cultured in osteoblast differentiation medium containing 100 μg/ml L-ascorbic acid and 5 mM β-glycerophosphate in the presence or absence of 40 ng/ml BMP-2 for 2 weeks. The cells were fixed, and mineralized bone nodules were identified by von-Kossa staining. The area of bone nodules was measured under light microscopy using point counting. The values are the mean ± S.E. of three wells. *, $p < 0.05$ *versus* wt cells. The same results were obtained from three pairs of TNF-Tg mice and wt littermates. *D*, mineralized bone nodules from one representative pair of TNF-Tg mice and wt littermates (magnification, ×2).

Statistics Analysis—All data are represented as the mean ± S.E. Comparisons of results were performed by paired Student's *t* tests, accepting $p < 0.05$ as the criterion of significance. All experiments were repeated at least twice with similar results.

RESULTS

TNF-Tg Mice Have Reduced Osteoblast Function—The TNF transgenic mouse is a well established animal model of rheumatoid arthritis, which exhibits polyarthritis because of chronic exposure to low levels of TNF (27). At 3–4 months of age, TNF-Tg mice develop a moderate to severe form of rheumatoid arthritis-like joint inflammation and destruction. This is characterized by chronic inflammation, local bone and cartilage erosion, and increased circulating TNF levels (27, 28). Apart from these well described features, animals develop general osteoporosis as show in Fig. 1*A*. Trabecular bone is markedly reduced in

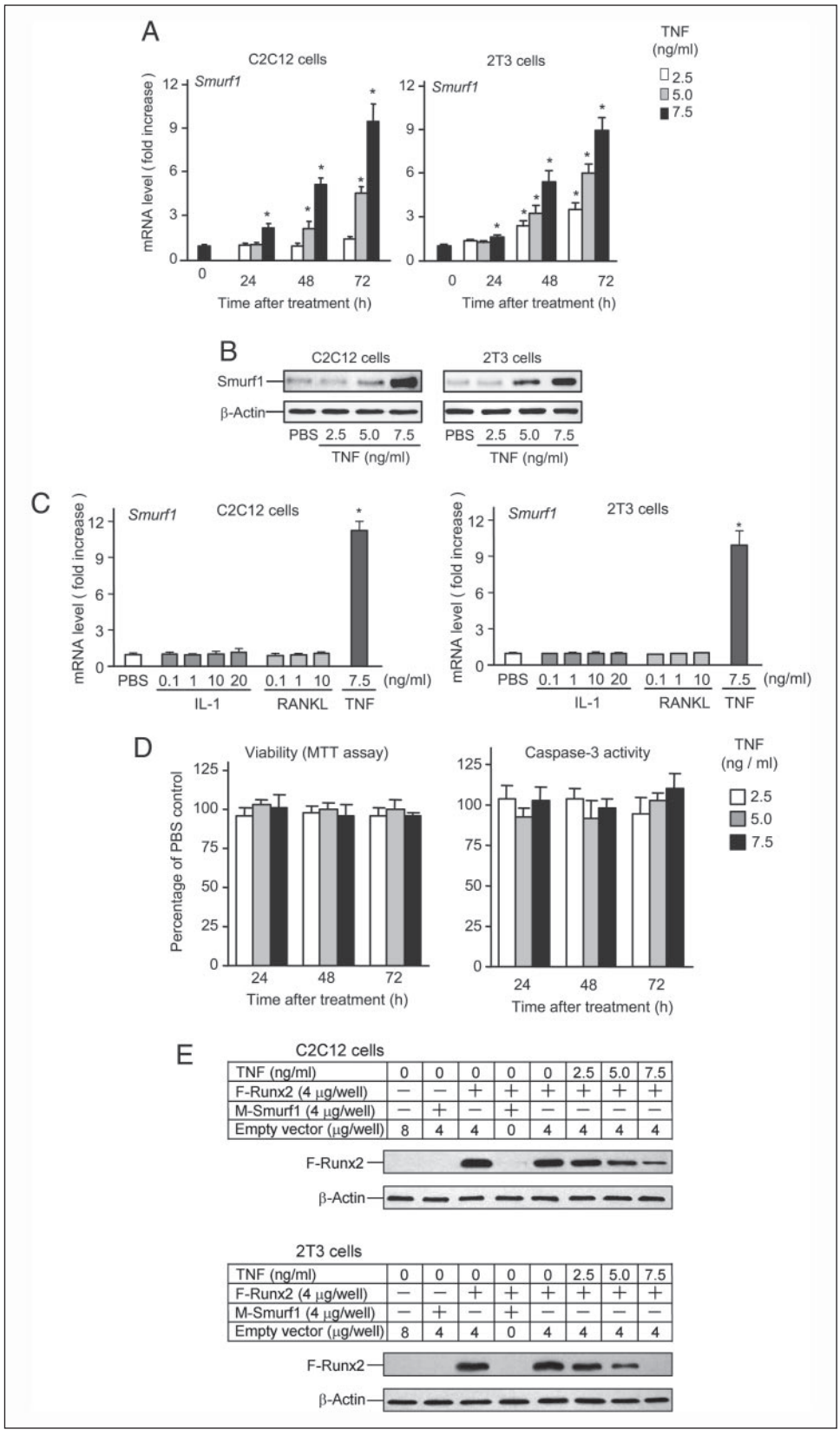

FIGURE 2. **TNF increases Smurf1 expression and induces Runx2 degradation.** *A*, C2C12 or 2T3 cells were treated with PBS or TNF (2.5–7.5 ng/ml) for 24, 48, and 72 h. *Smurf1* and *β-actin* mRNA levels were measured by real time RT-PCR. The relative expression level of *Smurf1* was normalized to *β-actin* in the same sample. The -fold increase was calculated as follows: (relative Smurf1 level in TNF-treated sample)/(relative Smurf1 level in PBS-treated sample). The values are the mean ± S.E. of three dishes. *, $p < 0.05$ *versus* the PBS-treated group. *B*, cells were treated with 2.5–7.5 ng/ml TNF for 72 h. Smurf1 and *β*-actin protein levels were examined by Western blot analysis. *C*, cells were treated with various doses of IL-1 and RANKL and with 7.5 ng/ml TNF for 72 h. The relative expression levels of *Smurf1* mRNA were determined by real time RT-PCR, as described in *A*. The values are the mean ± S.E. of three dishes. *, $p < 0.05$ *versus* the PBS-treated group. *D*, cells were treated with 2.5–7.5 ng/ml TNF for 24, 48, and 72 h. Cell lysates were used for measuring caspase-3 activity or MTT assay. The values are the mean ± S.E. of three dishes. *, $p < 0.05$ *versus* the PBS-treated group. *E*, cells were transfected with M-Smurf1 and/or F-Runx2 expression plasmids or empty vector for 24 h and cultured for 72 h in the presence of PBS or TNF (2.5–7.5 ng/ml). F-Runx2 expression was detected by Western blot using anti-FLAG antibody.

the metaphysis of long bones of TNF-Tg mice, compared with wt littermates (Fig. 1*B*). To examine whether osteoblast function is altered in TNF-Tg mice, bone marrow stromal cells were isolated from 4-month-old TNF-Tg mice and wt littermates. Cells were cultured in osteoblast differentiation medium to form mineralized bone nodules. Compared with wt mice, cells from TNF-Tg mice formed significantly fewer and smaller nodules under basal conditions and in the presence of BMP-2 (Fig. 1, *C* and *D*), indicating reduced osteoblast function.

TNF Increases Smurf1 Expression, Runx2 Degradation, and Ubiquitination of Runx2 Protein—Smurf1 is a negative regulator of the BMP signaling pathway and inhibits osteoblast function by promoting Runx2 degradation (17). To determine whether TNF affects Smurf1 expression, C2C12 myoblast/osteoblast precursor cells, 2T3 osteoblast precursors, and primary wt calvarial preosteoblasts were treated with PBS or 2.5–7.5 ng/ml TNF. Smurf1 expression was measured by real time RT-PCR at 24, 48, and 72 h. The highest dose of TNF (7.5 ng/ml) significantly increased *Smurf1* mRNA levels at 24 h in both cell lines, with the highest indication being observed at 72 h. At this time, the lowest dose of TNF (2.5 ng/ml) also had increased *Smurf1* mRNA expression (Fig. 2*A*). TNF-induced Smurf1 expression was similar in 2T3 and C2C12 cells. No significant increase in Smurf1 level was observed when the cells were treated with 7.5 ng/ml TNF for 2, 4, 8, and 12 h (data not shown). Consistent with these mRNA results, TNF increased Smurf1 protein expression in a dose-dependent manner after 24 h (Fig. 2*B*). Similarly, TNF also increased Smurf1 expression in primary preosteoblasts. TNF increased *Smurf1* mRNA levels in these cells by 4–5-fold over the PBS-treated cells at 48 h (the ratio of *Smurf1/β-actin* in TNF-treated group *versus* that from PBS group: 4.7 ± 0.14, $p < 0.002$). To determine the specificity of TNF for Smurf1, C2C12 and 2T3 cells were treated with IL-1 or receptor activator NF-κB ligand (RANKL) that activate intracellular signaling pathways similar to those activated by TNF. They did not alter *Smurf1* mRNA abundance (Fig. 2*C*). These doses of IL-1 and RANKL (10 ng/ml) stimulate osteoclast formation from osteoclast precursors (data not shown).

To examine whether TNF-induced apoptosis is associated with increased Smurf1 expression, 2T3 cells were treated with various doses of TNF for 24, 48, and 72 h. Apoptosis was determined by measuring caspase-3 activity and cell viability by MTT assay. *Smurf1* mRNA expression was examined by real time PCR in the same samples. At the doses (2.5–7.5 ng/ml) that TNF increased *Smurf1* expression (data not shown), osteoblasts were morphological normal with normal caspase-3 activity (Fig. 2*D*). In contrast, cells treated with 10 and 20 ng/ml TNF induced cell apoptosis, and dead cells were detached from the culture plates (data not shown).

To determine whether TNF induces Runx2 degradation, C2C12 or 2T3 cells were cotransfected with FLAG-tagged-Runx2 (F-Runx2) and/or Myc-tagged-Smurf1 (M-Smurf1) expression vectors or an empty vector in the presence of TNF. F-Runx2 expression was detected by Western blot analysis using an anti-FLAG antibody. As a positive control, Smurf1 overexpression decreased F-Runx2 protein levels. Similar to Smurf1 overexpression, TNF significantly reduced F-Runx2 protein levels in a dose-dependent manner (Fig. 2*E*).

Smurf1 induces Runx2 degradation by increasing its ubiquitination (17). If TNF-induced Runx2 degradation is mediated by Smurf1, we should be able to detect increased ubiquitinated-Runx2 complexes in TNF-treated cells. To test this hypothesis, 2T3 cells were treated with TNF in the presence and absence of the proteasomal inhibitor MG132, and endogenous Runx2 protein was immunoprecipitated with an anti-Runx2 antibody and followed by Western blot analysis using an anti-ubiquitin antibody. MG132 treatment revealed small amounts of ubiquitinated Runx2 in vehicle-treated cells. These were greatly increased in the presence of TNF (Fig. 3), indicating that TNF induces ubiquitination of Runx2 protein, leading to its rapid breakdown through proteasomal degradation.

TNF-induced Runx2 Degradation Is Dependent on Smurf1 and Smurf2—To determine whether TNF-induced Runx2 degradation is dependent on Smurf1, 2T3 cells were infected first with retroviral supernatant containing double-stranded siRNA specific for Smurf1 to knock down endogenous Smurf1. They were then transfected with F-Runx2 in the presence of TNF. Smurf1 siRNA decreased TNF-induced *Smurf1* mRNA by 95% and reduced *Smurf1* expression in PBS-treated cells to almost undetectable levels (Fig. 4*A*). Without changing the expression of *Smurf2* mRNA (Fig. 4*B*), Smurf1 siRNA partially blocked TNF-mediated inhibition of *ALP* mRNA expression compared with the empty vector control (Fig. 4*C*) and reduced TNF-induced Runx2 degradation by 30% (by a densitometric analysis, Fig. 4*D*). Interestingly, Smurf1 siRNA alone increased *ALP* mRNA levels by 58%, suggesting that Smurf1 may regulate osteoblast function under basal conditions.

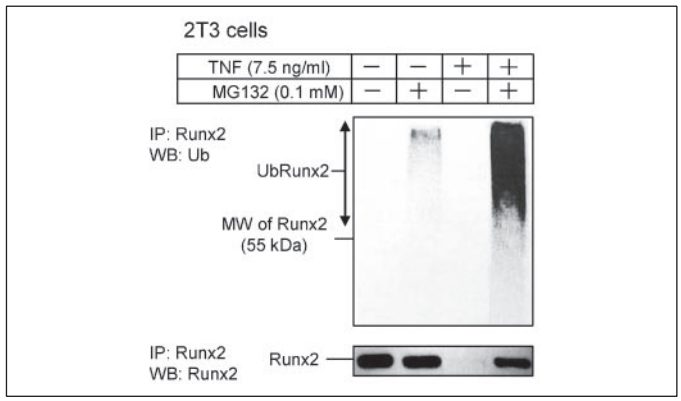

FIGURE 3. **TNF induces ubiquitination of Runx2 protein.** 2T3 cells were treated with 7.5 ng/ml TNF for 72 h in the presence or absence of 0.1 mM MG132 for the last 12 h of TNF treatment, and endogenous Runx2 was immunoprecipitated (*IP*) by anti-Runx2 antibody. Ubiquitinated Runx2 (*Ub-Runx2*) protein ladders were detected by anti-ubiquitin antibody (*upper panel*). After stripping the antibody, total un-ubiquitinated Runx2 protein levels were determined by anti-Runx2 antibody (*lower panel*). *MW*, molecular mass.

Smurf2 is another E3 ubiquitin ligase that affects osteoblast function by interfering with TGF-β signaling (20). To examine whether TNF regulates Smurf2 expression, 2T3 cells were treated with PBS or TNF (7.5 ng/ml) for 72 h, and *Smurf2* mRNA levels were examined by real time RT-PCR. Similar to, but to a lesser extent than *Smurf1*, TNF significantly increased *Smurf2* mRNA by 9.5 ± 0.88-fold ($p < 0.004$ *versus* PBS-treated cells). Because there is no Smurf2 antibody available to detect mouse Smurf2, the effect of TNF on Smurf2 protein levels cannot be assessed currently. To examine whether TNF-induced Runx2 degradation is also mediated by Smurf2, we used Smurf2 siRNA. Similar to Smurf1 siRNA, blocking endogenous Smurf2 led to reduced TNF-mediated inhibition of *ALP* expression and TNF-induced Runx2 degradation (Fig. 4, *C* and *D*) to a similar extent. Combining Smurf1 and Smurf2 siRNAs further prevented TNF-induced Runx2 degradation by 60% (Fig. 4*C*).

TNF Inhibits BMP and TGF-β Signaling through Individual Smurfs, and Its Inhibition on Runx2 Is Mediated by Both Smurf1 and Smurf2—Smurf1 recognizes and directs the ubiquitination and proteosomal degradation of Smad1 and 5 (15), whereas Smurf2 acts on both Smad1 and 2, but not Smad3 (20). Therefore, Smurf1 is thought to target BMP-2 and Smurf2 to target TGF-β signaling (14). Because TNF increases Smurf1 and Smurf2, it should target the BMP-2 and/or TGF-β signaling pathways. To test this, 2T3 cells were transfected with the Runx2, BMP, or TGF-β reporter constructs and a Runx2 expression vector or treated with BMP-2 or TGF-β, in the presence or absence of TNF in a luciferase reporter assay. Smurf1 and/or Smurf2, or control siRNA was used to determine whether blockade of Smurfs affects the effect of TNF. TNF significantly inhibited a Runx2-induced increase in Runx2 reporter by 86% (Fig. 5*A*). Smurf1 siRNA or Smurf2 siRNA alone reduced the inhibitory effect of TNF by 30–40%, and a combination of Smurf1 and

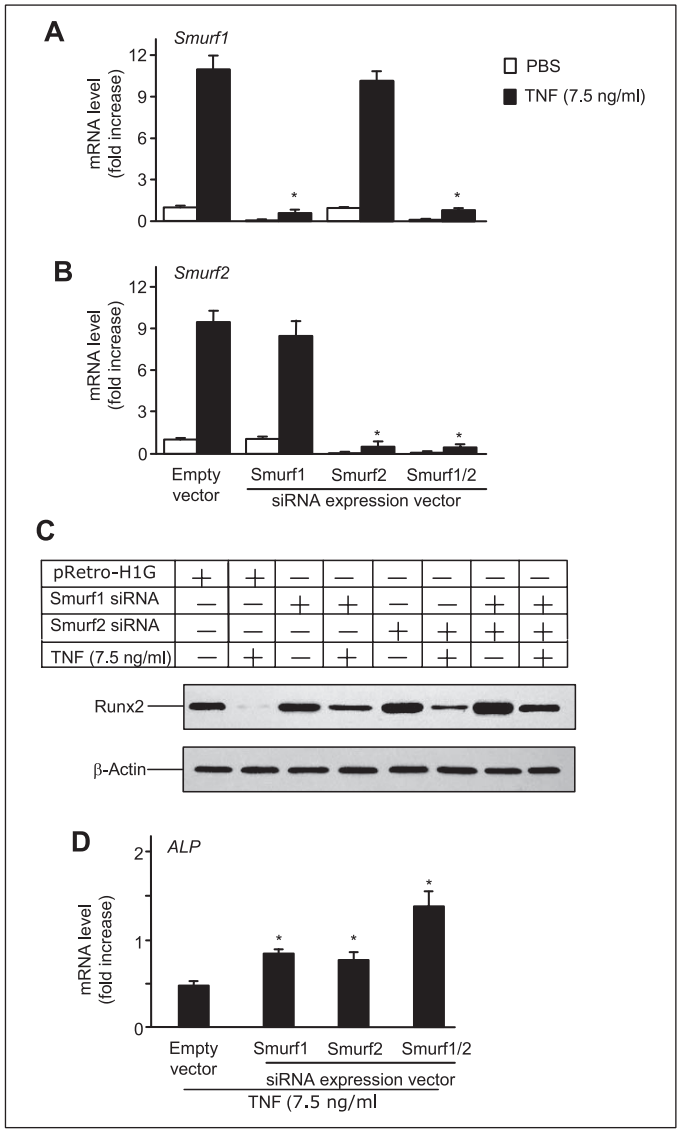

FIGURE 4. **Smurf1 or Smurf2 siRNA blocks TNF-induced Runx2 degradation.** 2T3 cells were infected with retroviral supernatant containing Smurf1 and/or Smurf2 siRNAs or empty vector, then cells were transfected with F-Runx2 expression plasmid (4 μg/dish) and treated with 7.5 ng/ml TNF for 72 h. *Smurf1* (*A*) and *Smurf2* (*B*) mRNA levels were measured by real time RT-PCR. The values are the mean ± S.E. of three dishes. The -fold increase was calculated as described in Fig. 2*A*. *, $p < 0.05$ *versus* the empty vector-infected TNF group. *C*, the expression of F-Runx2 was determined by Western blot analysis using anti-FLAG antibody as described in Fig. 2*E*. *D*, *ALP* mRNA expression was assessed by real time RT-PCR. The values are the mean ± S.E. of three dishes. The -fold increase was calculated as described in Fig. 2*A*. *, $p < 0.05$ *versus* empty vector-infected TNF group.

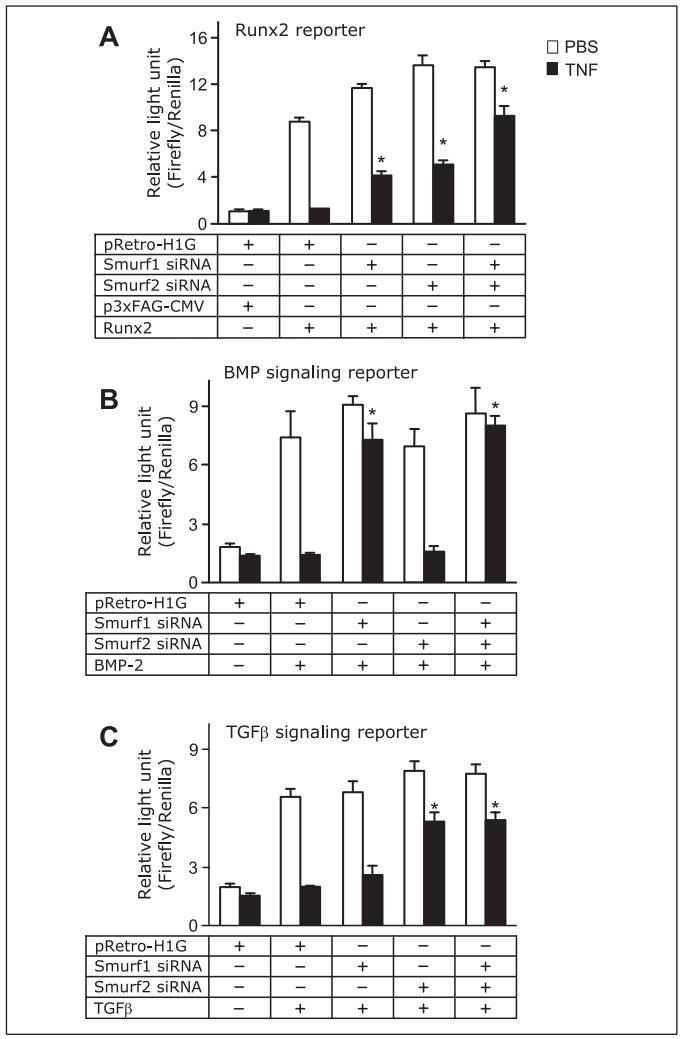

FIGURE 5. **TNF targets both BMP and TGF-β signaling pathways in osteoblasts.** *A*, 2T3 cells were infected with retroviral supernatant containing Smurf1 and/or Smurf2 siRNAs or empty vector, then cells were cotransfected with the Runx2 expression vector (Runx2), the empty expression vector (p3×FAG-CMV), and the Runx2 reporter vector (6×OSE2-OC-Luc) for 8 h and then treated with 7.5 ng/ml TNF for 48 h. *B* and *C*, 2T3 cells were infected with retroviral supernatant containing Smurf1 and/or Smurf2 siRNA or empty vector, then the BMP-2 and TGF-β signaling reporter constructs, 12×SBE-OC-Luc (*B*) or p3TP-Lux (*C*) were transfected into cells for 8 h. The cells were treated with 7.5 ng/ml TNF for 48 h and then stimulated with 50 ng/ml BMP-2 (*B*) or 2 ng/ml TGF-β (*C*) for 24 h in the presence of PBS or 10 ng/ml TNF. The values are the mean × S.E. of three dishes. *, $p < 0.05$ *versus* empty vector-infected TNF group.

Smurf2 siRNA further inhibited TNF action by 60–80%, indicating an additive effect (Fig. 5*A*). In contrast to the partial reduction of the effect of TNF on Runx2 reporter, Smurf1 siRNA alone reduced TNF-mediated inhibition of the BMP-2 signaling reporter by 90%, whereas Smurf2 siRNA had no effect (Fig. 5*B*). Smurf2 siRNA blocked TNF-mediated TGF-β signaling reporter inhibition by 60%, and Smurf1 siRNA had no effect (Fig. 5*C*). A combination of Smurf1 and Smurf2 siRNA had no additive effect on TNF inhibition on the BMP-2 or TGF-β signaling reporter. Thus, although TNF inhibits Runx2 activation through both Smurf1 and Smurf2, its inhibition in the BMP-2 and TGF-β signaling pathways is through Smurf1 and Smurf2, respectively.

TNF-overexpressing Mice Have Increased Smurf1 and Decreased Runx2 Expression—If Smurfs are responsible for reduced osteoblast function in conditions in which TNF is overexpressed, we should be able to detect elevated Smurf levels in TNF-Tg mice or mice receiving TNF treatment. To examine this, total RNA was extracted from the metaphysis of 4-month-old TNF-Tg mice and wt littermates, and the expression of *Smurf1*, *Smurf2*, *ALP*, and *OC* mRNA was examined by real time RT-PCR. Compared with that of wt mice, the expression of *Smurf1* was significantly increased, and *ALP* and *OC* expression was decreased in TNF-Tg mice (Fig. 6*A*). No change of *Smurf2* mRNA expression was observed (data not shown). Western blot analysis revealed that Smurf1 protein was increased, and Runx2 protein was decreased (Fig. 6*A*). To determine the acute effect of TNF on Smurf and osteoblast marker gene expression, wt mice were injected with TNF (0.25 μg/injection, three times/day × 3 days) or PBS over the calvarial bones. The expression of *Smurf1*, *Smurf2*, *ALP*, and *OC* mRNA was assessed. Similar to the results obtained from TNF-Tg mice, the expression of Smurf1 was increased at both mRNA and protein levels. Runx2 protein and *ALP* and *OC* mRNA levels were decreased in TNF-treated wt mice (Fig. 6*B*). These results suggest that TNF may inhibit osteoblast function *in vivo*

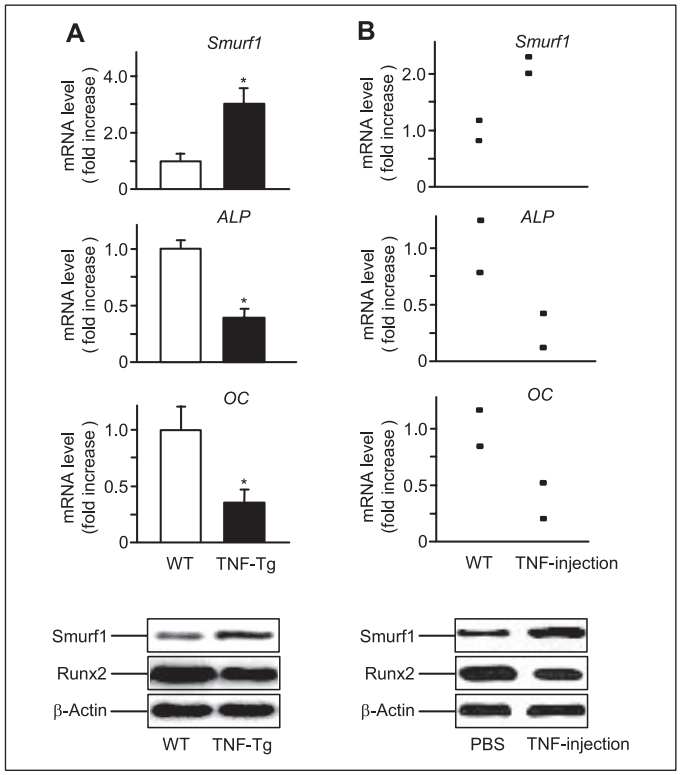

FIGURE 6. **TNF increases Smurf1 expression *in vivo*.** *A*, RNA and protein were extracted directly from the metaphyseal region of 4-month-old TNF-Tg mice and wt littermates. The relative expression levels of *Smurf1*, *ALP*, and *OC* were measured by real time RT-PCR (*upper panels*), as described in Fig. 2. The values are the mean ± S.E. of four pairs of TNF-Tg and wt mice. *, $p < 0.05$ *versus* wt mice. Smurf1 and β-actin protein levels were determined by Western blot analysis (*lower panels*). The data are representative of three pairs of TNF-Tg or wt mice. *B*, TNF (0.25 μg/injection, three times/day × 3 days, $n = 2$) or PBS was injected over the calvarial bones of wt mice. RNA and protein were extracted directly from calvarial bones. Expression levels of *Smurf1*, *ALP*, and *OC* mRNA and Smurf1 and β-actin protein were examined as described in *A*. The data show the values of individual mice.

by promoting Runx2 degradation through up-regulation of Smurf E3 ligases.

DISCUSSION

TNF is a central proinflammatory cytokine that contributes to local and systemic bone loss in inflammatory bone diseases, such as rheumatoid arthritis. Under these conditions, osteoblast-mediated bone formation cannot compensate for accelerated osteoclastic bone resorption, suggesting a direct inhibitory effect of TNF on osteoblasts. Here we provide evidence for the regulation of osteoblast-specific transcription factor Runx2 stability by TNF through the E3 ligases, Smurf1 and Smurf2. Although overexpression of Smurfs has been known to promote Runx2 degradation *in vitro*, our findings provide the first report that TNF inhibits osteoblast function by controlling the ubiquitination status of Runx2 protein through Smurfs. We have several lines of evidence implicating Smurfs in the regulation of TNF-induced Runx2 ubiquitination and degradation: (i) TNF promoted ubiquitination and degradation of transfected and endogenous Runx2; (ii) it increased the expression levels of Smurf1 and Smurf2; (iii) TNF-induced ubiquitination and degradation of Runx2 were attenuated in cells overexpressing Smurf1 and Smurf2 siRNA; (iv) expression of Smurf1 and Smurf2 siRNA rescued the inhibitory effect of TNF on Runx2 reporter; (v) bones of mice that have elevated TNF levels have increased Smurf1 and decreased Runx2 protein expression. In 2002, Gilbert *et al.* (10) reported that TNF reduced nuclear Runx2 protein in osteoblasts by 90%, but it inhibited Runx2 transcription only by 40–50%. They proposed that there may be other mechanism(s) accounting for the 90% reduction in Runx2 protein. Here, we found that overexpression of Smurf1 and Smurf2 siRNA can reverse TNF-induced down-regulation of Runx2 protein by 50–60% (Fig. 4*D*). We suspect that there may also be transcriptional inhibition of Runx2 to complement this TNF-induced reduction in protein expression. Thus, our data complement Gilbert's results and demonstrate that TNF regulates Runx2 by two distinct mechanisms: it inhibits Runx2 gene transcription and promotes Runx2 protein degradation through Smurf E3 ligases.

TNF has been implicated in mediating protein degradation through several E3 ligases in other cell types. For example, TNF induces TNF receptor-associated factor (TRAF)2 degradation in HeLa cells and mouse embryonic fibroblasts through a RING-type ubiquitin ligase, Siah2 (29). It stimulates expression of the gene for a F-box E3 ligase, atrogin1/MAFbx (30), which is involved in muscle atrophy (31) and sepsis (32). Interestingly, TNF-induced TRAF2 degradation or up-regulation of atrogin1/MAFbx occurs within 4 h, and this is within the same time frame that treatment of bone marrow cells with RANKL and interferon-γ resulted in degradation of TRAF6 (33). In contrast, TNF-induced Smurf up-regulation and Runx2 degradation take 24–72 h (Fig. 2), suggesting an indirect effect. We have attempted to dissect the possible requirements of transcription or translation for TNF-increased Smurf expression using pharmacological blockers. Unfortunately, blocking of transcription or translation by cycloheximide or actinomycin D in the presence of TNF causes massive apoptosis of cells, and thus we could not determine whether newly synthesized proteins are required for TNF-induced Smurf expression. Nevertheless, given that TNF induces various E3 ligases at different times, it is possible that TNF uses different types of E3 ligases to regulate the stability of specific targeting proteins in response to various stimuli. For example, TNF stimulates Siah2 and atrogin1/MAFbx E3 ligases in response to early signaling events during acute stress conditions and increases Smurf expression to regulate protein degradation in chronic conditions, such as rheumatoid arthritis and cancer (34).

TNF binds to TNF receptors and transduces the signals through TRAFs and various kinases to activate transcription factors, such as NF-κB and AP-1 family members. Activation of the IL-1 receptor via IL-1 or RANK through RANKL results in the activation of similar signaling pathways. Our finding that IL-1 and RANKL do not affect Smurf1 expression is interesting. There are several possible explanations: (i) osteoblasts do not express RANK, the receptor for RANKL, and thus they cannot respond to RANKL treatment. Whether osteoblasts express functional RANK is an issue of debate. It has been reported that glutathione *S*-transferase-RANKL stimulates osteoblast bone forming activity *in vitro* and *in vivo* (35). However, others argued that RANKL has no effect on osteoblasts because they do not express RANK. We have been unable to detect any effect of RANKL on osteoblast function in various assays,[3] suggesting that RANKL may not play an important role in this cell type. (ii) IL-1 may affect Smurfs in experimental conditions that differ from ours, given the fact that in some reports IL-1 has an inhibitory effect on osteoblast function. (iii) TNF may use a unique mechanism to regulate Smurf expression. Thus, characterization of the Smurf1 and Smurf2 promoters should have a great impact on our understanding of how Smurfs are regulated by TNF.

Unlike other cytokines, TNF is a strong apoptosis inducer (36, 37), and thus increased Smurf expression could be associated with TNF-

[3] H. Kaneki, R. Guo, D. Chen, Z. Yao, E. M. Schwarz, Y. E. Zhang, B. F. Boyce, and L. Xing, unpublished findings.

induced cell death. Because Smurf1-overexpressing 2T3 cells and osteoblasts in Col1a1-Smurf1 transgenic mice have rates of cell survival comparable with those of empty vector-overexpressing or wt cells (17, 18), elevated Smurf1 appears not to result in osteoblast apoptosis. Our finding that at the doses that TNF induced Smurf 1 expression, osteoblasts are normal suggests that increased Smurf1 is not associated with cell apoptosis (Fig. 2).

It is of interest to note that even though only increased Smurf1 expression was detected in bones of TNF transgenic mice or TNF-injected wt mice (Fig. 6), TNF increased both Smurf1 and Smurf2 expression *in vitro* (Figs. 2 and 4). One explanation is that Smurf1 and Smurf2 may have different response thresholds to TNF *in vivo*. Supporting this, our preliminary results showed that in joints of TNF-Tg mice where TNF levels were extremely high (40-fold over wt mice), both Smurf1 and Smurf2 levels were increased although the increase in Smurf2 was half of that of Smurf1. This is important because cells from Smurf1-null mice exhibit normal levels of Runx2 and BMP-Smads, which is explained by elevated Smurf2 expression in the absence of Smurf1 (23). By increasing both Smurf1 and Smurf2 in osteoblasts, TNF can overcome this compensatory effect between Smurf1 and Smurf2 to induce Runx2 degradation *in vivo* (Fig. 6). However, the real significance of Smurf1-mediated protein degradation in TNF-induced osteoblast inhibition needs to wait for *in vivo* data from TNF-Tg/Smurf1 knockout hybrid mice.

It is unlikely that increasing protein breakdown is the only mechanism by which TNF executes its effect in bone cells. We have found that TNF increased Smurf1 expression in several types of osteoblast precursors, including MC3T3E1 (data not shown), 2T3, and primary calvarial cells. Interestingly, TNF also increases Smurf1 expression in C2C12 cells (Fig. 2). Because untreated C2C12 cells have multiple potency to differentiate to other cell types, we do not know whether TNF-induced Smurf1/2 expression represents a generalized feature of connective tissue cell signaling response to TNF. However, TNF had no effect on Smurf1 expression in osteoclast precursors derived from bone marrow, spleen, and peripheral blood, or in ST2 murine stromal cells under the same experimental conditions (data not shown). Thus, TNF-induced Smurf expression does not appear as a common phenomenon for all cell types. Whether Smurfs have different target proteins in different cells needs to be investigated further.

In summary, our findings reveal a novel mechanism for TNF-induced osteoblast inhibition: through unregulation of Smurf1 and Smurf2 E3 ligases to promote the degradation of Runx2 protein. Better delineation of the role of TNF and perhaps other inflammatory cytokines in proteasomal regulation of protein function by Smurf E3 ligase in osteoblasts will enhance our understanding of the molecular mechanisms responsible for local or general bone loss in inflammatory bone diseases.

Acknowledgments—We thank Bianai Fan for technical assistance with the histological analysis.

REFERENCES

1. Goldring, S. R., and Gravallese, E. M. (2000) *Curr. Opin. Rheumatol.* **12,** 195–199
2. Srivastava, S., Weitzmann, M. N., Cenci, S., Ross, F. P., Adler, S., and Pacifici, R. (1999) *J. Clin. Invest.* **104,** 503–513
3. Nair, S. P., Williams, R. J., and Henderson, B. (2000) *Rheumatology* **39,** 821–834
4. Canalis, E. (1987) *Endocrinology* **121,** 1596–1604
5. Li, Y. P., and Stashenko, P. (1992) *J. Immunol.* **148,** 788–794
6. Taichman, R. S., and Hauschka, P. V. (1992) *Inflammation* **16,** 587–601
7. Kitajima, I., Soejima, Y., Takasaki, I., Beppu, H., Tokioka, T., and Maruyama, I. (1996) *Bone* **19,** 263–270
8. Jilka, R. L., Weinstein, R. S., Bellido, T., Parfitt, A. M., and Manolagas, S. C. (1998) *J. Bone Miner. Res.* **13,** 793–802
9. Gilbert, L., He, X., Farmer, P., Boden, S., Kozlowski, M., Rubin, J., and Nanes, M. S. (2000) *Endocrinology* **141,** 3956–3964
10. Gilbert, L., He, X., Farmer, P., Rubin, J., Drissi, H., van Wijnen, A. J., Lian, J. B., Stein, G. S., and Nanes, M. S. (2002) *J. Biol. Chem.* **277,** 2695–2701
11. Abbas, S., Zhang, Y. H., Clohisy, J. C., and Abu-Amer, Y. (2003) *Cytokine* **22,** 33–41
12. Gilbert, L. C., Rubin, J., and Nanes, M. S. (2005) *Am. J. Physiol.* **288,** E1011–E1018
13. Izzi, L., and Attisano, L. (2004) *Oncogene* **23,** 2071–2078
14. Datto, M., and Wang, X. F. (2005) *Cell* **121,** 2–4
15. Zhu, H., Kavsak, P., Abdollah, S., Wrana, J. L., and Thomsen, G. H. (1999) *Nature* **400,** 687–693
16. Ying, S. X., Hussain, Z. J., and Zhang, Y. E. (2003) *J. Biol. Chem.* **278,** 39029–39036
17. Zhao, M., Qiao, M., Oyajobi, B. O., Mundy, G. R., and Chen, D. (2003) *J. Biol. Chem.* **278,** 27939–27944
18. Zhao, M., Qiao, M., Harris, S. E., Oyajobi, B. O., Mundy, G. R., and Chen, D. (2004) *J. Biol. Chem.* **279,** 12854–12859
19. Lin, X., Liang, M., and Feng, X. H. (2000) *J. Biol. Chem.* **275,** 36818–36822
20. Zhang, Y., Chang, C., Gehling, D. J., Hemmati-Brivanlou, A., and Derynck, R. (2001) *Proc. Natl. Acad. Sci. U. S. A.* **98,** 974–979
21. Wang, H. R., Zhang, Y., Ozdamar, B., Ogunjimi, A. A., Alexandrova, E., Thomsen, G. H., and Wrana, J. L. (2003) *Science* **302,** 1775–1779
22. Zhang, Y., Wang, H. R., and Wrana, J. L. (2004) *Cell Cycle* **3,** 391–392
23. Yamashita, M., Ying, S. X., Zhang, G. M., Li, C., Cheng, S. Y., Deng, C. X., and Zhang, Y. E. (2005) *Cell* **121,** 101–113
24. Kavsak, P., Rasmussen, R. K., Causing, C. G., Bonni, S., Zhu, H., Thomsen, G. H., and Wrana, J. L. (2000) *Mol. Cell* **6,** 1365–1375
25. Boyce, B. F., Aufdemorte, T. B., Garrett, I. R., Yates, A. J., and Mundy, G. R. (1989) *Endocrinology* **125,** 1142–1150
26. Green, L. M., Reade, J. L., and Ware, C. F. (1984) *J. Immunol. Methods* **70,** 257–268
27. Keffer, J., Probert, L., Cazlaris, H., Georgopoulos, S., Kaslaris, E., Kioussis, D., and Kollias, G. (1991) *EMBO J.* **10,** 4025–4031
28. Li, P., Schwarz, E. M., O'Keefe, R. J., Ma, L., Looney, R. J., Ritchlin, C. T., Boyce, B. F., and Xing, L. (2004) *Arthritis Rheum.* **50,** 265–276
29. Habelhah, H., Frew, I. J., Laine, A., Janes, P. W., Relaix, F., Sassoon, D., Bowtell, D. D., and Ronai, Z. (2002) *EMBO J.* **21,** 5756–5765
30. Li, Y. P., Chen, Y., John, J., Moylan, J., Jin, B., Mann, D. L., and Reid, M. B. (2005) *FASEB J.* **19,** 362–370
31. Bodine, S. C., Latres, E., Baumhueter, S., Lai, V. K., Nunez, L., Clarke, B. A., Poueymirou, W. T., Panaro, F. J., Na, E., Dharmarajan, K., Pan, Z. Q., Valenzuela, D. M., DeChiara, T. M., Stitt, T. N., Yancopoulos, G. D., and Glass, D. J. (2001) *Science* **294,** 1704–1708
32. Dehoux, M. J. M., van Beneden, R. P., Fernandez-Celemin, L., Lause, P. L., and Thissen, J. M. (2003) *FEBS Lett.* **544,** 214–217
33. Takayanagi, H., Ogasawara, K., Hida, S., Chiba, T., Murata, S., Sato, K., Takaoka, A., Yokochi, T., Oda, H., Tanaka, K., Nakamura, K., and Taniguchi, T. (2000) *Nature* **408,** 600–605
34. Pray, T. R., Parlati, F., Huang, J., Wong, B. R., Payan, D. G., Bennett, M. K., Issakani, S. D., Molineaux, S., and Demo, S. D. (2002) *Drug Resist. Update* **5,** 249–258
35. Lam, J., Ross, F. P., and Teitelbaum, S. L. (2001) *J. Bone Miner. Res.* **16,** (Suppl. 1) S150
36. Tsuboi, M., Kawakami, A., Nakashima, T., Matsuoka, N., Urayama, S., Kawabe, Y., Fujiyama, K., Kiriyama, T., Aoyagi, T., Maeda, K., and Eguchi, K. (1999) *J. Lab. Clin. Med.* **134,** 222–231
37. Kitajima, I., Nakajima, T., Imamura, T., Takasaki, I., Kawahara, K., Okano, T., Tokioka, T., Soejima, Y., Abeyama, K., and Maruyama, I. (1996) *J. Bone Miner. Res.* **11,** 200–210
38. Xing, L., Venegas, A. M., Chen, A., Garrett-Beal, L., Boyce, B. F., Varmus, H. E., and Schwartzberg, P. L. (2001) *Genes Dev.* **15,** 241–253

nature medicine

Dimorphic effects of Notch signaling in bone homeostasis

Feyza Engin[1], Zhenqiang Yao[2,6], Tao Yang[1,6], Guang Zhou[1], Terry Bertin[1], Ming Ming Jiang[1,3], Yuqing Chen[1,3], Lisa Wang[4], Hui Zheng[1], Richard E Sutton[5], Brendan F Boyce[2] & Brendan Lee[1,3]

Notch signaling is a key mechanism in the control of embryogenesis. However, its *in vivo* function during mesenchymal cell differentiation, and, specifically, in bone homeostasis, remains largely unknown. Here, we show that osteoblast-specific gain of Notch function causes severe osteosclerosis owing to increased proliferation of immature osteoblasts. Under these pathological conditions, Notch stimulates early osteoblastic proliferation by upregulating the genes encoding cyclin D, cyclin E and Sp7 (osterix). The intracellular domain of Notch1 also regulates terminal osteoblastic differentiation by directly binding Runx2 and repressing its transactivation function. In contrast, loss of all Notch signaling in osteoblasts, generated by deletion of the genes encoding presenilin-1 and presenilin-2 in bone, is associated with late-onset, age-related osteoporosis, which in turn results from increased osteoblast-dependent osteoclastic activity due to decreased osteoprotegerin mRNA expression in these cells. Together, these findings highlight the potential dimorphic effects of Notch signaling in bone homeostasis and may provide direction for novel therapeutic applications.

Evolutionarily conserved Notch signaling has a crucial role in cell fate determination and various developmental processes, as it translates cell-cell interactions into specific transcriptional programs[1,2]. Temporal and spatial modulation of this pathway can markedly affect proliferation, differentiation and apoptotic events[3]. Moreover, the timing of Notch signaling can lead to diverse effects within the same cell lineage[4,5]. In mammals, activation of up to four Notch receptors by membrane-bound ligands initiates a process leading to presenilin-mediated cleavage and release from the membrane of the Notch intracellular domain (NICD), which then traffics to the nucleus. The NICD subsequently regulates the expression of genes, in cooperation with the transcription factor RBP-Jκ and Mastermind-like proteins.

The observation that mutations in the Notch ligand Delta-like–3 (Dll-3) and in the γ-secretase presenilin-1 cause axial skeletal phenotypes initially caused researchers to link Notch signaling with axial skeletal development[6,7]. Recently, several *in vitro* studies yielded conflicting results that implicated the Notch pathway in the regulation of osteoblast differentiation; however, the *in vivo* role of Notch signaling in bone homeostasis still remains unknown[8–12].

In this study, we investigate the tissue, cellular and molecular consequences of both gain and loss of function of Notch signaling in committed osteoblasts.

RESULTS

Gain of Notch function results in severe osteosclerosis

To determine the pathological consequences of *in vivo* gain of Notch function during bone formation and homeostasis, we generated transgenic mice expressing the Notch1 intracellular domain (N1ICD) under the control of the type I collagen (*Col1a1*) promoter (**Supplementary Fig. 1a,b** online). Here, gain of Notch function would occur in committed osteoblastic cells, as Col1a1 is both an early and a late marker of the osteoblastic lineage. Notably, founder mice expressing high levels of the transgene were small at birth and showed progressive growth retardation. Analysis of three established lines at 4 weeks of age showed increased bone mass on radiographs and a thickened, osteosclerotic appearance after skeletal preparations (**Fig. 1a** and **Supplementary Fig. 1c**). As determined by histology, marrow spaces in 4-week-old transgenic mice were filled with trabecular bone composed predominantly of immature woven, rather than lamellar, bone and surrounded by fibrotic marrow containing cells with morphologic features of early osteoblastic precursors, suggesting the increased proliferation of these cells (**Fig. 1b**). The cortices of the bones were also composed of woven bone, and this phenotype was present in 11-week-old mice as well. Toluidine blue staining of 11-week-old transgenic mice indicated an increased number of osteoblasts in vertebrae (**Fig. 1c**). Quantitative histomorphometry of an established mouse line confirmed the significant increase in trabecular bone volume and osteoblast surface area, which would be consistent with the high bone mass being due to increased osteoblastic activity (**Fig. 1d**). This increased osteoblastic activity led to increased production of osteoid (**Fig. 1d**) and bone formation (**Supplementary Fig. 1d**).

Because bone formation and resorption are coupled *in vivo*, we analyzed the status of osteoclasts by staining for tartrate-resistant acid phosphatase (TRAP) activity in osteoclasts from bone sections of 4-week-old mice. Although total TRAP staining was qualitatively increased in the limb sections of transgenic mice (**Supplementary**

[1]Department of Molecular and Human Genetics, Baylor College of Medicine, One Baylor Plaza, Houston, Texas 7703, USA. [2]Department of Pathology and Laboratory Medicine, University of Rochester Medical Center, 601 Elmwood Avenue, Rochester, New York 14642, USA. [3]Howard Hughes Medical Institute, One Baylor Plaza, Houston, Texas 77030, USA. [4]Department of Pediatrics and [5]Department of Molecular Virology and Microbiology, Baylor College of Medicine, One Baylor Plaza, Houston, Texas 77030, USA. [6]These authors contributed equally to this work. Correspondence should be addressed to B.L. (blee@bcm.tmc.edu).

Received 14 September 2007; accepted 19 December 2007; published online 24 February 2008; doi:10.1038/nm1712

Fig. 1e), consistent with increased bone mass and remodeling, the osteoclastic parameters normalized to bone surface (that is, osteoclast number per mm of bone surface and osteoclast surface) were significantly decreased in trabecular bone of transgenic mice (**Supplementary Fig. 1e**). Together, these data support the notion that gain of Notch function in committed osteoblastic lineage cells stimulates the proliferation of early osteoblastic precursors that differentiate into immature osteoblasts producing increased amounts of immature woven bone. Although osteoclastic activity was secondarily stimulated by this massive osteoblastic proliferation, bone formation much greatly outweighed bone resorption, leading to an osteosclerotic phenotype.

To determine the underlying cellular and molecular mechanism for the increase in early osteoblastic precursors in transgenic bone, we cultured postnatal day 6 (P6) calvarial osteoblasts and found significantly increased numbers of BrdU-positive cells, consistent with increased cellular proliferation (**Fig. 1e**). Quantitative real time RT-PCR (qRT-PCR) of 1-month-old calvarial total RNA showed an increased abundance of early osteoblastic differentiation markers, including osterix (encoded by *Sp7*), alkaline phosphatase and bone sialoprotein. In contrast, later markers of osteoblast differentiation, including osteocalcin, were downregulated (**Fig. 1f**). To exclude the possibility that the increased bone mass was due to decreased osteoclastic activity, we assessed the expression of markers that regulate macrophage differentiation along the osteoclastic lineage in the forelimbs of 4-week-old transgenic mice. RANK ligand (RANKL, encoded by *Tnfrsf11a*), osteoprotegerin, TRAP and macrophage colony–stimulating factor (M-CSF) were all highly expressed, suggesting that the hyperproliferation of the early osteoblastic pool was associated with increased production of both pro- (RANKL and M-CSF) and anti- (osteoprotegerin) osteoclastic differentiation factors by osteoblasts (**Fig. 1g**).

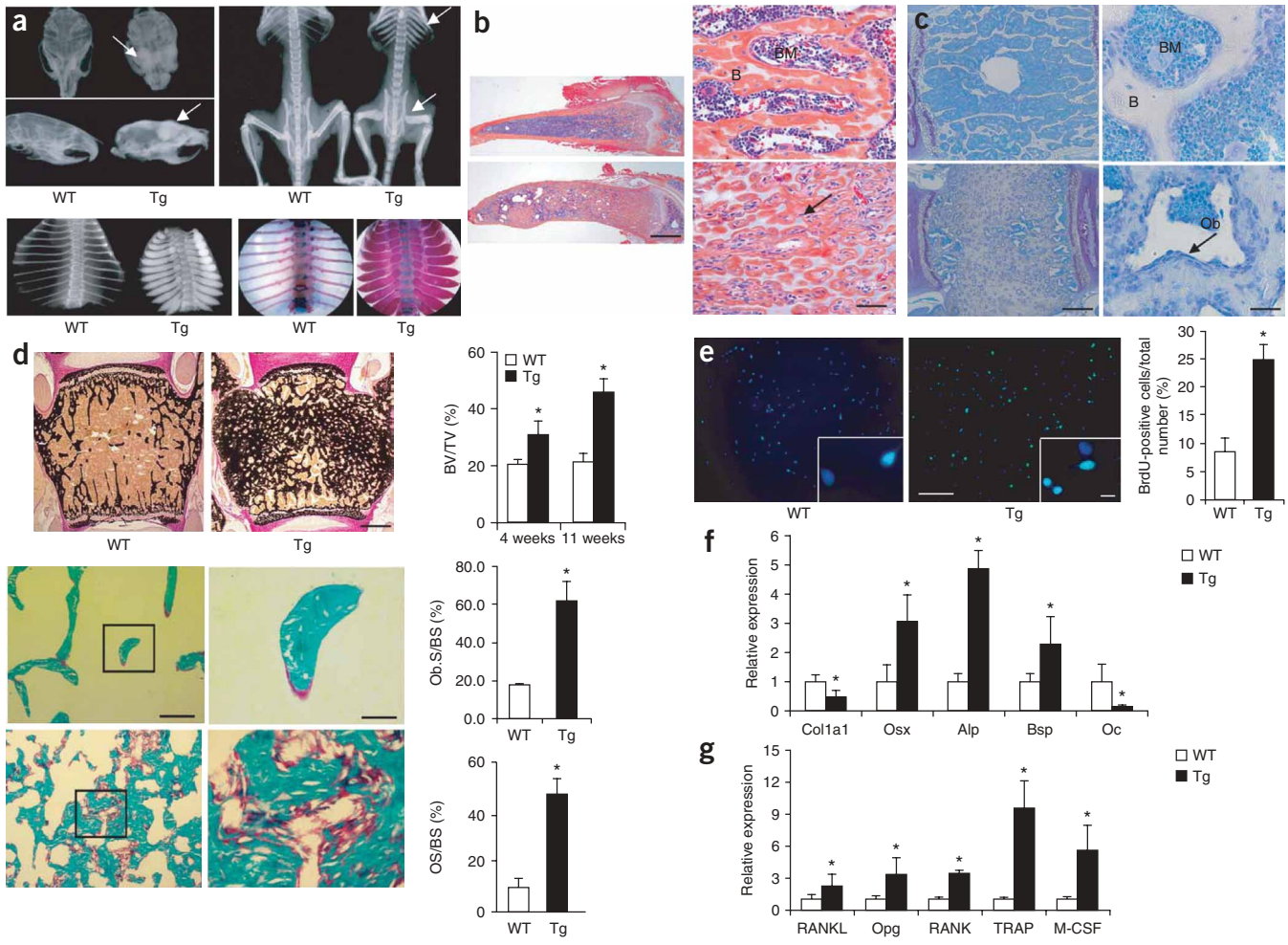

Figure 1 Gain of Notch function in transgenic mice cause osteosclerosis. (**a**) X-ray and skeletal preparations of 4-week-old transgenic mice show severe osteosclerosis (white arrows) in the skull, ribs and long bones. WT, wild-type mice; Tg, transgenic mice. (**b**) H&E staining of 4-week-old WT (top) and Tg (bottom) mouse hind limbs show immature woven bone formation with little distinction between cortex and marrow (black arrow). B, bone; BM, bone marrow. Scale bars, 500 μm (left) and 50 μm (right). (**c**) Toluidine blue staining of lumbar sections of 11-week-old WT (top) and Tg (bottom) mice reveals an increased number of osteoblasts (black arrow). Ob, osteoblasts lining bone. Scale bars, 500 μm (left) and 50μm (right). (**d**) Von Kossa staining of lumbar sections of 11-week-old mice (top left) and trabecular bone volume density (BV/TV) analyses of 4-week- and 11-week-old mice ($n = 4$; top right). Scale bar, 500 μm. Histomorphometric analyses of 4-week-old mice (bottom left) ($n = 5$) and Goldner's staining of spinal trabecular bone (bottom right). Boxed area is enlarged in the right panel. Scale bars, 500 μm (left) and 50 μm (right). Ob.S/BS, osteoblast surface per bone surface; OS/BS, osteoid per bone surface. (**e**) BrdU staining of osteoblastic cells from P6 calvaria ($n = 5$). Scale bars, 200 μm (left) and 20 μm (right). (**f**) qRT-PCR of total RNA from 4-week-old mouse calvaria ($n = 4$). Osx, osterix; Alp, alkaline phosphatase; Bsp: bone sialoprotein; Oc, osteocalcin. (**g**) qRT-PCR of total RNA from 4-week-old mouse calvaria and forelimbs ($n = 4$). Opg, osteoprotegerin. $^*P < 0.05$ between WT and Tg.

Notch regulates osteoblastic transcription factors

How Notch signaling regulates these processes on a biochemical level is unknown. Osteoblast differentiation from mesenchymal stem cells and subsequent maturation steps require the function of the runt-domain transcription factor Runx2 and the zinc-finger transcription factor osterix. Runx2 is required for commitment of mesenchymal osteochondroprogenitors to the osteoblastic lineage, differentiation into mature osteoblasts and terminal differentiation into osteocytes. In contrast, osterix is important in expansion of the early osteoblastic pool[13]. Whereas bone sialoprotein and alkaline phosphatase are markers of early osteoblasts, osteocalcin is a marker of later, mature osteoblasts. To determine the mechanistic basis of Notch action in this context, we tested the effects of Notch expression on these key transcriptional regulators of osteoblast differentiation and maturation. N1ICD alone was able to directly bind Runx2 and repress its transactivation of a reporter osteocalcin enhancer *in vitro* (in Cos7 and rat osteosarcoma Ros17/2.8 cells; **Fig. 2a–c** and **Supplementary Fig. 1f**). Electrophoretic mobility shift assays (EMSAs) showed that N1ICD could inhibit Runx2 binding to a target *cis* element in the type X collagen promoter (**Supplementary Fig. 1g**). Notably, there was marked downregulation of Runx2 protein in P2 calvaria of transgenic mice (**Fig. 2d**). Thus, the downregulation of osteocalcin and the delay in late osteoblast differentiation *in vivo* is probably due, in part, to direct repression of Runx2 by Notch at the protein level. At the same time, we observed upregulation of osterix mRNA expression in the P2 calvaria of transgenic mice (**Fig. 1f**). Moreover, N1ICD activated the *Sp7* promoter in transient transfection studies in C2C12 cells that were induced to differentiate into osteoblasts with bone morphogenic protein-2 treatment (**Fig. 2e**). These data suggest that Notch can induce proliferation of committed osteoblast precursors by directly upregulating transcription of *Sp7*, while inhibiting their maturation by repressing the function of Runx2.

To further understand the biochemical basis of the effects of Notch on osteoblastic proliferation, we analyzed the expression of cell cycle markers and detected increased mRNA expression of cyclin D and cyclin A by qRT-PCR in osteoblasts overexpressing N1ICD (**Fig. 2f**). This correlated with increased cyclin D and cyclin E expression at the protein level (**Fig. 2g**). We did not, however, observe significant differences in the abundance of two other important cell cycle regulators implicated in bone homeostasis, p53 and Rb. Of note, it has been shown with *in vitro* and *ex vivo* studies that Runx2 can suppress osteoblast proliferation and promote osteoblast maturation by supporting exit from the cell cycle[14,15]. Moreover, cyclin D1–cyclin-dependent kinase-4 (cdk4) can induce Runx2

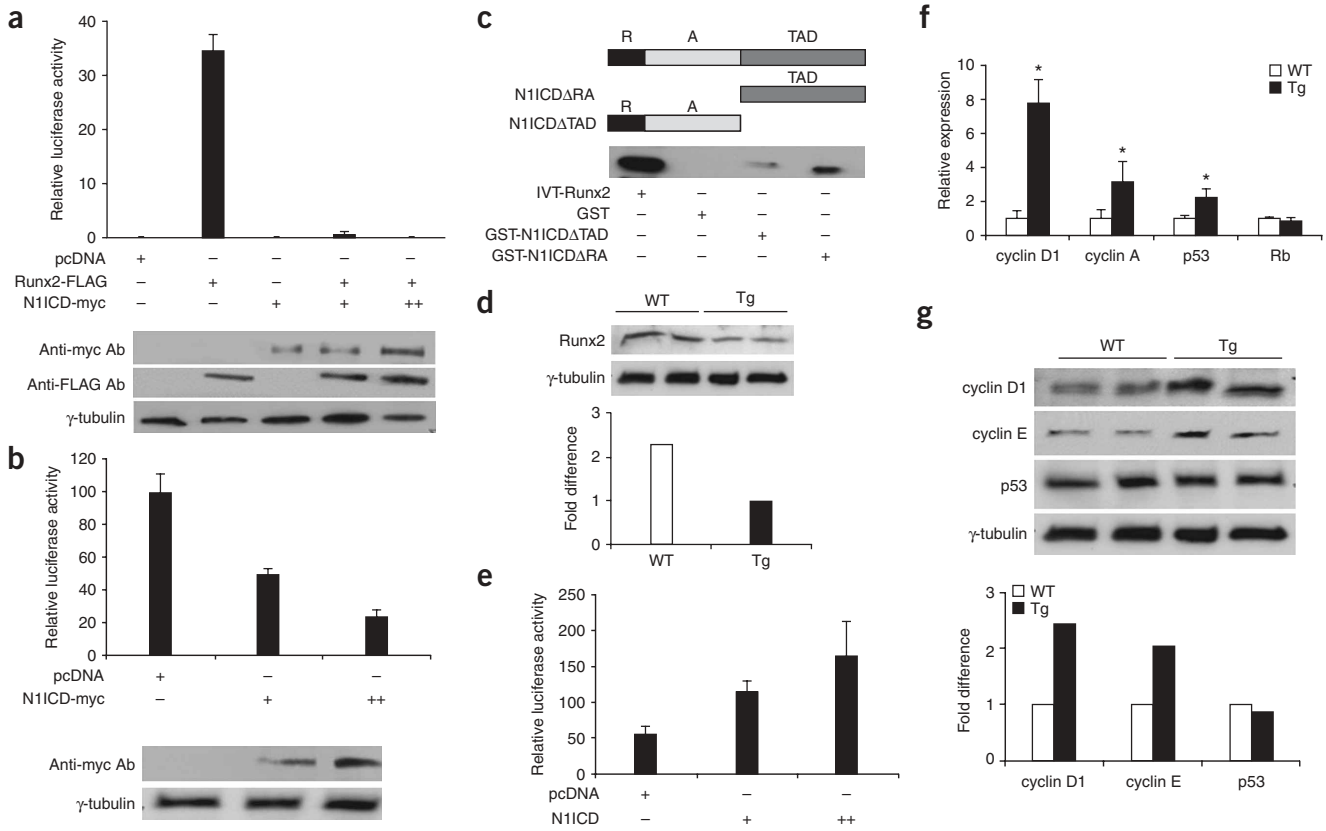

Figure 2 Notch regulates key osteoblast transcription factors and cell cycle proteins. (**a**) Relative luciferase activity in Cos7 cells transfected with Runx2 and Runx2-dependent osteocalcin enhancer luciferase reporter with increasing dosage of N1ICD. Western blot analyses of cell lysates using the indicated antibodies are shown. (**b**) Transfection of N1ICD inhibits endogenous Runx2 activity in ROS17/2.8 osteosarcoma cells as shown by relative luciferase activity of the Runx2-responsive osteocalcin enhancer. Western blot analyses of cell lysates using the indicated antibodies are shown. (**c**) GST pull-down assay with amino-terminal–truncated (GST-NICDRA) and carboxy-terminal–truncated (GST-NICDTAD) Notch fusion proteins and *in vitro* transcribed-translated, ^{35}S-methionine–labeled Runx2 (IVT-Runx2). Strongest binding is noted with the carboxy-terminal portion of Notch. (**d**) Decreased Runx2 protein abundance was detected by western blot analyses and quantified with densitometry on P2 calvarial protein extracts in Tg and WT mice. (**e**) Relative luciferase activity in C2C12 cells transfected with Osterix promoter luciferase reporter gene and N1ICD. (**f**) qRT-PCR of cell cycle markers on RNA obtained from 4-week-old mouse calvaria ($n = 4$). (**g**) Western blot analyses of P2 calvarial protein extracts to detect cell cycle markers and quantification by densitometry. $^*P < 0.05$ between WT and Tg.

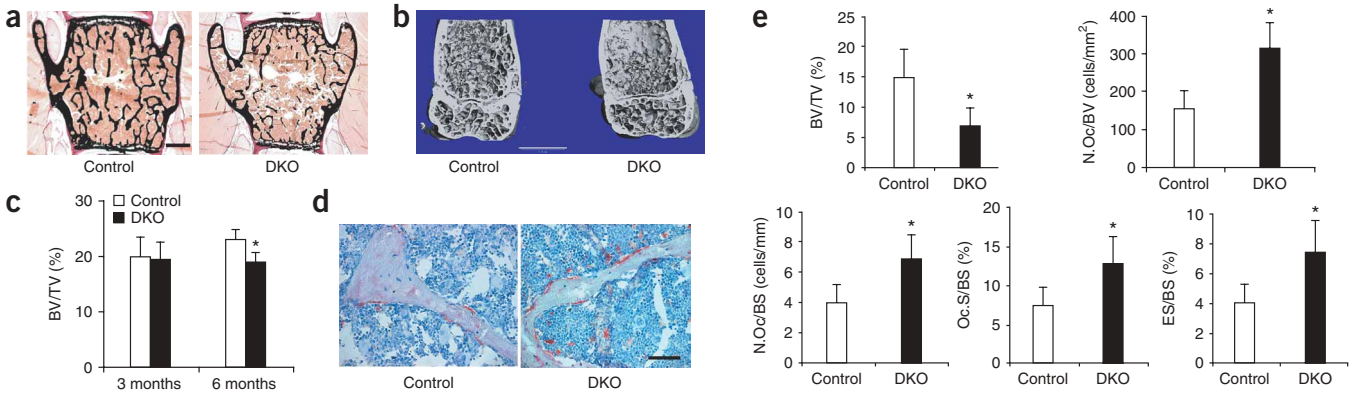

Figure 3 Loss of Notch signaling via presenilin deletion causes osteoporosis. (**a**) Von Kossa staining of 6-month-old lumbar vertebrae of *Psen1*$^{f/f}$*Ps2*$^{-/-}$ (Control) and DKO mice showed osteoporosis. Scale bar, 500 μm. (**b**) Micro-CT reconstruction of distal femur from 6-month-old DKO mice showing decreased trabecular bone. Scale bar, 1 mm. (**c**) Histomorphometry of 3-month-old and 6-month-old DKO L3–L4 spine showing age-related penetrance of low bone mass phenotype. (**d**) TRAP staining (red) of 6-month-old lumbar vertebral sections from DKO and control mice indicated increased osteoclast staining. Scale bar, 200 μm. (**e**) Histomorphometry of 6-month-old DKO and control ($n = 5$ per group) mouse tibiae revealed decreased BV/TV (top left) and increased osteoclast number per bone volume (N.Oc/BV; top right), osteoclast number per bone surface (N.Oc/BS), osteoclast surface per bone surface (Oc.S/BS) and eroded surface per bone surface (ES/BS) in DKO mice. $^*P < 0.05$.

ubiquitination and degradation, and thus Runx2 activity can be regulated by the cell cycle machinery[16]. Hence, gain of Notch function can inhibit osteoblast maturation by direct repression of Runx2 activity, as well as by repression of Runx2's antiproliferative effects via cyclin D1 upregulation.

Loss of Notch signaling leads to age-related osteoporosis

To determine whether the pathological effects of gain of Notch signaling reflect a physiological function during bone homeostasis, we generated a tissue-specific model of loss of Notch signaling in osteoblasts. Because all Notch receptors are expressed in osteoblasts

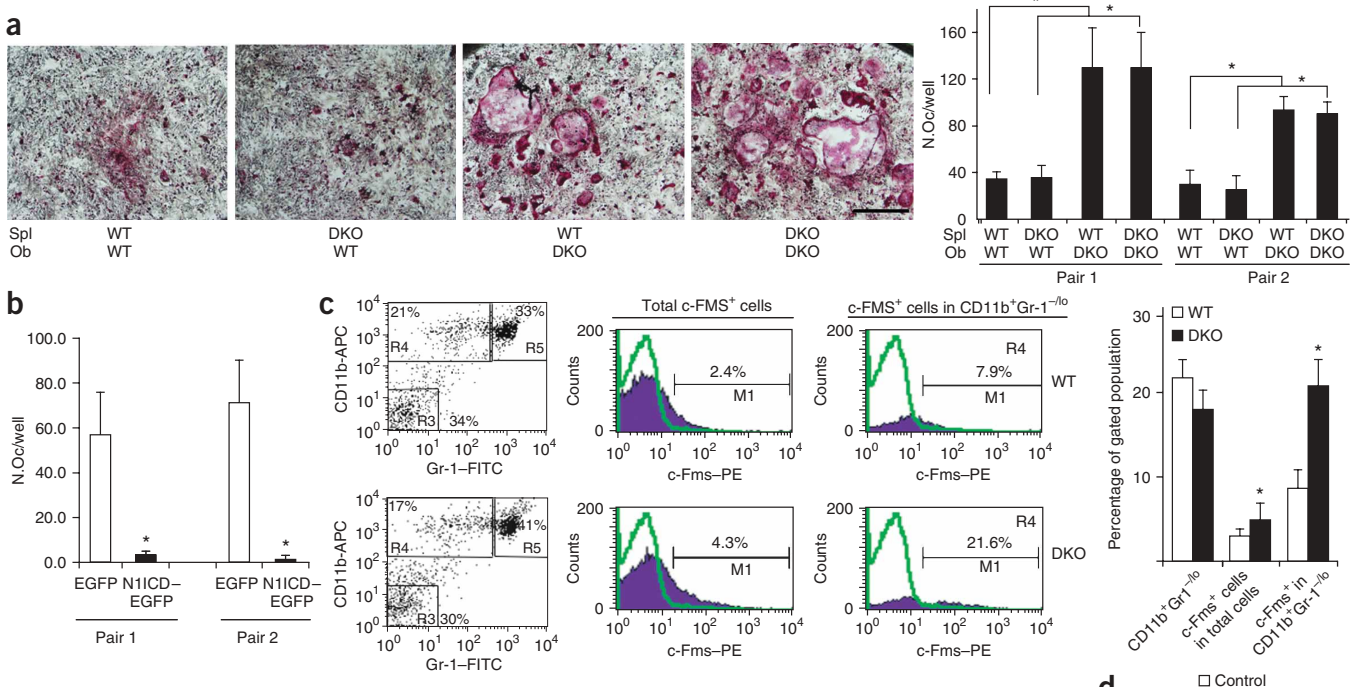

Figure 4 Loss of Notch signaling through presenilin deletion increases the osteoclastogenic pool. (**a**) Cocultures of WT or DKO P7 ($n = 2$, as indicated by 'Pair 1' and 'Pair 2') spleen cells (Spl) and osteoblasts (Ob) stained (images) and quantified (graph) for TRAP$^+$ osteoclasts. Scale bar, 250 μm. (**b**) Cocultures of P7 ($n = 2$, as indicated by 'Pair 1' and 'Pair 2') N1ICD lentivirus–transduced DKO osteoblasts with WT spleen cells quantified for TRAP$^+$ osteoclasts. (**c**) Bone marrow cells obtained from 3-month-old ($n = 3$) WT and DKO mice were stained and subjected to FACS to detect the CD11b$^+$Gr-1$^{-/lo}$ cells and the c-Fms$^+$ population specific for osteoclast precursors in both total gated and CD11b$^+$Gr-1$^{-/lo}$-gated populations. Representative histograms show total c-Fms$^+$ cells and c-Fms$^+$ cells in the CD11b$^+$Gr-1$^{-/lo}$ population. Percentages indicate the proportion of total cells in a given gate (indicated by boxes). (**d**) qRT-PCR for osteoblast markers in total RNA obtained from P4 mouse (DKO versus control calvaria ($n = 5$ per group)). $^*P < 0.05$.

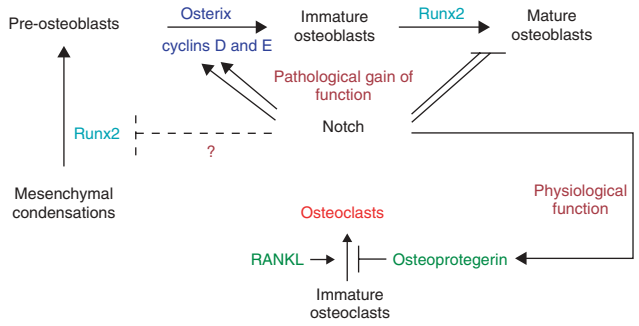

Figure 5 Model for Notch's dimorphic effects in bone homeostasis. In established osteoblastic lineages, pathological gain of Notch function activates expansion of the immature osteoblastic pool by increasing transcription of the genes encoding osterix, cyclin D and cyclin E and by repressing the function of Runx2 by direct interaction and inhibition of its binding. Physiologically, it inhibits osteoclastogenesis by increasing osteoprotegerin production over RANKL production.

(data not shown), we abolished Notch signaling by generating null mice for both presenilin-1 (*Psen1*) and presenilin-2 (*Psen2*). Because *Psen2*-null mice are viable and fertile, we generated double homozygotes for the *Psen2*-null allele and the *Psen1* floxed allele, but heterozygous for the type 1 collagen Cre recombinase transgene ($Psen1^{f/f}Psen2^{-/-}Col1a1^{Cre/+}$, or DKO). DKO mice were compared to their $Psen1^{f/f}Psen2^{-/-}$ littermates as controls, and efficient deletion of the $Psen1^{f/f}$ allele (approximately 92%) was confirmed by RT-PCR for presenilin mRNA expression and genomic PCR for DNA recombination in both calvarial osteoblasts and tail DNA, respectively (**Supplementary Fig. 2a,b** online). Moreover, we confirmed that this led to decreased NICD processing by western blot analysis (**Supplementary Fig. 2c**). Histomorphometric analyses of DKO mice showed that 6-month-old, but not 3-month-old, mice were osteoporotic, a decreased tissue bone mass phenotype that is the opposite of the osteosclerotic tissue phenotype in gain-of-Notch-function transgenic mice (**Fig. 3a–c**). Bone formation rates, osteoblast surfaces and mineralized surfaces in vertebrae and long bones in the DKO mice were similar to those in control mice (**Supplementary Fig. 3** online). However, osteoclast numbers, osteoclast surfaces and eroded surfaces were increased in DKO vertebrae and long bones at 6 months of age, but not at 3 months of age (**Fig. 3d,e** and **Supplementary Fig. 3**). These findings suggest that loss of *Psen1* and *Psen2*, and thus all Notch signaling in osteoblasts, led to osteoporosis through activation of osteoclastogenesis and the subsequent increased bone resorption over bone formation with age-related penetrance.

Activated osteoblasts support osteoclast formation and differentiation from osteoclast precursors by expressing M-CSF and RANKL, but they also inhibit this process through osteoprotegerin, which binds to and inactivates RANKL. To further examine the effects of loss of *Psen1* and *Psen2* in osteoblasts on osteoclastogenesis, we performed osteoblast-osteoclastic precursor (OCP) coculture studies. In this *ex vivo* assay, P7 DKO calvarial osteoblasts stimulated the formation of more osteoclasts from wild-type, spleen-derived OCPs than did wild-type osteoblasts, suggesting that *Psen1* and *Psen2* deletions can affect osteoclastogenesis in a non–cell-autonomous fashion (**Fig. 4a**). To determine whether this effect was specific for Notch signaling, we tested whether heterologous expression of N1ICD after lentiviral transduction of DKO osteoblasts could suppress osteoclastogenesis in coculture studies (**Fig. 4b** and **Supplementary Fig. 4a** online). Compared to control vector expressing EGFP, lentiviral transduction of N1ICD into *Psen1-Psen2* mutant osteoblasts was able to suppress osteoclastogenesis, suggesting that the DKO phenotype was primarily due to presenilin effects on Notch signaling.

The *in vivo* relevance of this was confirmed by flow cytometric analysis of markers on bone marrow cells from 3-month-old DKO mice. This showed increased staining of early OCPs in total cells ($cFMS^+$) and in more differentiated OCPs ($CD11b^+Gr\text{-}1^{-/lo}$) compared to controls, indicating an expansion of the OCP pool in DKO mice (**Fig. 4c**). To determine whether this increase in osteoclast differentiation was due to an imbalance of osteoblastic inductive (RANKL and M-CSF) versus suppressive (osteoprotegerin) signals, we analyzed their mRNA expression in DKO versus control bone at P4. We found comparable expression of RANKL mRNA in DKO and control mice, but expression of osteoprotegerin mRNA was markedly decreased (**Fig. 4d**) in DKO mice. Similarly, we found decreased osteoprotegerin production in cultured DKO calvarial osteoblasts as compared to wild-type calvarial osteoblasts (**Supplementary Fig. 4b**). Hence, under physiological conditions, Notch signaling enabled by Psen1 and Psen2 function in osteoblasts represses osteoclast differentiation by regulating osteoprotegerin expression.

Together, these *in vivo* gain-of-function and loss-of-function studies lend support for a central role of Notch and presenilin signaling in regulating both osteoclastogenesis and immature osteoblastic proliferation during bone homeostasis (**Fig. 5**).

DISCUSSION

Until now, few primary signaling mechanisms regulating osteoblast differentiation and function during bone homeostasis have been identified *in vivo* by genetic and biochemical studies. Wnt signaling via LRP5/6 coreceptors and canonical β-catenin activity are required for osteoblast lineage commitment and function[17–19]. Activation of this pathway leads to high bone mass[20,21]. Activating mutations in transforming growth factor-β in humans is associated with increased bone formation and inhibition of bone resorption[22]. However, and not unexpectedly, apparently discrepant results *in vivo* have been observed, depending on the timing of the gain versus the loss of transforming growth factor-β function. Similarly, Notch signaling probably has temporal and spatial dependence, as well.

In bone, our data suggest that Notch and presenilin signaling may be important in the physiological regulation of osteoclastogenesis by osteoblasts. Moreover, it raises the question of whether loss of Notch signaling contributes to age-related osteoporosis, as this type of osteoporosis is associated with increased resorption over bone formation[23], as is seen in our DKO model. We discovered that one function of Notch in committed osteoblasts is to regulate osteoclastogenesis via regulation of osteoprotegerin production. The magnitude of osteoprotegerin dysregulation and the age-related penetrance of the osteoporosis in the loss-of-function mouse phenotype correlate well with epidemiological data in humans, in which age-related osteoporosis has been associated with changes in osteoprotegerin production[24–27]. Furthermore, the report that heterozygote osteoprotegerin-mutant mice have an age-related osteoporotic phenotype suggests that this mechanism is sufficient for disease pathogenesis[28]. What is unclear is whether osteoprotegerin dysregulation is due to direct regulation by N1ICD or by its target transcription factors, given the still poorly characterized osteoprotegerin genetic regulatory region. Further studies showing chromatin immunoprecipitation analysis of a well-defined functional osteoprotegerin promoter with N1ICD or with its target genes would help to address this issue. Likewise, our studies do not address the potential role of Notch signaling before osteoblastic commitment in the mesenchymal stem cell (**Fig. 5**). Here, Runx2 has

the central role in osteoblastic commitment. Our data on the Notch-Runx2 interaction suggest that early loss of function of Notch would actually lead to increased commitment to the osteoblastic lineage and perhaps depletion of the mesenchymal stem cell compartment.

In a pathological disease context, our findings show that activation of Notch signaling in the committed osteoblastic lineage leads to expansion of an immature osteoblast pool. The primary mode of action is transcriptional upregulation of the early osteoblast transcription factor osterix and increase of cyclin D and cyclin E proteins. These data raise the question of the potential contribution of activation of Notch signaling in human diseases related to osteoblastic proliferation, such as in bone pathologies including human osteosarcomas. The substantial upregulation of cyclin D1 in the transgenic mice correlates with the observation in humans that 10% of osteosarcomas show amplification of the chromosomal region encoding cyclin D1(ref. 29). Although our data suggest that Notch can directly interact with Runx2 to inhibit its binding to target *cis* elements and its prodifferentiation function, this is probably not the main determinant of the gain-of-function phenotype in mice.

Finally, our data have key therapeutic implications. There are few anabolic bone agents for the treatment of osteoporosis, with most therapies targeted at inhibition of bone resorption. Upregulation of Notch signaling may represent a potential approach for increasing bone formation over bone resorption, as well as for inhibiting osteoclastogenesis. However, it is clear that temporal effects of Notch on other cellular compartments, such as the mesenchymal stem cell pool, would have to be considered; that is, Notch inhibition of Runx2 function could inhibit mesenchymal stem cell commitment to the osteoblastic lineage. In opposing fashion, inhibition of Notch signaling may be a therapeutic option to investigate for the treatment of proliferative disorders of the osteoblast, such as osteosclerotic diseases or bone cancers.

From a mechanistic perspective, the function of Notch signaling in bone constitutes an example of a signaling pathway capable of regulating both osteoblastic and osteoclastic lineages. Gain of Notch function in osteoblasts affects osteoblastic differentiation in a cell-autonomous fashion, whereas loss of Notch function in osteoblasts affects osteoclastogenesis in a non–cell-autonomous manner. A remaining question is how Notch-Notch ligand interactions with neighboring cells, such as stromal and osteoclastic cells, may further modify biological function in the respective lineages. For example, ephrin B2 signaling in bone is bidirectional, with consequences for both the cells expressing the ligand and the cells expressing the receptor. In this case, reverse signaling through ephrin B2 ligand expressed by osteoclasts suppresses osteoclast precursors, whereas forward signaling through EphB4 receptor expressed by osteoblasts enhances osteoblast formation[30,31]. Together, our data point to a dimorphic role for Notch signaling in osteoblast biology; that is, the stimulation of osteoblastic precursors in a pathological context and the inhibition of osteoclastogenesis in the physiological regulation of bone mass and homeostasis.

METHODS

Mice. We cloned Myc-His–tagged N1ICD, which includes amino acids 1760–2556 of Notch (gift of T. Kadesch), under the control of the 2.3–kilobase (kb) osteoblast-specific *Col1a1* promoter in a coat-color vector containing the tyrosinase minigene and the woodchuck posttranscriptional regulatory element (WPRE) sequences[32]. We generated transgenic founders by pronuclear injections using standard techniques. We maintained all transgenic lines on a FVB/N background. We identified the transgenic mice at birth by eye pigmentation and confirmed by PCR using primers specific for the WPRE. We crossed previously described *Psen1*$^{f/f}$ and *Psen2*$^{-/-}$ mice with *Col1a1*-Cre mice (gift of G. Karsenty) to generate osteoblast-specific *Psen1-Psen2* DKO mice. These studies were approved by the Baylor College of Medicine Institutional Animal Care and Use Committee.

Skeletal analyses, histology and bone histomorphometry. We cleared and stained skeletons from 1-month-old mice with Alcian blue for cartilage and Alizarin red for bone as described[33]. We killed the mice and fixed the whole skeleton in 10% neutral-buffered formalin for 18 h. For radiographic analyses, we analyzed the skeletons by contact radiography with a Faxitron X-ray cabinet (Faxitron X-ray). We sectioned paraffin-embedded tissues to a 4–7–μm thickness and stained the section with H&E. We performed toluidine blue, Von Kossa and Goldner's stains on 5–7–μm undecalcified lumbar vertebral plastic sections by using standard protocols. We performed all static and dynamic histomorphometry analyses according to standard protocols using the OsteoMeasure histomorphometry system (Osteometrics). We performed histomorphometric analyses on 4-week-old transgenic mice ($n = 3$) and 6-month-old knockout mice ($n = 5$–7).

We analyzed μ–computed tomography (μCT) scanning of the trabecular bone of the distal femur by the μCT system (μCT-40, Scanco Medical).

Plasmids. Osterix-luciferase was a gift of M.S. Nanes. For lentivirus vector production, we constructed plasmid pHIV-N1-IRES-eYFP by inserting a FLAG-tagged version of intracellular activated form of Notch1 (N1), just upstream of the 1.4-kb IRES-eYFP cassette (an internal ribosomal entry site fused to enhanced yellow fluorescence protein) of pHIV-IRES-eYFP[34]. For the primary osteoblasts, the lentiviral vectors used were self-inactivating and had the 0.5-kb mouse phosphoglycerate kinase promoter inserted upstream of either N1-IRES-eYFP or IRES-eYFP[35]. We produced vesicular stomatitis virus G protein–pseudotyped vector supernatants as previously described[36]. After 72 h, we harvested cell culture supernatants and clarified them. Typical titers after concentration by ultracentrifugation were in excess of 1×10^8 international units (IU)/ml for the two self-inactivating vectors as assessed on HOS cells by epifluorescence microscopy. Titers of unconcentrated non-SIN vectors were in excess of 1×10^7 IU/ml.

Coculture studies. We cocultured 5×10^3 calvarial osteoblasts from 1-week-old mice ($n = 3$) with 5×10^4 spleen cells per well in 96-well plates for 7 d in the presence 10^{-8} M vitamin D_3. We then stained the cells for TRAP activity and counted as described previously[37]. For the lentiviral rescue experiment, we cultured 5×10^3 osteoblasts isolated from calvaria of 10-d-old *Psen1-Psen2* DKO mice in a 96-well plate for 2 d. We then infected the cells with either 5 μl N1ICD lentivirus or the YFP lentiviral vector supernatant for 24 h in 100 μl α-MEM containing 10% FBS and 8 μg polybrene/ml. We then cocultured the infected cells with 5×10^4 spleen cells from 10-d-old WT mice for 7 d in the presence of 10^{-8} M vitamin D_3.

Fluorescence-activated cell sorting and cell sorting analyses. After lysis of erythrocytes with ammonium chloride solution, we incubated 2×10^6 cells from bone marrow or spleen for 5 min with antibody to murine CD16/32 to block Fc receptor–mediated antibody binding, and then followed with triple staining with allophycocyanin-conjugated antibody to mouse CD11b, FITC-conjugated antibody to Gr-1 and phycoerythrin-conjugated antibody to c-Fms for 30 min. We then subjected the cells to FACS to analyze the $CD11b^+Gr\text{-}1^{-/lo}$ cells that contain osteoclast precursors and c-Fms^+ cells in both the total gated and the $CD11b^+Gr\text{-}1^{-/lo}$ populations.

Bromodeoxyuridine incorporation. We isolated osteoblasts from calvaria of P6 transgenic mice and wild-type littermates ($n = 5$ per group) as previously described[33]. We replated cells 48 h after the initial culture and expanded them for an additional day. We treated cells with BrdU labeling reagent (Zymed) according to the manufacturer's instructions for 6 h, washed them with PBS and fixed them with 70% ethanol for 25 min at 4 °C. Three to five areas for each genotype ($n = 3$ slides) were counted by two independent observers blinded to genotype. We scored BrdU-positive cells over total cells visually and with Automeasure software (Zeiss Axiovision).

Western blot analysis. We extracted proteins from P2 mice by homogenizing the calvaria ($n = 3$ per group) in a buffer containing 5% SDS and 0.0625 M Tris HCl. We performed western blot analyses with antibody to p53 (gift of L. Donehower), polyclonal antibody to Runx2 (M70; Santa Cruz Biotechnology), antibody to cyclin D1 (H-2953; Santa Cruz Biotechnology) and antibody to cyclin E (ab-7959; Abcam). We normalized protein content using mouse monoclonal antibody to-γ-tubulin (Sigma).

Glutathione-*S*-transferase pulldown. We expressed GST, GST-NICDΔTAD, and GST-NICDΔRA (gift of T. Kadesch) in the BL21 strain of *Escherichia coli* (Stratagene). We induced production of the GST proteins were induced with 0.2 mM isopropyl β-D-thiogalactopyranoside (IPTG; Promega) and allowed the to grow an additional 4–5 h. After induction, we lysed the cells by sonication. We bound GST proteins to glutathione resin (Amersham Biosciences). We generated 625-μM Met-labeled, FLAG-tagged Runx2 proteins by a T7 *in vitro* transcription-translation kit (Novagen) and incubated them with GST or GST-NICDTAD or GST-NICDRA immobilized on glutathione-Sepharose beads at 4 °C for 2 h. We then washed the beads five times with TNN buffer (1 M TrisHCl, 5 M NaCl, 14.2 M 2-mercaptoethanol) containing 1% Nonidet P-40, boiled the proteins in 2× SDS sample loading buffer and separated them by SDS-PAGE. We performed western blotting to detect the FLAG-tagged Runx2 protein with M2 monoclonal antibody to FLAG (Sigma).

RNA extraction and quantitative reverse transcription PCR analysis. We extracted total RNA from calvaria and forelimbs of P4 and 4-week-old mice ($n = 5$ and $n = 3$, respectively) with TRIzol reagent (Invitrogen). We synthesized cDNAs from extracted RNA with the Superscript III First Strand RT-PCR kit (Invitrogen). We performed real-time quantitative PCR amplifications in a LightCycler (Roche) using a TaqMan assay (Applied Biosystems probe HS00172878-M1). We used the genes encoding β-actin and β2-microglobulin as internal controls for the quantity and quality of the cDNAs in real-time PCR assays.

DNA transfection. We transfected Cos7 and Ros17/2.8 cells with the 6XOSE2-luc reporter gene by using Lipofectamine Plus according to manufacturer's recommendations (Invitrogen). We assayed luciferase and β-galactosidase activities 48 h after transfection. We transfected C2C12 cells with –1269/91 Osx-p-luc (gift of M.S. Nanes) by using Fugene6 according to the manufacturer's instructions (Roche). We induced the cells 24 h after the transfection with 300ng/ml recombinant human bone morphogenic protein-2 (R&D Systems), and we harvested and assayed the cells the next day. We performed all transfections in triplicate with pSV2βgal as an internal control for transfection efficiency.

Statistical analyses. Data are expressed as mean values ± s.d. We computed statistical significance with Student's paired *t*-test. A P value of <0.05 was considered statistically significant.

Note: Supplementary information is available on the Nature Medicine website.

ACKNOWLEDGMENTS

We thank T. Kadesch (University of Pennsylvania) for Myc-His–tagged N1ICD, GST-NICDΔTAD and GST-NICDΔRA, G. Karsenty (Columbia University) for *Col1a1*-Cre mice, M.S. Nanes (Emory University) for osterix-luciferase and –1269/91 Osx-p-luc, and L. Donehower (Baylor College of Medicine) for antibody to p53. We thank M. Acar and O. Sirin for technical assistance. This work was supported by US National Institutes of Health grants ES11253 (B.L.), HD22657 (B.L.), DE016990 (B.L.) and AR43510 (B.F.B.).

Published online at http://www.nature.com/naturemedicine
Reprints and permissions information is available online at http://npg.nature.com/reprintsandpermissions

1. Artavanis-Tsakonas, S., Rand, M.D. & Lake, R.J. Notch signaling: cell fate control and signal integration in development. *Science* **284**, 770–776 (1999).
2. Bray, S.J. Notch signalling: a simple pathway becomes complex. *Nat. Rev. Mol. Cell Biol.* **7**, 678–689 (2006).
3. Weinmaster, G. The ins and outs of Notch signaling. *Mol. Cell. Neurosci.* **9**, 91–102 (1997).
4. Daudet, N. & Lewis, J. Two contrasting roles for Notch activity in chick inner ear development: specification of prosensory patches and lateral inhibition of hair-cell differentiation. *Development* **132**, 541–551 (2005).
5. Brennan, C.A. & Moses, K. Determination of *Drosophila* photoreceptors: timing is everything. *Cell. Mol. Life Sci.* **57**, 195–214 (2000).
6. Bulman, M.P. *et al.* Mutations in the human delta homologue, DLL3, cause axial skeletal defects in spondylocostal dysostosis. *Nat. Genet.* **24**, 438–441 (2000).
7. Shen, J. *et al.* Skeletal and CNS defects in presenilin-1–deficient mice. *Cell* **89**, 629–639 (1997).
8. Deregowski, V., Gazzerro, E., Priest, L., Rydziel, S. & Canalis, E. Notch 1 overexpression inhibits osteoblastogenesis by suppressing Wnt/β-catenin but not bone morphogenetic protein signaling. *J. Biol. Chem.* **281**, 6203–6210 (2006).
9. Sakamoto, K., Chao, W.S., Katsube, K. & Yamaguchi, A. Distinct roles of EGF repeats for the Notch signaling system. *Exp. Cell Res.* **302**, 281–291 (2005).
10. Sciaudone, M., Gazzerro, E., Priest, L., Delany, A.M. & Canalis, E. Notch 1 impairs osteoblastic cell differentiation. *Endocrinology* **144**, 5631–5639 (2003).
11. Tezuka, K. *et al.* Stimulation of osteoblastic cell differentiation by Notch. *J. Bone Miner. Res.* **17**, 231–239 (2002).
12. Zamurovic, N., Cappellen, D., Rohner, D. & Susa, M. Coordinated activation of Notch, Wnt, and transforming growth factor-β signaling pathways in bone morphogenic protein 2–induced osteogenesis. Notch target gene Hey1 inhibits mineralization and Runx2 transcriptional activity. *J. Biol. Chem.* **279**, 37704–37715 (2004).
13. Nakashima, K. *et al.* The novel zinc finger–containing transcription factor osterix is required for osteoblast differentiation and bone formation. *Cell* **108**, 17–29 (2002).
14. Galindo, M. *et al.* The bone-specific expression of Runx2 oscillates during the cell cycle to support a G1-related antiproliferative function in osteoblasts. *J. Biol. Chem.* **280**, 20274–20285 (2005).
15. Pratap, J. *et al.* Cell growth regulatory role of Runx2 during proliferative expansion of preosteoblasts. *Cancer Res.* **63**, 5357–5362 (2003).
16. Shen, R. *et al.* Cyclin D1–cdk4 induce Runx2 ubiquitination and degradation. *J. Biol. Chem.* **281**, 16347–16353 (2006).
17. Hill, T.P., Spater, D., Taketo, M.M., Birchmeier, W. & Hartmann, C. Canonical Wnt/β-catenin signaling prevents osteoblasts from differentiating into chondrocytes. *Dev. Cell* **8**, 727–738 (2005).
18. Day, T.F., Guo, X., Garrett-Beal, L. & Yang, Y. Wnt/β-catenin signaling in mesenchymal progenitors controls osteoblast and chondrocyte differentiation during vertebrate skeletogenesis. *Dev. Cell* **8**, 739–750 (2005).
19. Glass, D.A., II *et al.* Canonical Wnt signaling in differentiated osteoblasts controls osteoclast differentiation. *Dev. Cell* **8**, 751–764 (2005).
20. Krishnan, V., Bryant, H.U. & Macdougald, O.A. Regulation of bone mass by Wnt signaling. *J. Clin. Invest.* **116**, 1202–1209 (2006).
21. Tu, X. *et al.* Noncanonical Wnt signaling through G protein–linked PKC-δ activation promotes bone formation. *Dev. Cell* **12**, 113–127 (2007).
22. Janssens, K., ten Dijke, P., Janssens, S. & Van Hul, W. Transforming growth factor-β1 to the bone. *Endocr. Rev.* **26**, 743–774 (2005).
23. Mezquita-Raya, P. *et al.* The contribution of serum osteoprotegerin to bone mass and vertebral fractures in postmenopausal women. *Osteoporos. Int.* **16**, 1368–1374 (2005).
24. Fahrleitner-Pammer, A. *et al.* Osteoprotegerin serum levels in women: correlation with age, bone mass, bone turnover and fracture status. *Wien. Klin. Wochenschr.* **115**, 291–297 (2003).
25. Arko, B., Prezelj, J., Kocijancic, A., Komel, R. & Marc, J. Association of the osteoprotegerin gene polymorphisms with bone mineral density in postmenopausal women. *Maturitas* **51**, 270–279 (2005).
26. Choi, J.Y. *et al.* Genetic polymorphisms of OPG, RANK, and ESR1 and bone mineral density in Korean postmenopausal women. *Calcif. Tissue Int.* **77**, 152–159 (2005).
27. Hofbauer, L.C. *et al.* Estrogen stimulates gene expression and protein production of osteoprotegerin in human osteoblastic cells. *Endocrinology* **140**, 4367–4370 (1999).
28. Bucay, N. *et al.* Osteoprotegerin-deficient mice develop early onset osteoporosis and arterial calcification. *Genes Dev.* **12**, 1260–1268 (1998).
29. Wang, L.L. Biology of osteogenic sarcoma. *Cancer J.* **11**, 294–305 (2005).
30. Boyce, B.F. & Xing, L. Osteoclasts, no longer osteoblast slaves. *Nat. Med.* **12**, 1356–1358 (2006).
31. Zhao, C. *et al.* Bidirectional ephrinB2-EphB4 signaling controls bone homeostasis. *Cell Metab.* **4**, 111–121 (2006).
32. Zhou, G. *et al.* Dominance of SOX9 function over RUNX2 during skeletogenesis. *Proc. Natl. Acad. Sci. USA* **103**, 19004–19009 (2006).
33. Ducy, P. *et al.* A Cbfa1-dependent genetic pathway controls bone formation beyond embryonic development. *Genes Dev.* **13**, 1025–1036 (1999).
34. Segall, H.I., Yoo, E. & Sutton, R.E. Characterization and detection of artificial replication-competent lentivirus of altered host range. *Mol. Ther.* **8**, 118–129 (2003).
35. Dai, C., McAninch, R.E. & Sutton, R.E. Identification of synthetic endothelial cell–specific promoters by use of a high-throughput screen. *J. Virol.* **78**, 6209–6221 (2004).
36. Sutton, R.E., Wu, H.T., Rigg, R., Bohnlein, E. & Brown, P.O. Human immunodeficiency virus type 1 vectors efficiently transduce human hematopoietic stem cells. *J. Virol.* **72**, 5781–5788 (1998).
37. Xing, L. *et al.* NF-κB p50 and p52 expression is not required for RANK-expressing osteoclast progenitor formation but is essential for RANK- and cytokine-mediated osteoclastogenesis. *J. Bone Miner. Res.* **17**, 1200–1210 (2002).

ORIGINAL ARTICLE

JBMR®

NF-κB RelB Negatively Regulates Osteoblast Differentiation and Bone Formation

Zhenqiang Yao,[1,2] Yanyun Li,[1] Xiaoxiang Yin,[1] Yufeng Dong,[2] Lianping Xing,[1,2] and Brendan F Boyce[1,2]

[1]Department of Pathology and Laboratory Medicine, University of Rochester Medical Center, Rochester, NY, USA
[2]Center for Musculoskeletal Research, University of Rochester Medical Center, Rochester, NY, USA

ABSTRACT

RelA-mediated NF-κB canonical signaling promotes mesenchymal progenitor cell (MPC) proliferation, but inhibits differentiation of mature osteoblasts (OBs) and thus negatively regulates bone formation. Previous studies suggest that NF-κB RelB may also negatively regulate bone formation through noncanonical signaling, but they involved a complex knockout mouse model, and the molecular mechanisms involved were not investigated. Here, we report that RelB$^{-/-}$ mice develop age-related increased trabecular bone mass associated with increased bone formation. RelB$^{-/-}$ bone marrow stromal cells expanded faster in vitro and have enhanced OB differentiation associated with increased expression of the osteoblastogenic transcription factor, Runt-related transcription factor 2 (Runx2). In addition, RelB directly targeted the Runx2 promoter to inhibit its activation. Importantly, RelB$^{-/-}$ bone-derived MPCs formed bone more rapidly than wild-type cells after they were injected into a murine tibial bone defect model. Our findings indicate that RelB negatively regulates bone mass as mice age and limits bone formation in healing bone defects, suggesting that inhibition of RelB could reduce age-related bone loss and enhance bone repair. © 2014 American Society for Bone and Mineral Research.

KEY WORDS: RELB; NF-κB; MESENCHYMAL PROGENITOR CELLS; OSTEOBLASTS; BONE FORMATION

Introduction

Proinflammatory cytokines, such as receptor activator of NF-κB ligand (RANKL) and tumor necrosis factor (TNF), mediate bone destruction in common bone diseases, such as postmenopausal osteoporosis, rheumatoid arthritis, and periodontitis.[1] In these diseases, unlike in normal bone remodeling, bone formation by osteoblasts (OBs) does not match the bone lost,[1] resulting in localized and/or generalized bone loss. A role in bone for the NF-κB family of transcription factors, which includes NF-κB1 (p50 and its precursor p105), NF-κB2 (p52 and its precursor p100), RelA (p65), RelB, and c-Rel,[2] was first discovered when expression of both NF-κB1 and 2 was found unexpectedly to be required for osteoclast precursor (OCP) differentiation into osteoclasts (OCs).[3,4] Later it was discovered that they were required for RANKL-induced and TNF-induced OC formation.[5]

RANKL and TNF induce proteasomal processing of p105 to p50, which typically forms heterodimers with RelA to activate canonical NF-κB signaling.[2] RANKL, and to a much lesser extent TNF, activate noncanonical signaling in OCPs, leading to NF-κB–inducing kinase (NIK)-mediated processing of p100 to p52,[6] which typically forms heterodimers with RelB to activate noncanonical signaling and transcription of target genes. RelA promotes OC differentiation by blocking a RANKL-inducted apoptotic pathway in OCPs, but it is not involved in terminal OC differentiation.[7] RelB, in contrast, is not required for basal OC formation, but appears to play a role in the enhanced osteoclastogenesis observed in pathologic conditions such as osteolysis induced by metastatic cancer cells and inflammation.[8]

These previous studies have increased understanding of the role for NF-κB in OC formation and functions,[3–8] but the role of NF-κB signaling in bone formation is less well understood and the published data are conflicting. For example, several groups have shown that activation of canonical NF-κB signaling inhibits bone formation based on an inhibitory effect of TNF induction of p65 on OB differentiation.[9–12] Recently it was reported that inhibition of canonical signaling, specifically in mature OBs, by genetic manipulation results in a transient increase in bone mass in young mice.[13] Furthermore, the NF-κB inhibitor S1627 promotes murine calvarial defect repair and increased bone mineral density in ovariectomized mice,[14] providing additional evidence that canonical NF-κB signaling negatively regulates bone formation. However, several other groups reported that TNF-induced activation of canonical NF-κB signaling in mesenchymal progenitor cells (MPCs) promotes their differentiation into OBs[15–17] through bone morphogenic protein 2 (BMP-2)-mediated upregulation of Runt-related transcription factor 2 (Runx2) and Osterix (Osx) expression.[16] These findings indicate that there are complex interactions involving cytokines and canonical NF-κB signaling that can have positive or negative regulatory effects on OBs to influence bone mass depending

Received in original form April 14, 2013; revised form September 8, 2013; accepted September 19, 2013. Accepted manuscript online October 1, 2013.
Address correspondence to: Brendan F Boyce, MD, Department of Pathology and Laboratory Medicine, 601 Elmwood Ave, Box 626, Rochester, NY 14642, USA. E-mail: Brendan_Boyce@urmc.rochester.edu
Additional Supporting Information may be found in the online version of this article.
Journal of Bone and Mineral Research, Vol. 29, No. 4, April 2014, pp 866–877
DOI: 10.1002/jbmr.2108

upon the form of stimulation and the state of osteoblastic cell differentiation.

The role of noncanonical NF-κB signaling in bone formation has also been reported. For example, mice generated to have accumulation of a nonprocessable form of NF-κB2 p100 have enhanced osteoblastic differentiation,[18] and mice with deletion of p100, but retaining a functional p52, have osteopenia owing to increased OC activity and impaired OB parameters.[19] Interestingly, deletion of both RelB and p100 in the latter mice prevented the osteopenia in the $p100^{-/-}$ mice and actually increased bone mass accompanied by increased OB surfaces,[19] suggesting that an important role of RelB is to inhibit OB differentiation. However, these studies did not include reports of the OB phenotype of single $RelB^{-/-}$ mice and did not examine the molecular mechanisms whereby RelB regulates OB differentiation or function. We have found that bone mass increases in $RelB^{-/-}$ mice as they age owing to increased OB precursor proliferation associated with enhanced capacity of their MPCs to differentiate into OBs in vitro and to repair cortical bone defects in mice in vivo.

Subjects and Methods

Animals and reagents

$RelB^{+/-}$ and $RelB^{-/-}$ mice, including males and females for all experiments, on an inbred C57BL/6 background, were obtained from Dr. Mitchell Kronenberg and have been described.[20,21] Severe combined immunodeficiency (SCID) mice were purchased from Jackson Laboratory (Bar Harbor, ME, USA). The University of Rochester Medical Center Institutional Animal Care and Use Committee approved all animal studies. Labeled antibodies for fluorescence-activated cell sorting (FACS) (APC-CD45, PE-CD105, FITC-Sca-1) were purchased from eBioscience, San Diego, CA, USA. Ascorbic acid and β-glycerophosphate (β-GP) were purchased from Sigma, St. Louis, MO, USA. The 5-bromo-4-chloro-3-indolyl phosphate (BCIP)/4-nitro blue tetrazolium (NBT) alkaline phosphatase (ALP) substrate was purchased from ScyTek Laboratories, Logan, UT, USA. RelB antibody was purchased from Santa Cruz, Dallas, TX, USA.

OB differentiation

Bone marrow (BM) was flushed from long bones of mice with α modified essential medium (α-MEM) containing 20% fetal bovine serum (FBS) using a 25G needle. The cells were filtered with a 40-μm cell strainer, and 4×10^4 cells were cultured in 35-mm dishes at 37°C in 5% CO_2 for 4 days. Unattached cells were removed and replaced with 10% FBS in α-MEM containing 25 μg/mL L-ascorbic acid and 5 mM β-GP to induce OB differentiation. After 5 to 7 days in inducing medium, the cells were stained for ALP activity using the ALP substrate, BCIP/NBT. Mineralization typically occurs after 10 to 14 days in culture, and the cells were stained with the von Kossa method for measurement of mineralized nodule formation. Calvariae from 7-day-old wild-type (WT) and $RelB^{-/-}$ mice were cut into pieces and digested six times with a mixture of 0.5% collagenase I and 0.125% trypsin (both from Sigma) for 20 minutes at 37°C. Cells from the second to sixth digestions were collected for pre-OB cultures and OB differentiation experiments.

Generation of bone-derived MPCs

We cut mouse tibiae and femora into small pieces after BM had been flushed out and the cavities had been washed extensively with PBS using a modification of a previously described method.[22] The bone fragments were cultured for 4 days with α-MEM containing 20% FBS at 37°C. Bone pieces were transferred into a new dish and cultured for an additional 4 to 5 days with α-MEM containing 10% FBS. The cells grown on the dish were passaged twice when they were 90% confluent, each time excluding cells tightly attached to the dishes. Third-passage cells contained over 99% MPCs, sufficient for our experiments. We named these cells "bone-derived MPCs" (bMPCs) and they were frozen for use later in OB differentiation and mineralization experiments. mRNA expression levels of OB-related genes were tested using methods we described previously.[23]

FACS analysis

BM or cultured cells (2×10^6) were stained with APC-anti-CD45.2, PE-anti-CD105 and FITC-Sca-1 antibodies. For cell-cycle analysis, the collected bMPCs were incubated with 1 μM 4,6-diamidino-2-phenylindole (DAPI) with PBS containing 2% FBS for 20 minutes at 37°C. Data were acquired using a FACScanto (BM Bioscience, San Jose, CA, USA) flow cytometer and analyzed using FlowJo software (Ashland, OR, USA), as described.[24]

Micro–computed tomography and bone histomorphometric analysis

Mice were given injections of calcein (10 mg/kg) at 5 days and 1 day before euthanasia in a standard bone formation double-labeling protocol. Right tibiae were fixed in 10% neutral buffered formalin and micro–computed tomography (μCT) scanning using a VivaCT 40 mCT scanner (Scanco, Brüttisellen, Switzerland) was performed following guidelines for assessment of bone microstructure in rodents using μCT.[25] The bones were then processed through graded alcohols and embedded in plastic, and dynamic and static parameters of bone formation were assessed, according to standard methods using OsteoMeasure software (OsteoMetrics, Decatur, GA, USA). Left tibiae were fixed in 10% neutral buffered formalin for 2 days, decalcified in 10% EDTA for 3 weeks, and the bones were then processed and embedded in paraffin. Sections (4-μm-thick) were stained with hematoxylin and eosin (H&E) for analysis of bone volume, OB surface, and tartrate-resistant acid phosphatase–positive (TRAP +) OCs using OsteoMeasure software.

Tibial bone defects

A 2-mm × 5-mm full-thickness cortical defect was made on the anterior surface of the left and right tibiae of SCID mice. Briefly, a hole was pierced through the cortex ~1 mm below the growth plate using a 25G needle. Scissors were then inserted into the hole and a 2-mm × 5-mm defect was created by repeatedly cutting distally through the cortex. The defects were then almost completely filled with decalcified trabecular bone matrix, which had been extracted from bovine femoral necks using the following serial processing: 20% H_2O_2 for 2 days, 5 mmol Sodium Azide (NaN3) overnight, 1 mol NaOH containing 1% Triton X-100 overnight, methanol/chloroform (1:1) for 24 hours, ether overnight, and 10% EDTA for 2 weeks. bMPCs (5×10^5) in 5 μL of Hank's solution were then injected into the bone matrix in the defects. The muscle fascia and skin overlying the defects were then sutured closed. Mice were euthanized 2, 4, and 8 weeks postsurgery, and the tibiae were fixed in 10% neutral buffered formalin for 2 days. The volume of new bone formed in the defects was measured using a VivaCT 40 μCT scanner (Scanco, Brüttisellen, Switzerland). The bones were then processed

through alcohols, decalcified, and embedded in paraffin. The volume of newly formed bone and fibrous tissue was quantified in H&E-stained sections using OsteoMeasure software.

Quantitative real-time PCR

Total RNA was extracted from cultured cells using 1 mL TRIzol reagent, and 1 μg was used for synthesis of cDNA using a GeneAmp RNA PCR core kit. Quantitative PCR amplification was performed using an iCycler (Bio-Rad, San Diego, CA, USA) real-time PCR machine and iQ SYBR (Bio-Rad) Green. Relative mRNA expression levels of target genes were analyzed using the threshold cycle (C_T) value of the gene, normalized to β-actin.

Reporter constructs/luciferase assay

To clone the 5′ upstream region of the mouse Runx2 gene, 1997-bp (2-kb) fragments in the Runx2 promoter region were amplified by PCR from C57Bl6 mouse DNA extracted from bMPCs. The specific forward primer was: 5′-GTATTTCTGTGG-TTTTGTCATTAAAACT-3′, and the reverse primer was: 5′-AGAAAGTTTGCACCGCACTT-3′ overlapping the putative transcriptional start site (Fig. 5*B*). The 2-kb promoter was found with TFSEARCH software to contain two putative NF-κB binding sites. Overhangs containing the Kpn I restriction site were added to the forward primer and an overhang containing the Xho I site was added to the reverse primer at the 5′ end. PCR products were then subcloned into the pCRII TOPO vector (Invitrogen, Grand Island, NY, USA) and sequences were verified before their transfer into the Kpn I/Xho I backbone of pGL3-basic (Promega, Madison, WI, USA) driving the firefly Luciferase (Luc) gene. The Runx2 Luc reporter plasmid was cotransfected with either green fluorescent protein (GFP) control or RelB plasmid into C2C12 cells using a FuGene6 reagent (Roche, Indianapolis, IN, USA). A 0.1-μg aliquot of the SV40-Renilla Luc construct (Addgene, Cambridge, MA, USA) was also cotransfected with the above firefly reporters to standardize results for transfection efficiency. Cell lysates were prepared using a reporter lysis buffer (Promega). Luciferase activity was measured using a Microplate Luminometer (PerkinElmer, Waltham, MA, USA).

To perform site-directed mutagenesis of both κB binding sites in Runx2 promoter, two pairs of primers mRunx2-1fw 5′-AATATTT GTAAAGGACCCAGGCTAACACTT, mRunx2-1rv 5′-AAGTGTTAGCC TGGGTCCTTTACAAATATT; and mRunx2-2fw 5′-AGGAGAGAC-AGAGGACCCATAAGTAAAGAG, mRunx2-2rv 5′-CTCTTTACTTATG GGTCCTCTGTC-TCTCCT were designed using an Invitrogen software program and the GENEART Site-Directed Mutagenesis System (Invitrogen) was used to delete "ABC" and "ACA" in the 1 and 2 binding sites following the instruction manual. We followed this procedure to test the role of RelB on the mutated Runx2 promoter.

Chromatin immunoprecipitation

Chromatin immunoprecipitation (ChIP) was performed using a MAGnify ChIP kit (Invitrogen) following the instruction manual. Briefly, sheared chromatin from WT and RelB$^{-/-}$ bMPCs that had been fixed with 1% formaldehyde was immunoprecipitated with 5 μg of antibody to RelB, negative control rabbit immunoglobulin G (IgG) (Santa Cruz), or positive control H3 histone (Cell Signaling, Danvers, MA, USA). Immunoprecipitated DNA was then used as a template for quantitative PCR using primers specific for the NF-κB binding sites 1 (forward 5′-tcaactacacagc-catgatt and reverse 5′-taagcttggggatctgtaac) or 2 (forward 5′-cttctgaatgccaggaaggc and reverse 5′-tgggactgcctaccactgt) of the Runx2 promoter as well as a pair of unrelated primers (forward 5′-cactgctgactgaaacaagtc and reverse 5′-agtctgagt-gagcttcctgat) designed in the region that is 3 kb apart from the κB binding sites.

ELISA assay

Mouse serum osteocalcin (MyBioSource, San Diego, CA, USA) levels were assessed according to the manufacturer's instructions.

Statistics

All results are given as mean ± SD. Comparisons between two groups were analyzed using two-tailed unpaired Student's *t* test. One-way ANOVA and Dunnett's post hoc multiple comparisons were used for comparisons among three or more groups. Values of $p < 0.05$ were considered statistically significant.

Results

RelB$^{-/-}$ mice develop increased trabecular bone volume as they age

To fully investigate the role of RelB in bone remodeling, we analyzed the bone phenotype of RelB$^{-/-}$ mice of various ages. Consistent with a previous report that young RelB$^{-/-}$ mice do not appear to have a significant bone phenotype,[8] we found that 4-week-old RelB$^{-/-}$ mice have normal trabecular bone volume, as assessed by histomorphometric analysis (Fig. 1*A*). However, mean diaphyseal trabecular bone volume values in 6- to 8-week-old RelB$^{-/-}$ mice were double those of WT littermates. Importantly, their mean metaphyseal bone volumes remained within the normal range, similar to those of littermates (Fig. 1*A*), suggesting that OC function in the RelB$^{-/-}$ mice is normal. Furthermore, when the RelB$^{-/-}$ mice were 10 to 14 weeks old, their mean diaphyseal bone volumes had increased further to fourfold higher than those in WT littermates, whereas their mean metaphyseal bone volumes still remained within the normal range (Fig. 1*A*). These histomorphometric findings were confirmed by μCT when the mice were 10 to 14 weeks old (Fig. 1*B*), which showed that the increased bone mass was associated with increased trabecular number (Fig. 1*B*, $p < 0.01$), but not thickness. Ten- to 14-week-old RelB$^{-/-}$ mice also had increased vertebral trabecular bone volume associated with increased trabecular number, but not thickness, as assessed by μCT analysis (Fig. 1*C*), indicating that their increased bone mass was not restricted to diaphyseal bone. Interestingly, however, the RelB$^{-/-}$ mice had normal cortical thickness, and periosteal and endosteal surface areas of the cortical bone in the RelB$^{-/-}$ mice were also similar to that of the WT littermates (Fig. 1*D*).

RelB$^{-/-}$ mice have a transient increase in bone formation

The increased diaphyseal and vertebral trabecular bone observed in the RelB$^{-/-}$ mice as they aged could be caused by impaired OC and/or enhanced OB differentiation and function. We confirmed that metaphyseal OC numbers and surfaces are normal in young RelB$^{-/-}$ mice[8] (data not shown) and they remained similar to those in WT control mice in the metaphyseal bone as they aged to 8 weeks old (data not shown). However, in the proximal diaphyses of RelB$^{-/-}$ mice OC surfaces

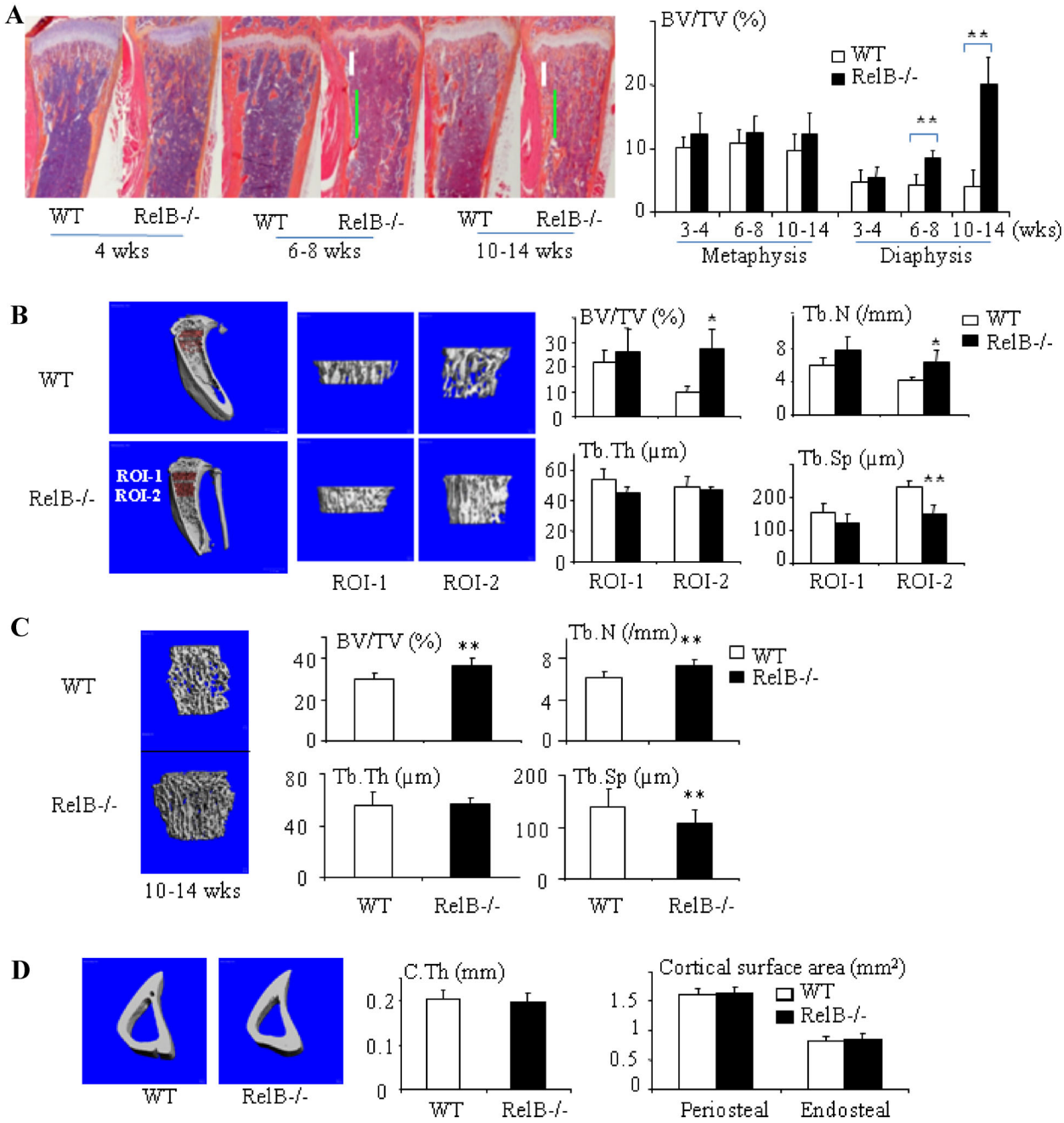

Fig. 1. Trabecular bone mass increases in RelB$^{-/-}$ mice as they age. (*A*) H&E-stained sections of tibiae from WT and RelB$^{-/-}$ mice and histomorphometric data showing trabecular BV/TV in the tibial metaphyses (area corresponding to the position of the white bar) and proximal diaphysis (vertical green bar) of 4- to 14-week-old mice. $n = 5$–8 mice/group. Metaphyseal bone (corresponding to ROI-1 of μCT) was defined as a 0.3-mm region along the long axis of the tibia beginning at 0.15 mm from the growth plate. Proximal diaphysis (corresponding to ROI-2 of μCT) was defined as a 0.6-mm region under ROI-1. (*B*) Representative μCT scans and BV/TV, Tb.N, Tb.Th, and Tb.Sp in the metaphysis (ROI-1) and in the proximal part of the diaphysis (ROI-2) of tibiae from 10-to 14-week-old mice. $n = 5$–8 mice/group. (*C*) μCT scans and data from fourth lumbar vertebrae from 10- to 14-week-old mice. $n = 10$ mice/group. (*D*) μCT scans and data from cortical bone at the junction between ROI-1 and ROI-2 from mice in *B*. All groups contained male and female mice. $^{*}p < 0.05$; $^{**}p < 0.01$ versus control. H&E = hematoxylin and eosin; WT = wild-type; BV/TV = bone volume/tissue volume; ROI = region of interest; μCT = micro–computed tomography; Tb.N = trabecular number; Tb.Th = trabecular thickness; Tb.Sp = trabecular separation.

were increased (15.6% ± 7.3% versus 7.8% ± 3.6% in WT littermates, $p < 0.05$), whereas OC numbers were not, presumably reflecting the increased bone mass in the RelB$^{-/-}$ mice. In fact, RelB regulation of OC differentiation is complicated. We found that RelB$^{-/-}$ mice have threefold to fivefold increase in monocyte-macrophages in their blood, BM, and spleen, and that sorted CD11b^{-}Gr-1^{-} BM cells from RelB$^{-/-}$ mice have significantly enhanced OC differentiation, but their

$CD11b^{+}Gr\text{-}1^{-/lo+}$ BM cells, the generally recognized OC precursors,[24] did not form OCs in response to RANKL and macrophage colony-stimulating factor (M-CSF) in in vitro culture (data not shown). Because the increased trabecular bone volume in $RelB^{-/-}$ mice is not associated with unresorbed islands of cartilage inside trabeculae, which is typically seen in osteopetrosis,[26,27] we concluded that the increased diaphyseal and vertebral bone mass likely resulted from enhanced OB formation or activity, as has been reported in RelB/p100 double knockout mice.[19] Indeed, mean values for OB and mineralizing surfaces and bone formation rates (BFR) in the trabecular bone in the diaphyses of 4-week-old $RelB^{-/-}$ mice are significantly higher than those in WT littermates (Fig. 2*A*, *B*). Surprisingly, however, mean values for OB surface and BFRs were reduced significantly in the tibial diaphyseal bone in older (8- to 9-week-old) $RelB^{-/-}$ mice (Fig. 2*C*), indicating that the increase in bone formation in the $RelB^{-/-}$ mice is transient. Consistent with this, serum osteocalcin levels were significantly increased in younger, but not in older $RelB^{-/-}$ mice (Fig. 2*D*), and mRNA levels of ALP, Runx2, RANKL and osteoprotegerin (OPG) were similar in femoral bone samples from 9-week-old $RelB^{-/-}$ and WT mice, wheras the osteocalcin mRNA levels were only slightly increased (Supplemental Fig. 1).

Murine MPCs have been defined as $CD45^{-}CD105^{+}$ cells,[28] and we have reported that $CD45^{-}$cells can be used as mesenchymal stem cell–enriched cells.[29] We found that $RelB^{-/-}$ and WT mice have similar numbers of $CD45^{-}CD105^{+}$ cells in freshly isolated BM from tibiae and femora (Fig. 3*A*, upper). However, these BM cells from $RelB^{-/-}$ mice generated twofold more $CD45^{-}CD105^{+}$ MPCs than WT cells 7 days after equal numbers of each were placed in culture dishes (Fig. 3*A*, lower), indicating that $RelB^{-/-}$ MPCs expanded faster in vitro. This was associated with formation of more ALP+ colonies and mineralized nodules (Fig. 3*B*) from the $RelB^{-/-}$ BM cell cultures and a 3-fold and 1.5-fold increase in osteocalcin and ALP mRNA expression levels (Fig. 3*C*) at day 10, respectively, compared to WT cells, consistent with the enhanced OB generation and function in the $RelB^{-/-}$ mice. The enhanced OB proliferation and differentiation persisted in BM cells cultured from 3-month-old $RelB^{-/-}$ mice, despite the reduced BFR in vivo. $RelB^{-/-}$ BM stromal cells formed threefold more ALP+ cell colonies than WT cells at day 7, but ALP mRNA expression levels were similar at day 6. This may reflect the fact that the increased numbers of ALP+ cells from $RelB^{-/-}$ stromal cells were mainly due to their faster expansion at an earlier stage of differentiation, as shown in Fig. 3*A*.

To determine if the enhanced differentiation of $RelB^{-/-}$ BM stromal cells contributed to the increased ALP+ colony numbers and mineralized nodule formation, we generated BM stromal cells, reseeded them onto culture plates, and induced OB differentiation when they were subconfluent to exclude the influence of proliferation. These reseeded stromal cells still had increased ALP+ cell formation (Fig. 3*D*), confirming their enhanced differentiation. Furthermore, we generated calvarial pre-OBs from 7-day-old WT and $RelB^{-/-}$ pups and found that $RelB^{-/-}$ calvarial pre-OBs also have enhanced ALP+ cell differentiation at day 10, but not after 5 days of induction of

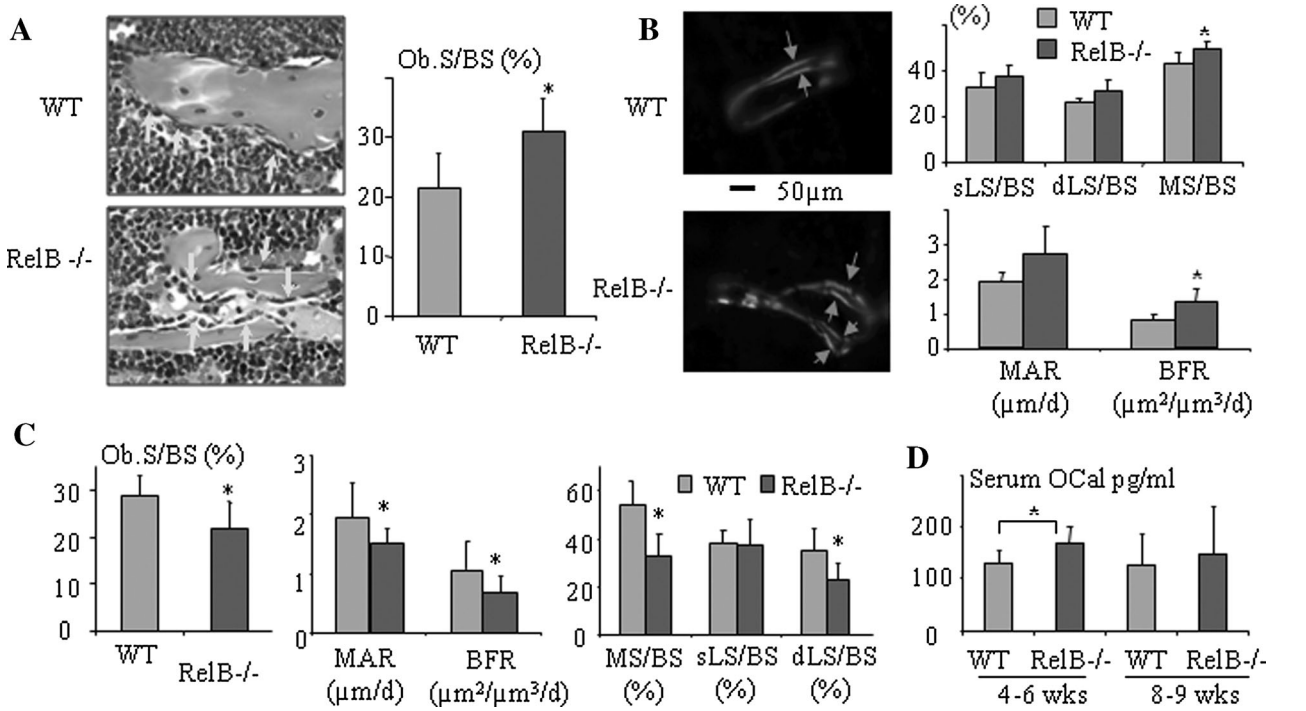

Fig. 2. $RelB^{-/-}$ mice have a transient increase in bone formation. (*A*) Histology and histomorphometric analysis of OBs (arrows) and Ob.S/BS (%) in the tibiae of 4-week-old $RelB^{-/-}$ mice and WT littermates ($n = 7$/group). (*B*) Double calcein labeling (arrows) in trabeculae in proximal tibial diaphyses corresponding to ROI-2 in Fig. 1 and analysis of dynamic parameters of bone formation: sLS/BS, dLS/BS, MS/BS, MAR, and BFR in 4-week-old $RelB^{-/-}$ and WT mice ($n = 8$/group). (*C*) Analysis of dynamic parameters of bone formation listed in *B* and Ob.S/BS in proximal tibial diaphyses of 7- to 8-week-old $RelB^{-/-}$ and WT mice ($n = 5$–6/group). (*D*) OCal levels from 4- to 5-week-old ($n = 9$) and 8- to 9-week-old ($n = 8$) male and female WT and $RelB^{-/-}$ mice tested by ELISA. OB = osteoblast; Ob.S/BS = osteoblast surface; WT = wild-type; ROI = region of interest; sLS/BS = single-labeled surface; dLS/BS = double-labeled surface; MS/BS = mineralization surface; MAR = mineral apposition rate; BFR = bone formation rate; OCal = osteocalcin.

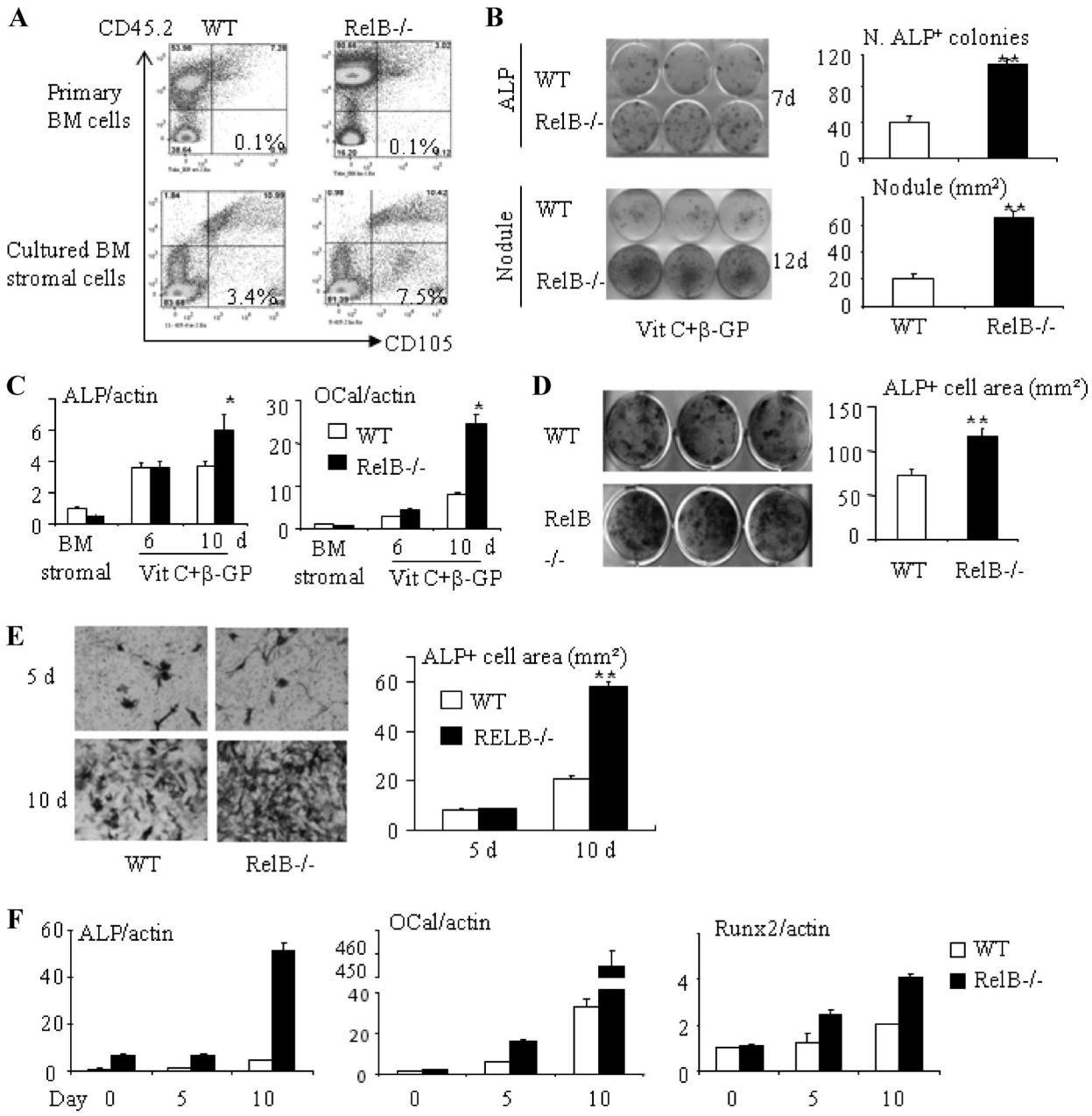

Fig. 3. RelB$^{-/-}$ mice have enhanced stromal cell proliferation and OB differentiation in vitro. (*A*) FACS analysis showing the % of CD45^{-}CD105^{+} MPCs in freshly isolated BM cells from 2-month-old WT and RelB$^{-/-}$ mice and BM stromal cells from the mice after being cultured for 7 days with growth-inducing medium. (*B*) Equal numbers of freshly isolated BM cells from 2 month-old RelB$^{-/-}$ and WT mice were cultured in OB differentiation medium containing 25 μg/mL Vit C and 5 mM β-GP for 7 and 12 days. ALP^{+} cells colonies (upper panel) and mineralized nodules (lower panel) were evaluated after ALP and von Kossa staining. (*C*) Expression of ALP and OCal was tested using real-time PCR in BM stromal cells and in differentiating OBs induced by Vit C and β-GP after 6 and 10 days of culture. (*D*) BM stromal cells generated from WT and RelB$^{-/-}$ mice were reseeded in 12-well plates. After the cells were subconfluent, they were induced for OB differentiation for 5 days and stained for ALP activity. (*E*) Calvarial pre-OBs generated from 7-day-old pups were cultured in OB differentiation medium for 5 and 10 days and stained for ALP activity. (*F*) Calvarial pre-OBs were cultured in OB differentiation medium for the indicated times, total RNA was extracted, and expression of ALP, OCal, and Runx2 mRNA was tested by real-time PCR. All mice in in vitro experiments were 1.5- to 2-month-old males or females except for those used for calvarial pre-OBss in E and *F*; 3 wells per group. $^{*}p < 0.05$ versus control. OB = osteoblast; FACS = fluorescence-activated cell sorting; MPC = mesenchymal progenitor cell; BM = bone marrow; WT = wild-type; Vit C = L-ascorbic acid; β-GP = β-glycerophosphate; ALP = alkaline phosphatase; OCal = osteocalcin; Runx2 = Runt-related transcription factor 2.

differentiation (Fig. 3*E*). Consistent with the findings in BM stromal cells, differentiating RelB$^{-/-}$ OBs from calvariae had significantly increased ALP, osteocalcin, and Runx2 mRNA expression, particularly at the later stage of differentiation (day 10; Fig. 3*F*).

RelB negatively regulates OB differentiation, associated with reduced Runx2 activity

Primary BM stromal cell cultures contain variable numbers of hematopoietic cells, including monocyte-macrophages,[30] which could influence stromal cell differentiation. To minimize this possibility, we employed a recently described method[22] in which bMPCs are used to study MPC differentiation. We confirmed that almost 100% of these cells from WT and RelB$^{-/-}$ long bones were of mesenchymal origin (ie, CD45–cells; Fig. 4*A*, left), and more than 90% of these cells expressed the stem cell marker, Sca-1 (Fig. 4*A*, right). These RelB$^{-/-}$ bMPCs grew faster than WT cells (Fig. 4*B*). Consistent with this, cell-cycle analysis using FACS (Fig. 4*C*) showed that the percentage of MPCs undergoing basal proliferation (S and G2/M phase cells) was higher in RelB$^{-/-}$ than in WT cells (36.3% versus 29.5%, $p < 0.05$) and they formed significantly more ALP+ cells (Fig. 4*D*), similar to primary BM stromal and calvarial cell cultures. Of note, the ratio of ALP+ cells to total cells was threefold higher in RelB$^{-/-}$ bMPCs cultures than in WT cells (Fig. 4*D*), indicating that RelB$^{-/-}$ bMPCs have enhanced OB differentiation. Importantly and consistently, RelB$^{-/-}$ bMPCs have significantly increased mineralized nodule formation (Fig. 4*E*) and increased expression of ALP and osteocalcin during their differentiation (Fig. 4*F*).

Runx2 and Osx are two critical transcription factors for OB differentiation and maturation. Osx is a downstream target of Runx2 and regulates expansion of an early osteoblastic pool derived from MPCs.[31,32] Runx2 is required for commitment of mesenchymal osteochondroprogenitors to the osteoblastic lineage and OB differentiation during both endochondral and intramembranous ossification.[33] We found that differentiated RelB$^{-/-}$ stromal cells have threefold higher Runx2 (Fig. 5*A*, left) and fourfold higher Osx (data not shown) mRNA expression levels than WT cells. Although the endogenous Runx2 protein level is low in osteoblastic cells,[23] we observed an increased Runx2 protein in the differentiating RelB$^{-/-}$ stromal cells compared to the WT cells tested by Western blot (Fig. 5*A*, right). Sequence analysis with TFSEARCH software showed that the mouse Runx2 promoter contains two putative NF-κB binding sites, at –653/–644 and –1262/–1253 (Fig. 5*B*). We constructed a 2-kb mouse Runx2 promoter Luc reporter, which contains two putative NF-κB binding sites (Fig. 5*B*). We then cotransfected the Runx2 Luc reporter with RelB plasmids into C2C12 preosteoblastic cells, and found that RelB dose-dependently inhibited Runx2 Luc activity (Fig. 5*C*). We performed the site-directed mutagenesis of both κB binding sites in the promoter by deleting "ATC" and "ACA" in binding sites 1 and 2, which was confirmed by sequencing. Then, using the mutated Runx2 reporter we found that RelB did not affect the Luc activity of the mutated Runx2 promoter reporter (Fig. 5*D*), confirming that RelB does indeed regulate Runx2 activity via κB binding sites.

To further test if RelB directly binds to the putative κB binding sites of the Runx2 promoter, we performed ChIP assays using WT and RelB$^{-/-}$ MPCs. As shown in Fig. 5*E*, immunoprecipitation of both binding sites with anti-RelB antibody followed by qPCR with specific primers for each of the putative binding sites yielded distinct enrichment in WT MPCs over the input chromatin compared to that of an IgG negative control antibody (Fig. 5*E*). No chromatin enrichment by the RelB antibody was observed in RelB$^{-/-}$ MPCs, indicating specific binding of RelB protein to the Runx2 promoter. Importantly, a Runx2 short-hairpin RNA (shRNA) abolished the enhanced OB differentiation by RelB$^{-/-}$ MPCs (Fig. 5*F*).

RelB$^{-/-}$ MPCs induce bone formation and repair in tibial bone defects more rapidly than WT MPCs

To test if RelB$^{-/-}$ MPCs have enhanced bone forming potential in vivo, we made 5-mm × 2-mm cortical defects in the anterior tibiae of SCID mice. We filled the defects with decalcified bovine bone matrix (DBM), which is used commonly to fill bone defects and stimulate bone formation. bMPCs from RelB$^{-/-}$ and WT littermates were then injected into the DBM in the left and right tibiae, respectively. We found that the defects injected with RelB$^{-/-}$ bMPCs had significantly more new bone formation than those injected with WT cells, as assessed by μCT and histologic analysis, at 4 weeks posttransplantation (Fig. 6*A*, *B*). The volume of new bone formed from transplanted WT MPCs almost matched that formed by the RelB$^{-/-}$ cells at 8 weeks postsurgery. However, at 8 weeks postsurgery almost all the area around the new bone and surviving fragments of bone matrix implanted before the injection of RelB$^{-/-}$ MPCs had become filled with hematopoietic marrow, whereas this space in the defects injected with WT MPCs was still largely filled with immature fibrous tissue and unresorbed DBM (Fig. 6*B*), indicating that the transplanted RelB$^{-/-}$ MPCs induced accelerated bone repair and resorption of the DBM. In addition, by 8 weeks postsurgery, new bone containing live osteocytes and partly covered with a periosteum-like membrane extended along ~70% of the surface of the DBM particles injected with RelB$^{-/-}$ MPCs. In contrast, only ~20% of the surface of DBM injected with WT MPCs was covered by viable new bone and the remainder of the surface was covered by fibrous tissue, indicating a marked delay in the healing process (Fig. 6*C*).

Discussion

Here, we report that RelB$^{-/-}$ mice have increased trabecular bone volume in the diaphyses of their long bones and in their vertebral bodies as they age. The mice have relatively normal OC numbers and functions in vivo, but impaired RANKL-induced OC formation in vitro, similar to findings reported in RelB$^{-/-}$ mice by other investigators.[8] Importantly, the metaphyseal bone in the RelB$^{-/-}$ mice does not have the typical histologic features of osteopetrosis, such as increased trabecular bone volume with unresorbed islands of cartilage inside trabeculae.[26,27] In contrast, young RelB$^{-/-}$ mice have significantly increased OB surfaces and BFRs in tibial and vertebral bone sections, consistent with an enhanced OB phenotype being responsible for the increased bone mass observed when the mice are older. The RelB$^{-/-}$ mice have normal numbers of BM MPCs, indicating that RelB does not have a role in the maintenance of these progenitor cells or in their differentiation from mesenchymal stem cells, as it does along with p52 in the maintenance of hematopoietic stem cells.[34] However, RelB$^{-/-}$ MPCs derived from either BM or bone have enhanced commitment of pre-OBs and their subsequent proliferation, OB differentiation, and mineralization potential in vitro accompanied by increased expression of Runx2, suggesting that RelB negatively regulates their differentiation in part at least by limiting expression of

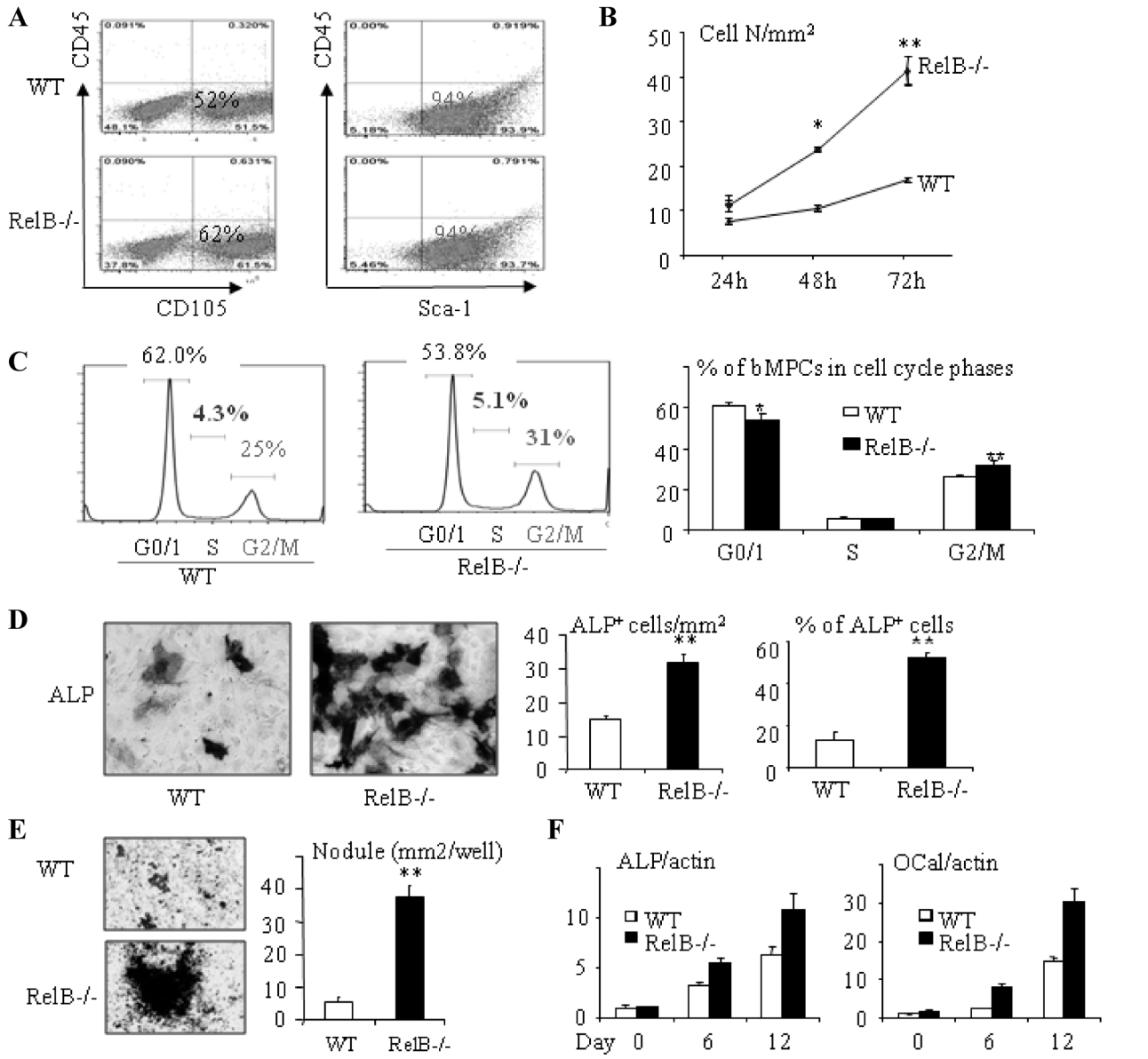

Fig. 4. RelB$^{-/-}$ bMPCs have enhanced proliferation and OB differentiation. (*A*) bMPCs generated from 8-week-old RelB$^{-/-}$ mice and WT littermates were analyzed by FACS using CD45, CD105, and Sca-1 antibodies. (*B*) A total of 2×10^4 bMPCs from WT and RelB$^{-/-}$ mice were seeded in 12-well plates for the indicated times. The cells were fixed with 10% formalin followed by H&E staining to count cell numbers (4 wells/time point). (*C*) Cultured bMPCs at 60% to 70% confluence were collected and incubated with DAPI (1 μg/mL). The cell cycle was analyzed by FACS; the data presented are from 3 pairs of mice. (*D*) bMPCs from RelB$^{-/-}$ and WT littermates were cultured in OB differentiation medium for 5 days and stained for ALP activity followed by eosin counterstaining. ALP+ and total cell numbers were counted and the ALP + /total cell ratio was calculated. (*E*) A total of 1×10^4 bMPCs were cultured in 12-well plates for 5 days to subconfluence, then OB differentiation medium was added for 21 days until nodules had formed. Von Kossa staining was performed to quantify nodule area. (*F*) bMPCs cultured in a 60-mm dish were induced for OB differentiation for the indicated times. Expression levels of ALP and OCal were tested using real-time PCR. All mice in in vitro experiments were 1.5- to 2-month-old males or females; 3 to 4 wells per group. $^*p < 0.05$; $^{**}p < 0.01$ versus control. bMPC = bone-derived mesenchymal progenitor cell; OB = osteoblast; WT = wild-type; FACS = fluorescence-activated cell sorting; H&E = hematoxylin and eosin; DAPI = 4,6-diamidino-2-phenylindole; ALP = alkaline phosphatase; OCal = osteocalcin.

this essential osteoblastogenic transcription factor. These findings suggest that RelB plays an important role to limit bone formation in the diaphysis, which could potentially reduce the strength of bone near the distal ends of long bones as mice and other mammals age, and increase the risk of fracture through them.

The role of Runx2 in the regulation of bone formation is complex. For example, it is required for commitment of progenitors to the OB lineage and for OB differentiation, but it also inhibits proliferation of MPCs and of mature OBs[33,35,36]; thus its presence reflects induction of differentiation of osteoblastic cells. We found that MPCs and neonatal calvarial

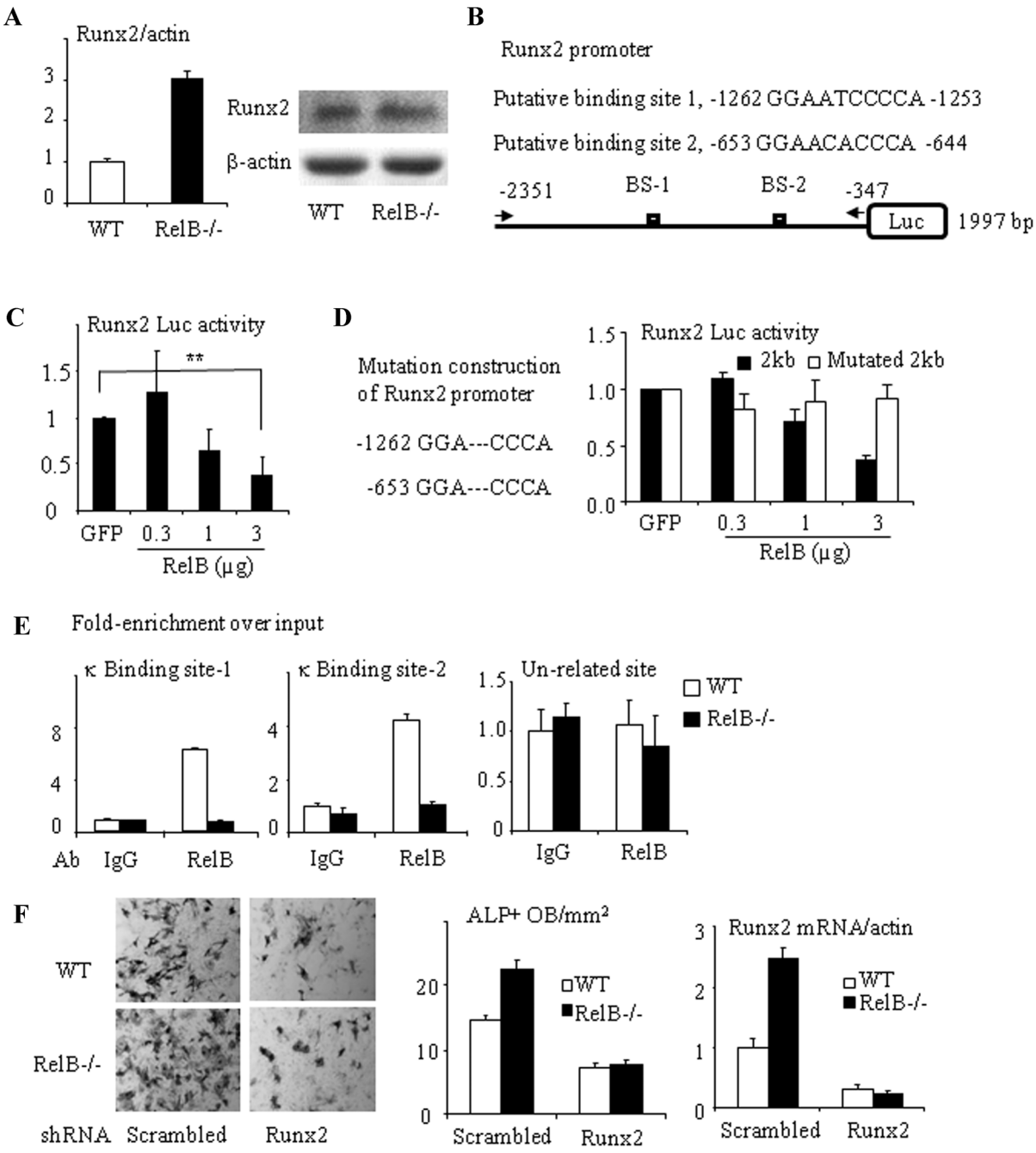

Fig. 5. RelB directly targets the Runx2 promoter and inhibits Runx2 expression. (*A*) mRNA (left panel) and protein (right panel) expression of Runx2 were tested by real-time PCR and Western blot from RelB$^{-/-}$ and WT BM stromal cells cultured with OB differentiation medium for 7 days. (*B*) Construction scheme of mouse Runx2 promoter Luc reporter. The 2-kb Runx2 promoter constructs contain two putative κB binding sites. (*C*) The 2-kb Runx2 promoter Luc reporter was cotransfected with RelB plasmid into C2C12 cells and the relative Luc activity was tested. (*D*) Site-directed mutagenesis of both κB binding sites 1 and 2 in the 2-kb Runx2 promoter was performed by deleting "ATC" and "ACA." A Luc activity assay was performed using C2C12 cells that were cotransfected with a RelB plasmid and the mutated Runx2 reporter. (*E*) ChIP assays were carried out using an anti-RelB or control IgG antibody on sheared chromatin from WT and RelB$^{-/-}$ MPCs. Immunoprecipitated DNA was analyzed by qPCR using primers covering either NF-κB binding sites 1 (left panel) or 2 (middle panel) in the Runx2 promoter region or a pair of unrelated primers (right panel) designed in the region that is 3 kb apart from the κB binding sites. Results are expressed as fold-enrichment compared with IgG normalized to input. (*F*) bMPCs from WT and RelB$^{-/-}$ mice were transfected with a scrambled or Runx2 mouse shRNA sequence for 2 days followed by puromycin selection to kill the uninfected cells. The cells were treated with OB differentiation medium for 5 days and stained for ALP activity to measure ALP+ cells (left and middle panel), and mRNA expression of Runx2 in these cells was tested by real-time PCR (right panel). All mice in in vitro experiments were 1.5- to 2-months-old. $^{*}p < 0.05$; $^{**}p < 0.01$ versus control. Runx2 = Runt-related transcription factor 2; WT = wild-type; BM = bone marrow; OB = osteoblast; Luc = luciferase; ChIP = chromatin immunoprecipitation; IgG = immunoglobulin G; MPC = mesenchymal progenitor cell; bMPC = bone-derived MPC; shRNA = short hairpin RNA; ALP = alkaline phosphatase.

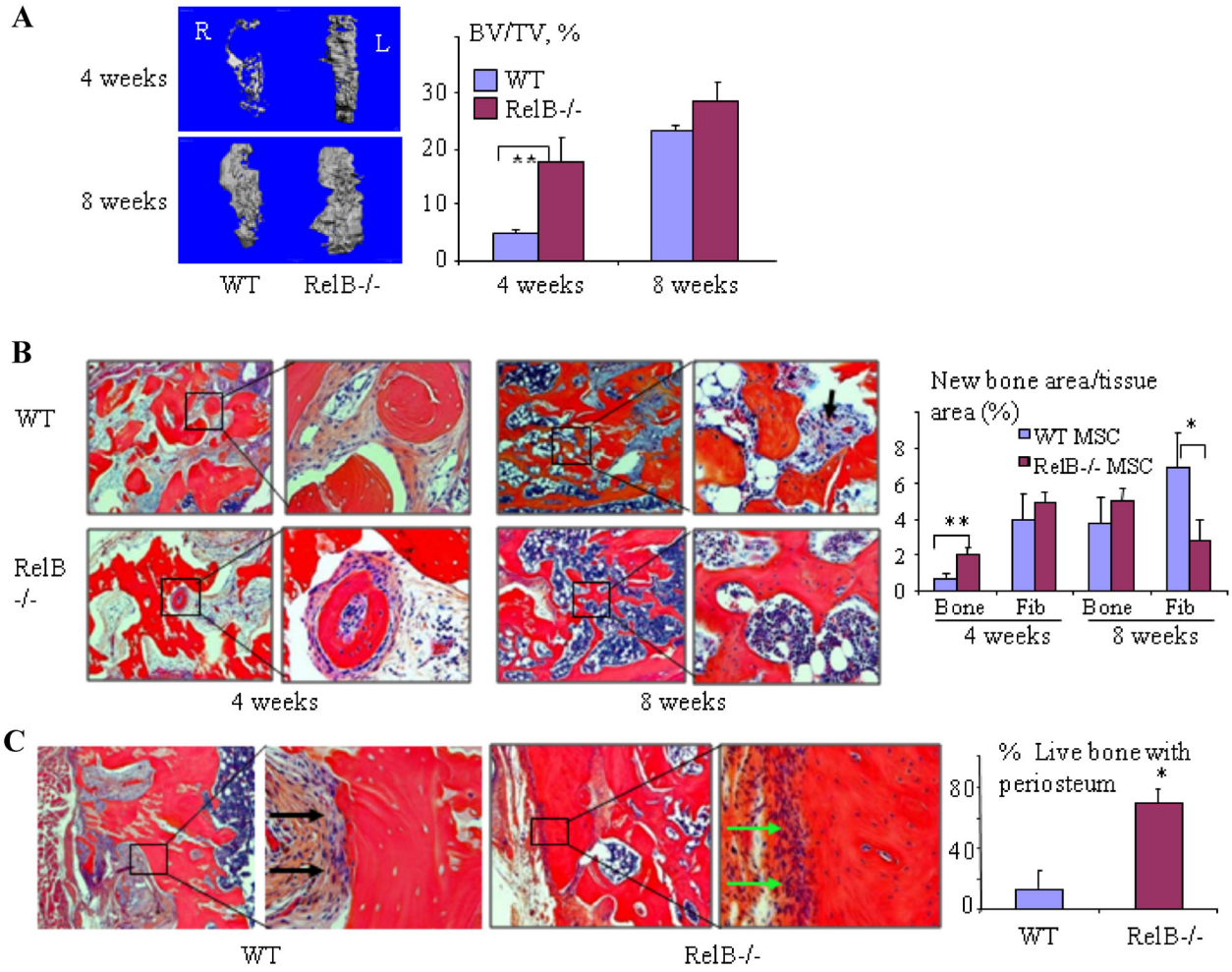

Fig. 6. RelB$^{-/-}$ MPCs induce bone formation and repair in tibial bone defects more rapidly than WT MPCs. Bilateral 2-mm × 5-mm cortical defects were made in the anterior proximal tibiae of SCID mice and filled with decalcified bovine bone matrix. A total of 5×10^5 bMPCs from 7-week-old RelB$^{-/-}$ and WT mice were injected into the bone matrix in the left and right tibial defects, respectively. The mice were euthanized 4 and 8 weeks postsurgery and the volume of new bone (BV/TV, expressed as a percentage of the total defect volume) formed in the defects was measured by μCT (*A*), followed by histomorphometric analysis of the area of newly formed trabecular bone (Trab) and fibrous tissue (Fib, black arrows) containing spindle-shaped fibroblast-like cells observed in decalcified H&E-stained sections of the bones (*B*). (*C*) Representative images of bone in the defect sites 8 weeks postsurgery, and the extent of new bone (with viable osteocytes and covered with a periosteum-like membrane, green arrow) formed on the DBM was quantified and expressed as a percentage of the total length of implanted DBM. The black arrow shows fibrous tissue covering the acellular DBM. $n = 5$/group. $^*p < 0.05$ versus control. MPC = mesenchymal progenitor cell; WT = wild-type; SCID = severe combined immunodeficiency; bMPC = bone-derived MPC; BV/TV = bone volume/tissue volume; μCT = micro–computed tomography; Trab = trabecular bone; Fib = fibrosis tissue; H&E = hematoxylin and eosin; DBM = decalcified bone matrix.

cells from RelB$^{-/-}$ mice have increased OB differentiation capacity and Runx2 mRNA expression levels (Figs. 3*F*, 5*A*) and that RelB inhibits Runx2 expression in osteoblastic cells by directly binding to κB binding sites in the Runx2 promoter. These findings suggest that by inhibiting Runx2 expression in MPCs, RelB plays an important contributory role to limit MPC proliferation and subsequent OB differentiation. In this way, RelB could limit trabecular bone formation in mice as they age. However, there are other possible mechanisms, including RelB regulation of expression of other genes that control proliferation, such as cyclin D1, p53, etc., and these will require further study.

The increase in bone formation rate and diaphyseal OB numbers in the RelB$^{-/-}$ mice is transient, indicating that the role of RelB in the regulation of OB differentiation and function is complex. This could reflect the fact that diaphyseal bone volume is not comparable between RelB$^{-/-}$ and WT mice as they age because very little trabecular bone remains in this region in WT mice. However, another possibility is that because RelB$^{-/-}$ mice develop multiorgan inflammation[21] and increased production of cytokines, such as TNF,[37] these could inhibit bone formation as the mice age. Importantly, BM cells from 3-month-old RelB$^{-/-}$ mice (which have reduced bone formation in vivo) have very significantly enhanced capacity to differentiate into ALP+ cells in vitro, suggesting that the reduced bone formation in older RelB$^{-/-}$ mice results from the effects of secondary factors. Further studies using mice with

tissue-specific deletion of RelB will be necessary to definitively address this issue.

Age-related bone loss is a major health problem associated with increased risk of fracture and morbidity and it will become more prevalent as the aging population increases. Thus, it is important to better understand the mechanisms that lead to loss of trabecular and cortical bone with aging so that novel therapeutic strategies can be developed to prevent it. Age-related osteoporosis is associated with so-called low-grade molecular inflammation induced by increased production of cytokines, including TNF, by immune cells and other cells as mice and humans age.[38–40] RelB could also play a role in this cytokine-associated bone loss with aging because it negatively regulates TNF expression.[37] Increased TNF production can lead to bone loss by a variety of mechanisms, including increased OC formation and activation, both directly[6] and indirectly,[41] and inhibition of OB differentiation and function.[9–11] Thus, increasing levels of cytokines, such as TNF, in blood and BM of RelB$^{-/-}$ mice could secondarily mediate inhibition of bone formation in the mice as they age and account for the decreased bone formation rate we observed in older mice. The enhanced differentiation of RelB$^{-/-}$ MPCs occurred in vitro in the absence of added TNF, and importantly, RelB$^{-/-}$ MPCs injected into tibial cortical bone defects experienced the same cytokine microenvironment as WT MPCs in recipient SCID mice, but they induced more bone formation in the defects, suggesting they have intrinsically enhanced OB differentiation.

Transplanted DBM, similar to allograft bone, is osteoinductive,[42] and likely undergoes creeping substitution, with new bone forming on it as bone defects are repaired. Once formed, new bone and some of the DBM to which it attaches is continually remodeled, but DBM typically is not fully resorbed even at 42 weeks after surgery.[43] Thus, although it is hard to predict when transplanted DBM will be resorbed completely to allow restoration of normal cortical structure in tibial cortical defects, the presence of new bone forming on and around DBM would be indicative of healing. Our observation that by 8 weeks after transplantation, 70% of the surface of DBM in defects injected with RelB$^{-/-}$ MPCs was covered by newly-formed viable bone compared with only ~20% of the surface of DBM injected with WT MPCs further supports an important negative regulatory role for RelB in bone defect repair. In addition to directly differentiating into bone tissue, donor MPCs injected into bone defects also produce cytokines and chemokines, which can recruit host MPCs, promote angiogenesis and cellular migration, and inhibit apoptosis,[44–46] to enhance tissue repair. Further studies will be required to determine how much of the new bone formed in the tibial bone defects in the SCID mice was derived directly from RelB$^{-/-}$ MSCs and if and how these injected MPCs recruited host MPCs or promoted angiogenesis and callus remodeling to enhance bone repair.

Interestingly, cortical thickness as well as the periosteal and endosteal surface area did not increase in the RelB$^{-/-}$ mice as they aged. This may explain why vertebral bodies from 10- to 14-month-old mice did not have increased biomechanical properties when we tested them ex vivo (data not shown). We do not have an explanation for this differential role for RelB in trabecular versus cortical bone, but we did not observe an increase in BFRs on the endosteal bone surfaces of the RelB$^{-/-}$ mice (data not shown) as we did on their trabecular surfaces. That OBs on trabecular and cortical bone surfaces may be regulated differentially is supported by a recent study reporting the in vivo effects of a peptide that inhibits OC formation by binding to RANKL[47]; it increased cortical, but not trabecular bone formation and mass in mice by activating Smad1/5/8 and working synergistically with BMP-2 signaling in osteoblasts to enhance OB differentiation and matrix mineralization.[47] Another study reported that TRAF family-member-associated NF-κB activator (TANK)-deficient mice have increased cortical bone mineral density and thickness, but trabecular osteopenia,[48] providing further support that signaling in trabecular and cortical OBs can be regulated differentially.

In summary, our findings indicate that RelB inhibits OB differentiation and bone formation directly, associated with reduced Runx2 activation, and contributes to age-related bone loss in mice. The enhanced bone formation in RelB$^{-/-}$ mice and from RelB$^{-/-}$ MPCs transplanted into SCID mice suggests that strategies to reduce or inhibit RelB functions in MPCs should increase bone mass and enhance repair of bone defects and possibly also of fractures.

Disclosures

All authors state that they have no conflicts of interest.

Acknowledgments

Research reported in this publication was supported by the National Institute of Arthritis and Musculoskeletal and Skin Diseases of the National Institutes of Health under Award Number AR43510 to B.F.B, AR48697 to L.X., P30AR061307 to E.S. (and a pilot grant to Z.Y. from P30AR061307), and grant number 1S10RR027340 to B.F.B. from the NIH. We thank Michael Thullen for help with μCT scanning and analysis. The content is solely the responsibility of the authors and does not necessarily represent the official views of the National Institutes of Health.

Authors' roles: Study design: ZY, BFB. Study conduct and data collection: ZY, YL, XY, YD. Data analysis and interpretation: ZY, LX and BFB. Manuscript preparation: ZY, LX and BFB. All authors approved final version of manuscript: ZY and BFB take responsibility for the integrity of the data analysis.

References

1. Mundy GR. Osteoporosis and inflammation. Nutr Rev. 2007;65(12 Pt 2):S147–51.
2. Vallabhapurapu S, Karin M. Regulation and function of NF-kappaB transcription factors in the immune system. Annu Rev Immunol. 2009;27:693–733.
3. Franzoso G, Carlson L, Xing L, et al. Requirement for NF-kappaB in osteoclast and B-cell development. Genes Dev. 1997;11(24):3482–96.
4. Iotsova V, Caamaño J, Loy J, Yang Y, Lewin A, Bravo R. Osteopetrosis in mice lacking NF-kappaB1 and NF-kappaB2. Nat Med. 1997;3(11):1285–9.
5. Yamashita T, Yao Z, Li F, et al. NF-kappaB p50 and p52 regulate receptor activator of NF-kappaB ligand (RANKL) and tumor necrosis factor-induced osteoclast precursor differentiation by activating c-Fos and NFATc1. J Biol Chem. 2007;282(25):18245–53.
6. Yao Z, Xing L, Boyce BF. NF-kappaB p100 limits TNF-induced bone resorption in mice by a TRAF3-dependent mechanism. J Clin Invest. 2009;119(10):3024–34.
7. Vaira S, Alhawagri M, Anwisye I, et al. RelA/p65 promotes osteoclast differentiation by blocking a RANKL-induced apoptotic JNK pathway in mice. J Clin Invest. 2008;118(6):2088–97.
8. Vaira S, Johnson T, Hirbe AC, et al. RelB is the NF-kappaB subunit downstream of NIK responsible for osteoclast differentiation. Proc Natl Acad Sci U S.A. 2008;105(10):3897–902.

9. Li Y, Li A, Strait K, et al. Endogenous TNF alpha lowers maximum peak bone mass and inhibits osteoblastic Smad activation through NF-kappaB. J Bone Miner Res. 2007;22(5):646–55.
10. Gilbert LC, Rubin J, Nanes MS. The p55 TNF receptor mediates TNF inhibition of osteoblast differentiation independently of apoptosis. Am J Physiol Endocrinol Metab. 2005;288(5):E1011–8.
11. Yamazaki M, Fukushima H, Shin M, et al. Tumor necrosis factor alpha represses bone morphogenetic protein (BMP) signaling by interfering with the DNA binding of Smads through the activation of NF-kappaB. J Biol Chem. 2009;284(51):35987–95.
12. Gilbert L, He X, Farmer P, et al. Expression of the osteoblast differentiation factor RUNX2 (Cbfa1/AML3/Pebp2alpha A) is inhibited by tumor necrosis factor-alpha. J Biol Chem. 2002;277(4):2695–701.
13. Chang J, Wang Z, Tang E, et al. Inhibition of osteoblastic bone formation by nuclear factor-kappaB. Nat Med. 2009;15(6):682–9.
14. Alles N, Soysa NS, Hayashi J, et al. Suppression of NF-κB increases bone formation and ameliorates osteopenia in ovariectomized mice. Endocrinology. 2010;151(10):4626–34.
15. Cho HH, Shin KK, Kim YJ, et al. NF-kappaB activation stimulates osteogenic differentiation of mesenchymal stem cells derived from human adipose tissue by increasing TAZ expression. J Cell Physiol. 2010;223(1):168–77.
16. Hess K, Ushmorov A, Fiedler J, et al. TNF alpha promotes osteogenic differentiation of human mesenchymal stem cells by triggering the NF-kappaB signaling pathway. Bone. 2009;45(2):367–76.
17. Lencel P, Delplace S, Hardouin P, Magne D. TNF-α stimulates alkaline phosphatase and mineralization through PPARγ inhibition in human osteoblasts. Bone. 2011;48(2):242–9.
18. Seo Y, Fukushima H, Maruyama T, et al. Accumulation of p100, a precursor of NF-κB2, enhances osteoblastic differentiation in vitro and bone formation in vivo in aly/aly mice. Mol Endocrinol. 2012;26(3):414–22.
19. Soysa NS, Alles N, Weih D, et al. The pivotal role of the alternative NF-kappaB pathway in maintenance of basal bone homeostasis and osteoclastogenesis. J Bone Miner Res. 2010;25(4):809–18.
20. Elewaut D, Shaikh RB, Hammond KJ, et al. NIK-dependent RelB activation defines a unique signaling pathway for the development of V alpha 14i NKT cells. J Exp Med. 2003;197(12):1623–33.
21. Burkly L, Hession C, Ogata L, et al. Expression of relB is required for the development of thymic medulla and dendritic cells. Nature. 1995;373(6514):531–6.
22. Zhu H, Guo ZK, Jiang XX, et al. A protocol for isolation and culture of mesenchymal stem cells from mouse compact bone. Nat Protoc. 2010;5(3):550–60.
23. Kaneki H, Guo R, Chen D, et al. Tumor necrosis factor promotes Runx2 degradation through up-regulation of Smurf1 and Smurf2 in osteoblasts. J Biol Chem. 2006;281(7):4326–33.
24. Yao Z, Li P, Zhang Q, et al. Tumor necrosis factor-alpha increases circulating osteoclast precursor numbers by promoting their proliferation and differentiation in the bone marrow through up-regulation of c-Fms expression. J Biol Chem. 2006;281(17):11846–55.
25. Bouxsein ML, Boyd SK, Christiansen BA, et al. Guidelines for assessment of bone microstructure in rodents using micro–computed tomography. J Bone Miner Res. 2010;25(7):1468–86.
26. Dougall WC, Glaccum M, Charrier K, et al. RANK is essential for osteoclast and lymph node development. Genes Dev. 1999;13(18): 2412–24.
27. Lowe C, Yoneda T, Boyce BF, Chen H, Mundy GR, Soriano P. Osteopetrosis in Src-deficient mice is due to an autonomous defect of osteoclasts. Proc Natl Acad Sci U S A. 1993;90(10):4485–9.
28. Mukherjee S, Raje N, Schoonmaker JA, et al. Pharmacologic targeting of a stem/progenitor population in vivo is associated with enhanced bone regeneration in mice. J Clin Invest. 2008;118(2):491–504.
29. Zhao L, Huang J, Zhang H, et al. Tumor necrosis factor inhibits mesenchymal stem cell differentiation into osteoblasts via the ubiquitin E3 ligase Wwp1. Stem Cells. 2011;29(10):1601–10.
30. Chang MK, Raggatt LJ, Alexander KA, et al. Osteal tissue macrophages are intercalated throughout human and mouse bone lining tissues and regulate osteoblast function in vitro and in vivo. J Immunol. 2008;181(2):1232–44.
31. Nishio Y, Dong Y, Paris M, et al. Runx2-mediated regulation of the zinc finger Osterix/Sp7 gene. Gene. 2006;372:62–70.
32. Nakashima K, Zhou X, Kunkel G, et al. The novel zinc finger-containing transcription factor osterix is required for osteoblast differentiation and bone formation. Cell. 2002;108(1):17–29.
33. Komori T. Signaling networks in RUNX2-dependent bone development. J Cell Biochem. 2011;112(3):750–5.
34. Zhao C, Xiu Y, Ashton J, et al. Noncanonical NF-κB signaling regulates hematopoietic stem cell self-renewal and microenvironment interactions. Stem Cells. 2012;30(4):709–18.
35. Pratap J, Galindo M, Zaidi SK, et al. Cell growth regulatory role of Runx2 during proliferative expansion of preosteoblasts. Cancer Res. 2003;63(17):5357–62.
36. Zaidi SK, Pande S, Pratap J, et al. Runx2 deficiency,defective subnuclear targeting bypass senescence to promote immortalization,tumorigenic potential. Proc Natl Acad Sci U S.A. 2007;104(50): 19861–6.
37. Kiebala M, Polesskaya O, Yao Z, et al. Nuclear factor-kappa B family member RelB inhibits human immunodeficiency virus-1 Tat-induced tumor necrosis factor-alpha production. PLoS One. 2010;5(7): e11875.
38. Kitaura H, Zhou P, Kim HJ, Novack DV, Ross FP, Teitelbaum SL. M-CSF mediates TNF-induced inflammatory osteolysis. J Clin Invest. 2005; 115(12):3418–27.
39. Clowes JA, Riggs BL, Khosla S. The role of the immune system in the pathophysiology of osteoporosis. Immunol Rev. 2005;208: 207–27.
40. Cao JJ, Wronski TJ, Iwaniec U, et al. Aging increases stromal/osteoblastic cell-induced osteoclastogenesis and alters the osteoclast precursor pool in the mouse. J Bone Miner Res. 2005;20(9): 1659–68.
41. Lam J, Takeshita S, Barker JE, et al. TNF-alpha induces osteoclastogenesis by direct stimulation of macrophages exposed to permissive levels of RANK ligand. J Clin Invest. 2000;106(12):1481–8.
42. Hosny M, Sharawy M. Osteoinduction in rhesus monkeys using demineralized bone powder allografts. J Oral Maxillofac Surg. 1985;43(11):837–44.
43. Tuli SM, Singh AD. The osteoninductive property of decalcified bone matrix. J Bone Joint Surg Br. 1978;60(1):116–23.
44. Boomsma RA, Geenen DL. Mesenchymal stem cells secrete multiple cytokines that promote angiogenesis and have contrasting effects on chemotaxis and apoptosis. PLoS One. 2012;7(4):e35685.
45. Schinköthe T, Bloch W, Schmidt A. In vitro secreting profile of human mesenchymal stem cells. Stem Cells Dev. 2008;17(1):199–206.
46. Oh JY, Kim MK, Shin MS, Wee WR, Lee JH. Cytokine secretion by human mesenchymal stem cells cocultured with damaged corneal epithelial cells. Cytokine. 2009;46(1):100–3.
47. Furuya Y, Inagaki A, Khan M, et al. Stimulation of bone formation in cortical bone of mice treated with a receptor activator of nuclear factor-κB ligand (RANKL)-binding peptide that possesses osteoclastogenesis inhibitory activity. J Biol Chem. 2013;288(8): 5562–71.
48. Maruyama K, Kawagoe T, Kondo T, Akira S, Takeuchi O. TRAF family member-associated NF-κB activator (TANK) is a negative regulator of osteoclastogenesis and bone formation. J Biol Chem. 2012;287(34): 29114–24.

NOTCH inhibits osteoblast formation in inflammatory arthritis via noncanonical NF-κB

Hengwei Zhang,[1] Matthew J. Hilton,[2] Jennifer H. Anolik,[3] Stephen L. Welle,[4] Chen Zhao,[1] Zhenqiang Yao,[1] Xing Li,[1,5] Zhiyu Wang,[5] Brendan F. Boyce,[1,2] and Lianping Xing[1,2]

[1]Department of Pathology and Laboratory Medicine, [2]Center for Musculoskeletal Research, [3]Division of Allergy/Immunology and Rheumatology, Department of Medicine, and [4]Functional Genomics Center, University of Rochester Medical Center, Rochester, New York, USA. [5]Department of Cancer Immunotherapy, The Fourth Hospital of Hebei Medical University, Shijiazhuang, China.

NOTCH-dependent signaling pathways are critical for normal bone remodeling; however, it is unclear if dysfunctional NOTCH activation contributes to inflammation-mediated bone loss, as observed in rheumatoid arthritis (RA) patients. We performed RNA sequencing and pathway analyses in mesenchymal stem cells (MSCs) isolated from transgenic *TNF*-expressing mice, a model of RA, to identify pathways responsible for decreased osteoblast differentiation. 53 pathways were dysregulated in MSCs from RA mice, among which expression of genes encoding NOTCH pathway members and members of the noncanonical NF-κB pathway were markedly elevated. Administration of NOTCH inhibitors to RA mice prevented bone loss and osteoblast inhibition, and CFU-fibroblasts from RA mice treated with NOTCH inhibitors formed more new bone in recipient mice with tibial defects. Overexpression of the noncanonical NF-κB subunit p52 and RELB in a murine pluripotent stem cell line increased NOTCH intracellular domain–dependent (NICD-dependent) activation of an RBPjκ reporter and levels of the transcription factor HES1. TNF promoted p52/RELB binding to NICD, which enhanced binding at the RBPjκ site within the *Hes1* promoter. Furthermore, MSC-enriched cells from RA patients exhibited elevated levels of HES1, p52, and RELB. Together, these data indicate that persistent NOTCH activation in MSCs contributes to decreased osteoblast differentiation associated with RA and suggest that NOTCH inhibitors could prevent inflammation-mediated bone loss.

Introduction

Patients with chronic inflammatory diseases, such as rheumatoid arthritis (RA), often have severe systemic bone loss and increased risk of fracture due to increased bone resorption and decreased bone formation, partially mediated by elevated TNF levels (1). We (1–4) and others (5, 6) have reported that TNF inhibits bone formation by affecting major osteoblast regulatory pathways, including BMP/SMAD/RUNX2 and WNT–β-catenin, but the role of TNF in osteoblast differentiation from MSCs has not been fully defined. The TNF transgenic (TNF-Tg) mouse model we use, line 3647, represents a good model of RA to study the influence of chronically elevated, but relatively low, levels of TNF and TNF-induced inflammation on bone cell function and MSC differentiation into osteoblasts (7). To attempt to identify molecules responsible for reduced differentiation of MSCs into osteoblasts in RA, we performed genome-wide screening and pathway analyses using data from RNA sequencing (RNA-Seq) of MSCs purified from TNF-Tg mice and WT littermates. We found that genes in the NOTCH and noncanonical NF-κB signaling pathways were markedly upregulated in TNF-Tg mouse MSCs, raising the possibility that NOTCH may interact with noncanonical NF-κB proteins in MSCs to inhibit their osteogenic differentiation.

NOTCH is a family of evolutionarily conserved receptors that regulate cell fate. NOTCH receptors are activated following direct contact with their ligands expressed on adjacent cells. In mammals, there are 4 NOTCH receptors (NOTCH1–NOTCH4) and 5 ligands (Jagged-1 [JAG1], JAG2, and Delta-like 1, 3, and 4). NOTCH receptors have extracellular, transmembrane, and intracellular domains. Upon ligand binding, the NOTCH intracellular domain (NICD) of the receptor is cleaved by γ-secretase and translocates to the nucleus, where it associates with the recombination signal–binding protein jκ (RBPjκ). RBPjκ is a key transcription factor in canonical NOTCH signaling and acts downstream of all 4 NOTCH receptors. In the absence of a NOTCH signal, RBPjκ inhibits transcription of target genes by binding to transcriptional corepressors. Following NOTCH activation, NICD binds to RBPjκ and displaces corepressors, leading to transcriptional activation of target genes such as *Hes1* and *Hey1*. Ligand binding also can lead to noncanonical NOTCH signaling, which is mediated through the interaction of NICD with factors other than RBPjκ to activate alternative signaling events.

Involvement of NOTCH in bone cells has been recognized since 2008 (8), when in vivo studies of genetically modified mice demonstrated that loss of NOTCH signaling in mesenchymal stem cells (MSCs) or osteoblast precursors resulted in increased bone mass (9, 10), whereas activation of NOTCH signaling decreased osteoblast numbers (11). NOTCH signaling maintains MSCs in a proliferative phase and inhibits osteoblast differentiation. NOTCH also inhibits osteoclast formation via indirect and direct mechanisms. Depletion of NOTCH (11) or γ-secretase (9) in osteoblasts decreased osteoprotegerin production, leading to increased osteoclast formation, whereas RBPjκ depletion specifically in myeloid cells increased osteoclast formation in response to inflammatory cytokines (12). Although a role for NOTCH signaling in MSC and osteoblast differentiation has been described in normal mice, little is known about its role or the effects of NOTCH inhibitors in these cells in common bone diseases, such as RA.

NF-κB is a family of transcription factors that regulate many aspects of normal cellular functions as well as innate and adaptive immunity in response to pathogens and autoimmune

Conflict of interest: The authors have declared that no conflict of interest exists.
Citation for this article: *J Clin Invest.* 2014;124(7):3200–3214. doi:10.1172/JCI68901.

stimuli (13, 14). The family includes NF-κB1 (also known as p50, and its precursor p105), NF-κB2 (p52, and its precursor p100), RELA, RELB, and c-REL. Homo- and heterodimers of these proteins activate transcription of target genes, typically through canonical (p50/RELA) and noncanonical (p52/RELB) signaling. NF-κB signaling (which typically refers to canonical RELA-mediated transcription) regulates many aspects of cellular activity (15). *Rela*$^{-/-}$ mice die during embryonic development, making direct study of the role of RELA in bone difficult (16), although rescue studies indicate that RELA prevents osteoclast precursor apoptosis (17). Inhibition of RELA in mature osteoblasts by a dominant-negative IKK-γ mutant increases bone mass (18). Double-knockout *Nfkb1*$^{-/-}$ *Nfkb2*$^{-/-}$ mice are severely osteopetrotic because they have no osteoclasts (19). Double-knockout *Nfkb2*$^{-/-}$ *Relb*$^{-/-}$ mice (referred to herein as p52/RELB dKO mice) have increased bone volume (20, 21), a phenotype also seen in *Relb*$^{-/-}$ mice due to enhanced RUNX2 activation and osteoblast precursor differentiation (22). Despite these advances in understanding of the role of NF-κB in bone, the relative roles of canonical versus noncanonical signaling in MSC functions in RA have not been defined. To date, the only reported interaction between NOTCH and NF-κB was in cells in the hematopoietic lineage and cancer cells. Most of these studies suggested that NOTCH regulates the transcription of *Nfkb* (23, 24). They focused on canonical NF-κB signaling (25), and consequently, it is not known whether there is a relationship between NOTCH and noncanonical NF-κB signaling in bone cells.

In the present study, we found persistent activation of the NOTCH and noncanonical NF-κB pathways in MSCs and in MSC-enriched cells from TNF-Tg mice. Enhanced NOTCH signaling in MSCs was associated with reduced osteoblast differentiation and bone formation, which was prevented by systemic administration of the NOTCH inhibitors N-[N-(3,5-difluorophenacetyl)-l-alanyl]-S-phenylglycine t-butyl ester (DAPT) and thapsigargin. At the molecular level, we found that TNF increased expression of the noncanonical NF-κB proteins p52 and RELB, which potentiated NOTCH activation by binding to and promoting nuclear translocation of NICD onto the *Hes1* promoter. Thus, inhibition of NOTCH represents a potential new therapeutic approach for inflammatory bone loss when NOTCH is activated in MSCs.

Results

Increased expression of NOTCH target genes in MSCs from TNF-Tg mice and TNF-treated MSCs. BM MSCs from TNF-Tg mice with inflammatory arthritis have significantly decreased osteoblast differentiation potential (1). To identify the molecules and pathways responsible for TNF-induced inhibition of osteoblast differentiation, we purified MSCs (CD45$^-$CD105$^+$SCA1$^+$) from 6-month-old TNF-Tg mice (which typically have developed severe systemic bone loss by this age; ref. 1) and WT littermates by flow sorting, and performed RNA-Seq using a single-cell protocol. We identified 965 differentially expressed genes (>1.5-fold change; $P < 0.05$) between TNF-Tg and WT cells from a total of 21,533 reference genes (Figure 1A; RNA-Seq results available at the NCBI Sequence Read Archive; accession no. SRX543086) and submitted them to 2 different pathway analyses: Ingenuity Pathway Analysis (IPA) and David Bioinformatics Resources Program (David program), according to the Ingenuity Pathways Knowledge and KEGG databases, respectively. For all analyses, Fisher exact test was used to calculate a *P* value determining the probability that each pathway assigned to the data set was due to chance alone. IPA analysis revealed 53 dysregulated pathways between TNF-Tg and WT cells (Supplemental Figure 1A; supplemental material available online with this article; doi:10.1172/JCI68901DS1). Among them, the NOTCH signaling pathway was in 14th place of 53 dysregulated pathways identified from the IPA analysis and in 7th place of 11 dysregulated pathways from the David program (Supplemental Figure 1B).

NOTCH signaling molecules contain 4 mammalian NOTCH receptors (NOTCH1–NOTCH4), 5 ligands (JAG1 and JAG2 and Delta-like 1, 3, and 4), 2 inhibitors (NUMB and NUMBL), and 4 coactivators (DTX1–DTX4) (26). In MSCs, RNA-Seq detected various expression levels of these NOTCH-related genes (Supplemental Figure 2). Interestingly, despite different levels of upstream NOTCH signaling molecules in cells from TNF-Tg mice, expression levels of the NOTCH target genes *Hes1* and *Hey1* were increased, which was confirmed by quantitative real-time RT-PCR (qPCR) in purified CD45$^-$CD105$^+$SCA1$^+$ MSCs (Figure 1B). Increased *Hes1* and *Hey1* expression was also demonstrated by qPCR in various TNF-treated MSC preparations, including: (a) 3rd-passage bone-derived MSCs from WT mice (Figure 1C), which we characterized as cells expressing MSC surface markers (93% CD45$^-$, 70% CD105$^+$, 72% SCA1$^+$, 90% CD44$^+$) and able to differentiate to osteoblasts, adipocytes, and chondrocytes in vitro (Supplemental Figure 3); (b) the murine MSC line C3H10T1/2 (Figure 1D); and (c) human MSCs purchased from Lonza and characterized as CD105$^+$CD166$^+$CD29$^+$CD44$^+$CD14$^-$CD34$^-$CD45$^-$ (Figure 1E). In a prior study, we demonstrated that mouse MSCs express *Hes1* among other NOTCH targets and that HES1 mediates much of the NOTCH effect on MSC-osteoblast differentiation (10), which indicates that *Hes1* is an important NOTCH downstream gene in MSCs. Thus, in subsequent experiments, we used *Hes1* as a readout measure for NOTCH activation.

TNF signals through TNF receptor 1 (TNFR1) and TNFR2 (27). To determine whether TNF receptors mediate *Hes1* expression upregulated by TNF, we injected murine TNF (0.5 μg/injection/d i.p.) into double-knockout *Tnfr1*$^{-/-}$ *Tnfr2*$^{-/-}$ (TNFR1/2 dKO) mice and WT littermates for 5 days. We examined the expression level of *Hes1* in CD45$^-$ MSC-enriched cells and in CD45$^+$ non-MSCs by qPCR. TNF increased *Hes1* expression in WT CD45$^-$ cells, but not CD45$^+$ cells, and had no effect on CD45$^-$ or CD45$^+$ cells in TNFR1/2 dKO mice (Figure 1F). Accordingly, TNF decreased alkaline phosphatase–positive CFU-fibroblast (CFU-ALP$^+$) numbers in WT cells, but had no effect in TNFR1/2 dKO cells (data not shown).

Short-term Notch inhibition by DAPT reverses decreased osteoblast differentiation of MSCs from TNF-Tg mice. NOTCH controls the fate of MSCs, including their osteoblast differentiation potential (10). However, the role of NOTCH in common bone disorders, such as osteoporosis, has not been well investigated. NOTCH inhibitors have not been tested in mouse osteoporotic models, perhaps reflecting concerns that sustained inhibition of NOTCH in the BM may have adverse effects, such as increased bone resorption (12). To investigate whether NOTCH inhibition can reverse the suppressed osteoblast differentiation in TNF-Tg mice, we administered the γ-secretase inhibitor DAPT to TNF-Tg mice and WT littermates by gavage for 4 days. The inhibitory effects of DAPT on NOTCH signaling was confirmed by decreased *Hes1* mRNA levels in popliteal lymph nodes (Figure 2A), an indicator of effective NOTCH inhibition in vivo, but not in spleen (Supplemental Figure 4), as described previously (28). Interestingly, CD45$^-$ MSC-enriched

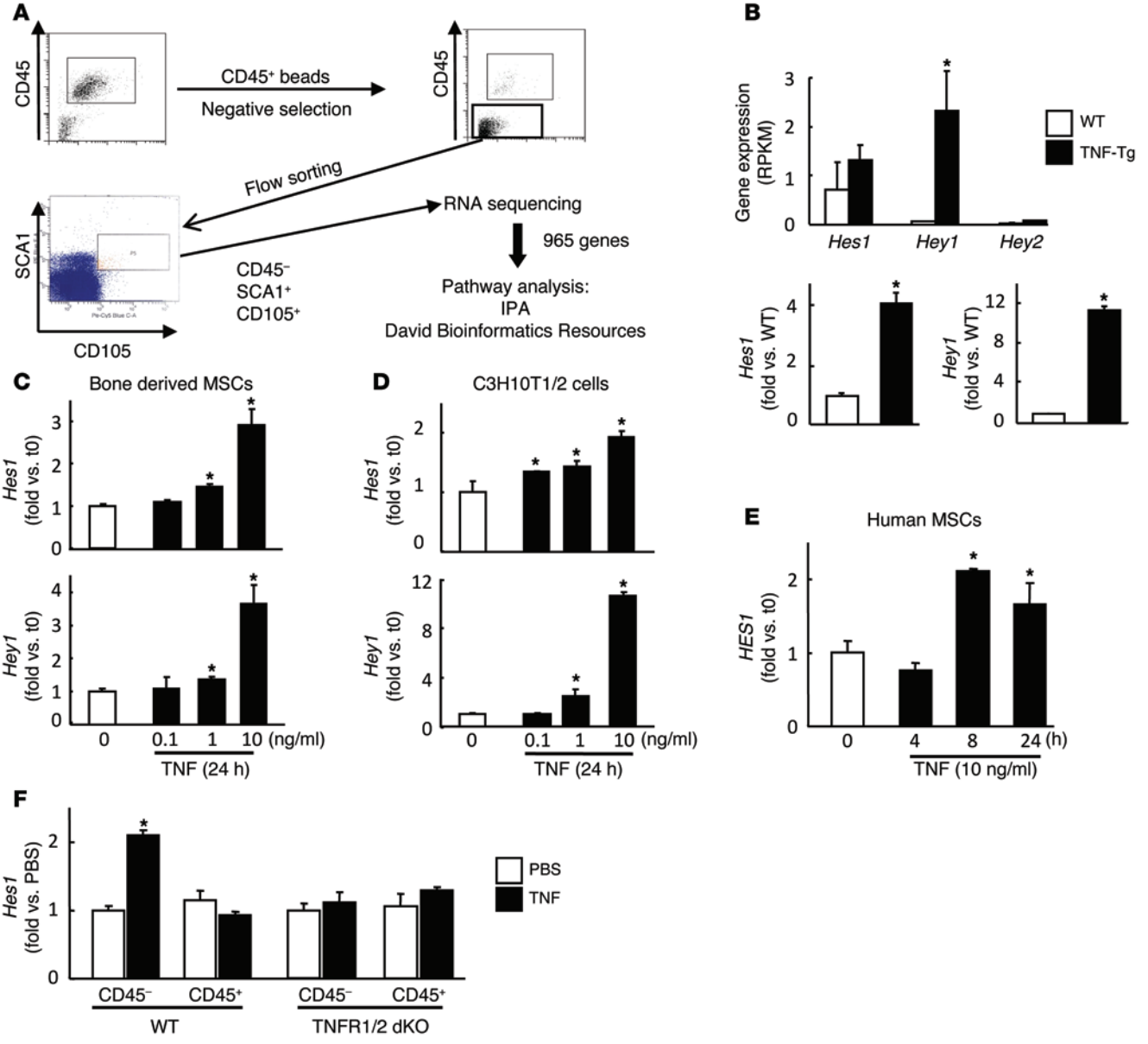

Figure 1

Increased expression of NOTCH target genes in MSCs from TNF-Tg mice and TNF-treated MSCs. (**A**) BM cells were isolated from 6-month-old TNF-Tg mice and WT littermates (n = 3 per genotype). CD45$^-$SCA1$^+$CD105$^+$ MSCs were subjected to RNA-Seq using a single-cell protocol. Differentially expressed genes between TNF-Tg and WT cells were subjected to pathway analysis. (**B**) RNA-Seq reads (top) and qPCR data (bottom) from CD45$^-$SCA1$^+$CD105$^+$ MSCs of TNF-Tg and WT mice. RPKM, reads per kilobase per million. (**C** and **D**) Expression of *Hes1* and *Hey1* in TNF-treated (24 hours) 3rd passage of bone-derived WT MSCs (**C**) and in the C3H10T1/2 murine MSC line (**D**) by qPCR. (**E**) Expression of *HES1* in TNF-treated (24 hours) human MSCs by qPCR. (**F**) 2-month-old TNFR1/2 dKO mice and WT littermates received TNF (0.5 μg/injection/d i.p.) or PBS for 5 days. BM cells were subjected to CD45$^-$ or CD45$^+$ cell isolation for *Hes1* expression by qPCR. *P < 0.05 vs. respective control.

cells from DAPT-treated WT mice had low levels of *Hes1* expression, similar to cells from vehicle-treated WT mice. CD45$^-$ MSC-enriched cells from vehicle-treated TNF-Tg mice had significantly increased *Hes1* levels compared with WT cells, and this was reduced by 50% in cells from DAPT-treated TNF-Tg mice (Figure 2B). To investigate whether DAPT affects osteoblastic differentiation of MSCs in TNF-Tg mice, we examined CFU-ALP$^+$ colony formation using BM stromal cells from DAPT- or vehicle-treated mice. As we previously reported (1), cells from TNF-Tg mice formed significantly decreased numbers of CFU-ALP$^+$ colonies compared with WT cells, an effect that was largely reversed with DAPT treatment. In contrast, CFU-ALP$^+$ colony numbers were similar in cells of DAPT- and vehicle- treated WT mice (Figure 2C).

To determine whether MSCs from DAPT-treated mice can form more new bone, and whether increased new bone formation is independent of the BM environment of TNF-Tg mice, we performed in vivo bone formation assays, as we described recently (22, 29), using cells from CFU mesenchymal colonies derived from

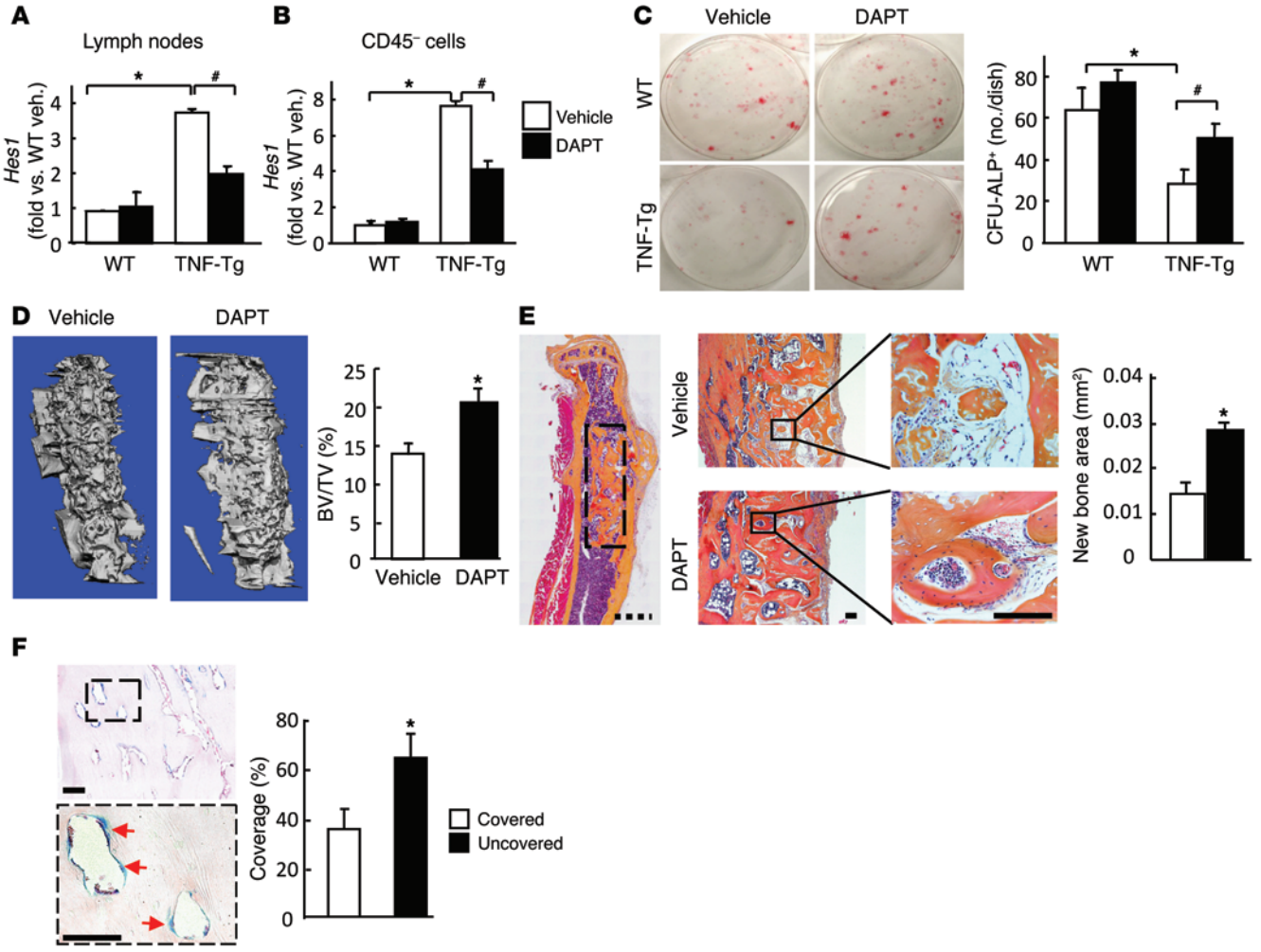

Figure 2

Short-term DAPT treatment revised decreased osteoblast differentiation of MSCs in TNF-Tg mice. (**A**–**C**) TNF-Tg mice and WT littermates were gavaged with DAPT (5 mg/kg each time) or vehicle daily for 4 days. The inhibitory effect of short-term DAPT treatment on NOTCH activation (*Hes1* mRNA) was confirmed in the popliteal lymph nodes (**A**; positive control) and in CD45⁻ MSC-enriched cells (**B**) by qPCR. (**C**) Representative images and number of CFU-ALP⁺ colonies in BM stromal cells. (**D** and **E**) CFU colony cells from vehicle- or DAPT-treated TNF-Tg mice were implanted to bone matrix in tibial cortical defects of SCID mice. Mice were sacrificed 6 weeks after surgery, and volume of new bone formed in the defects, relative to total defect volume (BV/TV), was measured by μCT (**D**), followed by histomorphometric analysis of the area of newly formed trabecular bone observed in decalcified H&E-stained bone sections (**E**). n = 8 per group. Scale bars: 1 mm (broken); 100 mm (solid). (**F**) CFU cells generated from BM stromal cells of *Rosa26-LacZ* mice were implanted to tibial cortical defects for 6 weeks as in **D**. Frozen sections were stained for LacZ enzymatic activity (blue) and counterstained with nuclear fast red (pink). Percent bone surface area covered by donor cells (LacZ⁺; red arrows) over total bone surface within the area of bone defect (green line) was assessed. n = 5 per group. Scale bars: 1 μm (broken); 100 μm (solid). *P < 0.05 vs. WT; #P < 0.05 vs. vehicle.

DAPT- or vehicle-treated TNF-Tg mice. We first demonstrated that a much higher percentage of CFU colony cells expressed MSC surface markers (50.4% CD45⁻, 89% SCA1⁺, 89% CD105⁺) compared with primary BM stromal cells (16% CD45⁻, 13% SCA1⁺, 7% CD105⁺) or freshly isolated BM cells (6% CD45⁻, 8% SCA1⁺, 2% CD105⁺) (Supplemental Figure 5). We loaded CFU colony cells from DAPT- or vehicle-treated TNF-Tg mice on decalcified bovine bone scaffolds and implanted them in tibial defects in recipient mice for 6 weeks. We examined the volume of newly formed bone by μCT and histomorphometric analysis and found that cells from DAPT-treated mice formed more new bone than cells from vehicle-treated mice (Figure 2, D and E).

To determine the fate of donor cells and their localization after they have been implanted in vivo for 6 weeks, we used CFU colony cells derived from *Rosa26-LacZ* mice in a separate experiment. LacZ⁺ cells were localized near the surfaces of newly formed bone, and they covered 37.3% of the total bone surface within the bone defect area (Figure 2F). To confirm that implanted MSCs were the major contributor to new bone formation, we compared mice that received only bone scaffolds with those that received bone scaffolds plus MSCs 6 weeks after implantation in WT mice (n = 5 per group). The implanting scaffold alone without MSCs could cause some degree of repair, perhaps via stimulation of MSCs from the host. However, the level of repair

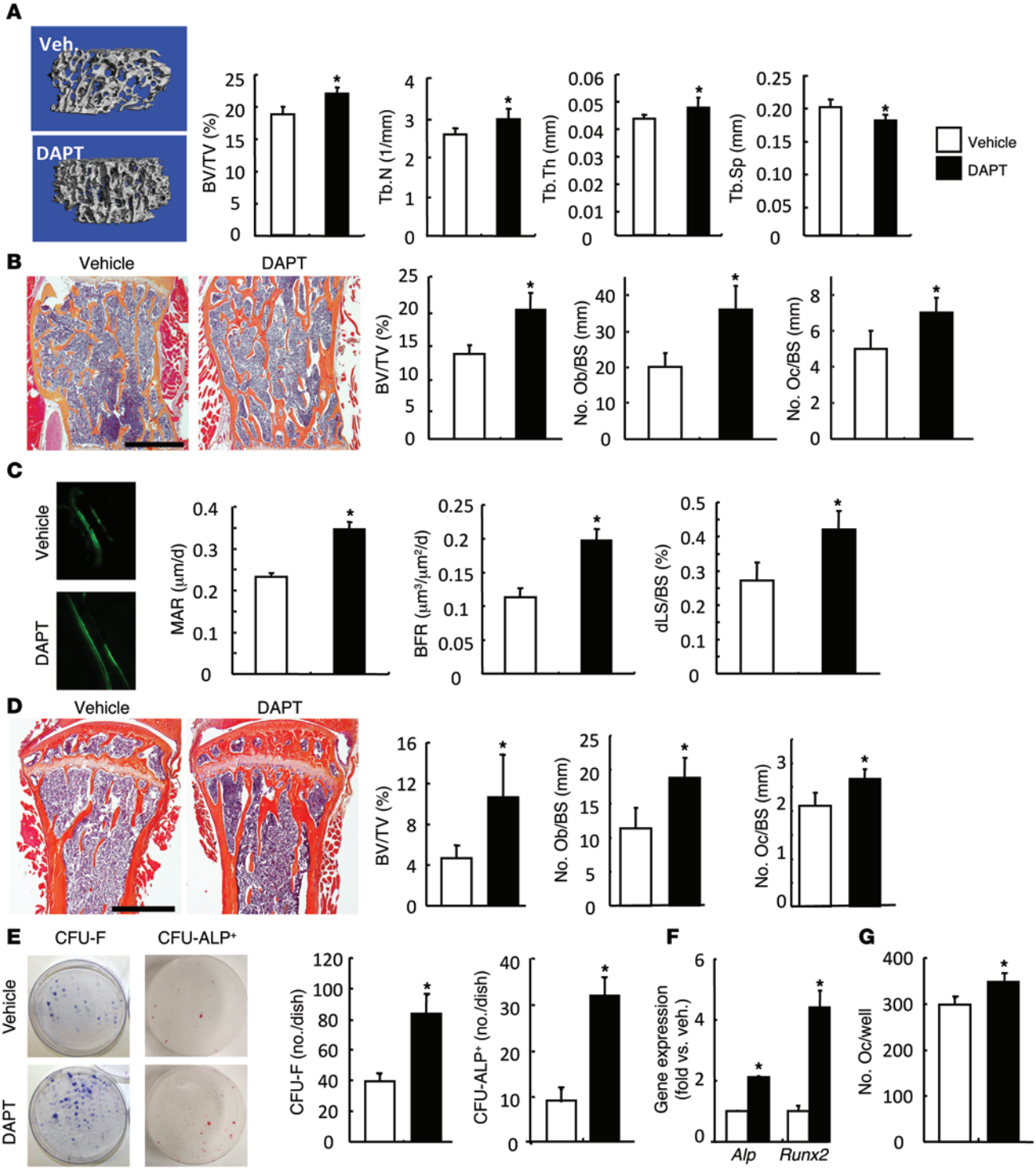

Figure 3

Long-term of DAPT treatment prevented bone loss in TNF-Tg mice. TNF-Tg mice were given with DAPT or vehicle as in Figure 2 for 3 months. (**A**) Representative μCT scans and morphometric data of BV/TV, trabecular number (Tb.N), trabecular thickness (Tb.Th), and trabecular separation (Tb.Sp) in L1 vertebrae. (**B**) Histology and histomorphometric analysis of BV/TV and number of osteoblasts (Ob) and osteoclasts (Oc) per bone surface (BS) in L1 vertebrae. (**C**) Calcein double-labeling in L1 vertebrae and analysis of dynamic parameters of bone formation: double labeled surface per bone surface (dLS/BS), mineral apposition rate (MAR), and bone formation rate (BFR). Original magnification, ×40. (**D**) Histology and histomorphometric analysis in the tibial metaphysis. Values are mean ± SD of 7–8 mice per group. (**E**) BM cells were cultured in the basal or osteoblast-inducing medium for 21 days in CFU colony formation assays. The number of CFU-F and CFU-ALP$^+$ colonies was evaluated. (**F**) Expression of *Alp* and *Runx2* in CFU-ALP$^+$ colonies, assessed by qPCR. (**G**) BM cells were cultured with RANKL and M-CSF for 5 days in osteoclastogenic assays. The number of TRAP$^+$ osteoclasts was counted. Values are mean ± SD of 4 dishes. Scale bars: 1 mm. *$P < 0.05$ vs. vehicle.

was much higher (5- to 6-fold) when MSCs were included along with scaffold (Supplemental Figure 6).

Long-term Notch inhibition by DAPT prevents bone loss in TNF-Tg mice. Patients and mice with inflammatory arthritis often have systemic bone loss due to increased bone resorption and decreased bone formation (1). Depletion of NOTCH in mice during embryonic development increased formation of both osteoblasts (10) and osteoclasts (12). We reasoned that NOTCH inhibition may have a different effect on bone mass of TNF-Tg mice compared with these genetically modified mice because MSCs from TNF-Tg mice have abnormally high NOTCH activation. Since persistent NOTCH inhibition (30) or activation (31) have detrimental effects on the skeleton, and high doses of NOTCH inhibitors have severe side effects in vivo, we decided to use low daily doses of DAPT. The half-life of DAPT in vivo is approximately 6 hours (32), and long-term, low-dose DAPT appears to have no notable side effects (28).

To determine whether DAPT prevents inflammatory bone loss, we treated TNF-Tg mice with DAPT or vehicle by daily gavage for 3 months. The efficacy of NOTCH inhibition was confirmed by demonstrating low expression of *Hes1* in popliteal lymph nodes (data not shown). DAPT treatment had no effect on mouse survival or body weight (data not shown). μCT of vertebral bones showed that DAPT treatment significantly increased the bone volume and the trabecular number and thickness and decreased the trabecular spacing compared with vehicle-treated mice (Figure 3A). Increased bone volume in DAPT-treated mice was confirmed by histomorphometric analysis in H&E-stained sections (Figure 3B). Bones from DAPT-treated mice had significantly increased osteoblast and osteoclast numbers on trabecular surfaces (Figure 3B). Calcein double-labeling in undecalcified sections showed that mineralization rate, bone formation rate, and mineral surface/bone surface were all increased in DAPT-treated mice compared with vehicle-treated controls (Figure 3C). In addition, bone volume, osteoblast number, and osteoclast number were increased in long bones from the same DAPT-treated mice (Figure 3D). DAPT treatment did not affect the severity of inflammation or bone erosion in joints of TNF-Tg mice (data not shown).

To determine whether long-term DAPT treatment increased bone formation by increasing MSC osteoblastic differentiation, we cultured BM stromal cells from DAPT- or vehicle-treated mice. Consistent with increased osteoblast-mediated bone formation, cells from DAPT-treated mice formed more CFU-fibroblast (CFU-F) and CFU-ALP$^+$ colonies compared with those from vehicle-treated mice (Figure 3E). mRNA expression of the osteoblast marker genes *Alp* and *Runx2* from CFU-ALP$^+$ colonies was increased in DAPT-treated mice (Figure 3F). We also found a small, but significant, increase in osteoclast formation when BM cells were cultured from DAPT-treated mice (Figure 3G).

Long-term treatment with high doses of DAPT causes damage to organs, including intestine and kidney, which could limit the potential clinical use of this class of reagents (33). Our DAPT regimen did not affect liver, lung, small intestine, or kidney at the microscopic level, nor did it affect body weight or survival (Supplemental Figure 7 and data not shown).

NOTCH inhibition by thapsigargin reverses decreased osteoblast differentiation and prevents bone loss in TNF-Tg mice. To further demonstrate that NOTCH inhibition reverses decreased osteoblast differentiation of MSCs and prevents bone loss in TNF-Tg mice, we used thapsigargin, which has been identified recently as a NOTCH inhibitor via complementary genomic screening (34). Thapsigargin regulates intracellular Ca^{2+} via inhibition of the endoplasmic reticulum in bone cells (35, 36) and interferes with processing of the NOTCH receptor in the endoplasmic reticulum, leading to accumulation of misfolded receptor, which inhibits NOTCH signaling (34). Thapsigargin-derived drugs have been tested in phase I clinical trails for breast, kidney, and prostate cancer (37). Thapsigargin is a much more potent inhibitor of NOTCH signaling than the γ-secretase activity inhibitor DAPT, requiring 0.4 mg/kg/injection (34) compared with 5 mg/kg/injection in vivo (28). However, the effects of thapsigargin on NOTCH signaling in osteoblasts have not previously been studied. We first demonstrated that administration of thapsigargin to TNF-Tg mice decreased *Hes1* mRNA levels in popliteal lymph nodes and CD45$^-$ MSC-enriched cells and also increased CFU-ALP$^+$ colony formation (Supplemental Figure 8, A and B), which suggests that thapsigargin could be used as a new NOTCH inhibitor in our model.

To investigate whether thapsigargin has a bone-anabolic effect in TNF-Tg mice similar to that of DAPT, we treated mice with thapsigargin using both short- and long-term regimens as we did using DAPT (Figures 2 and 3). In vivo bone formation assays using CFU colony cells indicated that cells derived from TNF-Tg mice subjected to short-term thapsigargin treatment (4 days) formed more new bone than cells derived from vehicle-treated mice (Figure 4A). Long-term treatment of TNF-Tg mice with thapsigargin (3 times per week for 2 months) rescued the decreased bone volume and trabecular number, as determined by μCT (Figure 4B).

Histomorphometric analyses confirmed the increased bone volume and osteoblast numbers in thapsigargin-treated mice (Figure 4C). We also tested whether long-term thapsigargin treatment increased bone formation by increasing MSC osteoblastic differentiation. Consistent with increased osteoblast-mediated bone formation, BM cells from thapsigargin-treated mice formed more CFU-F and CFU-ALP$^+$ colonies, which expressed higher levels of osteoblast-related genes and decreased NOTCH target gene levels compared with cells from vehicle-treated mice (Figure 4, D and E, and Supplemental Figure 8C). In this set of experiments, we also treated WT littermates of TNF-Tg mice in parallel to determine whether thapsigargin affects osteoblast function in WT mice. Long-term thapsigargin treatment slightly increased bone volume and osteoblast numbers in WT mice, despite its strong stimulatory effects on osteoblast differentiation in vitro (Figure 4).

The noncanonical NF-κB proteins p52 and RELB mediate TNF-induced NOTCH activation. NF-κB is a major signaling pathway downstream from TNFRs, and it interacts with NOTCH in hematopoietic cells (24). To investigate whether NF-κB proteins participate in TNF-induced NOTCH activation, we examined the expression pattern of *Nfkb* members in our RNA-Seq database. Expression of *Nfkb2* and *Relb*, but not *Nfkb1* or *Rela*, increased in MSCs from TNF-Tg mice (Figure 5A). To confirm this finding, we examined expression of p50, p52, RELA, and RELB proteins in CD45$^-$ MSC-enriched cells from TNF-Tg mice and WT littermates by Western blot. Similar to mRNA levels, expression of RELA and p50 was not markedly changed, but levels of p52, p100, and RELB increased substantially (Figure 5B). DAPT treatment did not affect p52 or RELB levels in CD45$^-$ MSC-enriched cells in WT and TNF-Tg mice, but it rescued the decreased expression of osteoblast-related genes in TNF-Tg cells (Figure 5C), whereas *Hes1* expression was significantly decreased in the same samples (Figure 2B). These data indicate that the change in p52 and RELB levels in MSCs from TNF-Tg mice is unlikely to be due to increased NOTCH activation.

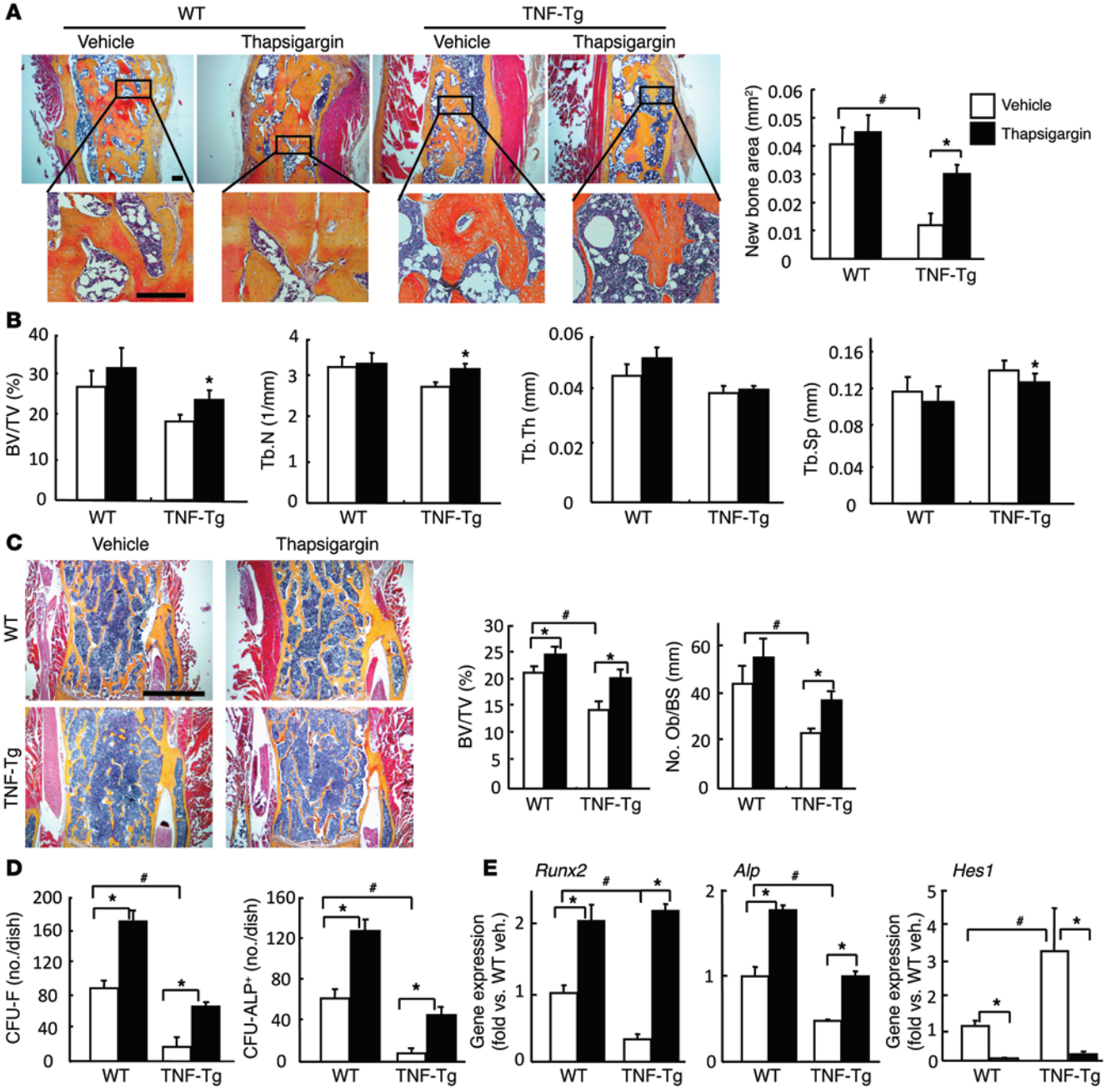

Figure 4

Effects of thapsigargin on osteoblast differentiation and bone volume. (**A**) 2.5-month-old TNF-Tg mice and WT littermates were given thapsigargin (0.4 mg/kg/injection i.p.) or vehicle daily for 4 days. CFU colony cells were derived from the mice and implanted to bone matrix in tibial cortical defects of SCID mice as in Figure 2. Mice were sacrificed 6 weeks after surgery. Shown are histomorphometric analyses and the calculated area of newly formed trabecular bone in decalcified H&E-stained bone sections. $n = 6$ per group. (**B**–**E**) 2.5-month-old TNF-Tg mice and WT littermates were given thapsigargin (0.4 mg/kg/injection i.p.) or vehicle 3 times per week for 2 months. The lumbar vertebrae were subjected to μCT and histological analyses as in Figure 3, and BM cells from long bones were used for biological analyses. $n = 6$ per group. (**B**) Morphometric data from μCT. (**C**) Histology and histomorphometric analysis. (**D**) BM cells were cultured in basal or osteoblast-inducing medium for 21 days in CFU colony formation assays. The number of CFU-F and CFU-ALP⁺ colonies was evaluated. Values are mean ± SD of 4 dishes. (**E**) Expression of osteoblast-related and NOTCH target genes in CFU-F colony cells, determined by qPCR. Scale bars: 100 μm (**A**); 1 mm (**C**). $^{*}P < 0.05$ vs. vehicle; $^{\#}P < 0.05$ vs. WT.

To examine whether p52 and RELB influence NOTCH activation, we overexpressed p52 and RELB in the presence or absence of low-dose NOTCH2-NICD in murine C3H10T1/2 cells with a RBPjκ-Luc reporter construct, which contains 6 RBPjκ response elements in front of the luciferase gene (10). Overexpression of p52 or RELB alone had no effect on RBPjκ-Luc activity, and low-dose NOTCH2-NICD increased RBPjκ-Luc reporter activity 4-fold. Importantly, overexpression of p52 or RELB markedly increased

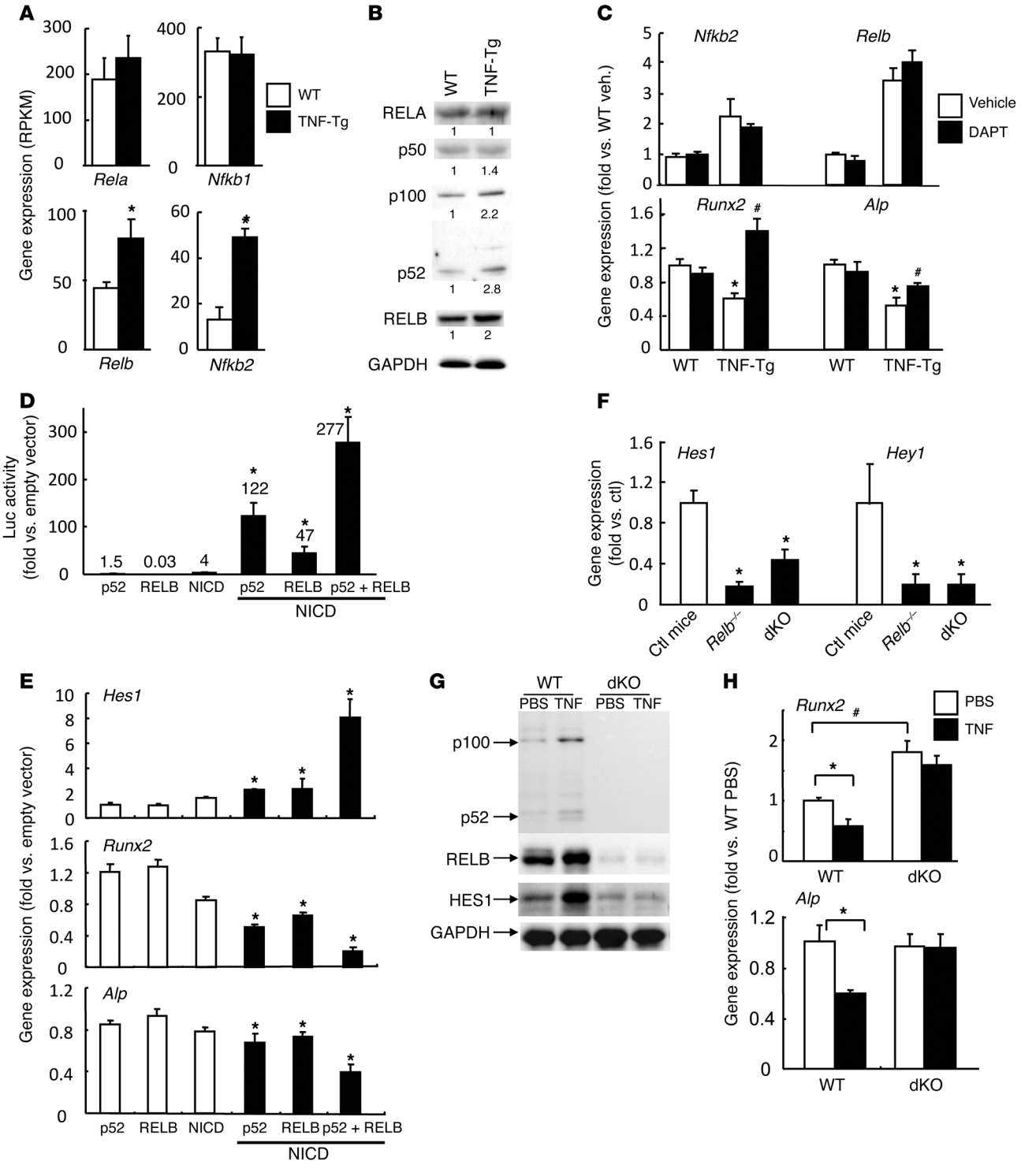

Figure 5

Noncanonical NF-κB proteins p52 and RELB mediate TNF-induced NOTCH activation. (**A**) *Nfkb* mRNA expression in CD45⁻SCA1⁺CD105⁺ MSCs from TNF-Tg mice and WT littermates by RNA-Seq. (**B**) NF-κB protein expression in CD45⁻ MSC-enriched cells from TNF-Tg mice and WT littermates by Western blot. Fold change in protein level (below) was determined by measuring band intensity. (**C**) *Nfkb2*, *Relb*, *Runx2*, and *Alp* mRNA expression in CD45⁻ MSC-enriched cells from DAPT- or vehicle-treated TNF-Tg mice by qPCR. (**D**) Reporter activity in C3H10T1/2 cells cotransfected with RBPjκ-Luc and with NOTCH2-NICD–, p52-, and/or RELB-expressing vectors. Fold increase versus empty vector was calculated. (**E**) Expression of *Hes1*, *Runx2*, and *Alp* in cells as in **D**. (**F**) Expression of *Hes1* and *Hey1* in CD45⁻Ter119⁻ MSCs from p52/RELB dKO mice, *Relb*$^{-/-}$ mice, and control littermates. Values are mean ± SD of 3 pairs of mice. (**G** and **H**) Bone-derived MSCs of p52/RELB dKO and control littermates were treated with TNF. (**G**) Expression of p52, RELB, and HES1 protein by Western blot. (**H**) Expression of *Runx2* and *Alp* by qPCR. **P* < 0.05, #*P* < 0.05 vs. control.

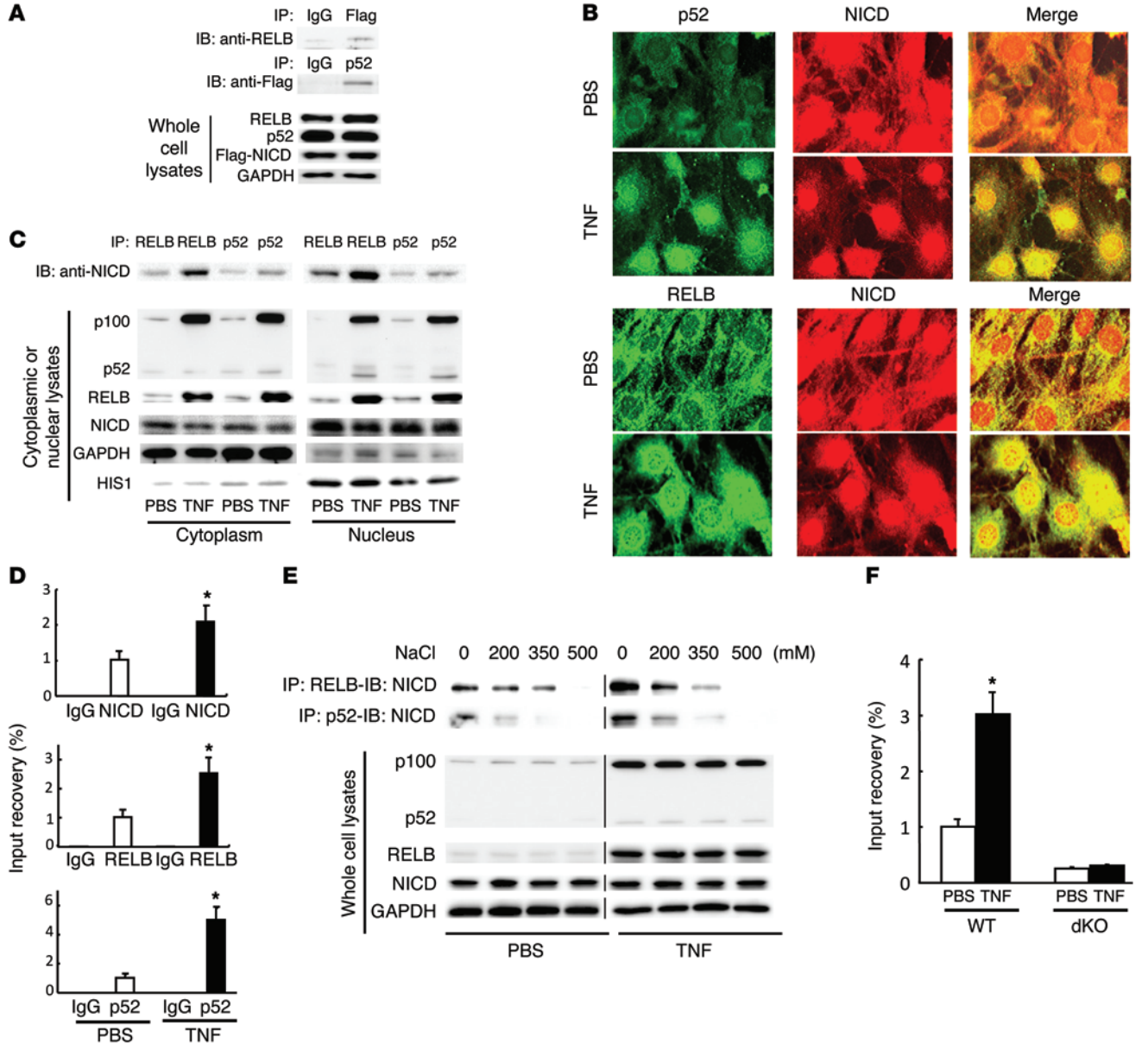

Figure 6

p52 and RELB bind to NICD and are recruited to the *Hes1* promoter. (**A**–**E**) C3H10T1/2 cells were treated with TNF for 24 hours in some experiments. (**A**) Cells were cotransfected with Flag-tagged NOTCH2-NICD, p52, and RELB expression vectors. Whole-cell lysates were subjected to IP with anti-Flag or anti-p52 antibodies and blotted with anti-RELB or anti-Flag antibodies. Experiments were repeated independently 4 times. (**B**) Colocalization of p52 or RELB with NICD was determined by immunofluorescent staining using anti-p52, -RELB, and –NOTCH2-NICD antibodies under confocal microscopy. (**C**) Nuclear and cytoplasm proteins were isolated. Protein lysates were subjected to IP with anti-p52 or anti-RELB antibodies. Immunocomplexes were blotted with anti–NOTCH2-NICD. Expression of p52, RELB and NICD proteins were examined in cytoplasmic and nuclear fractions. Experiments were repeated independently 4 times. (**D**) The ChIP assay was performed on immunocomplex subjected to IP with anti–NOTCH2-NICD, anti-RELB or anti-p52 antibodies. Rat IgG was used as control. Precipitated DNA was measured by qPCR using sequence-specific primers. (**E**) Total protein lysates were subjected to IP with anti-p52 or anti-RELB antibodies. Immunocomplexes were washed with concentration gradient of NaCl, then blotted with anti–NOTCH2-NICD. Experiments were repeated independently 3 times. Lanes were run on the same gel but were noncontiguous. (**F**) Bone-derived MSCs from p52/RELB dKO and WT mice were treated with TNF or PBS and subjected to ChIP as in **E**. Values are mean ± SD of triplicate determinants. **P* < 0.05 vs. respective control.

NOTCH2-NICD–induced RBPjκ-Luc reporter activity, and p52 and RELB combined had a synergistic effect, which was also observed in *Hes1* expression levels when total RNA from transfected cells was used (Figure 5, D and E). Consistent with the notion that NOTCH activation limits osteoblast differentiation, overexpression of p52, RELB, and NICD significantly reduced *Runx2* and *Alp* expression (Figure 5E). To investigate whether p52 and RELB regulate NOTCH signaling, we examined the gene expression lev-

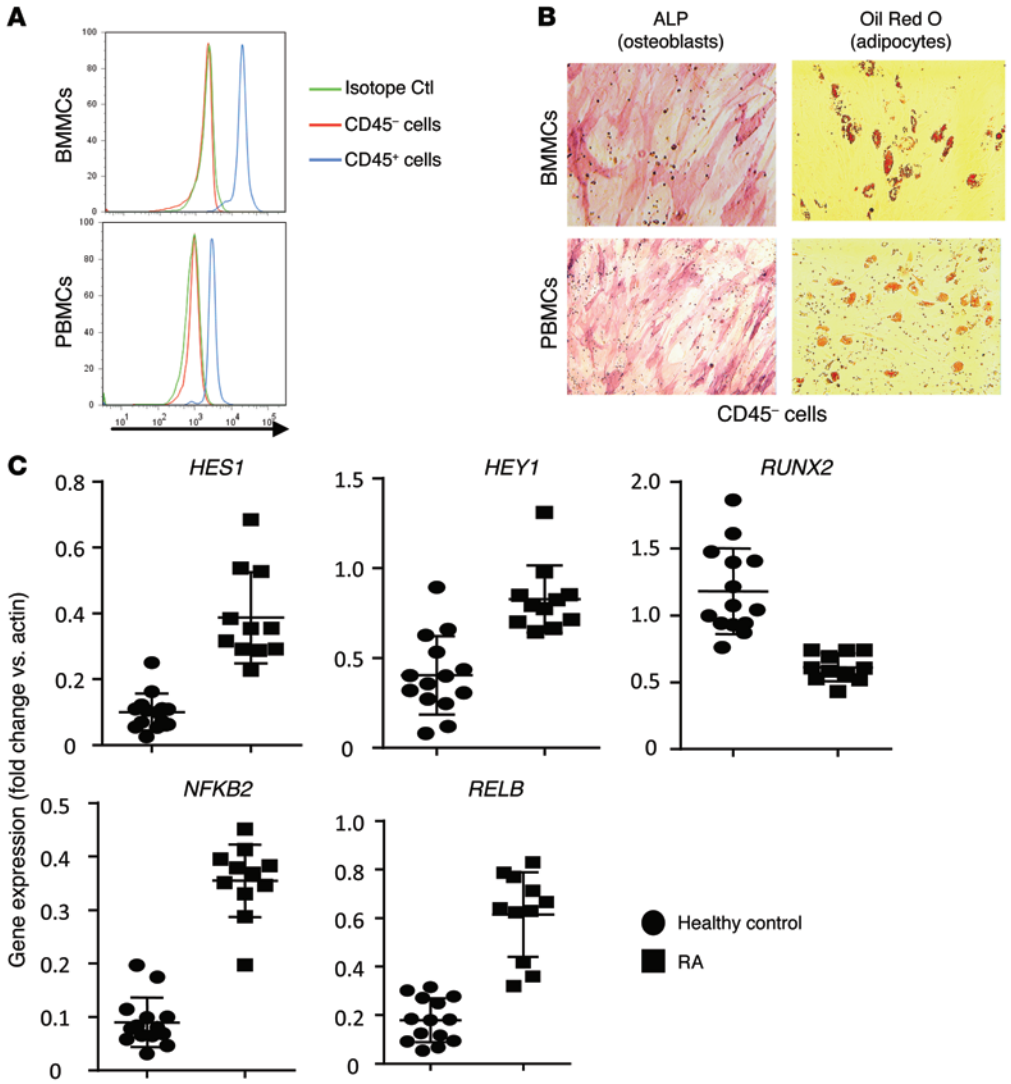

Figure 7
Increased NOTCH activation in CD45⁻ MSC/osteogenic precursors from RA patients. (**A**) CD45⁻ and CD45⁺ cells isolated from human BMMCs and PBMCs were stained with anti-CD45 antibody for FACS analysis. (**B**) CD45⁻ cells isolated from BMMCs and PBMCs were subjected to osteoblast (ALP) and adipocyte (Oil Red O) differentiation assays. Original magnification, ×10. (**C**) Expression levels of NOTCH target genes, *RUNX2*, and noncanonical NF-κB members were measured by qPCR in CD45⁻ cells isolated from PBMCs from healthy control subjects (n = 14) and patients with RA (n = 11). Values were calculated as $Ct_{gene\ of\ interest}/2 - Ct_{actin} \times 100$.

els of *Hes1* and *Hey1* in purified CD45⁻Ter119⁻ MSCs from p52/RELB dKO mice and found that they were reduced (Figure 5F). To determine whether p52 and RELB mediate TNF-induced upregulation of *Hes1*, we treated 3rd-passage bone-derived MSCs from p52/RELB dKO mice and control littermates with TNF. Western blot analysis showed that TNF increased HES1 protein expression in cells from control mice, but not from p52/RELB dKO mice (Figure 5G). qPCR analysis showed that TNF decreased expression of osteoblast-related genes in WT cells, but not in p52/RELB dKO cells (Figure 5H).

p52 and RELB bind to NICD and are recruited to the Hes1 promoter. To examine the molecular mechanism by which p52 and RELB activate NOTCH target gene transcription, we examined whether p52 and RELB bind to NICD, which associates with RBPjκ, the key transcription factor in canonical NOTCH signaling. We transfected C3H10T1/2 cells with Flag-tagged NOTCH2-NICD and with p52 and RELB expression plasmids, performed IP with anti-Flag antibody against NOTCH2-NICD or anti-p52 antibody against p52, and then blotted immunocomplexes with anti-RELB or anti-Flag antibody. Both p52 and RELB bound to NICD (Figure 6A). We hypothesized that TNF enhances the interaction between RELB or p52 and the NICD in MSCs to activate NOTCH signaling. To test this, we cultured C3H10T1/2 cells to confluence; under this culture condition, expression of endogenous NICD was increased due to cell-cell contact–mediated NOTCH activation (Supplemental Figure 9). We treated cells with TNF for 24 hours and examined colocalization of p52, RELB, and NICD by immunofluorescence staining with anti-p52, -RELB, or –NOTCH2-NICD antibodies. As reported previously (38), under basal conditions, RELB and p52 were expressed mainly in the cytoplasm and NICD mainly in the nucleus. After TNF treatment, colocalization of NICD with p52 or RELB increased markedly in the nucleus (Figure 6B). To examine whether TNF increases the interaction of RELB or p52 with NICD and whether this occurs in the cytoplasm or the nucleus, we treated cells with TNF, isolated cytoplasmic or nuclear fractions, performed IP with RELB or p52, and blotted the immunocomplexes with anti–NOTCH2-NICD. TNF increased the total amount of RELB and p100/p52 proteins in both cytoplasmic and nuclear fractions. TNF increased the binding of NICD to RELB and p52 in both the cytoplasm and the nuclei, despite the fact that it decreased the total amount of NICD protein in these compartments (Figure 6C). To determine whether TNF-induced NICD/

RELB or NICD/p52 interaction occurs on the native *Hes1* promoter, we performed ChIP assays using primers that flank the RBPjκ binding sites on the mouse *Hes1* promoter. TNF treatment significantly increased the amount of NICD, p52, and RELB that bound to the RBPjκ binding sites on the *Hes1* promoter (Figure 6D).

To determine whether the increased binding of NICD to RELB and p52 resulted from altered affinity in response to TNF or was due only to increased p52 and RELB expression, we performed an affinity assay (39) by washing the IP complex with gradient NaCl solutions. A high NaCl concentration (500 mM) dissociated the binding of NICD with p52 and RELB in both TNF- and PBS-treated samples (Figure 6E), which suggests that TNF does not affect the binding affinity of NICD for NF-κB proteins. To determine whether TNF increases NICD ChIP without overexpression of p52 or RELB, and whether knockdown of endogenous p52/RELB abolishes this increase, we performed ChIP assays using bone-derived cells from p52/RELB dKO and WT mice. TNF increased the binding of NICD to native RBPjκ binding sites on the *Hes1* promoter in WT cells, which was abolished in p52/RELB dKO cells (Figure 6F).

MSCs from patients with RA have elevated Notch activation. To determine the clinical relevance of our mouse findings, we next examined the expression levels of NOTCH, NF-κB, and osteoblast-related genes in MSCs of RA patients. We first examined properties of $CD45^-$ MSCs isolated from healthy human BM mononuclear cells (BMMCs) and PBMCs. We isolated $CD45^-$ and $CD45^+$ cells using magnetic beads as we did for mouse cells (Figure 1A) and stained them with FITC-conjugated anti-CD45 for fluorescence-activated cell sorting (FACS; Figure 7A). $CD45^-$ cells were cultured in osteoblast- or adipocyte-inducing medium. $CD45^-$ cells from both BMMCs and PBMCs gave rise to osteoblasts and adipocytes (Figure 7B), which indicates that $CD45^-$ cells from PBMCs contain MSC-enriched cells. Using $CD45^-$ MSC-enriched cells from PBMCs of 14 healthy controls and 11 RA patients (active disease, DAS28 score >5, not on bisphosphonates or biologics; see Methods), we measured gene expression levels by qPCR. Similar to our data from TNF-Tg RA mice, expression levels of NOTCH- and NF-κB–regulated genes were significantly increased in $CD45^-$ MSC-enriched cells from RA patients compared with those of healthy controls, whereas *RUNX2* expression levels were markedly decreased (Figure 7C). In addition, $CD45^-$ cells from BMMCs or PBMCs of TNF-Tg mice had similarly increased *Hes1* and decreased *Runx2* RNA expression levels (Supplemental Figure 10). $CD45^-$ PBMCs from RA patients had increased mRNA levels of NOTCH- and NF-κB–regulated genes and decreased *RUNX2* compared with cells from healthy subjects (Figure 7C), which indicates that elevated NOTCH in MSCs likely contributes to reduced osteoblast function in RA patients.

Discussion

Data from various genetically modified mice reveal a complicated role for NOTCH in MSC-osteoblast differentiation, which is tightly regulated both temporally and spatially. For example, NOTCH blocks MSC commitment to the osteoblast lineage when activated in MSCs, although it does not appear to have an important role in committed osteoblasts. Consequently, therapeutic targeting of this pathway is considered to be challenging, and thus the role of NOTCH in common bone diseases has not been studied extensively. Here, using unbiased pathway analysis of RNA-Seq data obtained from purified MSCs after chronic exposure to TNF in vivo, we found an increase in the expression of NOTCH signaling genes. MSCs from TNF-Tg mice, a model of chronic inflammatory arthritis, had significantly decreased osteoblast differentiation. The NOTCH inhibitors DAPT and thapsigargin increased bone volume and osteoblast number and activity in TNF-Tg mice. MSCs from DAPT-treated TNF-Tg mice had increased osteoblast differentiation in in vitro cultures and formed more new bone after injection into recipient mice in vivo. At the molecular level, TNF increased the expression levels of noncanonical NF-κB proteins p52 and RELB, which interacted with NICD on the *Hes1* promoter and upregulated NOTCH target gene expression. Thus, our findings revealed a new role of NOTCH in inflammatory bone loss, such as occurs in RA, in which persistent NOTCH activation in MSCs inhibits their differentiation into osteoblasts.

We speculate that there are 2 fundamental differences between our TNF-Tg mice and genetically modified *Notch* mouse models with respect to NOTCH activation in MSCs. First, in TNF-Tg mice, NOTCH activation resulted from chronic low-level systemic inflammation, rather than being driven by a specific promoter (i.e., NOTCH manipulation occurs only when cells express the promoter). Second, in TNF-Tg mice, the degree of NOTCH activation was low to moderate, which we found to be preventable by NOTCH inhibitor treatment. In contrast, in most animal models, NOTCH activation is persistent because the mice carry a constitutively activated NICD at very high levels that cannot be inhibited by NOTCH inhibitors unless very high doses are used.

NOTCH controls osteoclast function by negatively regulating osteoclastogenesis (40). Osteoclast-specific depletion of RBPjκ increases TNF-induced osteoclast formation (12) and local bone erosion in antibody-induced arthritis (41). The NOTCH/RBPjκ pathway promotes LPS-induced M1 inflammatory macrophage polarization (42), while osteoclasts are derived from M2 housekeeping macrophages (43). These findings suggest that NOTCH/RBPjκ inhibition might favor osteoclastogenesis and bone loss in an inflammatory environment, which appears at odds with the anabolic effect of NOTCH inhibition that we observed herein. In fact, we did observe a small increase in osteoclast numbers in DAPT-treated TNF-Tg mice. However, the overall effect was a significant increase in bone volume in these animals (Figure 3D), which indicates that the bone-anabolic effect of low-dose NOTCH inhibition in this study was greater than the bone-resorptive effects. NOTCH inhibition increases osteoclastogenesis (44), and myeloid-specific deletion of RBPjκ enhances TNF-induced osteoclast formation (41). However, NOTCH activation has been previously reported in synovial samples from RA patients and from mice in animal models of RA (45, 46). NOTCH mediates hypoxia-induced angiogenesis in RA by increasing the function of microvascular endothelial cells (47). Recent studies using DAPT (48) or an anti-mouse Delta-like 1–blocking monoclonal antibody (49) reported that NOTCH inhibition in mice with inflammatory arthritis reduces the severity of inflammation and inhibits osteoclastogenesis. These reports highlight the complexity of NOTCH signaling under normal and pathological conditions. We did not observe reduced joint inflammation in our present study. One potential reason why we did not find changes in inflammation or bone erosion in DAPT-treated mice is that the dose we used was low (5 mg/kg) compared with larger doses used previously (10–20 mg/kg; ref. 48).

Activation of NOTCH signaling is regulated at many levels. For example, TNF regulates NOTCH signaling in several cell types by different mechanisms: it regulates expression of NOTCH ligands (JAG2) and receptors (NOTCH1 and NOTCH4) in fibroblasts,

endothelial cells, and skeletal muscle cells (45, 50, 51) and induces HES1 expression in mouse embryonic fibroblasts (50). Our present results revealed a new molecular mechanism of TNF-induced NOTCH activation in MSCs: TNF activates NOTCH at a step after NICD release. Although TNF-treated cells had reduced NICD expression levels in both cytoplasm and nuclei, they had more NICD binding to the RBPjκ sequence on the *Hes1* promoter (Figure 6, C and D). In this model, the noncanonical NF-κB proteins RELB and p52 potentiated the effect of TNF, and in their absence, TNF-stimulated *Hes1* expression was abolished.

Studies of NOTCH interaction with NF-κB have focused mainly on canonical NF-κB p65 and p50 proteins (25) and how NOTCH regulates *Nfkb* transcription (23–25). We found that NOTCH inhibition did not affect *Nfkb2* expression, but MSCs from p52/RELB dKO mice had significantly reduced expression levels of NOTCH target genes (Figure 5, C and H), which indicates that RELB and p52 work upstream of NOTCH signaling in MSCs. NF-κB consensus sequences could interact with the RBPjκ binding site on target genes (52). However, our findings showed that overexpression of RELB and p52 did not affect RBPjκ-Luc reporter activity or *Hes1* expression, whereas RELB and p52 in combination with NICD significantly increased RBPjκ-Luc reporter activity as well as *Hes1* expression (Figure 5, D and E), which indicates that RELB and p52 need the NICD to regulate NOTCH target gene expression.

We used DAPT, a γ-secretase inhibitor, and thapsigargin, a newly identified NOTCH inhibitor (34), to inhibit NOTCH activation. Several γ-secretase inhibitors have been used in phase II clinical trails in diseases such as Alzheimer's disease (53) and cancer (31). It is unclear whether NOTCH inhibitors can be used to increase bone formation in RA patients; however, data from the genetically modified *Notch* mice demonstrated the complexity of the role of NOTCH in osteoblast differentiation: it functions early to block MSC commitment to the osteoblast lineage, and later promotes osteoblast maturation. Thus, therapeutic targeting of this pathway could be challenging. However, our present data indicated that the NOTCH inhibitor has a clearly beneficial bone-anabolic effect in an experimental model of RA in which NOTCH signaling is already elevated. A recent study demonstrated that osteoblasts are short-lived, nonreplicative cells, requiring continual replenishment from BM MSCs (54). Thus, if NOTCH signaling is elevated persistently in MSCs in RA patients, it will decrease the osteoblast pool by blocking the MSC-osteoblast transition and thereby inhibit bone formation. Under these conditions, NOTCH inhibition could lift this blockage to increase osteoblast numbers and thus bone volume. Our data showed that $CD45^-$ MSC-enriched cells from RA patients expressed increased levels of *HES1* and *HEY1* and decreased levels of *RUNX2* compared with those from healthy subjects, which indicates that the elevated NOTCH signaling in MSCs in RA mice likely occurs in human RA patients as well. Since patients with other types of chronic inflammatory diseases — such as systemic lupus erythematosus and Crohn's disease — often have systemic bone loss, it is possible that they also have abnormal NOTCH activation in their MSCs that contributes to reduced osteoblast function.

In summary, using TNF-Tg mice as a model of RA, we demonstrated that chronic inflammation caused persistent activation of the NOTCH pathway in MSCs, limiting their osteoblast differentiation, which was prevented by administration of a NOTCH inhibitor. At the molecular level, we found that inflammation increased the expression of noncanonical NF-κB proteins, which potentiated NOTCH activation by binding to and promoting nuclear translocation of NICD. Thus, NOTCH inhibition represents a potential new therapy for inflammation-induced bone loss associated with NOTCH activation in MSCs.

Methods

Reagents and animals. DAPT was from Calbiochem and thapsigargin was purchased from ENZO life sciences. M-CSF, RANKL, and TNF for cell culture were purchased from R&D Systems. TNF-Tg mice (line 3647), originally obtained from G. Kollias (Biomedical Sciences Research Centre "Alexander Fleming," Vari, Greece), carry a 3′-modified human *TNF* transgene in which the 3′-region of the *TNF* gene was replaced with that of the human β-globin gene. These mice develop arthritis starting at 2 months of age, and arthritis and bone loss progress with age. TNF-Tg 3647 mice can survive to 1 year or older, unlike the commonly used TNF-Tg 197 mice, which develop more severe arthritis and die within a few months of birth. We consider the chronic nature of the disease in TNF-Tg 3647 mice to be advantageous because it is more closely mimics human RA. *Nfkb2*$^{-/-}$ mice, and mice with a mutation-disrupted *Relb* locus by random integration of transgene sequences, have been described previously (21, 55). *Nfkb2*$^{+/-}$ *Relb*$^{+/-}$ mice were crossed with *Nfkb2*$^{-/-}$ *Relb*$^{+/-}$ mice to generate *Nfkb2*$^{-/-}$ *Relb*$^{-/-}$ mice (p52/RELB dKO). The mice used were in a mixed 129 and C57BL/6J background. *Tnfr1*$^{-/-}$ *Tnfr2*$^{-/-}$ mice (TNFR1/2 dKO) in a C57BL/6J background were provided by G.S. Pryhuber (Department of Pediatrics, University of Rochester School of Medicine and Dentistry, Rochester, New York, USA; ref. 56). Transplant recipients were 2-month-old SCID mice (strain B6.CB17-Prkdcscid/SzJ; stock no. 001913; Jackson Laboratories). *Rosa26-LacZ* mice (strain B6;129S-Gt[ROSA]26Sor/J; stock no. 002073; Jackson Laboratories) were used in in vivo tracking experiments.

MSC preparation. We used several types of cell preparations as MSCs and MSC-enriched cells based on individual experimental needs.

For FACS-sorted purified MSCs, we used the following antibodies (from eBioscience and BD Biosciences — Pharmingen): CD45, SCA1, CD105, Ter119. Whole BM cells were incubated with anti-CD45 antibody–conjugated microbeads (Miltenyi Biotec). The $CD45^-$ population was isolated by negative selection according to the manufacturer's instructions. $CD45^-$ cells were stained with a combination of SCA1 and CD105. $CD45^-SCA1^+CD105^+$ cells were isolated by FACS sorting and used in RNA-Seq and qPCR.

$CD45^-$ MSC-enriched cells were isolated by negative selection, as described above. We previously reported that $CD45^-$ cells express MSCs surface markers and can differentiate into multiple lineages (1). $CD45^-$ cells were used in qPCR and Western blot analysis.

Mesenchymal colony cells, generated by pooling cells from CFU colonies, were used for in vivo bone formation assays.

Bone-derived MSCs were isolated using a recently published protocol (57). Long bones were flushed several times with PBS, cut into small pieces, and cultured in a plastic dish for 3 days. The bone pieces were transferred into a clear dish as 1st-passage cells and continually cultured for another 7 days to allow the cells to become confluent. 3rd-passage cells were used for cell characterization and experiments. The MSC characteristics of bone-derived MSCs were confirmed by FACS and multilineage differentiation assays (Supplemental Figure 1). Bone-derived MSCs were used for Western blot and IP.

The C3H10T1/2 mouse MSC cell line was used in experiments involving transient transfection, Western blot, and ChIP assays.

Human MSCs (catalog no. PT-2501; Lonza) were used in qPCR analyses.

RNA-Seq and IPA. $CD45^-SCA1^+CD105^+$ MSCs were isolated from TNF-Tg mice and WT littermates. Cells (1×10^4) were subjected to mRNA isolation and RNA-Seq with SOLiD system (Applied Biosystems). Pathway analysis of statistically significant gene expression changes from mRNA sequenc-

ing was performed with IPA (Ingenuity System) and David Bioinformatics Resources program (Visualization and Integrated Discovery; http://david.abcc.ncifcrf.gov/home.jsp; ref. 58). Genes from the mRNA sequencing data set that met the 1.5-fold ($P < 0.05$) change cutoff and were associated with biological functions in the Ingenuity Pathways Knowledge Base or KEGG database were considered for analysis. For all analyses, Fisher exact test was used to calculate a P value determining the probability that each signal pathway assigned to that data set was due to chance alone. RNA-Seq data were deposited in the NCBI Sequence Read Archive (http://www.ncbi.nlm.nih.gov/sra; accession no. SRX543086).

Cell culture and analysis. For CFU-F and CFU-ALP assays, total BM cells were cultured in 10-cm dishes at 10^6 cells/dish in 10 ml α-MEM containing 10% FCS (Hyclone Laboratories) with or without 50 μg/ml ascorbic acid and 10 mM β-glycerophosphate for 28 days. At the end of the culture period, cells were stained for CFU-F or CFU-ALP activity. The stained CFU-F and CFU-AFP$^+$ colonies were counted (>20 cells in a single colony). For osteoclastogenic assays, BM cells were cultured with conditioned medium (1:50 dilution) from a M-CSF–producing cell line for 3 days in α-MEM with 10% FCS to enrich for osteoclast precursors. Osteoclast precursors were cultured with M-CSF conditioned medium and RANKL (10 ng/ml, R&D) for 2–3 days. After multinucleated cells were observed under a microscope, the cells were fixed, stained for TRAP activity to identify osteoclasts (TRAP$^+$ cells containing >3 nuclei), and counted, as described previously (55). For differentiation assay of human CD45$^-$ cells, PBMCs and BMMCs were cultured in 60-mm dishes at 2×10^6 cells/dish in 4 ml α-MEM culture medium containing 10% FCS with 50 μg/ml ascorbic acid and 10 mM β-glycerophosphate for osteoblast induction, or containing 10% FCS, 10 nM dexamethasone, 5 μg/ml insulin (Sigma-Aldrich), 100 nM indomethacin (Sigma-Aldrich), and 0.5 mM methylisobutylxanthine (Sigma-Aldrich) for adipocyte induction. Cells were stained for ALP activity for osteoblasts or with Oil Red for adipocytes.

qPCR. Total RNA was extracted from cell cultures using TRIzol reagent (Invitrogen). cDNAs were synthesized by iSCRIPT cDNA Synthesis Kit (Bio-Rad). qPCR amplifications were performed in an iCycler (Bio-Rad) real-time PCR machine using iQ SYBR Green supermix (Bio-Rad) according to the manufacturer's instructions. *Gapdh* was amplified on the same plates and used to normalize the data. Samples were prepared in triplicate, and each experiment was repeated at least 3 times. The relative abundance of each gene was calculated by subtracting the Ct value of each sample for an individual gene from the corresponding Ct value of *Gapdh* (ΔCt); ΔΔCt was obtained by subtracting the ΔCt of the reference point; and $2^{\Delta\Delta Ct}$ was then calculated to yield fold expression relative to the reference point. Representative data are presented as mean ± SD of the triplicates or of 4 wells of cell culture. See Supplemental Table 1 for sequence-specific primers.

μCT, histology, and histomorphometric analysis of bone sections. For μCT, lumbar 1 (L1) vertebrae and femora were dissected free of soft tissue, fixed overnight in 70% ethanol, and scanned at high resolution (10.5 μm) on a VivaCT40 μCT scanner (Scanco Medical) using 300 ms integration time, 55 kVp energy, and 145 uA intensity. 3D images were generated using a constant threshold of 275 for all samples. For histology and analysis, thoracic vertebrae and tibiae were removed from mice after sacrifice, fixed in 10% buffered formalin, decalcified in 10% EDTA, and embedded in paraffin. Sections (4 μm thick) were then stained with H&E and for TRAP activity. Histomorphometric analysis of osteoclast numbers and osteoblast numbers, expressed per millimeter bone surface in the vertebrae and tibiae, was carried out using an Osteometrics image analysis software system. Calcein double-labeling was performed by i.p. injection of calcein (10 mg/g body weight; C-0875; Sigma-Aldrich) at 6 and 1 days prior to sacrifice, as described previously (59). Bones were harvested and embedded in LR White acrylic resin. Serial sections were cut, and the freshly cut surface of each section was viewed and imaged using fluorescence microscopy. The calcein double-labeled morphometric analysis in trabecular bone was performed using Osteometrics image analysis software. The mineral apposition rate, bone formation rate, and double label surface/bone surface ratio were calculated as we previously described (1).

Confocal microscopy. Cells were treated with TNF for 24 hours, fixed with 4% paraformaldehyde, pretreated with 1% Triton X-100 and 0.5% BSA in PBST, and blocked in 10% BSA in PBST for 30 minutes at RT. Cells were immunostained with anti-NICD, anti-p52, or anti-RELB antibodies at 4°C overnight, incubated with secondary antibodies conjugated with Alexa Fluor 488 and Alexa Fluor 546 for 45 minutes at 37°C, and subjected to confocal microscopy. Confocal images were obtained with a MRC1024 confocal microscope (Bio-Rad). Laser beams with 488- and 543-nm excitation wavelengths were used for DAPI, FITC, and Cy5 imaging. Single confocal images were processed in Adobe Photoshop.

Transfection and luciferase reporter assay. Transient transfection was performed with Lipofectamine (Roche). 1×10^4 C3H10T1/2 cells were seeded in 24-well plates and cotransfected with NOTCH2-NICD (0.05 μg), p52, and/or RELB expressing constructs or the corresponding empty vectors along with RBPjκ-Luc (0.5 μg) and pRL-renilla (0.01 μg; Promega). Cells were cultured for a further 48 hours followed by harvesting for dual luciferase activity assays (Promega) according to the manufacturer's instruction. RBPjκ-Luc reporter activity was defined as the ratio of Firefly/Renilla luciferase activities.

IP and Western blot. For IP, C3H10T1/2 cells were seeded in 10-cm dishes and cotransfected with NICD, p52, or RELB expression vectors for 24 hours. Proteins from cell lysates were quantitated using a kit from Bio-Rad and subjected to IP as described in the technical bulletin from Sigma-Aldrich. Briefly, 300 μg of proteins in 1 ml cell lysis buffer were added with 1 μg antibody and incubated for 1 hour at 4°C, then incubated with prewashed EZview Red Protein A/G Affinity Gel beads (Sigma-Aldrich) for another hour at 4°C. To test whether TNF affected the binding affinity of NF-κB and NICD proteins, we performed an affinity assay according to a published protocol (39). In brief, the IP complex was washed 3 times with gradient concentrations of NaCl wash buffer containing 0, 200, 350, or 500 mM NaCl for 15 minutes. Eluted samples were fractionated by SDS-PAGE and transferred to PVDF membranes. For Western blot analysis, whole-cell lysates (10 μg) were loaded in 10% SDS-PAGE gels and blotted with antibodies against HES1, p52, RELB, p50, RELA (Santa Cruz Biotechnology Inc.) and NOTCH2-NICD (Developmental Studies Hybridoma Bank, University of Iowa) or mouse GAPDH (Santa Cruz Biotechnology Inc.).

ChIP. C3H10T1/2 cells and 3rd-passage bone-derived cells from WT and p52/RELB dKO mice were treated with TNF for 24 hours after reaching confluence. ChIP was performed with MAGnify Chromatin Immunoprecipitation System (Invitrogen) according to the manufacturer's instructions. A total of 3×10^6 C3H10T1/2 cells was used for each experiment. Cells were treated with 1% formaldehyde for 15 minutes and then sonicated on ice 16 times (30 seconds on, 30 seconds off) at high power using a Bioruptor UCD-200 sonicator. Antibodies against NOTCH2-NICD, RELB (Santa Cruz Biotechnology Inc.), or p52 (Cell Signaling Technology) and control rat IgG (Invitrogen) were used with 100 μg chromatin per ChIP procedure. The amounts of each specific DNA fragment in IPs were determined by qPCR. Primers used for this analysis were as follows: RBPjκ, –194 to +160, 5′-CTCAGGCGCGCGCCATTGGCC-3′ (forward), 5′-GCTTACGTCCTTTTACTTGAC-3′ (reverse); negative control, 1.5 kb downstream from the RBPjκ binding sites of the *Hes1* promoter, 5′-CCTAGGGAGAAGGAGCTGGGCT-3′ (forward), 5′-TGGCCGTCAGGAGCCGGCACC-3′ (reverse).

Tibial bone defect model. 2 month-old SCID mice ($n = 4$) were anesthetized, and bilateral 2 × 5 mm cortical bone defects were made in the anterior proximal tibiae and filled with bovine bone matrix. 5×10^5 cells from mesenchymal colony cells were injected into the bone matrix in defects. The right tibiae received cells from vehicle-treated mice and the left tibiae received cells from

DAPT-treated mice. Mice were sacrificed 6 weeks after surgery, and the volume of new bone formed in the defects (expressed as a percentage of the total defect volume) was measured by μCT, followed by histomorphometric analysis of the area of newly formed trabecular bone and associated spindle-shaped fibroblast-like cells observed in decalcified H&E-stained bone sections.

Patients and sampling. Patients (n = 11) met ACR criteria for RA, were seropositive (CCP^+), had a mean age of 56 years, mean disease duration of 3.25 years, and evidence of disease activity based on the presence of swollen and tender joints. Disease activity was measured by DAS28 scores (mean, 3.5; range, 2.19 to 5.85). Patients on biologics were excluded. Healthy controls (n = 14) were age matched, and subjects on bisphosphonates were excluded. BMMCs and PBMCs were isolated from heparinized BM aspirate and heparinized PB by Ficoll-Hypaque density gradient centrifugation (Pharmacia Biotech) (60, 61). PBMCs and BMMCs were incubated with anti-human CD45 antibody–conjugated microbeads (Miltenyi Biotec). $CD45^-$ and $CD45^+$ populations were collected according to the manufacturer's instructions.

Statistics. All results are given as mean ± SD. Comparisons between 2 groups were analyzed using 2-tailed unpaired Student's t test. 1-way ANOVA and Dunnett's post-hoc multiple comparisons were used for comparisons among 3 or more groups. P values less than 0.05 were considered statistically significant.

Study approval. All animal experiments were performed according to protocols approved by the University of Rochester Medical Center IACUC and conformed to the NIH *Guide for the Care and Use of Laboratory Animals*. For human studies, detailed written informed consent was obtained from all patients and healthy donors, in accordance with protocols approved by the Human Subjects IRB of the University of Rochester Medical Center (RSRB 29181 and 24888).

Acknowledgments

We thank G.S. Pryhuber for providing TNFR1/2 KO mice and Jixiang Shi and Lei Shu for histological analysis. This work was supported by NIH PHS awards AR48697 and AR63650 (to L. Xing); AR43510 (to B.F. Boyce); AR63071 (to M.J. Hilton); and AI077674, P01AI078907, and U19AI56390 (to J.H. Anolik). μCT was supported by NIH grant P30AR0613007. X. Li's salary was supported by a research grant from the National Natural Science Foundation of China (81202037 to Z. Wang).

Received for publication January 22, 2013, and accepted in revised form April 10, 2014.

Address correspondence to: Lianping Xing, Department of Pathology and Laboratory Medicine, 601 Elmwood Ave, Box 626, Rochester, New York 14642, USA. Phone: 585.273.4090; Fax: 585.756.4468; E-mail: Lianping_xing@urmc.rochester.edu.

1. Zhao L, et al. Tumor necrosis factor inhibits mesenchymal stem cell differentiation into osteoblasts via the ubiquitin E3 ligase Wwp1. *Stem Cells*. 2011;29(10):1601–1610.
2. Kaneki H, et al. Tumor necrosis factor promotes Runx2 degradation through up-regulation of Smurf1 and Smurf2 in osteoblasts. *J Biol Chem*. 2006; 281(7):4326–4333.
3. Guo R, et al. Ubiquitin ligase Smurf1 mediates tumor necrosis factor-induced systemic bone loss by promoting proteasomal degradation of bone morphogenetic signaling proteins. *J Biol Chem*. 2008; 283(34):23084–23092.
4. Li P, et al. Systemic tumor necrosis factor alpha mediates an increase in peripheral CD11bhigh osteoclast precursors in tumor necrosis factor alpha-transgenic mice. *Arthritis Rheum*. 2004; 50(1):265–276.
5. Diarra D, et al. Dickkopf-1 is a master regulator of joint remodeling. *Nat Med*. 2007;13(2):156–163.
6. Mukai T, et al. TNF-α inhibits BMP-induced osteoblast differentiation through activating SAPK/JNK signaling. *Biochem Biophys Res Commun*. 2007; 356(4):1004–1010.
7. Li P, Schwarz EM. The TNF-α transgenic mouse model of inflammatory arthritis. *Springer Semin Immunopathol*. 2003;25(1):19–33.
8. Zanotti S, Canalis E. Notch and the skeleton. *Mol Cell Biol*. 2010;30(4):886–896.
9. Engin F, et al. Dimorphic effects of Notch signaling in bone homeostasis. *Nat Med*. 2008;14(3):299–305.
10. Hilton MJ, et al. Notch signaling maintains bone marrow mesenchymal progenitors by suppressing osteoblast differentiation. *Nat Med*. 2008; 14(3):306–314.
11. Zanotti S, Smerdel-Ramoya A, Stadmeyer L, Durant D, Radtke F, Canalis E. Notch inhibits osteoblast differentiation and causes osteopenia. *Endocrinology*. 2008;149(8):3890–3899.
12. Zhao B, et al. Interferon regulatory factor-8 regulates bone metabolism by suppressing osteoclastogenesis. *Nat Med*. 2009;15(9):1066–1071.
13. Karin M, Greten FR. NF-κB: linking inflammation and immunity to cancer development and progression. *Nat Rev Immunol*. 2005;5(10):749–759.
14. Courtois G, Gilmore TD. Mutations in the NF-κB signaling pathway: implications for human disease. *Oncogene*. 2006;25(51):6831–6843.
15. Boyce BF, Yao Z, Xing L. Functions of nuclear factor κB in bone. *Ann N Y Acad Sci*. 2010;1192:367–375.
16. Beg AA, Sha WC, Bronson RT, Ghosh S, Baltimore D. Embryonic lethality and liver degeneration in mice lacking the RelA component of NF-κB. *Nature*. 1995;376(6536):167–170.
17. Vaira S, Alhawagri M, Anwisye I, Kitaura H, Faccio R, Novack DV. RelA/p65 promotes osteoclast differentiation by blocking a RANKL-induced apoptotic JNK pathway in mice. *J Clin Invest*. 2008; 118(6):2088–2097.
18. Chang J, et al. Inhibition of osteoblastic bone formation by nuclear factor-κB. *Nat Med*. 2009; 15(6):682–689.
19. Franzoso G, et al. Requirement for NF-κB in osteoclast and B-cell development. *Genes Dev*. 1997; 11(24):3482–3496.
20. Soysa NS, et al. The pivotal role of the alternative NF-κB pathway in maintenance of basal bone homeostasis and osteoclastogenesis. *J Bone Miner Res*. 2010;25(4):809–818.
21. Zhao C, et al. Noncanonical NF-κB signaling regulates hematopoietic stem cell self-renewal and microenvironment interactions. *Stem Cells*. 2012; 30(4):709–718.
22. Yao Z, Li Y, Yin X, Dong Y, Xing L, Boyce BF. NF-κB RelB negatively regulates osteoblast differentiation and bone formation. *J Bone Miner Res*. 2014; 29(4):866–877.
23. Osipo C, Golde TE, Osborne BA, Miele LA. Off the beaten pathway: the complex cross talk between Notch and NF-κB. *Lab Invest*. 2008;88(1):11–17.
24. Schwarzer R, Jundt F. Notch and NF-κB signaling pathways in the biology of classical Hodgkin lymphoma. *Curr Mol Med*. 2011;11(3):236–245.
25. Maniati E, et al. Crosstalk between the canonical NF-κB and Notch signaling pathways inhibits Pparγ expression and promotes pancreatic cancer progression in mice. *J Clin Invest*. 2011; 121(12):4685–4699.
26. Hansson EM, Lendahl U, Chapman G. Notch signaling in development and disease. *Semin Cancer Biol*. 2004;14(5):320–328.
27. Wright TW, Pryhuber GS, Chess PR, Wang Z, Notter RH, Gigliotti F. TNF receptor signaling contributes to chemokine secretion, inflammation, and respiratory deficits during Pneumocystis pneumonia. *J Immunol*. 2004;172(4):2511–2521.
28. Teachey DT, et al. Targeting Notch signaling in autoimmune and lymphoproliferative disease. *Blood*. 2008;111(2):705–714.
29. Zhang H, Xing L. Ubiquitin E3 ligase Itch negatively regulates osteoblast differentiation from mesenchymal progenitor cells. *Stem Cells*. 2013; 31(8):1574–1583.
30. Geling A, Steiner H, Willem M, Bally-Cuif L, Haass C. A γ-secretase inhibitor blocks Notch signaling in vivo and causes a severe neurogenic phenotype in zebrafish. *EMBO Rep*. 2002;3(7):688–694.
31. Shih Ie M, Wang TL. Notch signaling, γ-secretase inhibitors, and cancer therapy. *Cancer Res*. 2007; 67(5):1879–1882.
32. Tsao PN, et al. Lipopolysaccharide-induced Notch signaling activation through JNK-dependent pathway regulates inflammatory response. *J Biomed Sci*. 2011;18:56.
33. Wu W, Zhang L. γ-Secretase inhibitors for the treatment of Alzheimer's disease. *Drug Develop Res*. 2009; 70(2):94–100.
34. Roti G, et al. Complementary genomic screens identify SERCA as a therapeutic target in NOTCH1 mutated cancer. *Cancer Cell*. 2013;23(3):390–405.
35. Ishihara Y, et al. In situ imaging of the autonomous intracellular Ca(2+) oscillations of osteoblasts and osteocytes in bone. *Bone*. 2012;50(4):842–852.
36. Yip KH, et al. Thapsigargin modulates osteoclastogenesis through the regulation of RANKL-induced signaling pathways and reactive oxygen species production. *J Bone Miner Res*. 2005; 20(8):1462–1471.
37. Ghantous A, Gali-Muhtasib H, Vuorela H, Saliba NA, Darwiche N. What made sesquiterpene lactones reach cancer clinical trials? *Drug Discov Today*. 2010;15(15–16):668–678.
38. Sun SC. Non-canonical NF-κB signaling pathway. *Cell Res*. 2011;21(1):71–85.
39. Sumara I, Vorlaufer E, Gieffers C, Peters BH, Peters JM. Characterization of vertebrate cohesin complexes and their regulation in prophase. *J Cell Biol*. 2000; 151(4):749–762.
40. Duan L, Ren Y. Role of notch signaling in osteoimmunology — from the standpoint of osteoclast differentiation. *Eur J Orthod*. 2013;35(2):175–182.

41. Zhao B, Grimes SN, Li S, Hu X, Ivashkiv LB. TNF-induced osteoclastogenesis and inflammatory bone resorption are inhibited by transcription factor RBP-J. *J Exp Med*. 2012;209(2):319–334.
42. Xu H, et al. Notch-RBP-J signaling regulates the transcription factor IRF8 to promote inflammatory macrophage polarization. *Nat Immunol*. 2012; 13(7):642–650.
43. Brownlow N, Mol C, Hayford C, Ghaem-Maghami S, Dibb NJ. Dasatinib is a potent inhibitor of tumour-associated macrophages, osteoclasts and the FMS receptor. *Leukemia*. 2009;23(3):590–594.
44. Bai S, et al. NOTCH1 regulates osteoclastogenesis directly in osteoclast precursors and indirectly via osteoblast lineage cells. *J Biol Chem*. 2008; 283(10):6509–6518.
45. Ando K, et al. Induction of Notch signaling by tumor necrosis factor in rheumatoid synovial fibroblasts. *Oncogene*. 2003;22(49):7796–7803.
46. Okamoto T. The epigenetic alteration of synovial cell gene expression in rheumatoid arthritis and the roles of nuclear factor κB and Notch signaling pathways. *Mod Rheumatol*. 2005;15(2):79–86.
47. Gao W, et al. Notch-1 mediates hypoxia-induced angiogenesis in rheumatoid arthritis. *Arthritis Rheum*. 2012;64(7):2104–2113.
48. Park JS, et al. Inhibition of Notch signalling ameliorates experimental inflammatory arthritis [published online ahead of print November 19, 2013]. *Ann Rheum Dis*. doi:10.1136/annrheumdis-2013-203467.
49. Sekine C, Koyanagi A, Koyama N, Hozumi K, Chiba S, Yagita H. Differential regulation of osteoclastogenesis by Notch2/Delta-like 1 and Notch1/Jagged1 axes. *Arthritis Res Ther*. 2012;14(2):R45.
50. Fernandez L, et al. Tumor necrosis factor-α and endothelial cells modulate Notch signaling in the bone marrow microenvironment during inflammation. *Exp Hematol*. 2008;36(5):545–558.
51. Acharyya S, et al. TNF inhibits Notch-1 in skeletal muscle cells by Ezh2 and DNA methylation mediated repression: implications in duchenne muscular dystrophy. *PLoS One*. 2010;5(8):e12479.
52. Tao J, Chen S, Lee B. Alteration of Notch signaling in skeletal development and disease. *Ann N Y Acad Sci*. 2010;1192:257–268.
53. Zetterberg H, Mattsson N, Blennow K, Olsson B. Use of theragnostic markers to select drugs for phase II/III trials for Alzheimer disease. *Alzheimers Res Ther*. 2010;2(6):32.
54. Park D, et al. Endogenous bone marrow MSCs are dynamic, fate-restricted participants in bone maintenance and regeneration. *Cell Stem Cell*. 2012; 10(3):259–272.
55. Yao Z, Xing L, Boyce BF. NF-κB p100 limits TNF-induced bone resorption in mice by a TRAF3-dependent mechanism. *J Clin Invest*. 2009; 119(10):3024–3034.
56. Pryhuber GS, et al. Parenchymal cell TNF receptors contribute to inflammatory cell recruitment and respiratory failure in Pneumocystis carinii-induced pneumonia. *J Immunol*. 2008;181(2):1409–1419.
57. Zhu H, et al. A protocol for isolation and culture of mesenchymal stem cells from mouse compact bone. *Nat Protoc*. 2010;5(3):550–560.
58. Majeti R, et al. Dysregulated gene expression networks in human acute myelogenous leukemia stem cells. *Proc Natl Acad Sci U S A*. 2009; 106(9):3396–3401.
59. Zhang HW, et al. Defects in mesenchymal stem cell self-renewal and cell fate determination lead to an osteopenic phenotype in Bmi-1 null mice. *J Bone Miner Res*. 2010;25(3):640–652.
60. Kobie JJ, et al. Decreased influenza-specific B cell responses in rheumatoid arthritis patients treated with anti-tumor necrosis factor. *Arthritis Res Ther*. 2011;13(6):R209.
61. Palanichamy A, et al. Neutrophil-mediated IFN activation in the bone marrow alters B cell development in human and murine systemic lupus erythematosus. *J Immunol*. 2014;192(3):906–918.

OPEN ACCESS Freely available online

PLoS one

Nuclear Factor-Kappa B Family Member RelB Inhibits Human Immunodeficiency Virus-1 Tat-Induced Tumor Necrosis Factor-Alpha Production

Michelle Kiebala[1], Oksana Polesskaya[1], Zhenqiang Yao[2], Seth W. Perry[3], Sanjay B. Maggirwar[1]*

1 Department of Microbiology and Immunology, the University of Rochester School of Medicine and Dentistry, Rochester, New York, United States of America, **2** Department of Pathology and Laboratory Medicine, the University of Rochester School of Medicine and Dentistry, Rochester, New York, United States of America, **3** Center for Neural Development and Disease, Department of Neurology, the University of Rochester School of Medicine and Dentistry, Rochester, New York, United States of America

Abstract

Human Immunodeficiency Virus-1 (HIV-1)-associated neurocognitive disorder (HAND) is likely neuroinflammatory in origin, believed to be triggered by inflammatory and oxidative stress responses to cytokines and HIV protein gene products such as the HIV transactivator of transcription (Tat). Here we demonstrate increased messenger RNA for nuclear factor-kappa B (NF-κB) family member, transcription factor RelB, in the brain of doxycycline-induced Tat transgenic mice, and increased RelB synthesis in Tat-exposed microglial cells. Since genetic ablation of RelB in mice leads to multi-organ inflammation, we hypothesized that Tat-induced, newly synthesized RelB inhibits cytokine production by microglial cells, possibly through the formation of transcriptionally inactive RelB/RelA complexes. Indeed, tumor necrosis factor-alpha (TNFα) production in monocytes isolated from RelB deficient mice was significantly higher than in monocytes isolated from RelB expressing controls. Moreover, RelB overexpression in microglial cells inhibited Tat-induced TNFα synthesis in a manner that involved transcriptional repression of the TNFα promoter, and increased phosphorylation of RelA at serine 276, a prerequisite for increased RelB/RelA protein interactions. The Rel-homology-domain within RelB was necessary for this interaction. Overexpression of RelA itself, in turn, significantly increased TNFα promoter activity, an effect that was completely blocked by RelB overexpression. We conclude that RelB regulates TNFα cytokine synthesis by competitive interference binding with RelA, which leads to downregulation of TNFα production. Moreover, because Tat activates both RelB and TNFα in microglia, and because Tat induces inflammatory TNFα synthesis via NF-κB, we posit that RelB serves as a cryoprotective, anti-inflammatory, counter-regulatory mechanism for pathogenic NF-κB activation. These findings identify a novel regulatory pathway for controlling HIV-induced microglial activation and cytokine production that may have important therapeutic implications for the management of HAND.

Citation: Kiebala M, Polesskaya O, Yao Z, Perry SW, Maggirwar SB (2010) Nuclear Factor-Kappa B Family Member RelB Inhibits Human Immunodeficiency Virus-1 Tat-Induced Tumor Necrosis Factor-Alpha Production. PLoS ONE 5(7): e11875. doi:10.1371/journal.pone.0011875

Editor: Fatah Kashanchi, George Mason University, United States of America

Received January 22, 2010; **Accepted** July 6, 2010; **Published** July 29, 2010

Funding: This work was supported by the following National Institutes of Health grants: RO1 NS054578 and RO1 NS066801 (to SBM); R21 MH084718 (to SWP); T32 AI49105 (to MK). The funders had no role in study design, data collection and analysis, decision to publish, or preparation of the manuscript.

Competing Interests: The authors have declared that no competing interests exist.

* E-mail: sanjay_maggirwar@urmc.rochester.edu

Introduction

Human Immunodeficiency Virus-1 (HIV-1) enters the central nervous system (CNS) early after infection, and in many cases may ultimately result in HIV-1 associated neurologic disease (HAND) [1]. HAND can include neurocognitive impairments, motor deficits, or dementias [2], and continues to be a significant source of morbidity despite efficacious reduction of viral load by comprehensive anti-retroviral therapy (cART) [3–10]. Traditionally, onset of HAND correlated with CNS viral load, and was principally subcortical in origin, with neuropathology including multinucleated giant cells, reactive astrocytosis, myelin pallor, reduced dendritic complexity and synaptic density and neuronal loss [11–16]. Recent neuropathologic reports of severe white matter damage (i.e. leukoencephalopathy) in patients with HIV-1 infection and on cART [17–23], including significant frontostriatal and prefrontal cortex involvement in HAND [24–27], suggest that additional patterns of primary brain disease are emerging, either due to alterations in host cell signaling, or as yet unexplained interactions between virus, vulnerable populations of neural cells, and cART [6,28].

The pathogenesis of HAND likely arises from a toxic milieu of secretory neurotoxins released from HIV-1 infected, brain-resident mononuclear phagocytes and glia, and oxidative stress, which together adversely affect neuronal function. HIV productively infects microglia and perivascular macrophages, the resident phagocytes of the CNS, but does not infect neurons. This suggests that the neuropathology caused by HIV is indirect. Accordingly, neurologic deficits in HAND are more closely correlated with the presence of activated macrophages and microglia than with the amount of neuronal apoptosis or viral RNA [29–32]. Soluble viral proteins such as Tat and the glycoprotein gp120 can be released from infected microglia and macrophages [33]. Tat protein has been detected in blood plasma, serum, and cerebral spinal fluid (CSF) from HIV+ individuals, at levels ranging from 1–40 ng/ml [34,35], thus local extracellular concentrations in the CNS may be

much higher, particularly proximal to HIV+ pervivascular cells [36]. Tat also interacts with and activates neighboring, uninfected cells including microglia, astrocytes and neurons. Both infected and activated microglia and astrocytes produce the pro-inflammatory cytokines tumor necrosis factor-alpha (TNFα) and interleukin-1 beta (IL-1β), which further activate neighboring cells. Infected and activated cells also produce chemokines such as monocyte chemotactic protein-1 (MCP-1), attracting more inflammatory monocytes and macrophages [37–39]. Thus, circulating Tat has a high propensity to trigger this vicious cycle, leading to neurologic deficits [34].

HIV-1 Tat is necessary for viral replication and activates the nuclear factor-kappa B (NF-κB) signal transduction pathway in cells of the CNS [40,41]. Cytokine and chemokine gene expression in microglia, in turn, is also NF-κB dependent [41]. The NF-κB family of transcription factors is intricately involved in both innate and adaptive immune responses as well as in inflammation. In mammalian cells, there are five NF-κB family members including RelA (p65), RelB, cRel, p52 (with its precursor p100), and p50 (with its precursor p105). Homo- and hetero-dimeric combinations of the five NF-κB proteins activate transcription of NF-κB target genes. In resting cells, NF-κB dimers are retained in the cytoplasm through their inhibitory interaction with the inhibitor of kappa B (IκB) molecules [42]. Signals leading to activation of the NF-κB pathway include the pro-inflammatory cytokines TNFα and IL-1β [43]. Initiation of the NF-κB pathway is characterized by signal-induced activation of the inhibitory κB kinase (IKK) complex. IKK then phosphorylates IκBα leading to its subsequent ubiquitination and proteolytic degradation [44]. Degradation of IκBα frees NF-κB dimers to move to the nucleus, where they can then activate transcription. We, and others, have demonstrated that Tat-induced production of cytokines (e.g. TNFα) by microglia involves activation of the NF-κB pathway, as evidenced by the rapid degradation of IκBα in Tat treated microglial cells [41,45]. Indeed, overexpression of IκBα S32/36A, which is resistant to proteasomal degradation, blocks Tat-induced TNFα synthesis in microglial cells, thereby suggesting that Tat-induced TNFα synthesis is NF-κB dependent [45].

Here we show that Tat treatment of microglial cells induces *de novo* synthesis of RelB. The NF-κB family member RelB has many distinguishing features compared to the other NF-κB proteins, such as its unique amino-terminal leucine zipper motif [46]. RelB also preferentially interacts with p100 rather than the usual NF-κB inhibitory molecules (e.g. IκBα) [47,48]. RelB has lower relative DNA binding activity at prototypical response elements, and can both activate and inhibit transcription of target genes [49,50]. Specific nuclear DNA κB binding sites are efficiently recognized by RelB/p52 DNA heterodimers, allowing for transcription of certain κB-regulated target genes [49,51]. RelB also forms inactive complexes with RelA [52–55]. In addition, studies in $RelB^{-/-}$ mice have demonstrated impaired cellular immunity and development of multi-organ inflammation that involves activation of myeloid cells [56,57]. RelB has also been shown to be inhibitory to the TNFα promoter in fibroblasts [58,59]. Together these results strongly suggest that RelB has anti-inflammatory and cytokine-regulating properties. Herein we investigate these anti-inflammatory properties of RelB in the context of HIV-induced neuroinflammation.

Initial experiments in transgenic mice expressing Tat under a doxycycline (Dox)-inducible glial fibrillary acidic protein (GFAP) promoter demonstrated increased RelB message in the brains of Dox-induced mice, confirming that Tat increases RelB *in vivo*. Furthermore, Tat also enhanced TNFα release from monocytes isolated from $RelB^{-/-}$ mice as compared to monocytes from wild-type (WT) mice, which is in agreement with previous reports of anti-inflammatory properties of RelB. Next, in vitro experiments were conducted to determine the mechanisms of RelB inhibition of TNFα release from microglial cells. These experiments suggested that RelB binds RelA to inhibit RelA-dependent activation of the TNFα promoter, and that this RelB/RelA mechanism of interaction requires the entire RelB Rel Homology Domain (RHD). Taken together, these results suggest that RelB may regulate cytokine synthesis by counter-regulating NF-κB activated pathways, a finding that has important therapeutic implications for the management of HAND.

Methods

Reagents

Cycloheximide (CHX) and MG-132 were obtained from BioMol International/Enzo Life Sciences (Plymouth Meeting, PA, USA). CHX was used at concentrations of 10 and 25 μg/mL and MG-132 was used at a concentration of 50μM. Viral protein gp120 *SF162* was obtained from Immunodiagnostics (Woburn, MA, USA), and used at a concentration of 100nM. All other chemicals and regents were purchased from Sigma-Aldrich (St. Louis, MO, USA).

HIV-1 Tat 1–72 was expressed in Sf9 insect cells using a baculovirus system and was purified using Ni-NTA agarose according to the BD BaculoGold 6×His expression and purification protocol (BD Biosciences, San Jose, CA, USA). Briefly, the Tat 1–72 sequence (from HIV-1, YU-2 isolate) was PCR amplified and cloned into XhoI and NcoI sites in the pAcHLT-B baculovirus transfer vector. The recombinant plasmid was confirmed by sequencing. This transfer vector was then co-transfected into Sf9 cells along with BD BaculoGold linearized baculovirus backbone DNA. Resultant virus stock was propagated in Sf9 cells. Tat protein was then purified from lysates of infected Sf9 cells using Ni-NTA agarose beads.

Importantly, the Tat produced in this fashion and used for these studies was functionally indistinguishable from E. coli prepared Tat 1–72, and caused similar microglial activation of NF-κB related pathways as previously seen for E. coli Tat 1–72 (Text S1, Figure S1). Therefore this Sf9 Tat, hereafter referred to as "Tat," was used for these studies, allowing us to take advantage of this more efficient protocol for producing HIV-1 Tat in the high yields required for these studies.

Tat 1–101 (Immunodiagnostics,Woburn, MA, USA), Tat 1–72 (Sf9-Tat), Tat 1–72 (E. coli Tat; kind gift of Dr. A. Nath, Johns Hopkins University, Baltimore, MD, USA), Tat C31S (Diatheva, Fano, Italy), Tat Δ31–61 (obtained from Philip Ray, University of Kentucky, Lexington, KY, USA) and Tat peptides (Tat 48–72: G-R-K-K-R-R-Q-R-R-R-P-P-Q-D-S-Q-T-H-Q-S-S-L-S-K-Q; GenScript, Piscataway, NJ, USA; Tat 46–60: S-Y-G-R-K-K-R-R-Q-R-R-R-P-P-Q; and Tat 65–80: H-Q-V-S-L-S-K-Q-P-T-S-Q-P-R-G-D; Intracel Corp., Cambridge, MA, USA) were used at 100nM (~800 ng/ml) concentration unless otherwise described. It should be noted that soluble Tat levels in HIV patient sera have been measured up to 40 ng/mL [34,35]. It has also been shown that Tat can interact with endogenous glycosaminoglycans and heparin sulfates, thereby potentially lowering its measurable concentration *in vivo* [60]. Therefore, it is likely that Tat concentrations surrounding HIV-infected cells are much higher [36]. In addition, Tat's exceedingly strong affinity for other proteins and glass/plastic, and its temperature susceptibility, make it impossible to determine exactly what fraction of the Tat "starting dose" actually reaches the experimental specimen, thus likely leading to underestimation of Tat functions in vitro [61].

Finally, Tat's effects in vivo are likely to occur over long-term exposures. Chronic, low dose, in vivo effects of any reagent are often appropriately modeled in vitro, by proportionately higher doses of that same reagent, over more acute time frames. For these reasons, and in order to be consistent with previous experiments from our laboratories, and others, we use 100nM Tat for these experiments, which is at the lower end of the Tat dose range seen with many comparable studies, and which many studies have found to be an appropriate Tat dose by which to model Tat's in vivo effects in vitro.

Cell Cultures

Primary cultures. Human peripheral monocytes were isolated from commercially obtained soft-spun buffy coats (New York Blood Center, Long Island City, NY, USA) derived from HIV-1 and hepatitis B virus-seronegative donors, using immunomagnetic isolation methods as described [62,63]. Briefly, peripheral blood mononuclear cells (PBMCs) were isolated from buffy coats after centrifugation on a lymphoprep gradient (AXIS-Shield, Oslo, Norway). Monocytes were then isolated by positive selection with anti-CD14 MACS beads (Miltenyi Biotec, Bergisch Gladbach, Germany; Auburn, CA, USA), and cultured in RPMI 1640 medium supplemented with 10% fetal bovine serum (FBS), and antibiotics for 18–24h before use. The monocyte cultures used in our experiments were >95% pure as determined by morphologic criteria.

Mouse monocytes were isolated from bone marrow derived from age-matched C57BL/6 ($RelB^{+/+}$) or $RelB^{-/-}$ mice by positive selection with mouse/human anti-CD11b MACS beads (Miltenyi Biotec, Bergisch Gladbach, Germany; Auburn, CA, USA). These cells were cultured in RPMI 1640 medium supplemented with 10% FBS and antibiotics for 16h before use.

Human astrocytes were kindly supplied by Dr. Anuja Ghorpade (University of North Texas Health Science Center, Fort Worth, Texas, USA). Briefly, brain tissue was mechanically dissociated, centrifuged, and resuspended in Dulbecco's modified Eagle medium (DMEM) supplemented with 10% FBS and 1× penicillin-streptomycin-glutamine for 7 days. Non-adherent microglia and oligodendrocytes were removed by extensive agitation (260 rpm) on a rotating platform. Cultures of astrocytes were >98% pure as determined by immunocytochemical (ICC) staining for GFAP (rabbit polyclonal antibody, Chemicon/Millipore, Billerica, MA, USA).

Cell-lines: The murine microglial cell-line (BV-2) and human embryonic kidney cell line (HEK 293) were obtained from Dr. R. Donato (University of Perugia, Perugia, Italy) and American Type Culture Collection (ATCC, Manassas, VA, USA) respectively. These cells were maintained in DMEM containing 10% FBS, 2mM glutamine, and antibiotics, by standard procedures.

ELISA

TNFα levels were measured in culture supernatants (pre-cleared by brief centrifugation) by using a mouse TNFα ELISA kit (eBioscience, San Diego, CA, USA) according to the manufacturer's instructions. This kit has a minimum sensitivity threshold of 8 pg/ml. Briefly, 50 µl of cell culture supernatant was incubated in a 96-well plate pre-coated with a TNFα-specific monoclonal antibody for 1.5h. After extensive washing, binding of TNFα was detected by incubation with biotinylated antibodies, followed by streptavidin-peroxidase; colorimetric enzyme assays were performed to detect bound TNFα. Other cytokine levels were measured using Bio-Plex Multi-Plex analysis for detecting a panel of multiple cytokines from a single sample (Bio-Rad, Hercules, CA, USA). Briefly, this technology uses multiple spectrally identifiable polystyrene beads, each coated with a different anti-cytokine antibody, followed by target, then secondary antibody binding, to detect multiple cytokines from a single sample in typical sandwich-assay fashion. This assay was utilized to measure levels of IL-1β, IL-6, and MCP-1 in supernatant samples, as previously described [64–66]. TNFα ELISA results were also confirmed by this assay.

Electrophoretic Mobility Shift Assays

Nuclear extracts were prepared from BV-2 cells as previously described [67]. Electrophoretic mobility shift assays (EMSAs) were performed by incubating nuclear extracts with ^{32}P-radiolabeled high affinity, double-stranded DNA probe suspended in EMSA reaction buffer (12mM HEPES, pH 7.9, 100mM NaCl, 0.25mM EDTA, 1mM dithiothreitol, and 1mM phenylmethanesulfonyl fluoride) at room temperature for 10 min, followed by resolution of the protein-DNA complexes on native 4% polyacrylamide gels, then autoradiography. The double stranded oligonucleotide probes used in EMSA were as follows: (1) NF-κB: 5′-CAACGG-CAGGGGAATTCCCCTCTCCTT-3′ and (2) OCT-1: 5′-TG-TCGAATGCAAATCACTAGAA-3′. For antibody supershift assays, 1 µg of antiserum recognizing each of the NF-κB subunits (Santa Cruz Biotechnologies Inc., Santa Cruz, CA, USA) was added to the EMSA reaction 10 min prior to electrophoresis. Specificity and reactivity of the antibodies was confirmed as described previously [68,69].

Plasmids

The luciferase reporter construct driven by NF-κB as well as the RelA and cRel plasmids were obtained from Dr. S. C. Sun (MD Anderson Cancer Center, University of Texas, Houston, TX, USA). The plasmids expressing mouse RelB (mRelB) and influenza hemagglutinin (HA)-tagged derivative of RelA (HA-RelA) were obtained from Dr. Bernd Baumann (Ulm University, Ulm, Germany). We PCR amplified the mRelB sequence from this plasmid and inserted it into the pcDNA3.1-Myc/His(-)B vector (Invitrogen, Carlsbad, CA, USA). The luciferase reporter construct driven by the mouse TNFα (mTNFα) promoter was obtained from Dr. Dmitry Kuprash (Engelhardt Institute of Molecular Biology, Moscow, Russia).

Transient Transfections

HEK 293 cells were transfected with plasmid DNA using Lipofectamine 2000 (Invitrogen, Carlsbad, CA, USA). Cells were seeded at 1.8×10^5 cells/well in 24-well plates 18h prior to transfection. Each transfection reaction contained a total of 0.85 µg plasmid DNA. After addition of the transfection mixture to the cells, they were incubated at 37°C for 24h. BV-2 cells were transfected with plasmid DNA using Lipofectamine LTX (Invitrogen, Carlsbad, CA, USA) or Nucleofector (Amaxa/Lonza, Basel, Switzerland; Walkersville, MD, USA). For Lipofectamine transfections, cells were seeded at 1×10^5 cells/well in 24-well plates 18h prior to transfection, then transfected as for Lipofectamine 2000 above. For nucleofection, 5×10^6 cells were transfected with 10 µg NF-κB luciferase plasmid DNA. Transfected cells were plated at 5×10^5 cells/well in a 24-well plate and incubated for 24h prior to Tat treatment. Media was changed 4h after transfection and again prior to treatment to reduce cell toxicity. To determine nucleofection-based transfection efficiency, an aliquot of BV-2 cells was transfected with a GFP-expressing vector, pMax-GFP (Amaxa/Lonza, Basel, Switzerland; Walkersville, MD, USA), and 24h after transfection, greater than 90% of BV-2 cells were GFP-positive.

Luciferase assays

A luciferase reporter plasmid containing NF-κB responsive elements upstream of a firefly luciferase gene was transfected into BV-2 cells using Nucleofector (Amaxa/Lonza, Basel, Switzerland; Walkersville, MD, USA). 24h post-transfection, cells were either left untreated or incubated for 8h with 100nM Tat. Cell lysates were prepared using reporter lysis buffer (Promega Life Sciences, Madison, WI, USA), and luciferase activity was measured. A luciferase reporter plasmid with the mouse TNFα promoter region upstream of a luciferase reporter was transfected into either HEK 293 cells using Lipofectamine (Invitrogen, Carlsbad, CA, USA) or BV-2 cells using Nucleofector (Amaxa/Lonza, Basel, Switzerland; Walkersville, MD, USA). 24h post-transfection, cell lysates were prepared using reporter lysis buffer (Promega Life Sciences, Madison, WI, USA), and luciferase activity was measured with a Lumicount Microplate Luminometer (Packard Instrument Company, Meriden, CT; now PerkinElmer, Waltham, MA). In these assays, total protein amount as determined by Bradford assay (Bio-Rad, Hercules, CA, USA), was used to normalize the samples.

Immunoblotting assays

Following the indicated treatments, whole cell lysates were prepared in ELB buffer (50mM HEPES (pH 7), 250mM NaCl, 0.1% Nonidet P-40, 5mM EDTA, 10mM NaF, 0.1mM Na_3VO_4, 50μM $ZnCl_2$, supplemented with 0.1mM PMSF, 1mM DTT, and a mixture of protease and phosphatase inhibitors). Cellular debris was removed by high-speed centrifugation. Lysates were fractionated on 7.5% SDS-PAGE gels and protein was electrophoretically transferred to Hybond ECL nitrocellulose membrane (GE Healthcare Bio-Sciences Corporation, Piscataway, NJ, USA). The membranes were analyzed for immunoreactivity with primary antibodies raised against RelB (1:1000), RelA (1:1000), IκBα (1:1000), or α-Tubulin (1:1000; all from Santa Cruz Biotechnologies Inc., Santa Cruz, CA, USA), RelA P-S276 (1:1000), p100/p52 (1:1000, Cell Signaling Technology, Danvers, MA, USA), Actin (1:1000, Calbiochem/EMD Chemicals, Gibbstown, NJ, USA), or antiserum to HIV-1 Tat (1:3000; NIH AIDS Research & Reference Reagent Program, Germantown, MD, USA). Bound antibodies were detected by species-specific, horseradish peroxidase (HRP)-conjugated secondary antibodies (1:3000, GE Healthcare Bio-Sciences Corporation, Piscataway, NJ, USA), followed by addition of ECL reagent (Pierce Biotechnology/Thermo Fisher Scientific, Rockford, IL, USA) and subsequent exposure to x-ray film. Equal loading and uniformity of protein transfer to the nitrocellulose membrane were verified by stripping and reprobing the membranes with primary antibodies specific to α-Tubulin or Actin.

Tat transgenic mice and Real-Time RT-PCR analyses

Tat transgenic mice were kindly provided by Dr. Johnny He (Indiana University School of Medicine, Indianapolis, IN, USA) [70]. Briefly, 6-week old Tat transgenic mice were treated with 80 mg/kg of doxycycline in saline, injected intraperitoneally (IP) once daily for 0, 3, or 14 days. There were 4 mice per group for the 0 and 14 day groups, and 5 mice in the 3 day group. Mice were euthanized via cervical dislocation and brain tissue was immediately dissected at 4°C, flash frozen in isopentene, and stored at −80°C. RNA was isolated from half of each brain using the PureLink™ Total RNA Purification System (Invitrogen, Carlsbad, CA, USA) according to the manufacturer's protocol. Complementary DNA (cDNA) synthesis was performed using 2 μg total RNA, oligo-dT primers, and the Superscript III first-strand synthesis system (Invitrogen, Carlsbad, CA, USA). Gene-specific primer sequences were as follows: 1) Tat primers: forward 5′-GCATCCAGGGGATCAGCCTA-3′, reverse 5′-CTGATGAGCTCTTCGTCGCT-3′; 2) RelB primers: forward 5′-CCCCTACAATGCTGGCTCCCTGAA-3′, reverse 5′-CACGGCCCGCTCTCCTTGTTGATT-3′; 3) TNFα primers: forward 5′-ACTCCAGAACATCTTGGAAATAGC-3′, reverse 5′-GCGGATCATGCTTTCTGTGC-3′; 4) RelA primers: forward 5′-TCAAGATCAATGGCTACACAGG-3′, reverse 5′-GCATTCAAGTCATAGTCCCCG-3′; 5) GAPDH primers: forward 5′-TGATGACATCAAGAAGGTGGTGAA-3′, reverse 5′-TCCTTGGAGGCCATGTAGGCCAT-3′. Real-time RT-PCR was performed using iQ™ SYBR® Green PCR Supermix (Bio-Rad, Hercules, CA, USA) and 100nM gene-specific forward and reverse primers in 20 μL total volume. After denaturation for 3 min. at 95°C, the PCR was run for 40 cycles of 95°C for 30 sec., primer-specific melting temperature (T_m °C) for 1 min., and 72°C for 30 sec. using an iCycler instrument (Bio-Rad, Hercules, CA, USA). GAPDH served as an internal control in these experiments.

All animal experiments were carried out in accordance with the Animal Welfare Act and the National Institute of Health guidelines. The animal protocol was approved by the University Committee on Animal Resources of the University of Rochester Medical Center. The facilities and programs of the Vivarium and Division of Laboratory Animal Medicine of the School of Medicine and Dentistry are fully accredited by the Association for the Assessment and Accreditation of Laboratory Animal Care International (AAALAC) and are in compliance with state law, federal statute and NIH policy.

Immunoprecipitation

Samples containing equal amounts of protein were pre-cleared by incubation with 2 μg of normal rabbit serum and 20 μL of a 50/50 protein A/G+ agarose beads solution (both from Santa Cruz Biotechnologies Inc., Santa Cruz, CA, USA) at 4°C on a rotator for 1h. After the pre-clear step, the beads were removed by centrifugation and samples were transferred to tubes with specific antibodies (2 μg per sample). Samples were incubated with the antibodies at 4°C for 18h on a rotator. 30 μL of 50/50 protein A/G+ agarose beads were added to the samples, then they were incubated with rotation for an additional 2h at 4°C. The beads were then washed extensively with ELB lysis buffer supplemented with 0.1mM PMSF, 1mM DTT, and a mixture of protease and phosphatase inhibitors, and then boiled for 5 minutes in 20 μL of Laemmli buffer. Immunocomplexes were separated using SDS-PAGE (7.5%), transferred to a nitrocellulose membrane and probed with the indicated antibodies.

Statistical analysis

Mean data values and the standard error of the mean (SEM) were calculated for each variable. Data involving the analysis of multiple sample groups were analyzed by one-way ANOVA followed by Bonferroni's test for multiple comparisons. A value of $p<0.05$ was designated as statistically significant.

Results

Transgenic expression of Tat induces RelB synthesis in mouse brain

Tat transgenic (Tat-Tg) mice are used as a model of HIV-induced neurocognitive disorders, as they develop Tat-induced behavioral changes and neurological abnormalities including hunched posture, tremor, ataxia, slow motor movement, and seizures [70]. In addition, these mice exhibit neuropathologies including astrocytosis, degeneration of neuronal dendrites, neuronal apoptosis, and increased infiltration of activated monocytes

[70], all of which replicate features of HIV-associated neurologic disease (HAND). These mice express a Dox-inducible Tat gene driven by the GFAP promoter, which drives Tat protein production by astrocytes in the CNS [70].

RelB was originally identified as a protein that controls inflammation [56,57,59], leading us to hypothesize that RelB may mediate Tat's effects in models of HAND. Thus, we first used quantitative real-time PCR (qRT-PCR) to determine whether Tat altered RelB or RelA expression levels in the brains of the Tat-Tg mice. Total RNA isolated from brain tissue of mice induced with doxycycline for 0, 3, or 14 days was used to measure the abundance of Tat, RelB, and RelA transcripts. As compared to non-induced Tat-Tg mice (Day 0, Dox–), there was an approximately 20-fold increase in Tat mRNA levels in 14 day Dox-treated animals (Figure 1). Since Tat is known to activate TNFα production, in order to confirm the activity of Tat, we also measured TNFα synthesis in Dox-exposed mice. Our results revealed an increase in TNFα mRNA in the brains of Dox-induced mice, validating the functional activity of Tat in these animals (data not shown). Consistent with these effects, we also observed a nearly 5-fold increase in RelB mRNA levels by day 14 Dox treatment, confirming that Tat also increased RelB expression (Figure 1). Interestingly, under these conditions, RelA mRNA levels remained unchanged, suggesting that the Tat-mediated increase in RelB was not a generalized effect of Tat on NF-κB subunits (Figure 1). Since total RNA was isolated from whole brain tissue, we could not determine which cell type most contributed to this Tat-induced increase in RelB message in this *in vivo* model. However, our further experiments in BV-2 microglial cells, primary human monocytes, and primary human astrocytes suggest that both microglia and astrocytes contribute to this increase.

RelB inhibits TNFα and cytokine production triggered by Tat treatment

Microglia are believed to be principal mediators of HAND-associated neuropathology. Therefore, to explore the functional role of Tat-RelB induction in microglia, we examined Tat's ability to stimulate TNFα synthesis in magnetically sorted $CD11b^+$ monocytic cells derived from the bone marrow of RelB deficient ($RelB^{-/-}$) mice. We chose these cells to model microglia for three reasons: (1) microglia originate from myeloid lineage precursors in the bone marrow [71], (2) $CD11b^+$ bone marrow cells are sensitive to Tat [72], and (3) highly homogeneous monocyte cultures can be obtained from the bone marrow of genetically modified mice [73]. The vast majority of CD11b-positive cells (nearly 95% of the total isolated population) were monocytes, as determined by morphologic criteria. Using immunoblot analyses, we first verified that 8h 100 nM Tat treatment stimulated RelB synthesis in these murine monocytes, and that RelB is indeed absent in $RelB^{-/-}$ derived cells (Figure 2A). Again, following 8h 100 nM Tat treatment of these cells, we also collected culture supernatants and measured TNFα levels by ELISA. The results shown in Figure 2B reveal enhanced production of TNFα in Tat-treated $RelB^{-/-}$ monocytes as compared to their $RelB^{+/+}$ counterparts, strongly suggesting an anti-inflammatory role for RelB. The Bio-Plex Multi-Plex cytokine array assay was also used to measure additional inflammatory cytokine and chemokine levels in these same culture supernatants. Likewise, these results (Figure 2C) indicated enhanced production of IL-1β, IL-6, and MCP-1 in Tat-treated $RelB^{-/-}$ monocytes compared to Tat-treated $RelB^{+/+}$ cells, further supporting an anti-inflammatory role for RelB in the context of HIV. TNFα levels, as determined by ELISA above, were also validated using the Bio-Plex cytokine array, with similar results (data not shown).

We performed additional complementary experiments to test whether RelB overexpression in the microglial BV-2 cell line could reverse Tat's effects on TNFα synthesis. In contrast to cRel overexpression, which had no effect on Tat-induced TNFα production, RelB overexpression reduced Tat-induced TNFα release from BV-2 cells as we anticipated (Figure 3), further confirming the inhibitory properties of RelB.

Because RelB was over-expressed in these BV-2 cells, there is the possibility that over-expressing high levels of exogenous RelB could interfere with cells' ability to respond to Tat. This is not likely for two reasons: 1. cRel overexpression did not affect Tat's ability to induce TNFα production, and 2. Immunoblot analysis of transfected RelB levels, compared to RelB levels stimulated by 8h 100nM Tat treatment, showed no significant differences, thus suggesting that exogenous RelB levels resulting from transfection were similar to inducible RelB levels (data not shown). Together these data indicate that RelB's ability to reduce TNFα production in Tat-exposed cells results from a functional effect of RelB, and is not due to overexpression of RelB interfering with cells' ability to respond to Tat.

Tat induces de novo synthesis of RelB

Next we examined the mechanisms by which RelB regulates TNFα production through Tat. To do this we employed the easily genetically manipulatable microglial BV-2 cell line. First, we needed to confirm that the Tat-induced increases in RelB that we observed in our *in vivo* models, also translated to this *in vitro* model. Although activation of NF-κB involves cytosolic-nuclear redistribution of RelA (a major component of NF-κB) rather than *de novo* synthesis of this protein, NF-κB activation also positively regulates expression of other NF-κB family members, including RelB

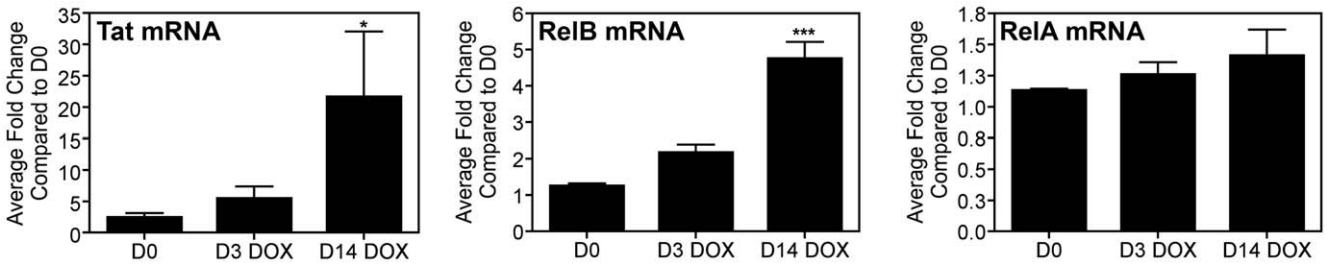

Figure 1. Transgenic expression of Tat induces RelB synthesis in mouse brain. 6-week old Tat-transgenic mice were induced with doxycycline for the indicated periods of time. Total RNA was extracted from brain tissue, reverse transcribed using oligo-dT primers, and subjected to Real-Time SYBR Green RT-PCR amplification. Fold induction of Tat, RelB and RelA mRNA species was normalized to GAPDH and presented as a function of the expression level in D0 samples. Data represent mean ± SEM of four replicates for D0 and D14 samples, and five replicates for D3 samples. Statistical significance (***, $p<0.001$ or *, $p<0.05$) is denoted as compared to D0 samples.
doi:10.1371/journal.pone.0011875.g001

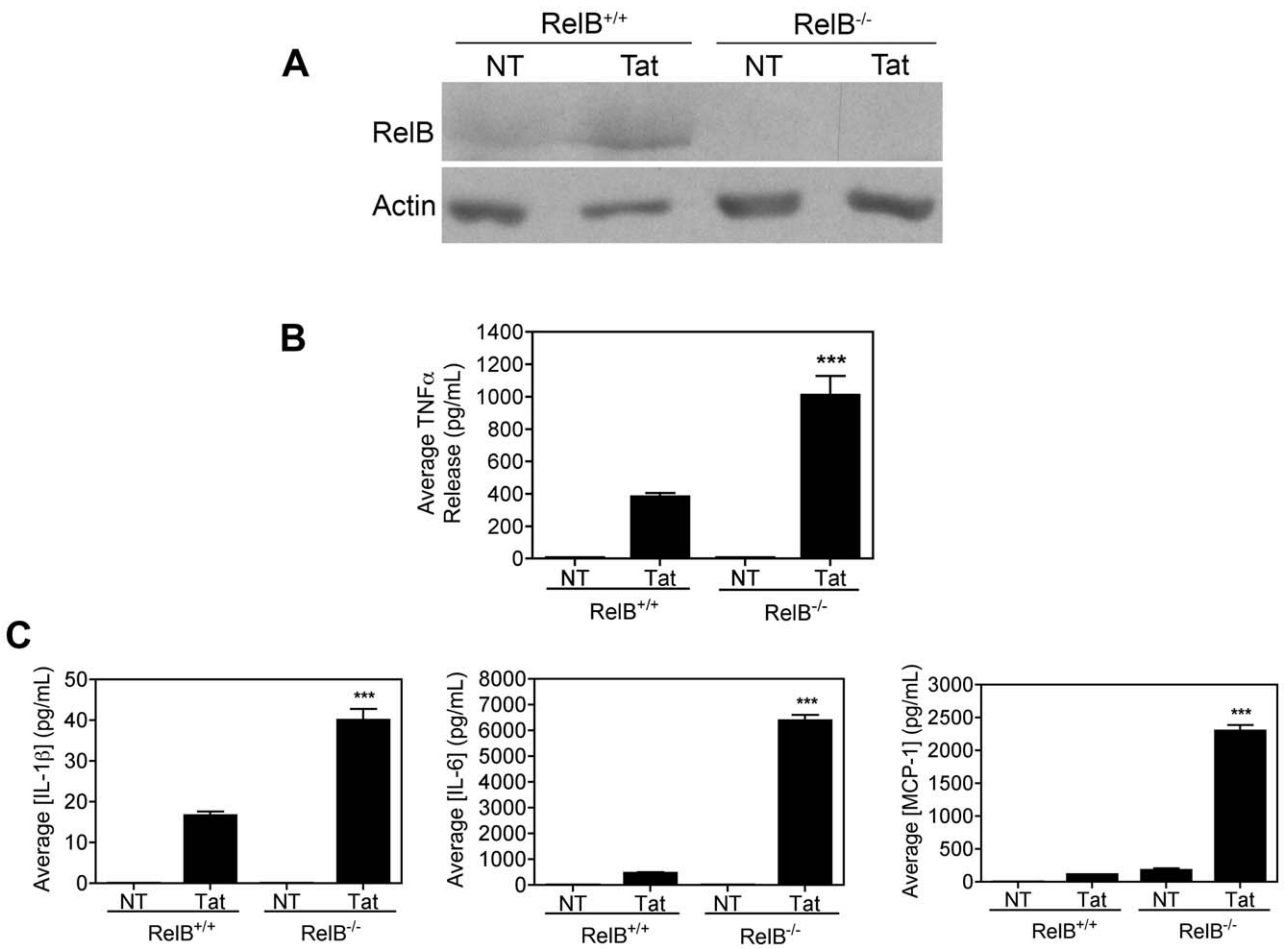

Figure 2. RelB inhibits Tat-induced TNFα and cytokine production in monocytes. *A,* Monocytes from RelB$^{+/+}$ or RelB$^{-/-}$ mice (3×10^5) treated with Tat (100nM) for 8h and subjected to immunoblot analysis with either RelB-specific (*upper panel*) or Actin-specific (*lower panel*) antibodies, confirmed that Tat induced RelB in these cells. Data are representative of results from two separate experiments. *B*, Levels of TNFα in culture supernatants from these cells were analyzed by ELISA, and *C,* Levels of IL-1β, IL-6, and MCP-1 were anlayzed by Multi-Plex cytokine array as described in Results. Data is shown as mean ± SEM of values derived from three replicates each from two combined experiments. Statistical significance ($p<0.001$) is indicated (***), as compared with Tat treated RelB$^{+/+}$ cells.
doi:10.1371/journal.pone.0011875.g002

[74,75]. Therefore, we speculated that Tat might be inducing *de novo* synthesis of RelB in our model systems. As shown in Figure 4A, relatively low levels of RelB were detected in untreated BV-2 cells. Within 4h, these levels were profoundly elevated by 100nM Tat and remained higher for up to 24h of Tat exposure. Under these conditions, Tubulin levels (protein loading control) were not altered. Further immunoblot analyses revealed that the Tat-induced increase in RelB expression resulted from enhanced RelB synthesis, as this effect was blocked by pre-treatment with the protein translation inhibitor Cycloheximide (CHX) (Figure 4B). Consistently, the Tat-induced increase in RelB expression was also blocked by pre-treatment of BV-2 cells with a proteasomal inhibitor, MG-132, or an inhibitor of chymotrypsin-like serine proteases, N-alpha-tosylphenylalanyl chloromethyl ketone (TPCK), suggesting that activation of the NF-κB signaling pathway might be crucial for this effect (Figure 4C). Furthermore, the increase in RelB levels was found to be a specific effect of Tat, as RelB was not increased by treatment with another HIV viral protein, gp120 (Figure 4D). However, gp120's failure to induce RelB synthesis was not due to failure of cellular activation by gp120, because, as expected [76], gp120 was able to induce TNFα release from BV-2 cells (data not shown).

Since microglia are a monocyte-derived cell type, we also examined RelB protein levels in primary human monocytes, to further translational relevance to primary human disease models. Analogous to the responses seen in BV-2 cells, treatment of primary human monocytes with Tat also resulted in increased RelB expression, albeit with delayed kinetics (Figure 4E), suggesting that Tat-mediated synthesis of RelB occurs in non-dividing cells as well. Active RelB is associated with NF-κB family member p52, which is proteolytically cleaved from the inhibitor p100 [48]. As such, further immunoblot analysis revealed increased p100 expression, and its processing into p52 molecules, in Tat-exposed primary human monocytes (Figure 4F), as well as in BV-2 cells (Figure 4G). Furthermore, we observed that this newly synthesized RelB rapidly relocates to the nucleus, and thus is functionally active (Figure 4H).

Astrocytes are the most abundant cell type in the brain, are non-productively infected with HIV-1 and, similar to microglia, can be activated by viral proteins such as Tat, thereby contributing to HIV-induced neuroinflammation [77]. For these reasons, we also measured RelB protein levels following Tat treatment of primary human astrocytes. As shown in Figure 4I, by 8h of Tat treatment there is increased RelB synthesis in astrocytes, while Tubulin levels remain unchanged.

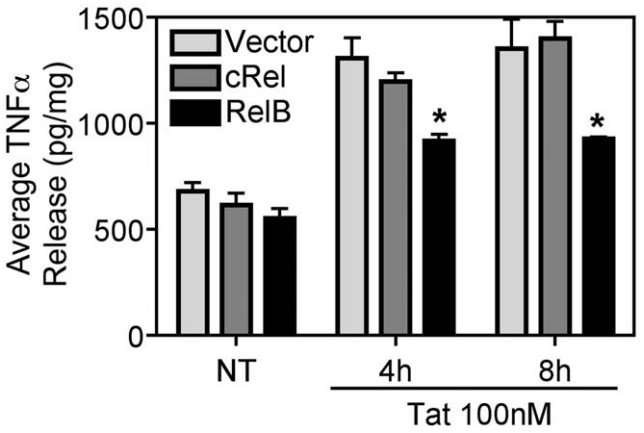

Figure 3. RelB inhibits Tat-induced TNFα production in BV-2 microglia. BV-2 cells (5×10^6) were transiently transfected with either empty vector (pcDNA3.1-Myc/His-B), cRel, or RelB (10 μg), using Nucleofector (Amaxa/Lonza), and treated with Tat (100nM) for the indicated periods of time. TNFα release was measured by ELISA and normalized to total cellular protein content in the culture wells. Results are shown as mean ± SEM of values derived from two replicates from one representative experiment; two total experiments were performed. Statistical significance ($p<0.05$) is indicated, as compared to empty vector transfected cells (*).
doi:10.1371/journal.pone.0011875.g003

RelB inhibits TNFα synthesis at the transcriptional level, but RelA increases TNFα synthesis

To better understand how RelB inhibits Tat-induced TNFα production, we used a reporter gene assay. To do this, BV-2 cells were transiently transfected with a TNFα-promoter luciferase reporter plasmid, either alone or together with increasing amounts of WT RelB plasmid. The total amount of DNA in each transfection was kept constant by addition of an appropriate amount of pcDNA3.1 empty vector plasmid. These results revealed that basal TNFα promoter activity was blocked by overexpression of RelB (Figure 5A). To compare the effects of RelA overexpression on TNFα promoter activity, we performed similar additional luciferase assays in which HEK 293 cells were transfected with the TNFα-promoter luciferase reporter, together with increasing amounts of either RelA or RelB. As shown in Figure 5B, in contrast to RelB, overexpression of increasing amounts of RelA led to dose-dependent *activation* of the TNFα promoter. These latter studies utilized HEK 293 cells for their high transfection yields, and their robust (and thus readily detectable) increases in TNFα promotor activity with RelA expression, thus allowing us to determine the effects of RelB expression on RelA transcriptional activity.

RelB interaction with RelA inhibits upregulation of the TNFα promoter by RelA

Previous reports have shown that RelB and RelA interact, and that this interaction can lead to inhibition of either RelA-dependent or RelB-dependent gene expression in multiple cell types [52–55]. Based on these reports, first we examined the effect of RelB overexpression on RelA-induced activation of the TNFα promoter. Overexpression of RelA alone resulted in an approximately 10-fold increase in TNFα promoter activation, an effect that was completely blocked by expressing increasing amounts of RelB (Figure 5C). Interestingly, consistent with Figure 3, overexpressing increasing amounts of cRel (relevant control), or β-galactosidase (irrelevant control), did not significantly inhibit RelA-dependent activation of the TNFα promoter (Figure 5D), suggesting that RelB exerts a selective inhibitory effect on RelA transcriptional activity.

Next, to determine whether RelB interacts with RelA to achieve these effects, we tested whether Tat stimulates protein-protein interactions between endogenous RelA and RelB in BV-2 cells. After addition of Tat for either 4h or 8h, whole cell lysates of BV-2 cells were collected, and RelA protein complexes were captured with a RelA-specific antibody using Protein A/G+ agarose beads. The bound proteins were then visualized by immunobloting with a RelB-specific antibody. By 4h of Tat treatment there was a significant increase in RelB protein that was pulled down with the RelA antibody, thus demonstrating that Tat treatment was stimulating interactions between RelA and RelB in BV-2 cells (Figure 6A, top panel). The blot was stripped and re-probed with a RelA-specific antibody to confirm that approximately equivalent amounts of RelA protein were pulled down in each sample (Figure 6A, bottom panel). Comparative densitometric analysis of these bands, normalized to the RelA IP/RelA IB bands (bottom panel), informed us that Tat increased RelB/RelA interactions by 4-fold at both 4h and 8h (Figure 6A, bar graph).

It was previously reported that RelA phosphorylation at serine 276 is required for the interaction between RelB and RelA to occur [53]. Accordingly, using an antibody that specifically recognizes serine 276 phosphorylated RelA, we were able to confirm that RelA is indeed phosphorylated at serine 276 in Tat-treated BV-2 cells (Figure 6B, blots). Quantification of these blots found a 20–40 fold increase in the phosphorylated form of RelA in Tat treated BV-2 cells versus controls (Figure 6B, graphs).

Thus, we predicted that this Tat-induced interaction between RelB and RelA would therefore inhibit Tat-induced, RelA-mediated transcriptional activation of NF-κB pathways. Indeed, using an NF-κB luciferase reporter plasmid in BV-2 cells, our results confirmed that overexpression of RelB inhibits activation of endogenous NF-κB induced by 8h 100 nM Tat treatment (Figure 6C). Likewise, analogous to the results shown in Figure 5C, we observed a dose-dependent inhibition of RelA-mediated NF-κB luciferase transcription following overexpression of RelB in BV-2 cells (Figure 6D).

The entire Rel Homology Domain of RelB is necessary for the interaction with RelA

To clarify how RelB might interact with RelA to inhibit activation of the TNFα promoter, sequential deletion mutants within RelB were made. These RelB deletion mutants were overexpressed in HEK 293 cells together with HA-tagged RelA. Co-immunoprecipitation (co-IP) was then used to test for interactions between these proteins. Parallel cultures were also co-transfected with the TNFα-promoter luciferase reporter, to determine which of these deletion mutated RelB derivatives failed to block transcriptional activity of RelA, which would suggest an inhibitory domain interaction with RelA. We first focused on the amino terminal leucine zipper domain of RelB, because this domain is unique to RelB among the NF-κB family members. Leucine zipper domains are also known to be involved with protein-protein interactions [46]. However, amino terminal truncation mutants of RelB, including deletion of the entire leucine zipper domain, still interacted with HA-RelA as shown by co-IP, and these mutants also inhibited RelA activity equally well (Figure 7A), suggesting that this region was not responsible for the transcription-inhibiting interactions of RelB on RelA.

We then introduced sequential deletions within the Rel Homology Domain (RHD) of RelB (Figure 7B). The RHD of NF-κB proteins is known to be responsible for homo- and

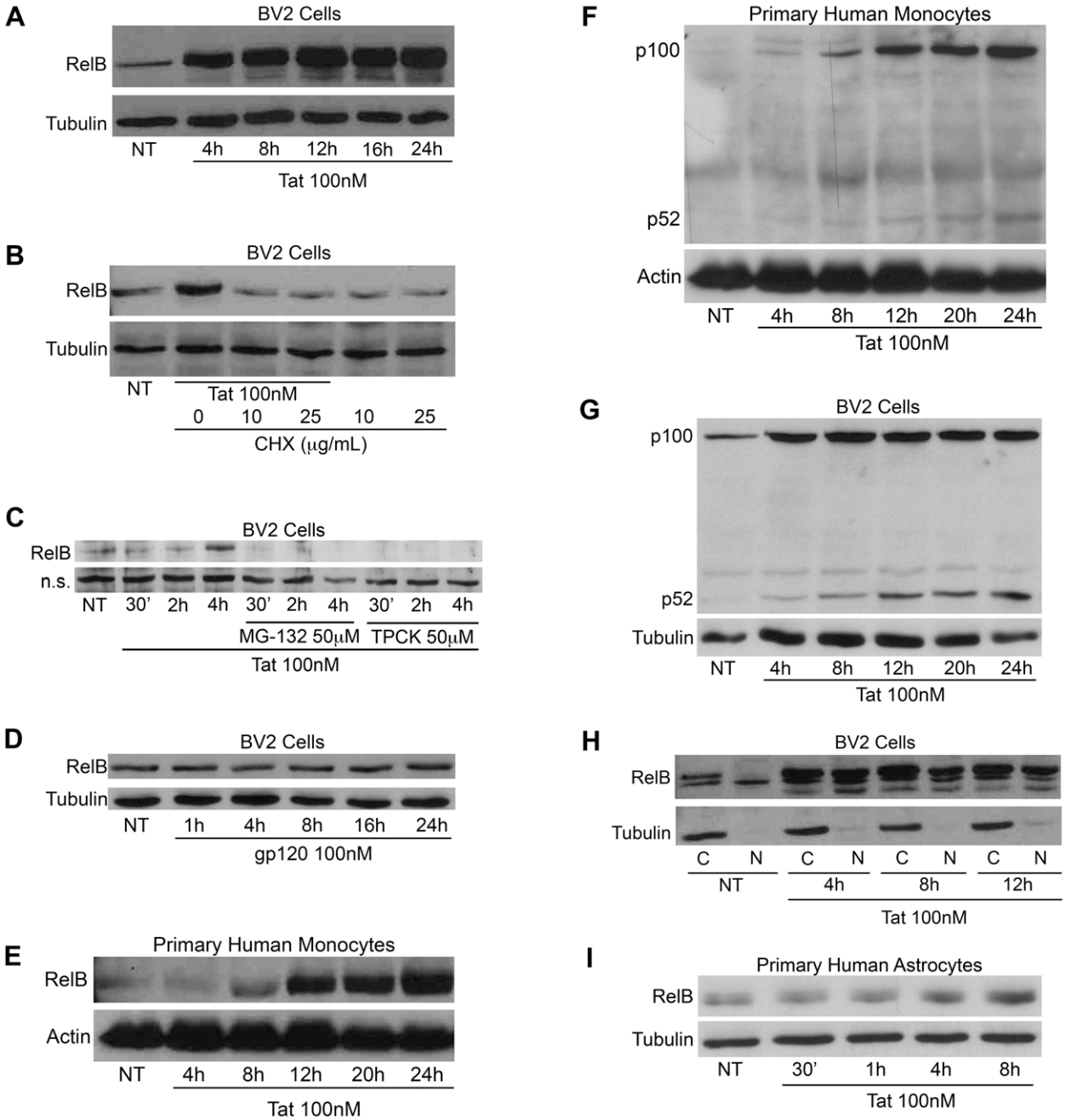

Figure 4. Tat induces de novo synthesis of RelB. *A,* BV-2 cells (1.2×10^5) were treated with Tat (100nM) for the indicated periods of time and whole cell lysates were subjected to immunoblot analysis using either RelB-specific (*upper panel*) or α-Tubulin-specific (*lower panel*) antibodies. *B,* BV-2 cells (1.2×10^5) were treated with Tat alone or together with CHX as indicated for 4h. Whole cell lysates were subjected to immunoblot analysis using either RelB-specific (*upper panel*) or α-Tubulin-specific (*lower panel*) antibodies. *C,* BV-2 cells (1.2×10^5) were treated with Tat (100nM) alone or together with MG-132 or TPCK both at a concentration of 50μM for the indicated periods of time. Whole cell lysates were subjected to immunoblot analysis using a RelB-specific (*upper panel*) antibody. Levels of a nonspecific (n.s.) band (*lower panel*) are shown to indicate equal protein loading. *D,* BV-2 cells (1.2×10^5) were treated with gp120 (SF162, 100nM) for the indicated periods of time and whole cell lysates were subjected to immunoblot analysis using either RelB-specific (*upper panel*) or α-Tubulin-specific (*lower panel*) antibodies. *E,* Primary human monocytes (2×10^5) were treated with Tat for the indicated periods of time and whole cell lysates were subjected to immunoblot analysis using either RelB-specific (*upper panel*) or Actin-specific (*lower panel*) antibodies. *F,* Primary human monocytes (2×10^5) were treated with Tat for the indicated periods of time and whole cell lysates were subjected to immunoblot analysis using either p100/p52-specific (*upper panel*) or Actin-specific (*lower panel*) antibodies. *G,* BV-2 cells (1.2×10^5) were treated with Tat for the indicated periods of time and whole cell lysates were subjected to immunoblot analysis using either p100/p52-specific (*upper panel*) or α-Tubulin-specific (*lower panel*) antibodies. *H,* BV-2 cells (1.2×10^5) were treated with Tat as indicated and cytosolic (labeled "C") and nuclear (labeled "N") extracts were subjected to immunoblot analysis with either RelB-specific (*upper panel*) or α-Tubulin-specific (*lower panel*) antibodies. *I,* Primary human astrocytes (4×10^4) were plated 72h prior to treatment. These cells were treated with Tat as indicated and whole cell lysates were subjected to immunoblot analysis using either RelB-specific (*upper panel*) or α-Tubulin-specific (*lower panel*) antibodies.
doi:10.1371/journal.pone.0011875.g004

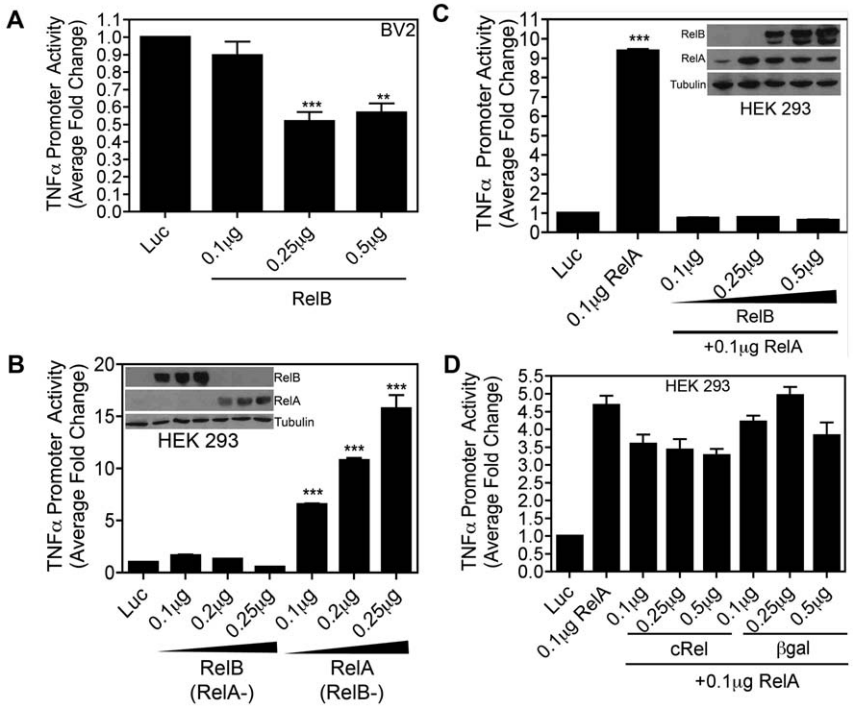

Figure 5. Opposing effects of RelA and RelB on TNFα promoter activity. *A,* BV-2 cells (1.2×10^5) were transiently transfected with 0.25 μg of plasmid DNA containing a luciferase reporter gene under transcriptional control of the mouse TNFα promoter region in the absence or presence of increasing amounts of a RelB-encoding plasmid. 24h later cells were lysed and luciferase activity was determined. Total protein amount, as determined by Bradford assay was used to normalize the samples. Data are presented as fold change compared to cells transfected with the luciferase reporter alone. ***, $p<0.001$, and **, $p<0.01$ as compared to cells transfected with the luciferase reporter alone. *B,* HEK 293 cells (1.8×10^5) were transiently transfected with the mouse TNFα promoter-luciferase reporter plasmid along with increasing amounts of a plasmid for RelA or RelB. The luciferase (i.e. TNFα promoter) activity in whole cell lysates was determined 24h post-transfection. Samples were subjected to immunoblot analysis using either RelA or RelB-specific antibodies to determine the expressed level of RelA and RelB protein. ***, $p<0.001$ as compared to cells transfected with the luciferase reporter alone. *C,* HEK 293 cells (1.8×10^5) were transiently transfected with the mouse TNFα promoter-luciferase reporter plasmid along with a plasmid for RelA in the absence or presence of increasing amounts of RelB-encoding plasmid. The luciferase activity in whole cell lysates was determined 24h post-transfection. Samples were subjected to immunoblot analysis using either RelA or RelB-specific antibodies to determine the expressed level of RelA and RelB protein. ***, $p<0.001$ as compared to cells transfected with the luciferase reporter alone. *D,* HEK 293 cells (1.8×10^5) were transiently transfected with the mouse TNFα promoter-luciferase reporter along with a plasmid for RelA in the absence or presence of increasing amounts of cRel or β-galactosidase-encoding plasmid. Luciferase activity in whole cell lysates was determined 24h post-transfection.
doi:10.1371/journal.pone.0011875.g005

hetero-dimer formation with other NF-κB proteins [78]. All of these sequential RelB RHD deletion mutants, as well as deletion of the proximal nuclear localization signal located between residues 388–392 within RelB, still formed complexes with RelA and inhibited its activity (Figure 7B). However, the ability of RelB to interact with RelA, and to inhibit RelA-dependent activation of the TNFα promoter, was lost following deletion of the entire RHD (Δ52–402, Figure 7B; aka ΔRHD RelB, Figures 7C and 7D). This is reported in tabular format in Figure 7B (bottom line), with Figures 7C and 7D illustrating the failure of ΔRHD RelB to interact with RelA (7C), and to inhibit RelA activation of TNFα transcriptional activity (7D), respectively. These results indicate that the entire RHD of RelB is necessary for its interaction with RelA.

Amino terminal region of Tat is necessary for RelB induction in microglia

The HIV-1 protein Tat is a multi-functional protein. Residues 1–72 are encoded by the first exon and residues 73–101 are encoded by a second exon [79]. It is released from infected microglia, macrophage and astrocytes in the CNS [80]. Despite its small size, Tat has multiple domains conferring different functional effects. For example, amino acids 1–48 contain protine-rich as well as cysteine-rich regions that represent a minimal activation domain of HIV-1 Tat required for activation of the HIV-1 promoter region, known as the long terminal repeat (LTR). The basic domain 49–72 contains an RKKRRQRRR motif, which confers the RNA binding activity of Tat and is also important for cellular uptake and nuclear distribution of this protein [81], while amino acids 65–80 of Tat include the RGD motif that is involved in binding to cellular integrins [81,82]. Sequences from 22–37, a cysteine-rich domain, bind with divalent cations like zinc and cadmium, thereby inducing the dimerization and subsequent inactivation of Tat [83]. Mutations in the region 1–21 are tolerant to changes without the loss of biologic activity; in contrast, changes in amino acids 25–40 are generally deleterious for transactivation. Moreover, substitution at cysteine residues 22, 25, 27 and 37 alters transactivation of the HIV LTR [81]. The cysteine residue at position 31 is critical for binding to the NMDA receptor on neurons and mediating neurotoxicity [84]. Chemotactic properties have also been attributed to this residue [85]. Here we have tested various length Tat proteins to determine which domains are necessary for induction of RelB synthesis in microglial cells. A diagram depicting the Tat peptides we used to treat BV-2 cells is shown in Figure 8A.

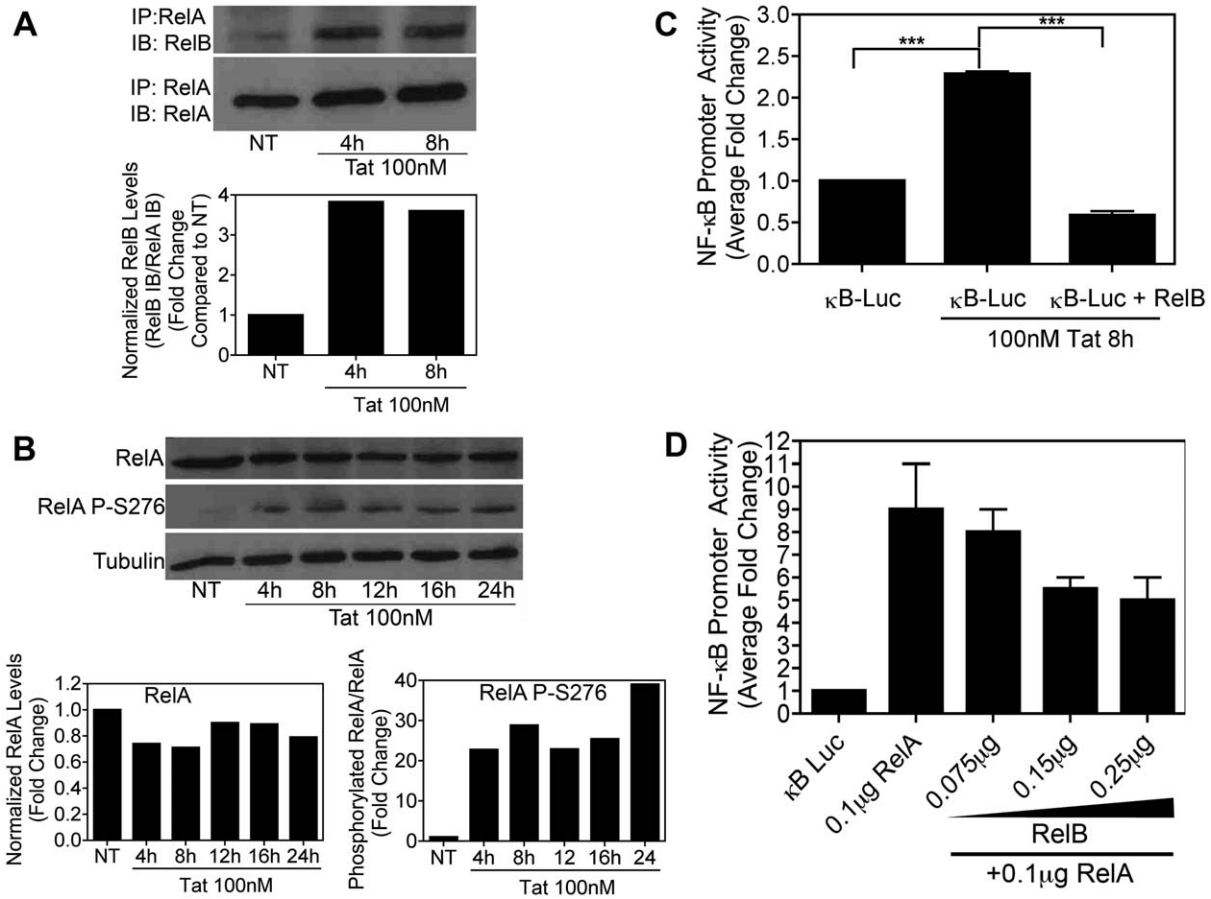

Figure 6. RelB inhibits NF-κB activation via physical interaction with RelA. *A,* BV-2 cells (8×10^5) were treated with Tat (100nM) for the indicated periods of time. Whole cell lysates were subjected to immunoprecipitation using a RelA-specific antibody and Protein A/G+ agarose beads. Immunocomplexes were separated by 7.5% SDS-PAGE and blotted onto nitrocellulose membrane and subjected to immunoblot analysis with antibodies specific for RelB or RelA. The plot below the bands represents densitometry values for each band, normalized as a ratio of RelA(IP)/RelB(IB) (i.e. top bands): RelA(IP)/RelA(IB) (i.e. bottom bands), to indicate the increase in RelB/RelA interactions at each time point. *B,* BV-2 cells (1.2×10^5) were treated with Tat (100nM) for the indicated periods of time and whole cell lysates were subjected to immunoblot analysis using either RelA-specific (*upper panel*), RelA phospho-serine 276-specific (*center panel*) or α-Tubulin-specific (*lower panel*) antibodies. Protein levels were quantified using ImageJ software (bottom graphs). The results of a single representative experiment are shown. *C,* BV-2 cells (5×10^6) were transiently transfected using Nucleofector (Amaxa/Lonza) with an NF-κB-dependent luciferase reporter plasmid either alone or together with a RelB-encoding plasmid. 16h post-transfection cells were either left untreated or were treated with Tat (100nM) for 8h. Luciferase activity in whole cell lysates was determined. Results are shown as mean ± SEM of values derived from three replicates from one representative experiment; two total experiments were performed. Statistical significance ($p<0.001$) is indicated (***). *D,* BV-2 cells (1.5×10^5) were transiently transfected using Lipofectamine (Invitrogen) with the NF-κB-luciferase reporter plasmid together with a plasmid for RelA in the absence or presence of increasing amounts of RelB-encoding plasmid. The luciferase activity in whole cell lysates was determined 18h post-transfection. Results are shown as mean ± SEM of values derived from two replicates from one representative experiment; two total experiments were performed.
doi:10.1371/journal.pone.0011875.g006

As shown in Figure 8, full-length Tat (Tat 1–101) and Tat 1–72 both induced an approximately 10–12-fold increase in RelB levels by 8h of treatment in BV-2 cells, suggesting that the first exon of Tat is required for RelB induction in microglia. Similarly, Tat C31S and Tat Δ31–61 treatments led to a 10–12-fold increase in RelB synthesis, suggesting that the altered residues in these variants are dispensible. In contrast, Tat 48–72, 46–60 and 65–80 did not induce RelB synthesis in BV-2 cells, indicating that the basic motif within Tat is not sufficient to stimulate RelB production. Our results suggest that the amino terminal region, consisting of amino acids 1–30 of Tat, is critical for Tat-dependent RelB activation in microglia. It may also be that multiple domains within the first exon of Tat are necessary for the Tat-induced increase in RelB synthesis. This possibility is currently under investigation in our laboratory.

Discussion

Neuroinflammatory responses and monocyte/macrophage CNS infiltration appear critical to the development of HAND even with cART, and are not significantly reduced by cART [86,87], thus, this remains a critical area of investigation in the pursuit of adjunctive therapies for reducing the impact of HIV on the nervous system. We, and colleagues, have previously shown that TNFα released from HIV infected or activated monocytes/microglia is a major contributor to HIV-induced neuroinflammation that leads to neuron damage and cognitive impairment [45,88–94]. Moreover, many key aspects of TNFα signaling occur via NF-κB [95,96], and NF-κB signaling is likely to be a key mediator of TNFα's neurotoxic actions in HAND, particularly in regards to activation and HIV infection of brain macrophages and microglia [97,98]. Accordingly, TNFα and NF-κB signal trans-

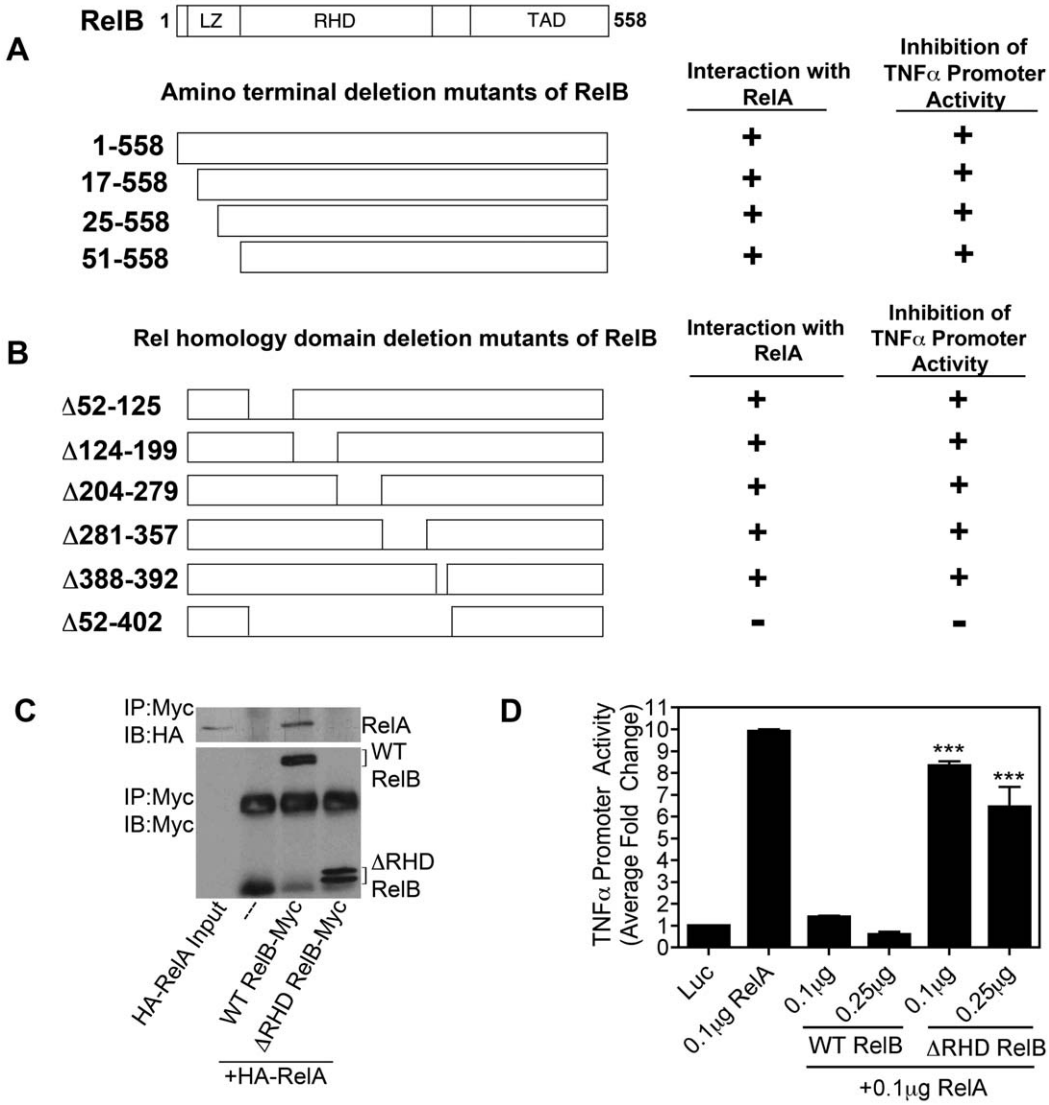

Figure 7. RelB Rel homology domain required for interaction with RelA and blockade of TNFα promoter activity. *A, B,* Diagrams show representation of full length and deletion mutants of RelB used to determine the domains of RelB necessary for interaction with RelA. HEK 293 cells (1.8×10^5) were transiently transfected with either HA-tagged RelA or Myc-tagged RelB deletion mutants alone or in combination. Interaction was determined by immunoprecipitation with Myc-specific antibody and Protein A/G+ agarose beads followed by immunoblot analysis with HA-specific or Myc-specific antibodies. Interacting (+) and non-interacting (−) mutants are indicated. These RelB deletion mutants were also analyzed using the TNFα promoter-luciferase reporter plasmid co-transfected into HEK 293 cells together with a plasmid for RelA in the absence or presence of increasing amounts of RelB-encoding plasmid (WT or deletion mutants). Inhibition of RelA activation of the TNFα promoter is indicated (+/−). *C,* HEK 293 cells (1.8×10^5) were transiently transfected with either HA-tagged RelA or Myc-tagged RelB Δ52–402 alone or in combination. Interaction was determined by immunoprecipitation with Myc-specific antibody and Protein A/G+ agarose beads followed by immunoblot analysis with HA-specific or Myc-specific antibodies. *D,* RelB Δ52–402 was also analyzed using the TNFα promoter-luciferase reporter plasmid co-transfected into HEK 293 cells along with a plasmid for RelA in the absence or presence of increasing amounts of RelB Δ52–402-encoding plasmid. Statistical significance ($p<0.001$) as compared to cells transfected with 0.1 μg WT RelB+RelA is indicated (***).
doi:10.1371/journal.pone.0011875.g007

duction are principal mechanistic pathways by which Tat and other viral proteins or mediators are thought to perpetuate HIV-induced nervous system damage [99–108]. RelB, in turn, is an NF-κB family molecule with known anti-inflammatory properties and modulatory roles in NF-κB signal transduction. While Rel family members have previously been implicated as possible mediators of HIV- and Tat-dependent transcription [100], the precise mechanisms of this regulation remain unclear. Furthermore, RelB modulation of cytokine and TNFα activation in microglial cells is an area that may have significant importance for understanding HAND pathology, yet until now has remained unexplored.

Herein we describe a novel inhibitory regulatory feedback loop for reducing inflammatory responses in microglial cells, whereby RelB protein-protein interactions with RelA inhibit RelA's transcriptional activity, to regulate NF-κB mediated cytokine synthesis. Early reports indicated that RelB exclusively formed heterodimers with p50 and p52. It was not until 2003 that Marienfeld et. al reported an interaction between RelB and RelA in multiple cell types [52]. RelB/RelA interactions may not have been reported earlier because this complex might not bind well to typical κB DNA binding elements, or the level of this complex might be low compared to levels of other RelB complexes.

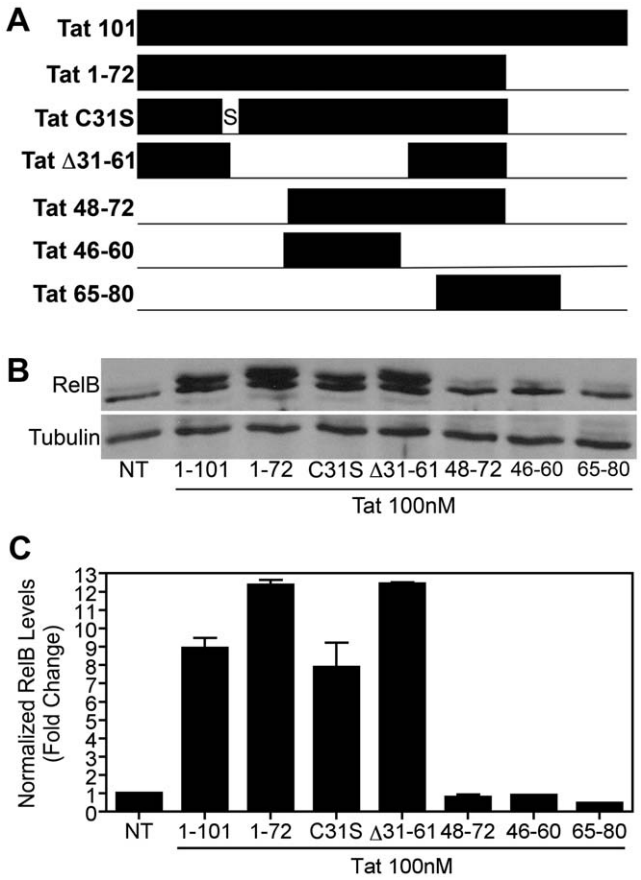

Figure 8. Amino terminal region of Tat is necessary for RelB induction in microglia. *A,* Diagram shows a representation of full length, mutated and truncated Tat proteins and peptides used in these experiments. *B,* BV-2 cells (1.2×10^5) were treated with Tat (100nM) for 8h and whole cell lysates were subjected to immunoblot analysis using either RelB-specific (*upper panel*) or α-Tubulin-specific (*lower panel*) antibodies. These results indicate that standard Tat 1–101, Tat 1–72, Tat C31S, and Tat Δ31–61 all activated RelB, whereas Tat peptides 48–72, 46–60 and 65–80 did not. *C,* Densitometry quantification of immunoblots shown in *B*. RelB levels were normalized to Tubulin levels and fold change compared to non-treated (NT) was calculated.
doi:10.1371/journal.pone.0011875.g008

Additional reports of an inhibitory RelB/RelA interaction have since been described in fibroblasts, dendritic cells, and THP-1 human monocyte cells [53–55].

Here we describe for the first time, direct inhibition of RelA-dependent TNFα transcription by RelB in microglia, as a result of RelB/RelA protein interactions. These findings are supported by other work showing that LPS stimulation of $RelB^{-/-}$ fibroblasts resulted in enhanced production of cytokines IL-1α, IL-1β, and TNFα [58], and chemokines RANTES, MIP-1α, MIP-1β, MIP-2, IP-10, JE/MCP-1, and KC/CINC [59]. In addition, another study demonstrated that RelB expression correlated with IL-1β repression in human monocyte THP-1 cells [55]. All these findings likely have parallels with our findings herein, that RelB deficiency leads to enhanced Tat-induced TNFα transcriptional activity, and that RelB expression reduces this activity. On the other hand, and in stark contrast, macrophages isolated from $RelB^{-/-}$ deficient mice demonstrated impaired TNFα production in response to LPS [57]. This study emphasizes that the exact consequences of RelB regulation of TNFα may be specifically dependent upon both the nature of the inflammatory insult, and upon the cell type affected – as is commonly the case with immunomodulatory signal transduction – thus highlighting the need for further studies of these effects in other cell types relevant to HIV neurologic disease, as we seek to further validate RelB as a potential therapeutic target in HAND.

Finally, since TNFα can be a downstream modulator of Tat's effects [104], it is possible that TNFα, rather than Tat directly, is the molecule responsible for inducing the RelA serine 276 phosphorylation that we observed in Tat-treated microglia. In addition, it is likely that either Tat- or TNFα-induced activation of NF-κB could also explain the increase in RelB, as RelB is known to be induced by NF-κB, and blockade of NF-κB signaling mechanisms with inhibitors MG-132 or TPCK inhibited the increase in microglial RelB. While additional studies are needed to further clarify these mechanisms, these possibilities do not conflict with our supposition that the RelB/RelA interactions shown here in Tat-treated microglial cells, represent a novel negative regulatory feedback loop for the resolution of inflammation in microglial cells, specifically by inhibiting RelA activation of pro-inflammatory cytokines such as TNFα. This mechanism may explain why more severe cognitive impairment is not present until late in the course of HIV infection, with HIV-induced inflammatory mediators provoking a constant "yin and yang" between inflammation and resolution of inflammation in the CNS.

Uncovering new mechanisms involved in resolving CNS inflammation has many potential benefits both in terms of reducing inflammation-induced neuronal damage, and also possibly limiting viral spread by reducing inflammation-induced influx of monocytes into the CNS. Moreover, TNFα and related cytokines have pleiotropic neuromodulatory, neurotoxic, and even neuroprotective functions [109], and are implicated in a wide range of CNS and peripheral disease states. Thus, identifying this novel negative regulatory feedback loop involving RelB could be particularly useful as an adjunctive therapeutic approach for HAND, peripheral HIV infection, or even other neurologic or immune diseases, since overexpression of RelB in microglial cells does not completely block Tat-induced release of TNFα, which would negatively impact TNFα's other endogenous functions. In total, these results described herein represent an important first-step toward furthering our understanding of RelB as a potentially important mediator of wide-ranging disease states.

Supporting Information

Text S1 Recombinant Tat produced in eukaryotic cells activates microglia.
Found at: doi:10.1371/journal.pone.0011875.s001 (0.04 MB DOC)

Figure S1 Recombinant Tat produced in eukaryotic cells activates microglia. A, HIV-1 Tat 1–72 protein was purified from recombinant baculovirus infected Sf9 insect cell cultures. Increasing volumes of the eluted protein were subjected to immunoblot analysis using antiserum to HIV-1 Tat. The Tat-specific band is indicated. B, BV-2 cells (1.2×10^5) were treated with Sf9-Tat (1–72, 100nM), or E.Coli-Tat (1–72, 100nM, from Dr. A. Nath) for 8h and levels of TNFα in the culture supernatant quantified by ELISA. Data correspond to mean ± SEM of three replicates, from a single representative experiment; the experiment was performed twice. C, BV-2 cells (1.2×10^5) were treated with Sf9-Tat (100nM) for the indicated periods of time and whole cell lysates were subjected to immunoblot analysis using either IκBα-specific (upper panel) or α-Tubulin-specific (lower panel) antibodies. Data are representative of results from two separate experiments. D, For the EMSA, 4 μL of nuclear protein extract from BV-2 cells treated

with Sf9-Tat (100nM) for the indicated times was incubated together with a ^{32}P-labeled palindromic NF-κB oligonucleotide. The samples were separated on a native polyacrylamide gel that was then fixed, dried, and exposed to x-ray film. The two major DNA binding complexes consisting of NF-κB family members, as labeled, were identified by antibody supershift analysis.
Found at: doi:10.1371/journal.pone.0011875.s002 (0.67 MB TIF)

Acknowledgments

We thank Drs. A. Nath, J. He, A. Ghorpade, S. C. Sun, R. Donato, B. Baumann, D. Kuprash, and P. Ray for generously providing us with valuable reagents.

Author Contributions

Conceived and designed the experiments: MK SBM. Performed the experiments: MK. Analyzed the data: MK SBM. Contributed reagents/materials/analysis tools: MK OP ZY SBM. Wrote the paper: MK SWP SBM.

References

1. Resnick L, Berger JR, Shapshak P, Tourtellotte WW (1988) Early penetration of the blood-brain-barrier by HIV. Neurology 38: 9–14.
2. Kaul M, Lipton SA (2006) Mechanisms of neuronal injury and death in HIV-1 associated dementia. Curr HIV Res 4: 307–318.
3. Masliah E, DeTeresa RM, Mallory ME, Hansen LA (2000) Changes in pathological findings at autopsy in AIDS cases for the last 15 years. AIDS 14: 69–74.
4. Nath A, Sacktor N (2006) Influence of highly active antiretroviral therapy on persistence of HIV in the central nervous system. Curr Opin Neurol 19: 358–361.
5. Tozzi V, Balestra P, Bellagamba R, Corpolongo A, Salvatori MF, et al. (2007) Persistence of neuropsychologic deficits despite long-term highly active antiretroviral therapy in patients with HIV-related neurocognitive impairment: prevalence and risk factors. J Acquir Immune Defic Syndr 45: 174–182.
6. Langford TD, Letendre SL, Marcotte TD, Ellis RJ, McCutchan JA, et al. (2002) Severe, demyelinating leukoencephalopathy in AIDS patients on antiretroviral therapy. AIDS 16: 1019–1029.
7. Gonzalez-Scarano F, Martin-Garcia J (2005) The neuropathogenesis of AIDS. Nat Rev Immunol 5: 69–81.
8. Kaul M, Garden GA, Lipton SA (2001) Pathways to neuronal injury and apoptosis in HIV-associated dementia. Nature 410: 988–994.
9. McArthur JC (2004) HIV dementia: an evolving disease. J Neuroimmunol 157: 3–10.
10. McArthur JC, Haughey N, Gartner S, Conant K, Pardo C, et al. (2003) Human immunodeficiency virus-associated dementia: an evolving disease. J Neurovirol 9: 205–221.
11. Ghafouri M, Amini S, Khalili K, Sawaya BE (2006) HIV-1 associated dementia: symptoms and causes. Retrovirology 3: 28.
12. Archibald SL, Masliah E, Fennema-Notestine C, Marcotte TD, Ellis RJ, et al. (2004) Correlation of in vivo neuroimaging abnormalities with postmortem human immunodeficiency virus encephalitis and dendritic loss. Arch Neurol 61: 369–376.
13. Bissel SJ, Wang G, Ghosh M, Reinhart TA, Capuano S, 3rd, et al. (2002) Macrophages relate presynaptic and postsynaptic damage in simian immunodeficiency virus encephalitis. Am J Pathol 160: 927–941.
14. Everall IP, Heaton RK, Marcotte TD, Ellis RJ, McCutchan JA, et al. (1999) Cortical synaptic density is reduced in mild to moderate human immunodeficiency virus neurocognitive disorder. HNRC Group. HIV Neurobehavioral Research Center. Brain Pathol 9: 209–217.
15. Masliah E, Heaton RK, Marcotte TD, Ellis RJ, Wiley CA, et al. (1997) Dendritic injury is a pathological substrate for human immunodeficiency virus-related cognitive disorders. HNRC Group. The HIV Neurobehavioral Research Center. Ann Neurol 42: 963–972.
16. Wiley CA, Masliah E, Morey M, Lemere C, DeTeresa R, et al. (1991) Neocortical damage during HIV infection. Ann Neurol 29: 651–657.
17. Oberdorfer P, Washington CH, Katanyuwong K, Jittamala P (2009) Progressive Multifocal Leukoencephalopathy in HIV-Infected Children: A Case Report and Literature Review. Int J Pediatr 2009: 348507.
18. Muller-Oehring EM, Schulte T, Rosenbloom MJ, Pfefferbaum A, Sullivan EV (2009) Callosal degradation in HIV-1 infection predicts hierarchical perception: A DTI study. Neuropsychologia.
19. Major EO (2009) Progressive Multifocal Leukoencephalopathy in Patients on Immunomodulatory Therapies. Annu Rev Med.
20. Cardenas V, Meyerhoff D, Studholme C, Kornak J, Rothlind J, et al. (2009) Evidence for ongoing brain injury in human immunodeficiency virus-positive patients treated with antiretroviral therapy. J Neurovirol. pp 1–10.
21. Letendre SL, Ellis RJ, Everall I, Ances B, Bharti A, et al. (2009) Neurologic complications of HIV disease and their treatment. Top HIV Med 17: 46–56.
22. Chen Y, An H, Zhu H, Stone T, Smith JK, et al. (2009) White matter abnormalities revealed by diffusion tensor imaging in non-demented and demented HIV+ patients. Neuroimage 47: 1154–1162.
23. Gongvatana A, Schweinsburg BC, Taylor MJ, Theilmann RJ, Letendre SL, et al. (2009) White matter tract injury and cognitive impairment in human immunodeficiency virus-infected individuals. J Neurovirol 15: 187–195.
24. Pfefferbaum A, Rosenbloom MJ, Rohlfing T, Kemper CA, Deresinski S, et al. (2009) Frontostriatal fiber bundle compromise in HIV infection without dementia. AIDS 23: 1977–1985.
25. Nguyen TP, Soukup VM, Gelman BB (2009) Persistent Hijacking of Brain Proteasomes in HIV-Associated Dementia. Am J Pathol.
26. Melrose RJ, Tinaz S, Castelo JM, Courtney MG, Stern CE (2008) Compromised fronto-striatal functioning in HIV: an fMRI investigation of semantic event sequencing. Behav Brain Res 188: 337–347.
27. Wohlschlaeger J, Wenger E, Mehraein P, Weis S (2009) White matter changes in HIV-1 infected brains: a combined gross anatomical and ultrastructural morphometric investigation of the corpus callosum. Clin Neurol Neurosurg 111: 422–429.
28. Langford TD, Letendre SL, Larrea GJ, Masliah E (2003) Changing patterns in the neuropathogenesis of HIV during the HAART era. Brain Pathol 13: 195–210.
29. Avison MJ, Nath A, Greene-Avison R, Schmitt FA, Bales RA, et al. (2004) Inflammatory changes and breakdown of microvascular integrity in early human immunodeficiency virus dementia. J Neurovirol 10: 223–232.
30. Bossi P, Dupin N, Coutellier A, Bricaire F, Lubetzki C, et al. (1998) The level of human immunodeficiency virus (HIV) type 1 RNA in cerebrospinal fluid as a marker of HIV encephalitis. Clin Infect Dis 26: 1072–1073.
31. Glass JD, Fedor H, Wesselingh SL, McArthur JC (1995) Immunocytochemical quantitation of human immunodeficiency virus in the brain: correlations with dementia. Ann Neurol 38: 755–762.
32. Everall IP, Glass JD, McArthur J, Spargo E, Lantos P (1994) Neuronal density in the superior frontal and temporal gyri does not correlate with the degree of human immunodeficiency virus-associated dementia. Acta Neuropathol 88: 538–544.
33. Rumbaugh JA, Nath A (2006) Developments in HIV neuropathogenesis. Curr Pharm Des 12: 1023–1044.
34. Westendorp MO, Frank R, Ochsenbauer C, Stricker K, Dhein J, et al. (1995) Sensitization of T cells to CD95-mediated apoptosis by HIV-1 Tat and gp120. Nature 375: 497–500.
35. Xiao H, Neuveut C, Tiffany HL, Benkirane M, Rich EA, et al. (2000) Selective CXCR4 antagonism by Tat: implications for in vivo expansion of coreceptor use by HIV-1. Proc Natl Acad Sci U S A 97: 11466–11471.
36. Hayashi K, Pu H, Andras IE, Eum SY, Yamauchi A, et al. (2006) HIV-TAT protein upregulates expression of multidrug resistance protein 1 in the blood-brain barrier. J Cereb Blood Flow Metab 26: 1052–1065.
37. D'Aversa TG, Weidenheim KM, Berman JW (2002) CD40-CD40L interactions induce chemokine expression by human microglia: implications for human immunodeficiency virus encephalitis and multiple sclerosis. Am J Pathol 160: 559–567.
38. D'Aversa TG, Yu KO, Berman JW (2004) Expression of chemokines by human fetal microglia after treatment with the human immunodeficiency virus type 1 protein Tat. J Neurovirol 10: 86–97.
39. Eugenin EA, Dyer G, Calderon TM, Berman JW (2005) HIV-1 tat protein induces a migratory phenotype in human fetal microglia by a CCL2 (MCP-1)-dependent mechanism: possible role in NeuroAIDS. Glia 49: 501–510.
40. Chen P, Mayne M, Power C, Nath A (1997) The Tat protein of HIV-1 induces tumor necrosis factor-alpha production. Implications for HIV-1-associated neurological diseases. J Biol Chem 272: 22385–22388.
41. Nath A, Conant K, Chen P, Scott C, Major EO (1999) Transient exposure to HIV-1 Tat protein results in cytokine production in macrophages and astrocytes. A hit and run phenomenon. J Biol Chem 274: 17098–17102.
42. Ghosh S, Karin M (2002) Missing pieces in the NF-kappaB puzzle. Cell 109 Suppl: S81–96.
43. Ghosh S, May MJ, Kopp EB (1998) NF-kappa B and Rel proteins: evolutionarily conserved mediators of immune responses. Annu Rev Immunol 16: 225–260.
44. Karin M, Ben-Neriah Y (2000) Phosphorylation meets ubiquitination: the control of NF-[kappa]B activity. Annu Rev Immunol 18: 621–663.
45. Sui Z, Sniderhan LF, Schifitto G, Phipps RP, Gelbard HA, et al. (2007) Functional synergy between CD40 ligand and HIV-1 Tat contributes to inflammation: implications in HIV type 1 dementia. J Immunol 178: 3226–3236.
46. Dobrzanski P, Ryseck RP, Bravo R (1993) Both N- and C-terminal domains of RelB are required for full transactivation: role of the N-terminal leucine zipper-like motif. Mol Cell Biol 13: 1572–1582.

47. Lernbecher T, Kistler B, Wirth T (1994) Two distinct mechanisms contribute to the constitutive activation of RelB in lymphoid cells. Embo J 13: 4060–4069.
48. Solan NJ, Miyoshi H, Carmona EM, Bren GD, Paya CV (2002) RelB cellular regulation and transcriptional activity are regulated by p100. J Biol Chem 277: 1405–1418.
49. Bonizzi G, Bebien M, Otero DC, Johnson-Vroom KE, Cao Y, et al. (2004) Activation of IKKalpha target genes depends on recognition of specific kappaB binding sites by RelB:p52 dimers. Embo J 23: 4202–4210.
50. Saccani S, Pantano S, Natoli G (2003) Modulation of NF-kappaB activity by exchange of dimers. Mol Cell 11: 1563–1574.
51. Fusco AJ, Huang DB, Miller D, Wang VY, Vu D, et al. (2009) NF-kappaB p52:RelB heterodimer recognizes two classes of kappaB sites with two distinct modes. EMBO Rep 10: 152–159.
52. Marienfeld R, May MJ, Berberich I, Serfling E, Ghosh S, et al. (2003) RelB forms transcriptionally inactive complexes with RelA/p65. J Biol Chem 278: 19852–19860.
53. Jacque E, Tchenio T, Piton G, Romeo PH, Baud V (2005) RelA repression of RelB activity induces selective gene activation downstream of TNF receptors. Proc Natl Acad Sci U S A 102: 14635–14640.
54. Gringhuis SI, den Dunnen J, Litjens M, van der Vlist M, Wevers B, et al. (2009) Dectin-1 directs T helper cell differentiation by controlling noncanonical NF-kappaB activation through Raf-1 and Syk. Nat Immunol 10: 203–213.
55. Yoza BK, Hu JY, Cousart SL, Forrest LM, McCall CE (2006) Induction of RelB participates in endotoxin tolerance. J Immunol 177: 4080–4085.
56. Weih F, Carrasco D, Durham SK, Barton DS, Rizzo CA, et al. (1995) Multiorgan inflammation and hematopoietic abnormalities in mice with a targeted disruption of RelB, a member of the NF-kappa B/Rel family. Cell 80: 331–340.
57. Weih F, Warr G, Yang H, Bravo R (1997) Multifocal defects in immune responses in RelB-deficient mice. J Immunol 158: 5211–5218.
58. Xia Y, Chen S, Wang Y, Mackman N, Ku G, et al. (1999) RelB modulation of IkappaBalpha stability as a mechanism of transcription suppression of interleukin-1alpha (IL-1alpha), IL-1beta, and tumor necrosis factor alpha in fibroblasts. Mol Cell Biol 19: 7688–7696.
59. Xia Y, Pauza ME, Feng L, Lo D (1997) RelB regulation of chemokine expression modulates local inflammation. Am J Pathol 151: 375–387.
60. Chang HC, Samaniego F, Nair BC, Buonaguro L, Ensoli B (1997) HIV-1 Tat protein exits from cells via a leaderless secretory pathway and binds to extracellular matrix-associated heparan sulfate proteoglycans through its basic region. AIDS 11: 1421–1431.
61. Nath A, Haughey NJ, Jones M, Anderson C, Bell JE, et al. (2000) Synergistic neurotoxicity by human immunodeficiency virus proteins Tat and gp120: protection by memantine. Ann Neurol 47: 186–194.
62. Biddison WE (2001) Preparation and culture of human lymphocytes. Curr Protoc Cell Biol Chapter 2: Unit 2 2.
63. Diamond TL, Roshal M, Jamburuthugoda VK, Reynolds HM, Merriam AR, et al. (2004) Macrophage tropism of HIV-1 depends on efficient cellular dNTP utilization by reverse transcriptase. J Biol Chem 279: 51545–51553.
64. Nichol KE, Poon WW, Parachikova AI, Cribbs DH, Glabe CG, et al. (2008) Exercise alters the immune profile in Tg2576 Alzheimer mice toward a response coincident with improved cognitive performance and decreased amyloid. J Neuroinflammation 5: 13.
65. de Jager W, te Velthuis H, Prakken BJ, Kuis W, Rijkers GT (2003) Simultaneous detection of 15 human cytokines in a single sample of stimulated peripheral blood mononuclear cells. Clin Diagn Lab Immunol 10: 133–139.
66. Bio-Rad Laboratories I, Life Sciences Group. Bio-Plex System and Technology. Bulletin #2890.
67. Sanchez JF, Sniderhan LF, Williamson AL, Fan S, Chakraborty-Sett S, et al. (2003) Glycogen synthase kinase 3beta-mediated apoptosis of primary cortical astrocytes involves inhibition of nuclear factor kappaB signaling. Mol Cell Biol 23: 4649–4662.
68. Maggirwar SB, Ramirez S, Tong N, Gelbard HA, Dewhurst S (2000) Functional interplay between nuclear factor-kappaB and c-Jun integrated by coactivator p300 determines the survival of nerve growth factor-dependent PC12 cells. J Neurochem 74: 527–539.
69. Maggirwar SB, Sarmiere PD, Dewhurst S, Freeman RS (1998) Nerve growth factor-dependent activation of NF-kappaB contributes to survival of sympathetic neurons. J Neurosci 18: 10356–10365.
70. Kim BO, Liu Y, Ruan Y, Xu ZC, Schantz L, et al. (2003) Neuropathologies in transgenic mice expressing human immunodeficiency virus type 1 Tat protein under the regulation of the astrocyte-specific glial fibrillary acidic protein promoter and doxycycline. Am J Pathol 162: 1693–1707.
71. Rezaie P, Patel K, Male DK (1999) Microglia in the human fetal spinal cord–patterns of distribution, morphology and phenotype. Brain Res Dev Brain Res 115: 71–81.
72. Quiterio S, Grant C, Hogan TH, Krebs FC, Wigdahl B (2003) C/EBP- and Tat-mediated activation of the HIV-1 LTR in CD34+ hematopoietic progenitor cells. Biomed Pharmacother 57: 49–56.
73. Iwata A, Stevenson VM, Minard A, Tasch M, Tupper J, et al. (2003) Over-expression of Bcl-2 provides protection in septic mice by a trans effect. J Immunol 171: 3136–3141.
74. Vallabhapurapu S, Karin M (2009) Regulation and function of NF-kappaB transcription factors in the immune system. Annu Rev Immunol 27: 693–733.
75. Bren GD, Solan NJ, Miyoshi H, Pennington KN, Pobst LJ, et al. (2001) Transcription of the RelB gene is regulated by NF-kappaB. Oncogene 20: 7722–7733.
76. Sui Z, Fan S, Sniderhan L, Reisinger E, Litzburg A, et al. (2006) Inhibition of mixed lineage kinase 3 prevents HIV-1 Tat-mediated neurotoxicity and monocyte activation. J Immunol 177: 702–711.
77. Minagar A, Shapshak P, Fujimura R, Ownby R, Heyes M, et al. (2002) The role of macrophage/microglia and astrocytes in the pathogenesis of three neurologic disorders: HIV-associated dementia, Alzheimer disease, and multiple sclerosis. J Neurol Sci 202: 13–23.
78. Hayden MS, Ghosh S (2008) Shared principles in NF-kappaB signaling. Cell 132: 344–362.
79. Ruben S, Perkins A, Purcell R, Joung K, Sia R, et al. (1989) Structural and functional characterization of human immunodeficiency virus tat protein. J Virol 63: 1–8.
80. Nath A, Geiger J (1998) Neurobiological aspects of human immunodeficiency virus infection: neurotoxic mechanisms. Prog Neurobiol 54: 19–33.
81. Jeang KT, Xiao H, Rich EA (1999) Multifaceted activities of the HIV-1 transactivator of transcription, Tat. J Biol Chem 274: 28837–28840.
82. Brake DA, Debouck C, Biesecker G (1990) Identification of an Arg-Gly-Asp (RGD) cell adhesion site in human immunodeficiency virus type 1 transactivation protein, tat. J Cell Biol 111: 1275–1281.
83. Frankel AD, Bredt DS, Pabo CO (1988) Tat protein from human immunodeficiency virus forms a metal-linked dimer. Science 240: 70–73.
84. Li W, Huang Y, Reid R, Steiner J, Malpica-Llanos T, et al. (2008) NMDA receptor activation by HIV-Tat protein is clade dependent. J Neurosci 28: 12190–12198.
85. Ranga U, Shankarappa R, Siddappa NB, Ramakrishna L, Nagendran R, et al. (2004) Tat protein of human immunodeficiency virus type 1 subtype C strains is a defective chemokine. J Virol 78: 2586–2590.
86. Kaul M (2009) HIV-1 associated dementia: update on pathological mechanisms and therapeutic approaches. Curr Opin Neurol 22: 315–320.
87. Anthony IC, Bell JE (2008) The Neuropathology of HIV/AIDS. Int Rev Psychiatry 20: 15–24.
88. Fine SM, Angel RA, Perry SW, Epstein LG, Rothstein JD, et al. (1996) Tumor necrosis factor alpha inhibits glutamate uptake by primary human astrocytes. Implications for pathogenesis of HIV-1 dementia. J Biol Chem 271: 15303–15306.
89. Perry SW, Hamilton JA, Tjoelker LW, Dbaibo G, Dzenko KA, et al. (1998) Platelet-activating factor receptor activation. An initiator step in HIV-1 neuropathogenesis. J Biol Chem 273: 17660–17664.
90. Gelbard HA, Dzenko KA, DiLoreto D, del Cerro C, del Cerro M, et al. (1993) Neurotoxic effects of tumor necrosis factor alpha in primary human neuronal cultures are mediated by activation of the glutamate AMPA receptor subtype: implications for AIDS neuropathogenesis. Dev Neurosci 15: 417–422.
91. Genis P, Jett M, Bernton EW, Boyle T, Gelbard HA, et al. (1992) Cytokines and arachidonic metabolites produced during human immunodeficiency virus (HIV)-infected macrophage-astroglia interactions: implications for the neuropathogenesis of HIV disease. J Exp Med 176: 1703–1718.
92. Merrill JE, Chen IS (1991) HIV-1, macrophages, glial cells, and cytokines in AIDS nervous system disease. FASEB J 5: 2391–2397.
93. Tornatore C, Nath A, Amemiya K, Major EO (1991) Persistent human immunodeficiency virus type 1 infection in human fetal glial cells reactivated by T-cell factor(s) or by the cytokines tumor necrosis factor alpha and interleukin-1 beta. J Virol 65: 6094–6100.
94. Brabers NA, Nottet HS (2006) Role of the pro-inflammatory cytokines TNF-alpha and IL-1beta in HIV-associated dementia. Eur J Clin Invest 36: 447–458.
95. Verstrepen L, Bekaert T, Chau TL, Tavernier J, Chariot A, et al. (2008) TLR-4, IL-1R and TNF-R signaling to NF-kappaB: variations on a common theme. Cell Mol Life Sci 65: 2964–2978.
96. Schutze S, Wiegmann K, Machleidt T, Kronke M (1995) TNF-induced activation of NF-kappa B. Immunobiology 193: 193–203.
97. Howard OM, Clouse KA, Smith C, Goodwin RG, Farrar WL (1993) Soluble tumor necrosis factor receptor: inhibition of human immunodeficiency virus activation. Proc Natl Acad Sci U S A 90: 2335–2339.
98. Swingler S, Morris A, Easton A (1994) Tumour necrosis factor alpha and interleukin-1 beta induce specific subunits of NFKB to bind the HIV-1 enhancer: characterisation of transcription factors controlling human immunodeficiency virus type 1 gene expression in neural cells. Biochem Biophys Res Commun 203: 623–630.
99. Westendorp MO, Shatrov VA, Schulze-Osthoff K, Frank R, Kraft M, et al. (1995) HIV-1 Tat potentiates TNF-induced NF-kappa B activation and cytotoxicity by altering the cellular redox state. Embo J 14: 546–554.
100. Harhaj E, Blaney J, Millhouse S, Sun SC (1996) Differential effects of I kappa B molecules on Tat-mediated transactivation of HIV-1 LTR. Virology 216: 284–287.
101. Beauparlant P, Kwon H, Clarke M, Lin R, Sonenberg N, et al. (1996) Transdominant mutants of I kappa B alpha block Tat-tumor necrosis factor synergistic activation of human immunodeficiency virus type 1 gene expression and virus multiplication. J Virol 70: 5777–5785.
102. Shatrov VA, Boelaert JR, Chouaib S, Droge W, Lehmann V (1997) Iron chelation decreases human immunodeficiency virus-1 Tat potentiated tumor

necrosis factor-induced NF-kappa B activation in Jurkat cells. Eur Cytokine Netw 8: 37–43.
103. Mayne M, Bratanich AC, Chen P, Rana F, Nath A, et al. (1998) HIV-1 tat molecular diversity and induction of TNF-alpha: implications for HIV-induced neurological disease. Neuroimmunomodulation 5: 184–192.
104. New DR, Maggirwar SB, Epstein LG, Dewhurst S, Gelbard HA (1998) HIV-1 Tat induces neuronal death via tumor necrosis factor-alpha and activation of non-N-methyl-D-aspartate receptors by a NFkappaB-independent mechanism. J Biol Chem 273: 17852–17858.
105. Guillemard E, Jacquemot C, Aillet F, Schmitt N, Barre-Sinoussi F, et al. (2004) Human immunodeficiency virus 1 favors the persistence of infection by activating macrophages through TNF. Virology 329: 371–380.
106. Devadas K, Hardegen NJ, Wahl LM, Hewlett IK, Clouse KA, et al. (2004) Mechanisms for macrophage-mediated HIV-1 induction. J Immunol 173: 6735–6744.
107. Ju SM, Song HY, Lee JA, Lee SJ, Choi SY, et al. (2009) Extracellular HIV-1 Tat up-regulates expression of matrix metalloproteinase-9 via a MAPK-NF-kappaB dependent pathway in human astrocytes. Exp Mol Med 41: 86–93.
108. Herbein G, Varin A, Larbi A, Fortin C, Mahlknecht U, et al. (2008) Nef and TNFalpha are coplayers that favor HIV-1 replication in monocytic cells and primary macrophages. Curr HIV Res 6: 117–129.
109. Perry SW, Dewhurst S, Bellizzi MJ, Gelbard HA (2002) Tumor necrosis factor-alpha in normal and diseased brain: Conflicting effects via intraneuronal receptor crosstalk? J Neurovirol 8: 611–624.

Research article

Open Access

Increased lymphangiogenesis in joints of mice with inflammatory arthritis

Qian Zhang[1], Yan Lu[1], Steven T Proulx[2], Ruolin Guo[1], Zhenqiang Yao[1], Edward M Schwarz[2], Brendan F Boyce[1,2] and Lianping Xing[1,2]

[1]Department of Pathology and Laboratory Medicine. University of Rochester Medical Center, 601 Elmwood Avenue, Rochester, NY 14642, USA
[2]Center for Musculoskeletal Research, University of Rochester Medical Center, 601 Elmwood Avenue, Rochester, NY 14642, USA

Corresponding author: Lianping Xing, Lianping_Xing@urmc.rochester.edu

Received: 7 Aug 2007 Revisions requested: 20 Sep 2007 Revisions received: 1 Oct 2007 Accepted: 12 Nov 2007 Published: 12 Nov 2007

Arthritis Research & Therapy 2007, **9**:R118 (doi:10.1186/ar2326)
This article is online at: http://arthritis-research.com/content/9/6/R118

Abstract

Angiogenesis is involved in the pathogenesis of inflammatory arthritis, but little is known about the role of lymphangiogenesis in this setting. Here, we examined whether tumor necrosis factor (TNF) stimulates osteoclast precursors (OCPs) to produce the lymphatic growth factor, vascular endothelial growth factor-C (VEGF-C), and induce lymphangiogenesis. We used TNF-transgenic (Tg) mice and mice with serum-induced arthritis. OCPs were purified by fluorescence-activated cell sorting of $CD11b^{+}/Gr\text{-}1^{-/lo}$ blood or bone marrow cells and subjected to microarray analysis or were generated from spleen or joint cells and treated with TNF. Expression of VEGFs was analyzed and examined by real-time reverse transcription-polymerase chain reaction and Western blotting. Immunostaining and magnetic resonance imaging were used to quantify lymphatic vessels and volumes of synovium and draining lymph nodes. TNF stimulated VEGF-C expression by OCPs and increased nuclear factor-kappa B (NF-κB) binding to an NF-κB sequence in the *VEGF-C* promoter. OCPs from joints of TNF-Tg mice express high levels of VEGF-C. Lymphatic vessel numbers and size were markedly increased in joint sections of TNF-Tg mice and mice with serum-induced arthritis. The severity of synovitis correlated with draining lymph node size. In summary, TNF induces OCPs to produce VEGF-C through NF-κB, leading to significantly increased lymphangiogenesis in joints of arthritic mice. The lymphatic system may play an important role in the pathogenesis of inflammatory arthritis.

Introduction

Joint disease in rheumatoid arthritis (RA) is characterized by inflamed hyperplastic synovial tissue or 'pannus' formation [1]. Pannus is composed of various cell types that produce a vast array of inflammatory mediators, including cytokines and chemokines that destroy the extracellular matrix in the joint by direct and indirect mechanisms. Pannus is extremely vascular, providing portals of entry for effector cells to enter the joint from the circulation and mediate joint destruction via autocrine and paracrine mechanisms. As a result of neovascularization, inflammatory cell infiltration, and concomitant synovial cell hyperplasia, the volumes of the synovium and synovial fluid increase, resulting in joint swelling and pain [2]. Thus, inhibition of new blood vessel formation has been proposed as an important therapeutic approach for patients with inflammatory-erosive arthritis [3].

The lymphatic circulation has been known for many years to be an important secondary vascular system to remove fluid, macromolecules, and cells from the interstitial spaces, and it functions as a 'compensatory' system for blood circulation. However, studies of the lymphatic system have been hampered until recently by the lack of markers that definitively distinguish blood from lymphatic vessels and a paucity of knowledge about growth factors specific to lymphatic endothelial cells. Gene array analysis comparing lymphatic endothelial cells and blood vascular endothelial cells has recently identified numerous previously unknown lineage-spe-

3D = three-dimensional; C_T = threshold cycle; EMSA = electrophoretic mobility shift assay; FACS = fluorescence-activated cell sorting; FITC = fluorescein isothiocyanate; IgG = immunoglobulin G; IL-1 = interleukin 1; LYVE-1 = lymphatic endothelial hyaluronan receptor 1; M-CSF = macrophage colony-stimulating factor; MRI = magnetic resonance imaging; NF-κB = nuclear factor-kappa B; OCP = osteoclast precursor; PBS = phosphate-buffered saline; PCR = polymerase chain reaction; PDGF = platelet-derived growth factor; RA = rheumatoid arthritis; SIA = serum-induced arthritis; Tg = transgenic; TNF = tumor necrosis factor; VEGF = vascular endothelial growth factor; VEGFR-3 = vascular endothelial growth factor receptor 3; WT = wild-type.

cific markers for blood and lymphatic vascular endothelium. Newly identified lymphatic endothelium-specific markers include [4] lymphatic endothelial hyaluronan receptor 1 (LYVE-1), prospero-related homeobox 1, vascular endothelial growth factor receptor 3 (VEGFR-3), and the mucin-type transmembrane glycoprotein, podoplanin [5-8].

In studies using these lymphatic markers, several factors, such as VEGF-A, platelet-derived growth factor (PDGF)-BB, and fibroblast growth factor, have been shown to affect lymphangiogenesis [9]. However, the most specific and potent lymphatic growth factors reported to date are VEGF-C and VEGF-D [10,11], members of the VEGF family. These differ from VEGF-A (also named VEGF) in that they promote proliferation, migration, and survival of lymphatic vascular endothelial cells through the VEGFR-3 signaling pathway [12]. This appears to be a non-redundant function because *VEGF-C*$^{-/-}$ mice are embryonic lethal due to the lack of lymphatic vessels [12]. Under physiologic conditions, VEGF-C is expressed most prominently in the heart, lymph nodes, placenta, and gut [13] but is also expressed by many cancer cells, which can induce lymphatics in metastases. Recent studies reported that VEGF-C is also expressed by CD11b^{+} myeloid cells that have migrated to inflammatory sites in several animal models of inflammation [14-17], such as corneal transplantation and bacterial lung infection. It was speculated that inflammatory cytokines, such as tumor necrosis factor (TNF) or interleukin 1 (IL-1), stimulate these CD11b^{+} cells to produce VEGF-C because TNF and IL-1 increase VEGF-C expression in human lung fibroblasts and human umbilical vein endothelial cells *in vitro* [18,19]. However, it has not been formally proven that these cytokines promote VEGF-C expression by CD11b^{+} cells, and the mechanisms involved are not known.

CD11b antigen is a pan marker for myeloid lineage cells, which also give rise to osteoclasts. We used a combination of fluorescence-activated cell sorting (FACS) and osteoclastogenesis and colony-forming assays to demonstrate that, in peripheral tissues, only CD11b^{+}/Gr-1$^{-/lo}$ cells have osteoclastogenic potential [20]. Thus, we termed CD11b^{+}/Gr-1$^{-/lo}$ cells osteoclast precursors (OCPs), although this population in bone marrow and spleen also contains macrophage and dendritic cell precursors. Over the last 2 to 3 years, immune cells and molecules that primarily function in immune responses have been demonstrated to affect the functions of cells involved in bone remodeling, particularly osteoclasts [21], which has led to development of the new field of osteoimmunology. We have pursued this line of investigation with OCPs because they belong to a subset of macrophages that can be activated to produce autocrine and paracrine factors that contribute to inflammation and autoimmunity [22]. In our microarray analysis of RNA from OCPs from TNF-transgenic (Tg) and wild-type (WT) mice, we found that VEGF-C expression is significantly increased in cells from TNF-Tg mice, suggesting that VEGF-C-mediated biologic events (for example, lymphangiogenesis) may be involved in the pathogenesis of arthritis. In this study, we used recently developed anti-lymphatic marker antibodies and contrast-enhanced magnetic resonance imaging (MRI) to demonstrate that TNF-Tg mice have a significant increase in the number and size of synovial lymphatic vessels compared with their WT littermates. Furthermore, the severity of erosive synovitis correlates with the lymphatic drainage capacity to local lymph nodes. Together, these findings demonstrate significant changes in lymphatic architecture and draining potential around inflamed joints of arthritic mice and suggest the possible involvement of the lymphatic system in the pathogenesis of inflammatory-erosive arthritis.

Materials and methods

Animals

TNF-Tg mice (Tg 3647 line) in a CBA × C57BL/6 background were originally obtained from George Kollias (The Biomedical Sciences Research Center, Greece). We backcrossed them with C57BL6 mice for seven generations [20]. All TNF-Tg mice used in this study were 4 to 8 months old with severe joint synovitis and bone and cartilage destruction. WT littermates were used as controls. TNF-Tg mice were identified by tail polymerase chain reaction (PCR) genotyping and paw deformation. KRN-TCR-Tg mice were obtained from Drs. Diane Mathis and Christophe Benoist (Harvard University, Cambridge, MA, USA) [23]. K/B × N mice were generated by breeding male KRN-TCR-Tg mice with female non-obese diabetic mice (The Jackson Laboratory, Bar Harbor, ME, USA). Serum was collected from 6- to 12-week-old K/B × N arthritic mice, pooled, and stored at -80°C. To generate mice with serum-induced arthritis (SIA), 4- to 5-week-old BALB/c mice were injected with K/B × N serum intraperitoneally (10 μL/gram body weight) on day 1 and day 3. Paw swelling and redness usually occurred the day after the first injection, peaked at 7 to 14 days, and declined thereafter. The Institutional Animal Care and Use Committee of the University of Rochester (Rochester, NY, USA) approved all studies.

Reagents

Recombinant murine TNF-α was purchased from R&D Systems, Inc. (Minneapolis, MN, USA). Allophycocyanin-, fluorescein isothiocyanate (FITC)-, and phycoerythrin-anti-mouse CD11b (M1/70) were purchased from eBiosciences (San Diego, CA, USA); FITC-anti-mouse Gr-1 (RB6-8C5) from BD Pharmingen (San Diego, CA, USA); rabbit polyclonal antibody to VEGF-C (H-190) from Santa Cruz Biotechnology, Inc. (Santa Cruz, CA, USA); rabbit polyclonal antibody to LYVE-1 from Abcam (Cambridge, MA, USA); mouse monoclonal antibody to CD31 (Mec13.3) from Biocare Medical LLC (Concord, CA, USA); Alexa Fluor 488 goat anti-hamster immunoglobulin G (IgG) from Molecular Probes Inc. (now part of Invitrogen Corporation, Carlsbad, CA, USA); and Alexa Fluor 546 F(ab')$_2$ fragment of goat anti-rabbit IgG (H+L) and

To-Pro-3 iodid (642/661) were purchased from Invitrogen Corporation.

Generation of osteoclast precursors

OCPs were generated from two sources:

(a) Spleen. Splenocytes were extracted from spleens of 8- to 12-week-old C57/B6 WT mice through a fine wire mesh, and red blood cells were lyzed with NH_4Cl (StemCell Technologies, Vancouver, BC, Canada) on ice for 10 minutes. The cells were then washed twice with medium and cultured with conditioned medium from a macrophage colony-stimulating factor (M-CSF)-producing cell line [24] (1:20 dilution) for 3 days to enrich for OCPs, as we described previously [25].

(b) Joints. Ankle and wrist joints were isolated from TNF-Tg mice and WT littermates according to published protocols [26,27] with minor modifications. In brief, mice were sacrificed and skin and muscle were removed from their limbs. Long bones together with a front or rear paw were cut from the limbs. Forceps were used to loosen the joints. The joints were then cut open and digested with 1 mg/mL of collagenase (Sigma-Aldrich, St. Louis, MO, USA) at 37°C for 3 hours with rotation. Cells were then filtered and used for cultures or FACS analysis.

Affymetrix gene chip analysis

$CD11b^+/Gr\text{-}1^{-/lo}$ OCPs were purified by flow sorting from peripheral blood and bone marrow of TNF-Tg mice and age-matched WT mice by a FACSVantage SE Turbo sorter (Becton, Dickinson and Company, Franklin Lakes, NJ, USA), as we described previously [20,28]. To obtain enough RNA from samples, bone marrow OCPs were pooled from 7 TNF-Tg mice or 11 WT mice and peripheral blood OCPs were from pooled from 7 TNF-Tg mice or 23 WT mice. Two completely independent experiments were performed. Total RNA was prepared using TRIzol (Invitrogen Corporation), processed, and hybridized to MG-U74Av2 gene chips according to Affymetrix protocols (Affymetrix, Santa Clara, CA, USA). Chips were scanned and analyzed using the GeneTraffic (version 3.2) microarray data analysis software (Lobion Informatics, La Jolla, CA, USA). In each group, WT samples were set as the baseline. Data were presented as the fold increase of samples from TNF-Tg mice over WT samples (baseline sample).

Real-time quantitative reverse transcription-polymerase chain reaction

Total RNA was extracted using TRIzol reagent, and cDNA was synthesized by an RNA PCR Core Kit (Applied Biosystems, Foster City, CA, USA). Quantitative PCR amplification was performed with gene-specific primers using an iCycler iQ Multiple-Color Real-Time PCR Detection System (Bio-Rad Laboratories, Inc., Hercules, CA, USA), as we described previously [25,28]. The primer sequences are listed in Table 1. Expression levels were normalized relative to β-*actin* in the same sample. For each sample, we first obtained the ΔC_T (difference in threshold cycle values), which is equal to C_T (target gene) – C_T (β-actin). We then used control (for example, phosphate-buffered saline [PBS]-treated) values as baseline to obtain the $\Delta\Delta C_T$, which is equal to the ΔC_T of the sample minus the ΔC_T of the baseline. Finally, we set the baseline as '1', and thus the fold change of each sample is equal to $2^{-\Delta\Delta CT}$.

Table 1

Sequences of primers used in the real-time reverse transcription-polymerase chain reaction

Genes	Sequences of primers	Accession number	Target sites	Size (base pairs)
VEGF-A	F: 5'-TTTACTGCTGTACCTCCACCA-3'	M95200	125–423	298
	R: 5'-ATCTCTCCTATGTGCTGGCTTT-3'			
VEGF-B	F: 5'-CCTGGAAGAACACAGCCAAT-3'	NM_011697	537–701	165
	R: 5'-GGAGTGGGATGGATGATGTC-3'			
VEGF-C	F: 5'-GGGAAGAAGTTCCACCATCA-3'	NM_009506	1258–1392	135
	R: 5'-ATGTGGCCTTTTCCAATACG-3'			
VEGF-D	F: 5'-GCTGTCACTGTTGCCCACTA-3'	NM_010216	1423–1611	207
	R: 5'-CCCTTCCTTTCTGAGTGCTG-3'			
PLGF	F: 5'-GGGAAGAAGCAAGACATGGA-3'	NM_008827	1055–1261	189
	R: 5'-ATGTCCTGTCCCATCTCCAG-3'			
β-actin	F: 5'-ACCCAGATCATGTTTGAGAC-3'	X03765	280–503	224
	R: 5'-GTCAGGATCTTCATGAGGTAGT-3'			

F, forward primer; PLGF, placental growth factor; R, reverse primer; VEGF, vascular endothelial growth factor.

Immunofluorescence staining and imaging cytometry

Cells were cytospun on glass slides and fixed by cold methanol at -20°C for 10 minutes. After washing with PBS, cells were incubated in 0.1% Triton and blocked with 1% bovine serum albumin/PBS for 30 minutes at room temperature. The fixed cells were stained with a mixture of FITC-anti-CD11b and anti-VEGF-C antibody followed by Alexa Fluor 546 $F(ab')_2$ fragment of goat anti-rabbit IgG (H+L) and by To-Pro-3 iodid.

Immunohistomorphometry of lymphatic vessels

Joint sections from TNF-Tg and WT mice were fixed in 4.5% phosphate-buffered formalin, decalcified in 14% ethylenediaminetetraacetic acid, and embedded in paraffin wax. Deparaffinized sections were quenched with 3% hydrogen peroxide and treated for antigen retrieval for 30 minutes. Adjacent serial sections were then stained with anti-LYVE-1 or anti-CD31 antibodies. Lymphatic vessels were quantified by a point-counting method, as we described previously [29]. For each mouse, two sections were cut at 250 μm apart and the area and size of LYVE-1$^+$ lymphatic vessels were measured within the synovial tissue. The size and area of lymphatic vessels were expressed per square millimeter of synovium.

Electrophoretic mobility shift assay

Raw 264.7 osteoclast/macrophage precursor cells were serum-starved overnight and then treated with 10 ng/mL of TNF for 30 and 60 minutes. Nuclear extract preparation and electrophoretic mobility shift assay (EMSA) were performed as described previously [30]. The following double-stranded oligonucleotides were used in this study according to the published mouse VEGF-C promoter sequence [18] (only the top strands are shown): VEGF-C nuclear factor-kappa B (NF-κB)-like sequence (WT), 5'-GCCCAGGGGGGTCCCCGGGAGG-3'; mutated VEGF-C NF-κB-like sequence (mutation underlined), 5'-GCCCAGGGG*AT*TC*I*CCGGGAGG-3'; and SP-1-binding sequence (control; Invitrogen Corporation), 5'-CGAGCCGGCCCCGCCCATC-3'. For competition assays, binding reactions were pre-incubated with unlabeled oligonucleotides for 15 minutes at room temperature.

In vivo contrast-enhanced magnetic resonance imaging

A detailed methodology of this new technique in mice will be published in a separate manuscript [31]. Briefly, mice were positioned with the right leg in a custom-designed murine knee coil and scanned in a Siemens 3 Tesla clinical magnet (Siemens AG, Munich, Germany). A high-resolution fat-suppressed T1-weighted sequence (Sagittal T1-weighted FLASH [fast low-angle shot], repetition time = 45 ms, echo time = 9.03 ms, 192 × 192 pixels, 20 mm × 20 mm field of view, 32 slices of 0.16-mm slice thickness, flip angle = 25°, 1 signal average, time: 8:28) was then initiated. An intravenous injection of Gd-DTPA contrast agent (Omniscan; Amersham Health, now part of GE Healthcare, Little Chalfont, Buckinghamshire, UK) was given, and a post-contrast high-resolution scan (same parameters) was collected. Analysis was performed with Amira 3.1 (TGS; Mercury Computer Systems, Inc., Chelmsford, MA, USA). An image registration and subtraction algorithm on the pre- and post-contrast images in Amira generated an image of the voxels of contrast enhancement. From this image, a three-dimensional (3D) region of interest of muscle tissue was used as a measure of delivered contrast agent, and a threshold of enhancing synovial tissue was generated from this value. Lymph nodes were traced manually and thresholded to define the margin between the node and surrounding fat. Tissue volumes (3D) were reconstructed using a surface generation module in Amira.

Statistics

Data are presented as mean ± standard deviation of three culture dishes, and all experiments were performed at least twice. Statistical analyses were performed with Statview statistical software (SAS Institute Inc., Cary, NC, USA). Differences among more than two groups were compared using one-way analysis of variance followed by the Mann-Whitney *U* test. *P* values of less than 0.05 were considered statistically significant. Each experiment was repeated at least twice with similar results.

Results

VEGF-C expression is upregulated in CD11b$^+$/Gr-1$^{-/lo}$ osteoclast precursors from tumor necrosis factor-transgenic mice

Previous studies demonstrated an increase in circulating OCPs in patients [32] and animals [20] with arthritis and that OCP frequency is reduced in response to anti-TNF therapy, suggesting that OCPs may play important roles in the pathogenesis of arthritis [33]. To screen for novel genes that are differentially expressed by OCPs between arthritic and normal mice, we performed microarrays on RNA isolated from CD11b$^+$/Gr-1$^{-/lo}$ OCPs from peripheral blood mononuclear cells and bone marrow pooled from TNF-Tg and WT mice. The purity of CD11b$^+$/Gr-1$^{-/lo}$ cells was confirmed by FACS. In our initial bioinformatic screen, we focused on genes encoding angiogenic factors because they are critical for development of inflammation and bone erosion in arthritic joints. Among more than 50 known angiogenic factors (including matrix metalloproteinases, adhesion molecules, enzymes, and growth factors), we found that expression levels of *PDGF-B*, *PDGF receptor β*, and *VEGF-C* were significantly increased in circulating OCPs of TNF-Tg mice (approximately six-fold in TNF-Tg over WT OCPs) (Figure 1). Expression levels of these genes were also increased in bone marrow OCPs but to a lesser extent. Since TNF is known to induce PDGF signaling [34], we decided to explore the possibility that VEGF-C has a novel role in inflammatory arthritis similar to its role in metastatic cancer [35,36].

Figure 1

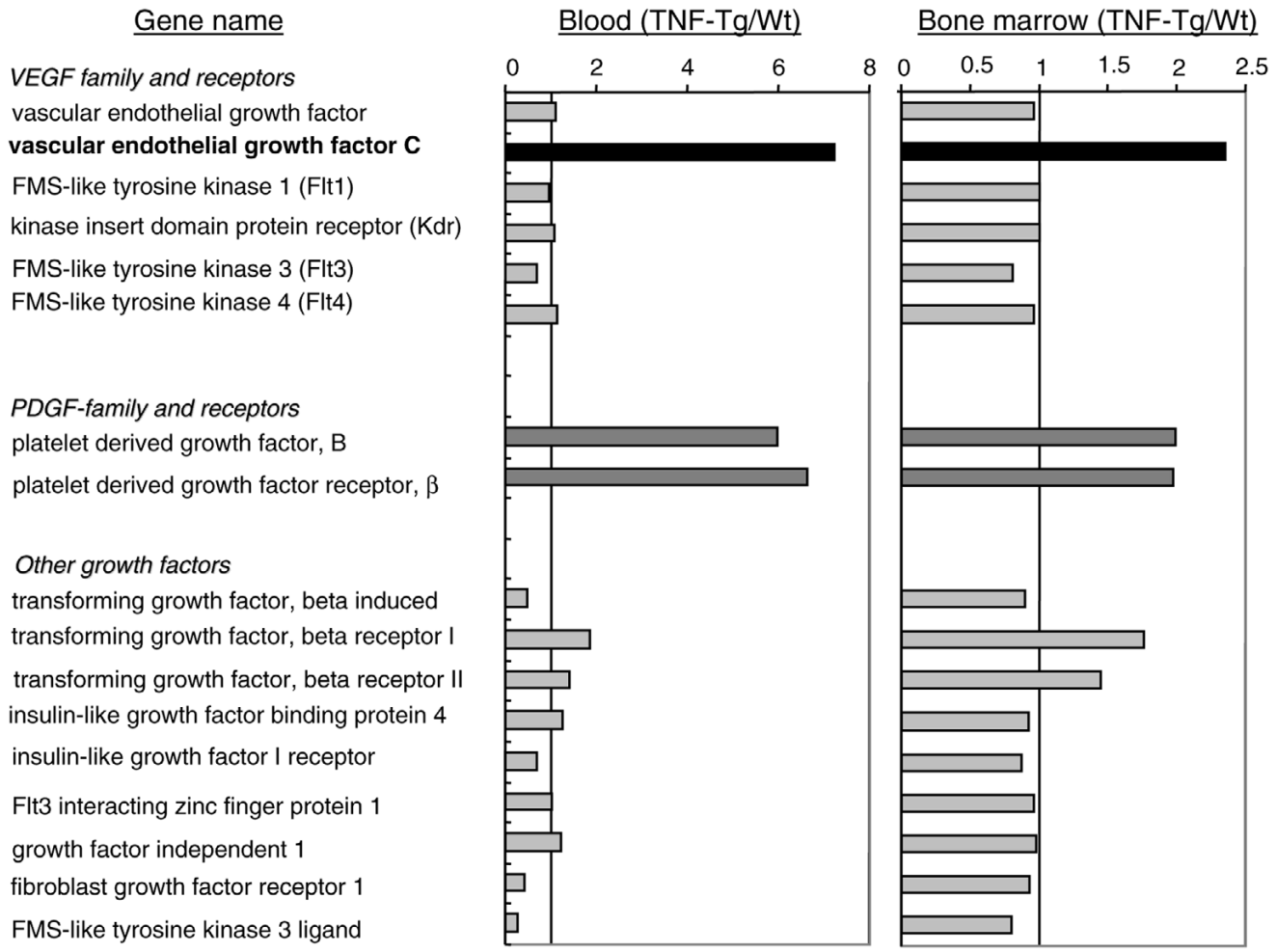

Differential expression of vascular endothelial growth factor (*VEGF*) and platelet-derived growth factor (*PDGF*) family genes in $CD11b^{+}/Gr\text{-}1^{-/lo}$ osteoclast precursors (OCPs) from tumor necrosis factor-transgenic (TNF-Tg) and wild-type (WT) mice. $CD11b^{+}/Gr\text{-}1^{-/lo}$ cells from peripheral blood and bone marrow from TNF-Tg (7 mice per array) and WT (23 mice per array) mice were pooled and purified by flow sorting. The RNA samples were subjected to microarray analysis using the GeneChip mouse genome 430A 2.0 array from Affymetrix. The array data on angiogenic gene expression were analyzed using GeneTraffic software. The expression ratio was calculated by dividing the mean value of the intensity of RNA signals from two separate arrays of TNF-Tg OCPs by that from WT cells.

Tumor necrosis factor stimulates osteoclast precursors to produce VEGF-C

To determine whether TNF directly upregulates expression of VEGF-C by OCPs, we cultured WT spleen cells with M-CSF for 3 days to generate OCPs, as we described previously [25]. The rationale for using spleen cells rather than bone marrow cells is that spleen-derived OCPs are closer to circulating OCPs than bone marrow OCPs in terms of their osteoclast-forming potency [37] and the increased *VEGF-C* expression level in circulating OCPs is more than three times higher than in bone marrow OCPs (Figure 1). TNF treatment increased *VEGF-C* mRNA levels by three- to four-fold in a time- and dose-dependent manner, beginning at between 4 and 8 hours, suggesting transcriptional regulation (left panel in Figure 2a). It also increased VEGF-C protein expression at 24 hours (right panels in Figure 2a). TNF did not significantly affect expression of other *VEGF* members (Figure 2b). Dose-response experiments demonstrated that a low dose of TNF (0.5 ng/mL) is sufficient to stimulate VEGF-C protein expression, supporting an *in vivo* role for TNF to induce VEGF-C expression (Figure 2c).

We also examined whether IL-1, another cytokine whose levels are increased significantly in joints of TNF-Tg mice, affects VEGF-C levels in OCPs. Similar to TNF, IL-1 treatment (by 24 hours) also increased *VEGF-C* mRNA by two- to three-fold, but IL-1 + TNF did not have an additive effect (Figure 2d). This suggests that TNF and IL-1 may use a similar signaling pathway to regulate VEGF-C expression.

Figure 2

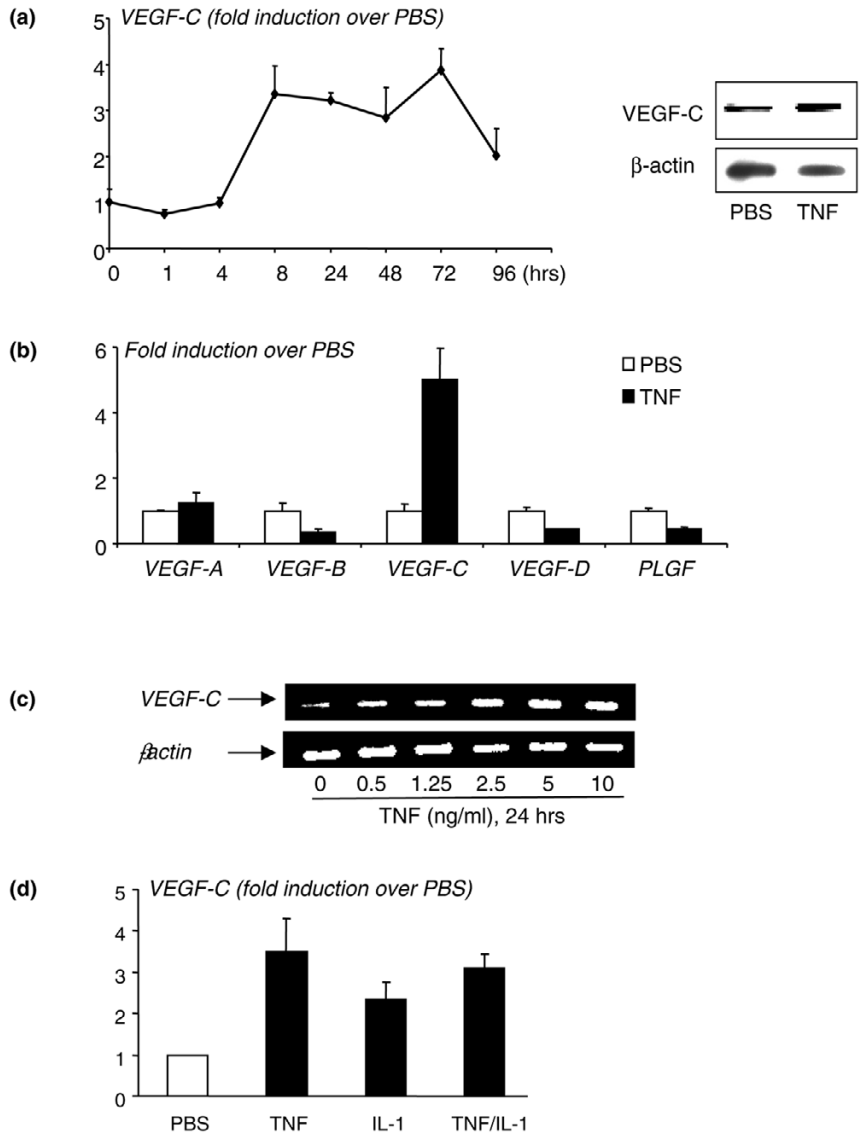

Tumor necrosis factor (TNF) increases expression of vascular endothelial growth factor-C (VEGF-C) by osteoclast precursors (OCPs). Wild-type (WT) spleen cells were cultured with macrophage colony-stimulating factor (M-CSF) for 3 days to enrich for OCPs. OCPs were cultured in 10% serum with M-CSF and treated with phosphate-buffered saline (PBS) or TNF (10 ng/mL). **(a)** Expression of *VEGF-C* and β-actin mRNA was measured by real-time reverse transcription-polymerase chain reaction (RT-PCR) at various times (left panel), and protein levels were measured by Western blot analysis (right panels). **(b)** Expression of *VEGF-A*, *-B*, -C, *-D*, and placental growth factor (*PLGF*) mRNA was examined in samples treated for 24 hours. The fold increases in TNF-treated over PBS-treated cells at a given time were calculated. Values are the means of triplicate loadings plus standard deviation. The effect of different doses of TNF **(c)** or a combination with interleukin 1 (IL-1) (TNF and IL-1 10 ng/mL) **(d)** on *VEGF-C* expression at 24 hours was examined by RT-PCR. Experiments were repeated twice with similar results.

Nuclear factor-kappa B mediates tumor necrosis factor-induced VEGF-C expression

NF-κB is a transcription factor that mediates induction of genes by TNF in many cell types, including OCPs [38]. NF-κB also mediates heregulin-beta-1-induced VEGF-C expression in human breast cancer cells [39]. We found that there is a putative NF-κB-binding element, GGGGTCCC, at the -108/-99 region of the mouse *VEGF-C* promoter, which is at a location similar to that in the human promoter [18]. Thus, to determine whether TNF stimulates binding of NF-κB proteins to this element in OCPs, we treated Raw 264.7 cells with TNF for 30 and 60 minutes and performed Western blot analysis and EMSA on nuclear extracts from the cells. TNF treatment for 30 minutes increased nuclear translocation of NF-κB p65 and p50 proteins (Figure 3a) and specific binding of NF-κB to the VEGF-C DNA probe (Figure 3b). To further confirm the involvement of NF-κB in TNF-induced VEGF-C expression, we treated WT OCPs with an NF-κB inhibitor (Calbiochem, now

part of EMD Biosciences, Inc., San Diego, CA, USA) and found that it inhibited TNF-induced VEGF-C expression in a dose-dependent manner (Figure 3c). These data support TNF induction of VEGF-C expression by activation of NF-κB.

CD11b$^+$/Gr-1$^{-/lo}$ cells isolated from joints of tumor necrosis factor-transgenic mice express high levels of VEGF-C

To examine whether OCPs at the site of inflammation express VEGF-C, we isolated cells from joints of TNF-Tg mice and WT littermates using a sequence enzyme digestion method [26,27]. We obtained, on average, a total of 1.5×10^6 cells from the four paws of a TNF-Tg mouse. FACS analysis revealed that approximately 60% of joint cells from TNF-Tg mice are CD11b$^+$ and almost all of them are Gr-1$^-$ (Figure 4a). Thus, in subsequent experiments, we used only CD11b as a single marker for OCPs. To determine whether CD11b$^+$ cells express VEGF-C, we performed double immunofluorescence staining using anti-CD11b and VEGF-C antibodies in a cytospin preparation of these cells. There were much more CD11b and VEGF-C double-stained cells in the joints of TNF-Tg mice than in WT mice (Figure 4b). We also found that most of the VEGF-C$^+$ cells are CD11b$^+$, whereas no CD11b$^-$ cells are VEGF-C$^-$, suggesting that VEGF-C is produced in arthritic joints by OCPs. To examine whether these joint CD11b$^+$ cells specifically produce more VEGF-C than other VEGFs, we cultured them with M-CSF for 3 days, harvested adherent cells, and performed real-time reverse transcription-PCR to assess the expression level of *VEGF-A*, *VEGF-C*, and *VEGF-D*. The rationale for using these M-CSF-dependent adherent cells is that they are composed mainly of OCPs and monocytes, as we described previously [25]. We found that M-CSF-dependent cells that were derived from joints of TNF-Tg mice expressed much higher levels of *VEGF-C* compared with those of WT mice (Figure 4c) whereas *VEGF-A* and *VEGF-D* levels were similar, suggesting that OCPs/monocytes are the major source of VEGF-C in arthritic joints of TNF-Tg mice. To confirm that there is elevated TNF or IL-1 expression in the joints of TNF-Tg mice, we measured the expression levels of *TNF* and *IL-1* mRNA and demonstrated that they were remarkably increased compared with levels in WT joints (Figure 4d), which supports the hypothesis that local increased cytokines stimulate VEGF-C production.

Increased lymphangiogenesis in joints of tumor necrosis factor-transgenic mice

Since VEGF-C is a specific lymphatic growth factor [40] and VEGF-C expression is increased in OCPs, we sought to determine whether there was increased lymphangiogenesis in joint sections from TNF-Tg mice compared with WT mice using immunohistochemistry and an antibody to the lymphatic endothelial cell marker, LYVE-1. We also assessed, as a positive control, blood vessels lined by endothelial cells using a CD31 antibody because these are known to be increased in TNF-Tg versus WT joints [41]. These results clearly demonstrated large LYVE-1$^+$ lymphatic vessels compared with smaller CD31$^+$ vessels in the pannus of TNF-Tg mice (Figure 5a). Histomorphometric quantitation of the area and number of these lymphatic vessels confirmed a significant increase in TNF-Tg versus WT joints (Figure 5b). To assess the functional significance of this increased lymphangiogenesis, we used a new *in vivo* MRI technology that we have developed [31] to see whether the draining popliteal lymph nodes from the knee and ankle joints of TNF-Tg mice with synovitis are increased versus WT littermates. Figure 6a demonstrates the remarkable differences in 2D MRI and 3D reconstructed images of the synovium and popliteal lymph nodes of TNF-Tg versus WT mice. Volumetric analyses confirmed that TNF-Tg mice have significantly larger synovial and popliteal lymph node volumes compared with WT mice (Figure 6b) and these were confirmed with histology (Figure 6c).

To demonstrate that increased lymphangiogenesis is not limited to the arthritis in TNF-Tg mice and to determine the association between joint inflammation and lymphatic vessel formation during the course of arthritis induction, we used mice with K/B × N SIA. This SIA model has clearly distinguishable phases of disease progression and uniform severity of joint lesions among animals compared with TNF-Tg mice. The SIA mice were sacrificed at 0, 14, and 35 days after K/B × N serum injection, and joint samples were subjected to histology and LYVE-1 immunostaining. At day 14 after serum injection, mice developed severe joint inflammation with pannus formation and inflammatory cell infiltration, which is accompanied with increased lymphatic vessel area and number (Figure 7). By day 35, the inflammation declined, but the lymphatic vessel formation had increased further (Figure 7) to a degree similar to that seen in TNF-Tg mice (Figure 5). These data suggest that increased lymphangiogenesis is a common phenotype of inflammatory-erosive arthritis.

Discussion

Patients with RA often accompany with enlarged draining lymph nodes [42] and increased lymph flow rates [43] in affected limbs, which are correlated with inflamed synovial volume. However, a cellular and molecular mechanism to explain these changes has yet to be postulated. In the present study, we demonstrated that CD11b$^+$/Gr-1$^{-/lo}$ OCPs from joints of TNF-Tg mice produce high levels of the lymphatic growth factor, VEGF-C, and that joints from mice in two models of RA have increased numbers of lymphatic vessels and enlargement of draining popliteal lymph nodes. Thus, lymphangiogenesis is also significantly increased in joints of mice with inflammatory arthritis. To date, most studies of inflammation-induced lymphangiogenesis have been performed in animal models in which the examined tissues have included cornea, lung, and skin [15,17,44], because frozen sections from these tissues can be prepared readily for immunostaining to identify lymphatic vessels and because dye injection can be used to examine the lymphatic drainage. However, it is difficult to apply

Figure 3

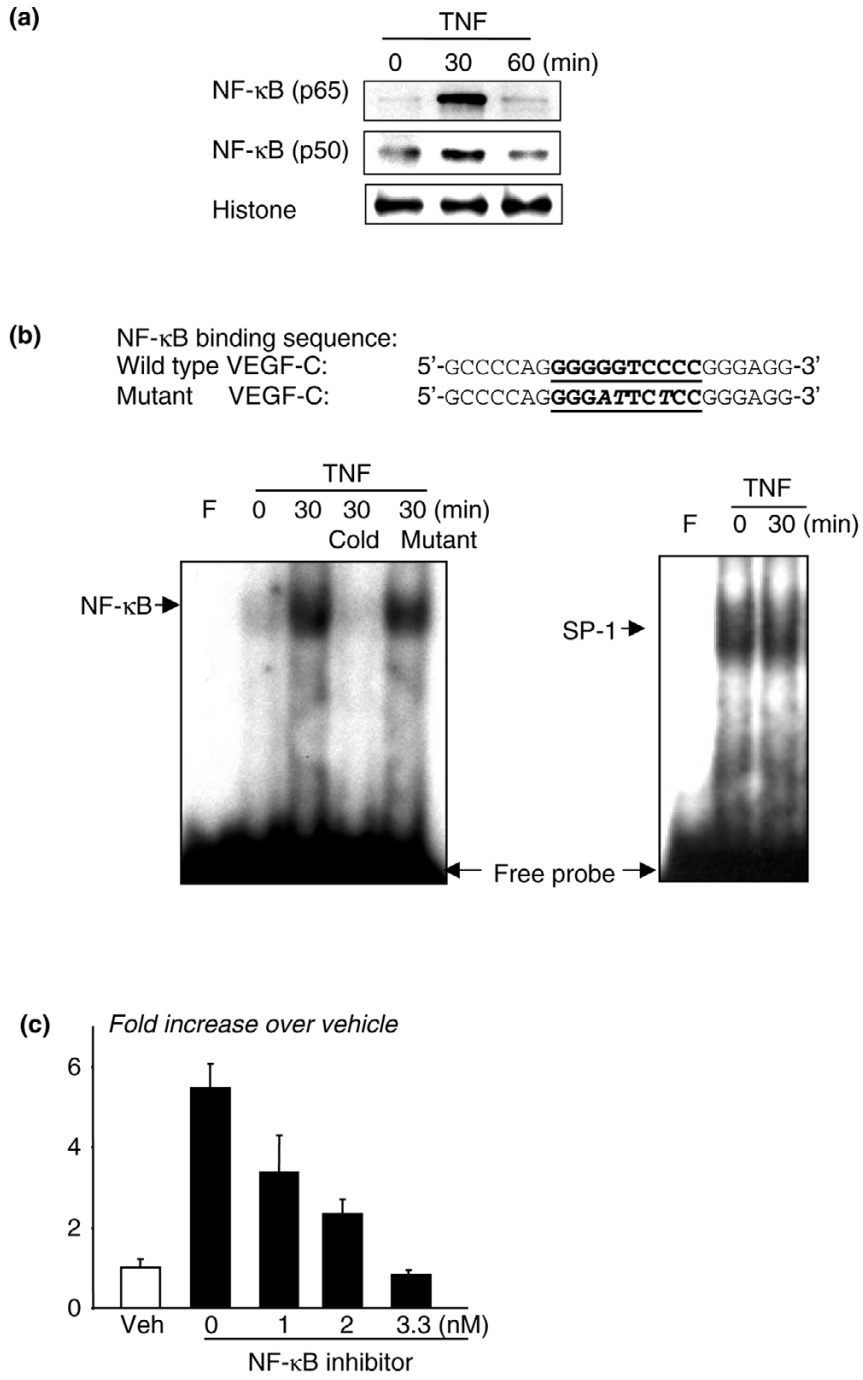

Tumor necrosis factor (TNF) promotes the binding of nuclear proteins to the nuclear factor-kappa B (NF-κB) binding sequences of the vascular endothelial growth factor-C (VEGF-C) promoter. Raw264.7 osteoclast/macrophage precursors were cultured in 0.5% bovine serum albumin overnight. Cells were treated with TNF for 30 to 60 minutes. Nuclear extracts were isolated and subjected to Western blot analysis using anti-NF-κB p65 and p50 antibodies **(a)** or to electrophoretic mobility shift assay using a ^{32}P-labeled probe consisting of the putative NF-κB binding sequence of the mouse VEGF-C promoter **(b)**. The specificity of binding was confirmed by using 50-fold more unlabeled wild-type (WT) or mutated probe in which the putative NF-κB binding sequence was mutated and could not be bound by NF-κB in a competition reaction. An SP-1 probe was used as a loading control. WT osteoclast precursors were treated with TNF ± an NF-κB inhibitor for 24 hours, and expression of *VEGF-C* was determined by real-time reverse transcription-polymerase chain reaction. Values are the means of three mice plus standard deviation. **(c)** The fold decrease in expression in the NF-κB inhibitor-treated over vehicle-treated cells was calculated. Experiments were repeated two times with similar results.

Figure 4

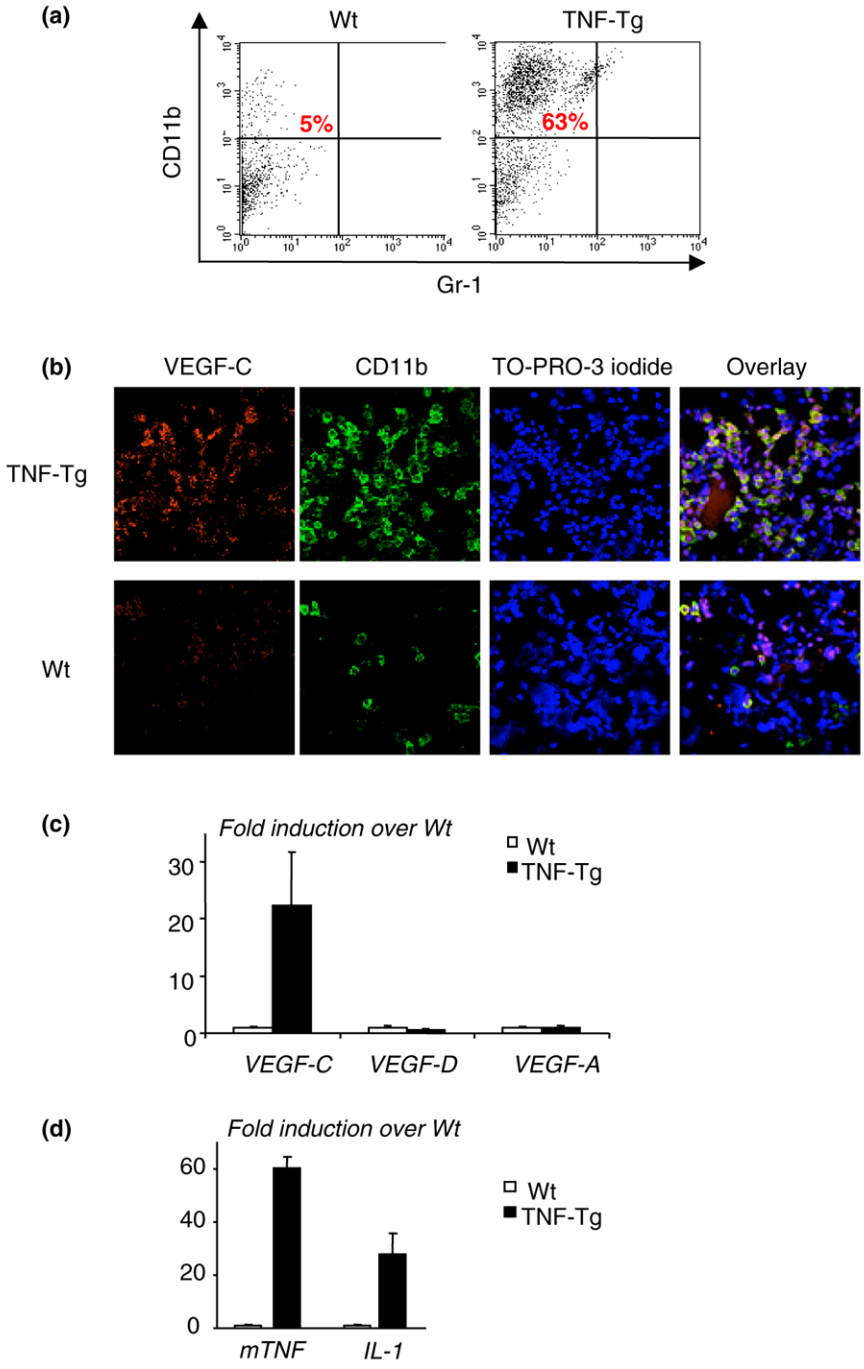

Cells from joints of tumor necrosis factor-transgenic (TNF-Tg) mice express high levels of vascular endothelial growth factor-C (VEGF-C). Ankle and wrist joints of TNF-Tg mice and wild-type (WT) littermates were subjected to collagenase digestion to isolate cells, which then were stained with fluorescein isothiocyanate (FITC)-anti-CD11b and phycoerythrin-anti-Gr-1 and subjected to fluorescence-activated cell sorting analysis. **(a)** The percentage of $CD11b^{+}/Gr\text{-}1^{-/lo}$ cells is shown in a representative histogram from one pair of TNF-Tg and WT mice. Cells (3×10^5) were cytospun onto glass slides and double-stained with FITC-anti-CD11b and rabbit anti-VEGF-C followed by anti-rabbit Alexa 546. TO-PRO-3 iodide was used as a DNA dye for nuclear staining. **(b)** Co-localization of CD11b and VEGF-C proteins was observed, and pictures were taken under a confocal microscope at a power of × 20. Cells were cultured with M-CSF for 3 days, and adherent cells were harvested. **(c)** Expressions of *VEGF-A*, *-C*, and *-D* mRNA were measured by real-time reverse transcription-polymerase chain reaction (RT-PCR). The fold increases in expression in TNF-Tg over WT cells were calculated. Values are the means of triplicate loadings plus standard deviation (SD). **(d)** The expression levels of TNF and IL-1 mRNA in joint extracts from TNF-Tg mice and WT littermates were determined by real-time RT-PCR. Values are the means of three mice plus SD. Experiments were repeated using four additional pairs of TNF-Tg and WT mice with similar results.

Figure 5

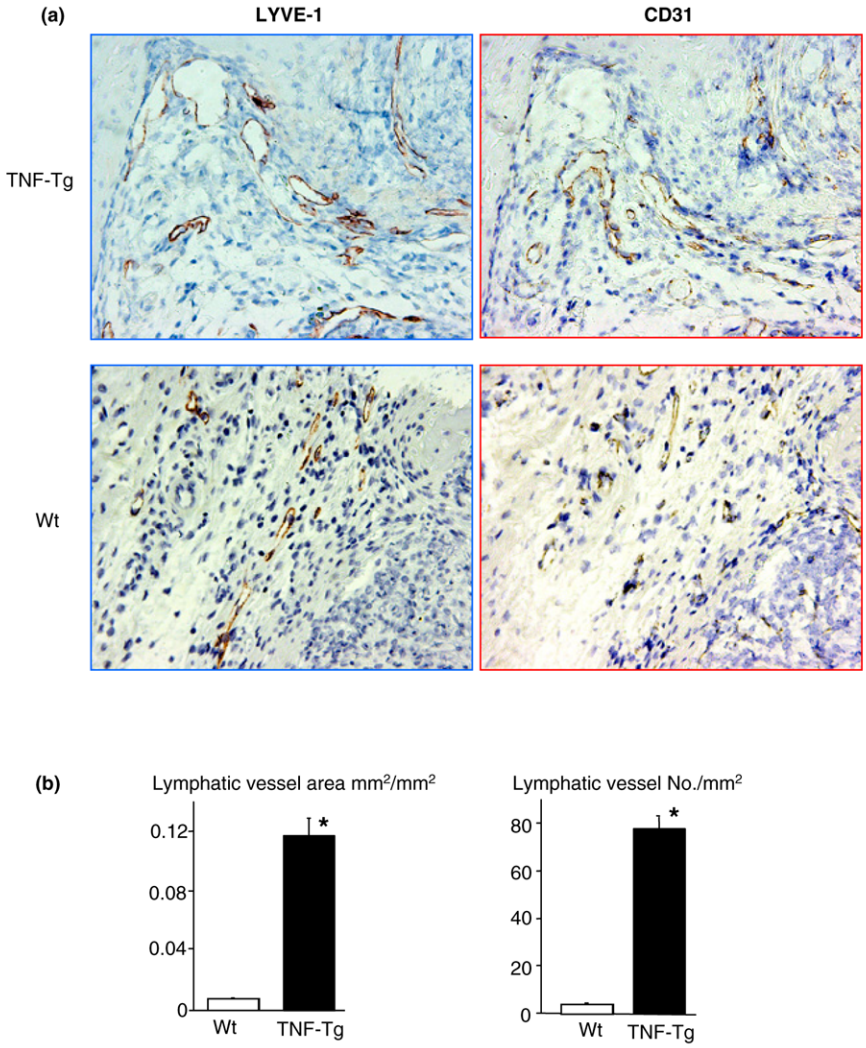

Enlargement of lymphatic vessels in the joints of tumor necrosis factor-transgenic (TNF-Tg) mice. Joint sections from TNF-Tg mice or wild-type (WT) littermates were immunostained with anti-LYVE-1 or CD31 antibody. **(a)** Micrographs (× 20) show increased numbers and diameters of LYVE-1$^+$ lymphatic vessels in the synovium of TNF-Tg mice. **(b)** The area and number of lymphatic vessels within the synovium were counted. Values are the means plus standard deviation of five TNF-Tg mice and six WT mice. *$p < 0.05$ versus WT samples. LYVE-1, lymphatic endothelial hyaluronan receptor 1.

these methods to joints. Here, we used a combination of microarrays, FACS, immunohistochemistry, and a novel *in vivo* contrast-enhanced-MRI technique to demonstrate that the lymphatic vasculature in inflamed joints and draining lymph nodes are significantly increased in mice with TNF and SIA. Our findings are consistent with those in clinical studies demonstrating increased VEGF-C expression in RA joints [45,46] and increased size of lymph nodes [43]. Furthermore, based on increased volume of collected lymph [42] and our demonstration of increased VEGF-C production by joint OCPs, we propose that the development of large lymphatic vessels in the pannus results from proliferation of lymphatic endothelial cells and their distention by increased amounts of lymph.

While the origin of lymphatic endothelia cells remains an area of active research, several studies on inflamed corneas, skin, and lung have reported the presence of CD11b$^+$ myeloid cells expressing VEGF-C in these tissues [15,47]. These studies speculated that inflammatory cytokines stimulate VEGF-C production by these CD11b$^+$ cells based on previous work in human lung fibroblasts and human umbilical vein endothelial cells [18,19]. Here, we demonstrated that TNF and IL-1 upregulate VEGF-C expression in CD11b$^+$ OCPs. To validate our microarray findings and provide insight into the mechanism of TNF-induced VEGF-C expression in OCPs, we provide preliminary evidence indicating that this response is mediated by NF-κB-dependent transcription. Since other signal transduction pathways could also be involved and TNF could be acting indi-

Figure 6

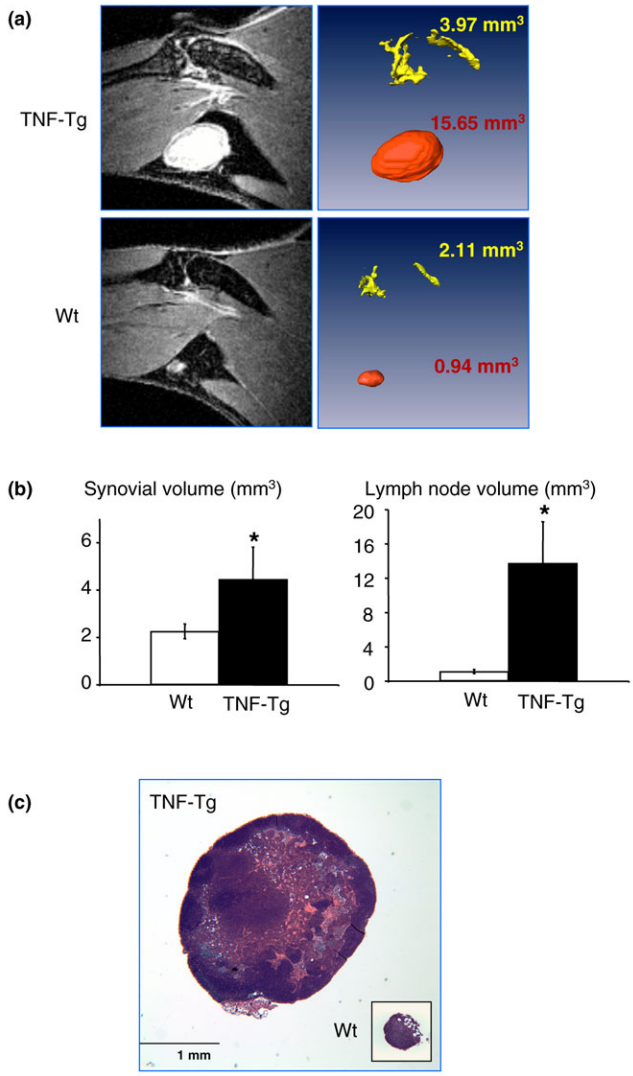

Increased volume of popliteal lymph nodes in tumor necrosis factor-transgenic (TNF-Tg) mice. **(a)** A representative post-contrast magnetic resonance imaging slice from a TNF-Tg and wild-type (WT) mouse (5 months old). **(b)** Using a semi-automated segmentation procedure in Amira software, the synovial (yellow) and lymph node (red) volumes were quantified and visualized in TNF-Tg and WT mice. *$p < 0.05$ versus WT samples ($n = 5$). **(c)** Representative hematoxylin-and-eosin sections (× 4) demonstrate differences in lymph node size between TNF-Tg and WT animals.

rectly through prostaglandins [48], which also mediate *VEGF-C* transcription in cancer cells [49], future studies are needed to elucidate the mechanisms of inflammation-induced VEGF-C expression in OCPs.

Considering the cellular heterogeneity of joint pannus, it is important to determine the primary source of VEGF-C in arthritic joints. While our studies focused on OCPs, others have shown that TNF and/or IL-1 stimulates VEGF-C expression by human lung fibroblasts, blood vascular endothelial cells, and synovial cells [19,46]. We found that TNF also stimulates VEGF-C expression in NIH3T3 and C2C12 fibroblast cell lines (data not shown), suggesting that fibroblast-like cells in synovium could perhaps be another source of VEGF-C in arthritic pannus. However, these results were obtained from *in vitro* treatment of cells with cytokines and may not precisely reflect the *in vivo* situation, particularly in the joint local microenvironment. Our immunocytochemistry studies using cells freshly isolated from joints demonstrated that most of the VEGF-C-expressing cells are CD11b$^+$ (Figure 4b). One potential concern with this approach is that primary joint cells are composed of a mixture of cell types. To address this limitation, we cultured these cells with M-CSF and used only adherent cells for further study. Under these culture conditions, more than 90% of adherent cells are CD11b$^+$/Gr-1$^{-/lo}$ OCPs (Q. Zhang, Y. Lu, S. Proulx, R. Guo, Z. Yao, E.M. Schwarz, B.F. Boyce, L. Xing, unpublished data). We found that these M-CSF-dependent joint cells express much higher levels of VEGF-C than cells treated *in vitro* (20- to 30-fold increase in joint cells in Figure 3c versus 3- to 5-fold increase in TNF-treated cells in Figure 2a). Thus, although other cell types may also be VEGF-C-producing cells, CD11b$^+$/Gr-1$^{-/lo}$ OCPs likely are one of the major sources of VEGF-C in joint pannus.

Our findings demonstrated that increased lymphangiogenesis is associated with the progression of joint inflammation, which occurs not only in dysregulated TNF-induced arthritis (Figure 5) but also in mice with SIA (Figure 7). A recent study reported that, in joint sections of collagen-induced arthritis, the number of LYVE-1$^+$ lymphatic vessels is increased [50]. Thus, elevated lymphangiogenesis likely is a common feature of inflammatory arthritis. Inflammation-induced lymphangiogenesis in joints appears to be a slow process, taking 2 to 3 weeks (Figure 7). Our explanation is that OCPs or other VEGF-C-producing cells may need to migrate to the inflamed joints first and then respond to elevated cytokine levels to produce VEGF-C, which then stimulates formation of lymphatic endothelial cells.

Interestingly, increased lymphatic vasculature persists even after serum-induced inflammation has resolved (Figure 7). This is consistent with our observation of no change in lymphatic vessel area or number in TNF-Tg mice with a significant reduction in their joint inflammation after anti-TNF therapy treatment (see Additional File 1). Persistent lymphangiogenesis was also reported in a mouse model of chronic respiratory tract infection in which inflammation has been cured by antibiotics [17]. Currently, there is no explanation why these lymphatic vessels do not disappear along with the reduction in inflammation. One speculation is that lymphatic enlargement makes affected tissues more susceptible to later inflammation by facilitating the accumulation of immune cells at the site of injury or infection [51]. However, it is also possible that an increased lymphatic network will prime tissues to respond to acute inflammation.

Figure 7

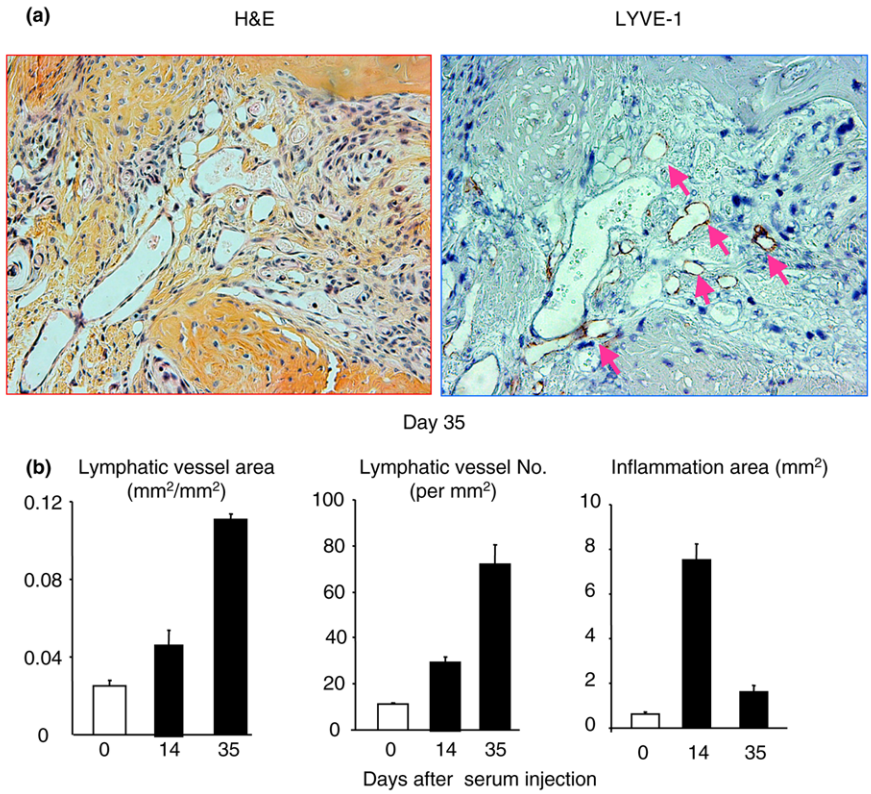

Increased lymphangiogenesis in joints of mice with serum-induced arthritis. Wild-type mice received serum from K/B × N mice to induce arthritis and were sacrificed at 0, 14, and 35 days after serum injection ($n = 3$ or 4 mice at each time point). Ankle joint sections were immunostained with anti-LYVE-1 antibody. **(a)** Representative pictures show inflamed pannus and large numbers of LYVE-1$^+$ lymphatic vessels in an adjacent section (pink arrows) at day 35. **(b)** The area and number of lymphatic vessels within the pannus were determined by histomorphometric analysis. Values are the means plus standard deviation of 3 or 4 mice at each time point. H&E, hematoxylin and eosin; LYVE-1, lymphatic endothelial hyaluronan receptor 1.

A central question that arises from our study and other recent studies regarding inflammation-induced lymphangiogenesis is whether lymphangiogenesis in arthritis is beneficial or harmful to affected joints. Early clinical studies proposed that inflammation-driven lymphangiogenesis induces the expansion of the lymphatic network in an exacerbated manner such that the lymphatic vessels may be dysfunctional, as reported in psoriasis and Crohn disease [52-54]. Recently, VEGF-C or VEGFR-3 antagonists have been used to directly stimulate or block VEGF-C/VEGFR-3-mediated lymphangiogenesis in several models of inflammation. In general, the effects of manipulating lymphangiogenesis in inflammatory conditions are not clear and appear to be largely dependent on the type of model used. For example, in the corneal transplantation model, lymphangiogenesis and angiogenesis are increased by grafting, and blockade of either form of new vessel formation has a similar beneficial effect and prevents graft rejection [55]. In contrast, UVB-induced skin inflammation is exacerbated by VEGF-C antagonism [56], suggesting that stimulation of the lymphatic system might reduce disease severity. Thus, the functional importance of lymphangiogenesis in the pathogenesis of RA remains to be determined.

Conclusion

Our findings demonstrate that lymphangiogenesis is significantly increased in joints of mice with inflammatory arthritis. TNF and OCPs appear to play a critical role in initiating this process through stimulation of VEGF-C production.

Competing interests

The authors declare that they have no competing interests.

Authors' contributions

LX participated in study design; acquisition, analysis, and interpretation of data; and manuscript preparation and had full access to all of the data in the study and takes responsibility for the integrity of the data and the accuracy of the data analysis. QZ and STP participated in study design; acquisition, analysis, and interpretation of data; manuscript preparation; and statistical analysis. YL participated in study design; acquisition, analysis, and interpretation of data; and statistical analysis. EMS and BFB participated in study design, analysis and interpretation of data, and manuscript preparation. RG and ZY participated in acquisition, analysis, and interpretation of data. All authors read and approved the final manuscript.

Additional files

The following Additional files are available online:

Additional file 1

Persistence of lymphatic vasculature in joints of tumor necrosis factor-transgenic (TNF-Tg) mice that received anti-TNF therapy. TNF-Tg mice (2.5 months old) received placebo or anti-TNF antibody (10 mg/kg per week × 8 weeks). Ankle sections were immunostained with anti-LYVE-1 antibody. The area and number of LYVE-1$^+$ lymphatic vessels within the pannus and the area of inflammation per ankle were assessed. Values are the means plus standard deviation of three placebo- or anti-TNF-treated mice. No statistically significant difference was observed between values in the placebo- and anti-TNF-treated group. TNF antibody treatment significantly reduced the inflammation. *$p < 0.05$ anti-TNF-treated group compared with placebo group. LYVE-1, lymphatic endothelial hyaluronan receptor 1.
See http://www.biomedcentral.com/content/supplementary/ar2326-S1.ppt

Acknowledgements

The authors thank Sunao Takeshita (National Institute for Longevity Sciences, Aichi, Japan) for an M-CSF-producing cell line, Diane Mathis and Christophe Benoist (Harvard University, Cambridge, MA, USA) for KRN-TCR-Tg mouse breeders, and Xiaoyun Zhang for technical assistance with the histology. This work was supported by research grants from the National Institutes of Health (Bethesda, MD, USA) (PHS AR48697 and AR53586 to LX, AR43510 to BFB, and DE17096 and AR54041 to EMS).

References

1. Firestein GS: **Evolving concepts of rheumatoid arthritis.** *Nature* 2003, **423:**356-361.
2. Maruotti N, Cantatore FP, Crivellato E, Vacca A, Ribatti D: **Angiogenesis in rheumatoid arthritis.** *Histol Histopathol* 2006, **21:**557-566.
3. De Bandt M, Ben Mahdi MH, Ollivier V, Grossin M, Dupuis M, Gaudry M, Bohlen P, Lipson KE, Rice A, Wu Y, *et al.*: **Blockade of vascular endothelial growth factor receptor I (VEGF-RI), but not VEGF-RII, suppresses joint destruction in the K/B × N model of rheumatoid arthritis.** *J Immunol* 2003, **171:**4853-4859.
4. Oliver G, Detmar M: **The rediscovery of the lymphatic system: old and new insights into the development and biological function of the lymphatic vasculature.** *Genes Dev* 2002, **16:**773-783.
5. Podgrabinska S, Braun P, Velasco P, Kloos B, Pepper MS, Skobe M: **Molecular characterization of lymphatic endothelial cells.** *Proc Natl Acad Sci USA* 2002, **99:**16069-16074.
6. Kriehuber E, Breiteneder-Geleff S, Groeger M, Soleiman A, Schoppmann SF, Stingl G, Kerjaschki D, Maurer D: **Isolation and characterization of dermal lymphatic and blood endothelial cells reveal stable and functionally specialized cell lineages.** *J Exp Med* 2001, **194:**797-808.
7. Mäkinen T, Veikkola T, Mustjoki S, Karpanen T, Catimel B, Nice EC, Wise L, Mercer A, Kowalski H, Kerjaschki D, *et al.*: **Isolated lymphatic endothelial cells transduce growth, survival and migratory signals via the VEGF-C/D receptor VEGFR-3.** *EMBO J* 2001, **20:**4762-4773.
8. Hirakawa S, Hong YK, Harvey N, Schacht V, Matsuda K, Libermann T, Detmar M: **Identification of vascular lineage-specific genes by transcriptional profiling of isolated blood vascular and lymphatic endothelial cells.** *Am J Pathol* 2003, **162:**575-586.
9. Cao R, Eriksson A, Kubo H, Alitalo K, Cao Y, Thyberg J: **Comparative evaluation of FGF-2-, VEGF-A-, and VEGF-C-induced angiogenesis, lymphangiogenesis, vascular fenestrations, and permeability.** *Circ Res* 2004, **94:**664-670.
10. Brown P: **Lymphatic system: unlocking the drains.** *Nature* 2005, **436:**456-458.
11. Alitalo K, Tammela T, Petrova TV: **Lymphangiogenesis in development and human disease.** *Nature* 2005, **438:**946-953.
12. Karkkainen MJ, Haiko P, Sainio K, Partanen J, Taipale J, Petrova TV, Jeltsch M, Jackson DG, Talikka M, Rauvala H, *et al.*: **Vascular endothelial growth factor C is required for sprouting of the first lymphatic vessels from embryonic veins.** *Nat Immunol* 2004, **5:**74-80.
13. Lee J, Gray A, Yuan J, Luoh SM, Avraham H, Wood WI: **Vascular endothelial growth factor-related protein: a ligand and specific activator of the tyrosine kinase receptor Flt4.** *Proc Natl Acad Sci USA* 1996, **93:**1988-1992.
14. Kerjaschki D, Huttary N, Raab I, Regele H, Bojarski-Nagy K, Bartel G, Kröber SM, Greinix H, Rosenmaier A, Karlhofer F, *et al.*: **Lymphatic endothelial progenitor cells contribute to *de novo* lymphangiogenesis in human renal transplants.** *Nat Med* 2006, **12:**230-234.
15. Maruyama K, Ii M, Cursiefen C, Jackson DG, Keino H, Tomita M, Van Rooijen N, Takenaka H, D'Amore PA, Stein-Streilein J, *et al.*: **Inflammation-induced lymphangiogenesis in the cornea arises from CD11b-positive macrophages.** *J Clin Invest* 2005, **115:**2363-2372.
16. Hamrah P, Chen L, Zhang Q, Dana MR: **Novel expression of vascular endothelial growth factor receptor (VEGFR)-3 and VEGF-C on corneal dendritic cells.** *Am J Pathol* 2003, **163:**57-68.
17. Baluk P, Tammela T, Ator E, Lyubynska N, Achen MG, Hicklin DJ, Jeltsch M, Petrova TV, Pytowski B, Stacker SA, *et al.*: **Pathogenesis of persistent lymphatic vessel hyperplasia in chronic airway inflammation.** *J Clin Invest* 2005, **115:**247-257.
18. Chilov D, Kukk E, Taira S, Jeltsch M, Kaukonen J, Palotie A, Joukov V, Alitalo K: **Genomic organization of human and mouse genes for vascular endothelial growth factor C.** *J Biol Chem* 1997, **272:**25176-25183.
19. Ristimäki A, Narko K, Enholm B, Joukov V, Alitalo K: **Proinflammatory cytokines regulate expression of the lymphatic endothelial mitogen vascular endothelial growth factor-C.** *J Biol Chem* 1998, **273:**8413-8418.
20. Li P, Schwarz EM, O'Keefe RJ, Ma L, Looney RJ, Ritchlin CT, Boyce BF, Xing L: **Systemic tumor necrosis factor alpha mediates an increase in peripheral CD11bhigh osteoclast precursors in tumor necrosis factor alpha-transgenic mice.** *Arthritis Rheum* 2004, **50:**265-276.
21. Kim N, Kadono Y, Takami M, Lee J, Lee SH, Okada F, Kim JH, Kobayashi T, Odgren PR, Nakano H, *et al.*: **Osteoclast differentiation independent of the TRANCE-RANK-TRAF6 axis.** *J Exp Med* 2005, **202:**589-595.
22. Xing L, Schwarz EM, Boyce BF: **Osteoclast precursors, RANKL/RANK, and immunology.** *Immunol Rev* 2005, **208:**19-29.
23. Kouskoff V, Korganow AS, Duchatelle V, Degott C, Benoist C, Mathis D: **Organ-specific disease provoked by systemic autoimmunity.** *Cell* 1996, **87:**811-822.
24. Takeshita S, Kaji K, Kudo A: **Identification and characterization of the new osteoclast progenitor with macrophage phenotypes being able to differentiate into mature osteoclasts.** *J Bone Miner Res* 2000, **15:**1477-1488.
25. Zhang Q, Badell IR, Schwarz EM, Boulukos KE, Yao Z, Boyce BF, Xing L: **Tumor necrosis factor prevents alendronate-induced osteoclast apoptosis *in vivo* by stimulating Bcl-xL expression through Ets-2.** *Arthritis Rheum* 2005, **52:**2708-2718.
26. Brühl H, Cihak J, Schneider MA, Plachý J, Rupp T, Wenzel I, Shakarami M, Milz S, Ellwart JW, Stangassinger M, *et al.*: **Dual role of CCR2 during initiation and progression of collagen-induced arthritis: evidence for regulatory activity of CCR2$^+$ T cells.** *J Immunol* 2004, **172:**890-898.
27. Kamata K, Kamijo S, Nakajima A, Koyanagi A, Kurosawa H, Yagita H, Okumura K: **Involvement of TNF-like weak inducer of apop-**

tosis in the pathogenesis of collagen-induced arthritis. *J Immunol* 2006, **177:**6433-6439.
28. Yao Z, Li P, Zhang Q, Schwarz EM, Keng P, Arbini A, Boyce BF, Xing L: **Tumor necrosis factor-{alpha} increases circulating osteoclast precursor numbers by promoting their proliferation and differentiation in the bone marrow through up-regulation of c-Fms expression.** *J Biol Chem* 2006, **281:**11846-11855.
29. Boyce BF: **Bone biopsy and histomorphometry in metabolic bone disease.** In *New Techniques in Metabolic Bone Disease* Edited by: Stevenson JC. London: Butterworths; 1990:110-131.
30. Feng JQ, Xing L, Zhang JH, Zhao M, Horn D, Chan J, Boyce BF, Harris SE, Mundy GR, Chen D: **NF-kappaB specifically activates BMP-2 gene expression in growth plate chondrocytes *in vivo* and in a chondrocyte cell line *in vitro*.** *J Biol Chem* 2003, **278:**29130-29135.
31. Proulx TS, Kwok E, Beck CA, Shealy D, Ritchlin CT, Awad HA, Boyce BF, Xing L, Schwarz EM: **Longitudinal assessment of synovial, lymph node, and bone volumes in inflammatory arthritis in mice using *in vivo* MRI and micro-CT.** *Arthritis Rheum* in press.
32. Ritchlin CT, Haas-Smith SA, Li P, Hicks DG, Schwarz EM: **Mechanisms of TNF-alpha- and RANKL-mediated osteoclastogenesis and bone resorption in psoriatic arthritis.** *J Clin Invest* 2003, **111:**821-831.
33. Xing L, Schwarz EM: **Circulating osteoclast precursors: a mechanism and a marker of erosive arthritis.** *Curr Rheumatol Rev* 2005, **1:**21-28.
34. Battegay EJ, Raines EW, Colbert T, Ross R: **TNF-alpha stimulation of fibroblast proliferation. Dependence on platelet-derived growth factor (PDGF) secretion and alteration of PDGF receptor expression.** *J Immunol* 1995, **154:**6040-6047.
35. Su JL, Yang PC, Shih JY, Yang CY, Wei LH, Hsieh CY, Chou CH, Jeng YM, Wang MY, Chang KJ, *et al.*: **The VEGF-C/Flt-4 axis promotes invasion and metastasis of cancer cells.** *Cancer Cell* 2006, **9:**209-223.
36. Roy H, Bhardwaj S, Yla-Herttuala S: **Biology of vascular endothelial growth factors.** *FEBS Lett* 2006, **580:**2879-2887.
37. Yao Z, Xing L, Qin C, Schwarz EM, Boyce BF: **Osteoclast precursors induce their differentiation to osteoclasts by interacting with bone matrix and secreting cytokines.** *JBMR* 2006, **21(Suppl 2):**S262.
38. Zhang YH, Heulsmann A, Tondravi MM, Mukherjee A, Abu-Amer Y: **Tumor necrosis factor-alpha (TNF) stimulates RANKL-induced osteoclastogenesis via coupling of TNF type 1 receptor and RANK signaling pathways.** *J Biol Chem* 2001, **276:**563-568.
39. Tsai PW, Shiah SG, Lin MT, Wu CW, Kuo ML: **Up-regulation of vascular endothelial growth factor C in breast cancer cells by heregulin-beta 1. A critical role of p38/nuclear factor-kappa B signaling pathway.** *J Biol Chem* 2003, **278:**5750-5759.
40. Tammela T, Enholm B, Alitalo K, Paavonen K: **The biology of vascular endothelial growth factors.** *Cardiovasc Res* 2005, **65:**550-563.
41. Yin G, Liu W, An P, Li P, Ding I, Planelles V, Schwarz EM, Min W: **Endostatin gene transfer inhibits joint angiogenesis and pannus formation in inflammatory arthritis.** *Mol Ther* 2002, **5(5 Pt 1):**547-554.
42. Olszewski WL, Pazdur J, Kubasiewicz E, Zaleska M, Cooke CJ, Miller NE: **Lymph draining from foot joints in rheumatoid arthritis provides insight into local cytokine and chemokine production and transport to lymph nodes.** *Arthritis Rheum* 2001, **44:**541-549.
43. Huh YM, Kim S, Suh JS, Song H, Song K, Shin KH: **The role of popliteal lymph nodes in differentiating rheumatoid arthritis from osteoarthritis by using CE 3D FSPGR MR imaging: relationship of the inflamed synovial volume.** *Korean J Radiol* 2005, **6:**117-124.
44. Goldman J, Le TX, Skobe M, Swartz MA: **Overexpression of VEGF-C causes transient lymphatic hyperplasia but not increased lymphangiogenesis in regenerating skin.** *Circ Res* 2005, **96:**1193-1199.
45. Wauke K, Nagashima M, Ishiwata T, Asano G, Yoshino S: **Expression and localization of vascular endothelial growth factor-C in rheumatoid arthritis synovial tissue.** *J Rheumatol* 2002, **29:**34-38.
46. Cha HS, Bae EK, Koh JH, Chai JY, Jeon CH, Ahn KS, Kim J, Koh EM: **Tumor necrosis factor-alpha induces vascular endothelial growth factor-C expression in rheumatoid synoviocytes.** *J Rheumatol* 2007, **34:**16-19.
47. Kerjaschki D: **Lymphatic neoangiogenesis in renal transplants: a driving force of chronic rejection?** *J Nephrol* 2006, **19:**403-406.
48. Tammali R, Ramana KV, Srivastava SK: **Aldose reductase regulates TNF-alpha-induced PGE_2 production in human colon cancer cells.** *Cancer Lett* 2007, **252:**299-306.
49. Timoshenko AV, Chakraborty C, Wagner GF, Lala PK: **COX-2-mediated stimulation of the lymphangiogenic factor VEGF-C in human breast cancer.** *Br J Cancer* 2006, **94:**1154-1163.
50. Silverman MD, Haas CS, Rad AM, Arbab AS, Koch AE: **The role of vascular cell adhesion molecule 1/very late activation antigen 4 in endothelial progenitor cell recruitment to rheumatoid arthritis synovium.** *Arthritis Rheum* 2007, **56:**1817-1826.
51. Bashyam H: **Vessel-widening by VEGF.** *J Exp Med* 2007, **204:**1240.
52. Braverman IM, Yen A: **Microcirculation in psoriatic skin.** *J Invest Dermatol* 1974, **62:**493-502.
53. Ryan TJ: **Microcirculation in psoriasis: blood vessels, lymphatics and tissue fluid.** *Pharmacol Ther* 1980, **10:**27-64.
54. Kovi J, Duong HD, Hoang CT: **Ultrastructure of intestinal lymphatics in Crohn's disease.** *Am J Clin Pathol* 1981, **76:**385-394.
55. Cursiefen C, Cao J, Chen L, Liu Y, Maruyama K, Jackson D, Kruse FE, Wiegand SJ, Dana MR, Streilein JW: **Inhibition of hemangiogenesis and lymphangiogenesis after normal-risk corneal transplantation by neutralizing VEGF promotes graft survival.** *Invest Ophthalmol Vis Sci* 2004, **45:**2666-2673.
56. Kajiya K, Detmar M: **An important role of lymphatic vessels in the control of UVB-induced edema formation and inflammation.** *J Invest Dermatol* 2006, **126:**919-921.